

**UNRAVELING THE FUNCTIONS OF DETOXIFICATION
ENZYMES AND DRUG TRANSPORTERS**

Yaogeng Wang

Printing of this thesis was financially supported by the Onderzoeksschool Oncologie Amsterdam and the Utrecht Institute for Pharmaceutical Science.

Copyright 2022 © **Yaogeng Wang**

The Netherlands. All rights reserved. No parts of this thesis may be reproduced, stored in a retrieval system or transmitted in any form or by any means without permission of the author.

ISBN: 978-94-6421-781-0

Printed by Ipskamp Printing | proefschriften.net

Cover design: Shuqing Yang

Layout and design: Eduard Boxem | persoonlijkproefschrift.nl

The graphic abstracts and part of figures in the current thesis are made with bio-render.com

UNRAVELING THE FUNCTIONS OF DETOXIFICATION ENZYMES AND DRUG TRANSPORTERS

Het ontrafelen van de functies van ontgiftende enzymen en geneesmiddel-
transporterende eiwitten
(met een samenvatting in het Nederlands)

Proefschrift

ter verkrijging van de graad van doctor aan de
Universiteit Utrecht
op gezag van de
rector magnificus, prof.dr. H.R.B.M. Kummeling,
ingevolge het besluit van het college voor promoties
in het openbaar te verdedigen op

dinsdag 12 juli 2022 des middags te 12.15 uur

door

YAOGENG WANG

geboren op 27 januari 1990
te Henan, China

Promotor:

Prof. dr. J.H. Beijnen

Copromotor:

Dr. A.H. Schinkel

“Progress is achieved through diligence and retarded by indolence. While success comes from thinking and destroyed by following.”

業精於勤而荒於嬉，行成於思而毀於隨。

-Han Yu (768-824 AD), a historian, poet and philosopher in Tang Dynasty

-韓愈

TABLE OF CONTENTS

PART I. PHARMACOLOGICAL AND PHYSIOLOGICAL FUNCTIONS OF THE CARBOXYLESTERASE 2 COMPLEX

| | |
|--|----|
| Chapter 1: Introduction of esterase enzymes | 11 |
| 1.1 Hepatic and intestinal esterases: insights into pharmacology | 13 |
| 1.2 Hepatic and intestinal esterases: insights into physiology | 39 |
| Chapter 2: Pharmacological and physiological functions of the Carboxylesterase 2 complex: new mouse models | 46 |

PART II. THE EFFECTS OF DRUG TRANSPORTERS AND CYP3A ENZYMES ON THE PHARMACOKINETICS OF SELECTIVE ANTI-TUMOR SMALL MOLECULAR INHIBITORS

| | |
|---|-----|
| Chapter 3: Introduction: The roles of drug transporters and metabolizing enzymes | 117 |
| Chapter 4: Pharmacokinetic studies on tyrosine kinase inhibitors | 131 |
| 4.1 OATP1A/1B, CYP3A, ABCB1, and ABCG2 limit oral availability of NTRK inhibitor larotrectinib, while ABCB1 and ABCG2 also restrict its brain accumulation | 133 |
| 4.2 Rifampin and ritonavir increase oral availability and elacridar enhances overall exposure and brain accumulation of the NTRK inhibitor larotrectinib | 175 |
| 4.3 P-glycoprotein (ABCB1/MDR1) and BCRP (ABCG2) limit brain accumulation and Cytochrome P450-3A (CYP3A) restricts oral availability of the RET inhibitor selpercatinib (RETEVMO) | 209 |
| 4.4 ABCB1 and ABCG2, but not CYP3A4 limit oral availability and brain accumulation of the RET inhibitor pralsetinib | 247 |
| Chapter 5: Conclusion and Perspectives | 289 |
| Chapter 6: Summary | 305 |
| Appendices | 317 |
| Chemical structures | 318 |
| Curriculum vitae | 319 |
| Publications | 320 |
| Acknowledgements | 322 |



PART I.

**PHARMACOLOGICAL AND PHYSIOLOGICAL
FUNCTIONS OF THE CARBOXYLESTERASE 2
COMPLEX**



CHAPTER 1

INTRODUCTION OF ESTERASE ENZYMES



CHAPTER 1.1

HEPATIC AND INTESTINAL ESTERASES: INSIGHTS INTO PHARMACOLOGY

Yaogeng Wang¹, Jos Beijnen^{1,2,3}, Alfred Schinkel^{1*}

**Corresponding author*

¹Division of Pharmacology, The Netherlands Cancer Institute, Plesmanlaan 121, 1066 CX Amsterdam, The Netherlands.

²Department of Pharmacy & Pharmacology, Plesmanlaan 121, 1066 CX Amsterdam, The Netherlands.

³Faculty of Science, Department of Pharmaceutical Sciences, Division of Pharmacoepidemiology & Clinical Pharmacology, Utrecht University, Universiteitsweg 99, 3584 CG Utrecht, The Netherlands.

Correspondence to:

Alfred H. Schinkel

Division of Pharmacology, The Netherlands Cancer Institute,
Plesmanlaan 121, 1066 CX Amsterdam, The Netherlands

Tel.: +31-20-512-2046, Fax: +31-20-5121792, E-mail: a.schinkel@nki.nl

ABSTRACT

Human carboxylesterase (CES) and arylacetamide deacetylase (AADAC) are two important serine esterase families expressed in liver and intestine. They can hydrolyze many carboxylester, amide, and thioester bonds in both endogenous molecules and xenobiotic compounds. Thus, they are involved in the activation or detoxification of many (pro-)drugs, influencing the absorption, distribution, metabolism and excretion (ADME) profiles for these drugs. Considering that CES and AADAC are abundant in both intestine and liver, they will play important roles in intestinal and subsequent liver metabolism of oral drugs (first-pass metabolism). This can profoundly influence the overall exposure, the efficacy, and the safety of specific ester (pro-)drugs. From this perspective, it is important to systematically understand the specific roles of each esterase, especially the hepatic and intestinal esterases, such as CES and AADAC. Such improved understanding will benefit rational drug design, development of new drugs and optimization of clinical drug regimens. In this review, we discuss the three different main hepatic and intestinal esterases (CES1, CES2 and AADAC), their specific substrates and inhibitors, their polymorphisms, and their hepatic or intestinal pharmacological roles in drug metabolism. We further discuss related pre-clinical mouse models that may help to meet currently unmet research needs on these esterases.

Keywords: Arylacetamide deacetylase, carboxylesterase, drug metabolism, esterase, prodrugs

Abbreviations:

AADAC: Arylacetamide deacetylase; CES: Carboxylesterase

1. INTRODUCTION

Drug absorption, distribution, metabolism and excretion (ADME) of specific medicines can be affected by different detoxification systems. Among these systems, drug-metabolizing enzymes (DMEs) play important roles¹. DMEs can be classified into two main groups: Phase I enzymes, which often catalyze oxidation, reduction, and hydrolysis reactions; and most phase II enzymes which catalyze conjugation reactions. Drugs are often metabolized by sequential reactions involving phase I and II enzymes². Cytochrome P450 (CYP) is one of the most important phase I enzyme superfamilies, which encodes an extensive range of enzymes involved in the metabolism of 70–80% of all clinically used drugs^{3,4}. Another important phase I enzyme superfamily encompasses esterases, including carboxylesterase (CES), arylacetamide deacetylase (AADAC), cholinesterase (CHE), paraoxonase (PON) and perhaps albumin, which contribute to the metabolism of ~10% of the clinical-therapeutic drugs containing ester, amide, or thioester bonds⁵.

Given their important pharmacological functions, the utilization of esterase enzymes has been increasingly incorporated into the drug development process to increase drug efficacy⁶. For instance, irinotecan, a semisynthetic camptothecin, was developed as a prodrug of SN-38 for colorectal cancer treatment⁷. The biotransformation from irinotecan to SN-38 is believed to be primarily mediated by CES enzymes^{8,9}. Moreover, abiraterone acetate was developed as an esterase-activated pro-drug to overcome the poor bioavailability of abiraterone, a potent inhibitor of cytochrome P450_{17 α} for treatment of metastatic castration-resistant prostate cancer¹⁰. And eslicarbazepine acetate was developed to efficiently generate the specific metabolite eslicarbazepine, an anticonvulsant medication¹¹. Recently, both abiraterone acetate and eslicarbazepine acetate were demonstrated to be rapidly converted during intestinal first-pass metabolism, predominantly mediated by AADAC^{12,13}. Thus, it is becoming more and more important to investigate the esterase enzyme functions in drug metabolism and distribution.

It has been well established that among these esterases, the CES and AADAC families have a broader hydrolytic substrate spectrum than others. When a drug is orally administered, it has to pass the intestinal wall and subsequently the liver before it reaches the systemic blood circulation (Figure 1). As both CES and AADAC are highly expressed in the intestine and liver, they can then make a major contribution to the pre-systemic elimination or activation of their substrate (pro-) drugs following oral administration by metabolism in intestine and liver (first-pass metabolism). This combined metabolism effect may thus profoundly influence the overall exposure and the efficacy of specific drugs. In the current review, we summarize the basic properties of three main hepatic and intestinal esterases (CES1, CES2 and AADAC), including, but not limited to, their amino acid sequences, tissue distribution, specific substrates and inhibitors, and genetic polymorphisms. In addition, the relationship between the pharmacological roles of hepatic

and intestinal esterases, the unmet pre-clinical research needs, and related pre-clinical mouse models are also discussed.

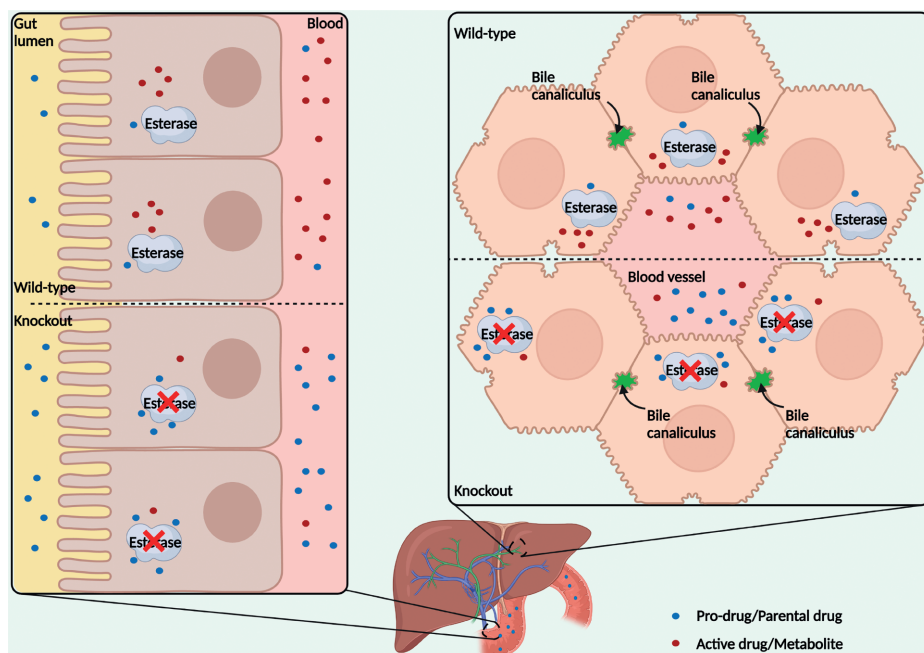


Figure 1. Systemic exposure to esterase enzyme substrate drugs is limited by the intestinal and hepatic localization of esterase enzymes. Metabolism of drug (dark blue circles) to its metabolite (red circles) by esterase enzymes is indicated. ✕: The deficiency (knockout or inhibition) of esterase enzymes.

2. CARBOXYLESTERASES

Mammalian carboxylesterases (CES, EC 3.1.1.1) belong to the serine (α/β) hydrolase superfamily of enzymes. They have broad substrate specificities and catalyze the ester cleavage of a large number of structurally diverse compounds containing ester-, thioester-, and amide bonds¹⁴⁻¹⁶. As hydrolytic enzymes, carboxylesterases (CES) can be involved in the activation, detoxification and further metabolism of (pro-)drugs and xenobiotic compounds¹⁷⁻²⁰. It is further well established that carboxylesterases can also hydrolyze endogenous ester and thioester compounds, such as triglyceride and cholesterol esters, and some of these enzymes have been shown to play important physiological roles in lipid metabolism and energy homeostasis²¹. To date, six human carboxylesterases (*CES1*, *CES1P1*, *CES2*, *CES3*, *CES4A* and *CES5A*) and twenty mouse carboxylesterases encoded in five gene clusters (*Ces1*, *Ces2*, *Ces3*, *Ces4* and *Ces5*) have been classified. Within these carboxylesterases, CES1 and CES2 appear to be the pharmacologically most important members.

2.1. CES1

The mouse harbors eight *Ces1* genes (from *Ces1a* to *Ces1h*). All genes are arranged in tandem within a 360-kb segment of mouse chromosome 8, with an average gene size of 28 kb. In contrast, human has only one dominant functional *CES1* gene (*CES1A1*) and one pseudogene (*CES1P1*), a polymorphism of which may generate a functional gene (*CES1A2*). Both of them are located on human chromosome 16. It is worth noting that except for mouse *Ces1a*, *Ces1b* and *Ces1c*, the other mouse *Ces1* and human *CES1* proteins all contain ER retrieval signal sequences (HXEL) at the C-terminus (Figure 2). This is essential for the localization of these enzymes to the ER lumen in mammalian cells^{14,21,22}. Likely related to this, mouse *Ces1c* was identified to be abundantly present in the blood, as it is secreted from the liver. Even though they also lack HXEL ER retention signals, no *Ces1a* or *Ces1b* was identified in the blood, which may relate to the (very) low expression of these genes in the liver. Mouse *Ces1* enzymes have a fairly wide and unique tissue distribution. For example, *Ces1h*, like *Ces1a*, is present in negligible amounts in liver, and *Ces1b* is undetectable in any tissue. However, the other five *Ces1* enzymes (*Ces1c* to *Ces1g*) are expressed in the liver to various extents, whereas *Ces1d* is most highly expressed in adipose tissue, and *Ces1f* in kidney²³. However, human *CES1*, an approximately 63 kDa protein, was found to be highly expressed in the liver and also observed in macrophages, adipose tissue, lung epithelia, heart, testis and other tissues^{16,24,25}. There is no human *CES1* detected in plasma, in line with the presence of an ER retention signal²⁶.

Given the high expression in the liver, *CES1*, rather than other esterase enzymes, is considered to be the most abundant hepatic esterase²⁰. The systemic exposure of ester (pro-)drugs therefore may be dominantly influenced by hepatic *CES1* metabolism, and the drug efficacy could thus be affected. However, a liver targeting oral pro-drug strategy to maximize drug exposure specifically in the liver could also be envisaged. Such a liver targeting ester (pro-)drug should be developed to be a *CES1* substrate and not a *CES2* substrate, avoiding intensive metabolizing occur in intestine. Upon oral administration, this could potentially have high oral absorption, low intestinal first-pass metabolism and then high conversion to the active drug in the liver due to the abundant hepatic *CES1* activity. Examples of such drugs could for instance be liver-targeted small-molecule inhibitors of proprotein convertase subtilisin/kexin Type 9 (PCSK9), which can be used to treat cardiovascular disease²⁷. On the other hand, the over-activation of some drugs by esterases may induce toxicity. Recently, as a drug for COVID-19, remdesivir was believed to be activated by *CES1*, not *CES2*. An *in vitro* study revealed that *CES1*-based hydrolysis contributes to both activation and cytotoxicity of remdesivir²⁸. Of significance, although remdesivir delivers benefits in the clinic, some adverse effects were also found, such as increased hepatic enzymes in serum, indicating potential hepatic injury²⁹⁻³¹. All in all, as a potential dominant esterase in the liver, *CES1* may dramatically influence the activation and/or inactivation of some specific (pro-)drugs, affecting the active drug systemic exposure, and consequently drug efficacy and/or toxicity.

Ces1a 1 **M**WLFALALAS LNTCMALGHL SSPVVDTLQ GKVMGKYISL EGSAQPVAVF LGVPFAKPPL
 Ces1b 1 **M**WLHALVWAS LALCPIWGHG PSSPVVDTTQ GKILGKYTSL EGFEHPVAVF LGVPFAKPPL
 Ces1c 1 **M**WLHALVWAS LAVCPILGHS LLPPVVDTTQ GKVLGKYISL EGFEQPVAVF LGVPFAKPPL
 Ces1d 1 **M**GLYPLIWL S LAAC TAWGYP SSPVVTNIVK GKVLGKYVNL EGFTQPVAVF LGVPFAKPPL
 Ces1e 1 **M**CLSALILVS LAAFTAGAGH PSSPPMVDTV QGKVLGKYIS LEGFTQPVAV FLGVFPAKPP
 Ces1f 1 **M**FLSTLFLVS LATCVICGNP SSPVVDTAH GKVLGKHVNV EGFSQPVAVF LGIPFAKPPL
 Ces1g 1 **M**WLCALSLIS LTACLSLGHF SLPPVVHTVH GKVLGKYVTL EGFSQPVAVF LGVPFAKPPL
 Ces1h 1 **M**CLYALILLS LSAMAWGGYP SSPVVTNTH GKVLGKYISL EGFTQPVAVF LGVPFAKPPL
 hCES1 1 **M**WLRAFILAT LSASAAGWHP SSPVVDTVH GKVLGKFSVL EGFAQPVAVF LGIPFAKPPL

Ces1a 61 GPLRFAPPQP AETWSSVKNT TSYPPMCSQI TGVGVLSDV FTNQLENVPL EYSEDCLYLN
 Ces1b 61 GSLRFAPPEP AEPWSFVKNA TSYPPMCSQD AVAVQLLSDM LSTKKEISPP LFSEDCLYLN
 Ces1c 61 GSLRFAPPQP AEPWSFVKNA TSYPPMCSQD AGWAKILSDM FSTEKEILPL KISEDCLYLN
 Ces1d 61 GSLRFAPPQP AEPWSFVKNT TSYPPMCSQD AVGGQVLSEL FTNRKENIPL QFSEDCLYLN
 Ces1e 61 LGS LRFAPPQ PAEPWSSVKN ATSYPPMCFQ DPVTGQIVND LLTNRKEKIP LQFSEDCLYL
 Ces1f 61 GSLRFAPPQP AEPWSSVKN TTYPPMCSQD AARGQAVNDL ITNRKEKIHL EYSEDCLYLN
 Ces1g 61 GSLRFAPPEP AEPWSFVKHT TSYPPMCSQD PEAALRLAEL FTNQRKIIPH KFSEDCLYLN
 Ces1h 61 GSLRFAPPQP PEPWSFVKNA TSYPPMCSQD AVLGQMVNDL IINNKEKIRL RFSEDCLYLN
 hCES1 61 GPLRFTPPQP AEPWSFVKNA TSYPPMCTQD PKAGQLLSEL FTNRKENIPL KISEDCLYLN

Ces1a 121 IYSPTDLTSK DRLPVMVWVH GGGLLSGGAS TFDGLALSTH ENVVIVVIQY RLGIWGFLST
 Ces1b 121 IYSPADLTKS SLLPVMVWIH GGGMLTGGAS LYNGLALSAH ENVVVVTIQY RLGIWGLFST
 Ces1c 121 IYSPADLTKS SLPVPMVWIH GGGLVIGGAS PYNGLALSAH ENVVVVTIQY RLGIWGLFST
 Ces1d 121 IYTPADLTKN SRLPVMVWIH GGGLVVGGAS TYDGLALSAH ENVVVVTIQY RLGIWGFST
 Ces1e 121 NIYTPADLTK SDRLPVMVWI HGGGLVLGGA STYDGLVLSH HENVVVVIQY YRLGIWGFSS
 Ces1f 121 IYTPADFSKN SRLPVMVWIH GGGKLVGGAS SFDGRALSAY ENVVVVAIQY RLSIWGFST
 Ces1g 121 IYTPADLTQN SRLPVMVWIH GGGLVIDGAS TYDGVPLAVH ENVVVVIQY RLGIWGFST
 Ces1h 121 VYTPVDLMKN TNRLPVMVWI HGGGLVVGGA SAYDGRTLSA HENVVVVTIQY YRLAIWGFSS
 hCES1 121 IYTPADLTKK NRLPVMVWIH GGGLMVGAAS TYDGLALAAH ENVVVVTIQY RLGIWGFST

Ces1a 181 GDEHSRGNWG HLDQVAALQW VQNNIANFGG DPSSVTLFGE SAGGESVSVL VLSPLTKNLF
 Ces1b 181 GDEHSRGNWA HLDQLAALRW VQDNIANFGG NPDSVTIFGS SAGGVSVSVL VLSPLAKNLF
 Ces1c 181 GDEHSPGNWA HLDQLAALRW VQDNIANFGG NPDSVTIFGE SGGISVSVL VLSPLGKDLF
 Ces1d 181 GDEHSRGNWG HLDQVAALRW VQDNIANFGG NPGSVTIFGE SAGGFSVSVL VLSPLAKNLF
 Ces1e 181 TGDEHSRGNW GHLDQVAALH WVQDNIAKFG GDPGSVTIFG ESAGGESVSV LVLSPAKNLF
 Ces1f 181 GDEHSRGNWG HLDQVAALHW VQDNIANFGG DPGSVTIFGE SAGGYSVSVL ILSPLSKNLF
 Ces1g 181 EDEHSRGNWG HLDQVAALHW VQDNIANFGG NPGSVTIFGE SAGGESVSVL VLSPLAKNLF
 Ces1h 181 TGDEHSRGNW GHLDQLAALH WIQDNIANFG GDPGSVTIFG QSAGGESVSV LVLSPAKNLF
 hCES1 181 GDEHSRGNWG HLDQVAALRW VQDNIAFGG NPGSVTIFGE SAGGESVSVL VLSPLAKNLF

Ces1a 241 QRAISESGVA LTPCLFRET RRAAEQVAIA TGCVATTSAD IVHCLREKTE EELLATTLKM
 Ces1b 241 HRAISESSV LENVITLDL VACDLSQMIA TVSGCNDTSS TAMVQCRLQK TENELLEITV
 Ces1c 241 HRAISESGV INTNVGKKN I QAVNEIATL SQCNDTSSAA MVQCRLQKTE SELLEISGKL
 Ces1d 241 HRAISESGV LTAALITTDV KPIAGLVATL SGCKTTTSAV MVHCLRQKTE DELLETSLK
 Ces1e 241 FQRAISESGV ALTAGLVKKN TRPLAEKIAV ISGCKNTTSA AMVHCLRQKTE EELLEITTLK
 Ces1f 241 HRAISESGVA FIPGMFTKDV RPIEQIAVT AGCKTTTSAV IVHCMRQKTE EELLEIMHKL
 Ces1g 241 HRAIAQSSVI FNPCLFGRAA RPLAKKIAAL AGCKTTTSA MVHCLRQKTE DELLEVSLKM
 Ces1h 241 FHRAISQSGV VFTSGLFMED ASSVTEQIAV TAGCKTTTSA VIVHCLRQKTE EELLEIMQK
 hCES1 241 HRAISESGVA LTSVLVKKGD VKPLAEQIAI TAGCKTTTSA VMVHCLRQKTE EELLEITTLK

Ces1a 301 KFFALDLLGD PRESYPFLTT VIDGVVLPKA PEEILAEKSF NTVPYIVGIN KQEFGWFIIPM
 Ces1b 301 KLEVTKVGG AAKDNTSM STVIDGVVLP KAPEEILAEK SFSTVPYIVG FNKQEFGWII
 Ces1c 301 VQYNISLSTM IDGVVLPKAP EEILAEKSFN TVPYIVGFNK QEFGWIIIPM LQNLLPEGKM

Ces1d 301 NLFKLDLLGN PKESYPFLPT VIDGVVLPKA PEEILAEKSF STVPYIVGIN KQEFGWIIPT
 Ces1e 301 NLFKLDLLHG DSRQSHFFVP TVLDGVVLPK MPEEILAEKN NTVPYIVGIN NKQEFGWILP
 Ces1f 301 NLYKLSLQGD TKNSDQFVTS VLDGVVLPKD PKEILAEKNF NTVPYIVGIN KQECGWLLPT
 Ces1g 301 KFGTVDFLGD PRESYPFLPT VIDGVVLPKA PEEILAEKSF NTVPYIVGIN KHEFGWIIIPM
 Ces1h 301 MNLFKLDQAQ NTKKNYFFLP TVLDGVVLPK APEAILAEKN NTVPYIVGIN NKQEFGWITLP
 hCES1 301 MKFLSLDLQG DPRESQPLLQ TVIDGMLLLK TPEELQAERN FHTVPYIVGI NKQEFGWILP

Ces1a 361 MMGYPLSEGK LDQKSATSLK WKSYPNTNIS KELTPVATEK YLGGSDCPDK KKDFLDMMG
 Ces1b 361 PTMLGDLLE GKMNEETASL LLRRFHSDLN ISESLIPAVI EKYLRGTDDP AKKRDLLLDM
 Ces1c 361 NEETASLLLR RFHSELNISE SMIPAVIEQY LRGVDDPAKK SELILDMFGD IFFGIPAVLL
 Ces1d 361 LMGYPLAEGK LDQKTANSLK WKSYPNTNIS ENMIPVVAEK YLGGTDDLTK KKDLFQDLMA
 Ces1e 361 TMMNYPPSDV KLDQMTAMSL LKSSSFLNLL PEDAIAVAIE KYLRDKDYTG RNKDQLLELI
 Ces1f 361 MTGFLPADVK LDKKKAIALL EQFASMTGIP EDIIPVAEK YTKGSDDDPQ IREGVLDAMG
 Ces1g 361 FLDFPLSERK LDQKTAASIL WQAYPILNIS EKLIPAAIEK YLGGTEDPAT MTDLFLDLIG
 Ces1h 361 MIMFPPPTDV KLDKKNVISL LKRLAYFFNI PEDGIPVAIE KYSKGTDDPI QNRVWLLQLI
 hCES1 361 MLMSYPLSEG QLDQKTAMSL LWKSYPLVCI AKELIPEATE KYLGGTDDTV KKKDLFLDLI

Ces1a 421 DVLFVAVSVI VARYHRDAGA PTYMYEFKYH PSFVSDMRPK TVIADHGDEV YSVWGTPFLK
 Ces1b 421 FSDVFFGIPA VLLSRSLRDA GVSTYMYEYR YRPSFVSDKR PQTVEGDHGD EIFSVFGIPL
 Ces1c 421 SRSLRDAGVS TYMYEYRYP SFVSDKRPQT VEGDHGDEIF FVFGAPLKE GASEEETNLS
 Ces1d 421 DVVFGVPSVI VSRSHRDAGA STYMYEYFYR PSFVSAMRPK AVIGDHGDEI FSVFSGPFLK
 Ces1e 421 GDVFGVPSV IVSRGHRDAG APTYMYEFQY SPSFSSMKP DTVVDHGDE IYSVFGAPIL
 Ces1f 421 DVAFVPSVI VSRGHRDAGA PTYMYEYQY PSFSSPQRPK NVVDGHADDV YSVFGAPILR
 Ces1g 421 DIMFGVPSVI VSRSHRDAGA PTYMYEYQY PSFVSDDRPQ ELLGDHDEL FSVWGAPFLK
 Ces1h 421 GDVMFGIPSV IVSRGHRDAG APTYMYEFQS RPSFSSSELKP KTVTGDHGD VYSVFGAPIL
 hCES1 421 ADVMFGVPSV IVARNHRDAG APTYMYEFQY RPSFSSDMKP KTVIGDHGD LFSVFGAPFL

Ces1a 481 EGASEEEINL STMMMKFWGN FARNGNPNGE GLPHWPEYGE KESYLQIGAT TQQAQRKDK
 Ces1b 481 LKEGTSEET NLSKVMKFW ANFARNGNPN GEGLPHWPEY DEKEGYLQIG ATTQQAQRK
 Ces1c 481 KMVMKFWANF ARNGNPNNEG LPHWPEYDEQ EGYLQIGAT TQQAQRKAE VAFWTELLAK
 Ces1d 481 DGASEEETNL SKMVMKFWAN FARNGNPNNG GLPHWPEYDQ KEGYLKIGAS TQQAQRKDK
 Ces1e 481 RGGTSEEEIN LSKMVMKFWA NFARNGNPNNG QGLPHWPEYD QKEGYLQIGA TQQAQRKKE
 Ces1f 481 EGASEEEINL SKMVMKFWAN FARNGNPNNG GLPHWPKYDQ KEGYLHIGGT TQQAQRKKEE
 Ces1g 481 EGASEEEINL SKMVMKFWAN FARNGNPNNG GLPHWPEYDQ KEGYLQIGVP AQAHRKDK
 Ces1h 481 REGSSEEEIN LSKMVMKFWA NFARNGNPNNG QGLPHWPEYN QKKGYLQIGA TQQAQRKDK
 hCES1 481 KEGASEEEIR LSKMVMKFWA NFARNGNPNNG EGLPHWPEYN QKEGYLQIGA NTQQAQRKDK

Ces1a 541 EVAFWTLRA MEVGEATKGD TQR-----
 Ces1b 541 AEEVAFWTEL LAKNPPETDP TEHREHK-----
 Ces1c 541 NPPETDPTEH TEHK-----
 Ces1d 541 EVSFAELRA KESAQRPSHR **EHVEL**-----
 Ces1e 541 KEVAFWTELL AKKQLPTE**HT EL**-----
 Ces1f 541 EVTFTWQSLA KKQPQPY**HNE I**-----
 Ces1g 541 EVDFWTELRA KETAERSSHR **EHVEL**-----
 Ces1h 541 KEVSLWTELR AKKPPQT**HT EL**-----
 hCES1 541 KEVAFWTLNF AKKAVEKPPQ **TEHIEL**-----

Figure 2. Amino acid sequence alignments of the human and murine carboxylesterase 1 family. The starting amino acid methionine (M) and the HXEL ER retrieval sequence are indicated with bold letters and highlighted with green and yellow color, respectively.

2.2. CES2

The mouse contains eight *Ces2* genes, from *Ces2a* to *Ces2h*, including one pseudogene designated *Ces2d-ps*. All these *Ces2* genes are located in a 286-kb gene cluster (*Ces2* cluster) on mouse chromosome 8. While human has only a single *CES2* gene, which, together with *CES3* and *CES4A*, is present in a cluster on human chromosome 16^{32,33}. Of note, unlike mouse *Ces1c*, which is primarily secreted into plasma due to lack of an ER retention signal, almost all mouse (except for *Ces2f*, which is hardly expressed in all tissues tested so far²²) and human *CES2* proteins carry the HXEL ER retrieval sequence at their C-terminus (such as HTEL for *CES2*, Figure 3)^{14,21,22}. However, presence of an ER retrieval sequence may not necessarily guarantee that proteins cannot be secreted at all from the ER lumen into blood. Almost all the mouse *Ces2* genes were most highly expressed in the small intestine, with in most cases a segmental distribution of mRNA at highest levels in the proximal (duodenum) small intestine, gradually decreasing towards the distal part of the small intestine (ileum), and lowest expression level in the colon. Besides in intestine, some *Ces2* enzymes are also substantially expressed in other organs, for instance, liver (*Ces2a*, *2e*), kidney (*Ces2c*), and spleen (*Ces2g*). Of note, *Ces2f* has extremely low expression in all tested tissues, including liver and intestine²³.

Like human *CES1*, human *CES2* (~62 kDa) can hydrolyze carboxyl ester as well as amide and thioester linkages in both exogenous and endogenous compounds, and there is substantial overlap in substrates. However, unlike *CES1*, *CES2* is mainly highly expressed in the intestine, and then liver. Because of this property, it may make a major contribution to the pre-systemic elimination of substrate drugs following oral administration (first-pass metabolism). The potential *CES2* mediated oral ester-drugs will be first metabolized within enterocytes where *CES2* is mainly present before arriving to the liver, in which substrate drugs will be further hydrolyzed by hepatocyte *CES2*. This two-step metabolism process can profoundly influence the overall exposure, the efficacy, and the safety of specific drugs. A good *CES2* substrate may be limited to a low systemic exposure due to enterocyte and hepatocyte *CES2*, while more metabolites accumulate in the local intestine tissue where they can potentially lead to local toxicity, such as chemotherapy-induced diarrhea (CID), in case the metabolite is toxic³⁴. In addition, *CES2* was found to be expressed in various types of cancer, including hepatocellular carcinoma, esophageal squamous carcinoma, colon adenocarcinoma, and renal adenocarcinoma, albeit with a significantly lower expression level than that in corresponding normal tissues. Besides this, the *CES2* expression and activity can vary considerably among different cancer types and individuals. These activity differences of *CES2* may therefore influence the response of tumor tissue to specific drugs, and thus affect anti-tumor therapy with esterase-activated drugs such as irinotecan and gemcitabine^{35,36}. In summary, *CES2* plays an important role in the metabolism of many exogenous compounds, such as (pro-)drugs, toxins and pesticides, and may thus directly influence pharmacology and toxicology in human.

| | | |
|--------------|-----|---|
| <i>Ces2a</i> | / | ----- |
| <i>Ces2b</i> | / | ----- |
| <i>Ces2c</i> | / | ----- |
| <i>Ces2e</i> | / | ----- |
| <i>Ces2f</i> | / | ----- |
| <i>Ces2g</i> | / | ----- |
| <i>Ces2h</i> | / | ----- |
| hCES2 | 1 | MTAQSRSPPT PTFPGPSQRT PLTPCPVQTP RLGKALIHCV TDPGQPLGEQ QRVRRQRTET |
| <i>Ces2a</i> | 1 | ----MPLARL PGWLCVVACG LLLLLQHVVHG QDSASPIRNT HRGQVRGSFV HVKDTKSGVH |
| <i>Ces2b</i> | 1 | ----MPRSQM HNWLDVLLFG LLLLLGHVQG QDSPEASPIR NTHTGQVRGS LVHVKDTKAG |
| <i>Ces2c</i> | 1 | ----MTRNQL HNWLNAGFFG LLLLLLIHVQG QDSPEANPIR NTHTGQIQGS LIHVKDTKAG |
| <i>Ces2e</i> | 1 | ----MPLYKL LGWLNNAVACG VLLLLLVHVQG QDSASPIRNT HTGQVRGSLV HVKDTDIAVH |
| <i>Ces2f</i> | 1 | ----MPVHRL PGWLDAAACG LLVLLLVHVKG LDSSEASPIR NTHTGQVRGK FVHLTDIKAG |
| <i>Ces2g</i> | 1 | ----MPRNQM HSWLDAVFFG LLLLLGHVQG HDSPETSPIR STHSGVQVGR LIHVKDTKAG |
| <i>Ces2h</i> | 1 | ----MRLEQI HARLTATCG LLLLLRVQGG DSTSPIRTH TQQLGSLIH MKDLVDVGVHS |
| hCES2 | 61 | SEPTMRLHRL RARLSAVACG LLLLLVVRGQG QDSASPIRTH HTGQVLGSLV HVKGANAGVQ |
| <i>Ces2a</i> | 57 | AFLGIPFAKP PVGLLRFAPP EDPEPWSGVR DGTSPQAMCL QPDIMNLEDA KEMNLILPPI |
| <i>Ces2b</i> | 57 | VHTFLGIPFA KPPVGPLRFA PPEAPEPWSG VRDGTGTAHPAM CLQNLGVMKE IKLKLPPVST |
| <i>CES2C</i> | 57 | VHTFLGIPFA KPPVGPLRFA PPEAPEPWSG VRDGTGTAHPAM CLQNLDMLE AGLPDMKMLL |
| <i>CES2E</i> | 57 | TFLGIPFAKP PVGPLRFAPP EAPEPWSGVR DGTSHPNMCL QNDNLMGSED LKMMNLILPP |
| <i>CES2F</i> | 57 | AHNFLGIPFA KPPVGPLRFA PPEAPEPWSG VRDGTSPQAM CLQNDDIVNL EGLKIKMIL |
| <i>CES2G</i> | 57 | VHTFLGIPFA KPPVGPLRFA PPEAPEPWSG VRDGTSPQAI CPQNVTMNME GLKELKLTLP |
| <i>CES2H</i> | 57 | FLGIPFAKPP VGPLRFAPPE PPEPWGGVVD GTSHFAMCLQ DITAMNMQAF KLLKLTLPFF |
| hCES2 | 121 | TFLGIPFAKP PLGPLRFAPP EPPESWSGVR DGTTHPAMCL QDLTAVESEF LSQFNMTFFS |
| <i>Ces2a</i> | 117 | SMSDCLYLN IYTPHAQEG SNLPVMVWIH GGLVVGVSAS MNDVSKLAAT EEIVIVAIQY |
| <i>Ces2b</i> | 117 | SEDCLYLNII TPAHAHEGSN LPVMVWIHGG GLVAGMASMY DGSLLAAIED LVVVVTIQYRL |
| <i>Ces2c</i> | 117 | SSFPMSEDCL YLNIYTPAHA HEGSNLPVMV WIHGALVIG MASMFDGSLT TVNEDLVVVT |
| <i>Ces2e</i> | 117 | ISMSEDCLYL NIYVPAHAHE GSNLPVMVWI HGGALTVGMA SMYDGSMLAA TEDVVVVAIQ |
| <i>Ces2f</i> | 117 | PPFSMEDCL YLNIYTPAHA QEGSNLPVMV WLHGGGLVAG MASMYDGSVL AATEDVVVVV |
| <i>Ces2g</i> | 117 | PVSMSEDCLY LNIYTPAHAQ EGSNLPVMVW IHGGALTVGM ASMYDGSVLA ATEDVVVVAI |
| <i>Ces2h</i> | 117 | PMSDCLYLN IYAPDHAHEG SNLPVMVWIH GGLVVGVSAS MYDGSMLAAM ENVVVVVTIQY |
| hCES2 | 181 | DSMEDCLYL SIYTPAHSHE GSNLPVMVWI HGGALVFGMA SLYDGSMLAA LENVVVVVIQ |
| <i>Ces2a</i> | 177 | RLGVLGFFST GDQHARGNWG YLDQVAALRW VQKNIAFFGG NRDRVTFVGF SAGGTSVSSH |
| <i>Ces2b</i> | 177 | GVLGFFSTGD QHARGNWGFL DQVAALRWIQ QNIAHFGGKP DRVTFVGFSA GGTSVSSHVV |
| <i>Ces2c</i> | 177 | IQYRLGVLGF FSTGDQHARG NWGYLDQAAA LRWVQONIAH FGGNPDVRTI FGESAGGTSV |
| <i>Ces2e</i> | 177 | YRLGVLGFFS TGDQHAKGNW GYLDQVAALR WVQONIVHFG GNPDRVTIFG ESAGGTSVSS |
| <i>Ces2f</i> | 177 | TQYRLGIPGF YSTGDEQARG NWGFLDQTAAL LHWVQONIAH FGGNPDVSTL FGQSAGGTSV |
| <i>Ces2g</i> | 177 | YRLGVLGFFS STGDEHARGN WGFLDQVAAL RWVQONIAHF GNPDRVTIFG GESAGGISVS |
| <i>Ces2h</i> | 177 | RLGVLGFFST GDERARGNWG YLDQVAALRW LQONIAFFGG NPDRVTFVGF SAGGTSVSSL |
| hCES2 | 241 | YRLGVLGFFS TGDKHATGNW GYLDQVAALR WVQONIAHFG GNPDRVTIFG ESAGGTSVSS |
| <i>Ces2a</i> | 237 | ILSPMSKGLF HGAIMQSGVA LLPDLISDTS EVVYKTVANL SGCEATDSEA LIHCLRAKSK |
| <i>Ces2b</i> | 237 | SPMSKGLFHG AIMESGVALL PYLITDTSSEM VSTTVAKLSG CEAMDSEALV RCLRGKSEAE |
| <i>Ces2c</i> | 237 | SSHVVSPMSQ GLFHGAIMES GVALLPDLIS ETSEMVSSTV AKLSGCEAMD SQALVRLRGL |
| <i>Ces2e</i> | 237 | HVVSPMSQGL FHGAIMESGV AVLPDLISS SEMVHRIVAN LSGCAAVNSE TLMCCLRGKN |
| <i>Ces2f</i> | 237 | SFHVLSPVSQ GLFHRAIMES GVALLPTIIP DSPEMIFTKV ANLSGCETSN SEALVRLRGL |
| <i>Ces2g</i> | 237 | SHVVSPMSKG LFHRAIMESG VALLPGTIFS FSEVVYQTVV KLSGCEAMDS EALVRLRGL |

```

Ces2h 237 VVSPMSQGLF RGAIMESGVA LISSLISVSS DVVYQTVANL SGCEQVDSEA LVNCLRKSE
hCES2 301 LVVSPISQGL FHGAIMESGV ALLPGLIASS ADVISTVVAN LSACDQVDSE ALVGCLRKGS

Ces2a 297 QEILAINQVF KMIPAVVDGE FLPKHPQELL TSMDFHPVPS IIGVNTDECG WGVPMFMGLD
Ces2b 297 ILAINKLQVM IPAVVDGEEF PRHPKELLAS EDFHPVPSII GVNND EFGWT IPVVMGSAQT
Ces2c 297 KSEAEILAIN KVFKMIPAVV DGEFFPRHPK ELLASEDFHP VPSIIGVNND EFGWSIPVVM
Ces2e 297 EAEMLAINKV FKIIIPGVVDG EFLPKHPQEL MASKDFHPVP SIIGINND EY GUILPTIMDP
Ces2f 297 KSEAEILAMS KAFRFMPAVV DGKFLPRHPK KLLASADFHP VPSIIGVNND EY GWIIPKIF
Ces2g 297 SEEEILAIK NFQMIPGVVD GEFLPKHPQE LLASADFHPV PSIIIGFNDE YGWIIVPKVIG
Ces2h 297 EEMAINKAF KIIPGIVDGI FLPRHPQELM ASADFHPVPS IIGVNND EY GWIIPSSMSMI
hCES2 361 KEEILAINKP FKMIPGVVDG VFLPRHPQEL LASADFQVPV SIVGVNNNEF GWLIPKVMRI

Ces2a 357 HIIKNITRET LPAVLKNTAA RMMLPPECCH LLVEEYMGDT EDPETLQAQF REMLGDFMFV
Ces2b 357 IKEITRENLO AVLKNTAQL MLPPECSDLL MEEYMGDTED AQTLLQIQFTE MMEDFMFVIP
Ces2c 357 GSAQMIKGIT RENLQAVLKD TAVQMLLPE CSDLLMEEYM GDTEDAQTLQ IQFTEMMGDF
Ces2e 357 AQKIEEITRK TLPVAVLKSTA LKMLLPPECG DLLMEEYMGD TEDPETLQAQ FREMKGDFMF
Ces2f 357 KFSQTIRKIN RNNLKAIMKI TTEQMMLPSE CGDLLIEEYL RDTEDPWTLO MQFREMIGDF
Ces2g 357 STQTIKIGITR ENLQAVLKD APQMLLPEEC SDLLMEEYME DIEDPKTLQI QFTEMMEDFM
Ces2h 357 DSKKGMDRQM VQAILQRRAT QMMWPPEVSD LLMEEYMGDN EDPQFLQVQF KEMMKDFTFV
hCES2 421 YDTQKEMDRE ASQAALQKML TLLMLPPTFG DLLREYIGD NGDPQTLQAQ FQEMMADSMF

Ces2a 417 IPALQVAHFQ RSQAPVYFYE FQHLSSFIKH VRPSHVKADH GDDVAVFVGS YLWDMNLDLT
Ces2b 417 ALQVAYFQRS HASVYFYEFO HQIASLKDVR PTHVKADHAD EIPFVFGYFF WDMKLDFTTEG
Ces2c 417 MFVIPALQVA HFQRSHAPVY FYEFQHPPSY FKDVRRPPHVK ADHADEIPFV FASFFWGMKL
Ces2e 417 VIPALQVAHF QRSHAPVYFY EFQHRPSFFK DFRPPYVKAD HGDEIFLVFG YQFGNIKLPY
Ces2f 417 LIIIPALQVA RFQRSHAPVY FYEFQHRSSL LKYFRPWHVK ADHGDELYLI FGSFFWGLKF
Ces2g 417 FVIPSQVAVY FQRSHAPVYF YEFQHQSFL KDVRPPHVNA DHGDEVFVVF GSFFWGMKLN
Ces2h 417 IPALQVAQFQ RSHAPVFFYE FQHRPSFFK SKPSHVKADH GDEILFIFRS FWGGTQVDFT
hCES2 481 VIPALQVAHF QCSRAPVYFY EFQHQPSWLK NIRPPHMKAD HGDELFPVFR SFFGGNYIKF

Ces2a 477 EEEELKRMK MKYWANFARN GNPNSEGLPS WPVLDHDEQY LQLDTQPAVG RALKARRLQF
Ces2b 477 EKLLSRMMK YWANFARHGN PNSEGLPYWP VMDHDEQYLQ LDTQPAVGRA LKSRRQLQFWT
Ces2c 477 DFTEEEELLS RRMMKYWANF ARHGNPNSEG LPYWPVMDHD EQYLQLDIQP AVGRALKAGR
Ces2e 477 TEEEEEQLSRR IMKYWANFAR HGPNNSEGLP YWPVMDHDEQ YLQLDIQPSV GRALKARRLQ
Ces2f 477 SFTAEEKLLS RKMMKYWANF ARYGNPNSED LPYWPASNQD DLYLQLDIHP SVGHALKARR
Ces2g 477 LTEEEKLLNR RMMKYWANFA RHGNPNSESL PYWPVFDHDE QYLQLNIQPA VGQFQKARKL
Ces2h 477 EEEELLSRRM MKYWANFARQ RNPNSEGLPY WPMFDQDEQY LQLDTQPAVG RALKTRRLQF
hCES2 541 TEEEEEQLSRK MMKYWANFAR NGPNNGEGLP HWPLFDQEEQ YLQLNLQPAV GRALKARRLQ

Ces2a 597 WTKTLPQKI ELKGSQDK HA EL-----
Ces2b 597 KTLKQIQEL RASQDK HTEL-----
Ces2c 597 LQFWTKTLPQ KIQLKASQD KHREL-----
Ces2e 597 FWTKTLQKI QELKGSQER H KEL-----
Ces2f 597 LPFWTKTLPQ KMLELKGND KIKAV-----
Ces2g 597 QFWTKTLPK IEELKRSQNV HKEL-----
Ces2h 597 WTKTLPQKI ELKDIEDR HK EL-----
hCES2 601 FWKALPQKI QELEEPEER H TEL-----

```

Figure 3. Amino acid sequence alignments of the human and murine carboxylesterase 2 family. The starting amino acid methionine (M) and the HXEL ER retrieval sequence are indicated with bold letters and highlighted with green and yellow color, respectively.

3. ARYLACETAMIDE DEACETYLASE (AADAC)

Besides CES1 and CES2, human arylacetamide deacetylase (AADAC), which has a molecular weight of 45 kDa, is another major serine esterase expressed in both liver and intestine (Figure 4)³⁷. AADAC contains an un-cleaved N-terminal signal anchor sequence which ensures its retention on the endoplasmic reticulum lumen side³⁸. AADAC was first identified as the deacetylation enzyme of 2-acetylaminofluorene³⁹. Subsequently, AADAC was classified as a lipase because of the high homology of its active site domain with that of hormone-sensitive lipase⁴⁰. Moreover, similar to CES2, AADAC prefers compounds with relatively small acyl groups, often acetyl⁴³. It was found that AADAC was responsible for hydrolysis of several clinical drugs, including aromatic amides/esters such as flutamide⁴¹, phenacetin⁴², vicagrel⁴³, prasugrel⁴⁴, ketoconazole⁴⁵ and aliphatic amides/esters such as rifamycins (rifampicin, rifabutin, and rifapentine)⁴⁶. Very recently, Hirosawa et al. found that eslicarbazepine acetate, an antiepileptic prodrug, can be dominantly hydrolyzed by AADAC to eslicarbazepine, an active form, and this hydrolysis efficiency was influenced by AADAC genetic polymorphisms⁴³. Moreover, AADAC over-activation decreased lipid storage in vascular smooth muscle cells, including triacylglycerol, diacylglycerol and cholesteryl esters. Probably related to this, over-expression of AADAC can reduce mouse cardiovascular disease risks⁴⁷. All of this indicates important functions of AADAC in both pharmacology and physiology.

The CES enzymes and AADAC have some overlap in their drug hydrolytic functions, and can be regarded as complementary to each other, but they still have their own specific roles in drug metabolism and elimination. Like human CES2, AADAC is expressed both in liver and intestine, so it can be involved in both the gut wall and hepatic first-pass metabolism. As described above, the presence of AADAC in both intestine and liver may decrease the parental drug exposure in the circulation, sometimes also affecting toxicity. Recently, Nagaoka et al. demonstrated that the deficiency of AADAC may induce sensitivity to ketoconazole-induced hepatotoxicity and adrenal insufficiency. This is due to the higher ketoconazole exposure in AADAC knockout mice, and subsequent inhibition of glucocorticoid synthesis and enhancement of the inflammatory response⁴⁵. Like with CES2, high expression of enterocyte AADAC may induce more local activation or inactivation of substrate drugs in intestine, leading to altered therapeutic effects or toxicity. From this perspective, pharmaceutical companies may use such properties to design and develop (pro-)drug candidates for different therapeutic purposes by appropriately engineering differential susceptibility to CES1, CES2, or AADAC.

```

mAadac 1 MGKTISLLIS VVLVAYLYI PLPDAIEEPW KVVWETAFVK IGTDLASFGE LLGISHFMET
hAADAC 1 MGRKSLYLLI VGILIAYYIY TPLPDNVVEEP WRMMWINAHL KTIQNLATFV ELLGLHHFMD

mAadac 61 IQLLMSFQEV PPTSDEHVTV METAFDSVPV RIYIPKRKSM ALRRGLFYIH GGGWCLGSAA
hAADAC 61 SFKVVGSFDE VPPTSDEHVTV VTETKFNNIL VRVYVPKRKS EALRRGLFYI HGGGWCVGSA

mAadac 121 HFSYDTLSRW TAHKLDVVV STDYGLAPKH HFPRQFEDVY RSLRWFLQED VLEKYGVDPDPR
hAADAC 121 ALSGYDLSR WTADRLDAVV VSTNYRLAPK YHFPIQFEDV YNALRWFLRK KVLAKYGVNP

mAadac 181 RVGVSGDSAG GNLA-AAVTQQ LIQDPDVKIK LKVQALIYPA LQALDTNVPS QQEGSHFPVL
hAADAC 181 ERIGISGDSA GGNLA-AAVTQ QLLDDPDVKI KLKIQSLIYP ALQPLDLDLP SYQENSNFLF

mAadac 241 TRSLMVRVFS EYFTTDRGLE KAMLLNQHPV MESSHLLQFV NWSLLPERY KKSVPYKNPT
hAADAC 241 LSKSLMVRVFS SEYFTTDRSL EKAMLSRQHV PVESHLLFKF VNWSLLPER FIKGHVYNNP

mAadac 301 PGSSELAQKY PGFIDVKACP LLANDNIIHH LPKTYIITCQ YDVLRRDDGLM YVKRLQNVGV
hAADAC 301 NYGSSELAKK YPGFLDVRAA PLLADDNKLK GLPLTYVITC QYDLLRRDDGL MYVTRLRNTG

mAadac 361 HVTHHHVEDG FHGTFSPFGL KLSERMKNQY LSWLIKNL-----
hAADAC 361 VQVTHNHVED GFHGAFSFLG LKISHRLINQ YIEWLKENL-----

```

Figure 4. Amino acid sequence alignment of human and mouse Arylacetamide Deacetylase (AADAC). The starting amino acid methionine (M) is indicated with bold letters and highlighted with green color.

4. SUBSTRATES AND INHIBITORS

Esterases contribute to the hydrolysis of ~10% of clinical-therapeutic drugs containing ester, amide, and thioester bonds⁴⁸. In particular, human carboxylesterase (CES) contributes to the hydrolysis of most of these drugs and xenobiotics. While they share 47% amino acid identity, human CES1 and CES2 exhibit distinct substrate specificities. CES1 preferentially catalyzes the hydrolysis of compounds esterified with a small alcohol group, whereas CES2 preferentially hydrolyzes compounds with a relatively small acyl group and large alcohol group²⁰. A series of studies has been performed to establish the specific substrates of esterases, including human CES1, CES2 and AADAC. It was found that CES1 had much more hydrolytic activity towards clofibrate⁴⁹, clopidogrel⁵⁰, fenofibrate⁴⁹ and oseltamivir⁵¹ than CES2 and AADAC. Imidapril⁵², temocapril⁵³, lidocaine⁵⁴ and mycophenolate mofetil⁵⁵ are also believed to be hydrolyzed mainly by CES1. CES2 also has its preferred substrate specificity, including procaine⁵⁶, heroin, and cocaine⁵⁷. With respect to AADAC, as described in the previous section, it has dominant functions towards rifampicin, rifabutin, rifapentine and phenacetin. However, there are also substrates that can be hydrolyzed by two or all three of these enzymes, for instance, N-acetyldapson, fluorescein diacetate and flutamide could be hydrolyzed by both CES2 and AADAC, whereas irinotecan, capecitabine, gemcitabine^{8,35,58,59}, prasugrel⁶⁰, oxybutynin and prilocaine are believed to be good substrates of both CES1 and CES2. Of note, p-nitrophenylacetate (PNPA) and 4-MUA can be hydrolyzed by all of these three esterases, and these are often used as non-selective

esterase substrate controls for selection of esterase inhibitors, usually together with specific recombinant-expressed esterase enzymes⁴⁹.

Inhibition studies often use specific inhibitors for each enzyme and can be helpful to determine the specific enzyme contribution for metabolism of a certain drug. On the other hand, such inhibitors or optimized derivatives thereof could be potentially used together with other esterase-affected drugs in the clinic, modulating their first-pass metabolism and aiming to increase or otherwise optimize target drug exposure in the system. Bis-(4-nitrophenyl) phosphate (BNPP) is a general esterase inhibitor, affecting CES1, CES2 and AADAC, as well as plasma esterases, such as cholinesterase and paraoxonase (PONs)⁶¹. Eserine, first found as a cholinesterase inhibitor⁶², can also inhibit CES2 and AADAC⁶³. Similarly, 100 nM diisopropyl fluorophosphate (DFP) can markedly limit both CES and AADAC activities⁶⁴. In contrast, phenylmethylsulfonyl fluoride (PMSF) could only inhibit CES enzymes, but not AADAC at a concentration of even 100 μM ^{41,55}. Some lipid-lowering medications, such as simvastatin and mevastatin also have potential inhibition functions for esterases^{65,66}. All the above-mentioned inhibitors are relatively general inhibitors for esterases. Thus, Nakajima and Yokoi and co-workers screened for specific inhibitors for CES1, CES2 and AADAC each by evaluating the inhibitory effects on the hydrolysis of PNPA and a specific probe substrate, respectively⁶⁷. The study revealed that only digitonin can specifically inhibit CES1, with an IC_{50} value of $9.2 \pm 0.4 \mu\text{M}$ and $25.8 \pm 3.7 \mu\text{M}$ for recombinant CES1 hydrolysis activity of PNPA and lidocaine, respectively. However, it cannot inhibit the lidocaine and fenofibrate hydrolysis processes in human liver samples, whereas these two drugs are considered as CES1-specific probe substrates. This might be influenced by other esterase proteins in liver, as it is extremely difficult to prove that a certain substrate (or inhibitor, for that matter) is completely specific for one enzyme. Flavoxate, loperamide, telmisartan and fenofibrate can quite specifically inhibit CES2. However, the metabolite of flavoxate can also inhibit AADAC, which may induce some extra inhibition complications. Telmisartan can inhibit hydrolysis of the specific probe substrate irinotecan with an IC_{50} of $0.5 \pm 0.1 \mu\text{M}$ in human liver microsomes (HLMs) and $0.4 \pm 0.1 \mu\text{M}$ in recombinant CES2 protein, indicating telmisartan is a quite efficient CES2 inhibitor. In addition, loperamide can also strongly inhibit CES2-mediated hydrolysis of capecitabine with an IC_{50} of $0.38 \mu\text{M}$ ⁶⁷. With respect to AADAC, it has been difficult to identify a specific inhibitor. However, very recently, epigallocatechin gallate appeared to be a promising AADAC inhibitor⁶⁸. Besides, vinblastine and physostigmine can efficiently inhibit AADAC as well as CES2^{63,67}.

5. GENETIC POLYMORPHISMS OF ESTERASES

There is substantial individual variation in the response to pharmacologic therapies. Many factors can contribute to this variability, but one of the main reasons can be genetic polymorphisms and splice variants⁶⁹. With respect to CES1, two human CES1 genes located in the CES1 locus, one functional gene *CES1A1* and one pseudogene (*CES1P1*) exist due to a stop codon present in exon

3. Moreover, alternative splicing in *CES1P1* results in another functional human CES1 isoform: *CES1A2*. However, *CES1A1* is the dominant splice form, resulting in most CES1 protein in the liver. *CES1A2* represents only 2% of the transcripts of *CES1A1*⁷⁰. Both yield the mature hCES1 protein⁷¹. With respect to CES2, there are two isoforms because of alternative splicing. Furthermore, with alternative transcription initiation (revealing a different (upstream) start codon in exon 1), there are another two isoforms with 64 additional amino acids at the N-terminus. The biological function of these extra 64 amino acids, if any, remains to be determined²¹. Compared to CES1 and CES2, less is known about AADAC, so far only one coding sequence and protein isoform has been reported.

Further genetic polymorphisms, including single nucleotide polymorphisms (SNPs), can influence the interindividual variation of a diverse group of therapeutic agents. As an oral anticoagulant to prevent stroke in patients with atrial fibrillation, dabigatran etexilate was designed as a dabigatran pro-drug, which can be hydrolyzed by esterases, including CES1⁷². Paré et al. demonstrated that the CES1 SNP (rs2244613) was associated with a decrease of active dabigatran plasma concentrations, and reduced risk of any bleeding cases, but not with ischemic events⁷³. This suggests that reduced activation of dabigatran etexilate by reduced CES1 activity limited the unwanted bleeding, but did not significantly affect the therapeutic benefit. Methylphenidate (MPH), a drug for attention deficit/hyperactivity disorder (ADHD) treatment, was believed to be inactivated through a de-esterification process by CES1⁷⁴. Both Zhu et al. and Nemoda et al. found two SNPs (rs71647871 and rs71647872) that were associated with a marked decrease in CES1 hydrolysis of MPH^{75,76}. Similarly, Zhu et al. and Tarkiainen et al. found that rs71647871 and rs121912777 could decrease the metabolism of the antiviral ester prodrug oseltamivir^{77,78}. In addition, clopidogrel, a prodrug to prevent platelet aggregation, is rapidly hydrolyzed for about 85% to its inactive metabolite, clopidogrel carboxylic acid, by CES1⁷⁹. Lewis et al. assessed the association between the SNP rs71647871 and clopidogrel clinical pharmacodynamic effects. The results suggested that this CES1 SNP (with reduced activity) may increase plasma clopidogrel exposure and also may increase the risk of potential toxic or adverse side effects⁸⁰. Similar studies were also applied for CES2. For instance, Tang et al. explored the association of aspirin (acetylsalicylic acid) and CES2 genetic polymorphisms, and found that the SNP A139T decreased CES2 hydrolytic function and lead to a 40% decrease in aspirin hydrolysis⁷⁹. Moreover, the CES2 variants (rs72547531 and rs72547532) reduced the expression of CES2, and were associated with lower CES2 activity in irinotecan-treated patients⁸¹. Although similar pharmacogenetic studies for AADAC are very limited, there is one study demonstrating that different SNPs of AADAC result in reduced hydrolytic activities towards flutamide, phenacetin and rifamycins⁸².

6. INTESTINAL VERSUS HEPATIC METABOLISM

When an ester (pro-)drug is orally administered, it would first be present in the gut lumen, then has to pass the intestinal wall and subsequently the liver via the portal vein before it reaches the systemic circulation. Of note, often not all the parental drug will be absorbed into enterocytes, the potential processes including: 1) Part of parental drug remains in the gut lumen and/or is metabolized by gut microbes, and further eliminated with feces. 2) Due to passive diffusion, facilitated and/or active transport by some uptake transporters, part of the drug will be taken up into enterocytes and can there be metabolized by intestinal esterases before entering the mesenteric and portal vein. 3) With the intestinal active apical ATP binding cassette (ABC) efflux transporters such as ABCB1 (P-glycoprotein: P-gp), ABCG2 (breast cancer resistance protein: BCRP) and ABCC2 (multidrug resistance-associated protein 2: MRP2), the absorbed drugs can also be discharged out of the enterocytes back into the intestinal lumen^{83,84}, which may reduce the parental drug accumulation in the enterocytes. This may have further consequences, as the reduced drug accumulation in enterocytes may prevent saturation of intestinal esterases, and allow for more complete metabolism of the drug in the enterocytes. The result would be poor survival of the drug during the first-pass absorption processes in the intestine. Indeed, the extruded drug may still reenter the enterocytes, but only at low concentration, again leading to extensive metabolism by intestinal esterases. In general, these three processes together might play a substantial role in the first-pass metabolism of ester (pro-)drugs, modulating the systemic exposure of the pharmacodynamically active compound.

After the intestinal first-pass metabolism, part of the residual fraction of the parental drug reaches the portal blood, where it may bind to plasma proteins. For some drugs substantial avid binding to these plasma proteins may reduce the fraction of drug available for diffusion into tissues⁸⁵. As with the enterocytes, with passive diffusion, facilitated and/or active uptake transport, the unbound drugs (and likely also partially plasma protein-bound drugs) can be taken up into hepatocytes. Within the hepatocytes, the following processes may occur: 1) The substrate ester (pro-)drug can be metabolized directly by hepatic esterases. 2) Due to the presence of efflux transporters in the apical membranes of hepatocytes, such as ABCB1, ABCG2, and ABCC2, the parental drug, in addition to its metabolite(s) produced in hepatocytes, can be transported into bile, and secreted back into the gut lumen. This hepatobiliary circulation may induce secondary absorption, but likely with a relatively reduced drug concentration, allowing more intensive metabolism in the intestine. All in all, in many cases only a fraction of the drug could pass through the enterocytes, reach the portal blood, further bypass the hepatocytes and consequently enter the systemic circulation.

This combined metabolism process by esterases (first-pass intestinal and hepatic metabolism) can not only cause complications for drug availability, but may also have implications for drug

design. The presence of esterase enzymes in both liver and intestine may decrease the overall systemic exposure of the ester drugs. In addition, on the one hand, local metabolism and accumulation of the drug and/or its metabolites may induce toxicity, for instance, as mentioned above, CES1-induced remdesivir hepatic toxicity and CES2-induced irinotecan (SN-38) intestinal toxicity. On the other hand, for some specific purposes, one might design an ester prodrug where the active drug accumulates and primarily works in the local tissue, such as intestine. Therapeutic agents commonly cause intestinal diarrhea³⁴, including chemotherapies such as irinotecan (CPT-11) and capecitabine⁸⁶; targeted therapies such as erlotinib, sorafenib and cetuximab⁸⁶; and immunotherapies such as ipilimumab, pembrolizumab and nivolumab⁸⁷. Considering this situation, some protective drug candidates specifically targeting the intestine are currently under development. If successful, these may meet the above-mentioned unmet medical needs (to prevent or alleviate the treatment-induced diarrhea), and help patients continue cancer treatment and have a better quality of life. Not limited to this, depending on different purposes, ester (pro-)drugs can be designed to “arrest in” or “escape from” the enterocytes enhancing their efficacy and/or limiting their toxicity as much as possible.

7. PRE-CLINICAL MODELS

7.1 Pre-clinical assessment complications

It is challenging to assess the relative role of hepatic versus intestinal esterase activity in drug metabolism and elimination. Such assessment has been usually done according to esterase protein levels or activity in hepatic and intestinal microsomes, or using prediction models incorporating *in vitro* and/or *in vivo* experimental data. Soto et al. evaluated the protein levels of human CES1 and CES2 in 16 individual human liver microsomes (HLMs) and found a variation of 4.7-fold (171–801 pmol/mg) and 3.5-fold (16.3–57.2 pmol/mg), respectively. The protein levels of CES1 correlated well with the hydrolysis rates of clopidogrel (5 μ M) and oxybutynin (10 μ M), and CES2 protein levels correlated strongly with the hydrolysis rates of irinotecan (1 μ M)⁸⁸. Wang et al. measured the mean expression level of hCES1 as 176.08 ± 75.6 pmol/mg in 102 individual liver samples using LC-MS/MS detection⁸⁹. Maybe due to the age difference and/or different method applied, Hines et al. obtained much lower CES1 and CES2 concentrations in pediatric liver samples by SDS-page⁹⁰. All of this indicates that there are individual expression differences and thus potential risks to evaluate the specific roles of carboxylesterases extrapolating from *in vitro* results. In addition, people used Caco-2 intestinal cell line monolayers to identify drugs with potential absorption problems and possibly also to predict the intestinal drug absorption *in vivo*^{91–93}. This *in vitro* system may reflect the permeability of specific drugs and determine whether there are any transporters involved in, or affecting the net absorption process⁹⁴.

In humans, there is very low CES1 expressed in the intestine, whereas there is abundant CES2 and AADAC. However, as human CES1 always showed higher expression levels than CES2 in the

Caco-2 cells, with respect to ester-drugs, this cell line may not be the best model to apply⁹⁵. Watanabe et al. and Kurokawa et al. estimated the relative percentage contributions of AADAC, CES1 and CES2 to specific drug hydrolysis activity by applying the relative activity factor (RAF) as the ratio of activity as measured in isolated human intestinal and hepatic microsomes (HIM and HLM, respectively). In brief, the RAF values for CES1, CES2 or AADAC in either intestine or liver (RAF_{HIM} or RAF_{HLM}) were determined as the ratios of the hydrolytic activity towards specific probe substrates in HIMs or HLMs to the values by recombinant human CES1, CES2 or AADAC, respectively. The obtained RAF values would be regarded as correction factors to predict targeted drug hydrolysis activity by CES1, CES2 or AADAC in HIMs or HLMs, respectively^{42,44}. With this method, the contribution of each esterase in specific drug hydrolytic activity can be estimated, although this may also introduce variation because of the different probe substrate selection. In addition, there are still some other detoxification systems present in the intestinal lumen, intestinal tissue, liver, kidney and/or systemic circulation, which may also markedly influence drug pharmacokinetic behavior. For instance, bacterial esterases present in the gut lumen or other esterases in the blood, such as butyrylcholinesterase, paraoxonase, acetylcholinesterase, and possibly albumin²⁶.

In conclusion, the aforementioned studies provided several approaches to estimate the contribution of hepatic and intestinal esterase hydrolysis activity. However, a clearly defined and accessible *in vivo* model to investigate the relative contributions of the specific esterases, and specifically intestinal and hepatic esterase-mediated first-pass metabolism of drugs was lacking thus far. Some new mouse models that might fill a large part of this gap will be described below.

7.2 CES1-related mouse models

There are several genetically modified *Ces1*-deficient or overexpression mouse models that have been reported. The research group of Lehner et al. has generated *Ces1d*^{-/-} and *Ces1g*^{-/-} mice by interrupting the exon 5 of each gene with targeting Neo cassettes, respectively^{96,97}. Also, Zhang and co-workers successfully knocked out mouse *Ces1g* specifically in liver or globally and further over-expressed *Ces1g* in the liver^{98,99}. However, all of these mouse models were applied only in physiological and metabolic disease research, not in pharmacology studies. Of note, all of the above-mentioned knockout mouse models were single knockout mice, which still have other mouse *Ces1* enzymes abundant in the body, especially *Ces1c* in blood. As humans lack plasma carboxylesterase, this will thus make the above-mentioned mouse models unsuitable for CES1 pharmacological studies. However, Duysen et al. generated a *Ces1c*-deficient mouse model, and demonstrated the increased sensitivity to soman coumarin, an organophosphate nerve agent compound, due to the absence of *Ces1c* from the blood¹⁰⁰. In addition, to better simulate the human situation, Lumley and coworkers obtained a *Ces1c* knockout mouse strain to study midazolam dose effects against soman¹⁰¹, and further modified it with a human acetylcholinesterase (AChE) knock-in, in order to obtain a better pre-clinical model of soman

toxicity and related therapy studies¹⁰². Of note, with 8 functional *Ces1* genes (although three of these are very lowly expressed), the single *Ces1* gene knockout situation cannot generate a clean *Ces1* enzyme deficiency background, which may thus over- or under- estimate *Ces1* enzyme functions, either in pharmacological or physiological studies.

Recently, our group generated and characterized two new CES1-related mouse models, including a *Ces1* cluster knockout strain (*Ces1*^{-/-}) lacking all functional *Ces1* genes and a transgenic human CES1 liver-specific expression strain in the mouse *Ces1*^{-/-} background (*Ces1*^{-/-}A). With these CES1-related mouse models, we found that mouse *Ces1* can dramatically influence irinotecan metabolism, and control SN-38 formation. In addition, even though *Ces1* was demonstrated to be very important in the first step in metabolizing capecitabine, a 5-FU prodrug activated in multiple steps, there was no effect on 5-FU exposure compared to wild-type mice. This was probably due to alternative esterases being sufficiently effective to substitute mostly for the *Ces1* deficiency. In general, these pre-clinical *Ces1* mouse models revealed the significant contributions of CES1 to drug metabolism and pharmacokinetic properties.

7.3 CES2-related mouse models

Like for CES1, some CES2-related genetically modified mouse strains have also been generated. Li et al. and Ruby et al. overexpressed mouse *Ces2c* or human CES2 specifically in liver with a recombinant adenovirus encoding m*Ces2c* and hCES2 cDNA, respectively^{103,104}. In addition, Lisa et al. generated and characterized a stable transgenic m*Ces2c* intestine-specific expression mouse strain with the intestine-specific 12.4-kb villin promoter¹⁰⁵. Again, all of these mouse models were applied in physiological studies, and considering that all the mouse *Ces2* proteins were still present, these mice might not be optimal for use for pharmacological research.

As a parallel project with the *Ces1* mouse models, we also generated and characterized several CES2-related mouse models. Like with *Ces1*, the *Ces2* cluster knockout (all *Ces2* genes deleted) strain (*Ces2*^{-/-}) and transgenic human CES2 liver-specific expression strain in the *Ces2*^{-/-} background (*Ces2*^{-/-}A) were constructed. Besides this, considering the high enterocyte CES2 expression, a transgenic human CES2 intestine-specific expression mouse strain in the *Ces2*^{-/-} background was also successfully generated (*Ces2*^{-/-}V). With these two transgenic mouse models, in theory we can analyze the specific roles of hepatic CES2 and intestinal CES2 pharmacological functions, and estimate the contributions of CES2 at different locations to the different ester (pro)-drug hydrolysis processes. We found that vinorelbine was a very good substrate of mouse *Ces2* protein(s), but much less so of human CES2. Mouse *Ces2* could markedly influence the vinorelbine metabolism into its active metabolite deacetylvinorelbine. In addition, like with CES1, CES2 was strongly involved in the first-step enzymatic activation of capecitabine, but without affecting ultimate 5-FU exposure, likely because of redundant esterase enzyme activity (Described in Chapter 2). All of this indicates the importance of optimal CES pre-clinical models, which may

provide powerful tools for the design, development, and investigation of ADME properties of specific drugs *in vivo*. In the future, a combined deletion of both *Ces1* and *Ces2* clusters can be generated, which could be used for CES pharmacological studies from a broader perspective.

7.4 AADAC-related mouse models

There are comparatively fewer studies related to AADAC, especially when concerning mouse models. Recently, the research group of Nakajima et al. published the generation and characterization of an *Aadac* knockout mouse model¹⁰⁶. They found, amongst others, that the deficiency of AADAC in mice can significantly increase ketoconazole exposure and decrease exposure of its metabolite N-deacetyl ketoconazole. The higher ketoconazole exposure induced hepatotoxicity and adrenal insufficiency¹⁰⁶.

This also brings up the theoretical possibility to generate a triple knockout mouse strain, which would be lacking all the *Ces1*, *Ces2* and *Aadac* genes, under the assumption that this would be viable. Further, based on this mouse model, transgenic human CES1 expressed in the liver, and transgenic human CES2 or AADAC expressed in both liver and intestine could be generated. With a more extensive esterase-deficiency mouse model, and three humanized esterase transgenic mouse models, perhaps more sensitive and accurate studies could be performed to evaluate the separate and specific roles of each esterase in drug ADME processes. However, there are (many) more esterases, and the possibility of partial functional compensation in these models by overexpression of such esterases or of other detoxifying proteins can certainly not be excluded.

8. CONCLUSION AND OUTLOOK

The esterase enzymes markedly contribute to drug metabolism and elimination, which may affect pro-drug activation, drug detoxification and hence toxicity. This is relevant to drug efficacy and safety. Carboxylesterase (CES) and arylacetamide deacetylase (AADAC) are two main esterase families present in liver and intestine. Even though they have some overlap in substrates, they still have their own preferential drug specificity. Moreover, their activities can be influenced by genetic polymorphisms and potential drug-drug interactions. The presence of esterases in both liver and intestine affects the pharmacological behavior of especially oral ester-drugs by the first-pass metabolic effects in intestine and liver. This combined metabolism process will thus influence efficacy and safety of the affected drug(s). For optimal understanding of the esterase pharmacological functions, suitable pre-clinical models are important. From this perspective, the CES1 and CES2 mouse models that we generated and characterized may help to better understand drug metabolism processes in humans. In the future, generation of more extensive genetically modified (combination) mouse models can be considered to investigate functions or specific roles of each esterase (CES1, CES2 and AADAC) in drug metabolism more specifically.

REFERENCE

- Lyubimov, A.V. *Encyclopedia of Drug Metabolism and Interactions*, (2011).
- Iyanagi, T. Molecular mechanism of phase I and phase II drug-metabolizing enzymes: implications for detoxification. *International Review of Cytology* **260**, 35-112 (2007).
- Zanger, U.M. & Schwab, M. Cytochrome P450 enzymes in drug metabolism: regulation of gene expression, enzyme activities, and impact of genetic variation. *Pharmacology and Therapeutics* **138**, 103-141 (2013).
- Guengerich, F.P. Cytochrome P450s and other enzymes in drug metabolism and toxicity. *The AAPS Journal* **8**, E101-111 (2006).
- Fukami, T. & Yokoi, T. The emerging role of human esterases. *Drug Metabolism and Pharmacokinetics* **27**, 466-477 (2012).
- Di, L. The Impact of Carboxylesterases in Drug Metabolism and Pharmacokinetics. *Current Drug Metabolism* **20**, 91-102 (2019).
- Rivory, L.P., Bowles, M.R., Robert, J. & Pond, S.M. Conversion of irinotecan (CPT-11) to its active metabolite, 7-ethyl-10-hydroxycamptothecin (SN-38), by human liver carboxylesterase. *Biochemical Pharmacology* **52**, 1103-1111 (1996).
- Humerickhouse, R., Lohrbach, K., Li, L., Bosron, W.F. & Dolan, M.E. Characterization of CPT-11 hydrolysis by human liver carboxylesterase isoforms hCE-1 and hCE-2. *Cancer Research* **60**, 1189-1192 (2000).
- Rivory, L.P., et al. Pharmacokinetic interrelationships of irinotecan (CPT-11) and its three major plasma metabolites in patients enrolled in phase I/II trials. *Clinical Cancer Research* **3**, 1261-1266 (1997).
- Chan, F.C.Y., et al. 3- and 4-Pyridylalkyl Adamantanecarboxylates: Inhibitors of Human Cytochrome P45017 α (17 α -Hydroxylase/C17,20-Lyase). Potential Nonsteroidal Agents for the Treatment of Prostatic Cancer. *Journal of Medicinal Chemistry* **39**, 3319-3323 (1996).
- Nunes, T., Rocha, J.F., Falcão, A., Almeida, L. & Soares-da-Silva, P. Steady-state plasma and cerebrospinal fluid pharmacokinetics and tolerability of eslicarbazepine acetate and oxcarbazepine in healthy volunteers. *Epilepsia* **54**, 108-116 (2013).
- Sakai, Y., et al. Arylacetylamide deacetylase as a determinant of the hydrolysis and activation of abiraterone acetate in mice and humans. *Life Sciences* **284**, 119896 (2021).
- Hirosawa, K., et al. Role of Human Arylacetylamide Deacetylase (AADAC) on Hydrolysis of Eslicarbazepine Acetate and Effects of AADAC Genetic Polymorphisms on Hydrolase Activity. *Drug Metabolism and Disposition* **49**, 322-329 (2021).
- Wang, D., et al. Human carboxylesterases: a comprehensive review. *Acta Pharmaceutica Sinica B* **8**, 699-712 (2018).
- Sanghani, S.P., Sanghani, P.C., Schiel, M.A. & Bosron, W.F. Human carboxylesterases: an update on CES1, CES2 and CES3. *Protein & Peptide Letters* **16**, 1207-1214 (2009).
- Satoh, T. & Hosokawa, M. The mammalian carboxylesterases: from molecules to functions. *Annual Review of Pharmacology and Toxicology* **38**, 257-288 (1998).
- Yoshida, T., et al. Difference in substrate specificity of carboxylesterase and arylacetamide deacetylase between dogs and humans. *European Journal of Pharmaceutical Sciences* **111**, 167-176 (2018).
- Casey Laizure, S., Herring, V., Hu, Z., Witbrodt, K. & Parker, R.B. The Role of Human Carboxylesterases in Drug Metabolism: Have We Overlooked Their Importance? *Pharmacotherapy* **33**, 210-222 (2013).
- Staudinger, J.L., Xu, C., Cui, Y.J. & Klaassen, C.D. Nuclear receptor-mediated regulation of carboxylesterase expression and activity. *Expert Opinion on Drug Metabolism & Toxicology* **6**, 261-271 (2010).
- Imai, T. Human carboxylesterase isozymes: catalytic properties and rational drug design. *Drug Metabolism and Pharmacokinetics* **21**, 173-185 (2006).
- Lian, J., Nelson, R. & Lehner, R. Carboxylesterases in lipid metabolism: from mouse to human. *Protein Cell* (2017).
- Robbi, M. & Beaufay, H. The COOH terminus of several liver carboxylesterases targets these enzymes to the lumen of the endoplasmic reticulum. *Journal of Biological Chemistry* **266**, 20498-20503 (1991).

- Jones, R.D., Taylor, A.M., Tong, E.Y. & Repa, J.J. Carboxylesterases are uniquely expressed among tissues and regulated by nuclear hormone receptors in the mouse. *Drug Metabolism and Disposition* **41**, 40-49 (2013).
- Satoh, T., et al. Current progress on esterases: from molecular structure to function. *Drug Metabolism and Disposition* **30**, 488-493 (2002).
- Munger, J.S., et al. A serine esterase released by human alveolar macrophages is closely related to liver microsomal carboxylesterases. *Journal of Biological Chemistry* **266**, 18832-18838 (1991).
- Li, B., et al. Butyrylcholinesterase, paraoxonase, and albumin esterase, but not carboxylesterase, are present in human plasma. *Biochemical Pharmacology* **70**, 1673-1684 (2005).
- McClure, K.F., et al. Liver-Targeted Small-Molecule Inhibitors of Proprotein Convertase Subtilisin/Kexin Type 9 Synthesis. *Angewandte Chemie. International Ed. In English* **56**, 16218-16222 (2017).
- Shen, Y., Eades, W. & Yan, B. The COVID-19 Medicine Remdesivir Is Therapeutically Activated by Carboxylesterase-1, and Excessive Hydrolysis Increases Cytotoxicity. *Hepatology communications* **5**, 1622-1623 (2021).
- Wang, Y., et al. Remdesivir in adults with severe COVID-19: a randomised, double-blind, placebo-controlled, multicentre trial. *Lancet* **395**, 1569-1578 (2020).
- Grein, J., et al. Compassionate Use of Remdesivir for Patients with Severe Covid-19. *New England Journal of Medicine* **382**, 2327-2336 (2020).
- Beigel, J.H., et al. Remdesivir for the Treatment of Covid-19 - Final Report. *New England Journal of Medicine* **383**, 1813-1826 (2020).
- Satoh, T. & Hosokawa, M. Carboxylesterases: structure, function and polymorphism in mammals. *Journal of Pesticide Science* **35**, 218-228 (2010).
- Holmes, R.S., et al. Recommended nomenclature for five mammalian carboxylesterase gene families: human, mouse, and rat genes and proteins. *Mammalian Genome* **21**, 427-441 (2010).
- Yu, Y., et al. Two birds, one stone: hesperetin alleviates chemotherapy-induced diarrhea and potentiates tumor inhibition. *Oncotarget* **9**, 27958-27973 (2018).
- Pratt, S.E., et al. Human Carboxylesterase-2 Hydrolyzes the Prodrug of Gemcitabine (LY2334737) and Confers Prodrug Sensitivity to Cancer Cells. *Clinical Cancer Research* **19**, 1159-1168 (2013).
- Xu, G., Zhang, W., Ma, M.K. & McLeod, H.L. Human carboxylesterase 2 is commonly expressed in tumor tissue and is correlated with activation of irinotecan. *Clinical Cancer Research* **8**, 2605-2611 (2002).
- Ross, M.K. & Crow, J.A. Human carboxylesterases and their role in xenobiotic and endobiotic metabolism. *Journal of Biochemical and Molecular Toxicology* **21**, 187-196 (2007).
- Frick, C., Atanasov, A.G., Arnold, P., Ozols, J. & Odermatt, A. Appropriate function of 11 β -hydroxysteroid dehydrogenase type 1 in the endoplasmic reticulum lumen is dependent on its N-terminal region sharing similar topological determinants with 50-kDa esterase. *Journal of Biological Chemistry* **279**, 31131-31138 (2004).
- Probst, M.R., Jenö, P. & Meyer, U.A. Purification and characterization of a human liver arylacetamide deacetylase. *Biochemical and Biophysical Research Communications* **177**, 453-459 (1991).
- Probst, M.R., et al. Human liver arylacetamide deacetylase. Molecular cloning of a novel esterase involved in the metabolic activation of arylamine carcinogens with high sequence similarity to hormone-sensitive lipase. *Journal of Biological Chemistry* **269**, 21650-21656 (1994).
- Watanabe, A., et al. Human arylacetamide deacetylase is a principal enzyme in flutamide hydrolysis. *Drug Metabolism and Disposition* **37**, 1513-1520 (2009).
- Watanabe, A., et al. Arylacetylamide deacetylase is a determinant enzyme for the difference in hydrolase activities of phenacetin and acetaminophen. *Drug Metabolism and Disposition* **38**, 1532-1537 (2010).
- Jiang, J., Chen, X. & Zhong, D. Arylacetylamide Deacetylase Is Involved in Vicagrel Bioactivation in Humans. *Frontiers in Pharmacology* **8**, 846 (2017).
- Kurokawa, T., Fukami, T., Yoshida, T. & Nakajima, M. Arylacetylamide Deacetylase is Responsible for Activation of Prasugrel in Human and Dog. *Drug Metabolism and Disposition* **44**, 409-416 (2016).
- Fukami, T., Iida, A., Konishi, K. & Nakajima, M. Human arylacetamide deacetylase hydrolyzes ketoconazole to trigger hepatocellular toxicity. *Biochemical Pharmacology* **116**, 153-161 (2016).
- Nakajima, A., et al. Human arylacetamide deacetylase is responsible for deacetylation of rifamycins: rifampicin, rifabutin, and rifapentine. *Biochemical Pharmacology* **82**, 1747-1756 (2011).

47. Misra, A. & Fisher, E.A. Translational Research in Culture: AADAC, Diabetes, and Cardiovascular Disease. *Cell Stem Cell* **27**, 6-7 (2020).
48. Williams, J.A., *et al.* Drug-drug interactions for UDP-glucuronosyltransferase substrates: a pharmacokinetic explanation for typically observed low exposure (AUC_i/AUC) ratios. *Drug Metabolism and Disposition* **32**, 1201-1208 (2004).
49. Fukami, T., Kariya, M., Kurokawa, T., Iida, A. & Nakajima, M. Comparison of substrate specificity among human arylacetamide deacetylase and carboxylesterases. *European Journal of Pharmaceutical Sciences* **78**, 47-53 (2015).
50. Farid, N.A., Kurihara, A. & Wrighton, S.A. Metabolism and disposition of the thienopyridine antiplatelet drugs ticlopidine, clopidogrel, and prasugrel in humans. *Journal of Clinical Pharmacology* **50**, 126-142 (2010).
51. Shi, J., *et al.* Association of Osetamivir Activation with Gender and Carboxylesterase 1 Genetic Polymorphisms. *Basic & Clinical Pharmacology & Toxicology* **119**, 555-561 (2016).
52. Imai, T., Imoto, M., Sakamoto, H. & Hashimoto, M. Identification of esterases expressed in Caco-2 cells and effects of their hydrolyzing activity in predicting human intestinal absorption. *Drug Metabolism and Disposition* **33**, 1185-1190 (2005).
53. Takahashi, S., Katoh, M., Saitoh, T., Nakajima, M. & Yokoi, T. Different Inhibitory Effects in Rat and Human Carboxylesterases. *Drug Metabolism and Disposition* **37**, 956-961 (2009).
54. Higuchi, R., Fukami, T., Nakajima, M. & Yokoi, T. Prilocaine- and lidocaine-induced methemoglobinemia is caused by human carboxylesterase-, CYP2E1-, and CYP3A4-mediated metabolic activation. *Drug Metabolism and Disposition* **41**, 1220-1230 (2013).
55. Fujiyama, N., *et al.* Involvement of carboxylesterase 1 and 2 in the hydrolysis of mycophenolate mofetil. *Drug Metabolism and Disposition* **38**, 2210-2217 (2010).
56. Jewell, C., *et al.* Specificity of procaine and ester hydrolysis by human, minipig, and rat skin and liver. *Drug Metabolism and Disposition* **35**, 2015-2022 (2007).
57. Hatfield, M.J., *et al.* Biochemical and molecular analysis of carboxylesterase-mediated hydrolysis of cocaine and heroin. *British Journal of Pharmacology* **160**, 1916-1928 (2010).
58. Xiao, D., *et al.* Regulation of carboxylesterase-2 expression by p53 family proteins and enhanced anti-cancer activities among 5-fluorouracil, irinotecan and doxazolidine prodrug. *British Journal of Pharmacology* **168**, 1989-1999 (2013).
59. Quinney, S.K., *et al.* Hydrolysis of capecitabine to 5'-deoxy-5-fluorocytidine by human carboxylesterases and inhibition by loperamide. *Journal of Pharmacology and Experimental Therapeutics* **313**, 1011-1016 (2005).
60. Williams, E.T., *et al.* The biotransformation of prasugrel, a new thienopyridine prodrug, by the human carboxylesterases 1 and 2. *Drug Metabolism and Disposition* **36**, 1227-1232 (2008).
61. Zou, L.W., *et al.* Carboxylesterase Inhibitors: An Update. *Current Medicinal Chemistry* **25**, 1627-1649 (2018).
62. Iwatsubo, K. STUDIES ON THE CLASSIFICATION OF THE ENZYMES HYDRO-LYZING ESTER-FORM DRUGS IN LIVER MICROSOMES. *The Japanese Journal of Pharmacology* **15**, 244-256 (1965).
63. Kobayashi, Y., Fukami, T., Higuchi, R., Nakajima, M. & Yokoi, T. Metabolic activation by human arylacetamide deacetylase, CYP2E1, and CYP1A2 causes phenacetin-induced methemoglobinemia. *Biochemical Pharmacology* **84**, 1196-1206 (2012).
64. Tabata, T., Katoh, M., Tokudome, S., Nakajima, M. & Yokoi, T. Identification of the cytosolic carboxylesterase catalyzing the 5'-deoxy-5-fluorocytidine formation from capecitabine in human liver. *Drug Metabolism and Disposition* **32**, 1103-1110 (2004).
65. Wang, X., Zhu, H.J. & Markowitz, J.S. Carboxylesterase 1-mediated drug-drug interactions between clopidogrel and simvastatin. *Biological and Pharmaceutical Bulletin* **38**, 292-297 (2015).
66. Fleming, C.D., *et al.* Structural insights into drug processing by human carboxylesterase 1: tamoxifen, mevastatin, and inhibition by benzil. *Journal of Molecular Biology* **352**, 165-177 (2005).
67. Shimizu, M., Fukami, T., Nakajima, M. & Yokoi, T. Screening of Specific Inhibitors for Human Carboxylesterases or Arylacetamide Deacetylase. *Drug Metabolism and Disposition* **42**, 1103-1109 (2014).
68. Yasuda, K., *et al.* Epicatechin gallate and epigallocatechin gallate are potent inhibitors of human arylacetamide deacetylase. *Drug Metabolism and Pharmacokinetics* **39**, 100397 (2021).

69. Merali, Z., Ross, S. & Paré, G. The pharmacogenetics of carboxylesterases: CES1 and CES2 genetic variants and their clinical effect. *Drug Metabolism and Drug Interactions* **29**, 143-151 (2014).
70. Zhu, H.J., Brinda, B., Froehlich, T.E. & Markowitz, J.S. A discriminative analytical method for detection of CES1A1 and CES1A2/CES1A3 genetic variants. *Pharmacogenetics and Genomics* **22**, 215-218 (2012).
71. Fukami, T., *et al.* Structure and characterization of human carboxylesterase 1A1, 1A2, and 1A3 genes. *Pharmacogenetics and Genomics* **18**, 911-920 (2008).
72. Blech, S., Ebner, T., Ludwig-Schwellinger, E., Stangier, J. & Roth, W. The metabolism and disposition of the oral direct thrombin inhibitor, dabigatran, in humans. *Drug Metabolism and Disposition* **36**, 386-399 (2008).
73. Paré, G., *et al.* Genetic determinants of dabigatran plasma levels and their relation to bleeding. *Circulation* **127**, 1404-1412 (2013).
74. Sun, Z., *et al.* Methylphenidate is stereoselectively hydrolyzed by human carboxylesterase CES1A1. *Journal of Pharmacology and Experimental Therapeutics* **310**, 469-476 (2004).
75. Zhu, H.J., *et al.* Two CES1 gene mutations lead to dysfunctional carboxylesterase 1 activity in man: clinical significance and molecular basis. *American Journal of Human Genetics* **82**, 1241-1248 (2008).
76. Nemoda, Z., Angyal, N., Tarnok, Z., Gadoros, J. & Sasvari-Szekely, M. Carboxylesterase 1 gene polymorphism and methylphenidate response in ADHD. *Neuropharmacology* **57**, 731-733 (2009).
77. Zhu, H.J., Appel, D.I., Jiang, Y. & Markowitz, J.S. Age- and sex-related expression and activity of carboxylesterase 1 and 2 in mouse and human liver. *Drug Metabolism and Disposition* **37**, 1819-1825 (2009).
78. Tarkiainen, E.K., *et al.* Carboxylesterase 1 polymorphism impairs osetamivir bioactivation in humans. *Clinical Pharmacology and Therapeutics* **92**, 68-71 (2012).
79. Tang, M., *et al.* Antiplatelet agents aspirin and clopidogrel are hydrolyzed by distinct carboxylesterases, and clopidogrel is transesterified in the presence of ethyl alcohol. *Journal of Pharmacology and Experimental Therapeutics* **319**, 1467-1476 (2006).
80. Lewis, J.P., *et al.* The functional G143E variant of carboxylesterase 1 is associated with increased clopidogrel active metabolite levels and greater clopidogrel response. *Pharmacogenetics and Genomics* **23**, 1-8 (2013).
81. Kubo, T., *et al.* Functional characterization of three naturally occurring single nucleotide polymorphisms in the CES2 gene encoding carboxylesterase 2 (HCE-2). *Drug Metabolism and Disposition* **33**, 1482-1487 (2005).
82. Shimizu, M., *et al.* A novel polymorphic allele of human arylacetamide deacetylase leads to decreased enzyme activity. *Drug Metabolism and Disposition* **40**, 1183-1190 (2012).
83. Nigam, S.K. What do drug transporters really do? *Nature Reviews Drug Discovery* **14**, 29-44 (2014).
84. Schinkel, A.H. & Jonker, J.W. Mammalian drug efflux transporters of the ATP binding cassette (ABC) family: an overview. *Advanced Drug Delivery Reviews* **55**, 3-29 (2003).
85. Banker, M.J. & Clark, T.H. Plasma/serum protein binding determinations. *Current Drug Metabolism* **9**, 854-859 (2008).
86. Stein, A., Voigt, W. & Jordan, K. Chemotherapy-induced diarrhea: pathophysiology, frequency and guideline-based management. *Therapeutic Advances in Medical Oncology* **2**, 51-63 (2010).
87. Weber, J.S., Yang, J.C., Atkins, M.B. & Disis, M.L. Toxicities of Immunotherapy for the Practitioner. *Journal of Clinical Oncology* **33**, 2092-2099 (2015).
88. Sato, Y., Miyashita, A., Iwatsubo, T. & Usui, T. Simultaneous absolute protein quantification of carboxylesterases 1 and 2 in human liver tissue fractions using liquid chromatography-tandem mass spectrometry. *Drug Metabolism and Disposition* **40**, 1389-1396 (2012).
89. Wang, X., Liang, Y., Liu, L., Shi, J. & Zhu, H.J. Targeted absolute quantitative proteomics with SILAC internal standards and unlabeled full-length protein calibrators (TAQSI). *Rapid Communications in Mass Spectrometry* **30**, 553-561 (2016).
90. Hines, R.N., Simpson, P.M. & McCarver, D.G. Age-Dependent Human Hepatic Carboxylesterase 1 (CES1) and Carboxylesterase 2 (CES2) Postnatal Ontogeny. *Drug Metabolism and Disposition* **44**, 959-966 (2016).
91. Artursson, P. & Karlsson, J. Correlation between oral drug absorption in humans and apparent drug permeability coefficients in human intestinal epithelial (Caco-2) cells. *Biochemical and Biophysical Research Communications* **175**, 880-885 (1991).

92. Rubas, W., *et al.* Correlation of solute flux across Caco-2 monolayers and colonic tissue in vitro. *S.T.P. Pharma Sciences* **5**, 93-97 (1995).
93. Wils, P., Warnery, A., Phung-Ba, V. & Scherman, D. Differentiated intestinal epithelial cell lines as in vitro models for predicting the intestinal absorption of drugs. *Cell Biology and Toxicology* **10**, 393-397 (1994).
94. Artursson, P., Palm, K. & Luthman, K. Caco-2 monolayers in experimental and theoretical predictions of drug transport. *Advanced Drug Delivery Reviews* **46**, 27-43 (2001).
95. Ohura, K., Sakamoto, H., Ninomiya, S. & Imai, T. Development of a novel system for estimating human intestinal absorption using Caco-2 cells in the absence of esterase activity. *Drug Metabolism and Disposition* **38**, 323-331 (2010).
96. Quiroga, A.D., *et al.* Deficiency of carboxylesterase 1/esterase-x results in obesity, hepatic steatosis, and hyperlipidemia. *Hepatology* **56**, 2188-2198 (2012).
97. Wei, E., *et al.* Loss of TGH/Ces3 in mice decreases blood lipids, improves glucose tolerance, and increases energy expenditure. *Cell Metabolism* **11**, 183-193 (2010).
98. Xu, Y., *et al.* Hepatocyte-Specific Expression of Human Carboxylesterase 1 Attenuates Diet-Induced Steatohepatitis and Hyperlipidemia in Mice. *Hepatology communications* **4**, 527-539 (2020).
99. Xu, J., Xu, Y., Xu, Y., Yin, L. & Zhang, Y. Global inactivation of carboxylesterase 1 (Ces1/Ces1g) protects against atherosclerosis in Ldlr (-/-) mice. *Scientific Reports* **7**, 17845 (2017).
100. Duysen, E.G., *et al.* Production of ES1 plasma carboxylesterase knockout mice for toxicity studies. *Chemical Research in Toxicology* **24**, 1891-1898 (2011).
101. Kundrick, E., *et al.* Delayed midazolam dose effects against soman in male and female plasma carboxylesterase knockout mice. *Annals of the New York Academy of Sciences* **1479**, 94-107 (2020).
102. Marrero-Rosado, B.M., *et al.* Novel Genetically Modified Mouse Model to Assess Soman-Induced Toxicity and Medical Countermeasure Efficacy: Human Acetylcholinesterase Knock-in Serum Carboxylesterase Knockout Mice. *International Journal of Molecular Sciences* **22**(2021).
103. Ruby, M.A., *et al.* Human Carboxylesterase 2 Reverses Obesity-Induced Diacylglycerol Accumulation and Glucose Intolerance. *Cell Reports* **18**, 636-646 (2017).
104. Li, Y., *et al.* Carboxylesterase 2 prevents liver steatosis by modulating lipolysis, endoplasmic reticulum stress, and lipogenesis and is regulated by hepatocyte nuclear factor 4 alpha in mice. *Hepatology* **63**, 1860-1874 (2016).
105. Maresch, L.K., *et al.* Intestine-Specific Overexpression of Carboxylesterase 2c Protects Mice From Diet-Induced Liver Steatosis and Obesity. *Hepatology communications* **3**, 227-245 (2019).
106. Nagaoka, M., *et al.* Arylacetamide deacetylase knockout mice are sensitive to ketoconazole-induced hepatotoxicity and adrenal insufficiency. *Biochemical Pharmacology* **195**, 114842 (2022).



CHAPTER 1.2

HEPATIC AND INTESTINAL ESTERASES: INSIGHTS INTO PHYSIOLOGY

Yaogeng Wang, Jos H. Beijnen, Alfred H. Schinkel

INTRODUCTION

As one of the main detoxification systems, esterases can metabolize massive current clinically used therapeutic drugs that contain ester, amide, and thioester bonds. This may drastically affect the net drug absorption, distribution, metabolism and excretion (ADME) processes of specific medicines^{1,2}. The group of esterases contains several quite divergent members, including carboxylesterases (CES), arylacetamide deacetylase (AADAC), cholinesterases (acetylcholinesterase (AChE) and butyrylcholinesterase (BChE)), paraoxonases (PON) and, perhaps, albumin. Among them, CES1 primarily resides in the liver, and CES2 and AADAC are highly expressed in both liver and intestine, whereas the rest is mainly present in the blood³. Thus CES1, CES2 and AADAC play important roles in intestinal elimination of oral drugs (intestinal first-pass metabolism) and subsequent liver metabolism effects (hepatic first-pass metabolism), which can profoundly influence the overall exposure, the efficacy, and even the safety of specific ester (pro-)drugs. Hepatic metabolism can further substantially affect exposure of parenterally administered drugs. Given these crucial pharmacological functions, esterases and especially carboxylesterase and AADAC attracted considerable attention in pre-clinical and clinical studies during the last decades⁴.

In addition, CES and AADAC can hydrolyze some endogenous compounds, such as triglyceride and cholesterol esters. This allows them to influence lipid metabolism, energy expenditure and homeostasis to a significant extent, which may relate variation in their activity to some metabolic syndromes, such as non-alcoholic fatty liver disease (NAFLD) and diabetes⁵. Notably, some clues have been obtained from clinical cases suggesting the important physiological functions of esterases³. It has been demonstrated that the protein expression and enzymatic activities of CES1 in adipose tissues from obese and type 2 diabetic patients are markedly elevated compared to those in lean subjects⁶. Another study found a reduced hepatic activity of CES2 and AADAC in human obesity compared to the activity in lean individuals⁷.

All of this indicates the important role of CES1, CES2 and AADAC enzymes in physiological processes and probably the generation or modulation of some metabolic disorders. A number of studies also explored the separate and specific individual roles of each enzyme in various metabolic processes. We briefly summarize these findings and their implications in the remainder of this Introduction.

PHYSIOLOGICAL FUNCTIONS OF CARBOXYLESTERASE 1

To date, six human carboxylesterase genes (*CES1*, *CES1P1*, *CES2*, *CES3*, *CES4A* and *CES5A*) and twenty mouse carboxylesterase genes in five clusters (*Ces1*, *Ces2*, *Ces3*, *Ces4* and *Ces5*) have been classified. Within these carboxylesterases, CES1 and CES2 (abundantly present in the liver

and/or intestine) are thought to be the most important members, profoundly affecting both pharmacology and physiology. CES1 has been well established to be, amongst others, a lipid lipase and substantially involved in lipid metabolism and energy homeostasis processes⁵. Lehner and coworkers made many contributions in understanding CES1 physiological functions, and performed a series of studies for two important *Ces1* members of the eight mouse *Ces1* genes, *Ces1d* and *Ces1g*. The deficiency of mouse *Ces1d* (thought to be a partial functional human CES1 ortholog) can decrease blood lipids, improve glucose tolerance, and increase energy expenditure⁸. Further, they found that *Ces1d* deficiency protected the mice from high sucrose diet-induced hepatic lipid accumulation⁹, and attenuated and potentially prevented progression from simple steatohepatitis to NAFLD¹⁰. Subsequently, it was demonstrated that attenuation of human CES1 activity in liver provided a beneficial effect on hepatic lipid metabolism, which is in line with the findings of the *Ces1d* mouse studies¹¹. In contrast, Zhang et al. found that hepatocyte-specific expression of human CES1 attenuated diet-induced steatohepatitis and hyperlipidemia in mice¹². The apparent discrepancy between these two studies may be due to the genetic background difference, as the Lehner group expressed human CES1 in a mouse *Ces1d*-deficient background, whereas the Zhang group induced human CES1 expression in wild-type mice. Perhaps different expression levels of CES1 or tissue-specific expression differences might also result in different phenotypes.

In contrast to the *Ces1d* knockout phenotype, the global absence of mouse *Ces1g* resulted in obesity, hepatic steatosis, and hyperlipidemia¹³, and a similar phenotype was observed in another globally inactivated mouse *Ces1g* study¹⁴. Moreover, hepatic expression of *Ces1g* ameliorated liver steatosis, dyslipidemia, and insulin signaling¹⁴⁻¹⁶. In addition, global inactivation of *Ces1g* ameliorates the atherosclerosis development via intestinal cholesterol absorption reduction, macrophage cholesterol efflux promotion, M2 macrophage polarization, and bile acid production in mice¹⁷. These results suggest quite different and at times even opposing roles of *Ces1d* and *Ces1g* in overall lipid and energy homeostasis.

All in all, these studies demonstrated the important role of CES1 in physiological processes and related metabolic syndromes, even though there are clearly still some substantial unresolved discrepancies. Therefore, in parallel to our CES2 studies, we also embarked on a CES1 project to systemically investigate the CES1 functions in both pharmacology and physiology using newly generated mouse models (this will be not discussed in this thesis).

PHYSIOLOGICAL FUNCTIONS OF CARBOXYLESTERASE 2

Similar to CES1, CES2 also possesses triglyceride and diacylglycerol lipase activities⁷. However, compared to CES1, human CES2 is highly expressed in both liver and intestine, albeit more abundantly and consistently in the intestine. Considering that the intestine is an important

organ related to lipid/glucose absorption and distribution, this may suggest an important role of CES2 in energy homeostasis. There are also some comparatively recent studies focused on the physiological role of carboxylesterase 2. Li et al. (2016) found that hepatic carboxylesterase 2 expression prevents liver steatosis by modulating lipolysis, endoplasmic reticulum (ER) stress, and lipogenesis, and potentially protects the liver from nonalcoholic fatty liver disease (NAFLD)¹⁸. Similarly, Ruby et al. (2017) found that obesity was associated with decreased hepatic activity of AADAC and CES2 in humans. Furthermore, CES2 depletion impaired lipid and glucose metabolism in primary human hepatocytes, whereas human CES2 hepatic-specific expression reversed liver steatosis and glucose intolerance in mice⁷. In addition, Maresch et al. (2019) demonstrated that mouse *Ces2c* (highly expressed in the intestine and a presumed partial human CES2 orthologue) played a critical role in intestinal lipid metabolism, highlighting the importance of intestinal lipolysis to protect mice from the development of hepatic insulin resistance, NAFLD, and excessive diet-induced weight gain during metabolic stress, such as lipid or glucose over-administration¹⁹.

However, the extent of CES2 physiological research is still limited. Especially the separate roles between hepatic and intestinal CES2 in energy homeostasis and relevant metabolic disorders are still unclear. Given the potential importance of physiological functions of CES2, we generated and characterized several CES2-related mouse models, including mouse *Ces2* cluster knockout mice, and transgenic human CES2 liver- or intestine-specific expression in a mouse *Ces2* knockout background, respectively. Based on these mouse models, some physiological studies were applied to explore the hepatic and/or intestinal CES2 functions in energy metabolism-related processes. The obtained results and implications will be discussed in this thesis.

PHYSIOLOGICAL FUNCTIONS OF ARYLACETAMIDE DEACETYLASE (AADAC)

Until now, there are few studies about AADAC physiological functions. Given the high homology of the active site domain of AADAC with that of hormone-sensitive lipase, AADAC has been classified as a lipase^{20,21}. Recently, it was reported that AADAC plays a protective role during cardiovascular disease generation in type 2 diabetes patients, illustrating the potential physiological functions of AADAC²². However, far too little is still known about AADAC functions in energy homeostasis and metabolic syndromes, which will need to be explored further in the future.

SUMMARY

Carboxylesterase and arylacetamide deacetylase are two main esterase families expressed in liver and intestine, and all of these have shown hydrolytic activities involving endogenous esters and thioesters, including lipids. Liver is one of the main organs of lipid/glucose metabolism and

distribution, markedly involved in energy homeostasis and balance, and its function is tightly associated with various related metabolic disorders. In its turn, the intestine is responsible for energy absorption, such as lipid and glucose from the diet, distribution, and metabolism. From this perspective, we generated and characterized several mouse models for CES2 to systemically explore the specific physiological roles of CES2, as well as the meaning of its expression at different locations (hepatic and intestinal CES2). An initial characterization of these mouse models is described in this thesis.

REFERENCE

1. Lyubimov, A.V. *Encyclopedia of Drug Metabolism and Interactions*, (2011).
2. Fukami, T. & Yokoi, T. The emerging role of human esterases. *Drug Metabolism and Pharmacokinetics* **27**, 466-477 (2012).
3. Wang, D., *et al.* Human carboxylesterases: a comprehensive review. *Acta Pharmaceutica Sinica B* **8**, 699-712 (2018).
4. Hatfield, M.J., *et al.* Carboxylesterases: General detoxifying enzymes. *Chemico-Biological Interactions* **259**, 327-331 (2016).
5. Lian, J., Nelson, R. & Lehner, R. Carboxylesterases in lipid metabolism: from mouse to human. *Protein Cell* (2017).
6. Dominguez, E., *et al.* Integrated phenotypic and activity-based profiling links Ces3 to obesity and diabetes. *Nature Chemical Biology* **10**, 113-121 (2014).
7. Ruby, M.A., *et al.* Human Carboxylesterase 2 Reverses Obesity-Induced Diacylglycerol Accumulation and Glucose Intolerance. *Cell Reports* **18**, 636-646 (2017).
8. Wei, E., *et al.* Loss of TGH/Ces3 in mice decreases blood lipids, improves glucose tolerance, and increases energy expenditure. *Cell Metabolism* **11**, 183-193 (2010).
9. Lian, J., *et al.* Ces1d deficiency protects against high-sucrose diet-induced hepatic triacylglycerol accumulation. *Journal of Lipid Research* (2019).
10. Lian, J., *et al.* Ces3/TGH Deficiency Attenuates Steatohepatitis. *Scientific Reports* **6**, 25747 (2016).
11. Lian, J., *et al.* Genetic variation in human carboxylesterase CES1 confers resistance to hepatic steatosis. *Biochimica et Biophysica Acta* **1863**, 688-699 (2018).
12. Xu, Y., *et al.* Hepatocyte-Specific Expression of Human Carboxylesterase 1 Attenuates Diet-Induced Steatohepatitis and Hyperlipidemia in Mice. *Hepatology communications* **4**, 527-539 (2020).
13. Quiroga, A.D., *et al.* Deficiency of carboxylesterase 1/esterase-x results in obesity, hepatic steatosis, and hyperlipidemia. *Hepatology* **56**, 2188-2198 (2012).
14. Xu, J., *et al.* Hepatic carboxylesterase 1 is essential for both normal and farnesoid X receptor-controlled lipid homeostasis. *Hepatology* **59**, 1761-1771 (2014).
15. Bahitham, W., Watts, R., Nelson, R., Lian, J. & Lehner, R. Liver-specific expression of carboxylesterase 1g/esterase-x reduces hepatic steatosis, counteracts dyslipidemia and improves insulin signaling. *Biochimica et Biophysica Acta* **1861**, 482-490 (2016).
16. Xu, J., *et al.* Hepatic carboxylesterase 1 is induced by glucose and regulates postprandial glucose levels. *PLoS One* **9**, e109663 (2014).
17. Xu, J., Xu, Y., Xu, Y., Yin, L. & Zhang, Y. Global inactivation of carboxylesterase 1 (Ces1/Ces1g) protects against atherosclerosis in Ldlr (-/-) mice. *Scientific Reports* **7**, 17845 (2017).
18. Li, Y., *et al.* Carboxylesterase 2 prevents liver steatosis by modulating lipolysis, endoplasmic reticulum stress, and lipogenesis and is regulated by hepatocyte nuclear factor 4 alpha in mice. *Hepatology* **63**, 1860-1874 (2016).
19. Maresch, L.K., *et al.* Intestine-Specific Overexpression of Carboxylesterase 2c Protects Mice From Diet-Induced Liver Steatosis and Obesity. *Hepatology communications* **3**, 227-245 (2019).
20. Tiwari, R., Köffel, R. & Schneider, R. An acetylation/deacetylation cycle controls the export of sterols and steroids from *S. cerevisiae*. *EMBO Journal* **26**, 5109-5119 (2007).
21. Probst, M.R., *et al.* Human liver arylacetamide deacetylase. Molecular cloning of a novel esterase involved in the metabolic activation of arylamine carcinogens with high sequence similarity to hormone-sensitive lipase. *Journal of Biological Chemistry* **269**, 21650-21656 (1994).
22. Misra, A. & Fisher, E.A. Translational Research in Culture: AADAC, Diabetes, and Cardiovascular Disease. *Cell Stem Cell* **27**, 6-7 (2020).



CHAPTER 2

Pharmacological and physiological functions of the carboxylesterase 2 complex: New mouse models

Yaogeng Wang¹, Changpei Gan¹, Joke Beukers², Hilde Rosing², Wenlong Li¹, Els Wagenaar¹, Maria C. Lebre¹, Ji-Ying Song³, Colin Pritchard⁴, Rahmen Bin Ali⁴, Ivo Huijbers⁴, Jos H. Beijnen^{1,2,5}, Alfred H. Schinkel^{1*}

**Corresponding author*

¹Division of Pharmacology, The Netherlands Cancer Institute, Plesmanlaan 121, 1066 CX Amsterdam, The Netherlands.

²Department of Pharmacy & Pharmacology, Plesmanlaan 121, 1066 CX Amsterdam, The Netherlands.

³Division of Experimental Animal Pathology, The Netherlands Cancer Institute, Plesmanlaan 121, 1066 CX Amsterdam, the Netherlands.

⁴Transgenic Core Facility, Mouse Clinic for Cancer and Aging (MCCA), The Netherlands Cancer Institute, 1066 CX Amsterdam, The Netherlands

⁵Faculty of Science, Department of Pharmaceutical Sciences, Division of Pharmacoepidemiology & Clinical Pharmacology, Utrecht University, Universiteitsweg 99, 3584 CG Utrecht, The Netherlands.

To be submitted

ABSTRACT

Background and Purpose

Carboxylesterase 2 (CES2) can hydrolyze carboxylester as well as amide and thioester linkages in both exogenous and endogenous compounds, including drugs and lipids. In this study, we aimed to generate and characterize several CES2-related mouse models, and investigate the pharmacological and physiological roles of CES2 *in vivo*, including metabolic syndrome parameters.

Experimental Approach

Ces2 gene cluster deletion mice (*Ces2*^{-/-}) and humanized hepatocyte or enterocyte CES2-transgenic mouse strains (*Ces2*^{-/-}A and *Ces2*^{-/-}V) were generated and characterized. Pharmacokinetic studies analyzing vinorelbine and capecitabine, and physiological analyses addressing lipid and glucose homeostasis were applied in these models.

Key Results

Vinorelbine was a specific and rapidly metabolized substrate of mouse *Ces2* but much less of human CES2. Both mouse and human CES2 could significantly limit capecitabine oral bioavailability, and mediate the conversion of capecitabine to its metabolites, but without influencing overall metabolite body exposure. Furthermore, CES2 decreased hepatic lipid accumulation, ameliorated white adipose tissue inflammation, and improved glucose tolerance and insulin sensitivity, probably by alleviating lipid burden in both liver and circulation.

Conclusions and Implications

Our results demonstrate the important role of CES2 in both pharmacology and physiology. The generated CES2 genetically engineered mouse models can provide powerful pre-clinical tools to help us develop drugs, improve drug administration regimens, obtain deeper physiological insights, and explore potential solutions for the metabolic syndrome.

Keywords: Carboxylesterase 2, vinorelbine, capecitabine, glucose homeostasis, lipid metabolism

Abbreviations:

CES: Carboxylesterase; *Ces2*^{-/-}: mouse *Ces2* cluster knockout mice; *Ces2*^{-/-}A: mouse *Ces2* cluster knockout mice with specific expression of human CES2 in liver; *Ces2*^{-/-}V: mouse *Ces2* cluster knockout mice with specific expression of human CES2 in intestine; LC-MS/MS: liquid chromatography coupled with tandem mass spectrometry.

1. INTRODUCTION

Mammalian carboxylesterases (EC 3.1.1.1) belong to a multigene superfamily encoding enzymes that have broad substrate specificity and catalyze the hydrolysis of ester-, thioester- and amide bonds¹⁻³. Carboxylesterases (CES) are mainly known as enzymes involved in detoxification and metabolism of (pro-)drugs and environmental toxicants⁴⁻⁷. However, carboxylesterases have also been demonstrated to hydrolyze endogenous esters and thioesters including lipids and some of these enzymes have been shown to play important physiological functions in lipid metabolism and energy homeostasis⁸. Carboxylesterase genes encoding six human carboxylesterases (CES1, CES1P1, CES2, CES3, CES4A and CES5A) and twenty mouse carboxylesterases in five clusters (Ces1, Ces2, Ces3, Ces4 and Ces5) have been identified. Within these carboxylesterases, CES1 and CES2 are thought to be the two most important members with the widest functional ramifications. With regard to CES2, the mouse contains eight *Ces2* genes (*Ces2a* to *Ces2h*), including one pseudogene designated *Ces2d-ps*. All these *Ces2* genes are located in a 286-kb gene cluster (*Ces2* cluster) on mouse chromosome 8. While human has only one single *CES2* gene, together with *CES3* and *CES4A*, these are located in a cluster on human chromosome 16^{9,10}. Of note, unlike mouse *Ces1c*, which is primarily secreted into plasma due to lack of an ER retention signal, almost all other mouse and human CES proteins carry the HXEL ER retrieval sequence at their C-terminus (such as HIEL and HTEL for human CES1 and CES2, respectively), which is essential for the localization of these enzymes to the ER lumen in mammalian cells^{1,8,11}. However, as we previously found that mouse *Ces2a* may also be present in the blood¹², and as protein disulfide isomerases (ER retention signal-containing) are found at the cell surface¹³, the ER retrieval sequence may not fully guarantee that protein cannot be secreted into blood.

Human (h) CES2 is expressed mainly in liver and intestine, but especially abundant in intestine, and can hydrolyze carboxylester as well as amide and thioester linkages in both exogenous and endogenous compounds. Although they share 47% amino acid identity, hCES1 and hCES2 exhibit distinct substrate specificities. hCES1 preferentially catalyzes the hydrolysis of compounds esterified with a small alcohol group, while hCES2 hydrolyzes compounds with a relatively small acyl group and large alcohol group⁷. hCES2 has a quite broad substrate specificity, including hydrolysis of narcotics (heroin, cocaine)¹⁴, chemotherapy (pro-)drugs (irinotecan, capecitabine and gemcitabine)¹⁵⁻¹⁸ and other drugs (procaine, prasugrel and flutamide)^{19,20}.

Considering the high expression of CES2 in intestine, it may make a major contribution to the pre-systemic elimination of substrate drugs following oral administration (first-pass metabolism). CES2 present inside the enterocytes could metabolize (part of) substrate drugs before they arrive to the liver, in which substrate drugs will subsequently be further hydrolyzed by hepatocyte CES2. This combined first-pass metabolism process may thus strongly influence the overall systemic exposure and the efficacy of specific substrate drugs, as is the case for CYP3A-metabolized drugs.

On the other hand, for CES-activated prodrugs, high CES2 levels in enterocytes may cause more active drug or metabolite accumulation in the intestinal tissue and thus local toxicity, such as chemotherapy-induced diarrhea (CID)²¹. CES2 is also expressed in various tumors, including hepatocellular carcinoma, esophageal squamous carcinoma, colon adenocarcinoma, renal adenocarcinoma, and others, although in most of these tumors CES2 expression is significantly lower than in the corresponding normal tissues. The expression of CES2 also varies among different cancer types and individuals, so activity differences of CES2 in tumors may influence the response of tumor tissue to specific drugs. In addition, systemic exposure changes may affect anti-tumor chemotherapies, such as irinotecan and gemcitabine^{16,22}, as well. In summary, CES2 plays an important role in the metabolism of many exogenous compounds, such as (pro-) drugs, toxins and pesticides, which directly influences pharmacology and toxicology in humans.

As CES2 can further hydrolyze endogenous lipids such as triglycerides, cholesteryl esters and retinyl esters, it is also involved in energy homeostasis, affecting lipid and glucose metabolism⁸. Li *et al.* demonstrated that hepatic CES2 plays an important role in controlling hepatic triglyceride homeostasis by regulating lipolysis, fatty acid oxidation (FAO), ER stress, and lipogenesis to alleviate liver steatosis, as well as improving glucose tolerance and energy expenditure. This process appeared to be mediated through hepatic HNF-4a²³. Similarly, another study suggested that CES2 promotes lipid oxidation to reverse hepatic steatosis and glucose intolerance²⁴. Besides hepatic CES2, intestinal *Ces2c* overexpression protected mice from excessive diet-induced weight gain and liver steatosis²⁵. These studies reveal important functions of CES2 in energy homeostasis, including lipid metabolism and glucose handling and a potential role of CES2 in protection from metabolic syndrome. However, compared to more substantial physiological studies of CES1 functions, such physiological research for CES2 is still limited.

In order to better understand the pharmacological and physiological functions of CES2, we generated and characterized mouse *Ces2* cluster knockout mice (*Ces2*^{-/-}). Considering the high CES2 expression in liver and intestine in humans, we also generated and characterized homozygous transgenic mice with stable liver- or intestine-specific expression of human *CES2* cDNA in a mouse *Ces2* knockout background (*Ces2*^{-/-}A or *Ces2*^{-/-}V), respectively. By analyzing the pharmacokinetics and metabolism of administered chemotherapy drugs (vinorelbine and capecitabine), we obtained better insights into the pharmacological functions of CES2. This will help us to develop a better understanding of the *in vivo* drug handling process and thus to potentially improve drug administration regimens. In addition, better understanding of the energy metabolism processes in which CES2 may be involved could provide clues on how to ameliorate aspects of the metabolic syndrome.

2. MATERIALS AND METHODS

2.1 Materials

Vinorelbine (GlaxoSmithKline) was obtained from the pharmacy of The Netherlands Cancer Institute. Capecitabine was purchased from Carbosynth (Berkshire, UK). The Lipid Extraction Kit was obtained from PromoCell GmbH (Heidelberg, Germany). The LabAssay Triglyceride Kit was from Wako Chemicals (Tokyo, Japan). Isoflurane was purchased from Pharmachemie (Haarlem, The Netherlands), heparin (5000 IU ml⁻¹) was from Leo Pharma (Breda, The Netherlands). All other chemicals and reagents were obtained from Sigma-Aldrich (Steinheim, Germany).

2.2 Animals

Mice were housed and handled according to institutional guidelines complying with Dutch and EU legislation. All experimental animal protocols were evaluated and approved by the institutional animal care and use committee. Wild-type, *Ces2* cluster knockout mice (*Ces2*^{-/-}), humanized *CES2* mice with specific expression of human *CES2* in liver (*Ces2*^{-/-}A) and humanized *CES2* mice with specific expression of human *CES2* in intestine (*Ces2*^{-/-}V) in a mouse *Ces2* cluster knockout background mice are all of a >99% FVB genetic background. Mice between 9 and 16 weeks of age were used for pharmacokinetic studies, between 4 and 20 weeks of age for body weight monitoring and basic physiology studies (hematology, plasma chemistry, histology/pathology, etc.), between 12 and 16 weeks old for VLDL (Very Low Density Lipoprotein) production, lipid tolerance test, glucose tolerance test and insulin resistance test, and aging mice of ~60 weeks old were used for basic physiology analysis. All the animals were kept in a temperature-controlled environment with 12-h light and 12-h dark cycle and they received a standard medium-fat diet (Transbreed, SDS Diets, Technilab-BMI, fat content 10% by weight, 24% by calories, Someren, The Netherlands) and acidified water *ad libitum*.

2.3 Generation of *Ces2*^{-/-}, *Ces2*^{-/-}A and *Ces2*^{-/-}V mice

Details of the development of *Ces2*^{-/-}, *Ces2*^{-/-}A and *Ces2*^{-/-}V mice are described in Supplemental Methods. Briefly, *Ces2*^{-/-} were generated using CRISPR-Cas9 technology, and transgenic *Ces2*^{-/-}A and *Ces2*^{-/-}V were generated using two tissue-specific human *CES2* cDNA expression plasmids with ApoE and Villin promoters, respectively.

2.4 Real-time PCR analysis.

RNA was isolated by RNeasy Mini Kit (Qiagen, Hilden, Germany) from mouse liver and small intestine. Subsequently cDNA synthesis was done by Maxima First Strand cDNA Synthesis Kit (Thermo Scientific, Waltham, US), and real-time (RT)-PCR using specific primers (Qiagen, Hilden, Germany) for mouse *Ces1a*, *Ces1b*, *Ces1c*, *Ces1d*, *Ces1e*, *Ces1f*, *Ces1g*, *Ces1h*, *Ces2a*, *Ces2b*, *Ces2c*, *Ces2e*, *Ces2f*, *Ces2g*, *Ces2h*, *Ces3a* and *Ces3b* was performed as described previously²⁶.

2.5 Western blot and immunohistochemical analysis.

Crude total cellular membrane fractions were isolated from mouse liver, kidney, and small intestine as described previously²⁷. Protein concentration was quantified by the BCA protein Assay Kit (Thermo Scientific, Waltham, MA, US). After size separation and transfer, proteins were probed with rabbit anti-human CES2 monoclonal antibody (ab184957, Abcam, Cambridge, UK) (diluted 1:2000) or rabbit anti- β -actin monoclonal antibody (#4970, Cell Signaling Technology, Danvers, MA, USA) (dilution 1:2,000), followed by HRP-labeled goat anti-rabbit second antibody (diluted 1:5000) (Agilent Dako, Santa Clara, CA, US). Immunohistochemistry on wild-type, *Ces2*^{-/-}, *Ces2*^{-/-}A and *Ces2*^{-/-}V tissues was conducted with the same rabbit anti-human CES2 monoclonal antibody (ab184957), and secondary antibody conjugated to HRP-labeled polymers (EnVision+ System-HRP; Agilent Dako, Santa Clara, CA, US).

2.6 Bodyweight monitoring, histology/pathology, plasma clinical chemistry and hematology analysis.

The bodyweights of mice (~20 female and ~20 male mice from each mouse strain) were monitored every week from 4 weeks to 20 weeks old. At week 20, mice were fasted overnight (16 h) and sacrificed for blood and organ collection. Isolated tissues were handled as described previously for Hematoxylin and Eosin (H&E)-staining, and Oil Red O-staining²⁸. Parts of liver samples were snap-frozen in dry ice for further lipid content analysis. The semi-quantitative assessment standard for H&E-staining of white adipose tissue and Oil Red O-staining of liver can be found in Supplemental Methods. Standard clinical-chemistry analyses on plasma were performed on a Roche Hitachi 917 analyzer to determine levels of alkaline phosphatase, alanine aminotransaminase, Na⁺, K⁺, Ca²⁺, Cl⁻, urea, uric acid, glucose, triglycerides and cholesterol. Hemoglobin, hematocrit, mean corpuscular volume, red and white blood cell counts, and platelets were analyzed in peripheral blood on a Cell Dyn 1200 analyzer (Abbott, Chicago, IL, US). The ageing mice at ~60 weeks (3 - 6 mice, either female or male) were sacrificed for histology, plasma clinical-chemistry and hematology analyses as well. Moreover, 12 - 13 weeks old young adult mice (~10 females and ~10 males from each strain) were sacrificed and different tissues, including organs and adipose tissues, were collected for absolute weight and tissue-to-body weight ratio analysis.

2.7 Drug solutions

Vinorelbine (10 mg/ml) was diluted with normal saline 5-fold to 2 mg/ml for intravenous injection and 10-fold to 1 mg/ml for oral administration. Capecitabine was first dissolved in dimethyl sulfoxide (DMSO) at a concentration of 500 mg/ml and further diluted with mixed buffer (polysorbate 20 : absolute ethanol = 1 : 1, v/v) and 40 mM Na-Acetate (NaAc, pH 4.2), to make up the final working solution of 50 mg/ml in [DMSO : Polysorbate 20 : absolute ethanol : 40 mM NaAc (pH 4.2) = 10 : 15 : 15 : 60, (v/v/v/v)]. All dosing solutions were prepared freshly on the day of experiment.

2.8 Plasma and organ pharmacokinetics of vinorelbine and capecitabine in mice

In order to minimize variation among individuals, mice were fasted for 3 h before drug was administered i.v. or orally. For the vinorelbine 4-h experiment, 6-7 male mice received vinorelbine intravenously (10 mg/kg, 5 μ l/g) or orally (10 mg/kg, 10 μ l/g) using a blunt-ended needle. Tail vein blood samples were collected at 0.125, 0.25, 0.5, 1 and 2 h after drug administration. For capecitabine 2-h experiments, 6-7 female mice received oral capecitabine (500 mg/kg, 10 μ l/g), and tail vein blood samples were collected at 0.125, 0.25, 0.5 and 1 h after drug administration. Tail vein blood sample collection (~50 μ l) was performed using microvettes containing dipotassium-EDTA. At the last time point in each experiment (2 or 4 h), mice were anesthetized with 5% isoflurane and blood was collected by cardiac puncture. Cardiac puncture blood samples (600 – 800 μ l) were collected in Eppendorf tubes containing heparin as an anticoagulant. The mice were then sacrificed by cervical dislocation and brain, liver, kidney, lung, small intestine and testis were rapidly removed. Plasma was isolated from the blood by centrifugation at 9,000g for 6 min at 4°C, and the plasma fraction was collected and stored at -30°C until analysis. Organs were homogenized with 4% (w/v) bovine serum albumin and stored at -30°C until analysis. Relative metabolite-to-parental drug ratio after drug administration was calculated by determining metabolite tissue concentration relative to corresponding parental drug concentration at the last time point of organ collection.

2.9 HPLC-MS analysis

Concentrations of vinorelbine and its metabolite and capecitabine and its metabolites in mouse plasma samples and organ homogenates were determined using two independent validated high-performance liquid chromatography-tandem mass spectrometry assays^{29,30}.

2.10 VLDL secretion and lipid tolerance test

For the VLDL secretion experiment, mice were fasted for 16 h and then Poloxamer-407 (1 g/kg) was injected intraperitoneally. Blood samples were collected from the tail vein before injection (0 h) and 1, 2, 3, and 4 h after injection of the lipase inhibitor. For the lipid tolerance test, mice were fasted for 16 h and olive oil (10 μ l/g) was then orally administered by a blunt-ended needle. Blood samples were collected from the tail vein at different time points as described above. All the plasma samples were processed and triglyceride levels were analyzed with the LabAssay Triglyceride Kit.

2.11 Glucose and insulin tolerance test

For the glucose tolerance test, mice fasted for 16 hours received orally administered glucose (1 g/kg). Blood glucose levels in tail vein samples were monitored at baseline (0 minutes, before glucose was administered) and various time points (15, 30, 60, 90, and 120 minutes) after glucose was administered with an ACCU-CHEK Performa glucose meter (Roche). For the insulin tolerance

test, mice were first fasted for 6 hours and then received an intraperitoneal injection with insulin (0.5 U/kg). Blood glucose levels were measured at different time points as described above.

2.12 Data and statistical analysis

Pharmacokinetic parameters were calculated by non-compartmental methods using the PK solver software³¹. The area under the plasma concentration-time curve (AUC) was calculated using the trapezoidal rule, without extrapolating to infinity. The peak plasma concentration (C_{max}) and the time of maximum plasma concentration (T_{max}) were estimated from the original (individual mouse) data. One-way analysis of variance (ANOVA) was used when multiple groups were compared and the Tukey's test *post hoc* correction was used to accommodate multiple testing. The two-sided unpaired Student's t-test was used when treatments or differences between two specific groups were compared. Kruskal-Wallis rank test was used for semi-quantitative assessment for (H&E)-staining of white adipose tissue and Oil Red O-staining of liver. All statistical analyses were performed using the software GraphPad Prism 8 (GraphPad Software Inc., La Jolla, CA, USA). All the linear data were log-transformed before statistical tests were applied. Differences were considered statistically significant when $P < 0.05$. All data are presented as mean \pm SD.

3. RESULTS

3.1 Generation of *Ces2* cluster knockout mice

In the mouse, 7 full-length *Ces2* genes (*Ces2a-2c*, *Ces2e-2h*) and 1 pseudogene (*Ces2d*) have been identified¹⁰. We originally aimed to obtain a conditional whole *Ces2* cluster (from *Ces2a* to *Ces2h*) deletion by insertion of 5' and 3' RoxP recombination sites flanking the *Ces2* locus using CRISPR/Cas9 methodology in fertilized oocytes (Figure 1A). Offspring with RoxP sites flanking the whole *Ces2* cluster could then further be cross-bred with Dre-expressing mice to generate a conditional *Ces2* knockout mouse strain³². In our first attempts we obtained just one candidate line with a RoxP site located upstream of *Ces2a*, but not downstream of *Ces2h*. However, PCR amplification and DNA sequencing of offspring revealed that a full *Ces2* cluster deletion resulting from direct ligation of the two CRISPR/Cas9 cutting sites without RoxP insertion had also been obtained. This complete *Ces2* cluster deletion allele was then backcrossed to wild-type (FVB/NRj) background for at least three generations to dilute any potential off-target mutations. Homozygotes of the complete *Ces2* cluster deletion (*Ces2*^{-/-}) were then generated by crossbreeding of heterozygous knockout mice and turned out to be viable and fertile, obviating the need for further generation of conditional *Ces2* knockout lines.

Deletion of the *Ces2* cluster genes was verified by comparing wild-type and *Ces2*^{-/-} mice by PCR for presence of each *Ces2* gene (except for the pseudogene *Ces2d*) (primers in Supplemental Table 1). PCR products of all functional *Ces2* genes (*Ces2a-2c* and *Ces2e-2h*) were present in

WT mice but absent in *Ces2*^{-/-} mice (Figure 1B). In addition, quantitative Real-Time PCR (qRT-PCR) analysis was performed for all functional *Ces1*, *Ces2* and *Ces3* genes in liver and small intestine of both wild-type and *Ces2*^{-/-} mice. The results revealed that in wild-type mice, *Ces1* genes were highly expressed in liver, especially *Ces1b-1g*, while *Ces2* was mainly highly expressed in small intestine, such as *Ces2a-2e*. Notably, *Ces2a-2e* were also expressed quite abundantly in liver, even though not as highly as some *Ces1* genes (Supplemental Table 2). All the functional *Ces2* mRNA signals were dramatically decreased in both liver and small intestine of *Ces2*^{-/-} mice compared with WT mice (Supplemental Table 2 and Supplemental Figure 1), without significant or meaningful changes in *Ces1* gene expression between WT and *Ces2*^{-/-} mice. This suggests that there was no compensatory up-regulation of the *Ces1* genes. However, we did find a significant decrease of *Ces3a* and *Ces3b* signal in small intestine, but this was down from an already very low basal expression level. Thus a homozygous *Ces2*^{-/-} mouse strain was generated which is viable and fertile with normal life spans and no prominent anatomic alterations. More extensive physiological analysis of this strain will be discussed later.

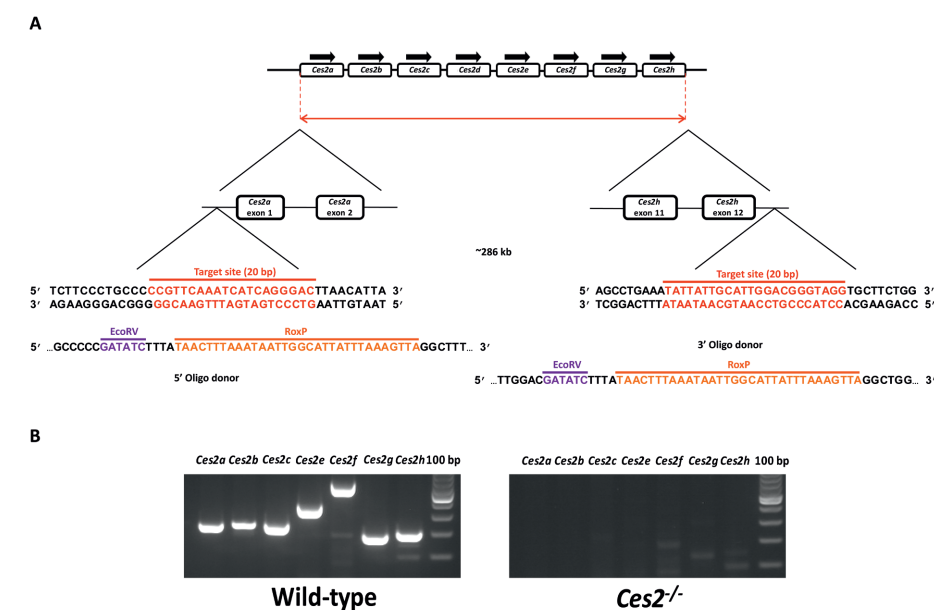


Figure 1. *Ces2* knockout mouse model generation and characterization. (A) Schematic overview of the CRISPR-Cas9 strategy for deletion of the *Ces2* cluster genes and (B) PCR analysis for all known functional *Ces2* genes in tail DNA of WT and *Ces2*^{-/-} mice.

3.2 Humanized mice with stable transgenic human *CES2* expression in liver or intestine in a mouse *Ces2* knockout background

Considering the substantial expression of *CES2* in human liver and intestine, homozygous transgenic mice containing human *CES2* cDNA specifically expressed either in liver or intestine

in a mouse *Ces2* cluster deletion background were generated using zygote injection of two expression cassettes (ApoE-hCES2-HCR-driven liver-specific and villin-hCES2-SV40-driven intestine-specific cassette, Figure 2A-B). The cross-breeding strategy from heterozygous to stable homozygous *hCES2* transgenic and *Ces2* knockout mice is described in the Supplemental Methods. We hereafter refer to these strains as *Ces2*^{-/-}A and *Ces2*^{-/-}V, respectively.

Crude membrane fractions of liver, kidney, small intestine and colon of wild-type, *Ces2*^{-/-}, *Ces2*^{-/-}A, and *Ces2*^{-/-}V mice, together with hCES2-expressing human donor tissues as positive controls, were analyzed for expression of human CES2 by western blotting using a specific rabbit anti-human CES2 monoclonal antibody. As expected, hCES2 was not detected in wild-type and *Ces2*^{-/-} mice in any of the tissues collected. hCES2 in *Ces2*^{-/-}A mice was expressed in the liver but not in the intestine, while in *Ces2*^{-/-}V mice, hCES2 was expressed in high amounts in the small intestine and relatively lower level in colon but not in the liver (Figure 2C). However, hCES2 in *Ces2*^{-/-}A and *Ces2*^{-/-}V mice was also somewhat detected in kidney, an expression site also observed in a previous study for these expression cassettes²⁸. The contribution of this renal CES2 to overall drug metabolism is probably modest, also considering that liver is the main detoxification organ and intestine is an important location for first-pass metabolism.

In order to further identify the location of hCES2 expression, immunohistochemical staining was performed with the same antibody. The results showed strong CES2 expression in nearly all hepatocytes, some expression in renal convoluted ducts and slight expression in the muscularis layer of intestine in *Ces2*^{-/-}A mice (Figure 2D). Whereas in *Ces2*^{-/-}V mice, hCES2 was highly expressed in all enterocytes, very slightly expressed in renal convoluted ducts, and undetectable in liver parenchyma. This is consistent with the western blot results. A similar localization and expression profile was previously seen for human CYP3A4 in analogous transgenic mouse models²⁸. Thus, two specific transgenic mouse strains with either liver-specific or intestine-specific expression of human CES2 were obtained. hCES2 expression was re-checked by western blot after 9 generations of breeding and found to be stable. Like for the *Ces2*^{-/-} mice, both *Ces2*^{-/-}A and *Ces2*^{-/-}V mouse strains are viable and fertile with normal life spans and no prominent anatomic alterations. More extensive physiological analysis will be discussed later together with *Ces2*^{-/-} mice.

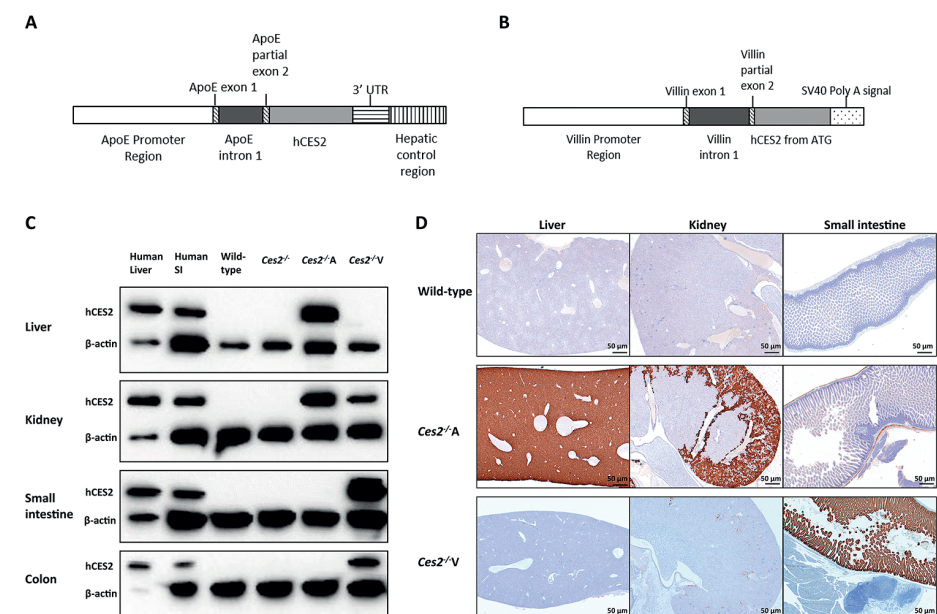


Figure 2. Generation and characterization of human CES2 liver- or intestine-specific transgene expressing mouse models. (A) Schematic structure of ApoE promoter-HCR1-driven expression cassette containing human CES2 cDNA; (B) Schematic structure of Villin promoter-driven expression cassette containing human CES2 cDNA; (C) Western blot analysis of crude membrane fractions of liver, kidney, small intestine and colon from wild-type, *Ces2*^{-/-}, human CES2 liver transgenic (*Ces2*^{-/-}A) and human CES2 intestine transgenic (*Ces2*^{-/-}V) mice; (D) Immunohistochemical staining of human CES2 in liver, small intestine and kidney of wild-type, *Ces2*^{-/-}A and *Ces2*^{-/-}V mice.

3.3 Mouse *Ces2* markedly but human CES2 only minimally affects vinorelbine metabolism

Vinorelbine (Navelbine), a semisynthetic vinca alkaloid agent, has been used for treatment of advanced non-small cell lung cancer (NSCLC) and breast cancer for several decades³³⁻³⁵. Two main vinorelbine metabolites have been identified in humans, CYP3A4-generated non-active vinorelbine N-oxide^{36,37} and active deacetylvinorelbine (4-O-deacetylvinorelbine) which is assumed to be formed by carboxylesterase enzymes³⁸ (Supplemental Figure 2). A preceding study suggested there was a high chance that in mice *Ces2a* was involved in this process¹². Thus, in order to study the metabolic impact of the mouse *Ces2* family and hCES2 on vinorelbine to deacetylvinorelbine conversion *in vivo*, we administered vinorelbine (10 mg/kg) either orally or intravenously (I.V.) to male wild-type, *Ces2*^{-/-}, *Ces2*^{-/-}A and *Ces2*^{-/-}V mice, and measured drug and metabolite levels in plasma and tissues.

For oral experiments, there was no significant difference in vinorelbine plasma AUC_{0-4h} between wild-type and *Ces2*^{-/-} mice, although at most time points concentrations were higher in the *Ces2*^{-/-} mice. Unexpectedly, we observed a significantly higher plasma exposure of vinorelbine

in *Ces2^{-/-}A* compared with wild-type, but not *Ces2^{-/-}* mice, whereas the *Ces2^{-/-}V* values were also higher than those in wild-type, but not significantly (Figure 3A). We further found that the plasma concentration of vinorelbine was rising between 1 and 2 h to yield a second plasma peak in all the mouse strains. This suggests re-absorption of vinorelbine from the gut lumen, presumably through enterohepatic circulation. Interestingly, the plasma AUC_{0-4h} of deacetylvinorelbine was profoundly decreased (238-fold) in *Ces2^{-/-}* mice compared to wild-type mice (1.0 ± 0.37 vs. 238 ± 112 ng/ml*h, $P < 0.001$), suggesting a dominant function of mouse *Ces2* in conversion of vinorelbine to deacetylvinorelbine (Figure 3B and Table 1). Somewhat unexpectedly, the deacetylvinorelbine plasma AUC_{0-4h} was, by comparison, only slightly (albeit significantly) increased in both *Ces2^{-/-}A* (3.7-fold, 3.7 ± 2.2 ng/ml*h, $P < 0.001$) and *Ces2^{-/-}V* (3.3-fold, 3.3 ± 2.3 ng/ml*h, $P < 0.001$) compared to *Ces2^{-/-}* mice (Figure 3B and Table 1). Transgenic human *CES2* thus had only a comparatively small impact on deacetylvinorelbine generation. These low plasma deacetylvinorelbine levels accordingly yielded a profoundly lower plasma AUC_{0-4h} ratio of deacetylvinorelbine-to-vinorelbine in *Ces2^{-/-}*, *Ces2^{-/-}A* and *Ces2^{-/-}V* compared to wild-type mice (Table 1). These data suggest that human *CES2* is probably far less proficient in hydrolyzing vinorelbine than one or more of the mouse *Ces2* enzymes. However, our previous study suggested that mouse *Ces2* proteins (likely *Ces2a*) may be secreted in part into the blood and contribute there to vinorelbine hydrolysis. This might disproportionately influence vinorelbine metabolism directly in the circulation, in contrast to the transgenic human *CES2* which is restricted to the liver or intestine.

With respect to tissues, similar to the plasma exposure, we observed that vinorelbine concentrations at 4 h were higher in all of the three gene-modified mouse strains compared with wild-type mice, but for most tissues without meaningful differences in tissue-to-plasma ratios (Supplemental Figure 3 - 4). This suggests that vinorelbine tissue concentrations mainly reflected plasma exposure. However, for the liver we observed significantly higher tissue-to-plasma ratios in *Ces2^{-/-}* and *Ces2^{-/-}V*, but not *Ces2^{-/-}A* mice (Supplemental Figure 3B). This might reflect significantly reduced hepatic metabolism of vinorelbine in the *Ces2^{-/-}* and *Ces2^{-/-}V* mice. Again, a pronounced decrease in deacetylvinorelbine generation was observed in *Ces2^{-/-}* mice compared with wild-type mice in all the tissues, with very limited increases in both *Ces2^{-/-}A* and *Ces2^{-/-}V* mice (Supplemental Figure 5 - 6). To better understand the transformation of vinorelbine to deacetylvinorelbine, we also calculated the ratios of deacetylvinorelbine to vinorelbine concentrations in all the tissues (Figure 4). In liver, the deacetylvinorelbine-to-vinorelbine ratio in wild-type was 5.0 ± 1.0 , suggesting a large amount of transformation of vinorelbine to deacetylvinorelbine in liver. This ratio was vastly reduced in *Ces2^{-/-}* mice (0.015 ± 0.008 , 333-fold decrease), *Ces2^{-/-}A* mice (0.019 ± 0.002 , 263-fold decrease) and *Ces2^{-/-}V* mice (0.021 ± 0.008 , 238-fold decrease) (Figure 4A and Supplemental Table 3). In small intestine tissue, the transformation was somewhat lower in wild-type with a ratio of 0.88 ± 0.22 . However, the deficiency of *Ces2* further markedly decreased this ratio to 0.034 ± 0.010 , and transgenic human *CES2* only slightly

increased the ratios to 0.039 ± 0.008 and 0.049 ± 0.015 in *Ces2^{-/-}A* and *Ces2^{-/-}V* mice, respectively (Figure 4B and Supplemental Table 3). Similar results were obtained in other tissues and matrices, including small intestine contents, colon, kidney and lung (Supplemental Figure 11A-E).

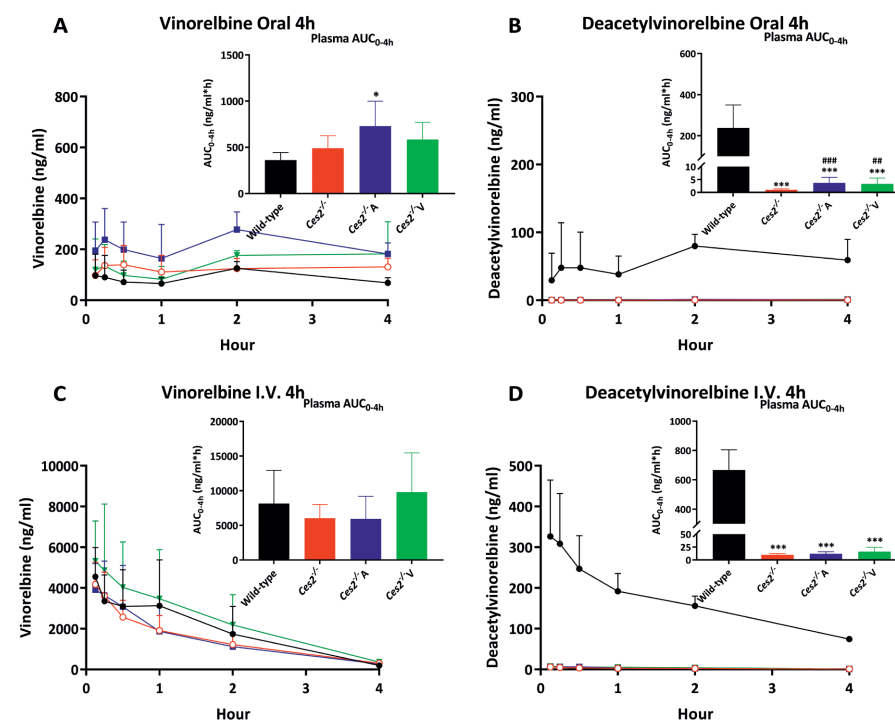


Figure 3. Vinorelbine plasma pharmacokinetic results in *CES2*-modified mouse models. Plasma concentration-time curves and AUC_{0-4h} of vinorelbine and its metabolite deacetylvinorelbine in male wild-type, *Ces2^{-/-}*, *Ces2^{-/-}A* and *Ces2^{-/-}V* mice over 4 h after oral administration (A and B) or intravenous injection (C and D) of 10 mg/kg vinorelbine. Data are given as mean \pm S.D. ($n = 6 - 7$). *, $P < 0.05$; **, $P < 0.01$; ***, $P < 0.001$ compared to wild-type mice; #, $P < 0.05$; ##, $P < 0.01$; ###, $P < 0.001$ compared to *Ces2^{-/-}* mice. ^, $P < 0.05$; ^^, $P < 0.01$; ^^, $P < 0.001$ for comparison between *Ces2^{-/-}A* and *Ces2^{-/-}V* mice. Statistical analysis was applied after log-transformation of linear data.

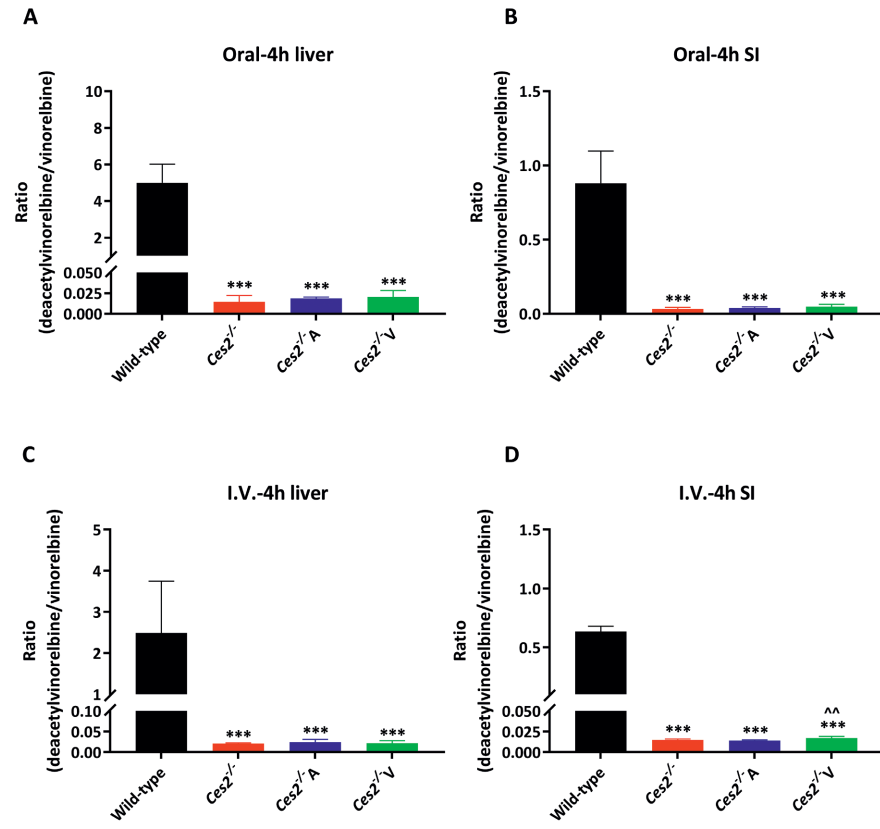


Figure 4. Vinorelbine conversion to deacetylvinorelbine in liver and small intestine. Deacetylvinorelbine-to-vinorelbine ratios in liver (A and C) and small intestine (B and D) after oral or i.v. administration, respectively, of 10 mg/kg vinorelbine. Data are given as mean \pm S.D. (n = 6 - 7). *, $P < 0.05$; **, $P < 0.01$; ***, $P < 0.001$ compared to wild-type mice; #, $P < 0.05$; ##, $P < 0.01$; ###, $P < 0.001$ compared to *Ces2*^{-/-} mice. ^, $P < 0.05$; ^^, $P < 0.01$; ^^, $P < 0.001$ for comparison between *Ces2*^{-/-}A and *Ces2*^{-/-}V mice. Statistical analysis was applied after log-transformation of linear data.

Table 1. Plasma pharmacokinetic parameters of vinorelbine and its active metabolite deacetylvinorelbine in male wild-type, *Ces2*^{-/-}, *Ces2*^{-/-}A and *Ces2*^{-/-}V mice over 4 h after oral administration or i.v. injection of 10 mg/kg vinorelbine.

| Vinorelbine Parameter | Oral administration | | | I.V. injection | | |
|---|---------------------|----------------------------|------------------------------|-----------------|----------------------------|------------------------------|
| | Wild-type | <i>Ces2</i> ^{-/-} | <i>Ces2</i> ^{-/-} A | Wild-type | <i>Ces2</i> ^{-/-} | <i>Ces2</i> ^{-/-} A |
| AUC _{0-4h} , ng/ml*h | 362 \pm 81 | 491 \pm 135 | 730 \pm 270* | 8143 \pm 4784 | 6043 \pm 1954 | 5949 \pm 3247 |
| C _{max} , ng/ml | 149 \pm 59 | 188 \pm 63 | 333 \pm 99**# | N.A. | N.A. | N.A. |
| T _{max} , h | 1.7 \pm 0.7 | 1.9 \pm 1.9 | 1.3 \pm 0.9 | N.A. | N.A. | N.A. |
| Deacetylvinorelbine Parameter | Oral administration | | | I.V. injection | | |
| | Wild-type | <i>Ces2</i> ^{-/-} | <i>Ces2</i> ^{-/-} A | Wild-type | <i>Ces2</i> ^{-/-} | <i>Ces2</i> ^{-/-} A |
| AUC _{0-4h} , ng/ml*h | 238 \pm 112 | 1.0 \pm 0.4*** | 3.7 \pm 2.2***### | 666 \pm 138 | 10.1 \pm 2.3*** | 12.0 \pm 3.8*** |
| AUC _{0-4h} ratio (x 10 ⁻³) (deacetylvinorelbine/vinorelbine) | 640 \pm 170 | 2.0 \pm 0.4 | 6.3 \pm 7.8***# | 110 \pm 60 | 1.7 \pm 0.2*** | 2.2 \pm 0.5*** |
| C _{max} , ng/ml | 91 \pm 44 | 0.42 \pm 0.15*** | 1.5 \pm 1.1***## | 346 \pm 104 | 5.9 \pm 1.4*** | 7.6 \pm 2.7*** |
| T _{max} , h | 1.7 \pm 0.7 | 3.7 \pm 0.8* | 2.6 \pm 1.0 | 0.46 \pm 0.76 | 0.13 \pm 0.00 | 0.25 \pm 0.19 |

Data are given as mean \pm S.D. (n = 6). AUC_{0-4h}, area under the plasma concentration-time curve; C_{max}, maximum concentration in plasma; T_{max}, time point (h) of maximum plasma concentration; N.A.: Not Applicable; *, $P < 0.05$; **, $P < 0.01$; ***, $P < 0.001$ compared to wild-type mice; #, $P < 0.05$; ##, $P < 0.01$; ###, $P < 0.001$ compared to *Ces2*^{-/-} mice; No statistical difference was found between *Ces2*^{-/-}A and *Ces2*^{-/-}V mice. Statistical analysis was applied after log-transformation of linear data and compared within either oral administration groups or i.v. injection groups.

Regarding the I.V. experiments, qualitatively similar results as for the oral administration were obtained. Even though the overall plasma exposure of i.v. vinorelbine was much higher, the plasma AUC_{0-4h} of deacetylvinorelbine was still highly decreased in *Ces2*^{-/-} mice (10.1 ± 2.3 ng/ml*h, 66-fold decrease), *Ces2*^{-/-}A mice (12.0 ± 3.8 ng/ml*h, 55.5-fold decrease) and *Ces2*^{-/-}V mice (16.2 ± 8.4 ng/ml*h, 41.1-fold decrease) compared to wild-type mice (666 ± 138 ng/ml*h) (Figure 3C-D and Table 1). With respect to tissues, the deficiency of *Ces2* drastically reduced the deacetylvinorelbine-to-vinorelbine ratio in liver from 2.5 ± 1.3 in wild-type mice to 0.021 ± 0.002 in *Ces2*^{-/-} mice, and human CES2 seemed not to alter the ratios much with 0.025 ± 0.0070 in *Ces2*^{-/-}A mice and 0.022 ± 0.007 in *Ces2*^{-/-}V mice. In small intestine, wild-type mice showed a somewhat lower conversion ratio (0.63 ± 0.05), and the ratio was decreased to 0.015 ± 0.001 in *Ces2*^{-/-} mice, 0.014 ± 0.001 in *Ces2*^{-/-}A mice and 0.017 ± 0.002 in *Ces2*^{-/-}V mice (Figure 4C-D and Supplemental Table 3). Similar profiles could be seen in kidney, lung, spleen, small intestine contents, and colon as well (Supplemental Figure 7-10 and Supplemental Figure 11F-J).

3.4 Mouse *Ces2* and human CES2 influence capecitabine metabolism in plasma and tissue distribution

Capecitabine, an oral anticancer prodrug, is biotransformed into active 5-fluorouracil (5-FU) in three steps, and carboxylesterases are believed to be involved in the first metabolism step from capecitabine to 5'-DFCR³⁹ (Supplemental Figure 12). *In vitro*, both human CES1 and CES2 can hydrolyze the carbamate bond in capecitabine to yield its first metabolite, 5'-DFCR, with roughly equal efficiency¹⁸. To study the impact of CES2 on capecitabine metabolism and disposition *in vivo*, 500 mg/kg capecitabine was orally administered to female wild-type, *Ces2*^{-/-}, *Ces2*^{-/-}A and *Ces2*^{-/-}V mice, and plasma and tissue concentrations of capecitabine and its four metabolite (5'-DFCR, 5'-DFUR, 5-FU and FBAL) were measured³⁰.

In plasma, we observed a 5.3-fold higher plasma AUC_{0-2h} of capecitabine in *Ces2*^{-/-} versus wild-type mice ($31,267 \pm 16,563$ vs $5,846 \pm 1,375$ ng*h/ml; $P < 0.001$), suggesting a marked role of mouse *Ces2* in limiting capecitabine levels (Figure 5A). The plasma AUC_{0-2h} of capecitabine in *Ces2*^{-/-}A mice ($31,533 \pm 19,150$ ng*h/ml) was similar to that in *Ces2*^{-/-} mice, whereas in *Ces2*^{-/-}V mice it was 1.8-fold reduced compared to *Ces2*^{-/-} mice ($17,535 \pm 9,707$ vs $31,267 \pm 16,563$ ng*h/ml) (Table 2), perhaps indicating an impact of the intestinal CES2, but still considerably higher than in wild-type mice. Somewhat surprisingly, the absolute values of the plasma AUC_{0-2h} for the first 3 metabolites (5'-DFCR, 5'-DFUR and 5-FU) were similar among these four strains, with only FBAL showing higher plasma exposure in *Ces2*^{-/-}A and *Ces2*^{-/-}V mice (Figure 5 and Table 2). Likely other esterases (possibly the abundant *Ces1* enzymes, with *Ces1c* prominent in plasma) still mediated extensive hydrolysis of capecitabine. Still, due to the differences in capecitabine plasma exposure (Figure 5A), the dynamic conversion from capecitabine to metabolites, as calculated by the metabolite-to-capecitabine ratios in plasma, was clearly impacted by mouse *Ces2* and human CES2 (data not shown).

Various tissues (liver, kidney, spleen, lung, SI, SIC and colon) were collected 2 h after drug administration and absolute drug concentrations and tissue-to-plasma ratios were analyzed. In liver, the absolute capecitabine concentration was 13.8-fold higher in *Ces2*^{-/-} mice than in wild-type mice ($P < 0.001$). Human CES2 could reduce this by 74.2% in *Ces2*^{-/-}A mice and by 63.5% in *Ces2*^{-/-}V mice compared with *Ces2*^{-/-} mice. The capecitabine liver-to-plasma ratios were also decreased due to the expression of hCES2 compared to *Ces2*^{-/-}, especially in *Ces2*^{-/-}A mice (Supplemental Figure 13A-B and Supplemental Table 4), indicating local hydrolysis of capecitabine by the hepatic transgenic hCES2. In small intestine, even though the absolute capecitabine concentration was again dramatically higher in *Ces2*^{-/-} mice than in wild-type mice (10.6-fold, $P < 0.001$), *Ces2*^{-/-}V mice profoundly reduced absolute capecitabine concentrations from $17,217 \pm 6,548$ ng/g to $2,411 \pm 1,191$ ng/g ($P < 0.001$) versus *Ces2*^{-/-} mice, thus reverting to the same magnitude as seen in wild-type mice. This suggests a strong function of the intestinal transgenic hCES2 in hydrolyzing capecitabine. In contrast, *Ces2*^{-/-}A mice still had a similar intestinal concentration as *Ces2*^{-/-} mice. Together with the similar trends in SI-to-plasma ratios, this indicates a clearly predominant impact of hCES2 on intestinal capecitabine metabolism in *Ces2*^{-/-}V but not in *Ces2*^{-/-}A mice (Supplemental Figure 13G-H and Supplemental Table 4). Similar results were further observed in kidney and colon (Supplemental Figure 13C-D and I-J and Supplemental Table 4). Notably, the reduced kidney-to-plasma ratios in transgenic mice were probably due to the renal expression of transgenic hCES2 as illustrated in Figure 2D. Spleen capecitabine concentration mainly reflected the plasma results, as the spleen-to-plasma ratio was not meaningfully altered. Again, for the 3 first metabolites (5'-DFCR, 5'-DFUR and 5-FU), the absolute tissue concentrations were similar among the strains in the collected organs (Supplemental Figure 14-16). The tissue 5'-DFCR-to-capecitabine ratios clearly reflected the tissue-specific activity of hCES2 in liver or intestine, respectively (Supplemental Figure 14C, F, I, L, O). FBAL showed somewhat higher tissue exposure in transgenic mice, especially *Ces2*^{-/-}A mice, but this entirely reflected the higher plasma levels as judged from the tissue-to-plasma ratios (Supplemental Figure 17).

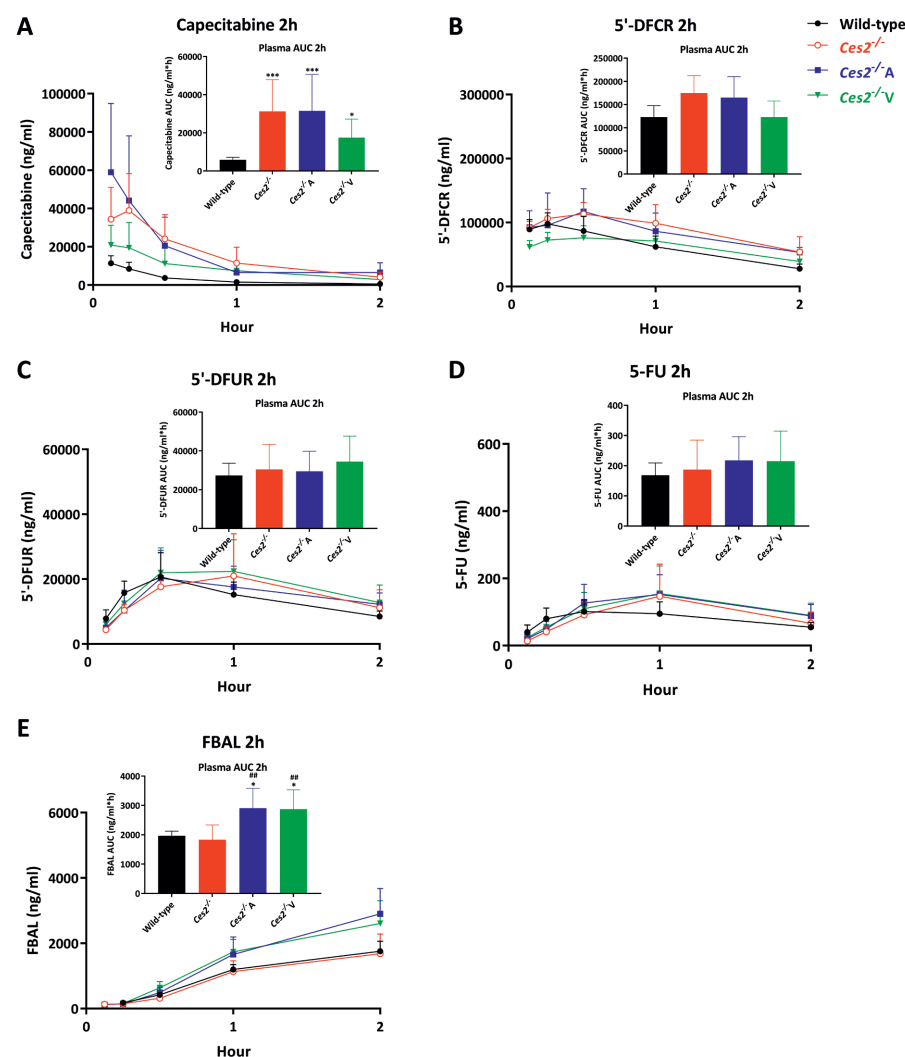


Figure 5. Capecitabine plasma pharmacokinetic results in CES2-modified mouse models. Plasma concentration-time curves and AUC_{0-2h} of capecitabine (A) and metabolites 5'-DFCR (B), 5'-DFUR (C), 5-FU (D) and FBAL (E) in female wild-type, *Ces2*^{-/-}, *Ces2*^{-/-A} and *Ces2*^{-/-V} mice over 2 h after oral administration of 500 mg/kg capecitabine. Data are given as mean \pm S.D. (n = 5 - 7). *, $P < 0.05$; **, $P < 0.01$; ***, $P < 0.001$ compared to wild-type mice; #, $P < 0.05$; ##, $P < 0.01$; ###, $P < 0.001$ compared to *Ces2*^{-/-} mice. No statistical differences were found between *Ces2*^{-/-A} and *Ces2*^{-/-V} mice. Statistical analysis was applied after log-transformation of linear data.

Table 2. Plasma pharmacokinetic parameters of capecitabine and its metabolites 5'-DFCR, 5'-DFUR, 5-FU and FBAL in female wild-type, *Ces2*^{-/-}, *Ces2*^{-/-A} and *Ces2*^{-/-V} mice over 2 h after oral administration of 500 mg/kg capecitabine.

| Capecitabine Parameter | Genotype/Groups | | | |
|---|--------------------|----------------------------|-----------------------------|-----------------------------|
| | Wild-type | <i>Ces2</i> ^{-/-} | <i>Ces2</i> ^{-/-A} | <i>Ces2</i> ^{-/-V} |
| AUC_{0-2h} , ng/ml*h | 5846 \pm 1375 | 31267 \pm 16563*** | 31533 \pm 19150*** | 17535 \pm 9707* |
| C_{max} , ng/ml | 12192 \pm 3796 | 42600 \pm 17764** | 47033 \pm 34131* | 23369 \pm 14079 |
| T_{max} , h | 0.19 \pm 0.07 | 0.21 \pm 0.06 | 0.17 \pm 0.07 | 0.16 \pm 0.06 |
| 5'-DFCR Parameter | Genotype/Groups | | | |
| | Wild-type | <i>Ces2</i> ^{-/-} | <i>Ces2</i> ^{-/-A} | <i>Ces2</i> ^{-/-V} |
| AUC_{0-2h} , ng/ml*h | 122720 \pm 24948 | 174979 \pm 37341 | 164965 \pm 45226 | 122870 \pm 34694 |
| AUC_{0-2h} ratio (5'-DFCR/capecitabine) | 21.3 \pm 3.5 | 6.4 \pm 1.9*** | 6.4 \pm 2.4*** | 8.0 \pm 2.2*** |
| C_{max} , ng/ml | 101350 \pm 18009 | 120557 \pm 23850 | 117133 \pm 35728 | 80014 \pm 18212# |
| T_{max} , h | 0.25 \pm 0.14 | 0.46 \pm 0.27 | 0.46 \pm 0.10 | 0.61 \pm 0.38 |
| 5'-DFUR Parameter | Genotype/Groups | | | |
| | Wild-type | <i>Ces2</i> ^{-/-} | <i>Ces2</i> ^{-/-A} | <i>Ces2</i> ^{-/-V} |
| AUC_{0-2h} , ng/ml*h | 27337 \pm 6291 | 30434 \pm 12950 | 29452 \pm 10370 | 34477 \pm 13143 |
| AUC_{0-2h} ratio (5'-DFUR/capecitabine) | 4.7 \pm 0.9 | 1.0 \pm 0.9*** | 1.1 \pm 0.3*** | 2.1 \pm 0.4***##^ |
| C_{max} , ng/ml | 21133 \pm 7207 | 22886 \pm 11936 | 21100 \pm 8366 | 23871 \pm 8673 |
| T_{max} , h | 0.42 \pm 0.13 | 0.64 \pm 0.24 | 0.58 \pm 0.20 | 0.79 \pm 0.27* |
| 5-FU Parameter | Genotype/Groups | | | |
| | Wild-type | <i>Ces2</i> ^{-/-} | <i>Ces2</i> ^{-/-A} | <i>Ces2</i> ^{-/-V} |
| AUC_{0-2h} , ng/ml*h | 168 \pm 41 | 187 \pm 98 | 218 \pm 79 | 215 \pm 100 |
| AUC_{0-2h} ratio ($\times 10^{-3}$) (5-FU/capecitabine) | 29 \pm 8.1 | 6.4 \pm 2.1*** | 8.0 \pm 2.7*** | 13 \pm 1.6***###^ |
| C_{max} , ng/ml | 105 \pm 36 | 147 \pm 96 | 159 \pm 56 | 156 \pm 81 |
| T_{max} , h | 0.50 \pm 0.27 | 0.93 \pm 0.19** | 0.92 \pm 0.20* | 0.86 \pm 0.24* |
| FBAL Parameter | Genotype/Groups | | | |
| | Wild-type | <i>Ces2</i> ^{-/-} | <i>Ces2</i> ^{-/-A} | <i>Ces2</i> ^{-/-V} |
| AUC_{0-2h} , ng/ml*h | 1966 \pm 158 | 1833 \pm 504 | 2910 \pm 671*## | 2874 \pm 659*## |
| AUC_{0-2h} ratio (FBAL/capecitabine) | 0.35 \pm 0.08 | 0.07 \pm 0.04*** | 0.12 \pm 0.06** | 0.20 \pm 0.09## |
| C_{max} , ng/ml | 1755 \pm 308 | 1684 \pm 597 | 2923 \pm 760*## | 2606 \pm 698# |
| T_{max} , h | 2.0 \pm 0.0 | 2.0 \pm 0.0 | 1.8 \pm 0.4 | 2.0 \pm 0.0 |

Data are given as mean \pm S.D. (n = 6). AUC_{0-2h} , area under plasma concentration-time curve; C_{max} , maximum concentration in plasma; T_{max} , time point (h) of maximum plasma concentration; *, $P < 0.05$; **, $P < 0.01$; ***, $P < 0.001$ compared to wild-type mice; #, $P < 0.05$; ##, $P < 0.01$; ###, $P < 0.001$ compared to *Ces2*^{-/-} mice; No statistical difference was found between *Ces2*^{-/-A} and *Ces2*^{-/-V} mice. Statistical analysis was applied after log-transformation of linear data.

3.5 Mouse *Ces2* and human CES2 affect body weight and white adipose tissue adipositis

A series of directed basic physiological studies was performed in the CES2-related gene-modified mouse strains (*Ces2*^{-/-}, *Ces2*^{-/-}A and *Ces2*^{-/-}V) and wild-type mice. Bodyweight was first monitored between 4 and 20 weeks of age for both female and male mice of all strains (n = 19-20 per gender per strain) fed a standard medium-fat diet. At the last time point (20 weeks old), all the mice were fasted overnight, sacrificed, and liver and gonadal white adipose tissue (gWAT) were collected and weighed in order to explore the potential bodyweight differences.

During the whole monitoring period, the body weight of *Ces2*^{-/-} mice showed no difference in either female or male mice compared with wild-type (Figure 6A - B). The absolute weights of liver and gWAT were also similar between wild-type and *Ces2*^{-/-} mice, reflecting the similar bodyweights. However, *Ces2*^{-/-}A mice (especially females) showed an average higher body weight than wild-type mice from 8 weeks on and *Ces2*^{-/-} mice from 11 weeks on, respectively, and these differences gradually increased further over time. *Ces2*^{-/-}A mice also displayed clearly higher weights of liver and gWAT. In contrast, *Ces2*^{-/-}V mice (especially females) always had an average lower body weight than the wild-type and *Ces2*^{-/-} mice, even starting from 4 weeks of age. After 10 weeks of age, these differences became more significant and clear (Figure 6A - B).

The *Ces2*^{-/-}V mice had significantly lower gWAT weights than *Ces2*^{-/-} mice in both genders (Supplemental Figure 18C). After correction for the bodyweights, gWAT-to-bodyweight ratio changes were much more pronounced than liver-to-bodyweight ratios, with *Ces2*^{-/-}A showing higher gWAT-to-bodyweight ratios (in female mice). In contrast, these ratios were significantly decreased in *Ces2*^{-/-}V mice compared to *Ces2*^{-/-} mice (Supplemental Figure 18E). This may indicate that the bodyweight differences were mainly due to changes in the adipose tissues (Supplemental Figure 18). Female and male aging mice (n = 3 - 6, each gender each strain) around 60 weeks old were also sacrificed and bodyweight and organ weights measured. The results were similar to those for the 20-week old mice, especially in females (data not shown).

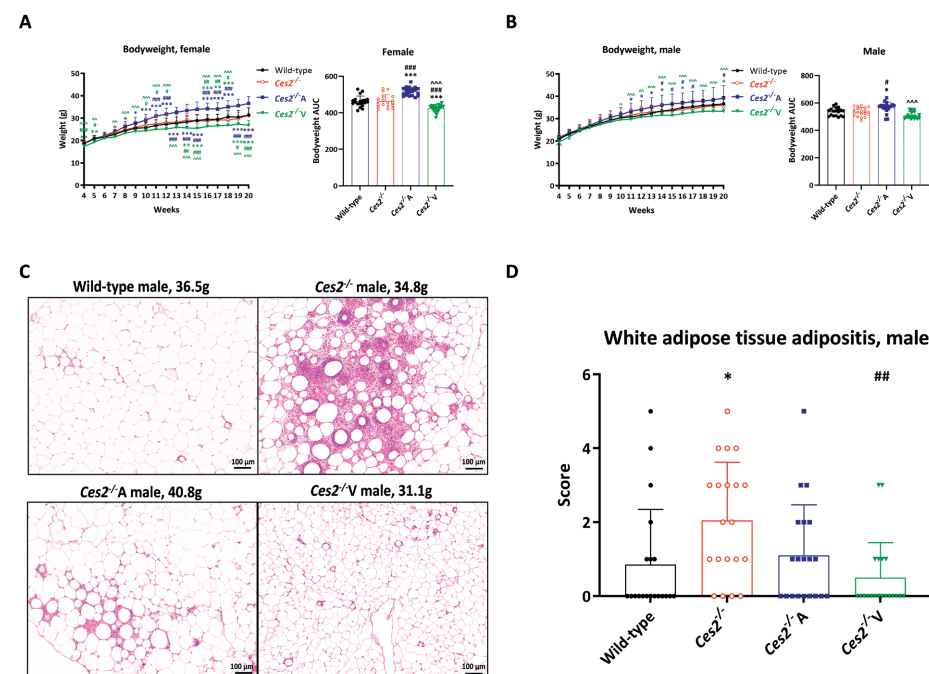


Figure 6. Basic physiological analysis of the *CES2* mouse models. Bodyweight development from 4 to 20 weeks of age for females (A) and males (B); Representative images of gonadal white adipose tissue of male mice from each mouse strain (C) and semi-quantified white adipose tissue adipositis levels (D) of 20-week old female and male wild-type, *Ces2*^{-/-}, *Ces2*^{-/-}A and *Ces2*^{-/-}V mice after bodyweight measurement from 4 weeks to 20 weeks of age. Data are given as mean \pm S.D. (n = 19 - 20). *, $P < 0.05$; **, $P < 0.01$; ***, $P < 0.001$ compared to wild-type mice; #, $P < 0.05$; ##, $P < 0.01$; ###, $P < 0.001$ compared to *Ces2*^{-/-} mice. ^, $P < 0.05$; ^^, $P < 0.01$; ^^, $P < 0.001$ for comparison between *Ces2*^{-/-}A and *Ces2*^{-/-}V mice. Statistical analysis was applied after log-transformation of linear data. For panel D, the Kruskal-Wallis rank test was used.

In order to better understand the reasons for the bodyweight differences, young adult mice between 12 and 13 weeks old (n = 9 - 16 for each gender and strain) were sacrificed and dissected. Bodyweights and different organ weights, including liver, kidney, spleen, lung, heart and different adipose tissue weights, including inguinal, perigonadal, mesenteric and retroperitoneal white adipose tissue (iWAT, gWAT, mWAT, and rWAT) and interscapular brown adipose tissue (iBAT) were measured (Supplemental Figure 19). The bodyweights were consistent with our earlier bodyweight monitoring results, showing no difference between wild-type and *Ces2*^{-/-} mice, both with respect to absolute organ and WAT weights and relevant ratios corrected by bodyweight. *Ces2*^{-/-}A mice had higher bodyweights than wild-type and *Ces2*^{-/-} mice, and this difference was also reflected in the organ and WAT weights. Further, after correction for the bodyweight, *Ces2*^{-/-}A male mice had slightly but significantly higher liver-to-body weight ratios and spleen-to-body weight ratios compared to wild-type and *Ces2*^{-/-} mice, respectively. *Ces2*^{-/-}A female mice did have

higher ratios for gWAT, mWAT and rWAT (albeit not statistically significant). In contrast, *Ces2^{-/-V}* mice were similar to, or slightly lighter than, *Ces2^{-/-}* mice, but overall less pronounced than at 20 weeks of age. The differences in absolute organ and WAT weights mostly corresponded to the bodyweight differences. *Ces2^{-/-V}* only showed a significantly lower ratio in mWAT compared to *Ces2^{-/-}* mice in females. No other differences were observed in organ or WAT-to-body weight ratios. Thus, in young-adult mice, the bodyweight differences were mainly due to a combination of both organ and white adipose tissue absolute weights, although WAT tissues may have contributed more, especially in females (Supplemental Figure 19).

A whole-body histology/pathology examination was performed for 20-week old mice and aging mice. For 20-week old mice, even though female mice showed clear and pronounced bodyweight differences between the strains, there were no marked abnormalities. However, we found a more severe gonadal white adipose tissue (gWAT) inflammation (adipositis) in *Ces2^{-/-}* male mice, and hCES2 could somewhat rescue this phenotype in both *Ces2^{-/-A}* and *Ces2^{-/-V}* mouse strains (for representative pictures see Figure 6C). After semi-quantification of the adipositis (Figure 6D), the results revealed that the deficiency of mouse *Ces2* resulted in a significantly higher adipositis compared with wild-type mice, and hepatocyte-specific expression of hCES2 could alleviate this back to a similar level as seen in wild-type mice, although the down-shift itself was not statistically significant. However, enterocyte-specific expression of hCES2 could profoundly rescue the adipositis, with an even lower average semi-quantification score than for wild-type male mice (Figure 6D). In contrast, no significant adipositis was observed in gWAT of females in any of the strains (data not shown), in spite of the significant changes in gWAT mass. A general histology/pathology examination was also applied in ~60-week old aging mice, but except for some basic geriatric disease phenotypes (like focal necrotizing hepatitis), no particular pathology was observed, whereas all strains at this age showed similar levels of mild to severe adipositis (data not shown).

3.6 Mouse *Ces2* and human CES2 alter plasma lipid concentrations

Plasma clinical chemistry and haematological examination were also applied for all the 20-weeks old mice. Remarkably, the total plasma cholesterol concentrations were significantly higher in *Ces2^{-/-}* mice than in wild-type mice, especially in female (Supplemental Figure 20L). A similar profile also showed up for plasma HDL cholesterol (the predominant form in mice) and LDL cholesterol. The plasma triglyceride levels were not significantly altered between *Ces2^{-/-}* and wild-type mice, nor any of the other parameters we analyzed (Supplemental Figure 20), indicating that deficiency of the mouse *Ces2* cluster may only affect plasma cholesterol exposure. Hepatic transgenic hCES2 could reduce the total plasma cholesterol level as well as HDL cholesterol level to some extent, especially in females. However, intestinal transgenic hCES2 had a much more pronounced effect in limiting cholesterol exposure, with clear decreases in total cholesterol, HDL cholesterol and LDL cholesterol compared to *Ces2^{-/-}* mice, especially in females. The reduced

values in either each or both of two transgenic mouse strains were also observed in a few other plasma parameters, such as triglyceride and alkaline phosphatase (ALP), alanine transaminase (ALAT) and glucose in males (Supplemental Figure 20). Although the differences were all small, the shifts always went into a relatively “healthy” direction. This may indicate that the two transgenic mouse strains had slightly “healthier” liver and circulation conditions than *Ces2^{-/-}* mice.

With respect to hematology, significantly lower mean corpuscular volume (MCV) and mean corpuscular hemoglobin (MCH) were observed in *Ces2^{-/-}* mice, and transgenic hCES2 could increase these values in both *Ces2^{-/-A}* and *Ces2^{-/-V}* mice. In contrast, the deficiency of mouse *Ces2* lead to higher red cell distribution width (RDW), and the presence of hCES2 somewhat reversed the situation (Supplemental Figure 21). Considering that the changes are limited, and all of these parameters are still within a normal physiological range, these differences are probably not pathologically meaningful. The basic plasma clinical chemistry and hematologic analyses for aging mice did not show any meaningful differences among the mouse strains (data not shown).

3.7 hCES2 protects mice from liver lipid accumulation without influencing triglyceride secretion from liver to blood

Oil-Red-O staining of the liver was performed and analyzed semi-quantitatively to assess neutral lipid content. Staining in female mice was quite high and not significantly altered due to deficiency of *Ces2*. However, this lipid accumulation was somewhat reduced by enterocyte but not hepatocyte expression of hCES2 (Supplemental Figure 22A-B). In contrast, absence of mouse *Ces2* in male mice profoundly increased hepatic lipid levels, and hCES2 significantly reduced these to a similar level as in wild-type mice, especially in *Ces2^{-/-A}* male mice (Figure 7A-B). The liver lipid was isolated and concentration was measured in both female and male mice. As with the Oil-Red-O staining, the liver lipid contents were not significantly altered in female strains (Supplemental Figure 22C). However, in male mice, lipid concentration was increased due to m*Ces2* absence (albeit not statistically significant because of high variation), whereas both hepatic and especially intestinal hCES2 expression reduced the liver lipid content back to wild-type levels (Figure 7C).

Considering that there were also plasma triglyceride concentration differences (increased in *Ces2^{-/-}* and then decreased especially in *Ces2^{-/-V}* mice), especially in males (Figure 7D), but also in females (Supplemental Figure 22D), we further explored whether there was altered triglyceride secretion from liver in the mouse models. We studied hepatic triglyceride production after inhibiting lipases by injecting poloxamer-407. However, we did not detect any significant differences among the mouse strains in either female or male mice at any time point (Figure 7E and Supplemental Figure 22E), also when we normalized the results (by subtraction of basal plasma triglyceride levels; Supplemental Figure 23A-B). We next explored whether lipid uptake and/or chylomicron clearance were altered in the various CES2 mouse strains. For this an oral

lipid tolerance test (oLTT) was performed in both female and male mice (n = 9 - 11). Mice were challenged with an olive oil gavage, and plasma triglyceride concentrations were measured hourly up to 4 hours after the gavage. *Ces2*^{-/-} mice had slightly higher plasma triglyceride concentrations during the experiments (0 - 4 h) compared to wild-type mice. Surprisingly, hepatocyte expression of hCES2 even further increased these values. In contrast, enterocyte expression of hCES2 could decrease plasma triglycerides (Figure 7F and Supplemental Figure 22F). Such phenotypes were further supported by the plasma triglyceride AUC_{0-4h} and were more obvious in male mice. However, normalization of the results by subtracting the baseline triglyceride concentrations revealed that *Ces2*^{-/-} mice had a similar absolute triglyceride absorption level as wild-type mice, and only hepatic hCES2 but not intestinal hCES2 could slightly increase this absorption, especially in male mice (Supplemental Figure 23C-D).

Of note, as the mice for the hepatic triglyceride production and oral lipid tolerance tests were all of the same age (~12-weeks old) and had undergone an overnight fast, we pooled the data and plotted the basal plasma triglyceride concentrations. The results show that mCes2 deficiency led to increased plasma triglyceride levels and hCES2 expression could decrease this in male mice, especially in the *Ces2*^{-/V} mouse strain (Figure 7D). Again, female mice showed a similar basal plasma triglyceride level profile among the mouse strains as the male mice, albeit less pronounced (Supplemental Figure 22D).

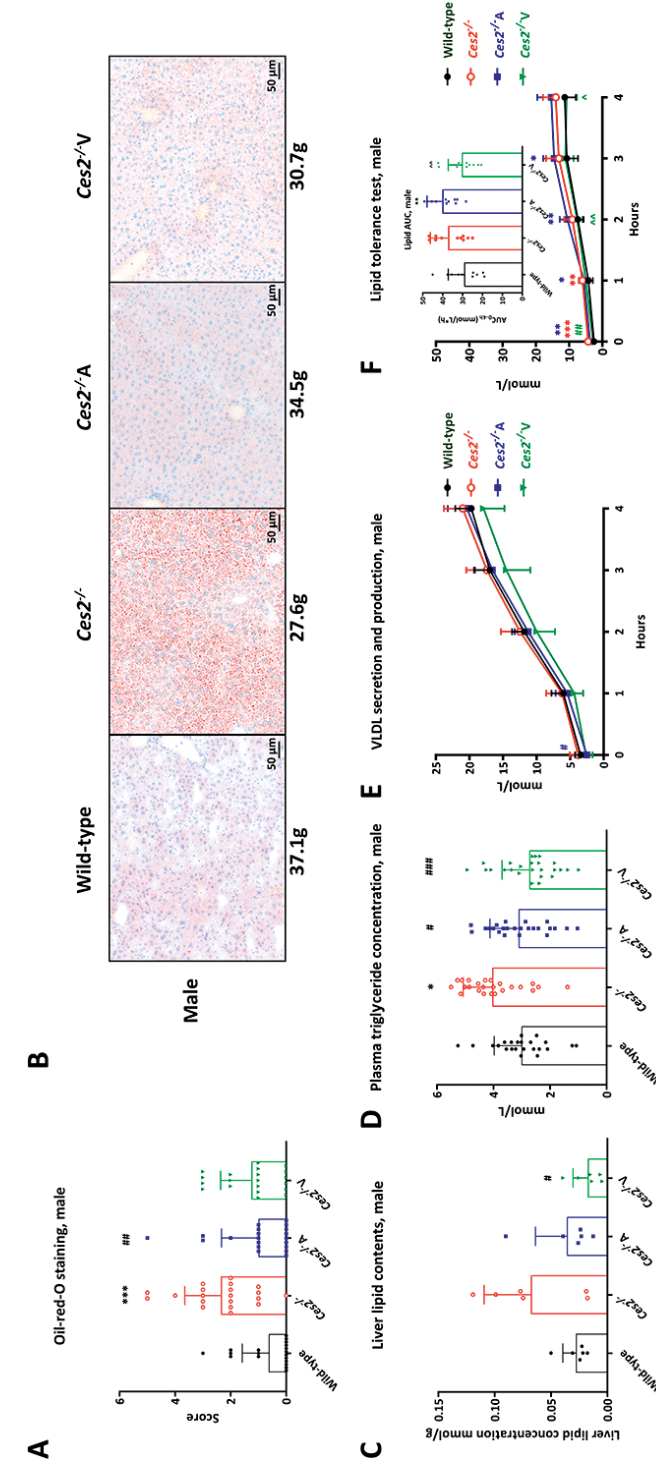


Figure 7. Lipid disposition, metabolism and homeostasis in the CES2 mouse models. Semi-quantified Oil-red-O staining lipid droplet levels (A) and representative Oil-red-O staining images for liver lipid accumulation for each mouse strain (B) in male wild-type, *Ces2*^{-/-}, *Ces2*^{-/-A} and *Ces2*^{-/V} 20-week old mice (n = 19 - 21; bodyweight of each individual mouse presented is indicated); Liver lipid contents in male wild-type, *Ces2*^{-/-}, *Ces2*^{-/-A} and *Ces2*^{-/V} 20-week old mice (n = 8) (C); Plasma triglyceride basal concentration (overnight fast) before VLDL production and secretion and oral lipid tolerance test in male wild-type, *Ces2*^{-/-}, *Ces2*^{-/-A} and *Ces2*^{-/V} 12-week old mice (n = 20 - 24) (D); VLDL production and secretion (E) and oral lipid tolerance test (F) in male wild-type, *Ces2*^{-/-}, *Ces2*^{-/-A} and *Ces2*^{-/V} 12-week old mice (n = 10 - 12). Data are given as mean \pm S.D. * $P < 0.05$, ** $P < 0.01$, *** $P < 0.001$ compared to wild-type mice; # $P < 0.05$; ## $P < 0.01$; ### $P < 0.001$ compared to *Ces2*^{-/-} mice; ° $P < 0.05$; °° $P < 0.01$; °°° $P < 0.001$ for comparison between *Ces2*^{-/-A} and *Ces2*^{-/V} mice. Statistical analysis was applied after log-transformation of linear data. For panel A, the Kruskal-Wallis rank test was used.

3.8 hCES2 improves glucose tolerance and insulin sensitivity

As CES2 expression induced changes in lipid metabolism, we also investigated the potential influence of CES2 on glucose homeostasis. We therefore performed both oral glucose tolerance tests and insulin tolerance tests. *Ces2*^{-/-} female mice showed marginally higher blood glucose levels in the glucose tolerance test than wild-type mice, but the blood glucose levels were reduced by hCES2 with even lower values than wild-type control before 1 h, especially in *Ces2*^{ΔV} female mice (Supplemental Figure 24A-C). The differences were more pronounced in male mice, where both hCES2 transgenic mouse strains, but especially the *Ces2*^{ΔV}, could decrease the plasma glucose levels compared to *Ces2*^{-/-} mice during the whole experimental period. These observations were further confirmed by the AUC data (Figure 8A-C).

In the insulin tolerance test, the responses to insulin challenge were relatively more sensitive in female mice. In both genders, *Ces2*^{-/-} mice displayed clearly higher glucose concentrations than wild-type mice. Hepatocyte expression of hCES2 significantly decreased glucose levels after insulin injection in both genders, while enterocyte expression of hCES2 had even more impact on this, but primarily in female mice (Figure 8D and Supplemental Figure 24D). The ratio of glucose concentration at each time point to the basal glucose level (T = 0) and AUC results also confirmed the differences (Figure 8E-F and Supplemental Figure 24E-F). Taken together, in our studies, under a medium-fat diet, the mouse *Ces2* and human CES2 enzymes can improve glucose tolerance and insulin sensitivity.

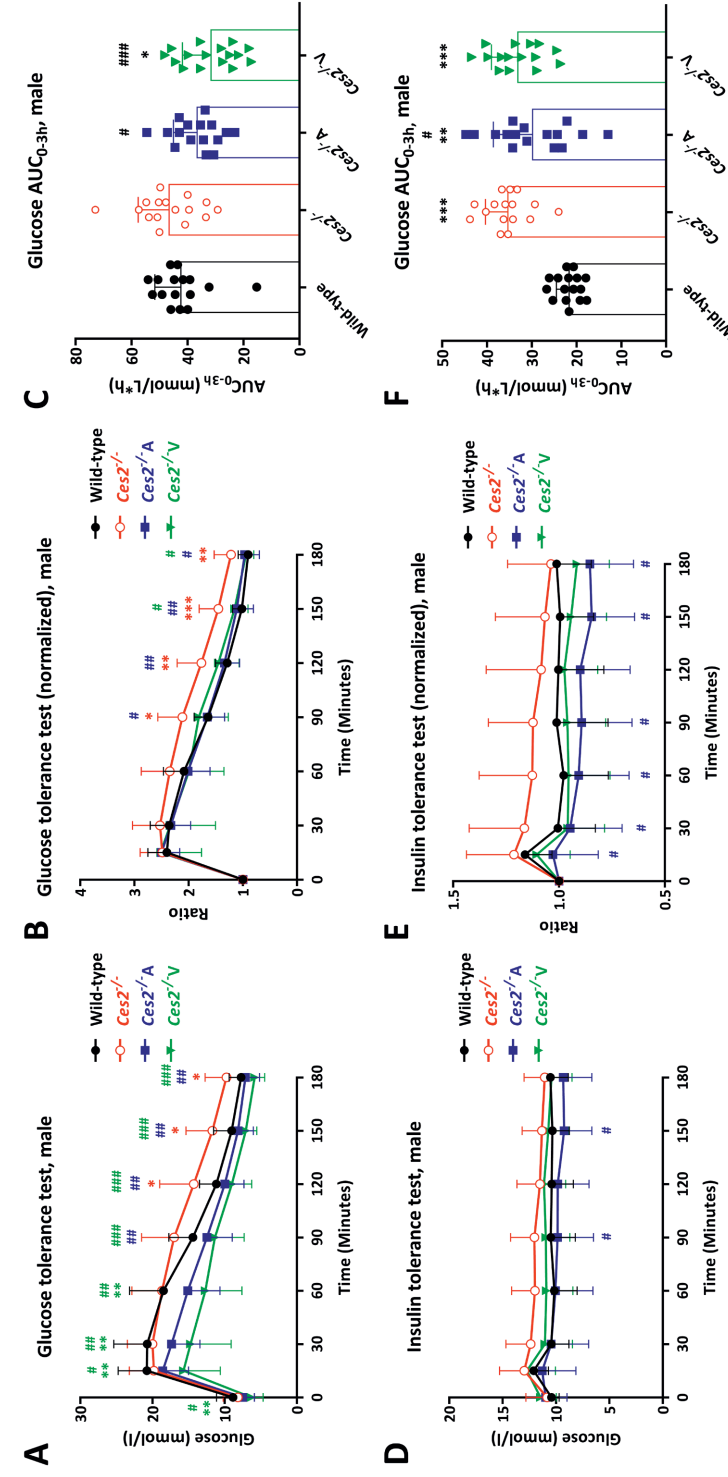


Figure 8. Glucose metabolism and homeostasis in the CES2 mouse models. The plasma glucose concentration time curve (A), plasma glucose concentration to basal glucose concentration (before glucose administration) ratio time curve (B) and glucose AUC_{0-3h} (C) in male wild-type, *Ces2*^{-/-}, *Ces2*^{ΔA} and *Ces2*^{ΔV} 12-week old mice over a 3 h glucose tolerance test after oral administration of 1 mg/g glucose; The plasma glucose concentration time curve (D), plasma glucose concentration to basal glucose concentration (before insulin injection) ratio time curve (E) and glucose AUC_{0-3h} (F) in male wild-type, *Ces2*^{-/-}, *Ces2*^{ΔA} and *Ces2*^{ΔV} 16-week old mice over a 3-h insulin tolerance test after i.p. injection of 0.5 U/kg insulin. Data are given as mean ± S.D. (n = 15 - 16). *, P < 0.05; **, P < 0.01; ***, P < 0.001 compared to wild-type mice; #, P < 0.05; ##, P < 0.01; ###, P < 0.001 compared to *Ces2*^{-/-} mice. ^, P < 0.05; ^^, P < 0.01; ^^, P < 0.001 for comparison between *Ces2*^{ΔA} and *Ces2*^{ΔV} mice. Statistical analysis was applied after log-transformation of linear data.

4. DISCUSSION

For several years, the key roles of CES, especially CES1 and CES2, in both endogenous and xenobiotic metabolism have garnered great interest in the discovery of CES modulators in order to regulate lipid metabolism or to optimize the activity of ester drugs^{1,4,19,40-44}. Lehner and co-workers studied the physiological functions of mouse *Ces1* by, amongst others, generating and analyzing single *Ces1d* or *Ces1g* knockout mouse strains⁴⁵⁻⁴⁹. Compared to CES1, CES2 physiological function research is still limited. Recently, several papers focused on mouse *Ces2c* and human CES2 functions in metabolic syndrome by knockdown of the *Ces2c* gene and/or overexpression of human CES2 using adenoviral vectors²³⁻²⁵. Until now, to the best of our knowledge, there is no full *Ces2* family knockout mouse model described, nor stable human CES2 transgenic mouse models either in liver or intestine in a complete mouse *Ces2*-deficient background. In this study, we generated and characterized a *Ces2* cluster knockout mouse model (*Ces2*^{-/-}), in which all eight *Ces2* genes are deficient, as well as two humanized CES2 transgenic (either hepatic or intestinal) strains in the mouse *Ces2* knockout background. All the obtained mouse strains were viable and fertile with normal appearance and behavior, and did not display marked abnormalities.

Using these CES2 related mouse models, we found that mouse *Ces2* enzymes markedly contributed to the conversion of vinorelbine to deacetylvinorelbine, affecting both plasma exposure and tissue distribution. Of note, even though there are still abundant mouse *Ces1* enzymes present in *Ces2*^{-/-} mice, including a high amount of *Ces1c* in blood, the deacetylvinorelbine generation was extremely low when *Ces2* was absent. This indicates that the conversion of vinorelbine to deacetylvinorelbine was primarily mediated by one or more of the mouse *Ces2* enzymes, but not *Ces1*, nor other esterases. However, somewhat unexpectedly, human CES2 had only a very limited impact on vinorelbine metabolism in mice. It is worth mentioning that when 80 mg/m² vinorelbine was orally administered in 24 patients, the plasma C_{max} of vinorelbine and deacetylvinorelbine were 133.4 ± 42.3 ng/ml and 9.1 ± 3.3, respectively³⁸. These results indicate an absolute exposure of vinorelbine and its metabolite deacetylvinorelbine that was still of a similar order of magnitude with that observed in our transgenic mice (Table 1). All in all, the vinorelbine results in our mouse models suggest that vinorelbine is a highly specific substrate of mouse *Ces2*, but less so of human CES2. In a previous study, we found that *in vitro* plasma incubation results showed a positive correlation between vinorelbine metabolism and *Ces2a* expression, suggesting that *Ces2a* probably is present to some extent in the blood, even though it contains an HXEL ER retention signal. Considering that there is no CES2 detected in human blood, the potentially secreted mouse *Ces2* may mediate more efficient vinorelbine metabolism directly in the blood than human CES2, which is always retained in tissues. On the other hand, CES2 is often expressed in both liver and intestine in human, which may induce more extensive hydrolysis effects than those in our single transgenic mouse models.

The present study further demonstrates that mouse *Ces2* can markedly limit the oral availability of capecitabine, whereas enterocyte human CES2, but not hepatocyte human CES2, can also substantially decrease capecitabine plasma exposure. This suggests that hCES2 plays an important role in the first-pass intestinal metabolism of capecitabine. However, neither mouse *Ces2* nor human CES2 activity could markedly influence levels of the further metabolites of capecitabine, including 5-FU. The plasma concentrations of 5'-DFCR, the first hydrolysis product of capecitabine, were considerably higher than those of capecitabine in all strains (Figure 5B), and the 5'-DFCR concentrations were not significantly different between the strains. It therefore seems most likely that other esterases (likely including *Ces1* enzymes) still catalyze very substantial formation of 5'-DFCR, converting most available capecitabine in plasma (perhaps 70-80% or more, given the plasma 5'-DFCR/capecitabine ratios we observed). However, *Ces2* can efficiently convert most of the remaining capecitabine, so deletion of *Ces2* still results in a marked increase in plasma capecitabine concentrations. Because in this interpretation the impact of *Ces2* on the total amount of 5'-DFCR formed is relatively limited, the levels of 5'-DFCR and hence further metabolites are not significantly affected by the absence of *Ces2*.

The different tissue capecitabine exposure profiles between the hepatocyte- and enterocyte-specific hCES2 expression mouse strains suggest specific local effects of hCES2 in capecitabine hydrolysis, in for instance liver, kidney, and small intestine. This is especially apparent from the 5'-DFCR/capecitabine ratios (Supplemental Figure 14). The significantly increased intestine 5'-DFCR/capecitabine ratios in *Ces2*^{-/V} mice suggest that enterocyte hCES2, but not hepatocyte hCES2, directly affects the first-pass metabolism of oral capecitabine and subsequently the exposure of other tissues. This may also apply for other esterase-sensitive drugs (or pro-drugs), potentially further inducing local toxicity in tissues (such as chemotherapy-induced diarrhea) or efficacy in solid tumors. In general, our capecitabine results demonstrate a clear role of CES2 in initial hydrolysis of capecitabine, but also suggest that this has only a very limited impact on formation and exposure of the active compound 5-FU, presumably because of the activity of alternative esterases. Of note, in several clinical pharmacokinetic studies with single oral doses of capecitabine (1250 to 1255 mg/m² or 2000 mg), the mean C_{max} of 5-FU was in the range of 218 ng/ml to 310 ng/ml⁵⁰. In our mouse models, the mean C_{max} of 5-FU was of the same order of magnitude, from 105 ng/ml to 159 ng/ml, at a dose of 500 mg/kg (Table 2).

Dietary lipids, including triglycerides and cholesterol, are mainly taken up by enterocytes from the small intestine and packaged into chylomicrons, which are subsequently secreted into the lymph stream, and then metabolized by lipoprotein lipase (LPL), releasing free fatty acids in the circulation. The remaining compounds are used in the formation of LDL and HDL, and then distributed in the various tissues, including liver. In the liver, free fatty acids are assembled, accumulated, re-esterified to glycerides and stored in lipid droplets (LDs). When secreted (again) into the circulation, this occurs mainly in the form of VLDL particles⁵¹⁻⁵⁴. As has emerged from

studies over the past years, carboxylesterases hydrolyze many lipids including triglycerides and cholesterol esters, thus affecting lipid homeostasis, atherosclerosis and inflammation, obesity, and type 2 diabetes (i.e., metabolic syndrome)^{23-25,45-49,55,56}. However, so far physiological studies on CES2 were not as substantial as those on CES1, and the lack of stable knockout and humanized transgenic mouse strains may also restrict such studies. We therefore applied a number of physiological studies in our CES2 modified mouse strains.

Upon 20 weeks regular monitoring, absence of mouse *Ces2* did not affect body weight development, in line with some other recent studies^{23,24}. However, the deficiency of mouse *Ces2*, especially hepatic *Ces2* loss, may increase local lipid accumulation in the liver. Probably related to this, the disruption of lipid homeostasis in liver may further induce remote white adipose tissue adipositis⁵⁷. A more detailed histology and plasma analysis revealed that the deficiency of mouse *Ces2* increased plasma cholesterol in both genders without changing plasma triglyceride levels. Somewhat contradictory, even though *Ces2* has no apparent direct influence on oral lipid absorption and hepatic lipid secretion, relatively higher basal plasma triglyceride concentrations in the VLDL and oLTT experiments were observed in *Ces2*^{-/-} male mice (Figure 7D). The reason behind this discrepancy is still not clear, but it suggests that *Ces2* may, at least partly, influence the triglyceride levels in circulation system in our mouse models.

Compromised lipid homeostasis may induce glucose dysregulation and insulin resistance⁵⁸. Indeed, *Ces2*^{-/-} mice showed slightly higher glucose exposure compared to wild-type mice in both GTT and ITT tests. Even though all our analyses were performed under medium-fat diet conditions, our results appear to be partly in line with a recent study, which revealed that knockdown of hepatic *Ces2c* had no effect on plasma triglyceride or cholesterol levels but increased hepatic triglyceride levels without affecting VLDL secretion²³. The higher plasma triglyceride and cholesterol levels in the *Ces2*^{-/-} mice observed in our study may be due to the multiple gene (the whole *Ces2* cluster) knockout effects or perhaps a strain difference (FVB background in our study and C57BL/6 background in the above-mentioned study²³).

Surprisingly, *Ces2*^{-/-}A mice showed relatively higher bodyweights compared to both wild-type and *Ces2*^{-/-} mice. Moreover, the hepatic human CES2 could slightly decrease both plasma triglyceride and cholesterol concentrations in both genders, and alleviated WAT adipositis and liver lipid over-accumulation to some extent in males compared to *Ces2*^{-/-} mice. In addition, hepatocyte hCES2 did not alter VLDL production but could further slightly (albeit not significantly) increase triglyceride exposure after oral lipid administration, especially in male mice (Supplemental Figure 23C-D). This may be in part because of the higher bodyweight of *Ces2*^{-/-}A mice, with more lipid administered due to the dosing regimen (10 µl/g). Of note, like in the plasma clinical chemistry analysis, hepatic human CES2 reduced the basal plasma triglyceride concentrations (as observed in the VLDL and oLTT experiments) compared to *Ces2*^{-/-} mice in males (Figure 7D).

Our data are again partly consistent with the above-mentioned study²³, which demonstrated that hepatic overexpression of human CES2 in HFD-fed mice (C57BL/6 background) had no effect on plasma triglyceride or cholesterol levels, but reduced hepatic triglyceride levels and improved glucose tolerance. It appears that the gain of hepatic CES2 function attenuates hepatic triglyceride accumulation, likely through both enhancing fatty acid oxidation and inhibition of lipogenesis, by reducing SREBP-1c transcription and processing²³. Another study revealed that hepatic expression of human CES2 (in otherwise C57BL/6J wild-type mice) enhanced TAG/DAG hydrolysis activity, reversed high-fat feeding-induced hepatic steatosis, reduced hepatic TAGs and decreased plasma cholesterol levels without affecting the mouse body weight²⁴. Despite activation of ER stress, as well as of the downstream effector proteins IKK and JNK, CES2 may promote Akt activation independently or IRS2-related, which further improves glucose tolerance²⁴. Consistent with this mechanism, improved glucose tolerance in *Ces2*^{-/-}A mice was also observed in our study. In general, it appears that hepatocyte hCES2 can directly ameliorate lipid homeostasis in the liver, as well as WAT adipositis. Furthermore, even though the potential mechanisms are unclear, it seems that hepatocyte hCES2 can enhance triglyceride clearance from the circulation, probably by increasing adipose tissue storage in a healthy condition, which induces a relatively heavier body weight in our study.

Interestingly, enterocyte-expressed human CES2 showed even more pronounced effects. It not only decreased the bodyweights, but also considerably reduced the plasma cholesterol levels, especially in females, and profoundly ameliorated WAT inflammation and liver lipid contents. Even though enterocyte hCES2 did not influence the overall lipid absorption and liver VLDL production, it could still markedly decrease the basal plasma triglyceride concentrations compared with *Ces2*^{-/-} mice. Similarly, a recent study indicated that after long-term high-fat diet feeding²⁵, transduced m*Ces2c* (considered an ortholog of hCES2) specifically in intestine also yielded a clear decrease in bodyweight, while reducing plasma cholesterol levels, and protecting mice from liver steatosis compared to wild-type mice. Just as seen with our results, the hepatic VLDL secretion, dietary fat absorption and chylomicron secretion rates were not altered in adenovirus-mediated *Ces2c* enterocyte overexpression or knockdown mice. However, postprandial triglyceride clearance was enhanced in *Ces2c* enterocyte overexpression mice. This could be related to increased chylomicron particle size and more lipid shuttling into skeletal muscle (mRNA expression of genes involved in fatty acid oxidation was increased in skeletal muscle but reduced in the liver of *Ces2c* enterocyte overexpression mice), thereby lowering lipid flux and triglyceride accumulation in the liver²⁵. Considering all the obtained lipid research results, our results suggest that enterocyte hCES2 may enhance the triglyceride clearance from circulation to muscle, and thus decrease hepatic triglyceride accumulation and alleviate the white adipose tissue inflammation. The improved lipid homeostasis may subsequently improve glucose tolerance and insulin resistance, which was observed in both our study and the above-mentioned study²⁵.

In summary, we have generated and characterized full mouse *Ces2* cluster deletion mice, and two humanized CES2 transgenic mouse strains with expression either in liver or intestine. The results show that our CES2 genetically engineered mouse models provide powerful pre-clinical tools to study pharmacological and physiological roles of the carboxylesterase 2 family. These mouse models are expected to facilitate development of several (pro-)drug classes and to improve drug administration regimens. In addition, using these models, a better understanding of CES2 involvement in energy metabolism processes and thus deeper physiological insights can be obtained. This could help us to further explore potential solutions for the metabolic syndrome problem.

REFERENCE

1. Wang, D., *et al.* Human carboxylesterases: a comprehensive review. *Acta Pharmaceutica Sinica B* **8**, 699-712 (2018).
2. Sanghani, S.P., Sanghani, P.C., Schiel, M.A. & Bosron, W.F. Human carboxylesterases: an update on CES1, CES2 and CES3. *Protein & Peptide Letters* **16**, 1207-1214 (2009).
3. Satoh, T. & Hosokawa, M. The mammalian carboxylesterases: from molecules to functions. *Annual Review of Pharmacology and Toxicology* **38**, 257-288 (1998).
4. Yoshida, T., *et al.* Difference in substrate specificity of carboxylesterase and arylacetamide deacetylase between dogs and humans. *European Journal of Pharmaceutical Sciences* **111**, 167-176 (2018).
5. Casey Laizure, S., Herring, V., Hu, Z., Witbrodt, K. & Parker, R.B. The Role of Human Carboxylesterases in Drug Metabolism: Have We Overlooked Their Importance? *Pharmacotherapy* **33**, 210-222 (2013).
6. Staudinger, J.L., Xu, C., Cui, Y.J. & Klaassen, C.D. Nuclear receptor-mediated regulation of carboxylesterase expression and activity. *Expert Opinion on Drug Metabolism & Toxicology* **6**, 261-271 (2010).
7. Imai, T. Human carboxylesterase isozymes: catalytic properties and rational drug design. *Drug Metabolism and Pharmacokinetics* **21**, 173-185 (2006).
8. Lian, J., Nelson, R. & Lehner, R. Carboxylesterases in lipid metabolism: from mouse to human. *Protein Cell* (2017).
9. Satoh, T. & Hosokawa, M. Carboxylesterases: structure, function and polymorphism in mammals. *Journal of Pesticide Science* **35**, 218-228 (2010).
10. Holmes, R.S., *et al.* Recommended nomenclature for five mammalian carboxylesterase gene families: human, mouse, and rat genes and proteins. *Mammalian Genome* **21**, 427-441 (2010).
11. Robbi, M. & Beaufay, H. The COOH terminus of several liver carboxylesterases targets these enzymes to the lumen of the endoplasmic reticulum. *Journal of Biological Chemistry* **266**, 20498-20503 (1991).
12. Lagas, J.S., *et al.* P-Glycoprotein, Multidrug-Resistance Associated Protein 2, Cyp3a, and Carboxylesterase Affect the Oral Availability and Metabolism of Vinorelbine. *Molecular Pharmacology* **82**, 636-644 (2012).
13. Bartels, A.K., *et al.* KDEL Receptor 1 Contributes to Cell Surface Association of Protein Disulfide Isomerases. *Cellular Physiology and Biochemistry* **52**, 850-868 (2019).
14. Hatfield, M.J., *et al.* Biochemical and molecular analysis of carboxylesterase-mediated hydrolysis of cocaine and heroin. *British Journal of Pharmacology* **160**, 1916-1928 (2010).
15. Xiao, D., *et al.* Regulation of carboxylesterase-2 expression by p53 family proteins and enhanced anti-cancer activities among 5-fluorouracil, irinotecan and doxazolidine prodrug. *British Journal of Pharmacology* **168**, 1989-1999 (2013).
16. Pratt, S.E., *et al.* Human Carboxylesterase-2 Hydrolyzes the Prodrug of Gemcitabine (LY2334737) and Confers Prodrug Sensitivity to Cancer Cells. *Clinical Cancer Research* **19**, 1159-1168 (2013).
17. Humerickhouse, R., Lohrbach, K., Li, L., Bosron, W.F. & Dolan, M.E. Characterization of CPT-11 hydrolysis by human liver carboxylesterase isoforms hCE-1 and hCE-2. *Cancer Research* **60**, 1189-1192 (2000).
18. Quinney, S.K., *et al.* Hydrolysis of capecitabine to 5'-deoxy-5-fluorocytidine by human carboxylesterases and inhibition by loperamide. *Journal of Pharmacology and Experimental Therapeutics* **313**, 1011-1016 (2005).
19. Fukami, T., Kariya, M., Kurokawa, T., Iida, A. & Nakajima, M. Comparison of substrate specificity among human arylacetamide deacetylase and carboxylesterases. *European Journal of Pharmaceutical Sciences* **78**, 47-53 (2015).
20. Williams, E.T., *et al.* The biotransformation of prasugrel, a new thienopyridine prodrug, by the human carboxylesterases 1 and 2. *Drug Metabolism and Disposition* **36**, 1227-1232 (2008).
21. Yu, Y., *et al.* Two birds, one stone: hesperetin alleviates chemotherapy-induced diarrhea and potentiates tumor inhibition. *Oncotarget* **9**, 27958-27973 (2018).
22. Xu, G., Zhang, W., Ma, M.K. & McLeod, H.L. Human carboxylesterase 2 is commonly expressed in tumor tissue and is correlated with activation of irinotecan. *Clinical Cancer Research* **8**, 2605-2611 (2002).

23. Li, Y., *et al.* Carboxylesterase 2 prevents liver steatosis by modulating lipolysis, endoplasmic reticulum stress, and lipogenesis and is regulated by hepatocyte nuclear factor 4 alpha in mice. *Hepatology* **63**, 1860-1874 (2016).
24. Ruby, M.A., *et al.* Human Carboxylesterase 2 Reverses Obesity-Induced Diacylglycerol Accumulation and Glucose Intolerance. *Cell Reports* **18**, 636-646 (2017).
25. Maresch, L.K., *et al.* Intestine-Specific Overexpression of Carboxylesterase 2c Protects Mice From Diet-Induced Liver Steatosis and Obesity. *Hepatology communications* **3**, 227-245 (2019).
26. Iusuf, D., *et al.* OATP1A/1B transporters affect irinotecan and SN-38 pharmacokinetics and carboxylesterase expression in knockout and humanized transgenic mice. *Molecular Cancer Therapeutics* **13**, 492-503 (2014).
27. van de Steeg, E., *et al.* Methotrexate pharmacokinetics in transgenic mice with liver-specific expression of human organic anion-transporting polypeptide 1B1 (SLCO1B1). *Drug Metabolism and Disposition* **37**, 277-281 (2009).
28. van Herwaarden, A.E., *et al.* Knockout of cytochrome P450 3A yields new mouse models for understanding xenobiotic metabolism. *Journal of Clinical Investigation* **117**, 3583-3592 (2007).
29. Damen, C.W.N., Lagas, J.S., Rosing, H., Schellens, J.H.M. & Beijnen, J.H. The bioanalysis of vinorelbine and 4-O-deacetylvinorelbine in human and mouse plasma using high-performance liquid chromatography coupled with heated electrospray ionization tandem mass-spectrometry. *Biomedical Chromatography* **23**, 1316-1325 (2009).
30. Deenen, M.J., Rosing, H., Hillebrand, M.J., Schellens, J.H. & Beijnen, J.H. Quantitative determination of capecitabine and its six metabolites in human plasma using liquid chromatography coupled to electrospray tandem mass spectrometry. *Journal of Chromatography. B: Analytical Technologies in the Biomedical and Life Sciences* **913-914**, 30-40 (2013).
31. Zhang, Y., Huo, M., Zhou, J. & Xie, S. PKSolver: An add-in program for pharmacokinetic and pharmacodynamic data analysis in Microsoft Excel. *Computer Methods and Programs in Biomedicine* **99**, 306-314 (2010).
32. Anastasiadis, K., *et al.* Dre recombinase, like Cre, is a highly efficient site-specific recombinase in E. coli, mammalian cells and mice. *Disease Models & Mechanisms* **2**, 508-515 (2009).
33. Gralla, R.J., *et al.* Oral vinorelbine in the treatment of non-small cell lung cancer: rationale and implications for patient management. *Drugs* **67**, 1403-1410 (2007).
34. Domenech, G.H. & Vogel, C.L. A review of vinorelbine in the treatment of breast cancer. *Clinical Breast Cancer* **2**, 113-128 (2001).
35. Wargin, W.A. & Lucas, V.S. The clinical pharmacokinetics of vinorelbine (Navelbine). *Seminars in Oncology* **21**, 21-27 (1994).
36. Beulz-Riche, D., *et al.* Characterization of human cytochrome P450 isoenzymes involved in the metabolism of vinorelbine. *Fundamental and Clinical Pharmacology* **19**, 545-553 (2005).
37. Kajita, J., Kuwabara, T., Kobayashi, H. & Kobayashi, S. CYP3A4 is mainly responsible for the metabolism of a new vinca alkaloid, vinorelbine, in human liver microsomes. *Drug Metabolism and Disposition* **28**, 1121-1127 (2000).
38. Marty, M., *et al.* Oral vinorelbine pharmacokinetics and absolute bioavailability study in patients with solid tumors. *Annals of Oncology* **12**, 1643-1649 (2001).
39. Tabata, T., *et al.* Bioactivation of capecitabine in human liver: involvement of the cytosolic enzyme on 5'-deoxy-5-fluorocytidine formation. *Drug Metabolism and Disposition* **32**, 762-767 (2004).
40. Shimizu, M., Fukami, T., Nakajima, M. & Yokoi, T. Screening of Specific Inhibitors for Human Carboxylesterases or Arylacetamide Deacetylase. *Drug Metabolism and Disposition* **42**, 1103-1109 (2014).
41. Imai, T., Takase, Y., Iwase, H. & Hashimoto, M. Involvement of Carboxylesterase in Hydrolysis of Propranolol Prodrug during Permeation across Rat Skin. *Pharmaceutics* **5**, 371-384 (2013).
42. Fukami, T. & Yokoi, T. The emerging role of human esterases. *Drug Metabolism and Pharmacokinetics* **27**, 466-477 (2012).
43. Fukami, T., *et al.* In Vitro Evaluation of Inhibitory Effects of Antidiabetic and Antihyperlipidemic Drugs on Human Carboxylesterase Activities. *Drug Metabolism and Disposition* **38**, 2173-2178 (2010).
44. Takahashi, S., Katoh, M., Saitoh, T., Nakajima, M. & Yokoi, T. Different Inhibitory Effects in Rat and Human Carboxylesterases. *Drug Metabolism and Disposition* **37**, 956-961 (2009).

45. Lian, J., *et al.* Ces1d deficiency protects against high-sucrose diet-induced hepatic triacylglycerol accumulation. *Journal of Lipid Research* (2019).
46. Lian, J., *et al.* Genetic variation in human carboxylesterase CES1 confers resistance to hepatic steatosis. *Biochimica et Biophysica Acta* **1863**, 688-699 (2018).
47. Lian, J., *et al.* Ces3/TGH Deficiency Attenuates Steatohepatitis. *Scientific Reports* **6**, 25747 (2016).
48. Quiroga, A.D., *et al.* Deficiency of carboxylesterase 1/esterase-x results in obesity, hepatic steatosis, and hyperlipidemia. *Hepatology* **56**, 2188-2198 (2012).
49. Wei, E., *et al.* Loss of TGH/Ces3 in mice decreases blood lipids, improves glucose tolerance, and increases energy expenditure. *Cell Metabolism* **11**, 183-193 (2010).
50. Reigner, B., Blesch, K. & Weidekamm, E. Clinical pharmacokinetics of capecitabine. *Clinical Pharmacokinetics* **40**, 85-104 (2001).
51. Rui, L. Energy metabolism in the liver. *Comprehensive Physiology* **4**, 177-197 (2014).
52. Walther, T.C. & Farese, R.V., Jr. Lipid droplets and cellular lipid metabolism. *Annual Review of Biochemistry* **81**, 687-714 (2012).
53. Guo, Y., Cordes, K.R., Farese, R.V., Jr. & Walther, T.C. Lipid droplets at a glance. *Journal of Cell Science* **122**, 749-752 (2009).
54. Giammanco, A., Cefalù, A.B., Noto, D. & Averna, M.R. The pathophysiology of intestinal lipoprotein production. *Frontiers in Physiology* **6**, 61 (2015).
55. Xu, Y., *et al.* Hepatocyte-Specific Expression of Human Carboxylesterase 1 Attenuates Diet-Induced Steatohepatitis and Hyperlipidemia in Mice. *Hepatology communications* **4**, 527-539 (2020).
56. Xu, J., Xu, Y., Xu, Y., Yin, L. & Zhang, Y. Global inactivation of carboxylesterase 1 (Ces1/Ces1g) protects against atherosclerosis in Ldlr (-/-) mice. *Scientific Reports* **7**, 17845 (2017).
57. Azzu, V., Vacca, M., Virtue, S., Allison, M. & Vidal-Puig, A. Adipose Tissue-Liver Cross Talk in the Control of Whole-Body Metabolism: Implications in Nonalcoholic Fatty Liver Disease. *Gastroenterology* **158**, 1899-1912 (2020).
58. Samuel, V.T., Petersen, K.F. & Shulman, G.I. Lipid-induced insulin resistance: unravelling the mechanism. *Lancet* **375**, 2267-2277 (2010).

SUPPLEMENTAL MATERIALS

Supplemental Methods

2.2 Generation of *Ces2*^{-/-}, *Ces2*^{-/-}A and *Ces2*^{-/-}V mice

2.2.1 *Ces2*^{-/-} mice generation

Mouse *Ces2* gene was searched at NCBI (<https://www.ncbi.nlm.nih.gov/>) and ENSEMBL database (<http://www.ensembl.org/index.html>), 5'-20 bp target sequence (5' - TCTCCCTGCCCGTTCAAATCATCAGGGACTTAACATTA - 3') and 3' - 20 bp target sequence (5' AGCCTGAAATATTATTGCATTGGACGGGTAGGTGCTTCTGG 3') were selected at ~3000 bp upstream of the *Ces2a* gene and ~2000 bp downstream of the *Ces2h* gene, respectively. In addition, two corresponding specifically designed (with EcoRV digestion site and RoxP sites introduced) homology-directed repair (HDR) oligos (5'-ATAGAGTGGAAACATCCTAAGTGGTCAATCTCACTGAGAGGAAGGTCTTCCCTGCCCGGATATCTTTATACTTTAAATAATTGGCATTATTTAAAGTTAGGCTTTCAAATCATCAGGACTTAACATTATCCTTGTAATGGCCTTGTTTACACATCTACCAG-3' and 5'-TTGCTTTGTATCCTCGCAAATCCTTAAAGTAGTGAGCCTGAAATATTATTGCATTGGACGATATCTTTATAACTTTAAATAATTGGCATTATTTAAAGTTAGGCTGGTAGGTGCTTCTGGTTGTAGATGTTCCCTAGATTTTATAGTGTCTGCTTCTAGAGAGA-3') were micro-injected mixed with gRNAs (obtained by PCR, target sequence as template) and Cas9 mRNA into zygotes isolated from the FVB/NRj mouse strain. The whole *Ces2* cluster (from *Ces2a* to *Ces2h*) deletion and/or independent 5'-RoxP and 3'-RoxP insertion lines were expected to be generated. A candidate whole *Ces2* cluster deletion from two CRISPR/Cas9 cutting sites without RoxP insertion was obtained and backcrossed to wild-type (>99% FVB background) at least three generations to dilute any potential off-target events. The homozygous complete deletion of the *Ces2* cluster (*Ces2*^{-/-}) was generated by crossbreeding among heterozygous knockout mice. *Ces2*^{-/-} mice were verified by PCR for 7 individual *Ces2* genes (except for the pseudogene *Ces2d*) with wild-type mice as positive control (primers listed in Supplemental Table 1).

2.2.2 Construction of the transgene liver-specific expression plasmid

In order to obtain liver-specific expression of human CES2, a transgene construct was generated as follows (Figure 2A). Briefly, pTarget Mammalian Expression Vector containing human CES2 cDNA (NM_003869 : 945 - 2889) (a gift from Prof. Nakajima, Kanazawa University, Kanazawa, Japan) (Fukami et al., 2010) was digested with Sall and MluI to obtain a human CES2 cDNA linear fragment (1972 bp). pLIV-LE6 vector containing a hepatic control region (HCR) (a gift from Dr. J. Taylor, Gladstone Institute, University of California, San Francisco, USA) (Simonet et al., 1993) was digested with XhoI to obtain a linearized fragment. Then these two linear fragments were purified by Qiaquick PCR Purification Kit, blunted by Klenow enzyme, purified again and followed by Calf

Intestinal Alkaline Phosphatase (CIP) treatment, and ligation using TaKaRa DNA Ligation Kit Ver. 2.1 (Catalog No: 6022) as last step. The ligated circular DNA product pLIV-LE6-hCES2-HCR was transformed into competent cell DH5a for mini-preparation. The resulting circular DNA product was digested with AclI and Sall to yield functional linearized ApoE-hCES2-HCR.

2.2.3 Construction of the transgene intestine-specific expression plasmid

Another transgene was constructed for intestine-specific expression of human CES2. Briefly, part of the hCES2 open reading frame was cloned behind the villin promoter by PCR. A forward 5'-CCTCTAGGCTCGTCCACCATGACTGCTCAGTCCCGCTCT-3' primer with the last bases of the villin promoter and the first bases of hCES2 (including ATG-start sequence) and a reverse 5'-AATAGCGACGTCTCCGGATGGGACTGGCTGAGT-3' primer aligning with the hCES2 sequence at its BspEI digestion site and followed by an introduced AatII digestion site was used, using pTarget-hCES2 as a template. Subsequently, the obtained PCR product was elongated at its 5' villin promoter side using pBluescript II KS-2kbvillin as a template (kindly provided by D. Louvard, Institut Curie, Paris, France) containing the last 2 kb 3' of the villin promoter (Pinto, D., Robine, S., Jaisser, F., El Marjou, F.E., Louvard, D. (1999) Regulatory sequences of the mouse villin gene that efficiently drive transgenic expression in immature and differentiated epithelial cells of small and large intestines. J. Biol. Chem. 274: 6476-6482). This elongated product was used as the template for a subsequent PCR with forward 5'-GCCTAAGCCGGCTGTGATAGC-3' primer, aligning with the villin promoter sequence at its AflII digestion site, and the earlier used reverse 5'-AATAGCGACGTCTCCGGATGGGACTGGCTGAGT-3' primer, aligning with the hCES2 sequence at its BspEI digestion site and introduced a AatII digestion site, and thereby a PCR product was generated spanning the last part of the villin promoter sequence connected with the ATG start sequence and subsequently the first part of hCES2, flanked by AflII and AatII digestion sites. The AflII and AatII digested fragment was then inserted into the digested AflII and AatII sites of pKS 9kbVill (kindly provided by D. Louvard) containing the full murine villin promoter that stops at the AatII site, yielding pBluescript II KS-9kbVill-ATG-partial hCES2. The pTarget-hCES2 was digested by BspEI to obtain the fragment containing the second part of hCES2 together with the SV40 region. This linearized fragment was subsequently inserted into the BspEI-digested pBluescript II KS-9kbVillin-ATG-partial hCES2, yielding pBluescript II KS-9kbVillin-ATG-hCES2-SV40 plasmid. An EcoRV-AatII excision of this clone was used to obtain functional linear insert Villin-hCES2-SV40 (Figure 2B).

2.2.4 *Ces2*^{-/-}A and *Ces2*^{-/-}V mice generation

The two functional linearized fragments were subsequently injected by pronuclear injection into fertilized oocytes of *Ces2*^{-/-} mice. Two-cell stage embryos were implanted into oviducts of pseudo-pregnant F1 fosters and carried to term. Transgenic founder lines among the offspring were detected by initial PCR screen with forward 5'-GCCTAAGCCGGCTGTGATAGC-3' and reverse 5'-CACCCTCAAGATTCAGGG-3' primers located in the villin promoter and hCES2 cDNA,

respectively. DNA was extracted from toe clips of mice. Obtained transgenic mice with either ApoE-hCES2-HCR-driven liver-specific or villin-hCES2-SV40-driven intestine-specific expression of human CES2 were first back-crossed with FVB/NRj at least three generations and subsequently crossed to *Ces2*^{-/-} mice in order to generate heterozygous hCES2 transgenics with homozygous *Ces2*^{-/-} background. Further cross-breeding yielded homozygous transgenic mice (both *Ces2*^{-/-} and human CES2 transgenes) referred to as *Ces2*^{-/-}A and *Ces2*^{-/-}V which were identified by real-time quantitative PCR with Qiagen human CES2 SYBR Green-based RT² qPCR Primer assays respectively. Transgenic hCES2 expression was monitored and was found to be stable around 9 generations (data not shown).

2.5 Bodyweight monitoring, histology/pathology, plasma clinical chemistry and hematology analysis.

2.5.1 Semi-quantitative assessment standard for (H&E)-staining of white adipose tissue

For white adipose tissue (WAT) adipositis, the following standard of semi-quantification for each slide was used and assessed independently by a pathologist blinded to the identity of the strain on the slides:

Normal WAT tissue: -, score: 0;

Normal WAT tissue with limited mild local adipositis: -/+, score: 1;

Mild adipositis: +, score: 2;

Mild local adipositis with limited moderate local adipositis: +/++, score: 3;

Moderate adipositis: ++, score: 4;

Moderate local adipositis with severe local adipositis: ++/+++, score: 5;

Severe adipositis: +++, score: 6;

2.5.2 Semi-quantitative assessment standard for Oil-red-O staining of liver lipid accumulation

For Oil-red-O staining of liver lipid accumulation, the following standard of semi-quantification for each slide was used and assessed independently by a pathologist blinded to the identity of the strain on the slides:

Negative Oil-red-O staining (no lipid droplets): -, score: 0;

Negative Oil-red-O staining with limited mild (small lipid droplets) local lipid droplets: -/+, score: 1;

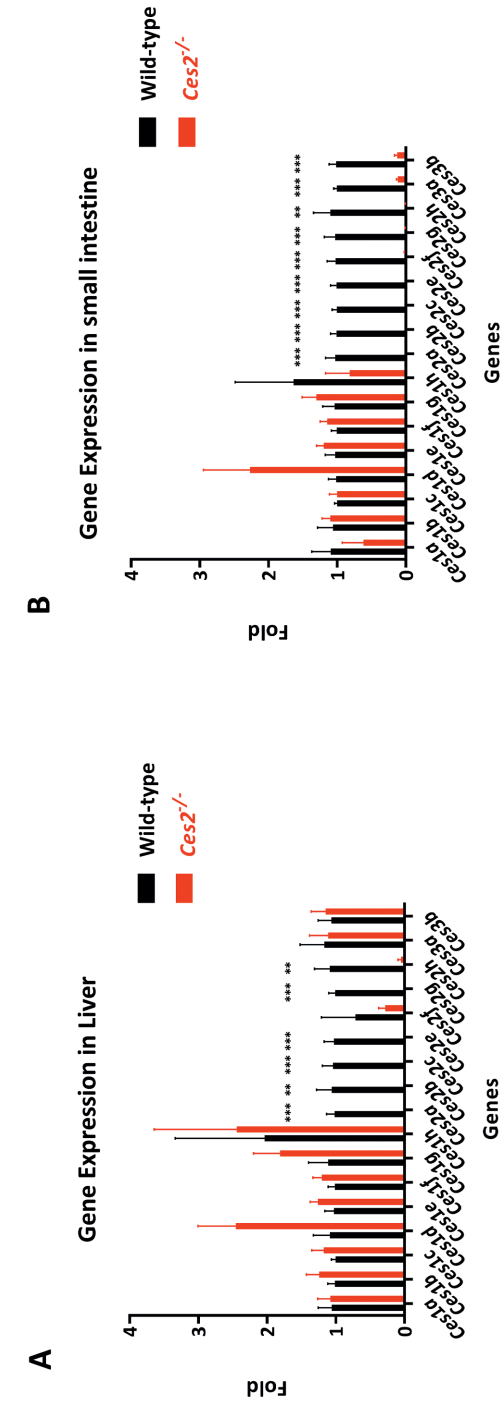
Mild Oil-red-O staining (small lipid droplets): +, score: 2;

Mild Oil-red-O staining with moderate (medium lipid droplets) local lipid droplets: +/++, score: 3;

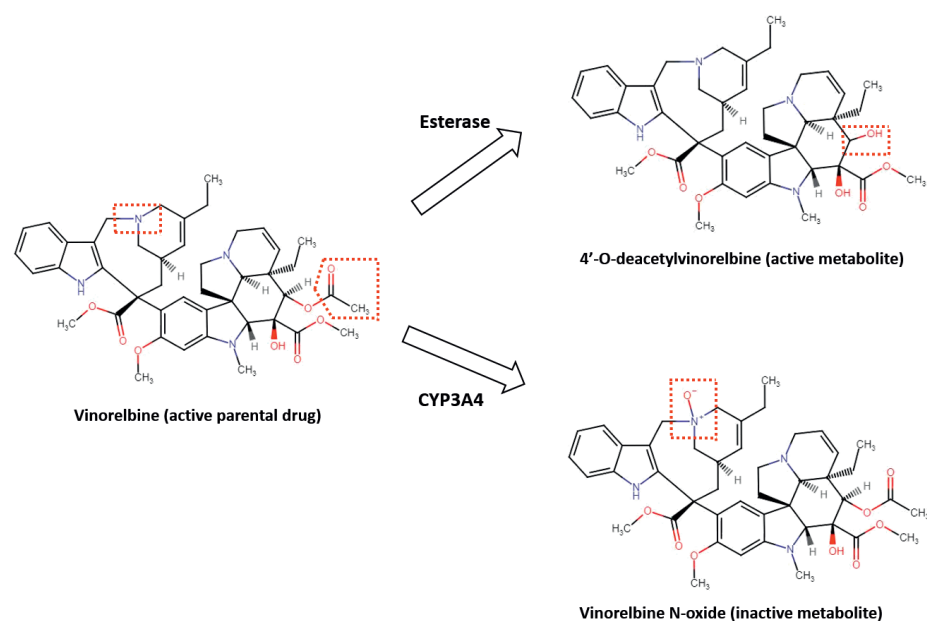
Moderate Oil-red-O staining (medium lipid droplets): ++, score: 4;

Moderate Oil-red-O staining with severe (large lipid droplets) local lipid droplets: ++/+++, score: 5;

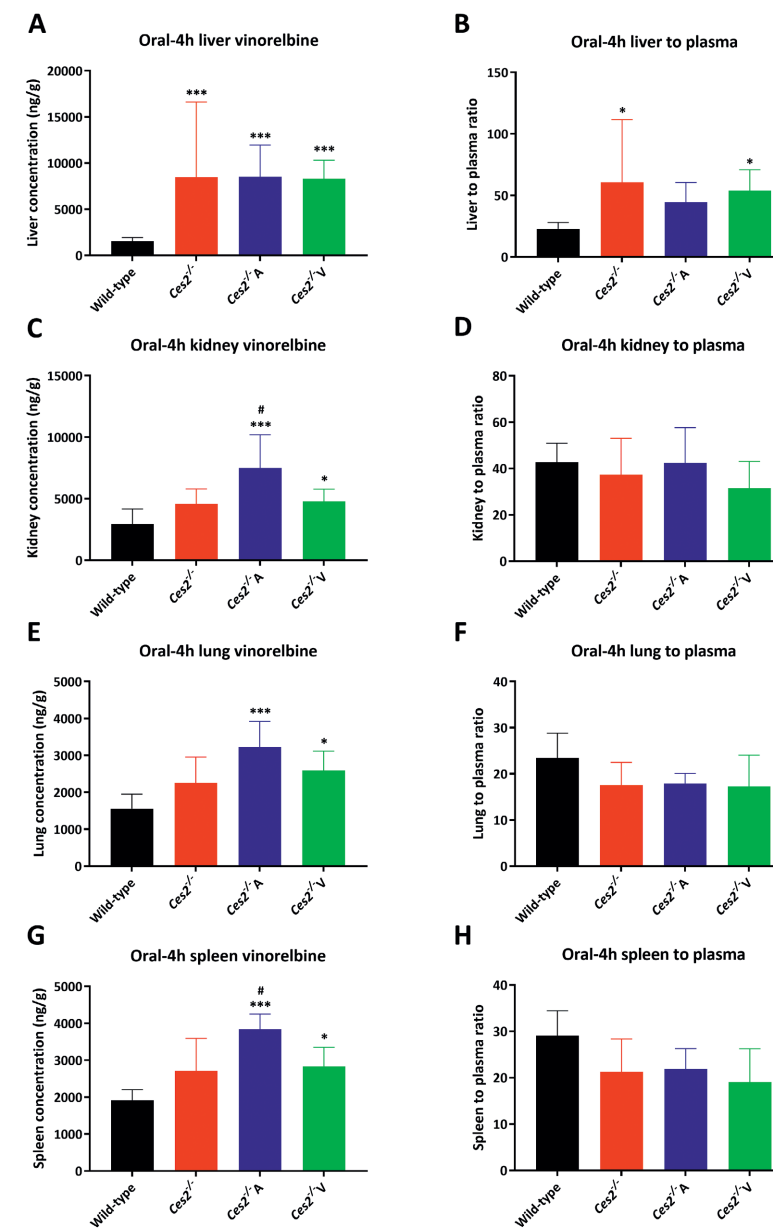
Severe Oil-red-O staining (large lipid droplets): +++, score: 6;



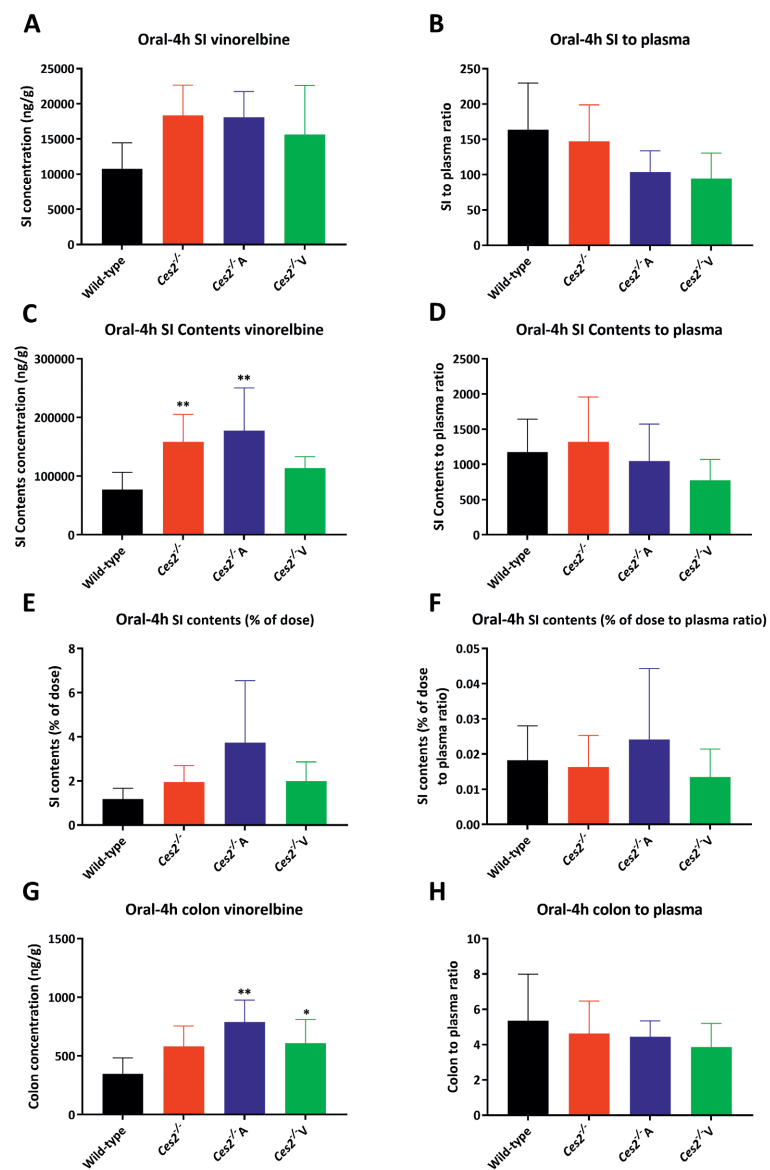
Supplemental Figure 1. Real-time PCR analysis of related carboxylesterase genes (*Ces1*, *Ces2*, and *Ces3*) for wild-type and *Ces2*^{-/-} mice in liver (A) and small intestine (B) tissues. Data (linear expression level normalized to the wild-type RNA level for each gene) are given as mean \pm S.D. (n = 4). Student's t-test was used for statistical analysis. *, P < 0.05; **, P < 0.01; ***, P < 0.001 compared to wild-type mice.



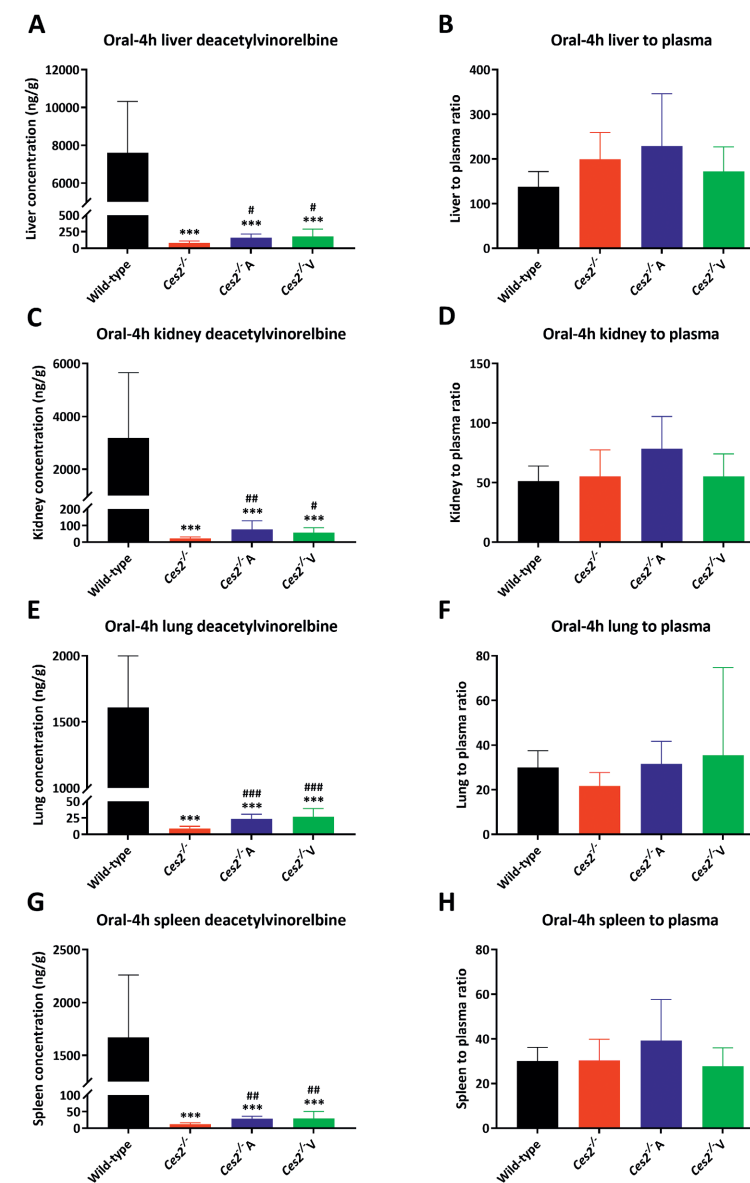
Supplemental Figure 2. Chemical structure and the conversion of vinorelbine to its metabolites vinorelbine N-oxide and 4'-O-deacetylvinorelbine. The red frame indicates where carboxylesterases and CYP3A4 effectively cleave or modify vinorelbine.



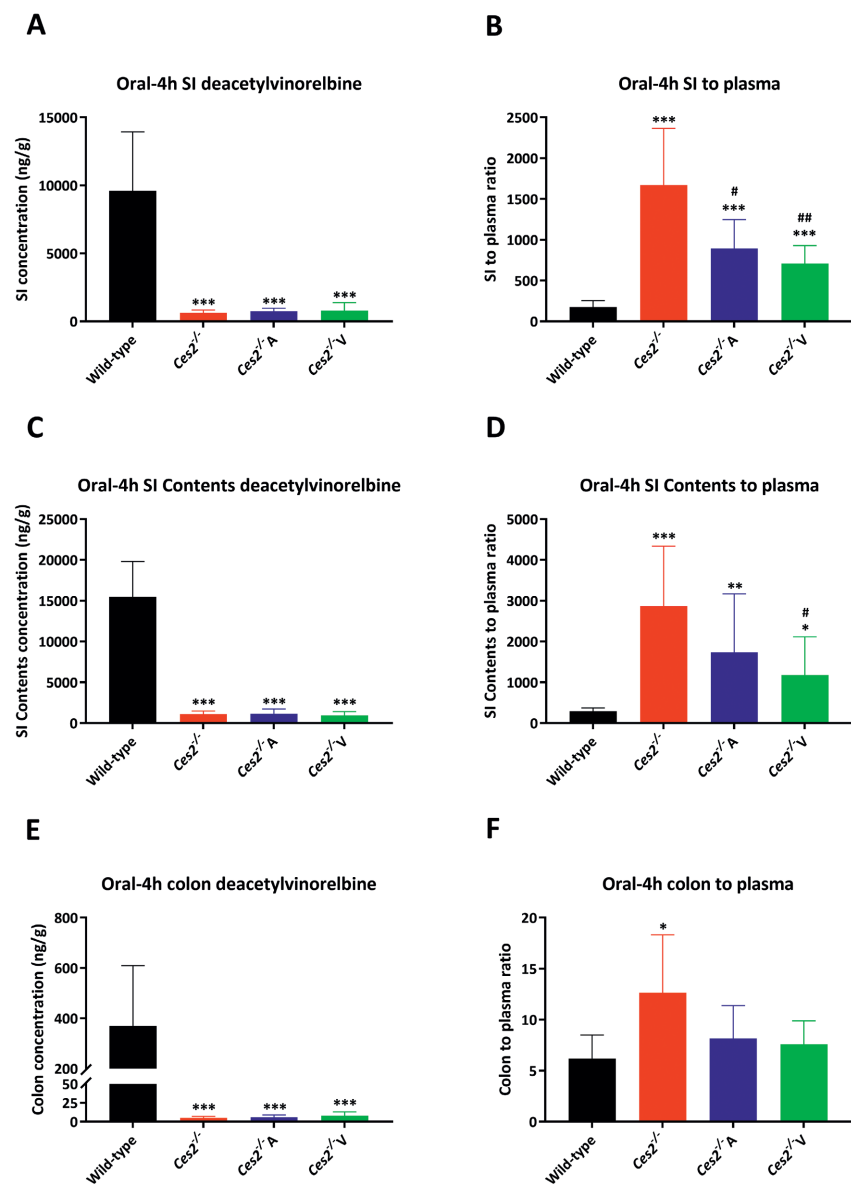
Supplemental Figure 3. Liver, kidney, lung and spleen vinorelbine concentrations (A, C, E and G), and vinorelbine tissue-to-plasma concentration ratios (B, D, F and H) in male wild-type, *Ces2*^{-/-}, *Ces2*^{-/-A} and *Ces2*^{-/-V} mice over 4 h after oral administration of 10 mg/kg vinorelbine. Data are given as mean \pm S.D. (n = 6 - 7). *, $P < 0.05$; **, $P < 0.01$; ***, $P < 0.001$ compared to wild-type mice; #, $P < 0.05$; ##, $P < 0.01$; ###, $P < 0.001$ compared to *Ces2*^{-/-} mice. ^, $P < 0.05$; ^^, $P < 0.01$; ^^, $P < 0.001$ for comparison between *Ces2*^{-/-A} and *Ces2*^{-/-V} mice. Statistical analysis was applied after log-transformation of linear data.



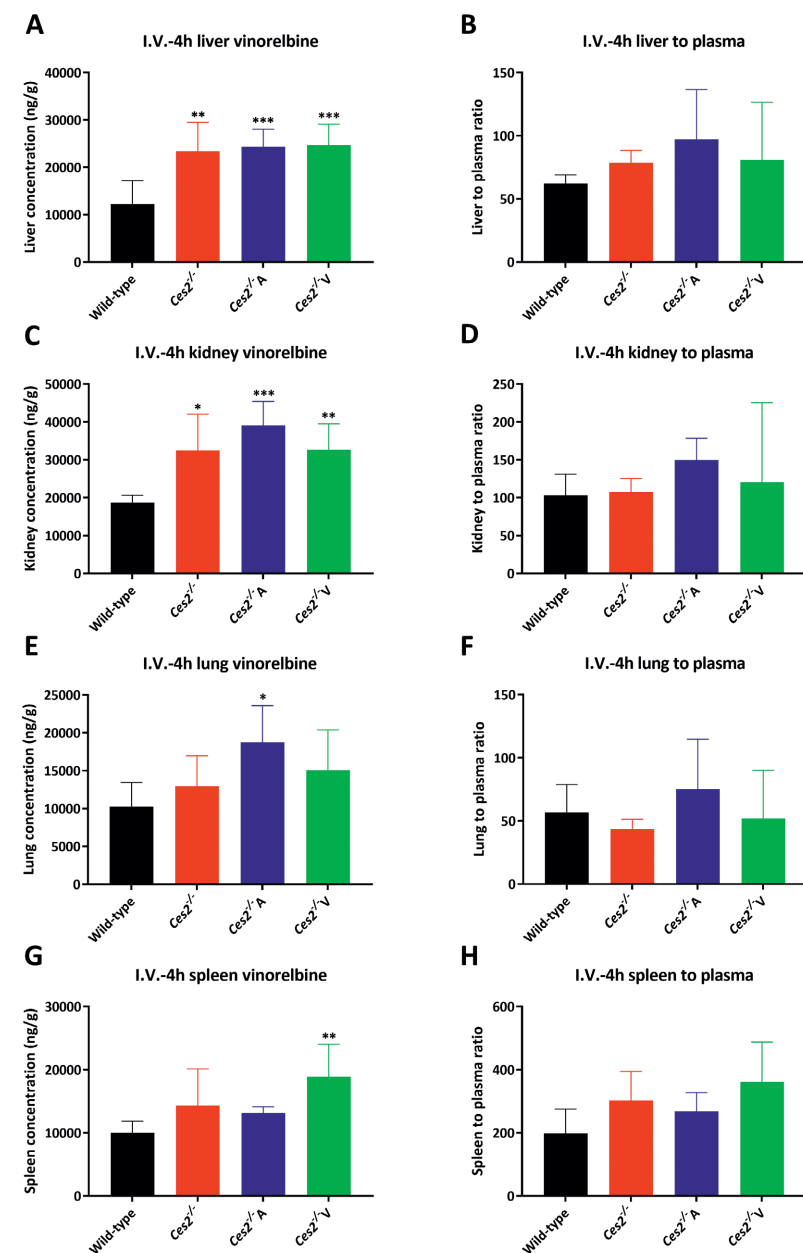
Supplemental Figure 4. Small intestine (SI), small intestine contents (SIC), small intestine contents percentage of total dose and colon vinorelbine concentrations (A, C, E and G), and vinorelbine tissue-to-plasma concentration ratios in SI, SIC, SIC (% of dose) and colon (B, D, F and H) in male wild-type, *Ces2*^{-/-}, *Ces2*^{-/-A} and *Ces2*^{-/-V} mice over 4 h after oral administration of 10 mg/kg vinorelbine. Data are given as mean \pm S.D. (n = 6 - 7). *, $P < 0.05$; **, $P < 0.01$; ***, $P < 0.001$ compared to wild-type mice; #, $P < 0.05$; ##, $P < 0.01$; ###, $P < 0.001$ compared to *Ces2*^{-/-} mice. ^, $P < 0.05$; ^^, $P < 0.01$; ^^, $P < 0.001$ for comparison between *Ces2*^{-/-A} and *Ces2*^{-/-V} mice. Statistical analysis was applied after log-transformation of linear data.



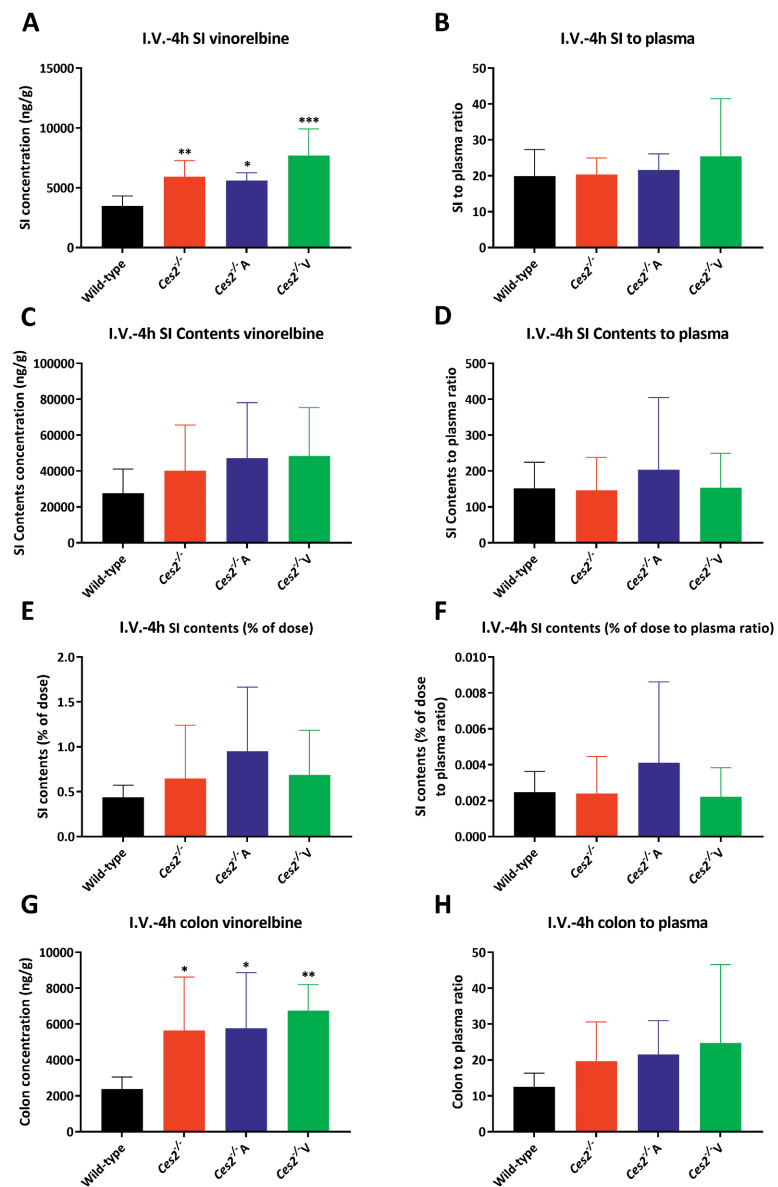
Supplemental Figure 5. Liver, kidney, lung and spleen deacetylvinorelbine concentrations (A, C, E and G), and deacetylvinorelbine tissue-to-plasma concentration ratios (B, D, F and H) in male wild-type, *Ces2*^{-/-}, *Ces2*^{-/-A} and *Ces2*^{-/-V} mice over 4 h after oral administration of 10 mg/kg vinorelbine. Data are given as mean \pm S.D. (n = 6 - 7). *, $P < 0.05$; **, $P < 0.01$; ***, $P < 0.001$ compared to wild-type mice; #, $P < 0.05$; ##, $P < 0.01$; ###, $P < 0.001$ compared to *Ces2*^{-/-} mice. ^, $P < 0.05$; ^^, $P < 0.01$; ^^, $P < 0.001$ for comparison between *Ces2*^{-/-A} and *Ces2*^{-/-V} mice. Statistical analysis was applied after log-transformation of linear data.



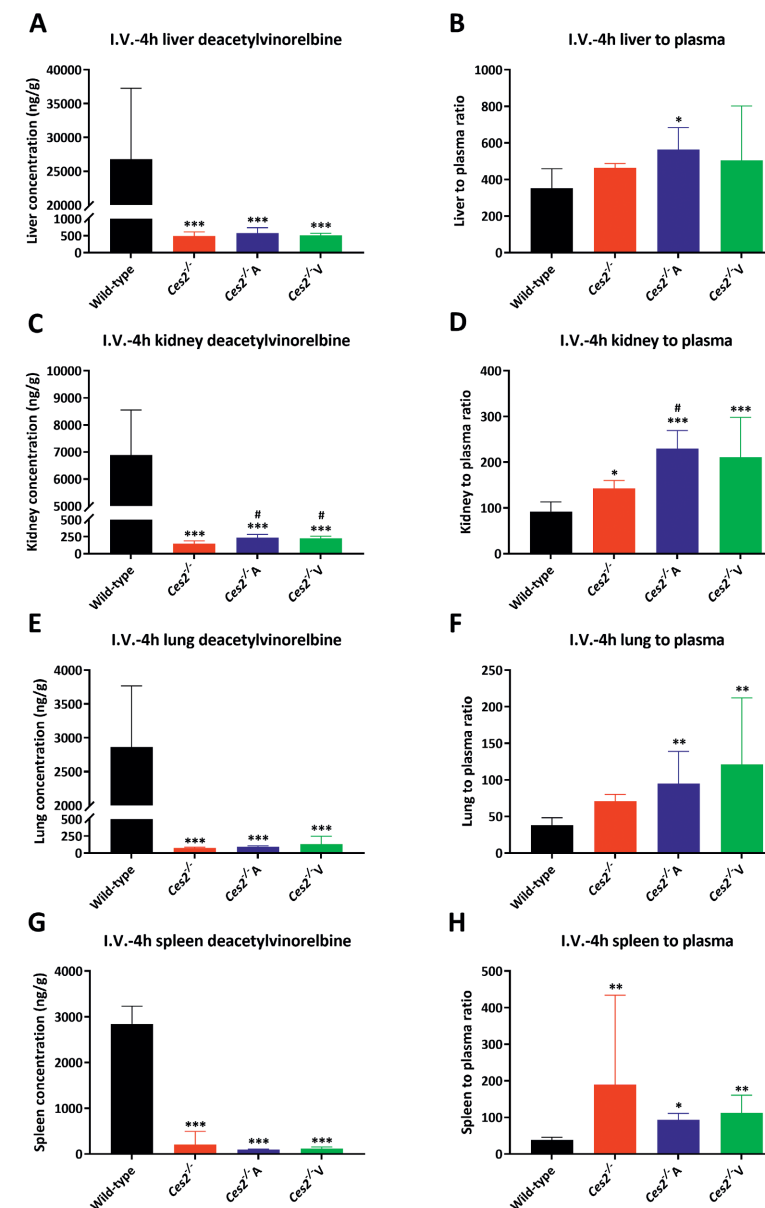
Supplemental Figure 6. Small intestine (SI), small intestine contents (SIC), small intestine contents percentage of total dose and colon deacetylvinorelbine concentrations (A, C, E and G), and deacetylvinorelbine tissue-to-plasma concentration ratios in SI, SIC, SIC (% of dose) and colon (B, D, F and H) in male wild-type, *Ces2*^{-/-}, *Ces2*^{-/-A} and *Ces2*^{-/-V} mice over 4 h after oral administration of 10 mg/kg vinorelbine. Data are given as mean \pm S.D. (n = 6 - 7). *, $P < 0.05$; **, $P < 0.01$; ***, $P < 0.001$ compared to wild-type mice; #, $P < 0.05$; ##, $P < 0.01$; ###, $P < 0.001$ compared to *Ces2*^{-/-} mice. ^, $P < 0.05$; ^^, $P < 0.01$; ^^, $P < 0.001$ for comparison between *Ces2*^{-/-A} and *Ces2*^{-/-V} mice. Statistical analysis was applied after log-transformation of linear data.



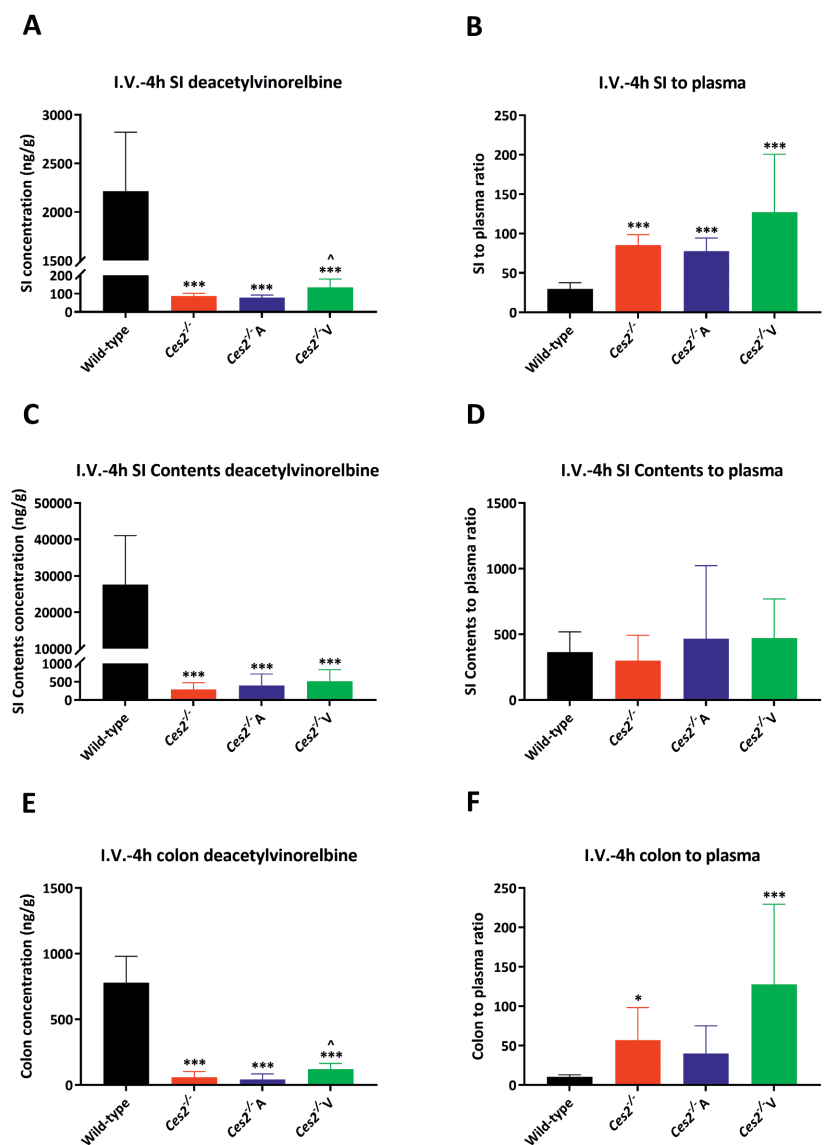
Supplemental Figure 7. Liver, kidney, lung and spleen vinorelbine concentrations (A, C, E and G), and vinorelbine tissue-to-plasma concentration ratios (B, D, F and H) in male wild-type, *Ces2*^{-/-}, *Ces2*^{-/-A} and *Ces2*^{-/-V} mice over 4 h after I.V. injection of 10 mg/kg vinorelbine. Data are given as mean \pm S.D. (n = 6 - 7). *, $P < 0.05$; **, $P < 0.01$; ***, $P < 0.001$ compared to wild-type mice; #, $P < 0.05$; ##, $P < 0.01$; ###, $P < 0.001$ compared to *Ces2*^{-/-} mice. ^, $P < 0.05$; ^^, $P < 0.01$; ^^, $P < 0.001$ for comparison between *Ces2*^{-/-A} and *Ces2*^{-/-V} mice. Statistical analysis was applied after log-transformation of linear data.



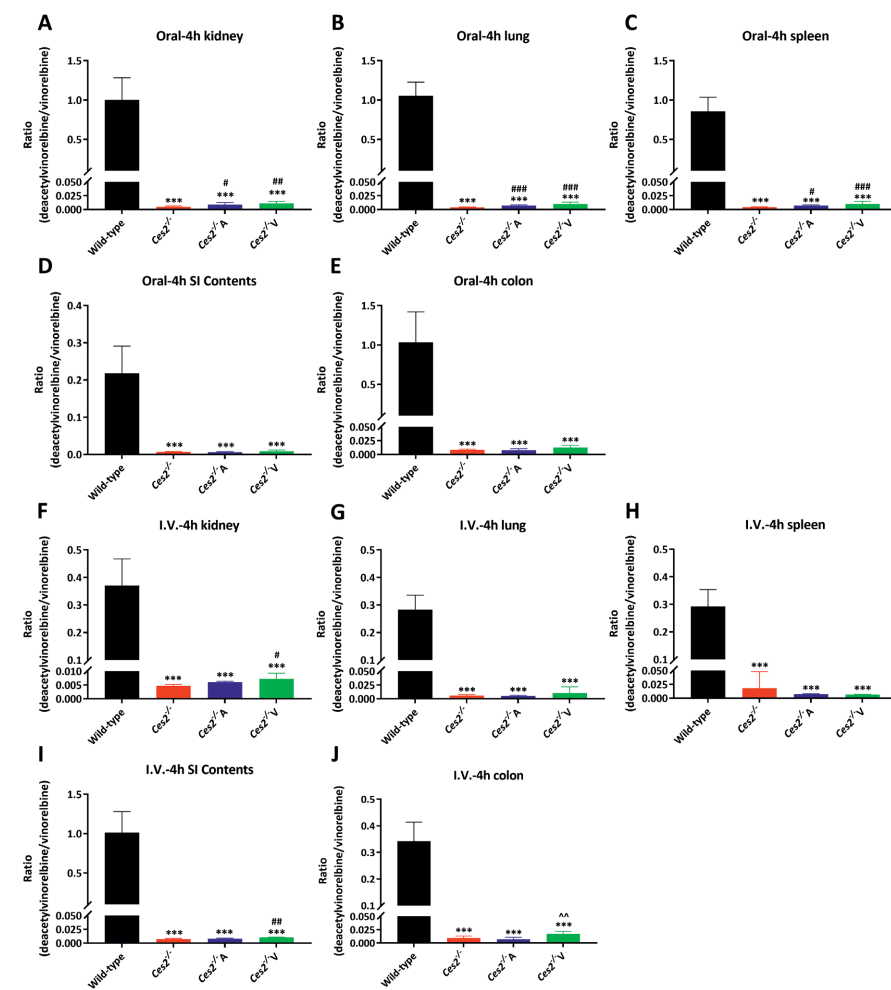
Supplemental Figure 8. Small intestine (SI), small intestine contents (SIC), small intestine contents percentage of total dose and colon vinorelbine concentrations (A, C, E and G), and vinorelbine tissue-to-plasma concentration ratios in SI, SIC, SIC (% of dose) and colon (B, D, F and H) in male wild-type, *Ces2*^{-/-}, *Ces2*^{-/-A} and *Ces2*^{-/-V} mice over 4 h after I.V. injection of 10 mg/kg vinorelbine. Data are given as mean \pm S.D. (n = 6 - 7). *, $P < 0.05$; **, $P < 0.01$; ***, $P < 0.001$ compared to wild-type mice; #, $P < 0.05$; ##, $P < 0.01$; ###, $P < 0.001$ compared to *Ces2*^{-/-} mice. ^, $P < 0.05$; ^^, $P < 0.01$; ^^, $P < 0.001$ for comparison between *Ces2*^{-/-A} and *Ces2*^{-/-V} mice. Statistical analysis was applied after log-transformation of linear data.



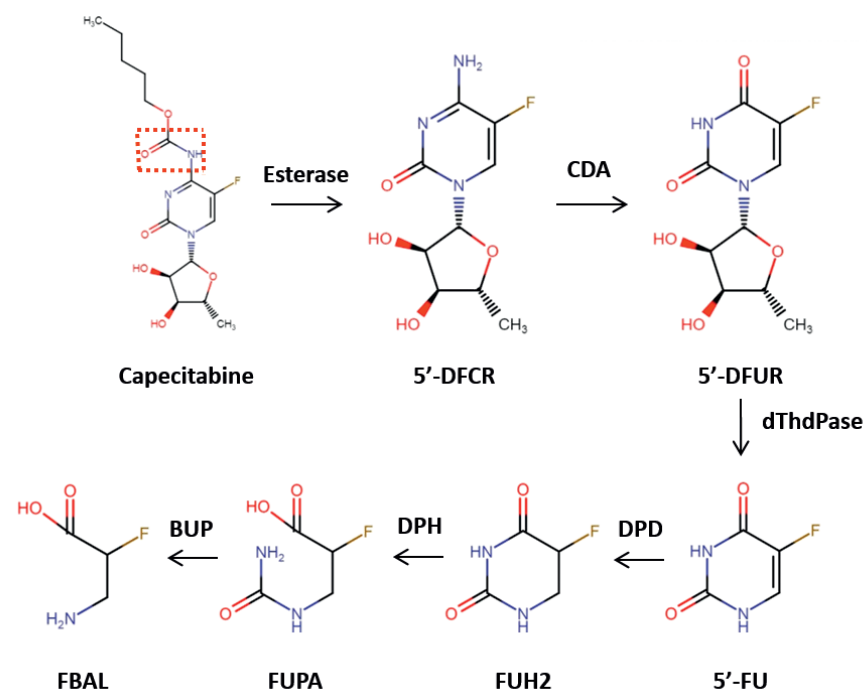
Supplemental Figure 9. Liver, kidney, lung and spleen deacetylvinorelbine concentrations (A, C, E and G), and deacetylvinorelbine tissue-to-plasma concentration ratios (B, D, F and H) in male wild-type, *Ces2*^{-/-}, *Ces2*^{-/-A} and *Ces2*^{-/-V} mice over 4 h after I.V. injection of 10 mg/kg vinorelbine. Data are given as mean \pm S.D. (n = 6 - 7). *, $P < 0.05$; **, $P < 0.01$; ***, $P < 0.001$ compared to wild-type mice; #, $P < 0.05$; ##, $P < 0.01$; ###, $P < 0.001$ compared to *Ces2*^{-/-} mice. ^, $P < 0.05$; ^^, $P < 0.01$; ^^, $P < 0.001$ for comparison between *Ces2*^{-/-A} and *Ces2*^{-/-V} mice. Statistical analysis was applied after log-transformation of linear data.



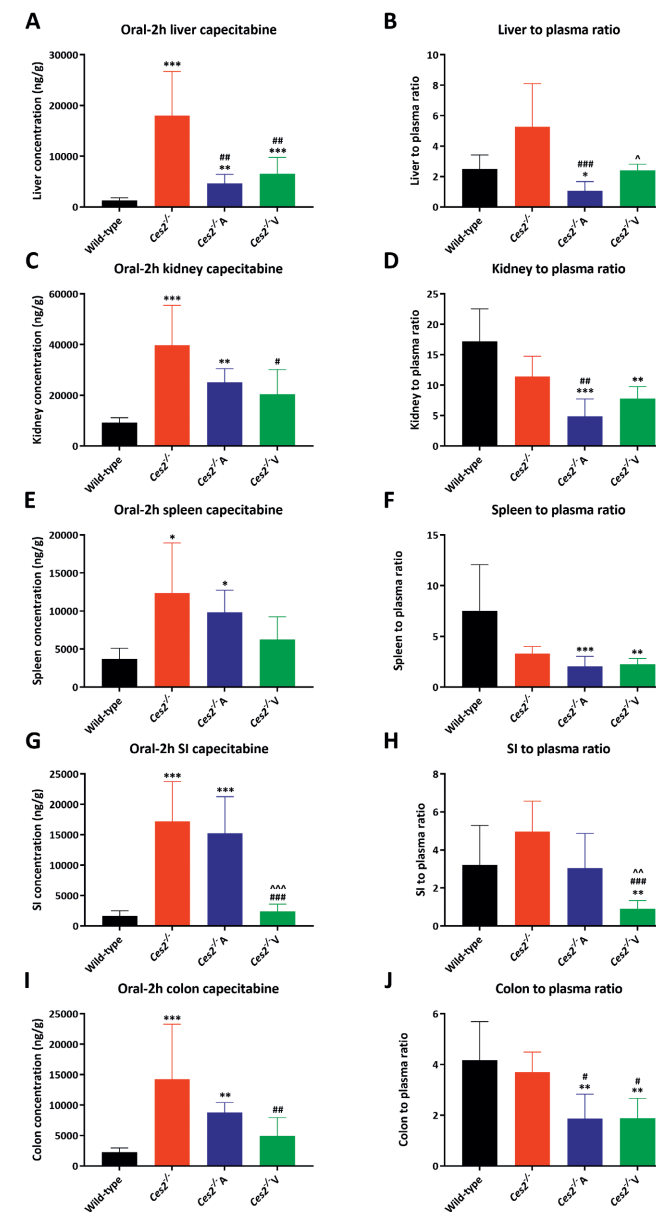
Supplemental Figure 10. Small intestine (SI), small intestine contents (SIC), small intestine contents percentage of total dose and colon deacetylvinorelbine concentrations (A, C, E and G), and deacetylvinorelbine tissue-to-plasma concentration ratios in SI, SIC, SIC (% of dose) and colon (B, D, F and H) in male wild-type, *Ces2*^{-/-}, *Ces2*^{-/-A} and *Ces2*^{-/-V} mice over 4 h after I.V. injection of 10 mg/kg vinorelbine. Data are given as mean \pm S.D. (n = 6 - 7). *, $P < 0.05$; **, $P < 0.01$; ***, $P < 0.001$ compared to wild-type mice; #, $P < 0.05$; ##, $P < 0.01$; ###, $P < 0.001$ compared to *Ces2*^{-/-} mice. ^, $P < 0.05$; ^^, $P < 0.01$; ^^, $P < 0.001$ for comparison between *Ces2*^{-/-A} and *Ces2*^{-/-V} mice. Statistical analysis was applied after log-transformation of linear data.



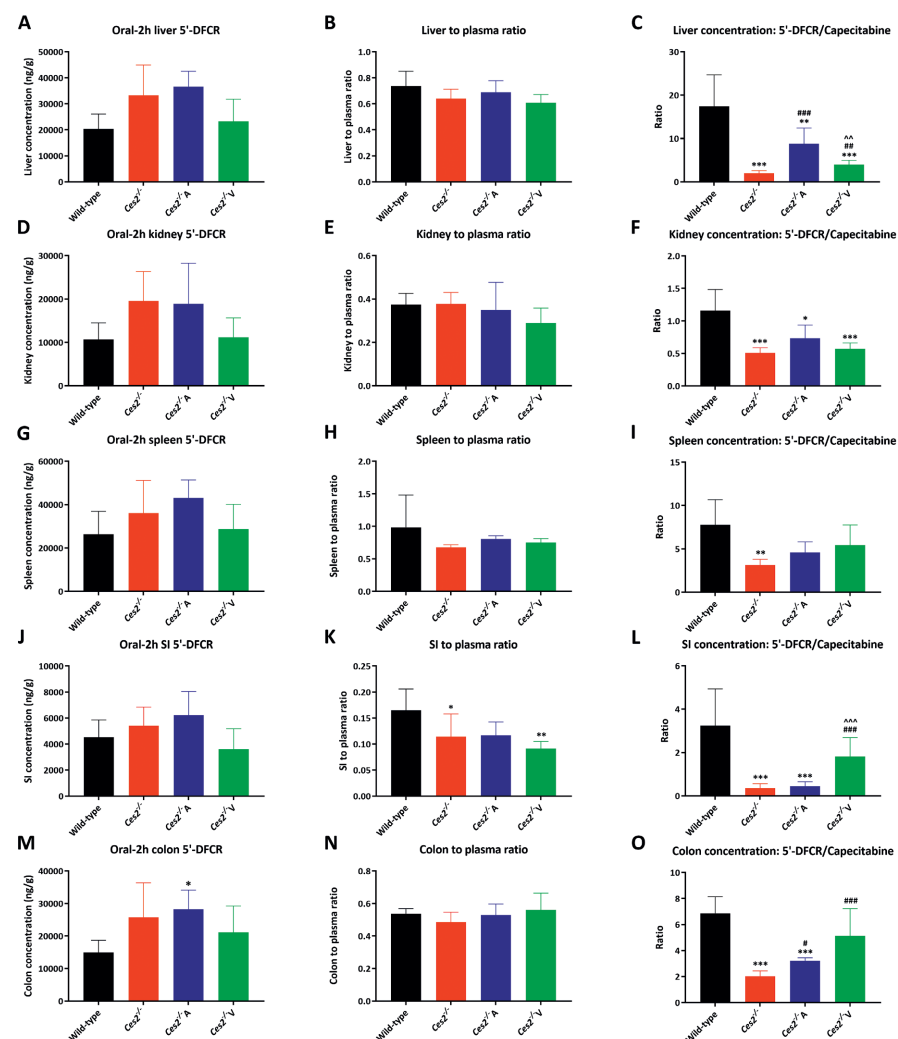
Supplemental Figure 11. Deacetylvinorelbine-to-vinorelbine ratios in kidney (A and F), lung (B and G), spleen (C and H), small intestine contents (D and I) and colon (E and J) after oral administration or I.V. injection, respectively, of 10 mg/kg vinorelbine. Data are given as mean \pm S.D. (n = 6 - 7). *, $P < 0.05$; **, $P < 0.01$; ***, $P < 0.001$ compared to wild-type mice; #, $P < 0.05$; ##, $P < 0.01$; ###, $P < 0.001$ compared to *Ces2*^{-/-} mice. ^, $P < 0.05$; ^^, $P < 0.01$; ^^, $P < 0.001$ for comparison between *Ces2*^{-/-A} and *Ces2*^{-/-V} mice. Statistical analysis was applied after log-transformation of linear data.



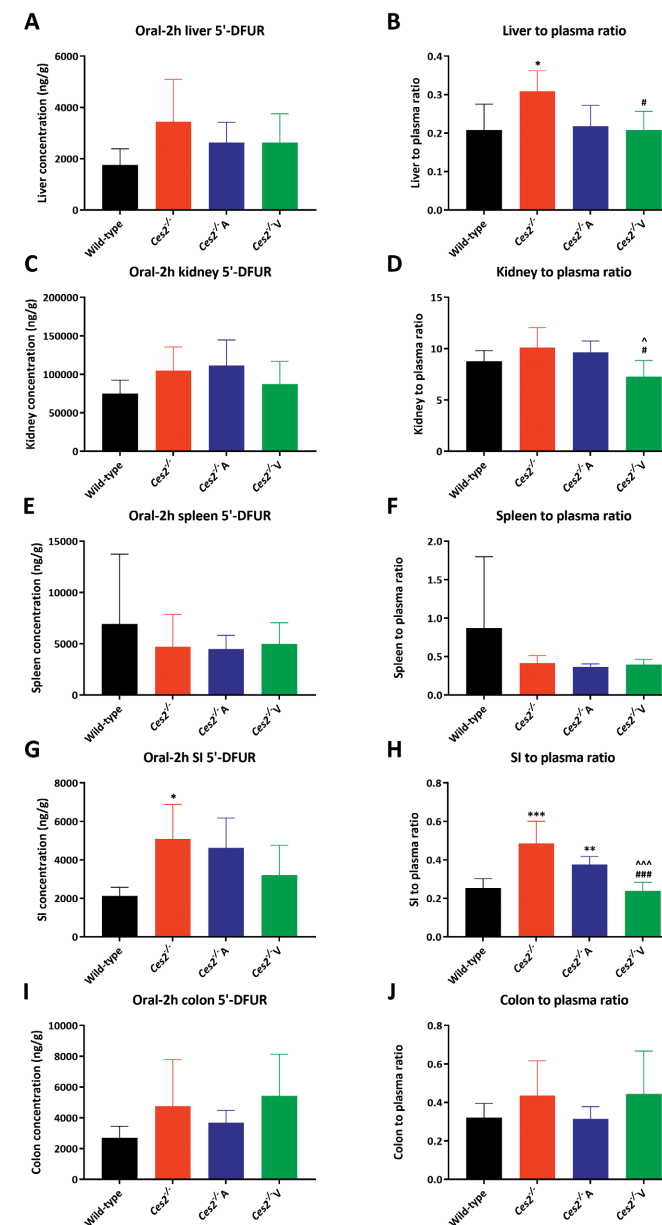
Supplemental Figure 12. Chemical structure and the bio-activation process of capecitabine to 5'-DFCR, 5'-DFUR, 5-FU and FBAL. The red frame indicates where esterases effectively cleave capecitabine. CDA: cytidine deaminase; dThdPase: thymidine phosphorylase; DPD: dihydropyrimidine dehydrogenase; DPH: dihydropyrimidinase; BUP: b-alanine synthase.



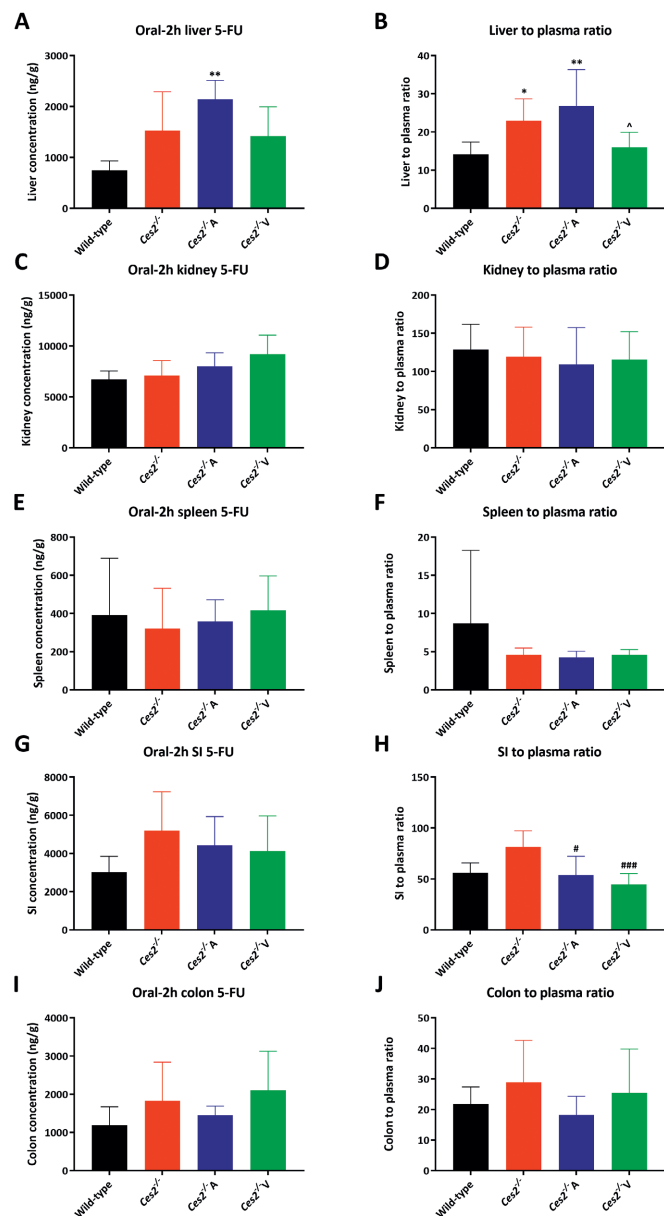
Supplemental Figure 13. Liver, kidney, spleen, small intestine (SI) and colon capecitabine concentrations (A, C, E, G and I), and capecitabine tissue-to-plasma concentration ratios (B, D, F, H and J) in female wild-type, *Ces2*^{-/-}, *Ces2*^{-/-A} and *Ces2*^{-/-V} mice over 2 h after oral administration of 500 mg/kg capecitabine. Data are given as mean ± S.D. (n = 5 - 7). *, $P < 0.05$; **, $P < 0.01$; ***, $P < 0.001$ compared to wild-type mice; #, $P < 0.05$; ##, $P < 0.01$; ###, $P < 0.001$ compared to *Ces2*^{-/-} mice. ^, $P < 0.05$; ^^, $P < 0.01$; ^^, $P < 0.001$ for comparison between *Ces2*^{-/-A} and *Ces2*^{-/-V} mice. Statistical analysis was applied after log-transformation of linear data.



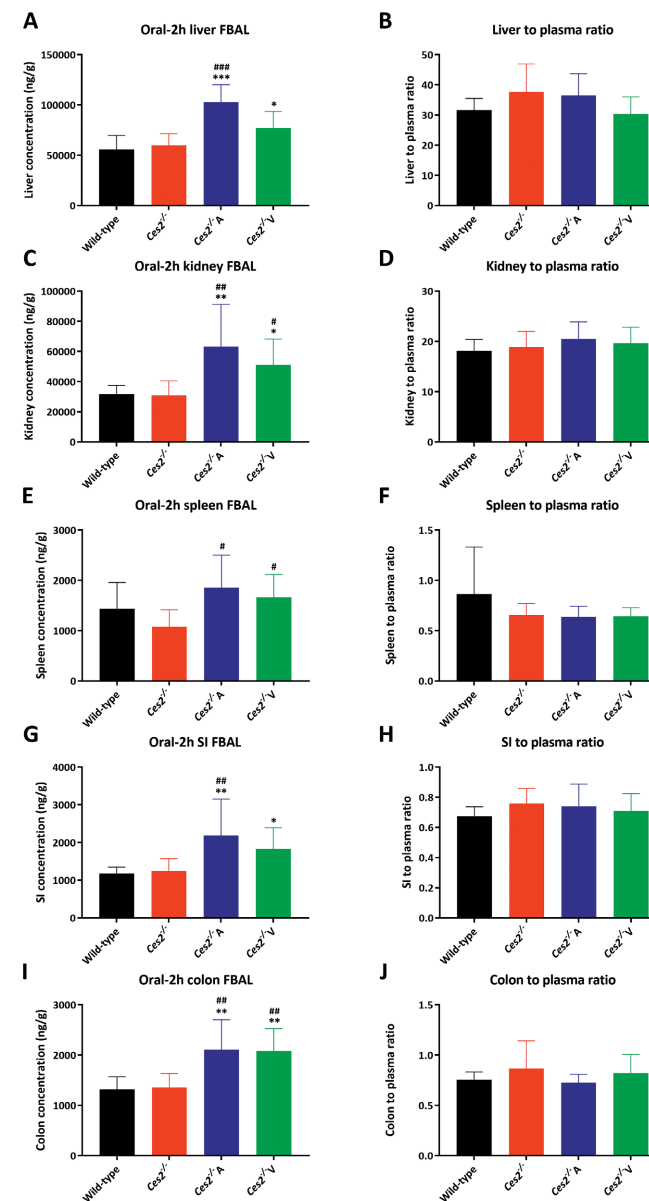
Supplemental Figure 14. Liver, kidney, spleen, small intestine (SI), colon 5'-DFCR concentrations (A, D, G, J and M), 5'-DFCR tissue-to-plasma concentration ratios (B, E, H, K and N), and 5'-DFCR-to-capecitabine conversion ratios in tissues (C, F, I, L and O) in female wild-type, *Ces2*^{-/-}, *Ces2*^{-/A} and *Ces2*^{-/V} mice over 2 h after oral administration of 500 mg/kg capecitabine. Data are given as mean \pm S.D. ($n = 5 - 7$). *, $P < 0.05$; **, $P < 0.01$; ***, $P < 0.001$ compared to wild-type mice; #, $P < 0.05$; ##, $P < 0.01$; ###, $P < 0.001$ compared to *Ces2*^{-/-} mice. ^, $P < 0.05$; ^^, $P < 0.01$; ^^, $P < 0.001$ for comparison between *Ces2*^{-/A} and *Ces2*^{-/V} mice. Statistical analysis was applied after log-transformation of linear data.



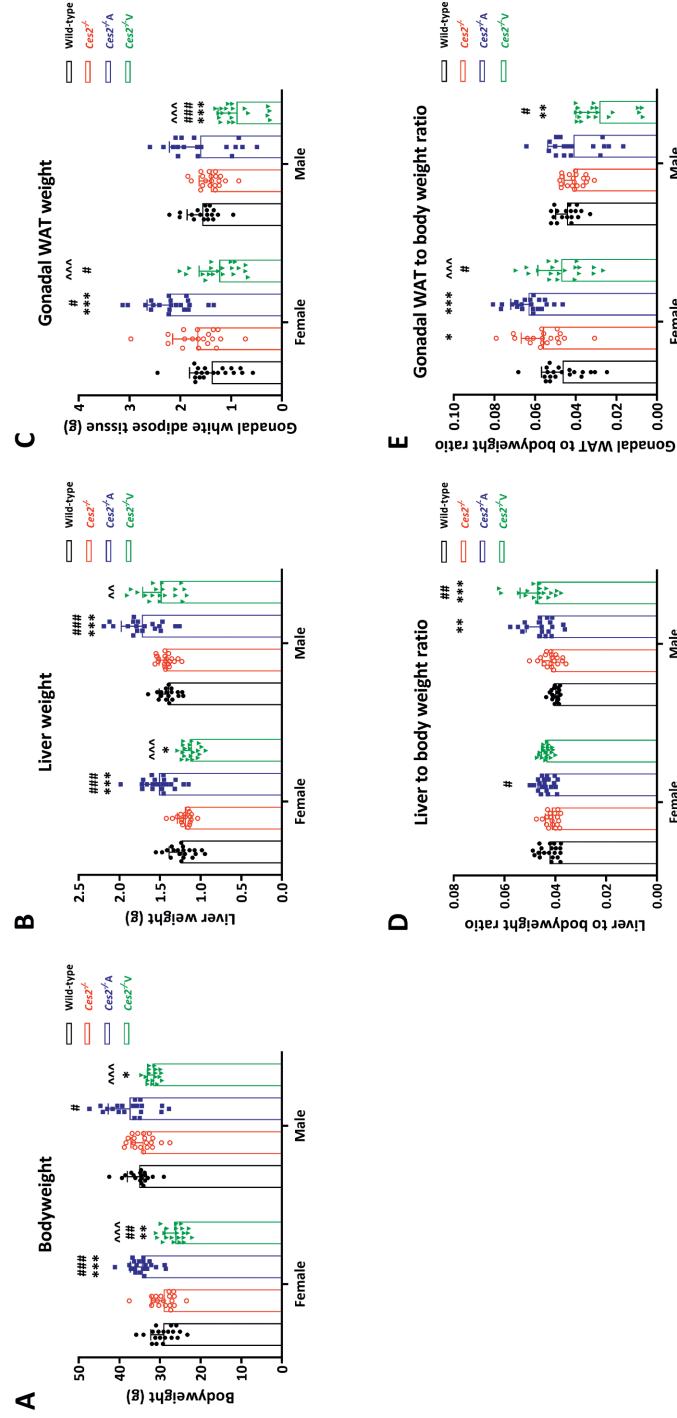
Supplemental Figure 15. Liver, kidney, spleen, small intestine (SI) and colon 5'-DFUR concentrations (A, C, E, G and I), and 5'-DFUR tissue-to-plasma concentration ratios (B, D, F, H and J) in female wild-type, *Ces2*^{-/-}, *Ces2*^{-/A} and *Ces2*^{-/V} mice over 2 h after oral administration of 500 mg/kg capecitabine. Data are given as mean \pm S.D. ($n = 5 - 7$). *, $P < 0.05$; **, $P < 0.01$; ***, $P < 0.001$ compared to wild-type mice; #, $P < 0.05$; ##, $P < 0.01$; ###, $P < 0.001$ compared to *Ces2*^{-/-} mice. ^, $P < 0.05$; ^^, $P < 0.01$; ^^, $P < 0.001$ for comparison between *Ces2*^{-/A} and *Ces2*^{-/V} mice. Statistical analysis was applied after log-transformation of linear data.



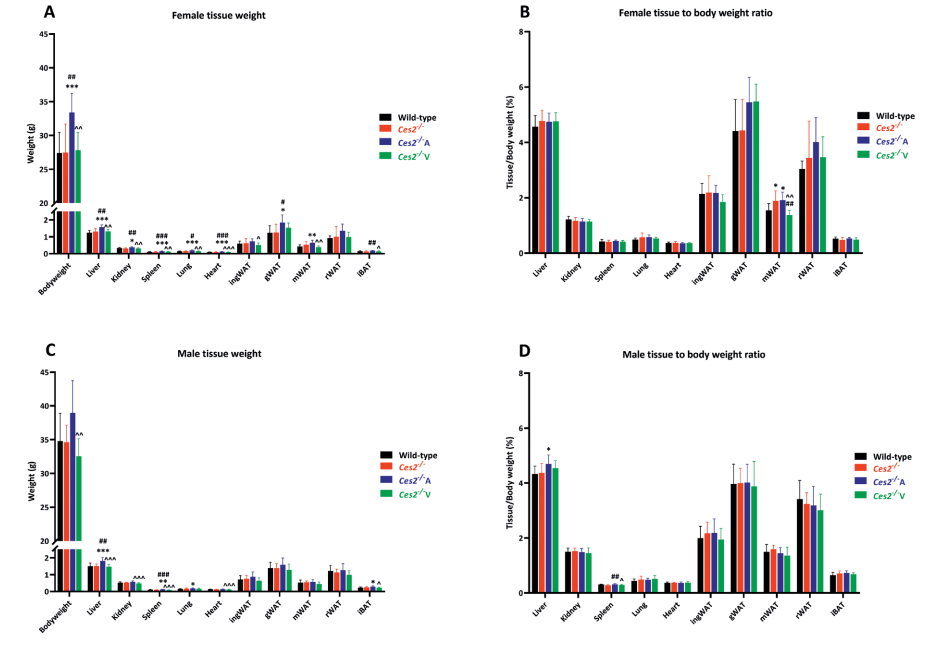
Supplemental Figure 16. Liver, kidney, spleen, small intestine (SI) and colon 5-FU concentrations (A, C, E, G and I), and 5-FU tissue-to-plasma concentration ratios (B, D, F, H and J) in female wild-type, *Ces2*^{-/-}, *Ces2*^{+A} and *Ces2*^{+V} mice over 2 h after oral administration of 500 mg/kg capecitabine. Data are given as mean \pm S.D. (n = 5 - 7). *, $P < 0.05$; **, $P < 0.01$; ***, $P < 0.001$ compared to wild-type mice; #, $P < 0.05$; ##, $P < 0.01$; ###, $P < 0.001$ compared to *Ces2*^{-/-} mice. ^, $P < 0.05$; ^^, $P < 0.01$; ^^, $P < 0.001$ for comparison between *Ces2*^{+A} and *Ces2*^{+V} mice. Statistical analysis was applied after log-transformation of linear data.



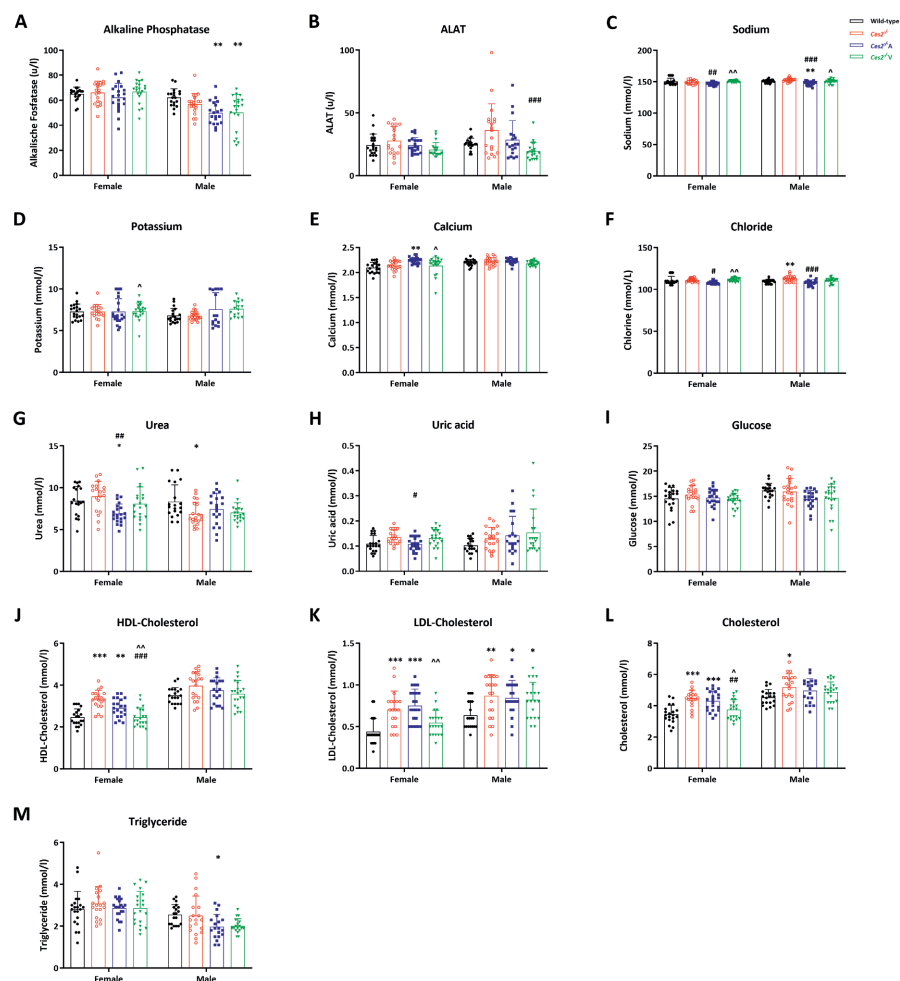
Supplemental Figure 17. Liver, kidney, spleen, small intestine (SI) and colon FBAL concentrations (A, C, E, G and I), and FBAL tissue-to-plasma concentration ratios (B, D, F, H and J) in female wild-type, *Ces2*^{-/-}, *Ces2*^{+A} and *Ces2*^{+V} mice over 2 h after oral administration of 500 mg/kg capecitabine. Data are given as mean \pm S.D. (n = 5 - 7). *, $P < 0.05$; **, $P < 0.01$; ***, $P < 0.001$ compared to wild-type mice; #, $P < 0.05$; ##, $P < 0.01$; ###, $P < 0.001$ compared to *Ces2*^{-/-} mice. ^, $P < 0.05$; ^^, $P < 0.01$; ^^, $P < 0.001$ for comparison between *Ces2*^{+A} and *Ces2*^{+V} mice. Statistical analysis was applied after log-transformation of linear data.



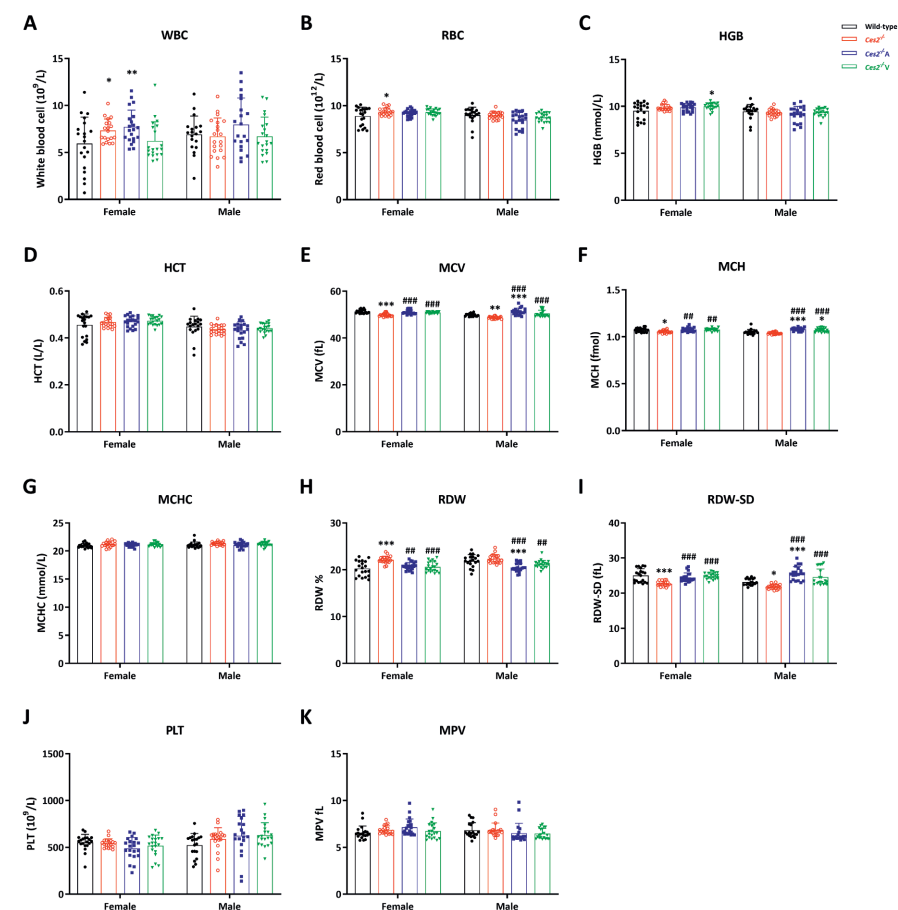
Supplemental Figure 18. Bodyweight (A), liver weight (B), gonadal white adipose tissue (gWAT) weight (C), liver to bodyweight ratio (D) and gWAT to bodyweight ratio (E) of 20 weeks old female and male wild-type, *Ces2^{-/-}*, *Ces2^{-/A}* and *Ces2^{-/V}* mice. Data are given as mean \pm S.D. (n = 19 - 20). *, $P < 0.05$; **, $P < 0.01$; ***, $P < 0.001$ compared to wild-type mice; #, $P < 0.05$; ##, $P < 0.01$; ###, $P < 0.001$ compared to *Ces2^{-/-}* mice. ^, $P < 0.05$; ^^, $P < 0.01$; ^^, $P < 0.001$ for comparison between *Ces2^{-/A}* and *Ces2^{-/V}* mice. Statistical analysis was applied after log-transformation of linear data.



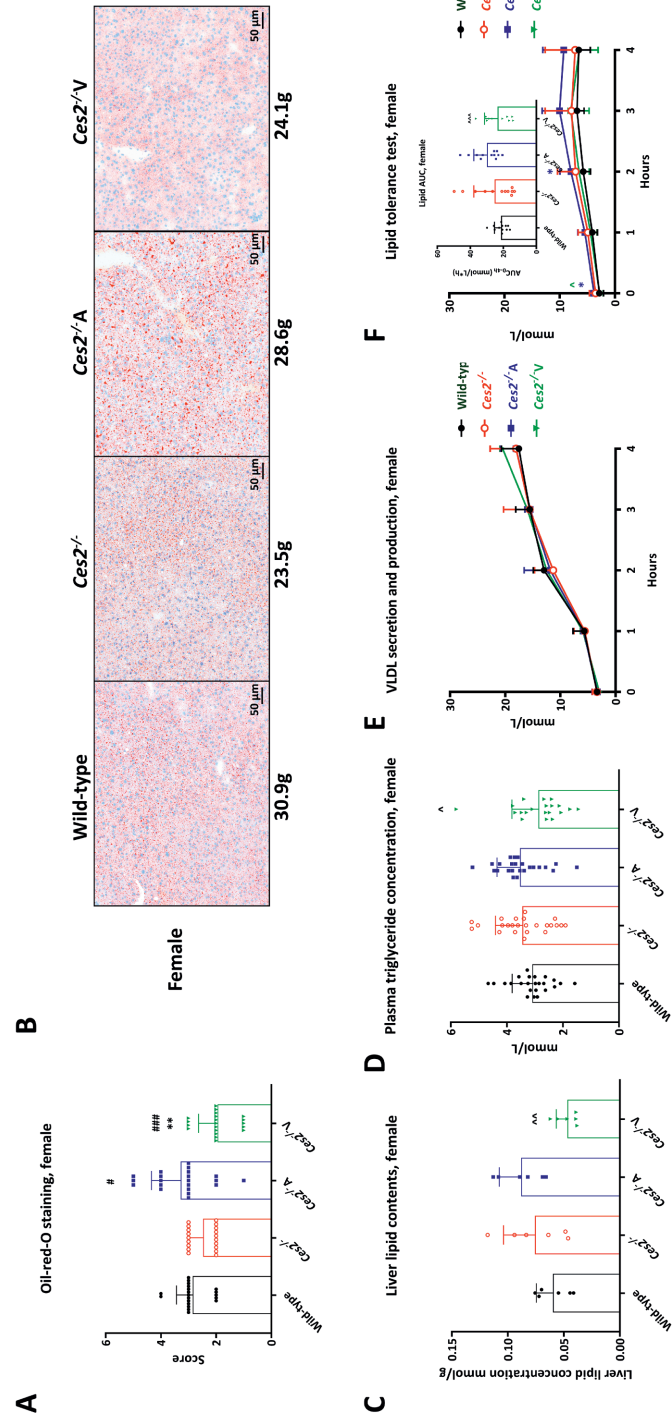
Supplemental Figure 19. Bodyweight and weights of different tissues and tissue to bodyweight ratios in young adult (12-weeks old) female (A and B) and male (C and D) mice from wild-type, *Ces2^{-/-}*, *Ces2^{-/A}* and *Ces2^{-/V}* mouse strains. IngWAT: inguinal white adipose tissue; gWAT: gonadal white adipose tissue; mWAT: mediastinal brown adipose tissue; rWAT: renal white adipose tissue; iBAT: interscapular brown adipose tissue. Data are given as mean \pm S.D. (n = 9 - 16). *, $P < 0.05$; **, $P < 0.01$; ***, $P < 0.001$ compared to wild-type mice; #, $P < 0.05$; ##, $P < 0.01$; ###, $P < 0.001$ compared to *Ces2^{-/-}* mice. ^, $P < 0.05$; ^^, $P < 0.01$; ^^, $P < 0.001$ for comparison between *Ces2^{-/A}* and *Ces2^{-/V}* mice. Statistical analysis was applied after log-transformation of linear data.



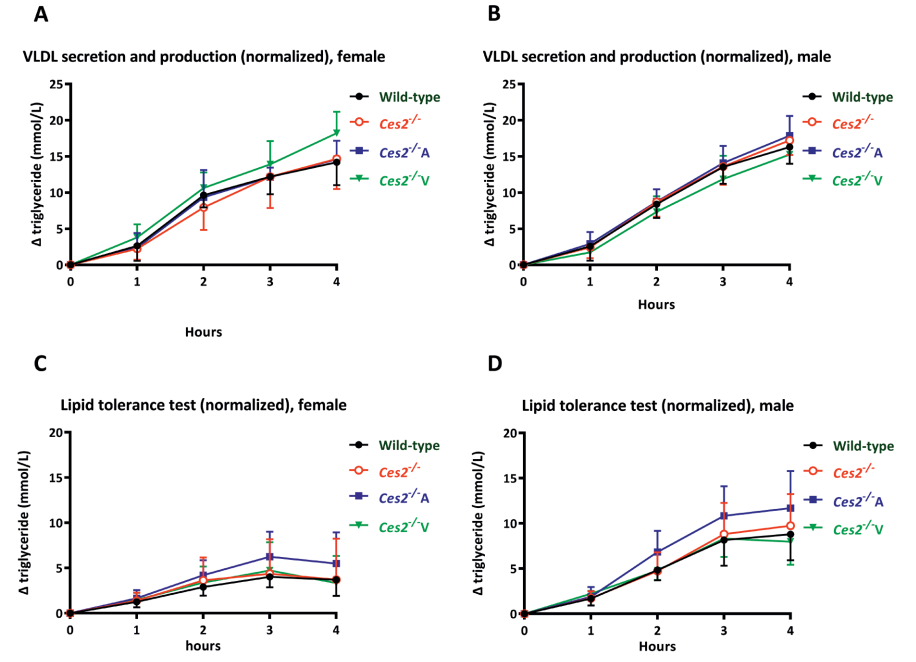
Supplemental Figure 20. Plasma alkaline phosphatase (A), ALAT (B), sodium (C), potassium (D), calcium (E), chloride (F), urea (G), uric acid (H), glucose (I), HDL-Cholesterol (J), LDL-Cholesterol (K), total cholesterol (L) and triglyceride (M) concentrations in female and male wild-type, *Ces2*^{-/-}, *Ces2*^{-/-A} and *Ces2*^{-/-V} 20-week old mice. Data are given as mean \pm S.D. (n = 15 - 21). *, $P < 0.05$; **, $P < 0.01$; ***, $P < 0.001$ compared to wild-type mice; #, $P < 0.05$; ##, $P < 0.01$; ###, $P < 0.001$ compared to *Ces2*^{-/-} mice. ^, $P < 0.05$; ^^, $P < 0.01$; ^^, $P < 0.001$ for comparison between *Ces2*^{-/-A} and *Ces2*^{-/-V} mice. Statistical analysis was applied after log-transformation of linear data.



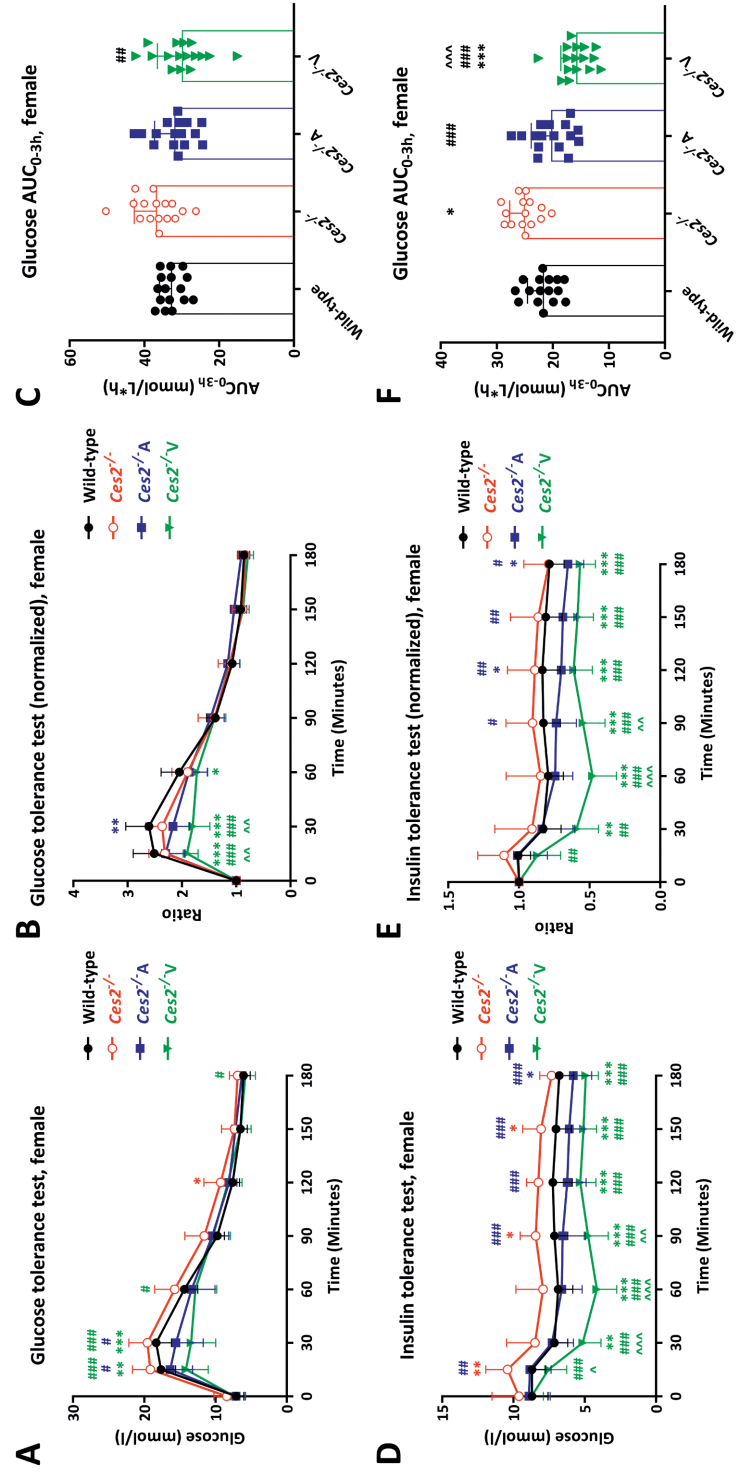
Supplemental Figure 21. Hematology analysis of WBC (A), RBC (B), HGB (C), HCT (D), MCV (E), MCH (F), MCHC (G), RDW (H), RDW-SD (I), PLT (J) and MPV (K) in female and male wild-type, *Ces2*^{-/-}, *Ces2*^{-/-A} and *Ces2*^{-/-V} 20-week old mice. Data are given as mean \pm S.D. (n = 19 - 21). WBC: white blood cells; RBC: red blood cells; HGB: hemoglobin; HCT: hematocrit (the relative volume of packed erythrocytes to whole blood); MCV: mean Corpuscular Volume (the average volume of individual erythrocytes derived from the RBC histogram, multiplied by a calibration factor); MCH: mean corpuscular hemoglobin (the weight of HGB in the average erythrocyte); MCHC: mean corpuscular hemoglobin concentration (the average weight of HGB in a measured dilution); RDW: red cell distribution width; RDW-SD: red cell distribution width - SD; PLT: platelet count or thrombocyte count; MPV: mean platelet volume; *, $P < 0.05$; **, $P < 0.01$; ***, $P < 0.001$ compared to wild-type mice; #, $P < 0.05$; ##, $P < 0.01$; ###, $P < 0.001$ compared to *Ces2*^{-/-} mice. ^, $P < 0.05$; ^^, $P < 0.01$; ^^, $P < 0.001$ for comparison between *Ces2*^{-/-A} and *Ces2*^{-/-V} mice. Statistical analysis was applied after log-transformation of linear data.



Supplemental Figure 22. Lipid disposition, metabolism and homeostasis in the CES2 mouse models. Oil-red-O staining lipid droplet levels (A) and representative Oil-red-O staining images for liver lipid accumulation for each mouse strain (B) in female wild-type, *Ces2^{-/-}*, *Ces2^{-/A}* and *Ces2^{-/V}* 20-week old mice (n = 19 - 21); Liver lipid contents in female wild-type, *Ces2^{-/-}*, *Ces2^{-/A}* and *Ces2^{-/V}* 20-week old mice (n = 8); Plasma triglyceride basal concentration (overnight fast) before VLDL production and secretion and oral lipid tolerance test in female wild-type, *Ces2^{-/-}*, *Ces2^{-/A}* and *Ces2^{-/V}* 12-week old mice (n = 20 - 24) (D), VLDL production and secretion (E) and oral lipid tolerance test (F) in female wild-type, *Ces2^{-/-}*, *Ces2^{-/A}* and *Ces2^{-/V}* 12-week old mice (n = 10 - 12). Data are given as mean \pm S.D. *, $P < 0.05$; **, $P < 0.01$; ***, $P < 0.001$ compared to wild-type mice; #, $P < 0.05$; ##, $P < 0.01$; ###, $P < 0.001$ compared to *Ces2^{-/-}* mice. ^, $P < 0.05$; ^^, $P < 0.01$; ^^, $P < 0.001$ for comparison between *Ces2^{-/A}* and *Ces2^{-/V}* mice. Statistical analysis was applied after log-transformation of linear data.



Supplemental Figure 23. Plasma triglyceride concentration above basal triglyceride concentration time curve in VLDL production and secretion test (A and B) or oral lipid tolerance test (C and D) in wild-type, *Ces2^{-/-}*, *Ces2^{-/A}* and *Ces2^{-/V}* 12-week old mice (n = 10 - 12). Mice were fasted overnight before the experiment. The base-line triglyceride plasma concentrations at the start of the experiment (t = 0) were subtracted from the measured triglyceride concentrations at each time point. Data are given as mean \pm S.D. *, $P < 0.05$; **, $P < 0.01$; ***, $P < 0.001$ compared to wild-type mice; #, $P < 0.05$; ##, $P < 0.01$; ###, $P < 0.001$ compared to *Ces2^{-/-}* mice. ^, $P < 0.05$; ^^, $P < 0.01$; ^^, $P < 0.001$ for comparison between *Ces2^{-/A}* and *Ces2^{-/V}* mice. Statistical analysis was applied after log-transformation of linear data.



Supplemental Figure 24. Glucose metabolism and homeostasis in the CES2 mouse models. The plasma concentration time curve (A), plasma glucose concentration to basal glucose concentration (before glucose administration) ratio time curve (B) and glucose AUC_{0-3h} (C) in female wild-type, *Ces2*^{-/-}, *Ces2*^{-/-A} and *Ces2*^{-/-V} 12-week old mice over a 3 h glucose tolerance test after oral administration of 1 mg/g glucose; The plasma glucose concentration time curve (D), plasma glucose concentration to basal glucose concentration (before insulin injection) ratio time curve (E) and glucose AUC_{0-3h} (F) in female wild-type, *Ces2*^{-/-}, *Ces2*^{-/-A} and *Ces2*^{-/-V} 16-week old mice over a 3-h insulin tolerance test after i.p. injection of 0.5 U/kg insulin. Data are given as mean \pm S.D. (n = 15 - 16). *, P < 0.05; **, P < 0.01; ***, P < 0.001 compared to wild-type mice; #, P < 0.05; ##, P < 0.01; ###, P < 0.001 compared to *Ces2*^{-/-} mice. ^, P < 0.05; ^^, P < 0.01; ^^, P < 0.001 for comparison between *Ces2*^{-/-A} and *Ces2*^{-/-V} mice. Statistical analysis was applied after log-transformation of linear data.

Supplemental Table 1. The primers for PCR analysis of each *Ces2* gene present in the genome, except for the *Ces2d* pseudogene.

| Genes | | Sequence | Length | Products |
|--------------|---------|----------------------|--------|----------|
| <i>Ces2a</i> | FORWARD | TGAGCCAAGCAGAACATCAG | 20 | 335 |
| | REVERSE | GCGAACCTAAGCCTGGTT | 19 | |
| <i>Ces2b</i> | FORWARD | TCAGCCTGGAGGCTAACTCT | 20 | 345 |
| | REVERSE | GAGAGCTGAGGAGTCCCCTA | 20 | |
| <i>Ces2c</i> | FORWARD | GCTTTACTGGTGTACGTGGC | 20 | 342 |
| | REVERSE | ACAAATGCCCTCTCCCAA | 20 | |
| <i>Ces2e</i> | FORWARD | TTCTTGAGCTGGATGGAGTT | 21 | 471 |
| | REVERSE | AGCAGTTGGGGGAAGGGTAA | 20 | |
| <i>Ces2f</i> | FORWARD | CATAGCACACTGGGGTCCAG | 20 | 695 |
| | REVERSE | TCCGCATGGCCTAGATGTTG | 20 | |
| <i>Ces2g</i> | FORWARD | GGCATGAAACGTGAGTCTCC | 21 | 285 |
| | REVERSE | TGCCACCTCATGTAAGTCT | 20 | |
| <i>Ces2h</i> | FORWARD | CTAACCCCGGACCTGTG | 20 | 302 |
| | REVERSE | TCTGCCACTCCTCAAACCC | 21 | |

Supplemental Table 2. Overview of ΔC_t values of the RT-qPCR analysis to investigate expression of *Ces1*, *Ces2* and *Ces3* cluster genes in liver and small intestine of wild-type and *Ces2*^{-/-} mice (n = 4). Quantification of the target cDNAs in all samples was normalized against the endogenous control GAPDH ($\Delta C_t = C_{\text{target}} - C_{\text{GAPDH}}$). Accordingly, the lower the value, the higher the expression level. *, $P < 0.05$; **, $P < 0.01$; ***, $P < 0.001$ compared to wild-type mice.

| Gene | Liver | | Small intestine | |
|--------------|--------------|----------------------------|-----------------|----------------------------|
| | Wild-Type | <i>Ces2</i> ^{-/-} | Wild-Type | <i>Ces2</i> ^{-/-} |
| <i>Ces1a</i> | 12.8 ± 0.6 | 12.7 ± 0.5 | 14.4 ± 0.7 | 15.5 ± 1.2 |
| <i>Ces1b</i> | -3.0 ± 0.3 | -3.2 ± 0.4 | 3.7 ± 0.6 | 3.6 ± 0.3 |
| <i>Ces1c</i> | -1.9 ± 0.2 | -2.1 ± 0.5 | 7.4 ± 0.1 | 7.5 ± 0.3 |
| <i>Ces1d</i> | 1.9 ± 0.7 | 0.8 ± 0.9 | 6.4 ± 0.3 | 5.5 ± 1.0 |
| <i>Ces1e</i> | 2.1 ± 0.4 | 1.8 ± 0.2 | 6.7 ± 0.4 | 6.4 ± 0.3 |
| <i>Ces1f</i> | 2.0 ± 0.3 | 1.8 ± 0.3 | 3.9 ± 0.2 | 3.7 ± 0.3 |
| <i>Ces1g</i> | 3.2 ± 0.8 | 2.5 ± 0.7 | 6.1 ± 0.5 | 5.8 ± 0.5 |
| <i>Ces1h</i> | 14.7 ± 2.1 | 13.8 ± 1.2 | 10.4 ± 1.8 | 11.1 ± 1.2 |
| <i>Ces2a</i> | 2.1 ± 0.3 | 15.2 ± 1.2*** | 2.6 ± 0.4 | 14.4 ± 1.1*** |
| <i>Ces2b</i> | 4.1 ± 0.6 | 13.4 ± 0.6*** | 1.6 ± 0.3 | 12.7 ± 0.4*** |
| <i>Ces2c</i> | 2.1 ± 0.5 | 16.6 ± 0.5*** | 1.0 ± 0.2 | 16.9 ± 0.8*** |
| <i>Ces2e</i> | 3.2 ± 0.4 | 18.9 ± 1.3*** | 0.4 ± 0.2 | 20.6 ± 0.9*** |
| <i>Ces2f</i> | 17.2 ± 2.9 | 18.8 ± 1.2 | 13.9 ± 0.4 | 19.9 ± 0.9*** |
| <i>Ces2g</i> | 5.5 ± 0.3 | 16.3 ± 2.1*** | 6.7 ± 0.4 | 13.7 ± 0.9*** |
| <i>Ces2h</i> | 12.9 ± 0.8 | 18.2 ± 2.0** | 8.9 ± 0.8 | 16.5 ± 0.8*** |
| <i>Ces3a</i> | -0.04 ± 0.97 | -0.09 ± 0.61 | 10.69 ± 0.14 | 13.83 ± 0.52*** |
| <i>Ces3b</i> | 2.11 ± 0.64 | 1.97 ± 0.47 | 14.71 ± 0.27 | 17.94 ± 1.03*** |

Supplemental Table 3. Tissue pharmacokinetic parameters of vinorelbine and its active metabolite deacetylvinorelbine in male wild-type, *Ces2*^{-/-}, *Ces2*^{-/-}A and *Ces2*^{-/-}V mice over 4 h after oral administration or i.v. injection of 10 mg/kg vinorelbine.

| Tissue Parameter | Genotype/Groups | | | |
|---|---------------------|----------------------------|------------------------------|------------------------------|
| | Oral administration | | I.V. Injection | |
| | Wild-type | <i>Ces2</i> ^{-/-} | <i>Ces2</i> ^{-/-} A | <i>Ces2</i> ^{-/-} V |
| $C_{\text{Vinorelbine}}$ ng/g | 1530 ± 409 | 8470 ± 8152*** | 8520 ± 3445*** | 8304 ± 2003*** |
| $C_{\text{Deacetylvinorelbine}}$ Ratio (x 10 ⁻³) | 7589 ± 2725 | 82 ± 29*** | 162 ± 52***## | 178 ± 110***## |
| C_{S1} ng/g | 5000 ± 1000 | 15 ± 7.5*** | 19 ± 1.7*** | 21 ± 7.8*** |
| C_{SIC} ng/g | 10755 ± 3700 | 18335 ± 4305 | 18081 ± 3649 | 15629 ± 6976 |
| C_{SIC} ng/g | 9590 ± 4337 | 625 ± 219*** | 748 ± 225*** | 808 ± 578*** |
| C_{SIC} ng/g | 880 ± 220 | 34 ± 10.0*** | 39 ± 8.0*** | 49 ± 15*** |
| C_{SIC} ng/g | 76985 ± 29328 | 158738 ± 46695** | 177344 ± 72971** | 113728 ± 19392 |
| C_{SIC} ng/g | 15491 ± 4320 | 1091 ± 405*** | 1120 ± 623*** | 957 ± 441*** |
| C_{SIC} ng/g | 220 ± 73 | 6.7 ± 1.4*** | 5.9 ± 1.6*** | 8.4 ± 3.4*** |
| C_{SIC} ng/g | 348 ± 136 | 581 ± 175 | 788 ± 189** | 608 ± 203* |
| C_{SIC} ng/g | 369 ± 240 | 5.0 ± 2.1*** | 6.0 ± 2.6*** | 8.1 ± 4.8*** |
| C_{SIC} ng/g | 1000 ± 390 | 8.4 ± 1.5*** | 7.8 ± 2.6*** | 13 ± 3.7*** |
| C_{SIC} ng/g | | | 340 ± 70 | 9.4 ± 3.8*** |
| C_{SIC} ng/g | | | 47236 ± 30865 | 7.0 ± 3.7*** |
| C_{SIC} ng/g | | | 400 ± 315*** | 48363 ± 27038 |
| C_{SIC} ng/g | | | 1000 ± 270 | 511 ± 322*** |
| C_{SIC} ng/g | | | 8.1 ± 1.1*** | 10 ± 1.0***## |
| C_{SIC} ng/g | | | 5625 ± 2998* | 6745 ± 1469** |
| C_{SIC} ng/g | | | 58 ± 45*** | 120 ± 45***A |
| C_{SIC} ng/g | | | 42 ± 43*** | 17 ± 2.2***AA |
| C_{SIC} ng/g | | | 25 ± 7.0*** | 17 ± 2.2***AA |
| C_{SIC} ng/g | | | 21 ± 1.9*** | 14 ± 1.0*** |
| C_{SIC} ng/g | | | 5925 ± 1348** | 22 ± 6.6*** |
| C_{SIC} ng/g | | | 5604 ± 644* | 7682 ± 2242*** |
| C_{SIC} ng/g | | | 79 ± 13*** | 134 ± 47***A |
| C_{SIC} ng/g | | | 14 ± 1.0*** | 17 ± 2.2***AA |
| C_{SIC} ng/g | | | 24326 ± 3721*** | 24682 ± 4451*** |
| C_{SIC} ng/g | | | 584 ± 157*** | 513 ± 61*** |
| C_{SIC} ng/g | | | 23365 ± 6113** | 22 ± 6.6*** |
| C_{SIC} ng/g | | | 487 ± 127*** | 22 ± 6.6*** |
| C_{SIC} ng/g | | | 2500 ± 1300 | 22 ± 6.6*** |
| C_{SIC} ng/g | | | 3466 ± 858 | 22 ± 6.6*** |
| C_{SIC} ng/g | | | 2214 ± 605 | 22 ± 6.6*** |
| C_{SIC} ng/g | | | 630 ± 46 | 22 ± 6.6*** |
| C_{SIC} ng/g | | | 27651 ± 13355 | 22 ± 6.6*** |
| C_{SIC} ng/g | | | 27594 ± 13421 | 22 ± 6.6*** |
| C_{SIC} ng/g | | | 1000 ± 270 | 22 ± 6.6*** |
| C_{SIC} ng/g | | | 2361 ± 692 | 22 ± 6.6*** |
| C_{SIC} ng/g | | | 780 ± 199 | 22 ± 6.6*** |
| C_{SIC} ng/g | | | 340 ± 70 | 22 ± 6.6*** |
| C_{SIC} ng/g | | | 47236 ± 30865 | 22 ± 6.6*** |
| C_{SIC} ng/g | | | 400 ± 315*** | 22 ± 6.6*** |
| C_{SIC} ng/g | | | 8.1 ± 1.1*** | 22 ± 6.6*** |
| C_{SIC} ng/g | | | 5625 ± 2998* | 22 ± 6.6*** |
| C_{SIC} ng/g | | | 58 ± 45*** | 22 ± 6.6*** |
| C_{SIC} ng/g | | | 42 ± 43*** | 22 ± 6.6*** |
| C_{SIC} ng/g | | | 7.0 ± 3.7*** | 22 ± 6.6*** |

Data are given as mean ± S.D. (n = 6). $C_{\text{Vinorelbine}}$, liver concentration; C_{S1} , small intestine (tissue); C_{SIC} , testis concentration; *, $P < 0.05$; **, $P < 0.01$; ***, $P < 0.001$ compared to wild-type mice; #, $P < 0.05$; ##, $P < 0.01$; ###, $P < 0.001$ compared to *Ces2*^{-/-} mice; A, $P < 0.05$; AA, $P < 0.01$; AAA, $P < 0.001$ for comparison between *Ces2*^{-/-}A and *Ces2*^{-/-}V mice. Statistical analysis was applied after log-transformation of linear data and compared within either oral administration groups or i.v. injection groups.

Supplemental Table 4. Tissue pharmacokinetic parameters of capecitabine and its metabolites 5'-DFCR, 5'-DFUR, 5'-FU and FBAL in female wild-type, *Ces2^{-/-}*, *Ces2^{-/-}* A and *Ces2^{-/-}* V mice over 2 h after oral administration of 500 mg/kg capecitabine.

| Tissue Parameter | Genotype/Groups | | |
|------------------------------|---------------------|---------------------------|-----------------------------|
| | Oral administration | | |
| | Wild-type | <i>Ces2^{-/-}</i> | <i>Ces2^{-/-}</i> V |
| Capecitabine | 1302 ± 522 | 18001 ± 8744*** | 4649 ± 1760***# |
| 5'-DFCR | 20310 ± 5741 | 33333 ± 11604 | 36650 ± 5867 |
| Ratio (5'-DFCR/capecitabine) | 17.4 ± 7.3 | 2.0 ± 0.6*** | 8.8 ± 3.6***## |
| 5'-DFUR | 1750 ± 637 | 3447 ± 1643 | 2628 ± 793 |
| Ratio (5'-DFUR/capecitabine) | 1.60 ± 0.96 | 0.21 ± 0.09*** | 0.66 ± 0.37***# |
| 5-FU | 747 ± 184 | 1525 ± 765 | 2141 ± 372** |
| Ratio (5-FU/Capecitabine) | 0.65 ± 0.31 | 0.09 ± 0.03*** | 0.52 ± 0.25### |
| FBAL | 55840 ± 13861 | 59839 ± 11722 | 102959 ± 17203***### |
| Ratio (FBAL /Capecitabine) | 48 ± 19 | 4.2 ± 2.7*** | 25 ± 11### |
| Capecitabine | 1631 ± 865 | 17217 ± 6548*** | 15234 ± 6017*** |
| 5'-DFCR | 4514 ± 1341 | 5414 ± 1430 | 6224 ± 1826 |
| Ratio (5'-DFCR/Capecitabine) | 3.20 ± 1.70 | 0.36 ± 0.20*** | 0.45 ± 0.21*** |
| 5'-DFUR | 2119 ± 460 | 5099 ± 1783* | 4632 ± 1545 |
| Ratio (5'-DFUR/Capecitabine) | 1.50 ± 0.62 | 0.32 ± 0.13*** | 0.33 ± 0.12*** |
| 5-FU | 3016 ± 835 | 5201 ± 2037 | 4427 ± 1508 |
| Ratio (5-FU/Capecitabine) | 2.1 ± 0.8 | 0.32 ± 0.10*** | 0.32 ± 0.11*** |
| FBAL | 1174 ± 174 | 1239 ± 335 | 2193 ± 960***# |
| Ratio (FBAL /Capecitabine) | 0.86 ± 0.38 | 0.08 ± 0.05*** | 0.15 ± 0.04*** |
| | | | 1.5 ± 2.0###^^^ |

Supplemental Table 4. Tissue pharmacokinetic parameters of capecitabine and its metabolites 5'-DFCR, 5'-DFUR, 5'-FU and FBAL in female wild-type, *Ces2^{-/-}*, *Ces2^{-/-}* A and *Ces2^{-/-}* V mice over 2 h after oral administration of 500 mg/kg capecitabine. (continued)

| Tissue Parameter | Genotype/Groups | | |
|---|---------------------|---------------------------|-----------------------------|
| | Oral administration | | |
| | Wild-type | <i>Ces2^{-/-}</i> | <i>Ces2^{-/-}</i> V |
| Capecitabine | 26460 ± 16294 | 97216 ± 37177** | 88454 ± 25100** |
| 5'-DFCR | 4408 ± 2348 | 10829 ± 5610 | 8123 ± 2843 |
| Ratio (5'-DFCR/Capecitabine) | 0.19 ± 0.08 | 0.11 ± 0.04 | 0.10 ± 0.06 |
| 5'-DFUR | 1759 ± 941 | 3905 ± 2357 | 2689 ± 1092 |
| Ratio (5'-DFUR/Capecitabine) | 0.077 ± 0.032 | 0.036 ± 0.016 | 0.035 ± 0.025 |
| 5-FU | 125 ± 90 | 200 ± 109 | 142 ± 64 |
| Ratio (x 10 ⁻³) (5-FU/Capecitabine) | 5.1 ± 3.4 | 2.1 ± 0.7 | 1.9 ± 1.6* |
| FBAL | N.A. | N.A. | N.A. |
| Ratio (FBAL /Capecitabine) | N.A. | N.A. | N.A. |
| Capecitabine | 2249 ± 712 | 14273 ± 9019*** | 8776 ± 1631** |
| 5'-DFCR | 14904 ± 3800 | 25745 ± 10651 | 28240 ± 5874 |
| Ratio (5'-DFCR/Capecitabine) | 6.9 ± 1.3 | 2.0 ± 0.4*** | 3.2 ± 0.2***# |
| 5'-DFUR | 2694 ± 755 | 4754 ± 3040 | 3692 ± 793 |
| Ratio (5'-DFUR/Capecitabine) | 1.2 ± 0.3 | 0.34 ± 0.06*** | 0.42 ± 0.06*** |
| 5-FU | 1186 ± 486 | 1829 ± 1013 | 1455 ± 233 |
| Ratio (5-FU/Capecitabine) | 0.53 ± 0.09 | 0.14 ± 0.03*** | 0.17 ± 0.02*** |
| FBAL | 1322 ± 249 | 1355 ± 281 | 2105 ± 600***# |
| Ratio (FBAL /Capecitabine) | 0.62 ± 0.16 | 0.12 ± 0.05*** | 0.24 ± 0.02*** |
| | | | 6.8 ± 3.0###^^ |
| | | | N.A. |
| | | | N.A. |
| | | | 4966 ± 2983## |
| | | | 21166 ± 8096 |
| | | | 5.1 ± 2.1### |
| | | | 5426 ± 27021.6 |
| | | | 1.2 ± 0.5###^^^ |
| | | | 2103 ± 1022 |
| | | | 0.50 ± 0.18###^^^ |
| | | | 2080 ± 446***# |
| | | | 0.60 ± 0.36###^^ |

Data are given as mean ± S.D. (n = 6). C_{liver}, liver concentration; S_I, small intestine (tissue); S_IC, small intestine contents; C_{testis}, testis concentration; N.A., Not applicable; *, P < 0.05; **, P < 0.01; ***, P < 0.001 compared to wild-type mice; #, P < 0.05; ##, P < 0.01; ###, P < 0.001 compared to *Ces2^{-/-}* mice; ^, P < 0.05; ^^, P < 0.01; ^^, P < 0.001 for comparison between *Ces2^{-/-}* A and *Ces2^{-/-}* V mice. Statistical analysis was applied after log-transformation of linear data and compared within either oral administration groups or i.v. injection groups.



PART II.

**THE EFFECTS OF DRUG TRANSPORTERS AND
CYP3A ENZYMES ON THE PHARMACOKINETICS
OF SELECTIVE ANTI-TUMOR SMALL MOLECULAR
INHIBITORS**



CHAPTER 3

Introduction: The roles of drug transporters and metabolizing enzymes

Yaogeng Wang, Jos H. Beijnen, Alfred H. Schinkel

INTRODUCTION

Drug absorption, distribution, metabolism and excretion (ADME) can be influenced by certain detoxification systems. Drug transporters and drug-metabolizing enzymes are two major detoxification systems that can be heavily involved in the ADME processes, influencing drug pharmacokinetic profiles, and hence efficacy and safety. As many endogenous compounds can also be modulated by these transmembrane transporters and metabolizing enzymes, they can also affect physiological balance, even metabolic disorders¹.

Efflux and influx transporters including many ATP-binding cassette (ABC) transporters and organic anion transporting polypeptides (OATPs) have been demonstrated to influence the drug ADME process with broad substrate specificity¹⁻³. Within the ABC efflux transporters, ABCB1 (P-glycoprotein: P-gp) and ABCG2 (breast cancer resistance protein: BCRP) are probably the best studied members. Both of them are mainly expressed at the apical membrane of enterocytes, hepatocytes and renal tubular epithelial cells, tissues which are all strongly related to drug detoxification and/or elimination. They could thus limit intestinal absorption of their substrates or mediate their direct intestinal, hepatobiliary or renal excretion. In addition, ABCB1 and ABCG2 are also highly expressed in some critical physiological barriers, for instance brain capillary endothelial cells of the blood-brain barrier (BBB). The efflux capacity of these transporters can protect the central nervous system (CNS) from exogenous toxic compounds⁴. On the other hand, this will also result in reduced exposure of the brain to substrate anticancer drugs, and subsequently potentially limit the drug therapeutic efficacy, especially against brain metastases⁵⁻⁸. Moreover, ABCB1 and ABCG2 are also expressed to various extents in many tumor types, potentially mediating multidrug resistance against anticancer drugs⁴.

Organic anion-transporting polypeptides (OATPs, encoded by *SLCO* genes) are sodium-independent transmembrane uptake transporters, which contribute to uptake of endogenous and exogenous compounds like hormones, toxins, and numerous drugs⁹. The *SLCO1A/1B* proteins are of particular interest in this thesis because of their broad substrate specificities and their high expression in the liver, where they may affect oral availability and liver disposition of certain drugs¹⁰⁻¹⁴.

Besides the various transporters, the Cytochrome P450 3A (CYP3A) enzyme complex is one of the most important multidrug-metabolizing enzyme families, responsible for most Phase I drug metabolism. CYP3A4, highly expressed in human liver, is involved in the metabolism of about 50% of the currently used drugs, resulting in drug inactivation or sometimes also activation¹⁵⁻¹⁷. The high variation in activity of CYP3A enzymes between, but also within, individuals due to drug-drug or diet-drug interactions or genetic polymorphisms can cause oral availability and

plasma exposure differences among patients, which may dramatically affect their therapeutic efficacy and toxicity.

In part II of this thesis we explored the roles of two ABC efflux transporters (ABCB1 and ABCG2), one group of *SLCO* uptake transporters (*SLCO1A/1B*), and the Cytochrome P450 3A4 (CYP3A4) enzyme in pharmacokinetic properties for several targeted small-molecule inhibitors, as well as the potential influence of drug-drug interactions (DDIs), using genetically modified cell lines and mouse strains. Obtained insights may provide useful information for future drug development and clinical pharmacotherapy regimes.

ABCB1 (P-GLYCOPROTEIN: P-GP) AND ABCG2 (BREAST CANCER RESISTANCE PROTEIN: BCRP)

The ATP-binding cassette (ABC) transporters utilize ATP hydrolysis and function as efflux transporters to translocate a variety of substrates across extra- and intra-cellular membranes¹. The human ABCB transporter subfamily consists of 11 members. Among them, ABCB1 (P-gp) was the first human ABC transporter cloned and characterized because of its ability to cause multidrug resistance in cancer cells¹⁸. With a broad substrate specificity (with generally preference for hydrophobic or amphipathic compounds), ABCB1 has been shown to recognize hundreds, if not thousands, of compounds ranging from small molecules to oligo- and perhaps even polypeptides. Humans have only one *ABCB1* gene, whereas rodents contain two drug-transporting P-gp homologues, encoded by *Abcb1a* and *Abcb1b*, respectively. These share approximately 85% amino acid identity with each other and > 80% amino acid identity with human ABCB1¹⁹.

ABCB1 is expressed highly in several important tissues, including liver and intestine, and at critical barrier positions, such as the blood-brain barrier (BBB). Thus it has quite prominent functions in several physiological and pharmacological processes. In liver, ABCB1 is abundantly present in the hepatocyte bile canalicular membrane, where it extrudes substrate drugs and other compounds from the hepatocyte into the bile. While in the intestine, ABCB1 is expressed in the apical side of the intestinal epithelium, where it may profoundly limit the drug substrate absorption from gut lumen into the bloodstream. ABCB1 is also present in the apical membranes of kidney epithelial cells (such as proximal tubule cells), where it can excrete substrates from these cells into the urine. The blood-brain-barrier (BBB) is formed by tightly joined endothelial cells in brain capillary microvessels, with high expression of ABCB1 in the luminal side, meaning that the brain is normally well protected from toxins in the circulation⁴. On the other hand, this may also limit the therapeutic effectiveness for specific medicines, especially those targeting cancer brain metastasis and/or central nervous system disease drugs. Because of this, the blood-brain-barrier is of particular interest in our studies. Especially the effects of ABCB1 in drug

brain accumulation, which is potentially clinically relevant. Like in the BBB, ABCB1 is highly expressed in some other critical blood-tissue barriers as well, including blood-testis-barrier (BTB) and blood-placental-barrier (BPB), preventing toxins from over-accumulation in the testis and fetus, respectively.

ABCG2, one of the five ABCG family members (ABCG1, ABCG2, ABCG4, ABCG5, and ABCG8), is involved in translocation of endogenous compounds, related to physiological functions, as well as contributing to efflux of numerous xenobiotic molecules. Both mouse and human harbor only one ABCG2 gene, encoding a 657 amino acid protein in mice and 655 amino acid protein in human, respectively, with 81% identity. Unlike ABCB1, ABCG2 first needs to form a homodimer to become functionally active¹⁹. Of note, the tissue locations of ABCG2 markedly overlap with those of ABCB1, for instance, the canalicular membrane of the hepatocytes, luminal membrane of villous epithelial cells in the intestine, apical membranes of kidney epithelial cells, and the blood-brain-barrier. The main expression locations of human ABCB1 and ABCG2 have been indicated in Figure 1. ABCG2 by itself, but, if there is substrate overlap, often together with ABCB1, can limit the absorption, alter the tissue distribution, and change the pharmacokinetic profiles of various drugs, including small-molecule inhibitors. This has been demonstrated by a number of previous studies including some from our group²⁰⁻²⁴.

In part II of this thesis, we investigate the specific functions of ABCB1 and ABCG2 with respect to the pharmacokinetics of the selective small-molecule inhibitors larotrectinib, selpercatinib and pralsetinib. For this purpose, an *in vitro* trans-well assay and mouse pharmacokinetic studies *in vivo* were performed. *In vitro*, polarized MDCK-II cells stably transduced with human (*h*)*ABCB1*, *hABCG2*, or mouse (*m*)*Abcg2* cDNA were used to investigate the potential transport effects of ABCB1 and ABCG2 for all of these inhibitors. Moreover, the related gene modified mouse strains, including *Abcb1a/1b*^{-/-} (mouse *Abcb1a/1b* deficiency), *Abcg2*^{-/-} (mouse *Abcg2* deficiency), and *Abcb1a/1b;Abcg2*^{-/-} (both mouse *Abcb1a/1b* and *Abcg2* deficiency) were used to study the relative effects *in vivo*.

SOLUTE CARRIER ORGANIC ANION UPTAKE TRANSPORTERS 1A/1B (SLCO1A/1B)

Organic anion-transporting polypeptides (OATPs), encoded by SLCO genes, are multispecific transporters located in a variety of epithelial cells throughout the body²⁵. So far, eleven human OATPs have been identified which can be classified into six families based on their amino acid identity, whereas mice and rats contain fifteen Oatp proteins²⁶. The SLCO1 family is the best characterized, which in humans harbors SLCO1A2, SLCO1B1, SLCO1B3 and SLCO1C1. Of note, rodents have gene duplications and divergences in this family compared to human. Human *SLCO1A2* has five rodent orthologues, including *Slco1a1*, *Slco1a3* (only in rats), *Slco1a4*, *Slco1a5*

and *Slco1a6*. Whereas human *SLCO1B1* and *SLCO1B3* have only a single rodent orthologue, *Slco1b2*^{26,27}. Considering the high expression of one or more SLCO1A/1B proteins in the most important organs/tissues related to drug ADME processes, such as liver, intestine, kidney and blood-brain-barrier, and their broad substrate specificity, they might substantially impact the pharmacokinetics of many drugs. Therefore in this thesis we will only focus on SLCO1A/1B functions in our pharmacokinetic studies.

SLCO1A/1B proteins (OATP1A/1B) are present in different kinds of epithelial cells throughout the body. In the liver, SLCO1B1 and SLCO1B3 are expressed in the basolateral side of hepatocytes, and the same applies to mouse *Slco1a1*, *1a4*, and *1b2*, which may be relevant for substrate drug uptake from blood into liver. However, human hepatic SLCO1A2 is found exclusively in the cholangiocytes and may be involved in the reabsorption of molecules excreted into bile²⁷. In the intestine, human SLCO1A2 is thought to be present at the apical membrane of enterocytes, where it can presumably mediate intestinal absorption of compounds, but its absolute intestinal expression level is contentious²⁸. Human SLCO1A2 and mouse *Slco1a1*, *1a4* and *1a6* have been demonstrated to be also located in the apical membrane of the renal proximal tubular cells, where they might be involved in reabsorption of substrates from the pre-urine. In brain capillary endothelial cells, human SLCO1A2 and mouse *Slco1a4* also show higher expression in comparison with the other SLCO transporters. Thus, they might mediate brain uptake or (in the case of *Oatp1a4*, which is thought to be expressed in both sides of brain capillary endothelial cells) efflux of substrates across the blood-brain barrier^{27,29}. Together with ABCB1 and ABCG2, we also showed the human SLCO1A/1B expression locations in Figure 1. SLCO1A/1B proteins (OATP1A/1B) are known to be involved in the translocation of various drugs, including chemotherapy drugs (paclitaxel, docetaxel, irinotecan, cisplatin, methotrexate, doxorubicin)³⁰, statins (atorvastatin, pravastatin, simvastatin)^{13,31} and various anticancer small-molecule inhibitors (sorafenib, larotrectinib, milciclib, repotrectinib)^{20,23,24,32}, as well as endogenous compounds, such as bilirubin and bile acid³³.

Considering the important pharmacological functions of OATP1A/1B proteins, we studied their influence on larotrectinib, selpercatinib and pralsetinib disposition in both *in vitro* uptake assays and *in vivo* mouse experiments. *In vitro*, HEK293 cells transduced with vector control and human *SLCO1A2*, *SLCO1B1*, or *SLCO1B3* cDNAs were used to assess the potential uptake functions of OATP1A/1B for larotrectinib and selpercatinib. *In vivo*, *Slco1a/1b*^{-/-} (*Slco1a/1b* deficient) mice are applied for all the three inhibitors, and further, *Slco1B1* and *Slco1B3* (human OATP1B1 or OATP1B3 specifically expressed in the liver in a mouse *Oatp1a/1b* knockout background) mice are also used to study the human OATP1B1 and -1B3 functions for larotrectinib.

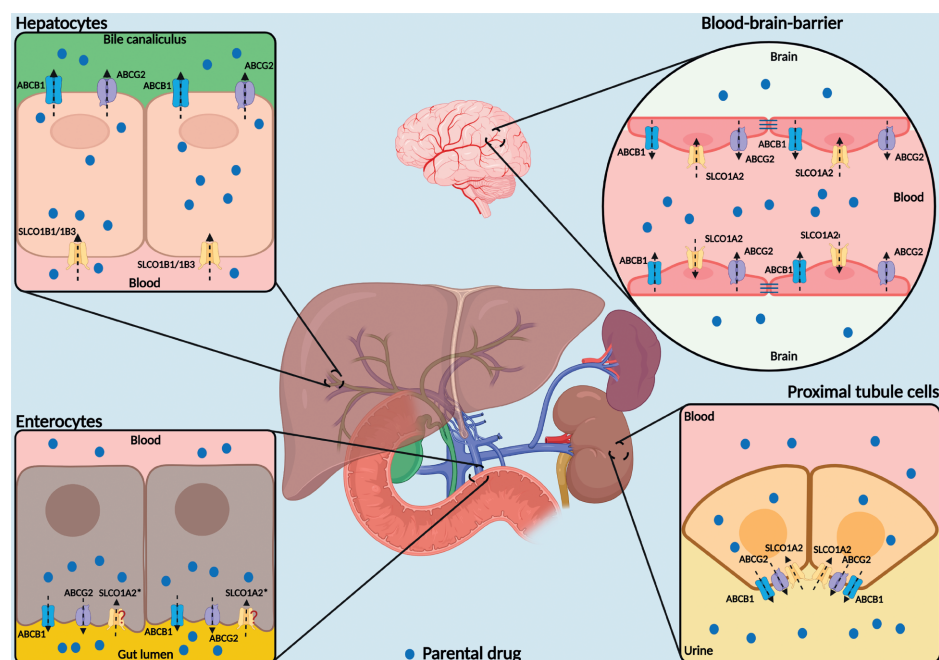


Figure 1. The locations of ABC efflux transporters (human ABCB1 and ABCG2) and human SLC01A/1B (OATP1A/1B) in different tissues. As indicated, in intestine, ABCB1, ABCG2 and SLC01A2 are expressed in the apical side (lumen side) of enterocytes, where ABCB1 and/or ABCG2 can efflux their substrates from enterocytes back to gut lumen. SLC01A2* in theory may take up its specific substrate from gut lumen into enterocytes, but its abundance in the small intestine is contentious. In liver, SLC01B1 and/or 1B3 take up their substrates from the blood circulation into the liver. Note that in the human liver, SLC01A2 is expressed only in cholangiocytes, where it may reabsorb its substrates from bile (not shown in the figure). However, ABCB1 and ABCG2 are abundantly present in the hepatocyte bile canaliculi, where they extrude substrate drugs from the liver hepatocyte into the bile. In kidney, ABCB1 and ABCG2 are also present in the apical membranes of epithelial cells (primarily proximal tubule cells), excreting substrates from the cells into urine. Whereas SLC01A2 in the apical membrane may reabsorb its own substrate back to the cells. In the blood-brain-barrier, ABCB1 and ABCG2 expressed in the apical membrane of brain microvessel endothelial cells, pump out their substrates from brain back into blood. In contrast, apical SLC01A2 may take up its substrates from blood into the brain.

THE CYTOCHROME P450 3A (CYP3A) ENZYME COMPLEX

The human genome contains 57 Cytochrome P450 (CYP) genes and about the same number of pseudogenes, which can be classified into 18 families and 44 subfamilies according to their sequence homology. The families CYP1, CYP2 and CYP3, but especially CYP3, are collectively responsible for most phase I biotransformations of drugs and other compounds in the human liver³⁴. In the last several decades, Cytochrome P450 3A (CYP3A) has been well studied and characterized as the oxidative metabolism enzyme for a vast number of endogenous and xenobiotic compounds, including toxins, carcinogens, bile acids, steroid hormones, and

approximately 50% of the drugs used in the clinic today¹⁷. As heme-containing monooxygenases, CYP3As are mainly expressed in the liver and intestine. Thus they are major determinants in drug metabolism and elimination, especially in the intestinal and liver metabolism of oral drugs (first-pass effects). This may dramatically influence the pharmacokinetic and pharmacodynamics profiles of specific substrate drugs, and hence drug efficacy and safety³⁵. The intestinal and hepatic CYP3A enzymes effects in the substrate drug systemic exposure are shown in Figure 2.

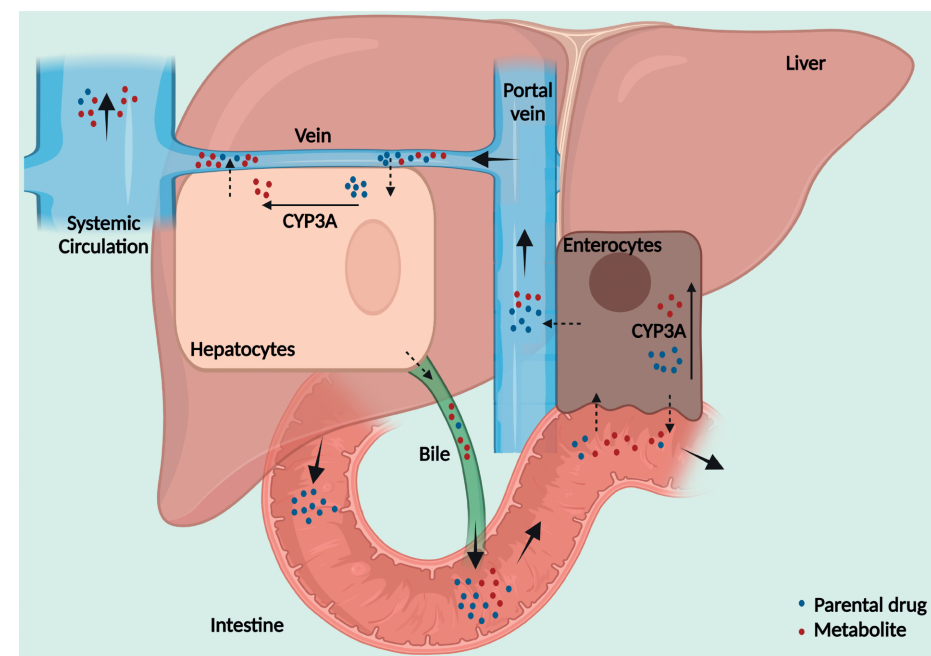


Figure 2. Systemic exposure to CYP3A substrate drugs is limited by the intestinal and hepatic localization of CYP3A enzymes. Bulk drug flow is indicated by black solid arrows. Metabolism of drug (dark blue circles) to its metabolite (red circles) by CYP3A is indicated. Black dotted arrows indicate transport of drug by uptake or efflux transporters (and/or simple transmembrane diffusion) into or out of the enterocyte or hepatocyte.

There are eight full-length *Cyp3a* genes and three pseudogenes grouped into two clusters in the mouse. Whereas in human, the CYP3A subfamily consists of four genes, *CYP3A4*, *3A5*, *3A7*, and *3A43*, which are located on chromosome 7^{34,36}. Enzymes of this subfamily are embedded in the endoplasmic reticulum and contribute to the metabolism of the most diverse group of substrates of all human P450s, as their active sites are large and flexible enough to bind and metabolize many preferentially lipophilic compounds with comparatively large structures. Among them, CYP3A4 is generally the most abundant hepatic and intestinal form, accounting on average for 95% of the combined liver CYP3A mRNA pool in white individuals^{15,35}. Of note, CYP3A levels among human donors can vary as much as 40-fold in both liver and small intestine,

which markedly affects the drug metabolism process and consequent drug therapeutic efficacy³⁷. These large inter- and intra-individual differences can come from various controlling factors of gene expression, such as circulating hormones, or drugs and food-derived xenobiotics, or from genetic polymorphisms³⁷.

The crucial pharmacological functions of CYP3A and especially CYP3A4 prompted us to investigate their relative roles in the metabolism of the above-mentioned selective small-molecule inhibitors. Thus we applied the *Cyp3a*^{-/-} (Cyp3a cluster deficiency) mice and Cyp3aXAV (human CYP3A4 expression in both liver and intestine in mouse Cyp3a knockout background) mice in our pharmacokinetic studies.

DRUG-DRUG INTERACTIONS

Genetic polymorphisms and potential drug-drug interactions (DDI) may extensively affect the drug ADME processes. As our pre-clinical mouse models have a clean genomic deficiency background, we will only focus on the potential drug-drug interaction issues in this thesis. DDIs are one of the commonest causes of adverse drug reactions, particularly in the elderly due to poly-therapy. DDIs can be classified into two main groups, pharmacokinetic DDIs and pharmacodynamic DDIs (the latter will be not discussed in the current thesis). The pharmacokinetic DDIs include, but are not limited to: 1) effects of drug metabolizing enzyme (CYP3A, CYP2C or esterase, etc.) inhibitors; 2) effects of drug metabolizing enzyme (CYP3A, CYP2C or esterase, etc.) inducers; 3) effects of drug transporter (like ABCB1 and ABCG2) inhibitors; 4) effects of drug transporter (like ABCB1 and ABCG2) inducers. All of these effects from (an)other drug(s) may cause over-exposure or reduced exposure of the victim drug, and subsequently result in treatment failure or toxicity³⁸.

As we have described in the above sections, drug transporters such as ABCB1 and ABCG2, the OATPs, and drug-metabolizing enzymes such as CYP3As can all be major determinants of pharmacokinetics of specific drugs. Drug-drug interactions interfering with these drug transporters or CYP3As, or even both, thus deserve serious consideration and in-depth exploration. There are a number of inhibitors and/or inducers specifically recognizing drug transporters or metabolizing enzymes that have been identified so far³⁹. As has been well studied, co-administration of elacridar, a dual inhibitor of ABCB1 and ABCG2, can improve both oral exposure and brain penetration (one of our particular interests) of several tyrosine kinase inhibitors (TKIs), such as sorafenib, crizotinib, vemurafenib, ribociclib, and others^{7,8,20,22,40,41}. Rifampin, an antibiotic used to treat several types of bacterial infections, could inhibit OATP uptake transporters, which leads to reduced uptake of many endogenous molecules and drugs, like statins⁴². Of note, rifampin can not only inhibit OATPs, but also ABCB1 to some extent. Rifampin further displays a kind of dual function in modulating pharmacokinetics, including acute inhibition of ABCB1 and OATPs, but also gene induction of ABCB1 and CYP3A, especially

upon chronic administration⁴³. With respect to CYP3As, these can be inhibited by various small-molecule drugs, including ritonavir, ketoconazole, itraconazole, and others³⁹. Among them, the HIV protease inhibitor ritonavir was demonstrated to very efficiently inhibit CYP3A activity and thus substantially boost systemic exposure of many drugs in our previous studies, such as docetaxel, paclitaxel, and lopinavir^{44,45}. However, like rifampin, ritonavir can also inhibit ABCB1 to a certain extent^{46,47}.

Given all these considerations, we performed drug-drug interaction studies using elacridar, rifampin and ritonavir, respectively, in relevant mouse models to explore the potential effects on larotrectinib pharmacokinetic profiles. Larotrectinib was chosen as a victim drug because its pharmacokinetics is simultaneously affected by the ABC transporters, OATPs, and CYP3A.

SUMMARY

Drug pharmacokinetic profiles, and hence drug efficacy and safety, can be markedly influenced by drug transporters (especially ABCB1/ABCG2 and OATP1A/1B) and drug-metabolizing enzymes (particularly CYP3A). In Part II of this thesis such potential effects were investigated for three small-molecule inhibitors, including larotrectinib (the first selective inhibitor for TRK receptors), selipercatinib and pralsetinib (the first two selective inhibitors for RET receptors) using relevant gene-modified mouse strains. In addition, in order to explore possible drug-drug interaction effects, we performed inhibition (boosting) experiments for larotrectinib and analyzed the resulting pharmacokinetic changes.

REFERENCE

- Nigam, S.K. What do drug transporters really do? *Nature Reviews Drug Discovery* **14**, 29-44 (2014).
- Russel, F.G.M. Transporters: Importance in Drug Absorption, Distribution, and Removal. 27-49 (2010).
- Giacomini, K.M., et al. Membrane transporters in drug development. *Nature Reviews Drug Discovery* **9**, 215-236 (2010).
- Schinkel, A.H. & Jonker, J.W. Mammalian drug efflux transporters of the ATP binding cassette (ABC) family: an overview. *Advanced Drug Delivery Reviews* **55**, 3-29 (2003).
- Tang, S.C., et al. Increased oral availability and brain accumulation of the ALK inhibitor crizotinib by coadministration of the P-glycoprotein (ABCB1) and breast cancer resistance protein (ABCG2) inhibitor elacridar. *International Journal of Cancer* **134**, 1484-1494 (2014).
- Tang, S.C., et al. Impact of P-glycoprotein (ABCB1) and breast cancer resistance protein (ABCG2) gene dosage on plasma pharmacokinetics and brain accumulation of dasatinib, sorafenib, and sunitinib. *Journal of Pharmacology and Experimental Therapeutics* **346**, 486-494 (2013).
- Lagas, J.S., et al. Breast cancer resistance protein and P-glycoprotein limit sorafenib brain accumulation. *Molecular Cancer Therapeutics* **9**, 319-326 (2010).
- Kodaira, H., Kusuhara, H., Ushiki, J., Fuse, E. & Sugiyama, Y. Kinetic analysis of the cooperation of P-glycoprotein (P-gp/Abcb1) and breast cancer resistance protein (Bcrp/Abcg2) in limiting the brain and testis penetration of erlotinib, flavopiridol, and mitoxantrone. *Journal of Pharmacology and Experimental Therapeutics* **333**, 788-796 (2010).
- Hagenbuch, B. & Meier, P.J. Organic anion transporting polypeptides of the OATP/SLC21 family: phylogenetic classification as OATP/SLCO superfamily, new nomenclature and molecular/functional properties. *Pflügers Archiv. European Journal of Physiology* **447**, 653-665 (2004).
- van de Steeg, E., van Esch, A., Wagenaar, E., Kenworthy, K.E. & Schinkel, A.H. Influence of human OATP1B1, OATP1B3, and OATP1A2 on the pharmacokinetics of methotrexate and paclitaxel in humanized transgenic mice. *Clinical Cancer Research* **19**, 821-832 (2013).
- van de Steeg, E., et al. Complete OATP1B1 and OATP1B3 deficiency causes human Rotor syndrome by interrupting conjugated bilirubin reuptake into the liver. *Journal of Clinical Investigation* **122**, 519-528 (2012).
- van de Steeg, E., et al. Organic anion transporting polypeptide 1a/1b-knockout mice provide insights into hepatic handling of bilirubin, bile acids, and drugs. *Journal of Clinical Investigation* **120**, 2942-2952 (2010).
- Kalliokoski, A. & Niemi, M. Impact of OATP transporters on pharmacokinetics. *British Journal of Pharmacology* **158**, 693-705 (2009).
- van de Steeg, E., et al. Methotrexate Pharmacokinetics in Transgenic Mice with Liver-Specific Expression of Human Organic Anion-Transporting Polypeptide 1B1 (SLCO1B1). *Drug Metabolism and Disposition* **37**, 277-281 (2008).
- van Herwaarden, A.E., et al. Knockout of cytochrome P450 3A yields new mouse models for understanding xenobiotic metabolism. *Journal of Clinical Investigation* **117**, 3583-3592 (2007).
- Lynch, T. & Price, A. The effect of cytochrome P450 metabolism on drug response, interactions, and adverse effects. *American Family Physician* **76**, 391-396 (2007).
- Guengerich, F.P. Cytochrome P-450 3A4: regulation and role in drug metabolism. *Annual Review of Pharmacology and Toxicology* **39**, 1-17 (1999).
- Dean, M., Rzhetsky, A. & Allikmets, R. The human ATP-binding cassette (ABC) transporter superfamily. *Genome Research* **11**, 1156-1166 (2001).
- Liu, X. ABC Family Transporters. *Advances in Experimental Medicine and Biology* **1141**, 13-100 (2019).
- Wang, Y., et al. OATP1A/1B, CYP3A, ABCB1, and ABCG2 limit oral availability of the NTRK inhibitor larotrectinib, while ABCB1 and ABCG2 also restrict its brain accumulation. *British Journal of Pharmacology* **177**, 3060-3074 (2020).
- Li, W., et al. P-glycoprotein (MDR1/ABCB1) restricts brain accumulation and cytochrome P450-3A (CYP3A) limits oral availability of the novel ALK/ROS1 inhibitor lorlatinib. *International Journal of Cancer* **143**, 2029-2038 (2018).

- Wang, Y., et al. ABCB1 and ABCG2, but not CYP3A4 limit oral availability and brain accumulation of the RET inhibitor pralsetinib. *Pharmacological Research* **172**, 105850 (2021).
- Martínez-Chávez, A., et al. The role of drug efflux and uptake transporters ABCB1 (P-gp), ABCG2 (BCRP) and OATP1A/1B and of CYP3A4 in the pharmacokinetics of the CDK inhibitor milciclib. *European Journal of Pharmaceutical Sciences* **159**, 105740 (2021).
- Li, W., Sparidans, R.W., Lebre, M.C., Beijnen, J.H. & Schinkel, A.H. ABCB1 and ABCG2 Control Brain Accumulation and Intestinal Disposition of the Novel ROS1/TRK/ALK Inhibitor Repotrectinib, While OATP1A/1B, ABCG2, and CYP3A Limit Its Oral Availability. *Pharmaceutics* **13**(2021).
- Cheng, X., Maher, J., Chen, C. & Klaassen, C.D. Tissue distribution and ontogeny of mouse organic anion transporting polypeptides (Oatps). *Drug Metabolism and Disposition* **33**, 1062-1073 (2005).
- Hagenbuch, B. & Meier, P.J. The superfamily of organic anion transporting polypeptides. *Biochimica et Biophysica Acta* **1609**, 1-18 (2003).
- Iusuf, D., van de Steeg, E. & Schinkel, A.H. Functions of OATP1A and 1B transporters in vivo: insights from mouse models. *Trends in Pharmacological Sciences* **33**, 100-108 (2012).
- Rodrigues, A.D., et al. Induction of Human Intestinal and Hepatic Organic Anion Transporting Polypeptides: Where Is the Evidence for Its Relevance in Drug-Drug Interactions? *Drug Metabolism and Disposition* **48**, 205-216 (2020).
- Oswald, S. Organic Anion Transporting Polypeptide (OATP) transporter expression, localization and function in the human intestine. *Pharmacology and Therapeutics* **195**, 39-53 (2019).
- Durmus, S., van Hoppe, S. & Schinkel, A.H. The impact of Organic Anion-Transporting Polypeptides (OATPs) on disposition and toxicity of antitumor drugs: Insights from knockout and humanized mice. *Drug Resistance Updates* **27**, 72-88 (2016).
- Hirota, T., Fujita, Y. & Ieiri, I. An updated review of pharmacokinetic drug interactions and pharmacogenetics of statins. *Expert Opinion on Drug Metabolism & Toxicology* **16**, 809-822 (2020).
- Zimmerman, E.J., et al. Contribution of OATP1B1 and OATP1B3 to the disposition of sorafenib and sorafenib-glucuronide. *Clinical Cancer Research* **19**, 1458-1466 (2013).
- van de Steeg, E., et al. Organic anion transporting polypeptide 1a/1b-knockout mice provide insights into hepatic handling of bilirubin, bile acids, and drugs. *Journal of Clinical Investigation* **120**, 2942-2952 (2010).
- Zanger, U.M., Turpeinen, M., Klein, K. & Schwab, M. Functional pharmacogenetics/genomics of human cytochromes P450 involved in drug biotransformation. *Analytical and Bioanalytical Chemistry* **392**, 1093-1108 (2008).
- van Herwaarden, A.E., van Waterschoot, R.A. & Schinkel, A.H. How important is intestinal cytochrome P450 3A metabolism? *Trends in Pharmacological Sciences* **30**, 223-227 (2009).
- Nelson, D.R., et al. Comparison of cytochrome P450 (CYP) genes from the mouse and human genomes, including nomenclature recommendations for genes, pseudogenes and alternative-splice variants. *Pharmacogenetics* **14**, 1-18 (2004).
- Lamba, J.K., Lin, Y.S., Schuetz, E.G. & Thummel, K.E. Genetic contribution to variable human CYP3A-mediated metabolism. *Advanced Drug Delivery Reviews* **54**, 1271-1294 (2002).
- Palleria, C., et al. Pharmacokinetic drug-drug interaction and their implication in clinical management. *Journal of Research in Medical Sciences* **18**, 601-610 (2013).
- Food and Drug Administration. Drug Development and Drug Interactions | Table of Substrates, Inhibitors and Inducers (2020). Available from: <https://www.fda.gov/drugs/drug-interactions-labeling/drug-development-and-drug-interactions-table-substrates-inhibitors-and-inducers>.
- Martínez-Chávez, A., et al. P-glycoprotein Limits Ribociclib Brain Exposure and CYP3A4 Restricts Its Oral Bioavailability. *Molecular Pharmaceutics* **16**, 3842-3852 (2019).
- Durmus, S., Sparidans, R.W., Wagenaar, E., Beijnen, J.H. & Schinkel, A.H. Oral availability and brain penetration of the B-RAFV600E inhibitor vemurafenib can be enhanced by the P-GLYCOPROTEIN (ABCB1) and breast cancer resistance protein (ABCG2) inhibitor elacridar. *Molecular Pharmaceutics* **9**, 3236-3245 (2012).
- Salphati, L., et al. Evaluation of organic anion transporting polypeptide 1B1 and 1B3 humanized mice as a translational model to study the pharmacokinetics of statins. *Drug Metabolism and Disposition* **42**, 1301-1313 (2014).

43. Reitman, M.L., *et al.* Rifampin's acute inhibitory and chronic inductive drug interactions: experimental and model-based approaches to drug-drug interaction trial design. *Clinical Pharmacology and Therapeutics* **89**, 234-242 (2011).
44. Hendriks, J.J., *et al.* Oral co-administration of elacridar and ritonavir enhances plasma levels of oral paclitaxel and docetaxel without affecting relative brain accumulation. *British Journal of Cancer* **110**, 2669-2676 (2014).
45. ter Heine, R., *et al.* An integrated pharmacokinetic model for the influence of CYP3A4 expression on the in vivo disposition of lopinavir and its modulation by ritonavir. *Journal of Pharmaceutical Sciences* **100**, 2508-2515 (2011).
46. Gutmann, H., Fricker, G., Drewe, J., Toeroek, M. & Miller, D.S. Interactions of HIV protease inhibitors with ATP-dependent drug export proteins. *Molecular Pharmacology* **56**, 383-389 (1999).
47. Drewe, J., *et al.* HIV protease inhibitor ritonavir: a more potent inhibitor of P-glycoprotein than the cyclosporine analog SDZ PSC 833. *Biochemical Pharmacology* **57**, 1147-1152 (1999).



CHAPTER 4

**PHARMACOKINETIC STUDIES ON TYROSINE
KINASE INHIBITORS**



CHAPTER 4.1

OATP1A/1B, CYP3A, ABCB1, AND ABCG2 LIMIT ORAL AVAILABILITY OF NTRK INHIBITOR LAROTRECTINIB, WHILE ABCB1 AND ABCG2 ALSO RESTRICT ITS BRAIN ACCUMULATION

Yaogeng Wang¹, Rolf W. Sparidans², Wenlong Li¹, Maria C. Lebre ¹, Jos H. Beijnen^{1,2,3}, Alfred H. Schinkel¹

¹The Netherlands Cancer Institute, Division of Pharmacology, Plesmanlaan 121, 1066 CX Amsterdam, The Netherlands.

²Utrecht University, Faculty of Science, Department of Pharmaceutical Sciences, Division of Pharmacology, Universiteitsweg 99, 3584 CG Utrecht, The Netherlands.

³The Netherlands Cancer Institute, Department of Pharmacy & Pharmacology, Plesmanlaan 121, 1066 CX Amsterdam, The Netherlands.

ABSTRACT

Background and Purpose

Larotrectinib is an FDA-approved oral small-molecule inhibitor for treatment of neurotrophic tropomyosin receptor kinase (NTRK) fusion-positive cancer. We here investigated the functions of the multidrug efflux transporters ABCB1 and ABCG2, the SLC01A/1B (OATP1A/1B) uptake transporters and the multispecific drug-metabolizing enzyme CYP3A in larotrectinib pharmacokinetic behavior.

Experimental Approach

In vitro, transepithelial drug transport and uptake assays were performed.

In vivo, larotrectinib (10 mg/kg) was administered orally to relevant genetically modified mouse models. Cell medium, plasma samples and organ homogenates were measured by a sensitive and specific liquid chromatography-tandem mass spectrometric larotrectinib assay.

Key Results

In vitro, larotrectinib was avidly transported by human (h)ABCB1 and mouse (m)Abcg2 efficiently by hABCG2, and modestly by hOATP1A2. *In vivo*, both mAbcb1a/1b and mAbcg2 markedly limited larotrectinib oral availability and brain and testis accumulation (by 2.1-, 10.4-, and 2.7-fold, respectively), with mAbcb1a/1b playing a more prominent role. mOatp1a/1b also restricted larotrectinib oral availability (by 3.8-fold) and overall tissue exposure, apparently by mediating substantial uptake into the liver, thus likely facilitating hepatobiliary excretion. Additionally, larotrectinib is an excellent substrate of CYP3A, which restricts the oral availability of larotrectinib, and hence its tissue exposure.

Conclusions and Implications

ABCG2 and especially ABCB1 limit the oral availability and brain and testis penetration of larotrectinib, while OATP1A/1B transporters restrict its systemic exposure by mediating hepatic uptake, thus allowing hepatobiliary excretion. CYP3A-mediated metabolism can strongly limit larotrectinib oral availability and hence its tissue concentrations. These insights may be useful in the further clinical development of larotrectinib.

Keywords: Larotrectinib, Cytochrome P450-3A, Oral availability, Neurotrophic tropomyosin receptor kinase, Slco1a/1b, P-glycoprotein, Brain accumulation

Abbreviations:

ABC: ATP-binding cassette; ABCB1: ATP-binding cassette sub-family B member 1; ABCG2: ATP-binding cassette super-family G member 2; BCRP: breast cancer resistance protein; CYP:

Cytochrome P450; Cyp3aXAV: Cyp3a knockout mice with specific expression of human CYP3A4 in liver and intestine; LC-MS/MS: liquid chromatography coupled with tandem mass spectrometry; MDCK: Madin-Darby canine kidney; m (as prefix): mouse; NTRK: Neurotrophic tropomyosin receptor kinase; OTAP: Organic-anion-transporting polypeptide; P-gp: P-glycoprotein; SLCO: solute carrier family; TKI: tyrosine kinase inhibitor.

1. INTRODUCTION

The Neurotrophic Tropomyosin Receptor Kinase (NTRK) family of three nerve growth factor receptor genes (NTRK1, NTRK2, and NTRK3), encodes the single-transmembrane receptor tyrosine kinases Trk A, B, and C, respectively¹. These receptors are composed of an extracellular domain for ligand binding, a transmembrane region and an intracellular kinase domain. Nerve growth factor (NGF), brain-derived growth factor (BDNF), and neurotrophin 3 (NTF-3) specifically bind to TrkA, TrkB and TrkC, respectively². This ligand binding triggers the oligomerization of the receptors and phosphorylation of tyrosine residues in the intracytoplasmic kinase domain, thus activating signal transduction pathways leading to growth, differentiation, and survival of neurons¹. Trk receptors, which are mainly expressed in human neuronal tissues, therefore play critical roles in the development and homeostasis of the nervous system.

Oncogenic fusions involving one or more of the NTRK genes occasionally occur in diverse adult malignancies and pediatric cancers, such as glioblastoma, non-small cell lung cancer (NSCLC), and colorectal cancer³⁻⁵. In certain rare pediatric tumors, including infantile fibrosarcoma, cellular congenital mesoblastic nephroma, and papillary thyroid cancer, the frequencies of Trk fusions are considerably higher. Thus, the presence of Trk fusions defines a unique molecular subgroup of advanced solid tumors in adult malignancies and pediatric cancers.

Several multikinase inhibitors inhibiting the function of TrkA, TrkB and TrkC fusion proteins are under evaluation in clinical trials, e.g., entrectinib (RXDX-101), altiratinib (DCC-2701), sitravatinib (MGCD516), TSR-011, PLX7486, DS-6051b, F17752 and cabozantinib⁶. Unlike those multikinase inhibitors, larotrectinib is the first selective pan-Trk inhibitor (Vitrakvi, LOXO-101, Supplemental Figure 1), and has been approved by the FDA in November 2018 (Food and Drug Administration, 2018). Larotrectinib is an orally administered ATP-competitive inhibitor of TrkA, TrkB, and TrkC and has been reported to induce marked tumor shrinkage in patients with NTRK-rearranged cancers. In Phase 1/2 clinical trials, larotrectinib showed marked and durable antitumor activity in patients with Trk fusion-positive cancers and an overall response rate of 75% regardless of tumor type, age or gender⁷.

Transmembrane transporters can affect drug absorption, distribution, metabolism and excretion (ADME). They can thus influence the pharmacokinetics, and hence the safety and efficacy profiles of specific drugs. There are two major super families of transmembrane transporters affecting drug disposition - the ATP-binding cassette (ABC) efflux transporter family and the solute carrier (SLC) uptake transporter family^{8,9}.

The ABC drug efflux transporters P-glycoprotein (P-gp; ABCB1) and breast cancer resistance protein (BCRP; ABCG2) are highly expressed in the luminal membrane of the small intestine,

blood-brain barrier, blood-testis barrier and blood-placenta barrier and in the apical membranes of excretory cells such as renal proximal tubule epithelial cells and hepatocytes¹⁰. ABCB1 and ABCG2 can therefore influence the intestinal absorption, biliary and urinary excretion and also the penetration in the central nervous system of specific drugs. Many anti-tumor drugs, including numerous tyrosine kinase inhibitors (TKIs) are transported substrates of ABCB1 and/or ABCG2. This interaction often results in reduced oral availability or poor brain penetration¹¹⁻¹⁴. As larotrectinib targets different tumor types with NTRK fusions, that may develop brain metastases or even occur primarily in the brain (glioblastoma), it is important to know whether larotrectinib interacts with ABCB1 and/or ABCG2 *in vivo*, potentially affecting its oral availability and brain accumulation.

Organic anion-transporting polypeptides (OATPs) are sodium-independent transmembrane uptake transporters encoded by SLCO genes. They are expressed mainly in organs like liver, kidney and small intestine, where they mediate the tissue uptake of many endogenous compounds, including bile acids and steroids, as well as exogenous compounds. The OATP1A/1B transporters have broad substrate specificities and are highly expressed in the liver¹⁵. They can therefore have key roles in hepatic uptake and hence plasma clearance of several drug substrates including statins, cardiac glycosides, antibiotics, and many chemotherapeutics with highly diverse structures¹⁶⁻²¹. While there are no direct one-to-one orthologues between the mouse and human OATP1A/1B proteins, mouse Oatp1a1, 1a4, 1a5, and 1a6 are most related to the single human OATP1A2 protein, whereas mouse Oatp1b2 is most related to human OATP1B1 and 1B3. Thus, we wanted to know whether larotrectinib is a substrate of OATP1A/1B and whether this can influence larotrectinib oral availability and organ distribution.

The multidrug-metabolizing Cytochrome P450 3A (CYP3A) enzyme complex is responsible for most phase I drug metabolism. CYP3A4 is the most abundant CYP enzyme in human liver, the main detoxification organ. Many (pro-) drugs are substrates of CYP3A4, resulting in drug inactivation or sometimes also activation^{22,23}. Thus, the oral availability and plasma exposure of many drugs can be strongly affected by CYP3A4, which may dramatically influence their therapeutic efficacy.

The primary aim of this study was to clarify the *in vivo* impact of ABCB1 and ABCG2, SLCO1A/1B (OATP1A/1B), and CYP3A enzymes on larotrectinib pharmacokinetic behavior, including oral availability and organ distribution by using appropriate genetically modified mouse models.

2. MATERIALS AND METHODS

2.1 Cell lines and transport assays

Polarized Madin-Darby Canine Kidney (MDCK-II) cells stably transduced with human (h) ABCB1, hABCG2, or mouse (m) *Abcg2* cDNA were used and cultured as described^{24,25}. Transepithelial transport assays were performed on microporous polycarbonate membrane filters (3.0 µm pore size, 12 mm diameter, Transwell 3414). Parental and variant subclones were seeded at a density of 2.5×10^5 cells per well and cultured for 3 days to form an intact monolayer. Membrane tightness was assessed by measurement of transepithelial electrical resistance (TEER) before and after the transport phase.

For inhibition experiments, 5 µM zosuquidar (ABCB1 inhibitor) and/or 5 µM Ko143 (ABCG2/*Abcg2* inhibitor) were used during the transport experiments. Cells were pre-incubated with one or combination of the inhibitors for 1 h in both apical and basolateral compartments. The transport phase was started ($t = 0$) by replacing the medium in either the apical or the basolateral compartment with fresh Dulbecco's modified Eagle's medium (DMEM) including 10% (v/v) fetal bovine serum (FBS) and larotrectinib at 5 µM, as well as the appropriate inhibitor(s). Plates then were kept at 37°C in 5% (v/v) CO₂ during the experiment, and 50 µl aliquots were taken from the acceptor compartment at 1, 2, 4, and 8 h, and stored at -30°C until LC-MS/MS measurement of the larotrectinib concentrations. Experiments were performed in independent triplicates and the mean transport is shown in the figure. Active transport was expressed using the transport ratio r , i.e., the amount of apically directed drug transport divided by basolaterally directed drug translocation after 8 hours (h). Our extensive previous studies with these cell lines have demonstrated that the transport data are highly reproducible. Transport ratios (r) above 3 therefore normally can be reliably assessed without the need for statistical analysis. For this reason $n = 3$ was considered sufficient for the larotrectinib transport results.

2.2 Cellular uptake assays

HEK293 cells (RRID: CVCL_0045) transduced with vector control, human SLCO1A2, SLCO1B1 or SLCO1B3 cDNAs were a kind gift from Prof. Werner Siegmund and Dr. Markus Keiser (University of Greifswald, Greifswald, Germany). HEK293 cells transduced with vector (mock) or human SLCO2B1 cDNA were a kind gift from Prof. Per Artursson and Dr. Maria Karlgren (Uppsala University, Uppsala, Sweden). All the HEK293 cell lines were grown in DMEM supplemented with 10% (v/v) FBS, 1% penicillin-streptomycin mix at 37°C in 5% (v/v) CO₂. Moreover, for HEK293-control, -SLCO1A2, -SLCO1B1 and -SLCO1B3 cell lines, 500 µg/ml G418 was added, while for HEK293-mock and -SLCO2B1 cell lines, 75 µg/ml hygromycin was added. For the uptake experiments, cells were first seeded in 12-well plates [coated with 50 mg/l poly (l-lysine) and 50 mg/l poly (l-ornithine)] at a density of 1.0×10^5 cells/well. For the transport study, the cell

culture medium was replaced with culture medium supplemented with 5 mM sodium butyrate 24 h before the uptake assay in order to induce the expression of OATP transporters.

The uptake transport study was carried out as described previously²⁶. After cells had been washed twice and pre-incubated with Krebs-Henseleit solution at 37°C for 15 min, uptake was initiated by adding Krebs-Henseleit buffer containing 5 µM larotrectinib or 0.2 µM rosuvastatin as positive control. The Krebs-Henseleit solution was prepared from Krebs-Henseleit buffer modified powder and supplemented with 25 mM NaHCO₃ and 2.5 mM CaCl₂ adjusted to pH 6.4 with 1 M HCL. At 2.5 min, the incubation buffer was removed and uptake was terminated by adding 1 ml of ice-cold Krebs-Henseleit buffer, followed by two times washing with 1 ml of ice-cold Krebs-Henseleit buffer. Afterwards, cells were lysed with 150 µl of 0.2 N NaOH 15 min at room temperature and cell lysates were transferred into 1.5 ml Eppendorf tubes and stored at -20°C until the next day. The cellular protein amount was determined by the Bradford method using 10 µl of the cell lysates with bovine serum albumin as a standard. LC-MS/MS measurements of the larotrectinib and rosuvastatin concentrations were performed for cell lysates. Experiments were performed in independent triplicates and the mean transport is shown in the figure. Like for the transepithelial transport assay, $n = 3$ was considered sufficient for the larotrectinib and rosuvastatin uptake results.

2.3 Animals

Wild-type, *Abcb1a/1b*^{-/-} (RRID:IMSR_TAC:1487), *Abcg2*^{-/-} (RRID:IMSR_TAC:2767), *Abcb1a/1b;Abcg2*^{-/-} (RRID:IMSR_TAC:3998), *Slco1a/1b*^{-/-} (RRID:MGI:4830142), *Cyp3a*^{-/-} (RRID:IMSR_TAC:9011) and *Cyp3aXAV* (RRID:IMSR_TAC:9049) male mice, all of a >99% FVB genetic background, were used between 9 and 16 weeks of age. All the mouse strains were well established and characterized before. The mouse strains are viable, fertile and stable and have previously been successfully used in extensive pharmacokinetic studies. The body weight was $30 \text{ g} \pm 5 \text{ g}$. Animals were kept in SPF animal facility, in a temperature-controlled environment with 12-h light and 12-h dark cycle and they received a standard diet (Transbreed, SDS Diets, Technilab – BMI) and acidified water *ad libitum*. Mice were housed and handled according to institutional guidelines complying with Dutch and EU legislation. Male and female mice were housed separately and 2-5 mice were housed per cage. In this study, only male mice were randomly allocated for experiments. Because the main read-out of these experiments was objective (larotrectinib plasma and tissue concentrations as measured by LC-MS/MS), we applied no blinding method. The mouse number may differ slightly among different groups in different experiments (usually 6 based on the power calculation and our extensive experience, but one more mouse was occasionally added when multiple mouse groups were tested and needed to be compared at the same time). All experimental animal protocols were evaluated and approved by the institutional animal care and use committee and experimental procedures were optimized to follow the principles of

3Rs (replacement, refinement or reduction), as also required by Dutch law, and carried out in accordance with the ARRIVE guidelines^{27,28}.

2.4 Drug solutions

For oral administration, larotrectinib was dissolved in dimethyl sulfoxide (DMSO) at a concentration of 50 mg/ml and further diluted with 5% glucose in water to yield a concentration of 1.0 mg/ml. Final concentrations for DMSO and glucose in the dosing solution were 2% (v/v) and 4.75% (w/v), respectively. All dosing solutions were prepared freshly on the day of experiment.

2.5 Plasma and organ pharmacokinetics of larotrectinib in mice

In order to minimize variation in absorption because of oral administration, mice were first fasted for 3 h before larotrectinib (10 mg/kg) was administered orally, using a blunt-ended needle. For the transporter 8 h or 1 h experiments, approximately 50 µl tail vein blood samples were collected at 0.25, 0.5, 1, 2, 4, and 8 h or 0.125, 0.25, 0.5, 0.75, and 1 h time points after oral administration, respectively, using microvettes containing dipotassium-EDTA. For the CYP3A 8 h or 4 h experiments, tail vein blood sampling was performed at 0.25, 0.5, 1, 2, and 4 h or 0.125, 0.25, 0.5, 1, and 2 h, respectively. At the last time point in each experiment (1 h, 4 h or 8 h), mice were anesthetized with 5% isoflurane and blood was collected by cardiac puncture. Blood samples were collected in Eppendorf tubes containing heparin as an anticoagulant. The mice were then sacrificed by cervical dislocation and brain, liver, kidney, lung, small intestine and testis were rapidly removed. Plasma was isolated from the blood by centrifugation at 9,000g for 6 min at 4°C, and the plasma fraction was collected and stored at -30°C until analysis. Organs were homogenized with 4% (w/v) bovine serum albumin and stored at -30°C until analysis. Relative tissue-to-plasma ratio after oral administration was calculated by determining the larotrectinib tissue concentration relative to larotrectinib plasma concentration at the last time point.

2.6 LC-MS/MS analysis

Larotrectinib concentrations in DMEM/FBS (9/1, v/v) (Invitrogen) cell culture medium, plasma samples, and organ homogenates were determined using a validated liquid chromatography-tandem mass spectrometry assay²⁹.

2.7 Materials

Larotrectinib was purchased from Carbosynth (Oxford, UK). Zosuquidar and elacridar HCl were obtained from Sequoia Research Products (Pangbourne, UK). Ko143 was from Tocris Bioscience (Bristol, UK). Bovine Serum Albumin (BSA) Fraction V was obtained from Roche Diagnostics GmbH (Mannheim, Germany). Glucose water 5% w/v was from B. Braun Medical Supplies, Inc. (Melsungen, Germany). Isoflurane was purchased from Pharmachemie (Haarlem, The Netherlands), heparin (5000 IU ml⁻¹) was from Leo Pharma (Breda, The Netherlands). All other

chemicals used in the larotrectinib detection assay were described before²⁹. All other chemicals and reagents were obtained from Sigma-Aldrich (Steinheim, Germany).

2.8 Data and Statistical analysis

Pharmacokinetic parameters were calculated by non-compartmental methods using the PK solver software³⁰. The area under the plasma concentration-time curve (AUC) was calculated using the trapezoidal rule, without extrapolating to infinity. The peak plasma concentration (C_{max}) and the time of maximum plasma concentration (T_{max}) were estimated from the original (individual mouse) data. For mouse experiments, one-way analysis of variance (ANOVA) was used when multiple groups were compared and the Bonferroni *post hoc* correction was used to accommodate multiple testing (with F achieved $P < 0.01$ and no significant variance inhomogeneity). This manuscript complies with BJP's recommendations and requirements on experimental design and analysis^{31,32}. The two-sided unpaired Student's t-test was used when treatments or differences between two specific groups were compared using the software GraphPad Prism7 (GraphPad Software Inc., La Jolla, CA, USA, RRID:SCR_002798). All the data were log-transformed before statistical tests were applied. Statistical analysis was undertaken only for studies where each group size was at least $n = 5$. For *in vitro* transport and uptake experiments, the number of each group is 3, no statistical analysis was performed for these data. Differences were considered statistically significant when $P < 0.01$. All data are presented as geometric mean \pm SD.

2.9 Nomenclature of Targets and Ligands

Key protein targets and ligands in this article are hyperlinked to corresponding entries in <http://www.guidetopharmacology.org>, the common portal for data from the IUPHAR/BPS Guide to PHARMACOLOGY³³, and are permanently archived in the Concise Guide to PHARMACOLOGY³⁴⁻³⁷.

3. RESULTS

3.1 *In vitro* transport of larotrectinib

Transepithelial transport of larotrectinib was tested using polarized monolayers of Madin-Darby Canine Kidney (MDCK-II) parental cells and its subclones overexpressing human (h) ABCB1, hABCG2, and mouse (m) Abcg2. Larotrectinib (5 µM) was modestly transported in the apical direction in the parental MDCK-II cell line ($r = 3.8$, Figure 1A), and this was virtually abrogated by addition of the ABCB1 inhibitor zosuquidar ($r = 1.1$, Figure 1B). These data are compatible with modest transport of larotrectinib by the low-level endogenous canine Abcb1 that is known to be present in the parental MDCK-II cells³⁸. In cells overexpressing hABCB1, there was strong apically directed transport of larotrectinib ($r = 33$, Figure 1C), which was extensively inhibited by zosuquidar ($r = 1.0$, Figure 1D).

Zosuquidar was added to inhibit any possible contribution of endogenous canine Abcb1 in subsequent experiments with MDCK-II cells overexpressing hABCG2 and mAbcg2. The ABCG2 inhibitor Ko143 was used to inhibit the transport activity of hABCG2 and mAbcg2. In hABCG2-overexpressing MDCK-II cells, there was clear apically directed transport of larotrectinib ($r = 9.6$, Figure 1E), and transport was inhibited by Ko143 ($r = 1.4$, Figure 1F). We also observed strong apically directed transport of larotrectinib in cells overexpressing mouse Abcg2 ($r = 41$) and this transport activity could be completely inhibited by Ko143 ($r = 1.1$, Figure 1G and H).

Larotrectinib thus appears to be avidly transported by hABCB1 and mAbcg2, and efficiently by hABCG2. It could also be modestly transported by canine ABCB1.

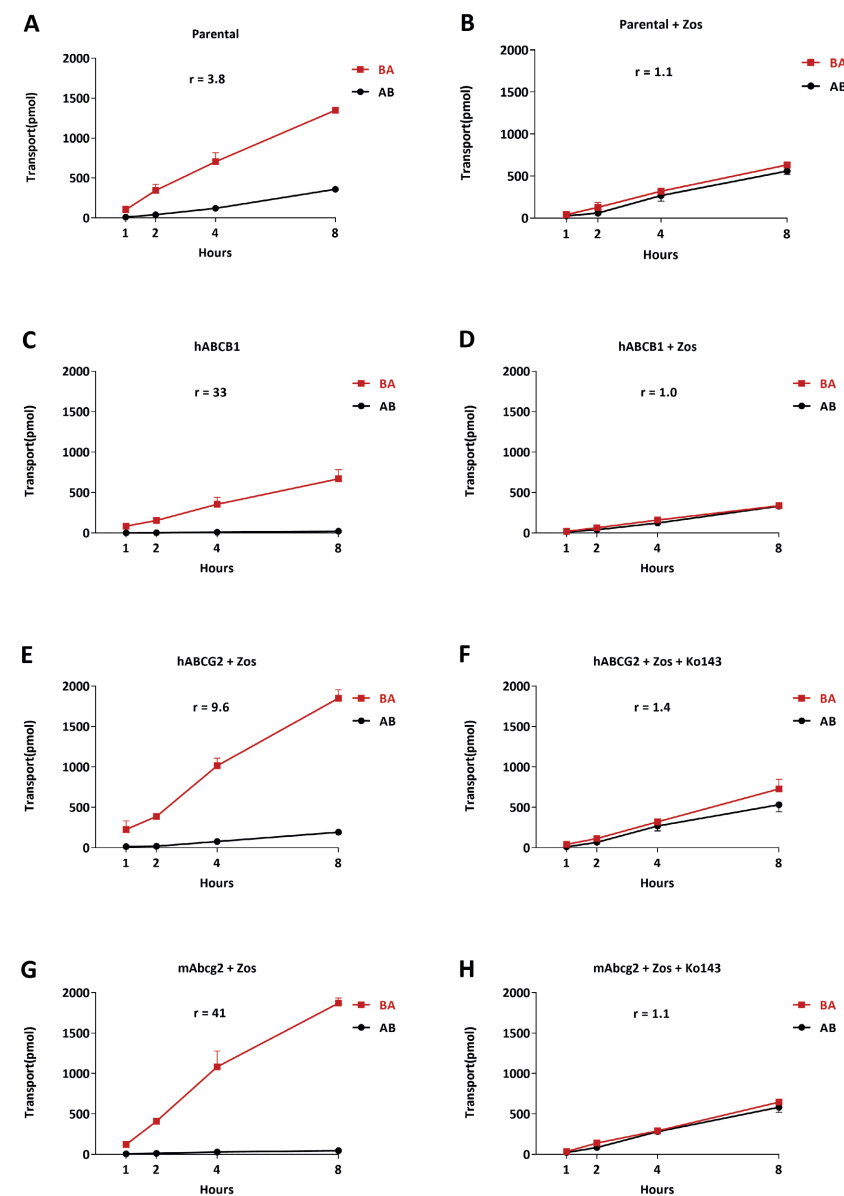


Figure 1. Transepithelial transport of larotrectinib (5 μM) assessed in MDCK-II cells either non-transduced (A, B), transduced with hABCB1 (C, D), hABCG2 (E, F) or mAbcg2 (G, H) cDNA. At $t = 0$ h, drug was applied in the donor compartment and the concentrations in the acceptor compartment at $t = 1, 2, 4$ and 8 h were measured and plotted as larotrectinib transport (pmol) in the graph ($n = 3$). B, D–H: Zosuquidar (Zos, 5 μM) was applied to inhibit human and/or endogenous canine ABCB1. F and H: the ABCG2 inhibitor Ko143 (5 μM) was applied to inhibit ABCG2/Abcg2-mediated transport. r , relative transport ratio. AB (●), translocation from the apical to the basolateral compartment; BA (■), translocation from the basolateral to the apical compartment. Points, mean; bars, S.D.

3.2 ABCB1 and ABCG2 limit larotrectinib plasma, brain, and testis exposure

To investigate the possible impact of ABCB1A/1B and ABCG2 on oral bioavailability and tissue disposition of larotrectinib, we performed an 8 h pharmacokinetic pilot study in male wild-type and *Abcb1a/1b;Abcg2*^{-/-} mice, using oral administration of 10 mg/kg larotrectinib. As shown in Supplemental Figure 2 and Supplemental Table 1, absorption was very rapid and the plasma exposure of larotrectinib over 8 h (AUC_{0-8h}) was significantly higher (2.1-fold) in *Abcb1a/1b;Abcg2*^{-/-} mice than in wild-type mice, especially before 4 h.

Brain, liver, kidney, lung, small intestine and testis concentrations of larotrectinib 8 h after oral administration were analyzed. The brain concentration and brain-to-plasma ratio in *Abcb1a/1b;Abcg2*^{-/-} mice were increased by 15.8-fold and 11.5-fold, respectively, compared to those in wild-type mice (Supplemental Figure 3; Supplemental Table 1). The larotrectinib brain-to-plasma ratio (0.09) in wild-type mice was quite low, suggesting poor brain penetration of larotrectinib at 8 h (Supplemental Table 1). We further observed a slightly lower liver-to-plasma ratio and a markedly lower small intestine-to-plasma ratio in *Abcb1a/1b;Abcg2*^{-/-} mice compared to wild-type mice (Supplemental Figure 4).

We next studied the separate and combined functions of *Abcb1a/1b* and *Abcg2* in oral bioavailability and tissue distribution of larotrectinib. Larotrectinib (10 mg/kg) was administered orally to wild-type, *Abcb1a/1b*^{-/-}, *Abcg2*^{-/-}, and *Abcb1a/1b;Abcg2*^{-/-} mice, and the experiment was terminated at 1 h, when larotrectinib plasma levels were still comparatively high. As shown in Figure 2 and Table 1, single deficiency of either *mAbcb1* or *mAbcg2* resulted in higher larotrectinib plasma exposure, with the plasma AUC_{0-1h} increased in both *Abcb1a/1b*^{-/-} (2.3-fold, *P* < 0.01) and *Abcg2*^{-/-} (1.7-fold, *P* < 0.01) mice (Table 1). In combination *Abcb1a/1b;Abcg2*^{-/-} mice, the larotrectinib plasma AUC_{0-1h} was even further increased up to 3.4-fold compared to wild-type mice (*P* < 0.01). The data suggest that *Abcb1a/1b*, but to some extent also *Abcg2*, can limit the oral availability of larotrectinib.

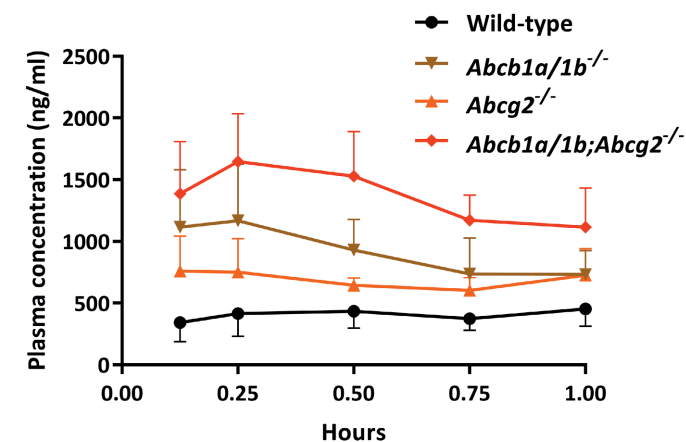


Figure 2. Plasma concentration-time curves of larotrectinib in male wild-type, *Abcb1a/1b*^{-/-}, *Abcg2*^{-/-} and *Abcb1a/1b;Abcg2*^{-/-} mice over 1 h after oral administration of 10 mg/kg larotrectinib. Data are given as mean ± S.D. (wild-type and *Abcb1a/1b*^{-/-} *n* = 7, *Abcg2*^{-/-} and *Abcb1a/1b;Abcg2*^{-/-} *n* = 6).

Table 1. Plasma, brain and testis pharmacokinetic parameters of larotrectinib over 1 h after oral administration of 10 mg/kg larotrectinib to male wild-type, *Abcb1a/1b*^{-/-}, *Abcg2*^{-/-}, and *Abcb1a/1b;Abcg2*^{-/-} mice.

| Parameter | Genotype | | | |
|---------------------------------|--------------|---------------------------------|-----------------------------|---------------------------------------|
| | Wild-type | <i>Abcb1a/1b</i> ^{-/-} | <i>Abcg2</i> ^{-/-} | <i>Abcb1a/1b;Abcg2</i> ^{-/-} |
| AUC _{0-1h} , ng/ml.h | 379 ± 120 | 867 ± 282* | 639 ± 129** | 1297 ± 266* |
| Fold change AUC _{0-1h} | 1.0 | 2.3 | 1.7 | 3.4 |
| C _{max} , ng/ml | 494 ± 156 | 1140 ± 431* | 856 ± 276* | 1684 ± 349* |
| T _{max} , h | 0.7 ± 0.3 | 0.2 ± 0.1 | 0.5 ± 0.4 | 0.3 ± 0.1 |
| C _{brain} , ng/g | 16.7 ± 3.9 | 69.7 ± 16.2** | 20.9 ± 2.7** | 393.3 ± 58.6* |
| Fold change C _{brain} | 1.0 | 4.4 | 1.3 | 25 |
| Brain-to-plasma ratio | 0.036 ± 0.01 | 0.10 ± 0.01** | 0.03 ± 0.01** | 0.38 ± 0.12* |
| Fold change ratio | 1.0 | 2.6 | 0.9 | 10.4 |
| C _{testis} , ng/g | 81.7 ± 15.8 | 301.2 ± 187.1** | 99.3 ± 17.3** | 564.6 ± 133.8* |
| Fold change C _{testis} | 1.0 | 3.7 | 1.2 | 6.9 |
| Testis-to-plasma ratio | 0.19 ± 0.06 | 0.41 ± 0.22* | 0.14 ± 0.03** | 0.52 ± 0.09* |
| Fold change ratio | 1.0 | 2.1 | 0.7 | 2.7 |

Data are given as mean ± S.D. (wild-type and *Abcb1a/1b*^{-/-} *n* = 7, *Abcg2*^{-/-} and *Abcb1a/1b;Abcg2*^{-/-} *n* = 6). AUC_{0-1h}, area under the plasma concentration-time curve; C_{max}, maximum concentration in plasma; T_{max}, time point (h) of maximum plasma concentration; C_{brain}, brain concentration; C_{testis}, testis concentration; *, *P* < 0.01 compared to wild-type mice. **, *P* < 0.01 compared to *Abcb1a/1b;Abcg2*^{-/-} mice. †, *P* < 0.01 compared between *Abcb1a/1b*^{-/-} and *Abcg2*^{-/-} mice. Statistical analysis was applied after log-transformation of linear data.

Interestingly, larotrectinib brain concentrations in *Abcb1a/1b*^{-/-} and *Abcb1a/1b/Abcg2*^{-/-} mice were profoundly increased by 4.4-fold and 25-fold, respectively, compared to wild-type mice, but not in single *Abcg2*^{-/-} mice. The brain-to-plasma ratio of larotrectinib was again very low (0.036) in wild-type mice, but could be increased to 0.10 (2.6-fold) due to single mAbcb1 deficiency and further up to 0.38 (10.4-fold) by combined mAbcb1 and mAbcg2 deficiency (Figure 3A-B; Table 1). The further increase in *Abcb1a/1b/Abcg2*^{-/-} brain demonstrates that, in the absence of *Abcb1a/1b* activity, *Abcg2* still markedly limits larotrectinib brain penetration. The apparent lack of *Abcg2* impact in the single *Abcg2* knockout strain can be readily explained if its absolute transport contribution is considerably lower than that of *Abcb1a/1b* in the mouse BBB. However, once this *Abcb1a/1b* transport background is removed, the more modest transport contribution of *Abcg2* becomes apparent (comparison *Abcb1a/1b* and *Abcb1a/1b/Abcg2* knockout data). A straightforward quantitative pharmacokinetic model to explain this behavior of shared *Abcb1a/1b* and *Abcg2* substrate drugs has been developed³⁹. Qualitatively similar results were obtained for larotrectinib testis penetration, although the wild-type testis-to-plasma ratio was substantially higher (0.19), and the relative increases in ratios in *Abcb1a/1b*^{-/-} (2.1-fold) and *Abcb1a/1b/Abcg2*^{-/-} (2.7-fold) mice were more modest than for brain (Figure 3C-D; Table 1). The data indicate that *Abcb1a/1b* and, to a lesser extent, *Abcg2* can strongly reduce the brain accumulation of larotrectinib, while testis accumulation was more modestly affected.

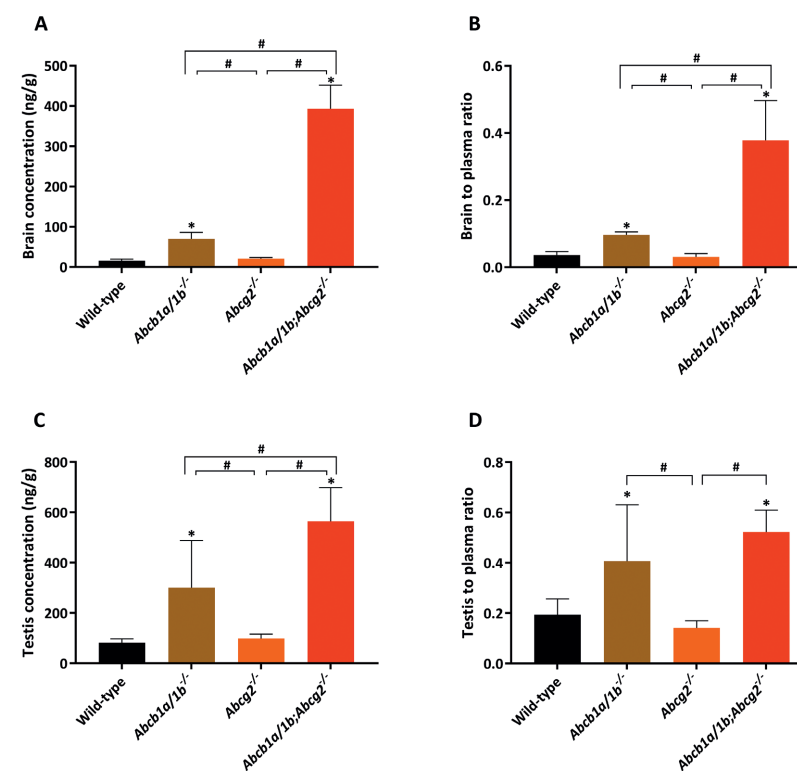


Figure 3. Organ concentration (A, C) and organ-to-plasma ratio (B, D) of larotrectinib in male wild-type, *Abcb1a/1b*^{-/-}, *Abcg2*^{-/-} and *Abcb1a/1b/Abcg2*^{-/-} mice 1h after oral administration of 10 mg/kg larotrectinib (wild-type and *Abcb1a/1b*^{-/-} n = 7, *Abcg2*^{-/-} and *Abcb1a/1b/Abcg2*^{-/-} n = 6). *, $P < 0.01$ compared to wild-type mice. #, $P < 0.01$ compared among knockout mouse strains. Statistical analysis was applied after log-transformation of linear data.

Whereas the liver-, kidney-, and lung-to-plasma ratios were not significantly altered between the four strains, we observed markedly lower small intestine-to-plasma ratios in all three knockout strains compared to wild-type mice, especially in the *Abcb1a/1b*^{-/-} and *Abcb1a/1b/Abcg2*^{-/-} mice (Supplemental Figure 5B, D, F, H). The latter result was also observed in the 8h experiment. The small intestinal tissue concentration often reflects the amount of drug still present in the intestinal lumen. These results may therefore point to more rapid absorption of intestinal larotrectinib in the absence of *Abcg2* and especially *Abcb1a/1b*, or to reduced hepatobiliary excretion of the absorbed larotrectinib, or to a combination of both processes.

It is worth noting that in wild-type mice the tissue-to-plasma ratios for liver, kidney, lung and small intestine (all >1) were far higher than observed for the brain (0.036) and even testis (0.19), illustrating the strong impact of the BBB and BTB on tissue accumulation of larotrectinib. In spite

of the clearly increased plasma and overall tissue exposure of larotrectinib in *Abcb1a/1b;Abcg2*^{-/-} mice, and the dramatically increased brain levels, we did not observe any sign of acute spontaneous toxicity. This contrasts with the TKI drug brigatinib, for which we recently observed severe and even lethal acute toxicity in *Abcb1a/1b;Abcg2*^{-/-} mice¹³.

3.3 *In vitro* uptake of larotrectinib

As the OATP1A/1B and OATP2B1 transporters, which are highly expressed in the liver, can have profound effects on tissue distribution and elimination of their substrates, we evaluated whether larotrectinib is a substrate of human OATP1A2, OATP1B1, OATP1B3 or OATP2B1 *in vitro* using HEK293 cells overexpressing these transporter proteins. Interestingly, OATP1A2 increased the *in vitro* uptake of larotrectinib (5 μ M) by 2.4-fold compared to the vector control cells (Supplemental Figure 6A). However, we observed no significant increase in the uptake of larotrectinib in OATP1B1- and OATP1B3-expressing cells compared to their vector control cells or OATP2B1-expressing cells compared to their mock control cells. The positive control substrate rosuvastatin was avidly taken up by all the OATP-overexpressing cell lines, confirming functional OATP expression in each cell line (Supplemental Figure 6B). These results suggest that *in vitro* larotrectinib is a transport substrate of human OATP1A2, but not of OATP1B1, OATP1B3 or OATP2B1 as measured in HEK293 cells.

3.4 Impact of SLCO1A/1B on larotrectinib plasma pharmacokinetics and tissue disposition

Following up on the *in vitro* OATP uptake results, we investigated whether *Slco1a/1b* deficiency would influence larotrectinib behavior *in vivo*. Aiming for a relatively high larotrectinib plasma level when assessing tissue distribution, we performed a 1 h pharmacokinetic experiment in wild-type and *Slco1a/1b*^{-/-} mice, receiving oral larotrectinib at 10 mg/kg. Interestingly, *Slco1a/1b*^{-/-} mice showed a markedly higher larotrectinib plasma AUC_{0-1h} than wild-type mice (3.8-fold, Figure 4 and Table 2). Larotrectinib tissue concentrations were likewise increased in *Slco1a/1b*^{-/-} mice compared to wild-type mice. In brain, testis, kidney and lung of *Slco1a/1b*^{-/-} mice, the larotrectinib tissue concentrations were 4.2-fold, 3.7-fold, 4.4-fold and 3.2-fold increased, respectively. No substantial meaningful changes were found in tissue-to-plasma ratios in these organs, suggesting that tissue concentrations mainly reflected the increased plasma levels of larotrectinib in *Slco1a/1b*^{-/-} mice (Figure 5, Supplemental Figure 7 and Table 2).

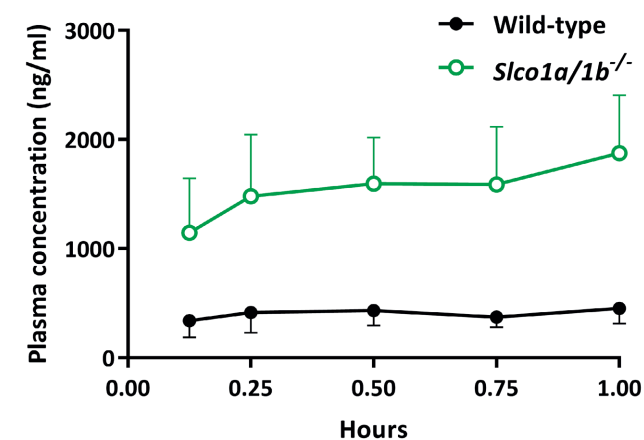


Figure 4. Plasma concentration-time curves of larotrectinib in male wild-type and *Slco1a/1b*^{-/-} mice over 1 h after oral administration of 10 mg/kg larotrectinib. Data are given as mean \pm S.D. (n = 7).

However, in liver, even though the absolute larotrectinib liver concentration was increased by 1.6-fold ($P < 0.01$) in *Slco1a/1b*^{-/-} mice compared to wild-type mice, the liver-to-plasma ratio was 2.9-fold decreased ($P < 0.01$), suggesting relatively reduced liver uptake of larotrectinib in *Slco1a/1b*^{-/-} mice. Perhaps related to this, in small intestinal tissue the absolute larotrectinib tissue concentration was also increased by 1.4-fold, but the tissue-to-plasma ratio was significantly decreased by 2.9-fold ($P < 0.01$) in *Slco1a/1b*^{-/-} mice compared to wild-type mice (Figure 5 and Table 2). It thus appears that mouse *Oatp1a/1b* proteins have a substantial impact on oral larotrectinib pharmacokinetics, most likely by mediating efficient liver uptake of (first-pass) absorbed larotrectinib. The *in vitro* uptake results suggested that larotrectinib is a substrate of OATP1A2. Considering that mouse *Oatp1a1*, -1a4, -1a5, and -1a6 are most related to the single human OATP1A2 protein and that *Oatp1a1* and *Oatp1a4* are both highly expressed in the sinusoidal (basolateral) membrane of hepatocytes^{40,41}, it is very likely that larotrectinib is an hepatic uptake transport substrate of *Oatp1a1* and/or -1a4. The deficiency of mouse *Oatp1a/1b* thus results in reduced uptake of larotrectinib into liver, which may further reduce the hepatobiliary excretion towards the small intestinal lumen. However, as we found that there was still a large amount of most likely unabsorbed larotrectinib (10-15 percent of the administered dose) present in small intestinal tissue plus contents at 1 h after administration in both wild-type and *Slco1a/1b*^{-/-} mice (data not shown), we could not directly test the latter idea.

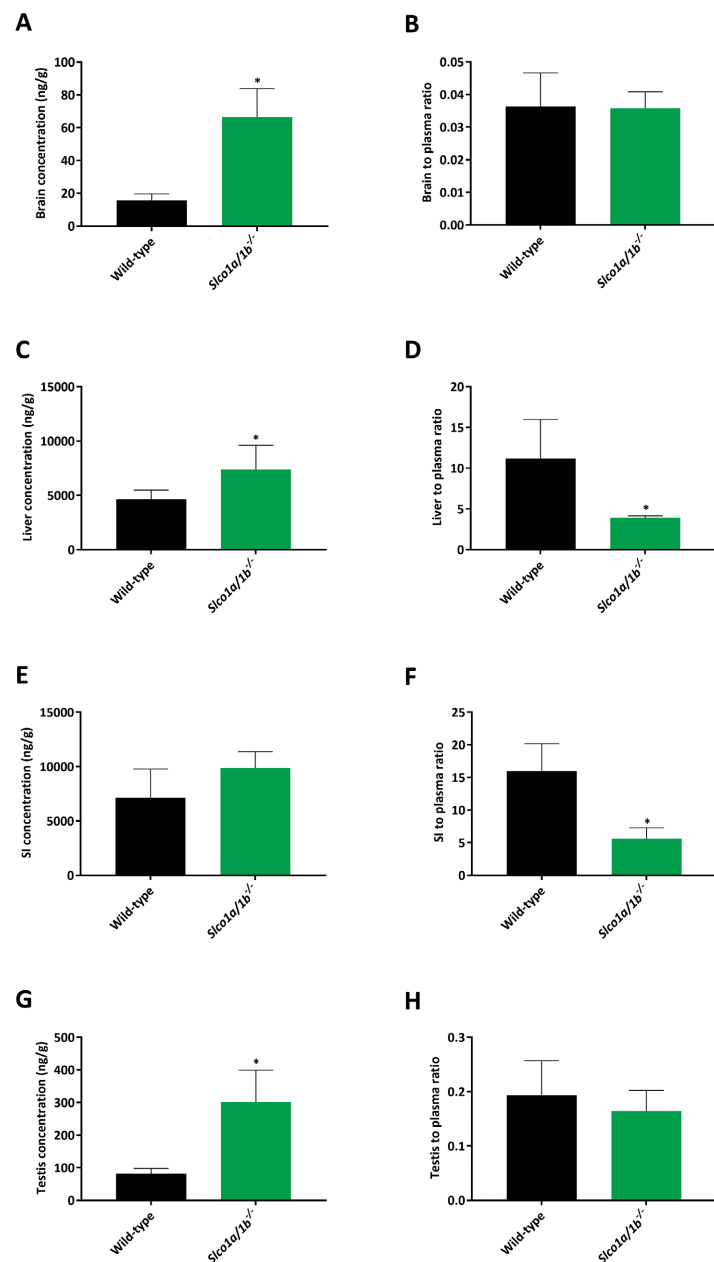


Figure 5. Tissue concentrations (A, C, E, G) and tissue-to-plasma ratios (B, D, F, H) of larotrectinib in male wild-type and *Slco1a1/1b*^{-/-} mice 1h after oral administration of 10 mg/kg larotrectinib (n = 7). SI, small intestinal tissue. *, P < 0.01 compared to wild-type mice. Statistical analysis was applied after log-transformation of linear data.

Table 2. Plasma and organ pharmacokinetic parameters of larotrectinib in male wild-type and *Slco1a1/1b*^{-/-} mice over 1 h after oral administration of 10 mg/kg larotrectinib.

| Parameter | Genotype | |
|-----------------------------------|--------------|----------------------------------|
| | Wild-type | <i>Slco1a1/1b</i> ^{-/-} |
| AUC _{0-1h} , ng/ml.h | 379 ± 120 | 1452 ± 443* |
| Fold change AUC _{0-1h} | 1.0 | 3.8 |
| C _{max} , ng/ml | 494 ± 156 | 1791 ± 494* |
| T _{max} , h | 0.7 ± 0.3 | 0.9 ± 0.2 |
| C _{brain} , ng/g | 16.7 ± 3.9 | 66.5 ± 17.4* |
| Fold increase C _{brain} | 1.0 | 4.2 |
| Brain-to-plasma ratio | 0.036 ± 0.01 | 0.046 ± 0.01 |
| Fold increase ratio | 1.0 | 1.0 |
| C _{liver} , ng/g | 4614 ± 862 | 7393 ± 2215* |
| Fold increase C _{liver} | 1.0 | 1.6 |
| Liver-to-plasma ratio | 11.2 ± 4.8 | 3.9 ± 0.2* |
| Fold change ratio | 1.0 | 0.35 |
| C _{SI} , ng/g | 7140 ± 2645 | 9879 ± 1487 |
| Fold increase C _{SI} | 1.0 | 1.4 |
| SI-to-plasma ratio | 16.0 ± 4.2 | 5.6 ± 1.7* |
| Fold change ratio | 1.0 | 0.35 |
| C _{testis} , ng/g | 81.7 ± 15.8 | 301.5 ± 98.0* |
| Fold increase C _{testis} | 1.0 | 3.7 |
| Testis-to-plasma ratio | 0.19 ± 0.06 | 0.16 ± 0.04 |
| Fold change ratio | 1.0 | 0.85 |

Data are given as mean ± S.D. (n = 7). AUC_{0-8h}, area under the plasma concentration-time curve; C_{max}, maximum concentration in plasma; T_{max}, time point (h) of maximum plasma concentration; C_{brain}, brain concentration; C_{liver}, liver concentration; SI, small intestine (tissue); C_{SI}, small intestine tissue concentration; C_{testis}, testis concentration; *, P < 0.01 compared to wild-type mice. Statistical analysis was applied after log-transformation of linear data.

3.5 Impact of CYP3A on larotrectinib plasma pharmacokinetics and tissue disposition

CYP3A plays an important role in metabolism of many (pro-) drugs, and therefore in restricting oral availability of its substrates. To assess its *in vivo* impact on larotrectinib we performed an 8 h pharmacokinetic pilot study in wild-type and *Cyp3a*^{-/-} mice. Larotrectinib (10 mg/kg) was administered orally after 2-3 h of fasting, blood samples were taken at several time points, and at 8 h organs were collected. The oral plasma larotrectinib AUC_{0-8h} in *Cyp3a*^{-/-} mice was significantly higher (1.7-fold, P < 0.01) than that in wild-type mice (Supplemental Figure 8 and Supplemental Table 2). Interestingly, as seen with the ABC transporter-deficient mice (Supplemental Figure 2), the main differences in plasma exposure occurred before 4 h. With respect to the tissue distribution at 8 h, there were no significant/meaningful differences in tissue concentrations

or tissue-to-plasma ratios between wild-type and *Cyp3a*^{-/-} mice for brain, liver, kidney, small intestine, lung and testis (Supplemental Table 2 and Supplemental Figure 9).

To study the *in vivo* effect of human CYP3A4 on larotrectinib metabolism, a 4 h experiment was performed in male wild-type, *Cyp3a*^{-/-} and *Cyp3aXAV* mice (*Cyp3a*^{-/-} mice with transgenic expression of human CYP3A4 in liver and intestine). After oral administration of 10 mg/kg larotrectinib, blood and organs were collected and processed as described above. As shown in Figure 6 and Table 3, the oral larotrectinib plasma AUC_{0-4h} in *Cyp3a*^{-/-} mice was 1.7-fold higher ($P < 0.01$) than that in wild-type mice. Moreover, larotrectinib plasma exposure in *Cyp3aXAV* mice was decreased by 2-fold ($P < 0.01$) relative to that in wild-type mice and by 3.5-fold ($P < 0.01$) relative to *Cyp3a*^{-/-} mice. Compared to the *Cyp3a*^{-/-} and wild-type mice, larotrectinib clearance from 30 min on was markedly higher in the *Cyp3aXAV* mice (Figure 6 B). With respect to the tissue distribution of larotrectinib at 4 h, the observed differences in absolute tissue concentrations between the strains in brain, liver, kidney, small intestine, lung, and testis mostly reflected the different plasma concentrations (Figure 7), as the tissue-to-plasma ratios were not substantially altered between the strains (Supplemental Figure 10). Note that the brain concentration at 4 h in *Cyp3aXAV* mice was below the lower limit of detection due to low plasma exposure of larotrectinib, and the associated brain parameters were therefore not plotted.

Collectively, these results indicate that larotrectinib is substantially metabolized by mouse CYP3A and human CYP3A4, which markedly affects the oral availability and, consequently, the tissue levels of larotrectinib.

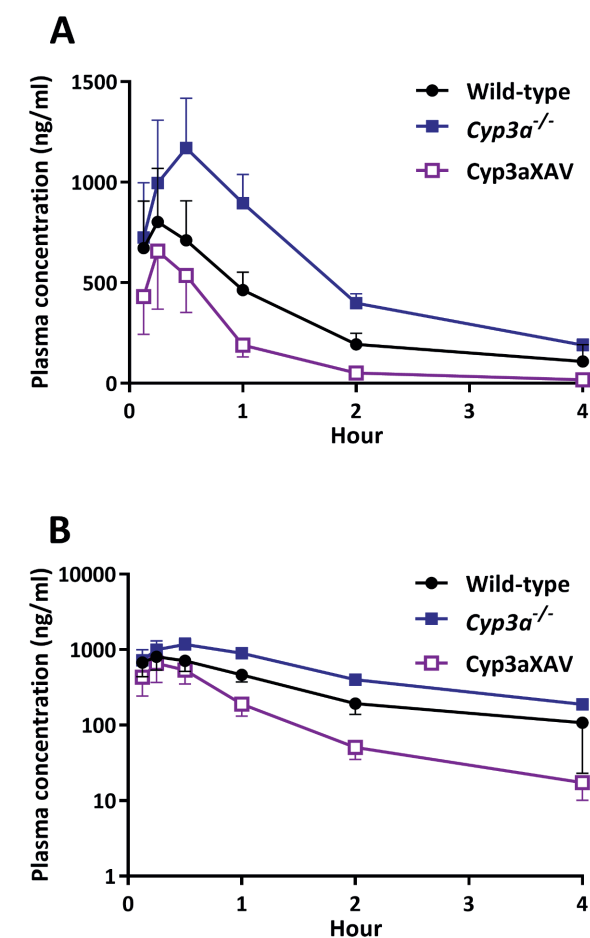


Figure 6. Plasma concentration-time curves (A) and semi-log plot of plasma concentration-time curves (B) of larotrectinib in male wild-type, *Cyp3a*^{-/-} and *Cyp3aXAV* mice 4h after oral administration of 10 mg/kg larotrectinib. Data are given as mean \pm S.D. ($n = 6$).

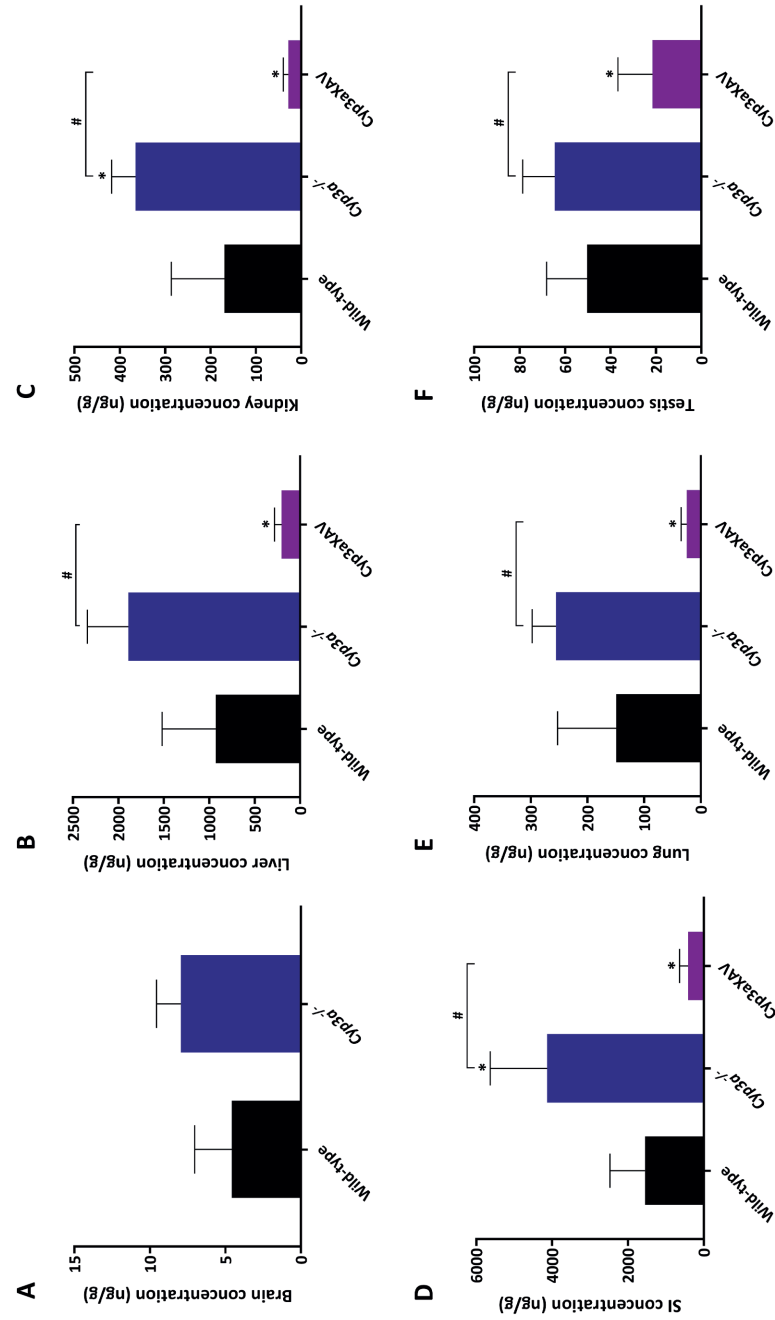


Figure 7. Tissue concentrations for brain (A), liver (B), small intestine (D), lung (E) and testis (F) of larotrectinib in male wild-type, *Cyp3a*^{-/-} and *Cyp3aXAV* mice 4 h after oral administration of 10 mg/kg larotrectinib (n = 6). * P < 0.01 compared to wild-type mice; #, P < 0.01 compared between *Cyp3a*^{-/-} and *Cyp3aXAV* mice. Statistical analysis was applied after log-transformation of linear data.

Table 3. Pharmacokinetic parameters, brain concentrations, and brain-to-plasma ratios of larotrectinib in male wild-type, *Cyp3a*^{-/-} and *Cyp3aXAV* mice over 4 h after oral administration of 10 mg/kg larotrectinib.

| Parameter | Genotype | | |
|---------------------------------|-------------|-----------------------------|-----------------|
| | Wild-type | <i>Cyp3a</i> ^{-/-} | <i>Cyp3aXAV</i> |
| AUC _{0-4h} , ng/ml.h | 1246 ± 228 | 2174 ± 286* | 614 ± 192** |
| Fold change AUC _{0-4h} | 1.0 | 1.7 | 0.5 |
| C _{max} , ng/ml | 816 ± 258 | 1187 ± 236 | 666 ± 278# |
| T _{max} , h | 0.3 ± 0.1 | 0.5 ± 0.2 | 0.3 ± 0.1 |
| C _{brain} , ng/g | 4.6 ± 2.5 | 8.0 ± 1.6 | N.D. |
| Fold change C _{brain} | 1.0 | 1.7 | N.A. |
| Brain-to-plasma ratio | 0.05 ± 0.02 | 0.04 ± 0.004 | N.A. |
| Fold change ratio | 1.0 | 0.8 | N.A. |
| C _{liver} , ng/g | 930 ± 591 | 1894 ± 450* | 206 ± 78# |
| Fold change C _{liver} | 1.0 | 2.0 | 0.2 |
| C _{SI} , ng/g | 1551 ± 925 | 4131 ± 1503* | 418 ± 223** |
| Fold change C _{SI} | 1.0 | 2.7 | 0.3 |
| C _{testis} , ng/g | 50.4 ± 17.8 | 64.6 ± 14.0 | 21.6 ± 15.1** |
| Fold change C _{testis} | 1.0 | 1.3 | 0.3 |
| Testis-to-plasma ratio | 0.8 ± 0.5 | 0.3 ± 0.05 | 1.3 ± 0.6 |
| Fold change ratio | 1.0 | 0.4 | 1.6 |

Data are given as mean ± S.D. (n = 6). AUC_{0-4h}, area under plasma concentration-time curve; C_{max}, maximum concentration in plasma; T_{max}, time point (h) of maximum plasma concentration; C_{brain}, brain concentration; C_{liver}, liver concentration; SI, small intestine (tissue); C_{SI}, small intestine tissue concentration; C_{testis}, testis concentration; *, P < 0.01 compared to wild-type mice; #, P < 0.01 compared between *Cyp3a*^{-/-} and *Cyp3aXAV* mice. N.D.: Not detectable, N.A.: Not applicable. Statistical analysis was applied after log-transformation of linear data.

4. DISCUSSION AND CONCLUSIONS

We found that *in vitro*, larotrectinib is highly effectively transported by human ABCB1 and mouse Abcg2 and efficiently by human ABCG2. *In vivo*, upon oral administration of 10 mg/kg larotrectinib, plasma AUCs were increased by 2.3-fold and 1.7-fold in *Abcb1a/1b*^{-/-} and *Abcg2*^{-/-} mice, respectively, and by 3.4-fold in *Abcb1a/1b;Abcg2*^{-/-} mice compared to wild-type mice. Thus, both mAbcb1a/1b and mAbcg2 can markedly limit the oral availability of larotrectinib, with a somewhat more pronounced role for Abcb1a/1b. Given our data, this effect of the ABC transporters may be either due to their limiting the net intestinal absorption of larotrectinib, or mediating the hepatobiliary elimination, or a combination of both processes. The brain-to-plasma ratio of larotrectinib was low (0.036) in wild-type mice, indicating poor brain penetration of larotrectinib. This could be increased to 0.10 (2.6-fold) in *Abcb1a/1b*^{-/-} mice and further up to 0.38 (10.4-fold) in *Abcb1a/1b;Abcg2*^{-/-} mice (Figure 3A-B; Table 1), but not in single *Abcg2*^{-/-} mice. The data indicate that ABCB1 P-glycoprotein in the blood-brain-barrier (BBB) can strongly restrict

the brain penetration of larotrectinib, while ABCG2 has a more modest effect. We obtained qualitatively similar results for larotrectinib testis penetration, indicating similar functions of ABCB1 and ABCG2 in the blood-testis-barrier (BTB). Despite the increased plasma and tissue exposure, no acute spontaneous toxicity was observed for larotrectinib in the *Abcb1a/1b;Abcg2*^{-/-} mice (nor in the *Slco1a/1b*^{-/-} and *Cyp3a*^{-/-} mice). We note that the plasma levels of larotrectinib we obtained in our mouse studies (C_{max} ~500-800 ng/ml in wild-type mice, Tables 1-3) were close to the average C_{max} obtained for larotrectinib during steady-state treatment of patients (788 ng/ml).

We observed a markedly decreased concentration and tissue-to-plasma ratio of larotrectinib in the small intestine in the absence of *Abcb1a/1b* or *Abcg2*, and when both *Abcb1a/1b* and *Abcg2* were deficient, these values were even lower ($P < 0.01$). As explained above, since small intestinal tissue concentrations often reflect the amount of drug still present in the intestinal lumen, this suggests that *Abcb1a/1b* and *Abcg2* can mediate either the direct efflux of larotrectinib across the intestinal wall (also reducing net intestinal uptake) or the hepatobiliary excretion of larotrectinib or a combination of both processes. No noticeable changes in tissue distribution due to the ABC transporter deficiencies were found in other tissues including liver, kidney and lung.

Although infrequent, NTRK fusions can occur in diverse types of cancer, including glioblastoma, NSCLC, and colorectal cancer, and frequencies are even higher in certain rare pediatric tumors, such as infantile fibrosarcoma, cellular congenital mesoblastic nephroma, and papillary thyroid cancer³⁻⁵. As brain metastases can easily occur in NSCLC, and glioblastoma is a primary brain tumor, it is important to know whether larotrectinib can achieve high intrinsic BBB permeability, and how it interacts with ABCB1 and ABCG2 in the BBB. While this project was ongoing, the FDA approved larotrectinib (Food and Drug Administration, 2018). According to its guidelines, larotrectinib is a good substrate of ABCB1 and ABCG2, in accordance with our data. The observed strong interactions with ABCB1 and ABCG2 could well result in poor brain penetration also in humans, potentially limiting therapeutic efficacy. So far, there is little documentation about human larotrectinib brain penetration or accumulation. Ziegler et al. reported that larotrectinib penetrates the BBB and may have potent activity in TRK-driven high-grade glioma in a 3-year old child⁴², but there is no evidence such activity could be translated to other cases and the drug concentration and activity in brain are still unclear. Based on our data and previous *in vivo* inhibition studies, brain penetration of larotrectinib could perhaps be enhanced by up to 10-fold by co-administering an efficacious ABCB1 and ABCG2 inhibitor such as elacridar. As also tumors that express significant levels of ABCB1 and/or ABCG2 themselves might become relatively drug resistant, there could be an added benefit to such an inhibitor approach.

Unexpectedly, we found that larotrectinib is a likely substrate of human OATP1A2 *in vitro*, but not of human OATP1B1 or -1B3, the latter negative result in line with the FDA registration

documentation. An *in vivo* pharmacokinetic study revealed a pronounced impact of mouse *Slco1a/1b* transporters on the oral availability and tissue distribution of larotrectinib. *Slco1a/1b*-deficient mice showed a 3.8-fold higher larotrectinib plasma AUC_{0-1h} than wild-type mice, with concomitantly increased tissue concentrations in brain, testis, kidney and lung, but without changes in tissue-to-plasma ratios. However, in liver and small intestine, although absolute tissue concentrations were slightly higher in *Slco1a/1b*^{-/-} mice due to the higher larotrectinib plasma exposure, we observed a clear decrease (both 2.9-fold) in tissue-to-plasma ratios in *Slco1a/1b*^{-/-} compared to wild-type mice.

These data indicate that larotrectinib is a good *in vivo* transport substrate of mOatp1a/1b. Taking the *in vitro* uptake results into consideration, we assume that this uptake effect is mainly due to mOatp1a1 and/or mOatp1a4 in the mouse liver. The deficiency of hepatic sinusoidal mOatp1a leads to relatively reduced larotrectinib uptake into the liver and consequently more larotrectinib retention in the blood. The decreased accumulation of larotrectinib in the liver may then also result in relatively reduced hepatobiliary excretion of larotrectinib, restricting the amount of larotrectinib returned to the intestinal lumen. However, we could not confirm the latter effect due to the high levels of remaining larotrectinib in the intestinal lumen 1 h after administration. The unchanged tissue-to-plasma ratios in all other tested tissues further suggest that, despite the significant expression of some *Slco1a/1b* transporters in BBB and BTB, they do not have noticeable effects on larotrectinib brain and testis penetration. Also kidney and lung appeared to just passively follow the larotrectinib plasma concentration. It is worth noting that in most cases we used single-time-point data for tissue-to-plasma ratios, which may not necessarily reflect the behavior over the whole exposure time. However, by choosing time points where plasma levels were still very substantial, and close to the C_{max} for the transporter studies (see e.g. Figures 2 and 4), we think that we obtained a reasonable estimate of qualitative changes in tissue exposure due to the transporter inactivation.

Larotrectinib is, to our knowledge, the first targeted TKI anticancer drug for which the disposition of the parent compound is demonstrated to be strongly affected by mouse *Oatp1a/1b* proteins. For some targeted drugs, such as sorafenib, the disposition of the negatively charged glucuronide metabolite can be strongly affected, but impact on the parent compound is minimal^{43,44}. It appears that pharmaceutical companies are relatively efficient in developing targeted anticancer drugs that are minimal OATP substrates. This contrasts with efforts to develop drugs that are not significantly transported by ABCB1 and/or ABCG2, as we and others have found that the vast majority of new TKIs is transported by ABCB1 and/or ABCG2 to such an extent that their brain penetration is markedly restricted by these transporters^{45,46}. As this study was being finalized, larotrectinib was approved by the FDA, and the registration documentation states that larotrectinib was not significantly transported by human OATP1B1 or -1B3, in line with our own findings. It may therefore be that the OATP1A/1B impact is more limited in humans, and perhaps

absent. It should be noted, however, that OATP-mediated uptake of certain substrates can be cell-type dependent for as yet unknown reasons⁴⁷, so a negative result does not necessarily mean that a substrate cannot be transported under any circumstances. We therefore would still recommend vigilance in recognizing possible OATP-mediated drug-drug interactions during the clinical application of larotrectinib.

We further found that larotrectinib oral availability in mice was markedly restricted by mouse Cyp3a (1.7-fold) and especially by human CYP3A4 (3.5-fold), demonstrating that human CYP3A can play a substantial role in the metabolic clearance of larotrectinib. We did not observe any meaningful changes in tissue-to-plasma ratios, suggesting that the differences in tissue concentrations simply reflected the different plasma concentrations among the mouse strains. Our results are in line with the FDA data, indicating that larotrectinib is a good substrate of CYP3A4. The substantial intestinal and hepatic first-pass metabolism and elimination functions of CYP3A for larotrectinib will likely markedly influence its overall tissue exposure and thus efficacy. Various well-known drug-drug interactions affecting CYP3A activity as well as some genetic polymorphisms may drastically affect the oral availability and subsequent tissue and tumor accumulation of larotrectinib, potentially compromising its therapeutic effect and safety. On the other hand, the clear *in vivo* interactions of larotrectinib with the ABCB1, ABCG2, and OATP1A/1B transporters, as well as with CYP3A4 that we observed raise the possibility that larotrectinib may also partially inhibit these detoxifying systems in clearing other substrate anticancer drugs, and this might affect their efficacy and toxicity. Indeed, the FDA documentation cautions against coadministering larotrectinib with CYP3A(4)-sensitive substrates. However, at least *in vitro*, larotrectinib did not substantially inhibit ABCB1, ABCG2, OATP1B1, and OATP1B3, suggesting that these transporters may present less of a drug interaction risk with larotrectinib as perpetrator.

In summary, ABCG2 and especially ABCB1 can limit the oral availability and brain penetration of larotrectinib. To the best of our knowledge, this is the first study documenting that OATP1A/1B (most likely OATP1A proteins) can restrict larotrectinib systemic exposure by mediating hepatic uptake and thus, presumably, facilitating hepatobiliary excretion. Additionally, CYP3A-mediated metabolism can strongly reduce larotrectinib oral availability and thus its tissue concentrations. The obtained insights and principles may potentially be used to further enhance the therapeutic application and efficacy of larotrectinib, especially for brain metastases in NSCLC and for glioblastoma patients.

ACKNOWLEDGEMENTS

This work was funded in part by the Chinese Scholarship Council (CSC Scholarship No. 201506240107 to Yaogeng Wang).

AUTHOR CONTRIBUTIONS

Yaogeng Wang and Alfred H. Schinkel designed the study, analyzed the data and wrote the manuscript. Yaogeng Wang, Rolf W. Sparidans, and Wenlong Li performed the experimental parts of the study. Maria C. Lebre contributed reagents, materials, and mice. Jos H. Beijnen and Rolf W. Sparidans supervised the bioanalytical part of the studies and checked the content and language of manuscript. All authors commented on and approved the manuscript.

CONFLICT OF INTEREST STATEMENT

The research group of Alfred Schinkel receives revenue from commercial distribution of some of the mouse strains used in this study. The remaining authors declare no conflict of interest.

DECLARATION OF TRANSPARENCY AND SCIENTIFIC RIGOUR

This Declaration acknowledges that this paper adheres to the principles for transparent reporting and scientific rigour of preclinical research as stated in the BJP guidelines for Design & Analysis, and Animal Experimentation, and as recommended by funding agencies, publishers and other organisations engaged with supporting research.

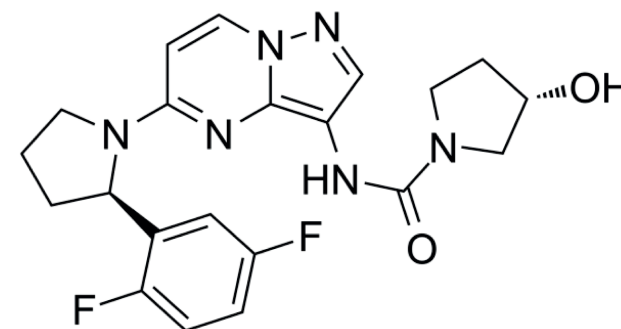
REFERENCE

- Nakagawara, A. Trk receptor tyrosine kinases: a bridge between cancer and neural development. *Cancer Letters* **169**, 107-114 (2001).
- Huang, E.J. & Reichardt, L.F. Trk receptors: roles in neuronal signal transduction. *Annual Review of Biochemistry* **72**, 609-642 (2003).
- Créancier, L., *et al.* Chromosomal rearrangements involving the NTRK1 gene in colorectal carcinoma. *Cancer Letters* **365**, 107-111 (2015).
- Wu, G., *et al.* The genomic landscape of diffuse intrinsic pontine glioma and pediatric non-brainstem high-grade glioma. *Nature Genetics* **46**, 444-450 (2014).
- Stransky, N., Cerami, E., Schalm, S., Kim, J.L. & Lengauer, C. The landscape of kinase fusions in cancer. *Nature Communications* **5**, 4846 (2014).
- Amatu, A., Sartore-Bianchi, A. & Siena, S. NTRK gene fusions as novel targets of cancer therapy across multiple tumour types. *ESMO Open* **1**, e000023 (2016).
- Drilon, A., *et al.* Efficacy of Larotrectinib in TRK Fusion-Positive Cancers in Adults and Children. *New England Journal of Medicine* **378**, 731-739 (2018).
- Nigam, S.K. What do drug transporters really do? *Nature Reviews Drug Discovery* **14**, 29-44 (2014).
- Giacomini, K.M., *et al.* Membrane transporters in drug development. *Nature Reviews Drug Discovery* **9**, 215-236 (2010).
- Schinkel, A.H. & Jonker, J.W. Mammalian drug efflux transporters of the ATP binding cassette (ABC) family: an overview. *Advanced Drug Delivery Reviews* **55**, 3-29 (2003).
- Tang, S.C., *et al.* Impact of P-glycoprotein (ABCB1) and breast cancer resistance protein (ABCG2) gene dosage on plasma pharmacokinetics and brain accumulation of dasatinib, sorafenib, and sunitinib. *Journal of Pharmacology and Experimental Therapeutics* **346**, 486-494 (2013).
- Tang, S.C., *et al.* Increased oral availability and brain accumulation of the ALK inhibitor crizotinib by coadministration of the P-glycoprotein (ABCB1) and breast cancer resistance protein (ABCG2) inhibitor elacridar. *International Journal of Cancer* **134**, 1484-1494 (2014).
- Li, W., *et al.* P-glycoprotein and breast cancer resistance protein restrict brigatinib brain accumulation and toxicity, and, alongside CYP3A, limit its oral availability. *Pharmacological Research* **137**, 47-55 (2018a).
- Li, W., *et al.* P-glycoprotein (MDR1/ABCB1) restricts brain accumulation and cytochrome P450-3A (CYP3A) limits oral availability of the novel ALK/ROS1 inhibitor lorlatinib. *International Journal of Cancer* **143**, 2029-2038 (2018b).
- Hagenbuch, B. & Meier, P.J. Organic anion transporting polypeptides of the OATP/ SLC21 family: phylogenetic classification as OATP/ SLCO superfamily, new nomenclature and molecular/functional properties. *Pflügers Archiv. European Journal of Physiology* **447**, 653-665 (2004).
- van de Steeg, E., van Esch, A., Wagenaar, E., Kenworthy, K.E. & Schinkel, A.H. Influence of human OATP1B1, OATP1B3, and OATP1A2 on the pharmacokinetics of methotrexate and paclitaxel in humanized transgenic mice. *Clinical Cancer Research* **19**, 821-832 (2013).
- Shitara, Y., *et al.* Clinical significance of organic anion transporting polypeptides (OATPs) in drug disposition: their roles in hepatic clearance and intestinal absorption. *Biopharmaceutics and Drug Disposition* **34**, 45-78 (2013).
- van de Steeg, E., *et al.* Complete OATP1B1 and OATP1B3 deficiency causes human Rotor syndrome by interrupting conjugated bilirubin reuptake into the liver. *Journal of Clinical Investigation* **122**, 519-528 (2012).
- van de Steeg, E., *et al.* Organic anion transporting polypeptide 1a/1b-knockout mice provide insights into hepatic handling of bilirubin, bile acids, and drugs. *Journal of Clinical Investigation* **120**, 2942-2952 (2010).
- Kalliokoski, A. & Niemi, M. Impact of OATP transporters on pharmacokinetics. *British Journal of Pharmacology* **158**, 693-705 (2009).
- van de Steeg, E., *et al.* Methotrexate Pharmacokinetics in Transgenic Mice with Liver-Specific Expression of Human Organic Anion-Transporting Polypeptide 1B1 (SLCO1B1). *Drug Metabolism and Disposition* **37**, 277-281 (2008).

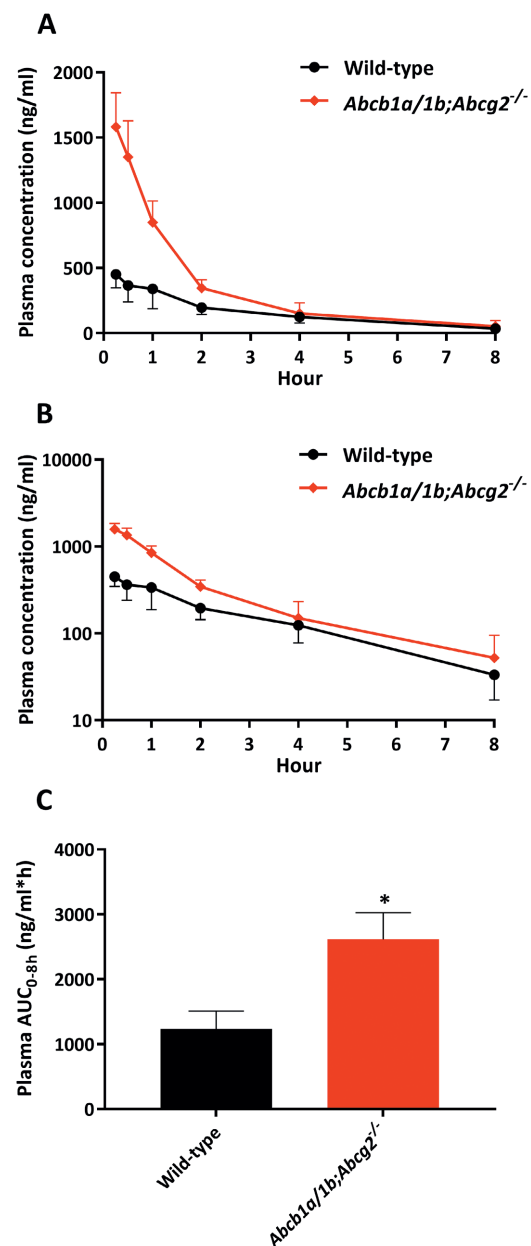
- Guengerich, F.P. Cytochrome P-450 3A4: regulation and role in drug metabolism. *Annual Review of Pharmacology and Toxicology* **39**, 1-17 (1999).
- van Herwaarden, A.E., *et al.* Knockout of cytochrome P450 3A yields new mouse models for understanding xenobiotic metabolism. *Journal of Clinical Investigation* **117**, 3583-3592 (2007).
- Evers, R., *et al.* Drug export activity of the human canalicular multispecific organic anion transporter in polarized kidney MDCK cells expressing cMOAT (MRP2) cDNA. *Journal of Clinical Investigation* **101**, 1310-1319 (1998).
- Bakos, E., *et al.* Characterization of the amino-terminal regions in the human multidrug resistance protein (MRP1). *Journal of Cell Science* **113 Pt 24**, 4451-4461 (2000).
- Durmus, S., *et al.* In vivo disposition of doxorubicin is affected by mouse Oatp1a/1b and human OATP1A/1B transporters. *International Journal of Cancer* **135**, 1700-1710 (2014).
- McGrath, J.C. & Lilley, E. Implementing guidelines on reporting research using animals (ARRIVE etc.): new requirements for publication in BJP. *British Journal of Pharmacology* **172**, 3189-3193 (2015).
- Kilkenny, C., Browne, W., Cuthill, I.C., Emerson, M. & Altman, D.G. Animal research: reporting in vivo experiments: the ARRIVE guidelines. *British Journal of Pharmacology* **160**, 1577-1579 (2010).
- Sparidans, R.W., Wang, Y., Schinkel, A.H., Schellens, J.H.M. & Beijnen, J.H. Quantitative bioanalytical assay for the tropomyosin receptor kinase inhibitor larotrectinib in mouse plasma and tissue homogenates using liquid chromatography-tandem mass spectrometry. *Journal of Chromatography. B: Analytical Technologies in the Biomedical and Life Sciences* **1102-1103**, 167-172 (2018).
- Zhang, Y., Huo, M., Zhou, J. & Xie, S. PKSolver: An add-in program for pharmacokinetic and pharmacodynamic data analysis in Microsoft Excel. *Computer Methods and Programs in Biomedicine* **99**, 306-314 (2010).
- Curtis, M.J., *et al.* Experimental design and analysis and their reporting II: updated and simplified guidance for authors and peer reviewers. *British Journal of Pharmacology* **175**, 987-993 (2018).
- Curtis, M.J., *et al.* Experimental design and analysis and their reporting: new guidance for publication in BJP. *British Journal of Pharmacology* **172**, 3461-3471 (2015).
- Southan, C., *et al.* The IUPHAR/BPS Guide to PHARMACOLOGY in 2016: towards curated quantitative interactions between 1300 protein targets and 6000 ligands. *Nucleic Acids Research* **44**, D1054-1068 (2016).
- Alexander, S.P.H., *et al.* THE CONCISE GUIDE TO PHARMACOLOGY 2019/20: Transporters. *British Journal of Pharmacology* **176 Suppl 1**, S397-s493 (2019).
- Alexander, S.P.H., *et al.* THE CONCISE GUIDE TO PHARMACOLOGY 2019/20: Catalytic receptors. *British Journal of Pharmacology* **176 Suppl 1**, S247-s296 (2019).
- Alexander, S.P.H., *et al.* THE CONCISE GUIDE TO PHARMACOLOGY 2019/20: Enzymes. *British Journal of Pharmacology* **176 Suppl 1**, S297-s396 (2019).
- Alexander, S.P., *et al.* THE CONCISE GUIDE TO PHARMACOLOGY 2017/18: Overview. *British Journal of Pharmacology* **174 Suppl 1**, S1-s16 (2017).
- Simoff, I., *et al.* Complete Knockout of Endogenous Mdr1 (Abcb1) in MDCK Cells by CRISPR-Cas9. *Journal of Pharmaceutical Sciences* **105**, 1017-1021 (2016).
- Kodaira, H., Kusuhara, H., Ushiki, J., Fuse, E. & Sugiyama, Y. Kinetic analysis of the cooperation of P-glycoprotein (P-gp/Abcb1) and breast cancer resistance protein (Bcrp/Abcg2) in limiting the brain and testis penetration of erlotinib, flavopiridol, and mitoxantrone. *Journal of Pharmacology and Experimental Therapeutics* **333**, 788-796 (2010).
- Cheng, X., Maher, J., Chen, C. & Klaassen, C.D. Tissue distribution and ontogeny of mouse organic anion transporting polypeptides (Oatps). *Drug Metabolism and Disposition* **33**, 1062-1073 (2005).
- Iusuf, D., van de Steeg, E. & Schinkel, A.H. Functions of OATP1A and 1B transporters in vivo: insights from mouse models. *Trends in Pharmacological Sciences* **33**, 100-108 (2012).
- Ziegler, D.S., *et al.* Brief Report: Potent clinical and radiological response to larotrectinib in TRK fusion-driven high-grade glioma. *British Journal of Cancer* **119**, 693-696 (2018).
- Zimmerman, E.I., *et al.* Contribution of OATP1B1 and OATP1B3 to the disposition of sorafenib and sorafenib-glucuronide. *Clinical Cancer Research* **19**, 1458-1466 (2013).
- Vasilyeva, A., *et al.* Hepatocellular Shuttling and Recirculation of Sorafenib-Glucuronide Is Dependent on Abcc2, Abcc3, and Oatp1a/1b. *Cancer Research* **75**, 2729-2736 (2015).

45. van Hoppe, S. & Schinkel, A.H. What next? Preferably development of drugs that are no longer transported by the ABCB1 and ABCG2 efflux transporters. *Pharmacological Research* **123**, 144 (2017a).
46. van Hoppe, S., Sparidans, R.W., Wagenaar, E., Beijnen, J.H. & Schinkel, A.H. Breast cancer resistance protein (BCRP/ABCG2) and P-glycoprotein (P-gp/ABCB1) transport afatinib and restrict its oral availability and brain accumulation. *Pharmacological Research* **120**, 43-50 (2017b).
47. de Graan, A.J., *et al.* Influence of polymorphic OATP1B-type carriers on the disposition of docetaxel. *Clinical Cancer Research* **18**, 4433-4440 (2012).

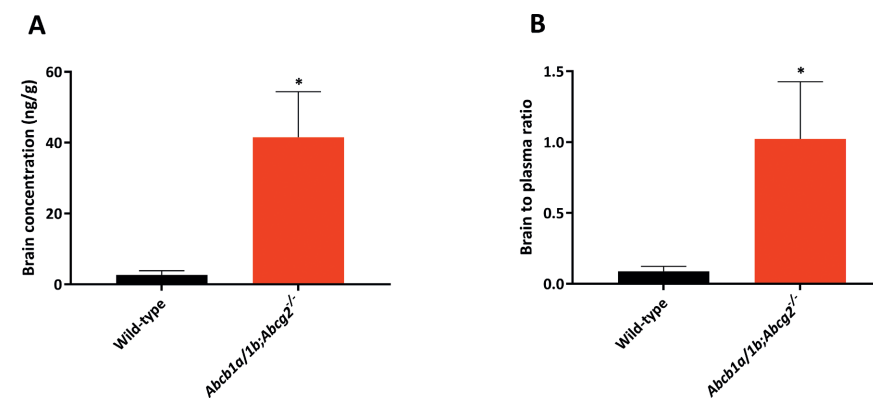
SUPPLEMENTAL MATERIALS



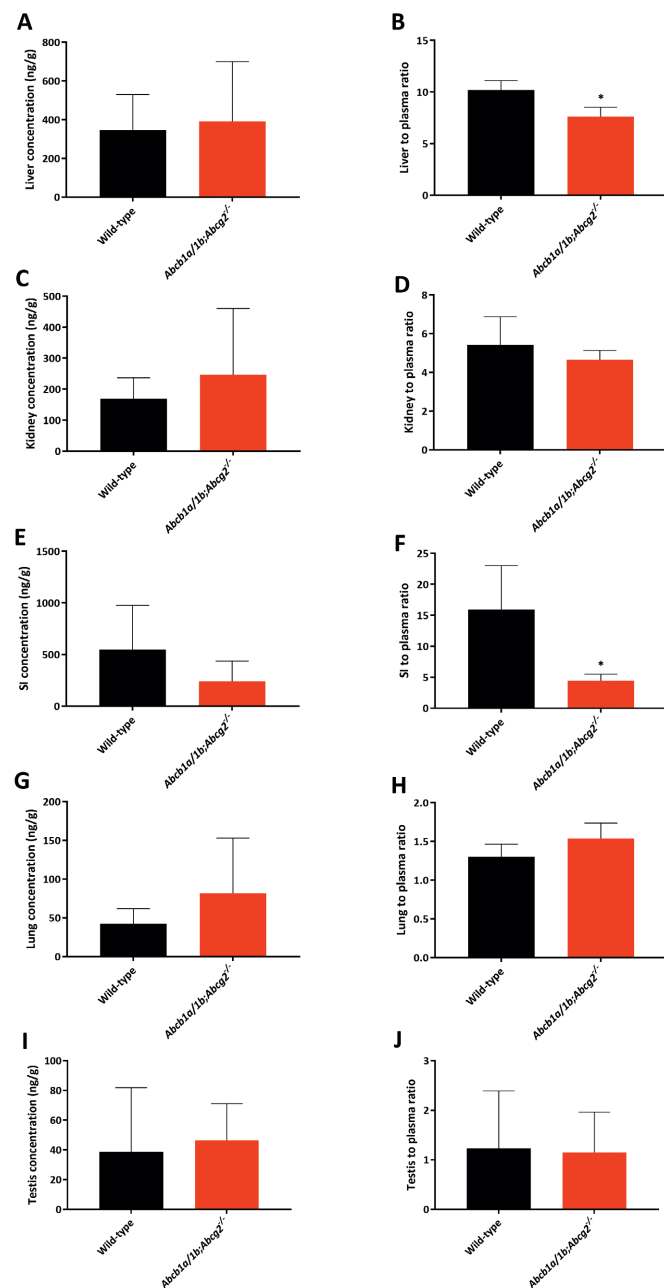
Supplemental Figure 1. Molecular structure of larotrectinib (VITRAKVI, LOXO-101, 428.44 g/mol).



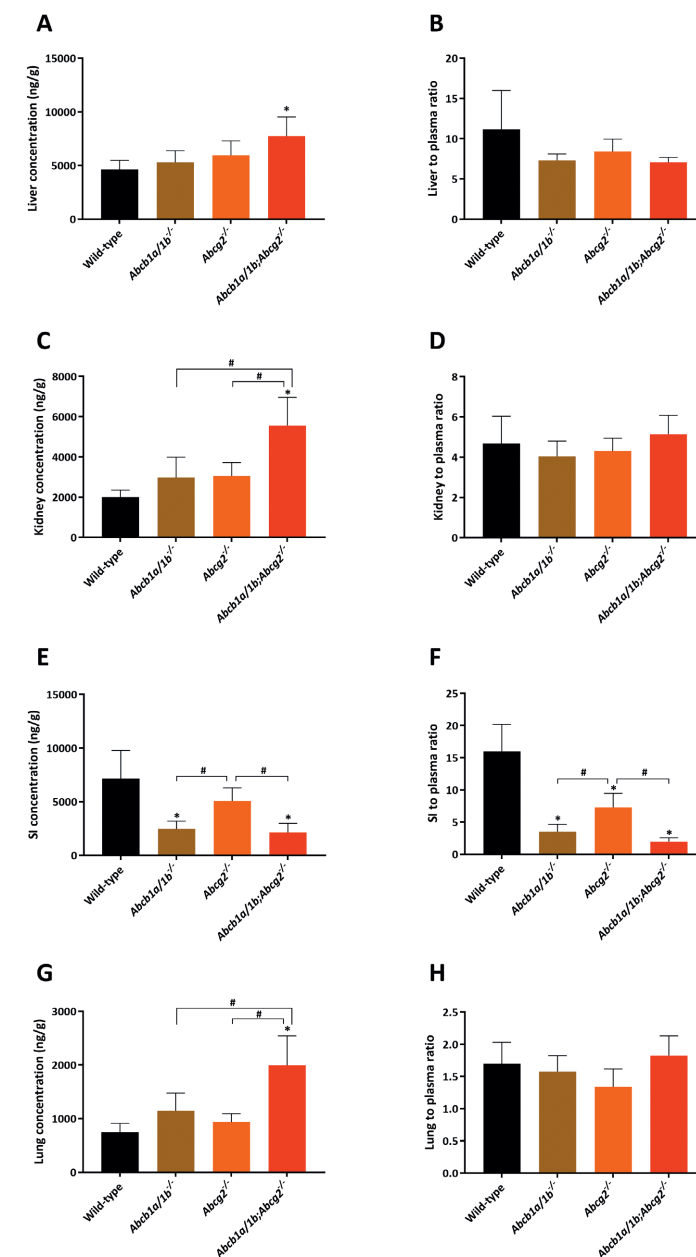
Supplemental Figure 2. Plasma concentration-time curves (A), semi-log plot of plasma concentration-time curves (B) and plasma AUC_{0-8h} (C) of larotrectinib in male wild-type and *Abcb1a/1b;Abcg2^{-/-}* mice over 8 h after oral administration of 10 mg/kg larotrectinib. Data are given as mean \pm S.D. (wild-type n = 6, *Abcb1a/1b;Abcg2^{-/-}* n = 7). *, $P < 0.01$ compared to wild-type mice. Statistical analysis was applied after log-transformation of linear data.



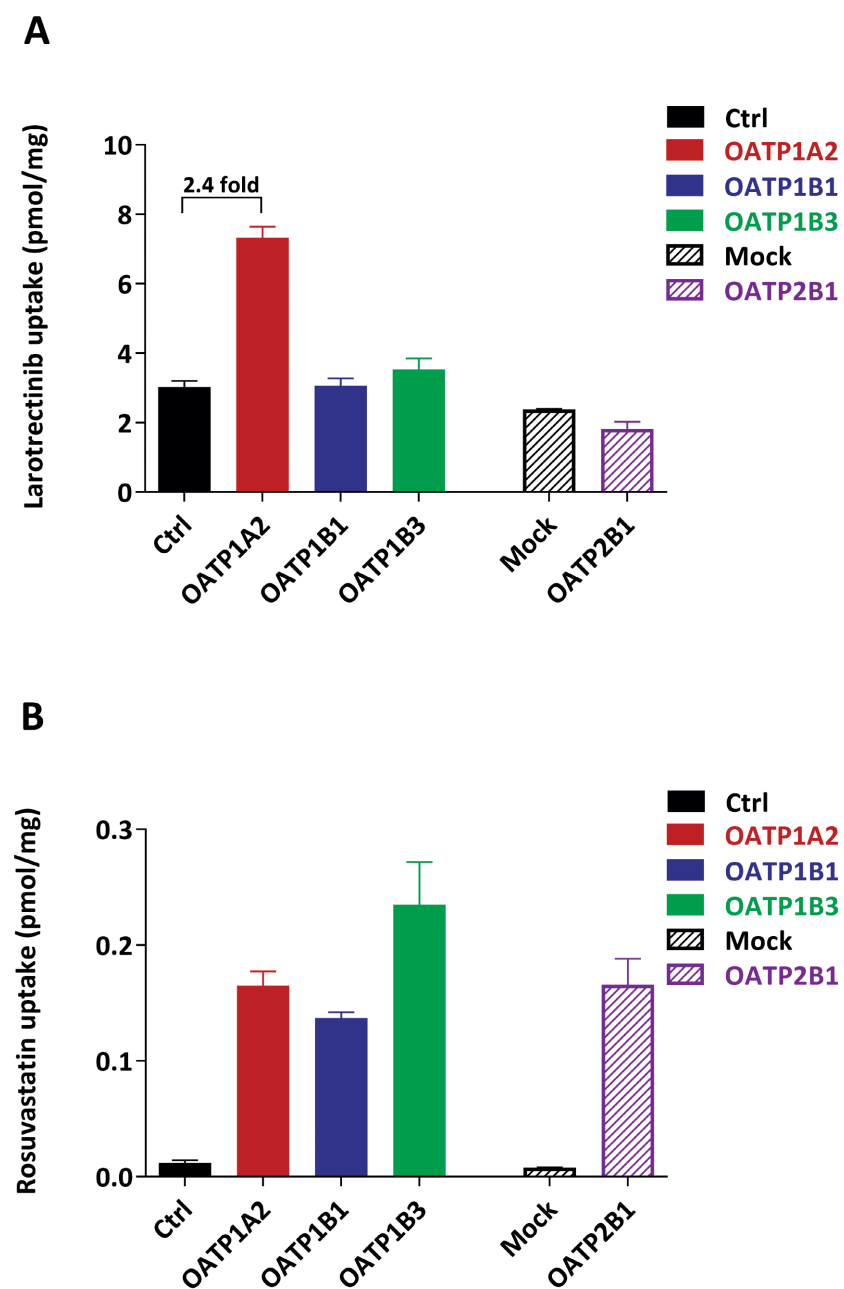
Supplemental Figure 3. Brain concentration (A) and brain-to-plasma ratio (B) of larotrectinib in male wild-type and *Abcb1a/1b;Abcg2^{-/-}* mice 8 h after oral administration of 10 mg/kg larotrectinib (wild-type n = 6, *Abcb1a/1b;Abcg2^{-/-}* n = 7). *, $P < 0.01$ compared to wild-type mice. Statistical analysis was applied after log-transformation of linear data.



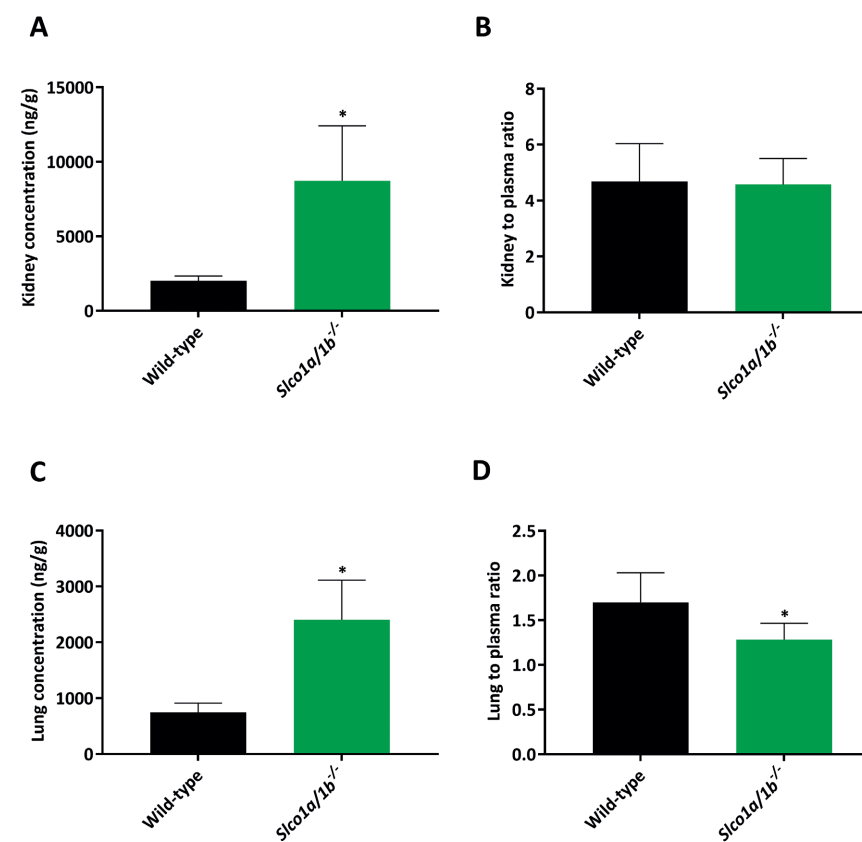
Supplemental Figure 4. Tissue concentrations (A, C, E, G, I) and tissue-to-plasma ratios (B, D, F, H, J) of larotrectinib in male wild-type and *Abcb1a/1b;Abcg2^{-/-}* mice 8 h after oral administration of 10 mg/kg larotrectinib (wild-type $n = 6$, *Abcb1a/1b;Abcg2^{-/-}* $n = 7$). SI, small intestinal tissue. *, $P < 0.01$ compared to wild-type mice. Statistical analysis was applied after log-transformation of linear data.



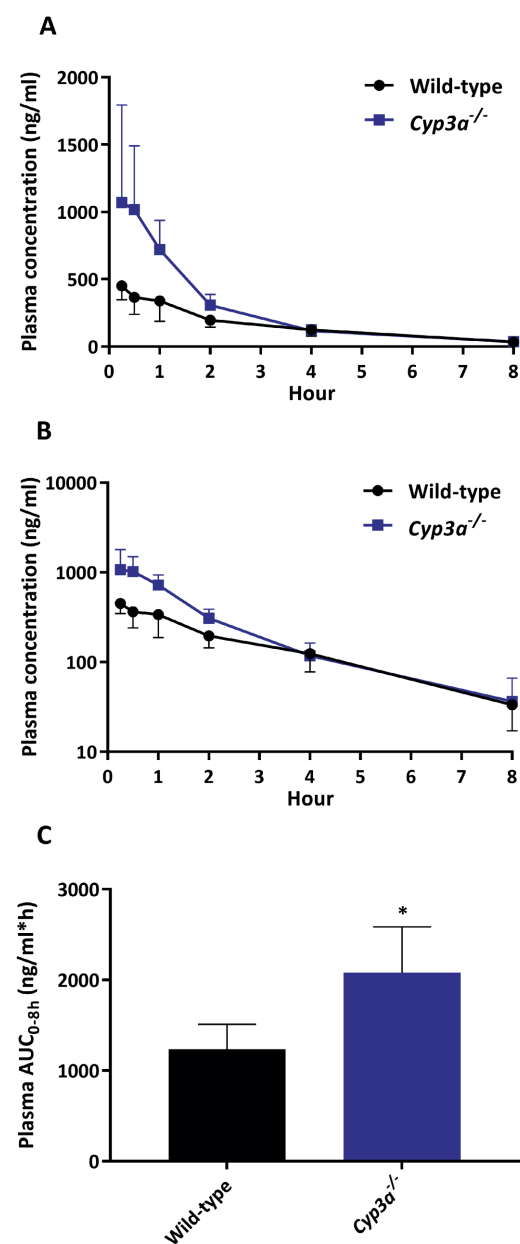
Supplemental Figure 5. Tissue concentrations (A, C, E, G) and tissue-to-plasma ratios (B, D, F, H) of larotrectinib in male wild-type, *Abcb1a/1b^{-/-}*, *Abcg2^{-/-}* and *Abcb1a/1b;Abcg2^{-/-}* mice 1 h after oral administration of 10 mg/kg larotrectinib (wild-type $n = 7$, *Abcb1a/1b^{-/-}* $n = 7$, *Abcg2^{-/-}* and *Abcb1a/1b;Abcg2^{-/-}* $n = 6$). SI, small intestinal tissue. *, $P < 0.01$ compared to wild-type mice. #, $P < 0.01$ among knockout mouse strains. Statistical analysis was applied after log-transformation of linear data.



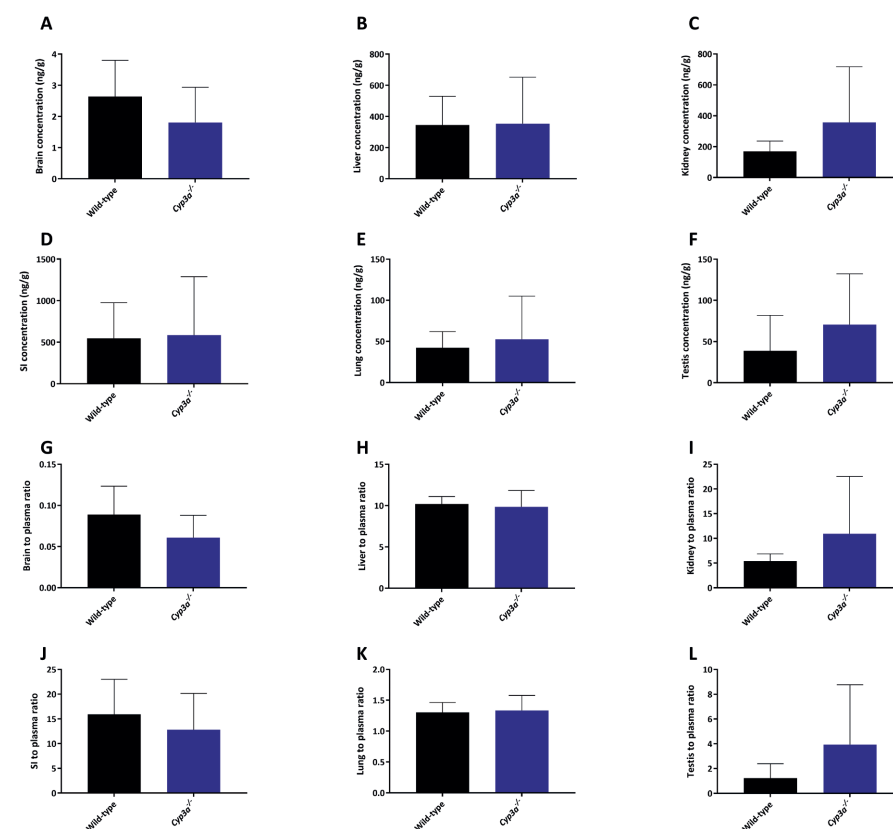
Supplemental Figure 6. *In vitro* uptake of larotrectinib (A) and positive control rosuvastatin (B) by human OATP1A2, OATP1B1, OATP1B3 and OATP2B1. Uptake of 5 μ M larotrectinib and 0.2 μ M rosuvastatin were measured after 2.5 min incubation using vector-transfected (control) or OATP1A2-, OATP1B1- or OATP1B3- overexpressing HEK293 cells and vector-transfected (mock) or OATP2B1-overexpressing HEK293 cells. $n = 3$, data are given as mean \pm S.D.



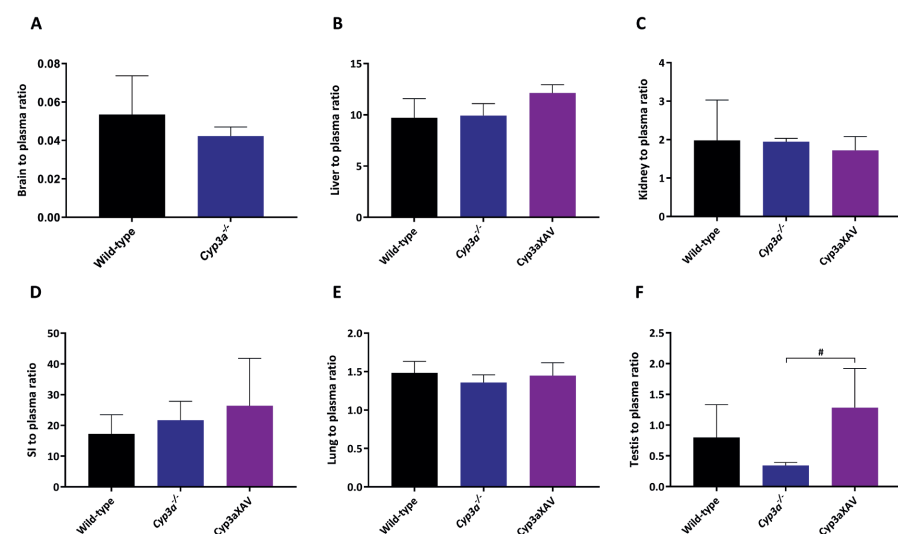
Supplemental Figure 7. Tissue concentrations (A, C) and tissue-to-plasma ratios (B, D) of larotrectinib in male wild-type and *Slco1a1/1b*^{-/-} mice 1 h after oral administration of 10 mg/kg larotrectinib ($n = 7$). *, $P < 0.01$ compared to wild-type mice. Statistical analysis was applied after log-transformation of linear data.



Supplemental Figure 8. Plasma concentration-time curves (A), semi-log plot of plasma concentration-time curves (B) and plasma AUC_{0-8h} (C) of larotrectinib in male wild-type and *Cyp3a*^{-/-} mice over 8 h after oral administration of 10 mg/kg larotrectinib. Data are given as mean ± S.D. (wild-type n = 6, *Cyp3a*^{-/-} n = 7). *, P < 0.01 compared to wild-type mice. Statistical analysis was applied after log-transformation of linear data.



Supplemental Figure 9. Tissue concentrations for brain, liver, kidney, small intestine, lung and testis (A-F) and tissue-to-plasma ratio (G-L) of larotrectinib in male wild-type and *Cyp3a*^{-/-} mice 8 h after oral administration of 10 mg/kg larotrectinib (wild-type n = 6, *Cyp3a*^{-/-} n = 7). SI, small intestinal tissue. Statistical analysis was applied after log-transformation of linear data.



Supplemental Figure 10. Tissue-to-plasma ratio for brain (A), liver (B), kidney (C), small intestine (D), lung (E) and testis (F) of larotrectinib in male wild-type, *Cyp3a*^{-/-} and *Cyp3aXAV* mice 4 h after oral administration of 10 mg/kg larotrectinib (n = 6). SI, small intestinal tissue. *, *P* < 0.01 compared to wild-type mice. #, *P* < 0.01 compared between *Cyp3a*^{-/-} and *Cyp3aXAV* mice. Statistical analysis was applied after log-transformation of linear data.

Supplemental Table 1. Pharmacokinetic parameters, brain concentrations, and brain-to-plasma ratios of larotrectinib in male wild-type and *Abcb1a/1b;Abcg2*^{-/-} mice over 8 h after oral administration of 10 mg/kg larotrectinib.

| Parameter | Genotype | |
|--|-------------|---------------------------------------|
| | Wild-type | <i>Abcb1a/1b;Abcg2</i> ^{-/-} |
| AUC _{0-8h} [†] ng/ml.h | 1235 ± 275 | 2614 ± 412* |
| Fold change AUC _{0-8h} | 1.0 | 2.1 |
| C _{max} [†] ng/ml | 478 ± 109 | 1589 ± 252* |
| T _{max} [†] h | 0.4 ± 0.3 | 0.3 ± 0.1 |
| C _{brain} [†] ng/g | 2.6 ± 1.2 | 41.5 ± 12.8* |
| Fold increase C _{brain} | 1.0 | 15.8 |
| Brain-to-plasma ratio | 0.09 ± 0.03 | 1.02 ± 0.40* |
| Fold increase ratio | 1.0 | 11.5 |

AUC_{0-8h}[†] area under plasma concentration-time curve; C_{max}[†] maximum concentration in plasma; T_{max}[†] time point (h) of maximum plasma concentration; C_{brain}[†] brain concentration. Data are given as mean ± S.D. (wild-type n = 6, *Abcb1a/1b;Abcg2*^{-/-} n = 7). *, *P* < 0.01 compared to wild-type mice. Statistical analysis was applied after log-transformation of linear data.

Supplemental Table 2. Pharmacokinetic parameters, brain concentrations and brain-to-plasma ratios of larotrectinib in male wild-type and *Cyp3a*^{-/-} mice over 8 h after oral administration of 10 mg/kg larotrectinib.

| Parameter | Genotype | |
|--|-------------|-----------------------------|
| | Wild-type | <i>Cyp3a</i> ^{-/-} |
| AUC _{0-8h} [†] ng/ml.h | 1235 ± 275 | 2078 ± 507* |
| Fold change AUC _{0-8h} | 1.0 | 1.7 |
| C _{max} [†] ng/ml | 478 ± 109 | 1146 ± 683 |
| T _{max} [†] h | 0.4 ± 0.3 | 0.5 ± 0.25 |
| C _{brain} [†] ng/g | 2.6 ± 1.2 | 1.8 ± 1.1 |
| Fold increase C _{brain} | 1.0 | 0.7 |
| Brain-to-plasma ratio | 0.09 ± 0.03 | 0.06 ± 0.03 |
| Fold increase ratio | 1.0 | 0.7 |

AUC_{0-8h}[†] area under the plasma concentration-time curve; C_{max}[†] maximum concentration in plasma; T_{max}[†] time point (h) of maximum plasma concentration; C_{brain}[†] brain concentration. Data are given as mean ± S.D. *, *P* < 0.01 compared to wild-type mice (wild-type n = 6, *Abcb1a/1b;Abcg2*^{-/-} n = 7). Statistical analysis was applied after log-transformation of linear data.



CHAPTER 4.2

RIFAMPIN AND RITONAVIR INCREASE ORAL AVAILABILITY AND ELACRIDAR ENHANCES OVERALL EXPOSURE AND BRAIN ACCUMULATION OF THE NTRK INHIBITOR LAROTRECTINIB

Yaogeng Wang¹, Rolf W. Sparidans², Jing Wang¹, Maria C. Lebre¹, Jos H. Beijnen^{1,2,3}, Alfred H. Schinkel¹

¹The Netherlands Cancer Institute, Division of Pharmacology, Plesmanlaan 121, 1066 CX Amsterdam, The Netherlands.

²Utrecht University, Faculty of Science, Department of Pharmaceutical Sciences, Division of Pharmacology, Universiteitsweg 99, 3584 CG Utrecht, The Netherlands.

³The Netherlands Cancer Institute, Department of Pharmacy & Pharmacology, Plesmanlaan 121, 1066 CX Amsterdam, The Netherlands.

ABSTRACT

Introduction

Larotrectinib is an FDA-approved oral small-molecule inhibitor for neurotrophic tropomyosin receptor kinase (NTRK) fusion-positive cancer treatment. Here we investigated larotrectinib pharmacokinetic behavior upon co-administration with prototypical inhibitors of the efflux transporters ABCB1/ABCG2 (elacridar), the SLCO1A/1B (OATP1A/1B) uptake transporters (rifampin), and the drug-metabolizing enzyme CYP3A (ritonavir), respectively.

Methods

Inhibitors were orally administered prior to oral larotrectinib (10 mg/kg) to relevant genetically modified mouse models. Larotrectinib plasma and tissue homogenate concentrations were measured by a liquid chromatography-tandem mass spectrometric assay.

Results

Elacridar increased oral availability (2.7-fold) and drastically improved brain penetration (13.8-fold) of larotrectinib in wild-type mice. Mouse (m)Oatp1a/1b but not hepatic transgenic human (h)OATP1B1 or -1B3 restricted larotrectinib oral availability and affected its tissue distribution. Rifampin enhanced larotrectinib oral availability not only in wild-type mice (1.9-fold), but surprisingly also in *Slco1a/1b*^{-/-} mice (1.7-fold). Similarly, ritonavir increased the larotrectinib plasma exposure in both wild-type (1.5-fold) and *Cyp3a*^{-/-} mice (1.7-fold). Intriguingly, both rifampin and ritonavir decreased liver and/or intestinal larotrectinib levels in all related experimental groups, suggesting additional inhibition of enterohepatic Abcb1a/1b activity.

Conclusions

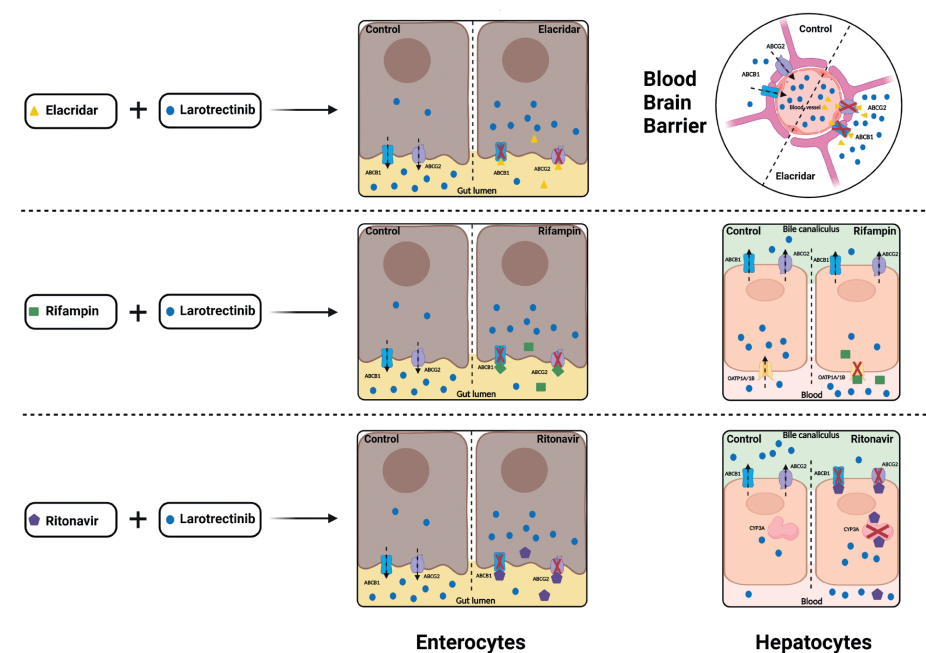
Elacridar enhances both larotrectinib plasma and tissue exposure and especially relative brain penetration, which might be therapeutically relevant. Hepatic mOatp1a/1b but not hOATP1B1 or -1B3 transported larotrectinib. Additionally, rifampin enhances larotrectinib systemic exposure, most likely by inhibiting mOatp1a/1b, but probably also hepatic and/or intestinal mAbcb1. Similar to rifampin, dual-inhibition functions of ritonavir affecting both CYP3A enzymes and enterohepatic Abcb1 transporters enhanced larotrectinib oral availability. The obtained insights may be used to further optimize the clinical-therapeutic application of larotrectinib.

Keywords: Larotrectinib, ABCB1, OATP1A, Elacridar, Rifampin, Ritonavir, Cytochrome P450-3A, Oral availability

Abbreviations:

ABC: ATP-binding cassette; ABCB1: ATP-binding cassette sub-family B member 1; ABCG2: ATP-binding cassette super-family G member 2; BBB: Blood-brain-barrier; BTB: Blood-testis-barrier;

CYP: Cytochrome P450; Cyp3aXAV: Cyp3a knockout mice with specific expression of human CYP3A4 in liver and intestine; DDI: drug-drug interaction; LC-MS/MS: liquid chromatography coupled with tandem mass spectrometry; NTRK: Neurotrophic tropomyosin receptor kinase; OATP: Organic anion-transporting polypeptide; P-gp: P-glycoprotein; SLCO: OATP solute carrier family; SI + SIC : Small intestine together with small intestinal contents; TKI: tyrosine kinase inhibitor.



1. INTRODUCTION

The Neurotrophic Tropomyosin Receptor Kinase (NTRK) family contains three nerve growth factor receptor genes, NTRK1, NTRK2 and NTRK3, which encode the single-transmembrane receptor tyrosine kinases TRK A, B, and C, respectively¹. These receptors are essential for proliferation and survival of neurons. However, albeit infrequently, oncogenic fusions among the NTRK genes may occur in a variety of adult malignancies and pediatric cancers, including glioblastoma, non-small cell lung cancer (NSCLC), and colorectal cancer²⁻⁴. In November 2018, the FDA approved a first selective pan-TRK inhibitor, larotrectinib (Vitrakvi, LOXO-101, Supplemental Figure 1)⁵, which could induce marked tumor shrinkage in patients with NTRK-rearranged cancers.

As two important members of the ABC drug efflux transporters, P-glycoprotein (P-gp; ABCB1) and breast cancer resistance protein (BCRP; ABCG2) are highly expressed in the blood-facing luminal membrane of the physiological barriers protecting pharmacological sanctuary compartments, including blood-brain barrier (BBB) and blood-testis barrier (BTB), and in the apical membranes of epithelial cells in organs that are responsible for drug absorption and elimination, such as enterocytes and hepatocytes⁶. Organic anion-transporting polypeptides (SLCO; OATPs) are expressed mainly in liver, kidney and small intestine, where they mediate the tissue uptake of many endogenous and exogenous compounds. Thus, these transmembrane transporters could influence the distribution of molecules between blood and tissues.

We previously found that mAbcb1a/1b and mAbcg2 together can markedly limit larotrectinib oral availability and brain accumulation in mice by 2.1- and 10.4-fold, respectively. Interestingly, mSlco1a/1b (Oatp1a/1b) also restricted larotrectinib oral availability (by 3.8-fold), apparently by mediating substantial uptake into the liver⁷. *In vitro* uptake assays suggested that larotrectinib is very likely a substrate of human OATP1A2 (SLCO1A2), but not of human OATP1B1 (SLCO1B1) or -1B3. However, OATP-mediated uptake of certain substrates can be cell-type dependent for as yet unknown reasons⁸, so a negative result does not necessarily mean that a substrate cannot be transported under all circumstances. For this reason *in vivo* studies and vigilance in recognizing possible OATP-mediated drug-drug interactions during the clinical application of larotrectinib are still advisable.

The multidrug-metabolizing Cytochrome P450 3A (CYP3A) enzyme complex is responsible for most phase I drug metabolism. CYP3A4 is the most highly expressed CYP enzyme in human liver, one of the main detoxification organs, but also in the small intestine. It therefore profoundly contributes to the oxidative metabolism of nearly half of the drugs currently in clinical use, resulting in drug inactivation or sometimes also activation^{9,10}. Larotrectinib was demonstrated to be an excellent *in vivo* substrate of CYP3A enzymes in our previous study⁷. However, many ABCB1 and/or ABCG2 substrates are also substrates and/or inhibitors for CYP3A, and it has been

hypothesized that the combined activity of drug efflux transporters and CYP3A results in efficient first-pass metabolism of orally administered drugs¹¹⁻¹⁵. As larotrectinib is an excellent substrate of ABC efflux and OATP1 uptake transporters, as well as CYP3A enzymes, these properties may complicate larotrectinib pharmacokinetics: activity variation through gene polymorphisms or exogenous factors such as inhibitors or inducers of transporters and metabolizing enzymes could all affect larotrectinib behavior.

Drug-drug interactions (DDIs) may cause changes in the absorption, distribution, metabolism and excretion (ADME) of a drug and can result in variable drug exposure leading to potential toxicities or altered efficacy. This includes interfering with drug transporters such as ABCB1 and ABCG2, or the OATPs, or interfering with drug-metabolizing enzymes such as CYP3A, or even both. Co-administration of elacridar, a dual inhibitor of ABCB1 and ABCG2, could improve both oral exposure and brain penetration of several tyrosine kinase inhibitors (TKIs), such as sorafenib, crizotinib, vemurafenib, ribociclib, and others¹⁶⁻¹⁹. Besides, OATP uptake transporters could be inhibited by the prototypical Oatp1a/1b inhibitor rifampin, which leads to reduced uptake of many endogenous molecules and drugs, like statins²⁰. Of note, rifampin can not only inhibit OATPs, but also ABCB1 to some extent. Rifampin further displays a kind of dual function, including acute inhibition of ABCB1 and OATPs, but also chronic gene induction of ABCB1 and CYP3A²¹. With respect to CYP3A inhibitors, the HIV protease inhibitor ritonavir can efficiently inhibit CYP3A activity and thus substantially boost systemic exposure of many drugs, such as docetaxel, paclitaxel, and lopinavir^{22,23}. However, like rifampin, ritonavir can also inhibit ABCB1^{24,25}.

In the present study, using different genetically modified mouse models, we examined whether larotrectinib is a substrate of human OATP1B1 and OATP1B3 *in vivo* using human OATP transgenic mice. As larotrectinib can be transported by ABCB1, ABCG2 and OATP1A, and can also be metabolized by CYP3A, potentially endogenous genetic polymorphisms and exogenous inhibitors/inducers of all these systems may influence the pharmacokinetics, and hence the safety and efficacy profiles of larotrectinib. We therefore further explored whether we could substantially alter oral availability and tissue distribution of larotrectinib, including brain penetration, by inhibition of ABCB1/ABCG2, OATP1A/1B, or CYP3A using oral co-administration of elacridar, rifampin, or ritonavir, respectively.

2. MATERIALS AND METHODS

2.1 Chemicals

Larotrectinib was purchased from Carbosynth (Oxford, UK). Ritonavir and elacridar HCl were obtained from Sequoia Research Products (Pangbourne, UK). Rifampin was from Sigma-Aldrich (Steinheim, Germany). Bovine Serum Albumin (BSA) Fraction V was obtained from Roche

Diagnosics GmbH (Mannheim, Germany). Glucose water 5% w/v was from B. Braun Medical Supplies (Melsungen, Germany). Isoflurane was purchased from Pharmachemie (Haarlem, The Netherlands), heparin lithium (5000 IU ml⁻¹) was from Leo Pharma (Breda, The Netherlands). All chemicals used in the larotrectinib LC-MS/MS assay were described before²⁶. All other chemicals and reagents were obtained from Sigma-Aldrich (Steinheim, Germany).

2.2 Animals

Wild-type, *Abcb1a/1b;Abcg2*^{-/-27}, *Slco1a/1b*^{-/-28}, *Slco1B1*²⁹, *Slco1B3*³⁰, *Cyp3a*^{-/-9} and *Cyp3aXAV*⁹ male mice, all of a >99% FVB genetic background, were used between 9 and 16 weeks of age. All the mouse strains were established and characterized before. Animals were kept in an SPF animal facility, in a temperature-controlled environment with 12-h light and 12-h dark cycle. They received a standard diet (Transbreed, SDS Diets, Technilab – BMI, Someren, The Netherlands) and acidified water *ad libitum*. Mice were housed and handled according to institutional guidelines complying with Dutch and EU legislation. In this study, only male mice were randomly allocated for experiments. Because the main read-out of these experiments was objective (larotrectinib plasma and tissue concentrations as measured by LC-MS/MS), we applied no blinding method. All experimental animal protocols were evaluated and approved by the institutional animal care and use committee and experimental procedures were optimized to follow the 3R principles (replacement, refinement, reduction).

2.3 Drug solutions

For oral administration, larotrectinib was dissolved in dimethyl sulfoxide (DMSO) at a concentration of 50 mg/ml and further diluted with 5% (w/v) glucose in water to yield a concentration of 1.0 mg/ml. Final concentrations for DMSO and glucose in the dosing solution were 2% (v/v) and 4.75% (w/v), respectively. Elacridar hydrochloride was dissolved in DMSO (106 mg/ml) in order to get 100 mg elacridar base per ml DMSO. The stock solution was further diluted with a mixture of polysorbate 20, ethanol and water [20:13:67, (v/v/v)] to yield a concentration of 10 mg/ml elacridar. Rifampin was first dissolved in DMSO to yield a 100 mg/ml stock solution, and further diluted with polysorbate 20, absolute ethanol and 5% glucose water, to obtain a final working solution of 10 mg/ml [in DMSO : polysorbate 20 : ethanol : 5% glucose water = 10:15:15:60, (v/v/v/v)]. For the ritonavir boosting experiment, 30 mg/ml ritonavir was dissolved in polysorbate 20/ethanol (1:1, v/v) and stored at -30 °C. This was then further diluted with 5 parts of water (1:5, v/v) to obtain a 5 mg/ml working solution for administration. All dosing solutions were prepared freshly on the day of experiment.

2.4 Larotrectinib administration schedules with targeted inhibitors

To minimize variation in absorption upon oral administration, all the mice were fasted for 3 h before any inhibitors and larotrectinib were administered orally. Larotrectinib was administered at a dose of 10 mg/kg, while elacridar and rifampin were both administered at a dose of 100

mg/kg. For ritonavir boosting, 15 mg/kg of larotrectinib was used after 50 mg/kg ritonavir was administered. All the drug working solutions were administered by gavage using a blunt-ended needle, applying 10 µl/g of body weight. Elacridar was orally administered 3 hours prior to oral larotrectinib administration in wild-type and *Abcb1a/1b;Abcg2*^{-/-} mice. For the rifampin inhibition experiments, rifampin was administered first, and larotrectinib was administered orally 15 min later in wild-type, *Slco1a/1b*^{-/-}, *Slco1B1* and *Slco1B3* mice. Similarly, for ritonavir inhibition experiments, ritonavir was administered orally 15 min prior to oral larotrectinib in wild-type, *Cyp3a*^{-/-} and *Cyp3aXAV* mice.

2.5 Plasma and organ pharmacokinetics of larotrectinib in mice

For all the inhibition experiments, approximately 50 µl tail vein blood samples were collected at 7.5 min (0.125 h), 15 min (0.25 h), 30 min (0.5 h) and 45 min (0.75 h) after oral larotrectinib administration, using microvettes containing dipotassium-EDTA. At the last time point (1 h), mice were anesthetized with 5% isoflurane and blood was collected by cardiac puncture. Blood samples were collected in Eppendorf tubes containing heparin as an anticoagulant. The mice were then sacrificed by cervical dislocation and brain, liver, kidney, small intestine together with small intestine contents (SI + SIC) and testis were rapidly removed. Plasma was isolated from the blood by centrifugation at 9,000 × g for 6 min at 4°C, and the plasma fraction was collected and stored at -30°C until analysis. Organs were homogenized with 4% (w/v) bovine serum albumin and stored at -30°C until analysis. Relative tissue-to-plasma ratios after oral administration were calculated by determining the larotrectinib tissue concentration relative to larotrectinib plasma concentration at the last time point.

2.6 LC-MS/MS analysis

Larotrectinib concentrations in plasma samples and organ homogenates were determined using a validated liquid chromatography-tandem mass spectrometry assay²⁶.

2.7 Data and statistical analysis

Pharmacokinetic parameters were calculated by non-compartmental methods using the PK Solver software³¹. The area under the plasma concentration-time curve (AUC) was calculated using the trapezoidal rule, without extrapolating to infinity. The peak plasma concentration (C_{max}) and the time of maximum plasma concentration (T_{max}) were estimated from the original (individual mouse) data. One-way analysis of variance (ANOVA) was used when multiple groups were compared and the *Tukey post hoc* correction was used to accommodate multiple testing. The two-sided unpaired Student's t-test was used when treatments or differences between two specific groups were compared using the software GraphPad Prism 9 (GraphPad Software Inc., La Jolla, CA, USA). All the data were log-transformed before statistical tests were applied. Differences were considered statistically significant when $P < 0.05$. All data are presented as geometric mean ± SD.

3. RESULTS

3.1 Effect of the dual ABCB1 and ABCG2 inhibitor elacridar on larotrectinib pharmacokinetics

We previously demonstrated that mAbcb1a/1b and mAbcg2 together can markedly limit larotrectinib oral availability and brain accumulation⁷. In view of the potential benefit of further enhancing larotrectinib overall exposure and brain accumulation and drug disposition in other organs, we wanted to assess to what extent the dual ABCB1 and ABCG2 inhibitor elacridar could modulate the pharmacokinetics, especially plasma exposure and brain accumulation of oral larotrectinib. For this purpose, we administered elacridar (100 mg/kg) orally 3 hours prior to oral larotrectinib (10 mg/kg) to male wild-type and *Abcb1a/1b;Abcg2*^{-/-} mice, and assessed plasma and organ larotrectinib levels 1 hour later. This 3-hour time span was used to obtain sufficiently high elacridar exposure in plasma throughout the larotrectinib exposure, ensuring complete inhibition of the BBB apical ABC transporters. In vehicle-treated mice, the larotrectinib plasma AUC_{0-1h} was significantly higher (2.3-fold) in *Abcb1a/1b;Abcg2*^{-/-} compared to wild-type mice. Pre-treatment with elacridar increased the larotrectinib plasma exposure in wild-type mice to a similar level as seen in vehicle-treated *Abcb1a/1b;Abcg2*^{-/-} mice, whereas it did not affect the plasma levels in *Abcb1a/1b;Abcg2*^{-/-} mice (Figure 1A-B). These results indicate that larotrectinib plasma exposure and oral availability in wild-type mice are markedly increased by elacridar, to the same levels as observed for the genetic knockout of *Abcb1a/1b* and *Abcg2*. This suggests effectively complete inhibition of these ABC transporters.

In the absence of elacridar, brain concentrations and brain-to-plasma ratios of larotrectinib were 15.9-fold and 6.3-fold higher in *Abcb1a/1b;Abcg2*^{-/-} mice than in wild-type mice. Elacridar substantially increased the brain concentrations and brain-to-plasma ratios of larotrectinib in wild-type mice by 13.8-fold and 5.0-fold, respectively (Figure 1C-D and Table 1), resulting in levels similar to those observed in *Abcb1a/1b;Abcg2*^{-/-} mice with or without elacridar pretreatment. Elacridar did not significantly affect these parameters in *Abcb1a/1b;Abcg2*^{-/-} mice, further supporting the specificity of elacridar in inhibiting *Abcb1* and *Abcg2* in the BBB. In view of the functional presence of ABCB1 and ABCG2 in the blood-testis barrier, testis distribution of larotrectinib was also analyzed. As shown in Supplemental Figure 2B and Table 1, we did not find significant differences in testis-to-plasma ratios among these groups, likely due in part to the high experimental variation in wild-type mice.

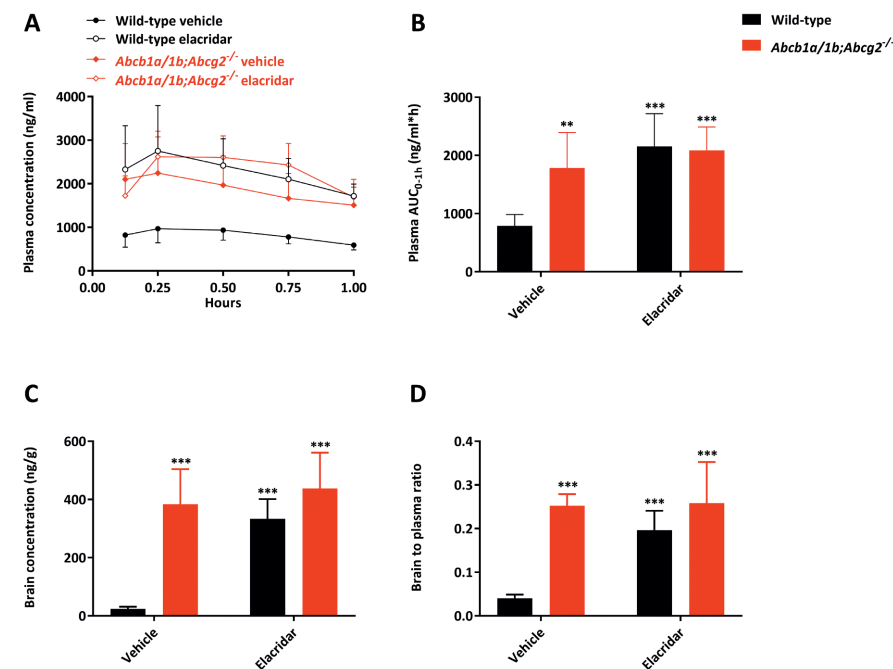


Figure 1. Plasma concentration-time curves (A), plasma AUC_{0-1h} (B), brain concentration (C) and brain-to-plasma ratio of larotrectinib in male wild-type and *Abcb1a/1b;Abcg2*^{-/-} mice over 1 h after oral administration of 10 mg/kg larotrectinib with or without co-administration of elacridar. Data are given as mean ± S.D. (n = 6). *, $P < 0.05$; **, $P < 0.01$; ***, $P < 0.001$ compared to vehicle-treated wild-type mice.

Table 1. Plasma and tissue pharmacokinetic parameters of larotrectinib in male wild-type and *Abcb1a/1b;Abcg2*^{-/-} mice over 1 h after oral administration of 10 mg/kg larotrectinib with or without inhibitor elacridar.

| Parameter | Genotype/Groups | | |
|-------------------------------------|-----------------|---------------------------------------|------------------|
| | Vehicle | Wild-type | Elacridar |
| | Wild-type | <i>Abcb1a/1b;Abcg2</i> ^{-/-} | Wild-type |
| AUC _{0-3h} , ng/ml*h | 787 ± 196 | 1781 ± 611** | 2153 ± 563*** |
| Fold change AUC _{0-3h} | 1.0 | 2.3 | 2.7 |
| C _{max} , ng/ml | 1008 ± 304 | 2262 ± 832** | 2871 ± 963*** |
| T _{max} , h | 0.38 ± 0.14 | 0.27 ± 0.12 | 0.36 ± 0.23 |
| C _{brain} , ng/g | 24.1 ± 7.2 | 383.4 ± 121*** | 333.0 ± 68.3*** |
| Fold increase C _{brain} | 1.0 | 15.9 | 13.8 |
| Brain-to-plasma ratio | 0.040 ± 0.009 | 0.25 ± 0.03*** | 0.20 ± 0.04*** |
| Fold increase ratio | 1.0 | 6.3 | 5.0 |
| C _{liver} , ng/g | 4564 ± 410 | 6458 ± 1516* | 8746 ± 2147*** |
| Fold increase C _{liver} | 1.0 | 1.4 | 1.9 |
| Liver-to-plasma ratio | 7.9 ± 1.2 | 4.3 ± 0.5*** | 5.1 ± 0.6*** |
| Fold change ratio | 1.0 | 0.54 | 0.65 |
| C _{SI + SIC} , ng/g | 42565 ± 7747 | 3060 ± 427*** | 5770 ± 1169*** |
| Fold increase C _{SI + SIC} | 1.0 | 0.072 | 0.14 |
| SI + SIC-to-plasma ratio | 73.9 ± 17.8 | 2.1 ± 0.6*** | 3.5 ± 1.1*** |
| Fold change ratio | 1.0 | 0.028 | 0.047 |
| C _{testis} , ng/g | 170.6 ± 99.6 | 578.4 ± 177.1*** | 502.5 ± 125.8*** |
| Fold increase C _{testis} | 1.0 | 3.4 | 2.9 |
| Testis-to-plasma ratio | 0.29 ± 0.19 | 0.38 ± 0.02 | 0.29 ± 0.07 |
| Fold change ratio | 1.0 | 1.3 | 1.0 |

Data are given as mean ± S.D. (n = 6). AUC_{0-3h}, area under the plasma concentration-time curve; C_{max}, maximum concentration in plasma; T_{max}, time point (h) of maximum plasma concentration; C_{brain}, brain concentration; C_{liver}, liver concentration; SI, small intestine (tissue); SIC, small intestine contents; C_{SI + SIC}, small intestine tissue together with small intestine contents concentration; C_{testis}, testis concentration; *, P < 0.05; **, P < 0.01; ***, P < 0.001 compared to vehicle-treated wild-type mice. Statistical analysis was applied after log-transformation of linear data.

In liver, we observed significantly lower liver-to-plasma ratios in vehicle-treated *Abcb1a/1b;Abcg2*^{-/-} mice compared to vehicle-treated wild-type mice. These results confirm a trend we observed in the previous larotrectinib study. A reduced liver-to-plasma ratio in *Abcb1a/1b;Abcg2*^{-/-} liver may indicate reduced accumulation of larotrectinib in intrahepatic bile due to the absence of the canalicular ABC transporters. Elacridar treatment yielded a similarly decreased liver-to-plasma ratio in wild-type mice as seen in vehicle- or elacridar-treated *Abcb1a/1b;Abcg2*^{-/-} mice (Supplemental Figure 2F and Table 1), consistent with specific inhibition of the hepatic ABC transporters. Somewhat similar results might perhaps occur in kidney, with the ABC transporters concentrating larotrectinib in the intrarenal pre-urine, but experimental variation did not allow a statistically significant conclusion here (Supplemental Figure 2D).

We previously observed about 3-fold reduced larotrectinib tissue-to-plasma ratios in the small intestinal tissue of *Abcb1a/1b;Abcg2*^{-/-} mice⁷, which usually reflects a strongly reduced drug concentration in the small intestinal content (SIC). In this experiment we therefore collected SI and SIC combined. We observed a profoundly decreased concentration (13.9-fold), tissue-to-plasma ratio (35.2-fold), percentage of dose (6.0-fold) and percentage of dose-to-plasma ratio (16.9-fold) of larotrectinib in SI + SIC in vehicle-treated *Abcb1a/1b;Abcg2*^{-/-} compared to wild-type mice. Pre-treatment with elacridar of wild-type mice led to very similar results, with concentration, tissue-to-plasma ratio, percentage of dose and percentage of dose-to-plasma ratio of larotrectinib decreased by 7.4-fold, 21.1-fold, 14.1-fold and 35.7-fold, respectively, compared to vehicle-treated wild-type mice (Supplemental Figure 2G-J and Table 1). These results point to a more rapid and extensive absorption of intestinal larotrectinib upon inhibition of both *Abcb1a/1b* and *Abcg2*, or to reduced hepatobiliary excretion of the absorbed larotrectinib, or to a combination of both processes. Despite the overall increased plasma and tissue exposure, we did not observe any sign of spontaneous toxicity of larotrectinib in any of the mouse strains that we tested with oral larotrectinib at 10 mg/kg, either in the absence or presence of elacridar.

Collectively, these data indicate that oral elacridar treatment can extensively and specifically inhibit the activity of mouse *Abcb1* and *Abcg2* in the BBB, leading to markedly increased larotrectinib distribution to the brain at an early time point, when the larotrectinib exposure was relatively high. Moreover, elacridar could markedly enhance the general oral exposure of larotrectinib, presumably mainly due to increased net drug absorption from the gut or reduced hepatobiliary excretion, or both.

3.2 Impact of human SLCO1B1 and 1B3 on larotrectinib pharmacokinetics

To investigate the possible impact of human OATP1B1 and OATP1B3 on oral bioavailability and tissue disposition of larotrectinib, we performed a 1 h pharmacokinetic study in male wild-type, *Slco1a/1b*^{-/-}, SLCO1B1 and SLCO1B3 mice, using oral administration of 10 mg/kg larotrectinib. SLCO1B1 and SLCO1B3 mice are *Slco1a/1b*^{-/-} mice that transgenically overexpress human OATP1B1

or -1B3 in the liver, respectively. As shown in Figure 2A-B and Supplemental Table 1, absorption was very rapid and the T_{max} occurred between 0.25 and 0.75 h in all four strains. The plasma exposure of larotrectinib over 1 h (AUC_{0-1h}) was significantly higher (2.5-fold) in *Slco1a/1b*^{-/-} mice than in wild-type mice, in line with our previous study. However, SLCO1B1 and SLCO1B3 did not decrease the plasma exposure of larotrectinib, with the plasma AUC_{0-1h} still 2.7-fold and 2.5-fold increased, respectively, compared to wild-type mice.

Brain, liver, kidney, lung, small intestine and testis concentrations of larotrectinib 1 h after oral administration were also analyzed. Due to the higher plasma exposure of larotrectinib in *Slco1a/1b*^{-/-}, SLCO1B1 and SLCO1B3 mice, brain, kidney, lung and testis had higher drug concentrations in all of these three mouse strains. However, the relative tissue-to-plasma ratios revealed no meaningful differences among all the mouse strains for brain, testis, and kidney, although there was a consistent modest reduction in relative lung distribution in all the *Oatp1a/1b*-deficient mouse strains (Supplemental Figure 3). The latter finding is in line with what we observed in the preceding larotrectinib study⁷, and suggests that possibly *Oatp1a/1b* proteins play a limited role in distribution of larotrectinib to lung tissue. Whereas the liver concentrations showed no differences between all strains, this translated into significantly lower liver-to-plasma ratios in *Slco1a/1b*^{-/-}, *Slco1B1* and *Slco1B3* compared to wild-type mice (2.7-fold, 2.7-fold and 2.4-fold, respectively (Figure 2C-D and Supplemental Table 1). This is in line with a clear role for mOatp1a/1b proteins in the liver uptake of larotrectinib, but not for human OATP1B1 or -1B3. With respect to small intestinal tissue concentration, even though this was 1.7-fold higher in *Slco1a/1b*^{-/-} mice than in wild-type mice, and slightly higher in SLCO1B1 (1.2-fold) and SLCO1B3 (1.3-fold) mice, no significant difference showed up among all the mouse strains. However, as also seen for the liver, small intestine-to-plasma ratios were significantly reduced in *Slco1a/1b*^{-/-}, SLCO1B1 and SLCO1B3 mice compared to wild-type mice (2-fold, 2.8-fold and 2.4-fold, respectively. Figure 2E-F and Supplemental Table 1). Such intestinal tissue data shortly after oral administration of drugs often primarily reflect the intestinal content levels (which were not measured in this experiment). These data therefore suggest that the uptake function of mouse *Oatp1a/1b* proteins for larotrectinib in the liver indirectly also affects the intestinal (content) exposure through hepatobiliary excretion, but that human OATP1B1 and OATP1B3 do not. All in all, the collected data thus further support that larotrectinib is not a transport substrate of hepatic human OATP1B1 and OATP1B3 *in vivo*.

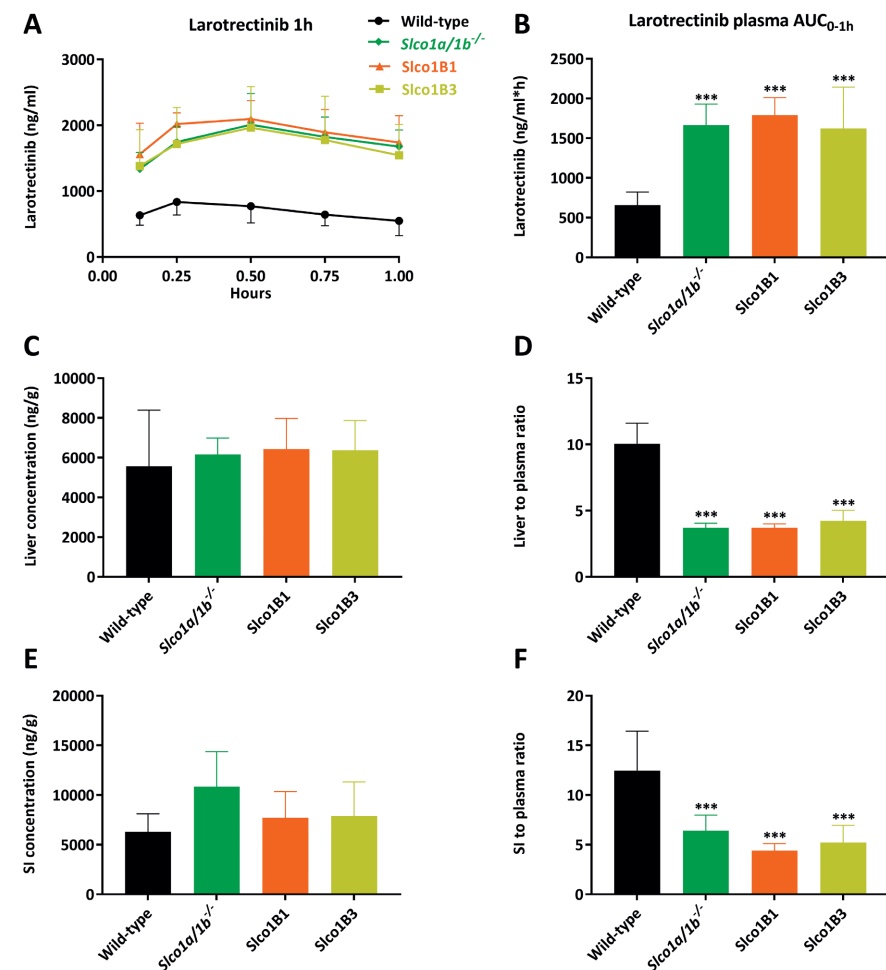


Figure 2. Plasma concentration-time curves (A), plasma AUC_{0-1h} (B), liver concentration (C), liver-to-plasma ratio (D), small intestine concentration (E) and small intestine-to-plasma ratio (F) of larotrectinib in male wild-type, *Slco1a/1b*^{-/-}, *Slco1B1* and *Slco1B3* mice over 1 h after oral administration of 10 mg/kg larotrectinib. SI: Small intestine. Data are given as mean \pm S.D. (n = 6 - 7). *, $P < 0.05$; **, $P < 0.01$; ***, $P < 0.001$ compared to wild-type mice.

3.3 Larotrectinib pharmacokinetic behavior after co-administration of the OATP inhibitor rifampin

We next investigated whether the *Slco1a/1b* inhibitor rifampin could influence larotrectinib pharmacokinetics *in vivo*. Aiming for a relatively high larotrectinib plasma level when assessing tissue distribution, we performed a 1 h pharmacokinetic experiment in wild-type, *Slco1a/1b*^{-/-}, SLCO1B1 and SLCO1B3 mice, with rifampin (100 mg/kg) or vehicle orally administered 15 min

prior to oral larotrectinib at 10 mg/kg. Both, vehicle-treated *Slco1a/1b*^{-/-} mice and rifampin-treated wild-type mice showed a higher larotrectinib plasma AUC_{0-1h} than vehicle-treated wild-type mice (each 1.9-fold higher), suggesting that rifampin could inhibit mouse Oatp1a/1b and thus increase larotrectinib plasma exposure (Figure 3A-B). However, we also noticed that after pre-treatment with rifampin, larotrectinib plasma exposure increased in *Slco1a/1b*^{-/-} mice compared with vehicle-treated *Slco1a/1b*^{-/-} mice. Meanwhile, SLCO1B1 and SLCO1B3 mice showed a significantly higher plasma AUC_{0-1h} compared to wild-type mice and a similar plasma AUC_{0-1h} of larotrectinib no matter whether in the vehicle- or rifampin-treated group (Figure 3).

To try and come to a better mechanistic understanding of these observations, organs were collected after 1 hour and larotrectinib concentrations were measured. Brain, testis and kidney mostly reflected the plasma larotrectinib exposure and no meaningful changes showed up in tissue-to-plasma ratios in either vehicle- or rifampin-treated groups (Supplemental Figure 4). While there were no differences in absolute larotrectinib concentrations among all four mouse strains in either vehicle- or rifampin-treated groups, the liver-to-plasma ratios were significantly decreased in *Slco1a/1b*^{-/-}, SLCO1B1 and SLCO1B3 mice in the vehicle-treated group. This suggests a relatively reduced liver uptake of larotrectinib in *Slco1a/1b*^{-/-} mice and no substantial uptake functions of human OATP1B1 and OATP1B3. Importantly, the rifampin-treated group wild-type mice had a similar liver-to-plasma ratio as the vehicle-treated *Slco1a/1b*^{-/-} mice (3.7 ± 0.5 vs 3.6 ± 0.6). This suggests that rifampin could effectively inhibit the mouse hepatic *Slco1a/1b* proteins and thus restrict liver uptake of larotrectinib (Supplemental Figure 5B and Table 2).

In this experiment we also measured the small intestine (SI) and its content (SIC) combined (SI + SIC). In vehicle-treated groups, SI + SIC-to-plasma ratios in *Slco1a/1b*^{-/-} (37.2 ± 14.2), SLCO1B1 (25.1 ± 8.0) and SLCO1B3 (25.7 ± 8.5) mice were not significantly changed compared to wild-type mice (43.7 ± 27.2) (Supplemental Figure 5D). Interestingly, pre-treatment with rifampin could markedly decrease these ratios in all the groups to a similar level. Similarly, the amount of larotrectinib recovered from SI + SIC as percentage of the dose-to-plasma ratios was also clearly reduced in all the rifampin-treated groups compared to corresponding vehicle-treated groups (Supplemental Figure 5F). These data suggest that rifampin had an additional impact on larotrectinib intestinal disposition that was not directly related to inhibition of Oatp1a/1b-mediated liver uptake. The most likely explanation is that the high intestinal concentration of (oral) rifampin also inhibited the intestinal Abcb1 and perhaps Abcg2 proteins, thus increasing the net rate of uptake of larotrectinib from the intestinal lumen. Furthermore, likely the extent of inhibition of ABC transporters in other organs that were only exposed to rifampin through the blood did not affect larotrectinib excretion much, resulting in only a limited increase in overall plasma exposure in *Slco1a/1b*^{-/-}, Slco1B1 and Slco1B3 mice. Nonetheless, considering that the elimination phase started within 1 h, it may be that additional Abcb1 inhibition by rifampin was responsible for the relative increase in plasma AUC in the *Slco1a/1b*^{-/-} mice (Figure 3B). Of note,

we did not observe any acute toxicity complications of larotrectinib in any of the mouse strains that we tested with oral larotrectinib at 10 mg/kg, either in the absence or in the presence of rifampin.

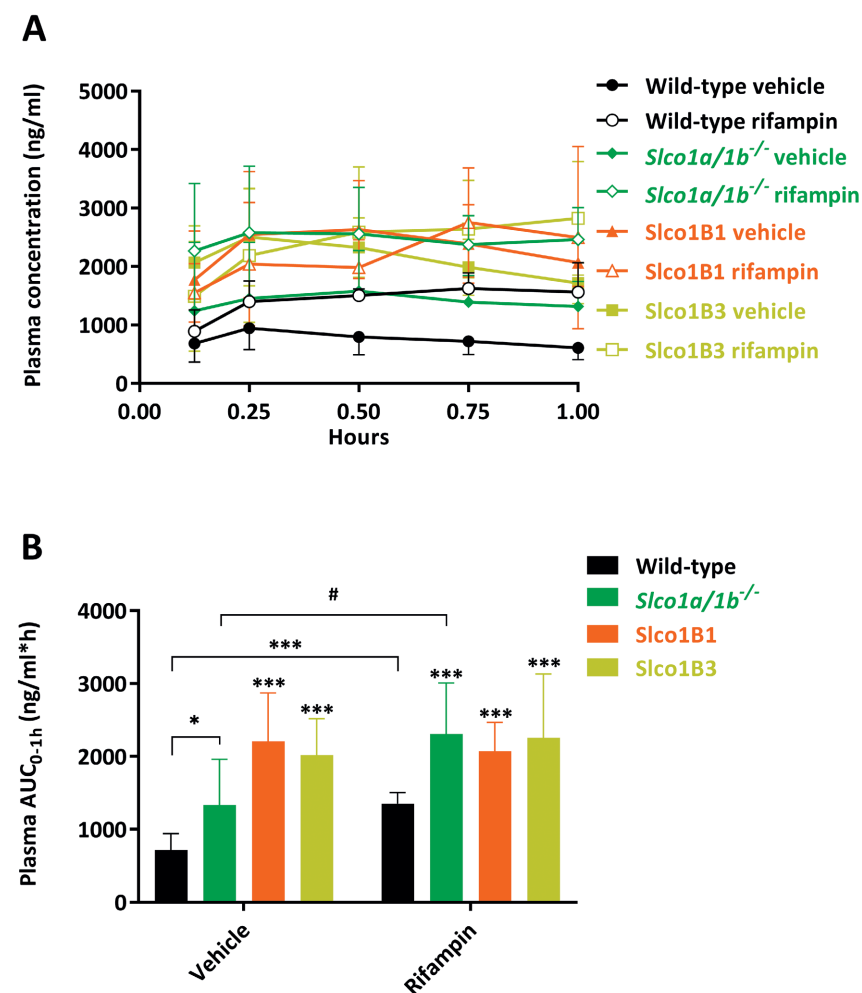


Figure 3. Plasma concentration-time curves (A) and plasma AUC_{0-1h} (B) of larotrectinib in male wild-type, *Slco1a/1b*^{-/-}, Slco1B1 and Slco1B3 mice over 1 h after oral administration of 10 mg/kg larotrectinib with or without co-administration of rifampin. Data are given as mean ± S.D. (n = 6 - 7). *, P < 0.05; **, P < 0.01; ***, P < 0.001 compared to vehicle-treated wild-type mice; #, P < 0.05 compared between vehicle-treated and rifampin-treated *Slco1a/1b*^{-/-} mice; No significant differences were observed between vehicle-treated Slco1B1 and rifampin-treated Slco1B1 mice or between vehicle-treated Slco1B3 and rifampin-treated Slco1B3 mice.

Table 2. Plasma and tissue pharmacokinetic parameters of larotrectinib in male wild-type, *Sico1a/1b^{-/-}*, *Sico1B1* and *Sico1B3* mice over 1 h after oral administration of 10 mg/kg larotrectinib with or without inhibitor rifampin.

| Parameter | Genotype/Groups | | | | | | | |
|-----------------------------------|-----------------|--------------------------------|-----------------|----------------|----------------|--------------------------------|-------------------|--------------------|
| | Vehicle | | | Rifampin | | | | |
| | Wild-type | <i>Sico1a/1b^{-/-}</i> | <i>Sico1B1</i> | <i>Sico1B3</i> | Wild-type | <i>Sico1a/1b^{-/-}</i> | <i>Sico1B1</i> | <i>Sico1B3</i> |
| AUC _{0-3h} , ng/ml.h | 715 ± 227 | 1333 ± 627* | 2210 ± 662** | 2019 ± 499** | 1351 ± 155*** | 2306 ± 703*** | 2071 ± 399*** | 2255 ± 875*** |
| Fold change AUC _{0-3h} | 1.0 | 1.9 | 3.1 | 2.8 | 1.9 | 3.2 | 2.9 | 3.2 |
| C _{max} , ng/ml | 977 ± 321 | 1779 ± 881* | 2800 ± 962*** | 2557 ± 781*** | 1857 ± 329** | 2955 ± 702***# | 3197 ± 1457*** | 3026 ± 1052*** |
| T _{max} , h | 0.46 ± 0.3 | 0.46 ± 0.4 | 0.54 ± 0.3 | 0.33 ± 0.1 | 0.71 ± 0.3 | 0.54 ± 0.4 | 0.67 ± 0.3 | 0.71 ± 0.4 |
| C _{brain} , ng/g | 21.2 ± 2.8 | 44.9 ± 16.7 | 68.0 ± 27.2*** | 70.2 ± 19.6*** | 84.9 ± 30.4*** | 139.6 ± 45.7***### | 102.9 ± 52.9*** | 129.7 ± 69.9*** |
| Fold increase C _{brain} | 1.0 | 2.1 | 3.2 | 3.3 | 4.0 | 6.6 | 4.9 | 6.1 |
| Brain-to-plasma ratio | 0.039 ± 0.02 | 0.037 ± 0.02 | 0.033 ± 0.01 | 0.042 ± 0.01 | 0.057 ± 0.02 | 0.057 ± 0.01# | 0.052 ± 0.03 | 0.045 ± 0.02 |
| Fold change ratio | 1.0 | 0.95 | 0.85 | 1.1 | 1.5 | 1.5 | 1.3 | 1.2 |
| C _{liver} , ng/g | 4812 ± 1392 | 4628 ± 1584 | 6265 ± 1393 | 6676 ± 2124 | 5555 ± 1192 | 8316 ± 946***# | 6383 ± 1084 | 6875 ± 810** |
| Fold increase C _{liver} | 1.0 | 1.0 | 1.3 | 1.4 | 1.2 | 1.7 | 1.3 | 1.1 |
| Liver-to-plasma ratio | 8.1 ± 0.8 | 3.6 ± 0.6*** | 3.0 ± 0.2*** | 3.9 ± 1.1*** | 3.7 ± 0.5*** | 3.5 ± 0.5*** | 3.2 ± 1.2***^^ | 2.2 ± 1.4*** |
| Fold change ratio | 1.0 | 0.44 | 0.37 | 0.48 | 0.46 | 0.43 | 0.40 | 0.27 |
| C _{SI+SIc} , µg/g | 23.7 ± 10.5 | 44.3 ± 5.4* | 50.4 ± 11.1** | 42.7 ± 12.8* | 13.0 ± 3.7 | 20.3 ± 4.5### | 18.6 ± 2.7^^ | 27.2 ± 7.6^ |
| Fold change C _{SI+SIc} | 1.0 | 1.9 | 2.1 | 1.8 | 0.5 | 0.9 | 0.8 | 1.1 |
| SI + SIC-to-plasma ratio | 43.7 ± 27.2 | 37.2 ± 14.2 | 25.1 ± 8.0 | 25.7 ± 8.5 | 8.4 ± 1.2*** | 8.5 ± 1.7***### | 9.3 ± 3.5***###^^ | 9.9 ± 1.6***###^^^ |
| Fold change ratio | 1.0 | 0.85 | 0.57 | 0.59 | 0.19 | 0.19 | 0.21 | 0.23 |
| C _{testis} , ng/g | 175.2 ± 103.7 | 328.4 ± 148.7 | 534.3 ± 128.8** | 411.5 ± 71.6** | 358.4 ± 141.3* | 326.3 ± 72.9* | 337.8 ± 74.5^^ | 369.1 ± 112.0* |
| Fold increase C _{testis} | 1.0 | 1.9 | 3.0 | 2.3 | 2.0 | 1.9 | 1.9 | 2.1 |
| Testis-to-plasma ratio | 0.35 ± 0.32 | 0.26 ± 0.12 | 0.26 ± 0.04 | 0.25 ± 0.08 | 0.23 ± 0.04 | 0.13 ± 0.03# | 0.17 ± 0.07 | 0.14 ± 0.04^^ |
| Fold change ratio | 1.0 | 0.74 | 0.74 | 0.71 | 0.66 | 0.37 | 0.49 | 0.40 |

Data are given as mean ± S.D. (n = 6 - 7). AUC_{0-3h}, area under the plasma concentration-time curve; C_{max}, maximum concentration in plasma; T_{max}, time point (h) of maximum plasma concentration; C_{brain}, brain concentration; C_{liver}, liver concentration; SI, small intestine (tissue); SIC, small intestine contents; C_{SI+SIc}, small intestine tissue together with small intestine contents concentration; C_{testis}, testis concentration; *, P < 0.05; **, P < 0.01; ***, P < 0.001 compared to vehicle-treated wild-type mice; #, P < 0.05; ##, P < 0.01; ###, P < 0.001 compared between vehicle-treated and rifampin-treated *Sico1a/1b^{-/-}* mice; ^, P < 0.05; ^^, P < 0.01; ^^, P < 0.001 compared between vehicle-treated *Sico1B1* and rifampin-treated *Sico1B1* mice or between vehicle-treated *Sico1B3* and rifampin-treated *Sico1B3* mice. Statistical analysis was applied after log-transformation of linear data.

3.4 Larotrectinib exposure and tissue distribution upon co-administration with the CYP3A inhibitor ritonavir

In order to examine whether we could increase the oral availability of larotrectinib by inhibition of CYP3A, we administered the irreversible CYP3A inhibitor ritonavir (50 mg/kg) or vehicle orally 15 min prior to oral larotrectinib (15 mg/kg) to male wild-type, *Cyp3a^{-/-}*, and *Cyp3aXAV* mice, which express transgenic human CYP3A4 in liver and intestine of *Cyp3a^{-/-}* mice. In vehicle-treated mice, although the plasma AUC_{0-1h} was not statistically significantly different among the three mouse strains, it was modestly increased (1.4-fold) in *Cyp3a^{-/-}* mice and then relatively decreased (by 1.7-fold) in *Cyp3aXAV* mice (Figure 4 and Table 3), similar to the previously observed significant plasma AUC_{0-4h} differences among these strains measured over 4 h⁷. While the plasma AUC differences were not significant, the larotrectinib tissue concentrations at 1 h among these three strains clearly supported an increase in exposure in *Cyp3a^{-/-}* mice relative to wild-type mice, and a subsequent strong decrease in *Cyp3aXAV* mice (Supplemental Figures 6 and 7). This applied to all tested tissues, i.e. brain, testis, kidney, liver, and SI + SIC.

In the absence of ritonavir, brain-, testis- and kidney-to-plasma ratios of larotrectinib were similar among wild-type, *Cyp3a^{-/-}* and *Cyp3aXAV* mice, suggesting that the CYP3A genotype did not influence the distribution between tissue and blood in these organs (Supplemental Figure 6). However, there were clear increases in liver- and SI + SIC-to-plasma ratios in *Cyp3a^{-/-}* mice (1.3-fold, P < 0.05 and 2.0-fold, P < 0.01) compared to wild-type mice and then downward shifts in *Cyp3aXAV* mice (0.7-fold, P < 0.01 and 0.3-fold, P < 0.001) relative to *Cyp3a^{-/-}* mice (Supplemental Figure 7 and Table 3). These effects might be related to the direct metabolism of larotrectinib by Cyp3a and CYP3A4 enzymes in liver and intestinal tissue. Overall, these data support our earlier finding that transgenic human CYP3A4 has a substantial impact on larotrectinib pharmacokinetics, as does endogenous mouse Cyp3a.

Unexpectedly, pre-treatment with ritonavir resulted in plasma larotrectinib exposure increases not only in wild-type mice (1.5-fold compared to vehicle-treated wild-type mice) and *Cyp3aXAV* mice (2.2-fold compared to vehicle-treated *Cyp3aXAV* mice), but also in *Cyp3a^{-/-}* mice (1.7-fold compared to vehicle-treated *Cyp3a^{-/-}* mice) (Figure 4 and Table 3). These shifts suggest that ritonavir must have additional effects beyond the possible inhibition of mouse Cyp3a (and human CYP3A4). Brain, testis and kidney absolute drug concentrations were also increased, but ritonavir had no substantial influence on the relative brain-, testis- and kidney-to-plasma ratios in these three mouse strains (Supplemental Figure 6). The increases in concentrations in these tissues therefore mainly reflected the higher plasma levels of larotrectinib due to ritonavir treatment. In contrast, for both liver and small intestine with intestinal contents, we observed a marked decrease in tissue-to-plasma ratios to a similar level in all of the three mouse strains upon pre-treatment with ritonavir (Supplemental Figure 7). These results suggest that, in addition to Cyp3a/CYP3A4, also some other larotrectinib-handling systems were noticeably affected

by ritonavir in liver and intestine. Given that Abcb1a/1b/Abcg2 deficiency likewise resulted in decreased liver-to-plasma ratios and SI + SIC-to-plasma ratios (Supplemental Figure 2), and as ritonavir is known to inhibit ABCB1 P-glycoprotein, a likely explanation is that ritonavir also inhibited Abcb1a/1b activity in intestine and liver.

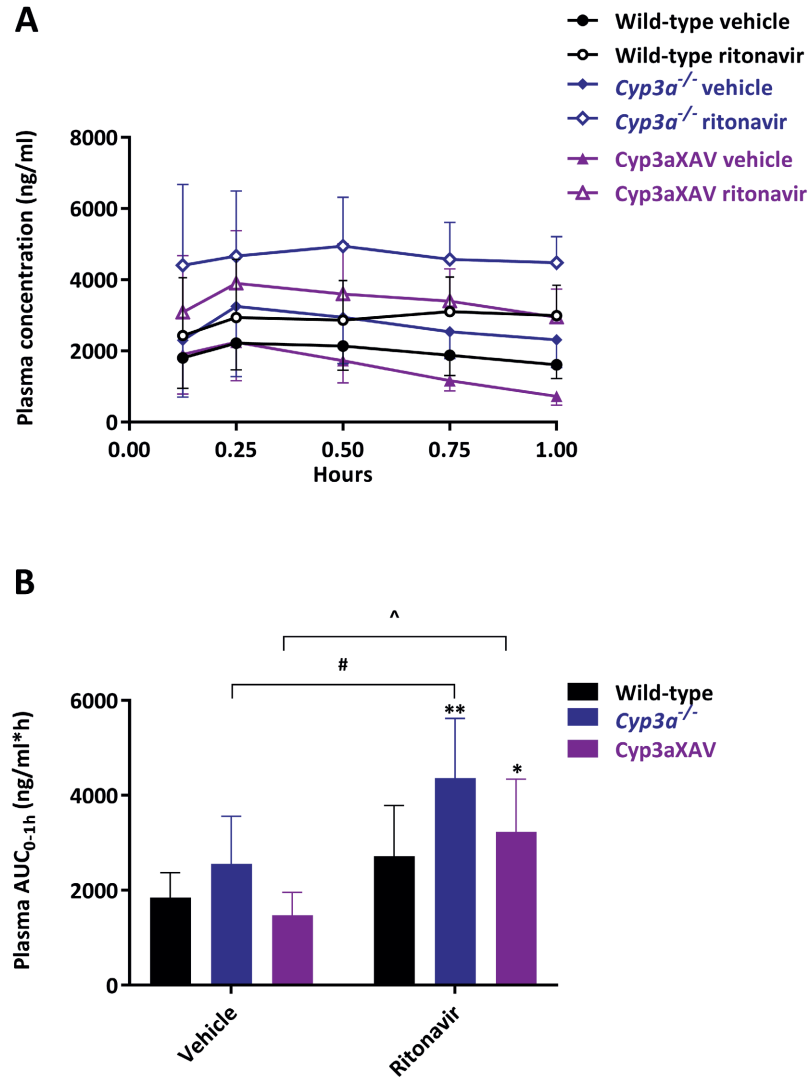


Figure 4. Plasma concentration-time curves (A) and plasma AUC_{0-1h} (B) of larotrectinib in male wild-type, *Cyp3a^{-/-}* and *Cyp3aXAV* mice over 1 h after oral administration of 15 mg/kg larotrectinib with or without co-administration of ritonavir. Data are given as mean \pm S.D. (n = 6). *, $P < 0.05$; **, $P < 0.01$ compared to vehicle-treated wild-type mice; #, $P < 0.05$ compared between vehicle-treated and ritonavir-treated *Cyp3a^{-/-}* mice; ^, $P < 0.05$ compared between vehicle-treated and ritonavir-treated *Cyp3aXAV* mice.

Table 3. Pharmacokinetic parameters, brain concentrations, and brain-to-plasma ratios of larotrectinib in male wild-type, *Cyp3a^{-/-}* and *Cyp3aXAV* mice over 1 h after oral administration of 15 mg/kg larotrectinib with or without inhibitor ritonavir.

| Parameter | Vehicle | | Ritonavir | |
|----------------------------------|-------------------|----------------------------|-------------------|----------------------------|
| | Wild-type | <i>Cyp3a^{-/-}</i> | Wild-type | <i>Cyp3a^{-/-}</i> |
| | Mean \pm S.D. | Mean \pm S.D. | Mean \pm S.D. | Mean \pm S.D. |
| AUC _{0-1h} , ng/ml/h | 1845 \pm 530 | 2557 \pm 1006 | 2719 \pm 1067 | 4362 \pm 1262**# |
| Fold change AUC _{0-1h} | 1.0 | 1.4 | 1.5 | 2.4 |
| C _{max} , ng/ml | 2395 \pm 763 | 3916 \pm 1046* | 3562 \pm 1033 | 5314 \pm 1377** |
| T _{max} , h | 0.50 \pm 0.31 | 0.50 \pm 0.39 | 0.63 \pm 0.34 | 0.52 \pm 0.32 |
| C _{brain} , ng/g | 63.0 \pm 35.7 | 84.1 \pm 29.8 | 143.8 \pm 49.0* | 284.1 \pm 120.5***### |
| Fold change C _{brain} | 1.0 | 1.3 | 2.3 | 4.5 |
| Brain-to-plasma ratio | 0.037 \pm 0.01 | 0.039 \pm 0.02 | 0.046 \pm 0.02 | 0.064 \pm 0.03* |
| Fold change ratio | 1.0 | 1.1 | 1.3 | 1.7 |
| C _{liver} , μ g/g | 15.0 \pm 3.0 | 30.2 \pm 14.6* | 11.5 \pm 2.9 | 19.3 \pm 3.8 |
| Fold change C _{liver} | 1.0 | 2.0 | 0.77 | 1.3 |
| Liver-to-plasma ratio | 9.4 \pm 1.5 | 12.5 \pm 2.5* | 3.9 \pm 0.4*** | 4.3 \pm 0.4***### |
| Fold change ratio | 1.0 | 1.3 | 0.41 | 0.46 |
| C _{SI+ SIC} , μ g/g | 76.9 \pm 40.1 | 222.5 \pm 98.2** | 24.2 \pm 6.8** | 58.5 \pm 6.4### |
| Fold change C _{SI+ SIC} | 1.0 | 2.9 | 0.31 | 0.76 |
| SI + SIC-to-plasma ratio | 47.3 \pm 19.0 | 94.5 \pm 21.0** | 8.4 \pm 1.9*** | 13.2 \pm 1.7***### |
| Fold change ratio | 1.0 | 2.0 | 0.18 | 0.28 |
| C _{testis} , ng/g | 381.9 \pm 240.8 | 699.8 \pm 359.2 | 772.1 \pm 474.6 | 1518 \pm 579.1***# |
| Fold change C _{testis} | 1.0 | 1.8 | 2.0 | 4.0 |
| Testis-to-plasma ratio | 0.23 \pm 0.13 | 0.40 \pm 0.38 | 0.25 \pm 0.11 | 0.35 \pm 0.16 |
| Fold change ratio | 1.0 | 1.7 | 1.1 | 1.5 |

Data are given as mean \pm S.D. (n = 6). AUC_{0-1h}, area under the plasma concentration-time curve; C_{max}, maximum concentration in plasma; T_{max}, time point (h) of maximum plasma concentration; C_{brain}, brain concentration; C_{liver}, liver concentration; SI, small intestine (tissue); SIC, small intestine contents; C_{SI+ SIC}, small intestine tissue together with small intestine contents concentration; C_{testis}, testis concentration; *, $P < 0.05$; **, $P < 0.01$; ***, $P < 0.001$ compared to vehicle-treated wild-type mice; #, $P < 0.05$; ##, $P < 0.01$; ###, $P < 0.001$ compared between vehicle-treated and ritonavir-treated *Cyp3a^{-/-}* mice; ^, $P < 0.05$; ^^, $P < 0.01$; ^^, $P < 0.001$ compared between vehicle-treated and ritonavir-treated *Cyp3aXAV* mice. Statistical analysis was applied after log-transformation of linear data.

4. DISCUSSION AND CONCLUSIONS

In a preceding study⁷, larotrectinib was shown to be efficiently transported by ABCB1 and ABCG2. Here we found that the dual ABCB1 and ABCG2 inhibitor elacridar could extensively enhance the plasma exposure and especially the brain penetration of larotrectinib in wild-type mice, but not in *Abcb1a/1b;Abcg2*^{-/-} mice. This suggests that these pharmacokinetic effects of elacridar were specifically mediated by virtually complete inhibition of these ABC transporters. In contrast, in liver elacridar decreased the liver-to-plasma ratios in wild-type mice, yielding similarly reduced ratios as seen in vehicle-treated *Abcb1a/1b;Abcg2*^{-/-} mice. We previously noticed similar hepatic distribution effects for some other small-molecular inhibitors (TKIs) that are ABC transporter substrates. The likely cause is high accumulation of larotrectinib in intrahepatic bile due to the concentrative effect of the ABC transporters, resulting in higher overall liver concentration of larotrectinib in wild-type liver than in ABC-transporter-deficient liver³². These results thus suggest extensive inhibition of bile canalicular *Abcb1a/1b* and *Abcg2* by elacridar treatment. Pre-treatment with elacridar further lead to a marked decrease in drug concentration and percentage of dose in SI + SIC and related parameters, also after correction for the plasma levels in wild-type mice compared to vehicle-treated wild-type mice. This indicates that elacridar could further extensively inhibit intestinal *Abcb1a/1b* and *Abcg2* activity. No noticeable changes in tissue distribution due to the ABC transporter deficiencies were found in other tissues. As several of the cancers indicated for larotrectinib treatment reside in the brain or readily form brain metastases, it may be considered to coadminister elacridar in order to improve the brain penetration and thus possibly therapeutic efficacy of larotrectinib.

We further previously found that larotrectinib was a likely substrate of human OATP1A2 *in vitro*, but not of human OATP1B1 or -1B3⁷. To further investigate the possible impact of OATPs on larotrectinib behavior *in vivo*, we performed a distribution study in human SLCO1B1 or SLCO1B3 transgenic mice with wild-type and *Slco1a/1b*^{-/-} mice as controls. Our results confirmed that larotrectinib is taken up into the liver by the mouse *Oatp1a/1b* proteins, and that this secondarily results in higher intestinal levels of larotrectinib. However, we found no indications for an analogous function of hepatic transgenic human OATP1B1 or OATP1B3. This indicates that larotrectinib is not a substrate of human OATP1B1 or 1B3 *in vivo*, consistent with the FDA registration documentation⁵. A modest reduction in larotrectinib uptake was further observed in lungs of *Slco1a/1b*^{-/-} mice, as also seen in our previous study⁷. This suggests a limited impact of *mOatp1a/1b* on larotrectinib lung uptake.

Rifampin, a well-studied OATP inhibitor, can dramatically influence the pharmacokinetics of OATP substrate drugs. We previously demonstrated that in mice rifampin was an effective and specific *Oatp1a/1b* inhibitor in controlling methotrexate pharmacokinetics²⁸. Studying the effects of rifampin on larotrectinib exposure and distribution, we found that rifampin decreased the

relative liver uptake in wild-type mice by about 2.2-fold to similar levels as seen in *Slco1a/1b*^{-/-} mice (Supplemental Figure 5B), resulting in a concomitant (~1.9-fold) increase in larotrectinib plasma levels (Figure 3). As rifampin did not affect relative liver distribution of larotrectinib in *Slco1a/1b*^{-/-} mice, this inhibitory effect appeared to be specific for the hepatic *Oatp1a/1b* proteins, with no other hepatic uptake or efflux transporters noticeably inhibited.

Based on the reduced relative liver uptake of larotrectinib and thus presumably reduced hepatobiliary excretion, we expected that the SI + SIC values would also be reduced by rifampin treatment, as seen when comparing vehicle-treated wild-type and *Slco1a/1b*^{-/-} mice. To our surprise, however, the larotrectinib concentration and percentage of the dose in SI + SIC were significantly decreased in all the groups upon rifampin treatment, even in *Slco1a/1b*^{-/-} mice, and these decreases were even more obvious after plasma correction (Supplemental Figure 5D). These results indicate that, besides inhibiting hepatic *Oatp1a/1b* transporters, other larotrectinib-handling systems must have been influenced by rifampin. It is known that oral rifampin can inhibit enterocyte ABCB1 (P-gp), without affecting hepatic ABCB1 or renal transporters^{21,33}, thus inhibiting the efflux of digoxin, an excellent ABCB1 substrate, into the intestinal lumen. As larotrectinib is also an excellent ABCB1 substrate, it is very likely that a similar process applies in our mouse models: inhibition of intestinal ABCB1 by the high concentration of oral rifampin results in reduced direct intestinal excretion and increased net absorption of larotrectinib, thus explaining the strongly reduced SI + SIC levels of larotrectinib upon rifampin treatment. Comparison of the rifampin SI + SIC data as larotrectinib percentage of dose in wild-type mice (5.2 %) with those obtained with elacridar treatment (2.0 %) show that elacridar is still a more effective inhibitor of intestinal ABCB1. The absence of clear shifts in brain- or other tissue distribution (apart from liver and SI + SIC) of larotrectinib suggests that, for instance, ABCB1 in the BBB was not markedly inhibited upon oral rifampin treatment (Supplemental Figures 4 and 5), presumably due to lower systemic concentrations of rifampin. Overall, the data suggest that in mice oral rifampin does not only inhibit hepatic *Oatp1a/1b* proteins, but also intestinal ABCB1 activity to some extent.

As FDA guidelines⁵ indicate, coadministration of a strong CYP3A inhibitor (itraconazole) with a single 100 mg dose of larotrectinib in humans could increase the larotrectinib plasma $AUC_{0-\infty}$ by 4.3-fold and the C_{max} by 2.8-fold as compared to larotrectinib administered alone. Ritonavir, another strong CYP3A inhibitor, could profoundly enhance both paclitaxel and docetaxel oral availability in mice²². In this study, given the prominent role of CYP3A in the pharmacokinetics of larotrectinib, we investigated the influence of oral ritonavir on oral larotrectinib pharmacokinetics. After pre-treatment with ritonavir, wild-type and *Cyp3aXAV* mice showed increased plasma exposure to a similar level as seen in vehicle-treated *Cyp3a*^{-/-} mice. Interestingly, ritonavir also enhanced the overall exposure of larotrectinib in *Cyp3a*^{-/-} mice, suggesting additional effects of ritonavir on non-Cyp3a larotrectinib clearance mechanisms. While ritonavir primarily inhibits

CYP3A-mediated metabolism, it is known that it can also inhibit ABCB1^{24,25}. As we found that ritonavir strongly reduced both liver and SI + SIC distribution of larotrectinib even in *Cyp3a*^{-/-} mice, the most likely explanation is that ritonavir could also inhibit ABCB1 in both small intestine and liver, thus enhancing the larotrectinib exposure even when *Cyp3a* is absent. These results could not be logically explained by reduced metabolism of larotrectinib, for instance if ritonavir would inhibit another non-*Cyp3a* larotrectinib-metabolizing enzyme, as one would then expect relative increases in tissue levels of larotrectinib.

Strikingly, the relative effect of ritonavir on liver- and SI + SIC-to-plasma ratios was highest in the *Cyp3a*^{-/-} mice, and lowest in the *Cyp3aXAV* mice (Supplemental Figure 7B, D, F). This suggests that ritonavir-mediated inhibition of *Abcb1a/1b* was strongest in the *Cyp3a*^{-/-} mice, lowest in the *Cyp3aXAV* mice, with the wild-type mice in between. This could in part relate to relative ritonavir exposure in liver and intestine of these strains. As ritonavir itself is also metabolized by and/or irreversibly bound to mouse and human CYP3A, the amount of available ritonavir in these organs may well be highest in the *Cyp3a*^{-/-} mice, and lowest in the *Cyp3aXAV* mice. In contrast to its intestinal and hepatic disposition, the brain penetration of larotrectinib was not influenced by ritonavir. Like for rifampin, it may well be that the effective plasma concentration of ritonavir was too low to achieve noticeable inhibition of the ABC transporters in the BBB.

The combined activity of drug transporters and CYP3A results in efficient first-pass metabolism of orally administered drugs, and this phenomenon was also observed for many other drugs^{11-15,23,34}. Considering that ritonavir inhibits both *Cyp3a* and ABCB1 proteins, it is difficult to conclude which inhibition function predominates for the increase of larotrectinib exposure in ritonavir-treated wild-type mice, but it seems likely that inhibition of ABCB1 by ritonavir does contribute to the increased oral bioavailability of larotrectinib.

Unlike some other drugs that are primarily affected by one or a few of the main detoxification systems, larotrectinib pharmacokinetics behavior can be affected by multiple factors, including but perhaps not limited to ABC transporters, OATP1A, and CYP3A. On the one hand, these properties may make it more likely that larotrectinib is affected by drug-drug interactions or genetic polymorphisms, thus possibly influencing its safety and efficacy profiles. On the other hand, being handled by multiple detoxification systems may make it less likely that one system will be very dominant, and have a disproportionate impact of larotrectinib pharmacokinetics. Still, the fact that some known possibly co-administered drugs such rifampin and ritonavir can simultaneously affect larotrectinib through multiple detoxification systems does pose a potential risk that needs to be carefully considered. Even though no signs of spontaneous toxicity of larotrectinib showed up in any of the tested mouse strains in our experiments, given the complications we observed, any attempt to apply “specific” inhibitors or combination therapy regimes in patients together with larotrectinib should be carefully monitored.

In summary, we confirmed that larotrectinib is a substrate of mouse *Oatp1a/1b*, but not of human OATP1B1 and -1B3 *in vivo*. To the best of our knowledge, this is the first study documenting that elacridar could enhance larotrectinib plasma exposure as well as brain penetration. We further found that rifampin can increase larotrectinib systemic exposure, most likely by inhibiting OATP1A, as well as by acute inhibition of enterocyte ABCB1. Similarly, ritonavir can also increase larotrectinib oral availability and thus its tissue exposure by inhibition of not only CYP3A enzymes, but also ABCB1 transporters in both small intestine and liver. The obtained drug-drug interaction insights and principles in this study may potentially be used to further optimize the therapeutic application and efficacy of larotrectinib in the clinic.

ACKNOWLEDGEMENTS

This work was funded in part by the Chinese Scholarship Council (CSC Scholarship No. 201506240107 to Yaogeng Wang).

AUTHOR CONTRIBUTIONS

Yaogeng Wang and Alfred H. Schinkel designed the study, analyzed the data and wrote the manuscript. Yaogeng Wang, Rolf W. Sparidans, and Jing Wang performed the experimental parts of the study. Maria C. Lebre contributed reagents, materials and mice, and checked the content and language of the manuscript. Jos H. Beijnen and Rolf W. Sparidans supervised the bioanalytical part of the studies and checked the content and language of manuscript. All authors commented on and approved the manuscript.

CONFLICT OF INTEREST STATEMENT

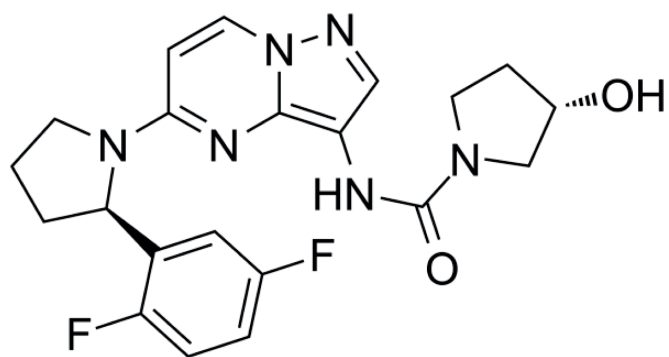
The research group of Alfred Schinkel receives revenue from commercial distribution of some of the mouse strains used in this study. The graphical abstract was made with biorender.com. The remaining authors declare no conflict of interest.

REFERENCE

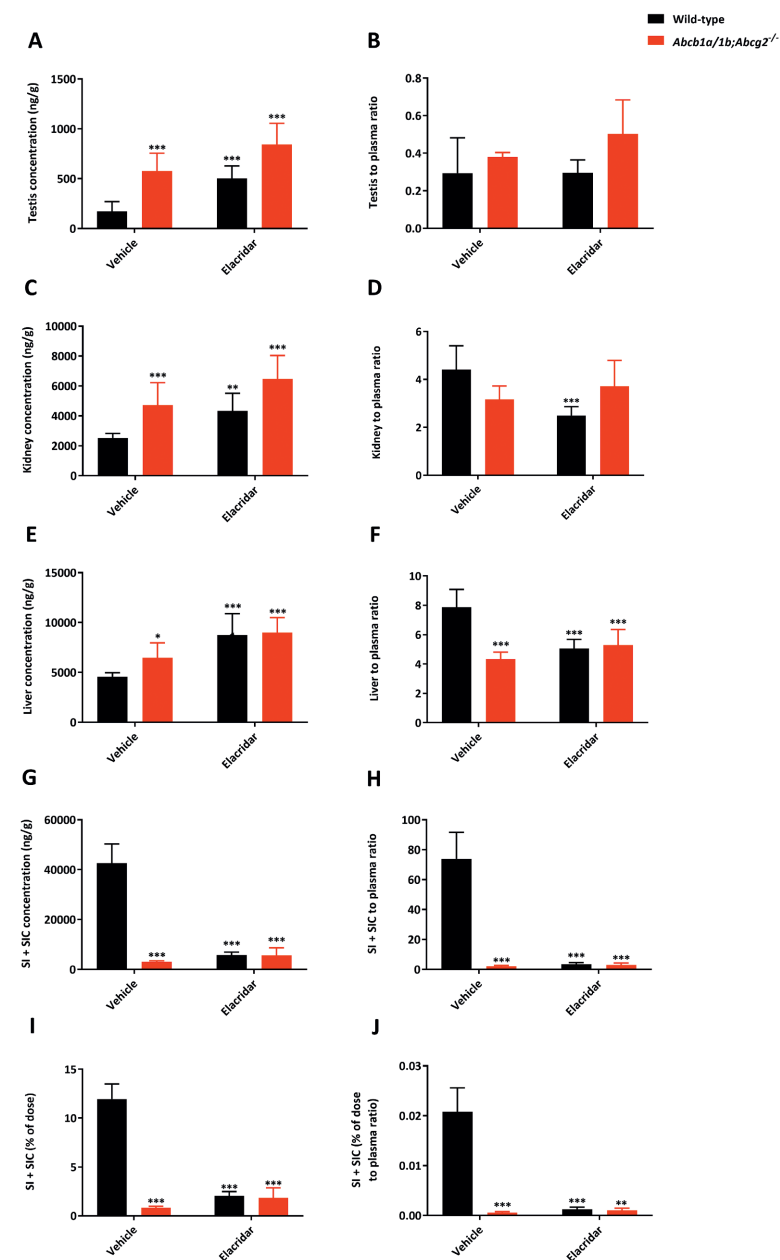
- Nakagawara, A. Trk receptor tyrosine kinases: a bridge between cancer and neural development. *Cancer Letters* **169**, 107-114 (2001).
- Créancier, L., *et al.* Chromosomal rearrangements involving the NTRK1 gene in colorectal carcinoma. *Cancer Letters* **365**, 107-111 (2015).
- Wu, G., *et al.* The genomic landscape of diffuse intrinsic pontine glioma and pediatric non-brainstem high-grade glioma. *Nature Genetics* **46**, 444-450 (2014).
- Stransky, N., Cerami, E., Schalm, S., Kim, J.L. & Lengauer, C. The landscape of kinase fusions in cancer. *Nature Communications* **5**, 4846 (2014).
- Food and Drug Administration. Center for Drug Evaluation and Research of the US Department of Health and Human Service, Food and Drug Administration. Multi-discipline Review (2018). Available from: https://www.accessdata.fda.gov/drugsatfda_docs/label/2018/211710s000lbl.pdf.
- Schinkel, A.H. & Jonker, J.W. Mammalian drug efflux transporters of the ATP binding cassette (ABC) family: an overview. *Advanced Drug Delivery Reviews* **55**, 3-29 (2003).
- Wang, Y., *et al.* OATP1A/1B, CYP3A, ABCB1, and ABCG2 limit oral availability of the NTRK inhibitor larotrectinib, while ABCB1 and ABCG2 also restrict its brain accumulation. *British Journal of Pharmacology* **177**, 3060-3074 (2020).
- de Graan, A.J., *et al.* Influence of polymorphic OATP1B-type carriers on the disposition of docetaxel. *Clinical Cancer Research* **18**, 4433-4440 (2012).
- van Herwaarden, A.E., *et al.* Knockout of cytochrome P450 3A yields new mouse models for understanding xenobiotic metabolism. *Journal of Clinical Investigation* **117**, 3583-3592 (2007).
- Guengerich, F.P. Cytochrome P-450 3A4: regulation and role in drug metabolism. *Annual Review of Pharmacology and Toxicology* **39**, 1-17 (1999).
- Garmire, L.X. & Hunt, C.A. In silico methods for unraveling the mechanistic complexities of intestinal absorption: metabolism-efflux transport interactions. *Drug Metabolism and Disposition* **36**, 1414-1424 (2008).
- Kivistö, K.T., Niemi, M. & Fromm, M.F. Functional interaction of intestinal CYP3A4 and P-glycoprotein. *Fundamental and Clinical Pharmacology* **18**, 621-626 (2004).
- Wandel, C., *et al.* P-glycoprotein and cytochrome P-450 3A inhibition: dissociation of inhibitory potencies. *Cancer Research* **59**, 3944-3948 (1999).
- Ito, K., Kusuhara, H. & Sugiyama, Y. Effects of intestinal CYP3A4 and P-glycoprotein on oral drug absorption--theoretical approach. *Pharmaceutical Research* **16**, 225-231 (1999).
- Watkins, P.B. The barrier function of CYP3A4 and P-glycoprotein in the small bowel. *Advanced Drug Delivery Reviews* **27**, 161-170 (1997).
- Martínez-Chávez, A., *et al.* P-glycoprotein Limits Ribociclib Brain Exposure and CYP3A4 Restricts Its Oral Bioavailability. *Molecular Pharmaceutics* **16**, 3842-3852 (2019).
- Durmus, S., Sparidans, R.W., Wagenaar, E., Beijnen, J.H. & Schinkel, A.H. Oral availability and brain penetration of the B-RAFV600E inhibitor vemurafenib can be enhanced by the P-GLYCOPROTEIN (ABCB1) and breast cancer resistance protein (ABCG2) inhibitor elacridar. *Molecular Pharmaceutics* **9**, 3236-3245 (2012).
- Lagas, J.S., *et al.* Breast cancer resistance protein and P-glycoprotein limit sorafenib brain accumulation. *Molecular Cancer Therapeutics* **9**, 319-326 (2010).
- Kodaira, H., Kusuhara, H., Ushiki, J., Fuse, E. & Sugiyama, Y. Kinetic analysis of the cooperation of P-glycoprotein (P-gp/Abcb1) and breast cancer resistance protein (Bcrp/Abcg2) in limiting the brain and testis penetration of erlotinib, flavopiridol, and mitoxantrone. *Journal of Pharmacology and Experimental Therapeutics* **333**, 788-796 (2010).
- Salphati, L., *et al.* Evaluation of organic anion transporting polypeptide 1B1 and 1B3 humanized mice as a translational model to study the pharmacokinetics of statins. *Drug Metabolism and Disposition* **42**, 1301-1313 (2014).
- Reitman, M.L., *et al.* Rifampin's acute inhibitory and chronic inductive drug interactions: experimental and model-based approaches to drug-drug interaction trial design. *Clinical Pharmacology and Therapeutics* **89**, 234-242 (2011).

- Hendrikx, J.J., *et al.* Oral co-administration of elacridar and ritonavir enhances plasma levels of oral paclitaxel and docetaxel without affecting relative brain accumulation. *British Journal of Cancer* **110**, 2669-2676 (2014).
- ter Heine, R., *et al.* An integrated pharmacokinetic model for the influence of CYP3A4 expression on the in vivo disposition of lopinavir and its modulation by ritonavir. *Journal of Pharmaceutical Sciences* **100**, 2508-2515 (2011).
- Gutmann, H., Fricker, G., Drewe, J., Toeroek, M. & Miller, D.S. Interactions of HIV protease inhibitors with ATP-dependent drug export proteins. *Molecular Pharmacology* **56**, 383-389 (1999).
- Drewe, J., *et al.* HIV protease inhibitor ritonavir: a more potent inhibitor of P-glycoprotein than the cyclosporine analog SDZ PSC 833. *Biochemical Pharmacology* **57**, 1147-1152 (1999).
- Sparidans, R.W., Wang, Y., Schinkel, A.H., Schellens, J.H.M. & Beijnen, J.H. Quantitative bioanalytical assay for the tropomyosin receptor kinase inhibitor larotrectinib in mouse plasma and tissue homogenates using liquid chromatography-tandem mass spectrometry. *Journal of Chromatography. B: Analytical Technologies in the Biomedical and Life Sciences* **1102-1103**, 167-172 (2018).
- Jonker, J.W., *et al.* Contribution of the ABC transporters Bcrp1 and Mdr1a/1b to the side population phenotype in mammary gland and bone marrow of mice. *Stem Cells* **23**, 1059-1065 (2005).
- van de Steeg, E., *et al.* Organic anion transporting polypeptide 1a/1b-knockout mice provide insights into hepatic handling of bilirubin, bile acids, and drugs. *Journal of Clinical Investigation* **120**, 2942-2952 (2010).
- van de Steeg, E., *et al.* Methotrexate pharmacokinetics in transgenic mice with liver-specific expression of human organic anion-transporting polypeptide 1B1 (SLCO1B1). *Drug Metabolism and Disposition* **37**, 277-281 (2009).
- van de Steeg, E., van Esch, A., Wagenaar, E., Kenworthy, K.E. & Schinkel, A.H. Influence of human OATP1B1, OATP1B3, and OATP1A2 on the pharmacokinetics of methotrexate and paclitaxel in humanized transgenic mice. *Clinical Cancer Research* **19**, 821-832 (2013).
- Zhang, Y., Huo, M., Zhou, J. & Xie, S. PKSolver: An add-in program for pharmacokinetic and pharmacodynamic data analysis in Microsoft Excel. *Computer Methods and Programs in Biomedicine* **99**, 306-314 (2010).
- Wang, J., *et al.* Brain accumulation of tivozanib is restricted by ABCB1 (P-glycoprotein) and ABCG2 (breast cancer resistance protein) in mice. *International Journal of Pharmaceutics* **581**, 119277 (2020).
- Greiner, B., *et al.* The role of intestinal P-glycoprotein in the interaction of digoxin and rifampin. *Journal of Clinical Investigation* **104**, 147-153 (1999).
- Benet, L.Z. & Cummins, C.L. The drug efflux-metabolism alliance: biochemical aspects. *Advanced Drug Delivery Reviews* **50 Suppl 1**, S3-11 (2001).

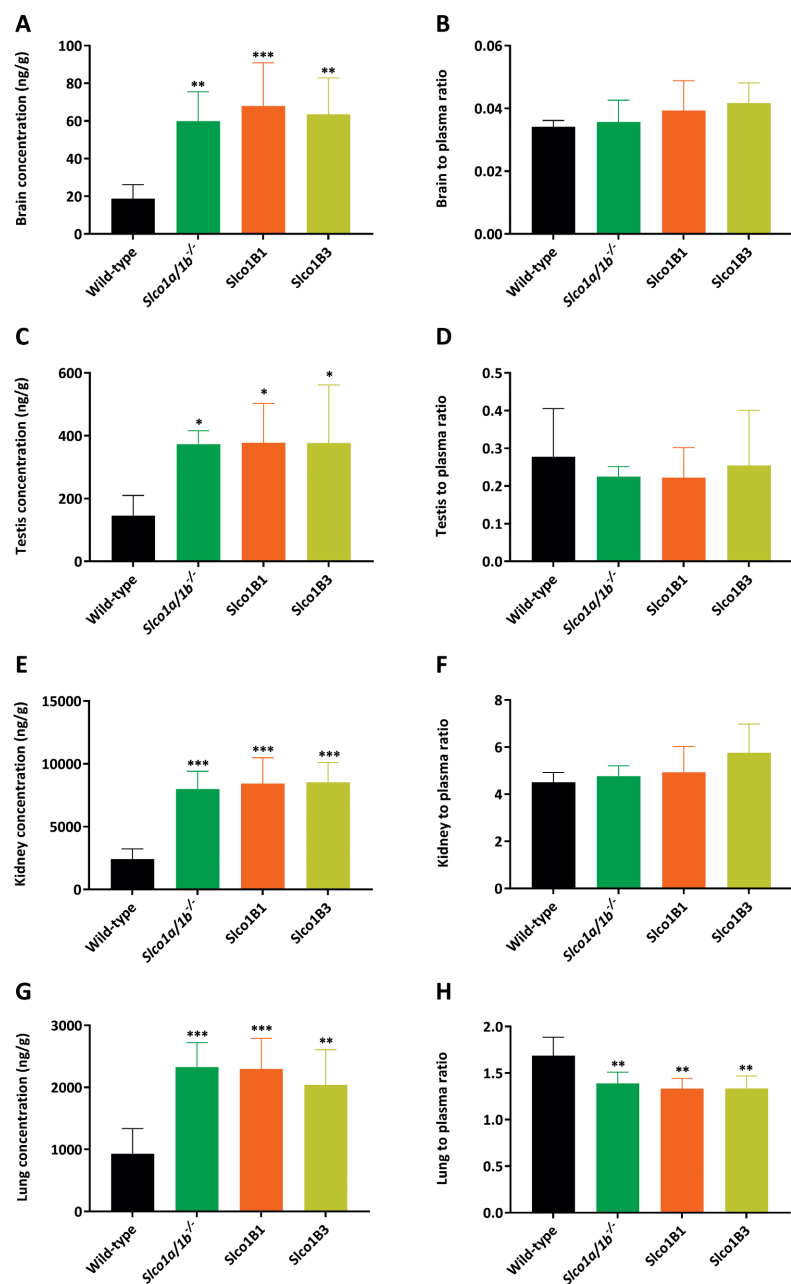
SUPPLEMENTAL MATERIALS



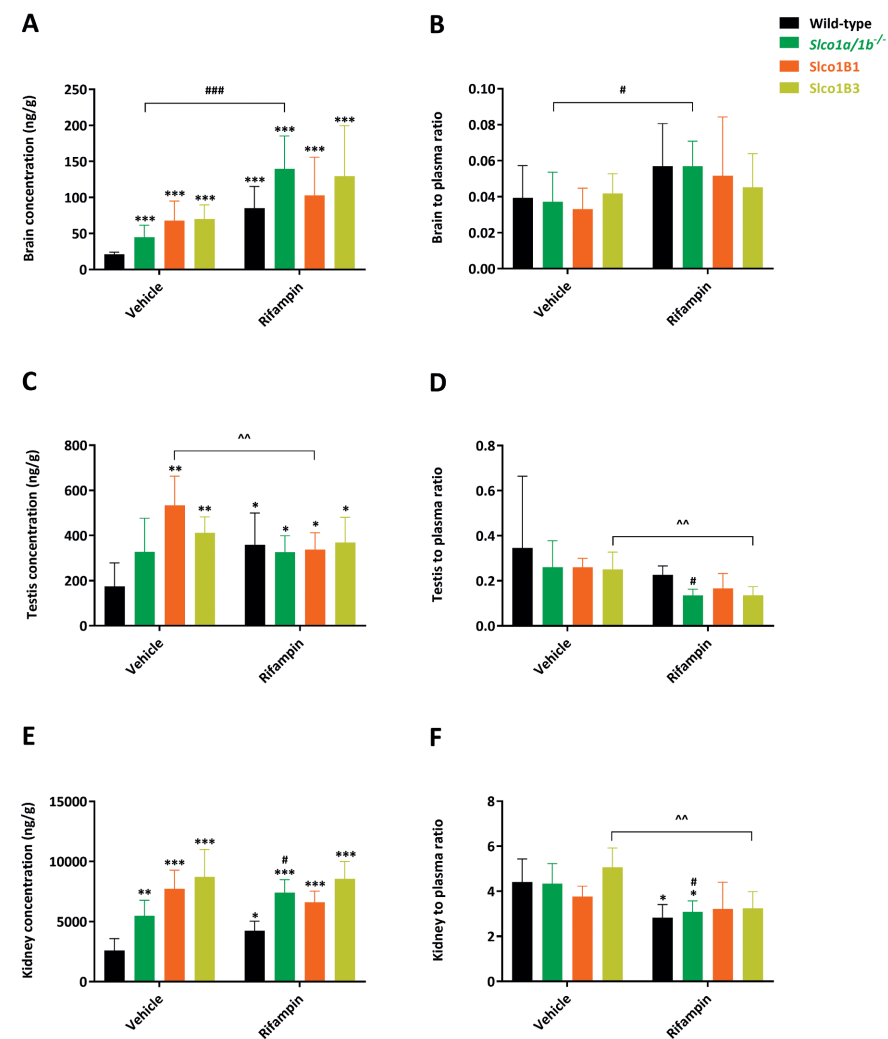
Supplemental Figure 1. Molecular structure of larotrectinib (VITRAKVI, LOXO-101, 428.44 g/mol).



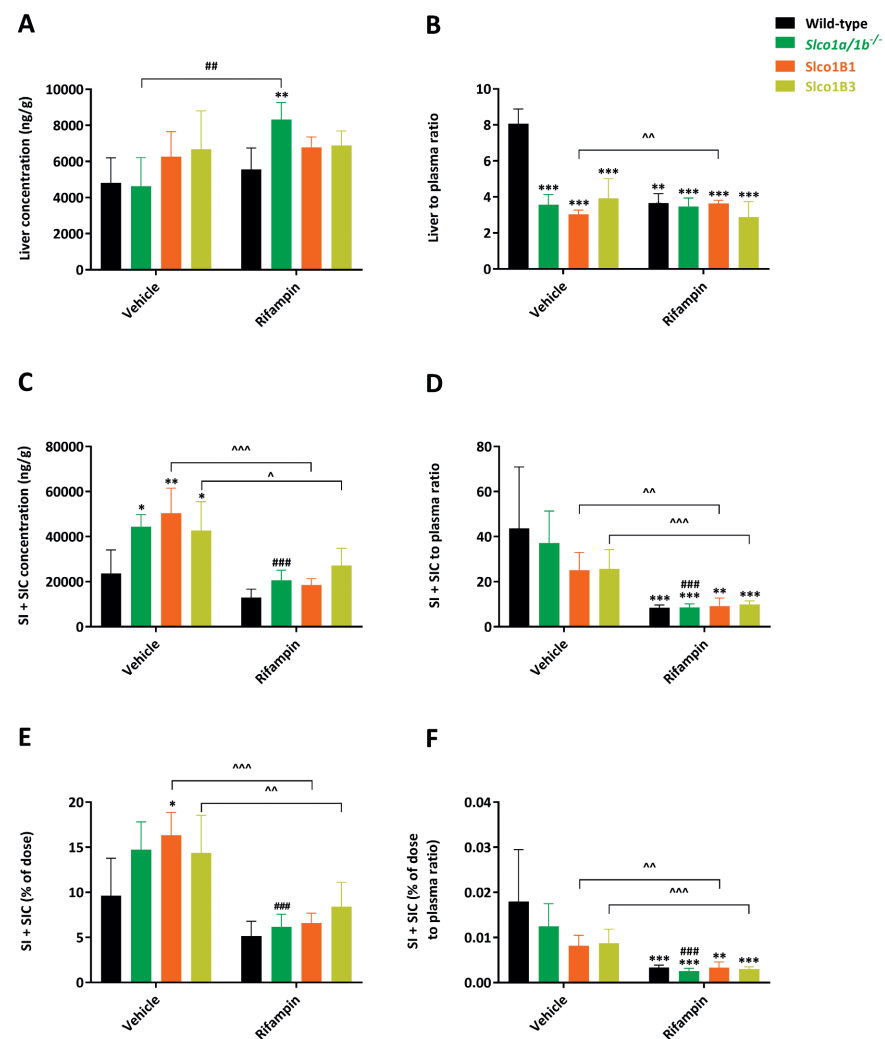
Supplemental Figure 2. Tissue concentrations (A, C, E, G) and tissue-to-plasma ratios (B, D, F, H), SI+SIC percentage of total dose (I) and SI+SIC percentage of total dose to plasma ratio (J) of larotrectinib in male wild-type and *Abcb1a/1b;Abcg2^{-/-}* mice over 1h after oral administration of 10 mg/kg larotrectinib with or without co-administration of elacridar (n = 6). SI, small intestinal tissue; SIC, small intestine contents. *, $P < 0.05$; **, $P < 0.01$; ***, $P < 0.001$ compared to wild-type mice.



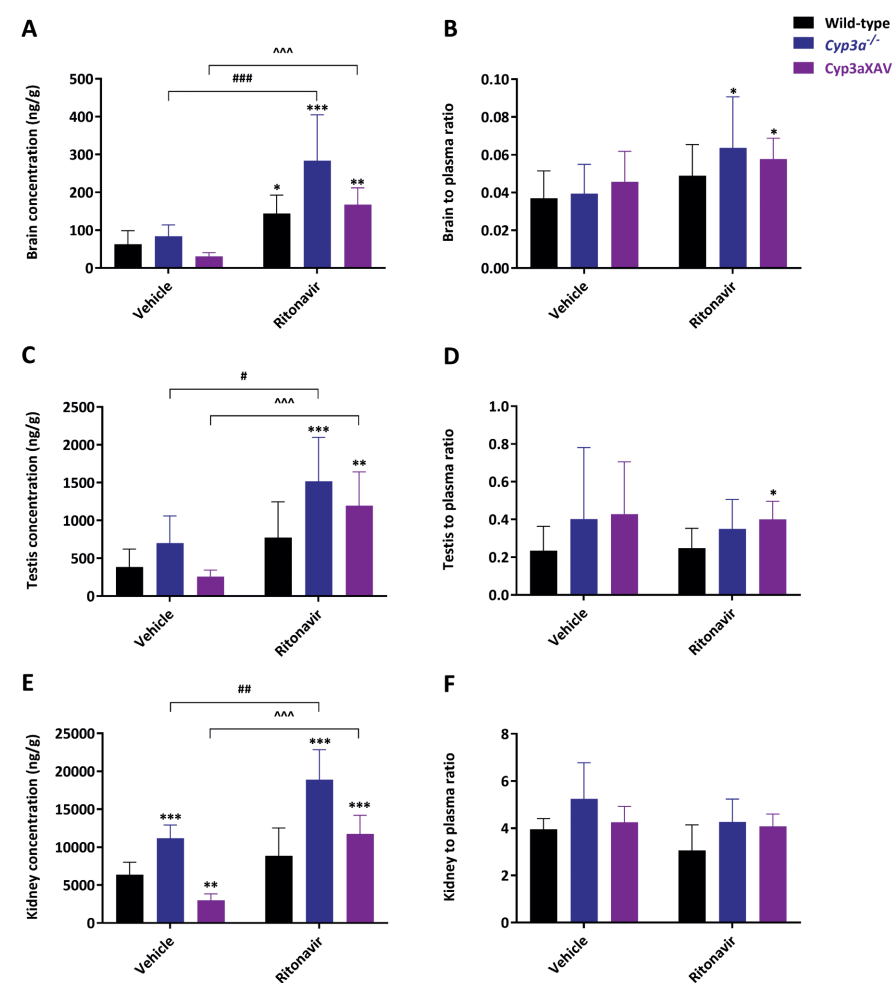
Supplemental Figure 3. Tissue concentrations (A, C, E, G) and tissue-to-plasma ratios (B, D, F, H) of larotrectinib in male wild-type, *Slco1a/1b*^{-/-}, *Slco1B1* and *Slco1B3* mice over 1h after oral administration of 10 mg/kg larotrectinib (n = 6 - 7). SI, small intestinal tissue. *, $P < 0.05$; **, $P < 0.01$; ***, $P < 0.001$ compared to wild-type mice; #, $P < 0.05$; ##, $P < 0.01$; ###, $P < 0.001$ compared to vehicle-treated *Slco1a/1b*^{-/-} mice.



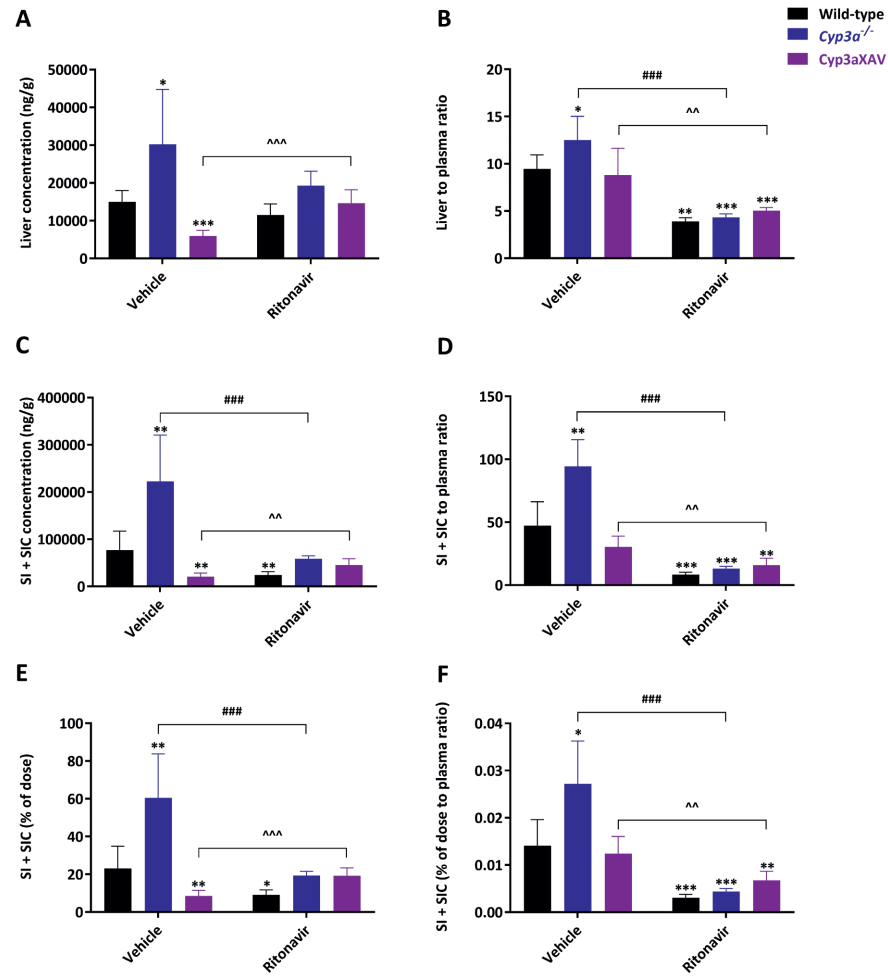
Supplemental Figure 4. Tissue concentrations (A, C, E) and tissue-to-plasma ratios (B, D, F) of larotrectinib in male wild-type, *Slco1a/1b*^{-/-}, *Slco1B1* and *Slco1B3* mice over 1h after oral administration of 10 mg/kg larotrectinib with or without co-administration of rifampin (n = 6 - 7). *, $P < 0.05$; **, $P < 0.01$; ***, $P < 0.001$ compared to vehicle-treated wild-type mice; #, $P < 0.05$; ##, $P < 0.01$; ###, $P < 0.001$ compared between vehicle-treated and rifampin-treated *Slco1a/1b*^{-/-} mice; ^, $P < 0.05$; ^^, $P < 0.01$; ^^, $P < 0.001$ compared between vehicle-treated *Slco1B1* and rifampin-treated *Slco1B1* mice or between vehicle-treated *Slco1B3* and rifampin-treated *Slco1B3* mice.



Supplemental Figure 5. Tissue concentrations (A and C), tissue-to-plasma ratios (B and D), SI+SIC percentage of total dose (E) and SI+SIC percentage of total dose to plasma ratio (F) of larotrectinib in male wild-type, *Slco1a/1b*^{-/-}, *Slco1B1* and *Slco1B3* mice over 1h after oral administration of 10 mg/kg larotrectinib with or without co-administration of rifampin (n = 6 - 7). SI, small intestinal tissue; SIC, small intestine contents. *, $P < 0.05$; **, $P < 0.01$; ***, $P < 0.001$ compared to vehicle-treated wild-type mice; #, $P < 0.05$; ##, $P < 0.01$; ###, $P < 0.001$ compared between vehicle-treated and rifampin-treated *Slco1a/1b*^{-/-} mice; ^, $P < 0.05$; ^^, $P < 0.01$; ^^, $P < 0.001$ compared between vehicle-treated *Slco1B1* and rifampin-treated *Slco1B1* mice or between vehicle-treated *Slco1B3* and rifampin-treated *Slco1B3* mice.



Supplemental Figure 6. Tissue concentrations (A, C, E) and tissue-to-plasma ratios (B, D, F) of larotrectinib in male wild-type, *Cyp3a*^{-/-} and *Cyp3aXAV* mice over 1h after oral administration of 10 mg/kg larotrectinib with or without co-administration of ritonavir (n = 6). *, $P < 0.05$; **, $P < 0.01$; ***, $P < 0.001$ compared to vehicle-treated wild-type mice; #, $P < 0.05$; ##, $P < 0.01$; ###, $P < 0.001$ compared between vehicle-treated and ritonavir-treated *Cyp3a*^{-/-} mice; ^, $P < 0.05$; ^^, $P < 0.01$; ^^, $P < 0.001$ compared between vehicle-treated and ritonavir-treated *Cyp3aXAV* mice.



Supplemental Figure 7. Tissue concentrations (A and C), tissue-to-plasma ratios (B and D), SI+SIC percentage of total dose (E) and SI+SIC percentage of total dose to plasma ratio (F) of larotrectinib in male wild-type, *Cyp3α^{-/-}* and *Cyp3αXAV* mice over 1h after oral administration of 10 mg/kg larotrectinib with or without co-administration of ritonavir (n = 6). SI, small intestinal tissue; SIC, small intestine contents. *, $P < 0.05$; **, $P < 0.01$; ***, $P < 0.001$ compared to vehicle-treated wild-type mice; #, $P < 0.05$; ##, $P < 0.01$; ###, $P < 0.001$ compared between vehicle-treated and ritonavir-treated *Cyp3α^{-/-}* mice; ^, $P < 0.05$; ^^, $P < 0.01$; ^^, $P < 0.001$ compared between vehicle-treated and ritonavir-treated *Cyp3αXAV* mice.

Supplemental Table 1. Plasma and tissue pharmacokinetic parameters of larotrectinib in male wild-type, *Slico1a/1b^{-/-}*, *Slico1B1* and *Slico1B3* mice over 1 h after oral administration of 10 mg/kg larotrectinib.

| Parameter | Genotype | | |
|---------------------------|---------------|---------------------------------|-----------------|
| | Wild-type | <i>Slico1a/1b^{-/-}</i> | <i>Slico1B3</i> |
| AUC_{0-3h} , ng/mLh | 658 ± 164 | 1663 ± 266*** | 1622 ± 521*** |
| Fold change AUC_{0-3h} | 1.0 | 2.5 | 2.5 |
| C_{max} , ng/ml | 877 ± 227 | 2024 ± 457*** | 1980 ± 621*** |
| T_{max} , h | 0.33 ± 0.13 | 0.63 ± 0.21 | 0.42 ± 0.13 |
| C_{brain} , ng/g | 18.7 ± 7.5 | 60.0 ± 15.5** | 63.5 ± 19.4** |
| Fold change C_{brain} | 1.0 | 3.2 | 3.4 |
| Brain-to-plasma ratio | 0.034 ± 0.002 | 0.036 ± 0.007 | 0.041 ± 0.006 |
| Fold change ratio | 1.0 | 1.0 | 1.2 |
| C_{liver} , ng/g | 5561 ± 2836 | 6163 ± 825.7 | 6371 ± 1501 |
| Fold increase C_{liver} | 1.0 | 1.1 | 1.1 |
| Liver-to-plasma ratio | 10.0 ± 1.6 | 3.7 ± 0.4*** | 4.2 ± 0.8*** |
| Fold change ratio | 1.0 | 0.37 | 0.42 |
| C_{SI} , ng/g | 6290 ± 1818 | 10849 ± 3516 | 7899 ± 3423 |
| Fold increase C_{SI} | 1.0 | 1.7 | 1.3 |
| SI-to-plasma ratio | 12.5 ± 4.0 | 6.4 ± 1.6** | 5.2 ± 1.7*** |
| Fold change ratio | 1.0 | 0.51 | 0.42 |
| C_{testis} , ng/g | 145.7 ± 63.9 | 373.2 ± 43.0* | 376.6 ± 185.2* |
| Fold change C_{testis} | 1.0 | 2.6 | 2.6 |
| Testis-to-plasma ratio | 0.28 ± 0.13 | 0.22 ± 0.03 | 0.25 ± 0.15 |
| Fold change ratio | 1.0 | 0.79 | 0.89 |

Data are given as mean ± S.D. (n = 6). AUC_{0-3h} , area under the plasma concentration-time curve; C_{max} , maximum concentration in plasma; T_{max} , time point (h) of maximum plasma concentration; C_{brain} , brain concentration; C_{liver} , liver concentration; C_{SI} , small intestine (tissue) concentration; C_{testis} , testis concentration; *, $P < 0.05$; **, $P < 0.01$; ***, $P < 0.001$ compared to wild-type mice; #, $P < 0.05$; ##, $P < 0.01$; ###, $P < 0.001$ compared to wild-type mice; ^, $P < 0.05$; ^^, $P < 0.01$; ^^, $P < 0.001$ compared between vehicle-treated and ritonavir-treated *Cyp3α^{-/-}* mice. Statistical analysis was applied after log-transformation of linear data.



CHAPTER 4.3

P-GLYCOPROTEIN (ABCB1/MDR1) AND BCRP (ABCG2) LIMIT BRAIN ACCUMULATION AND CYTOCHROME P450-3A (CYP3A) RESTRICTS ORAL EXPOSURE OF THE RET INHIBITOR SELPERCATINIB (RETEVMO)

Yaogeng Wang¹, Rolf W. Sparidans², Sander Potters³, Rahime Şentürk², Maria C. Lebre¹, Jos H. Beijnen^{1,2,4}, Alfred H. Schinkel¹

¹The Netherlands Cancer Institute, Division of Pharmacology, Plesmanlaan 121, 1066 CX Amsterdam, The Netherlands.

²Utrecht University, Faculty of Science, Department of Pharmaceutical Sciences, Division of Pharmacology, Universiteitsweg 99, 3584 CG Utrecht, The Netherlands.

³Leiden University, Faculty of Science, Leiden Academic Centre for Drug Research (LACDR), Einsteinweg 55, 2300 RA Leiden, The Netherlands.

⁴The Netherlands Cancer Institute, Department of Pharmacy & Pharmacology, Plesmanlaan 121, 1066 CX Amsterdam, The Netherlands.

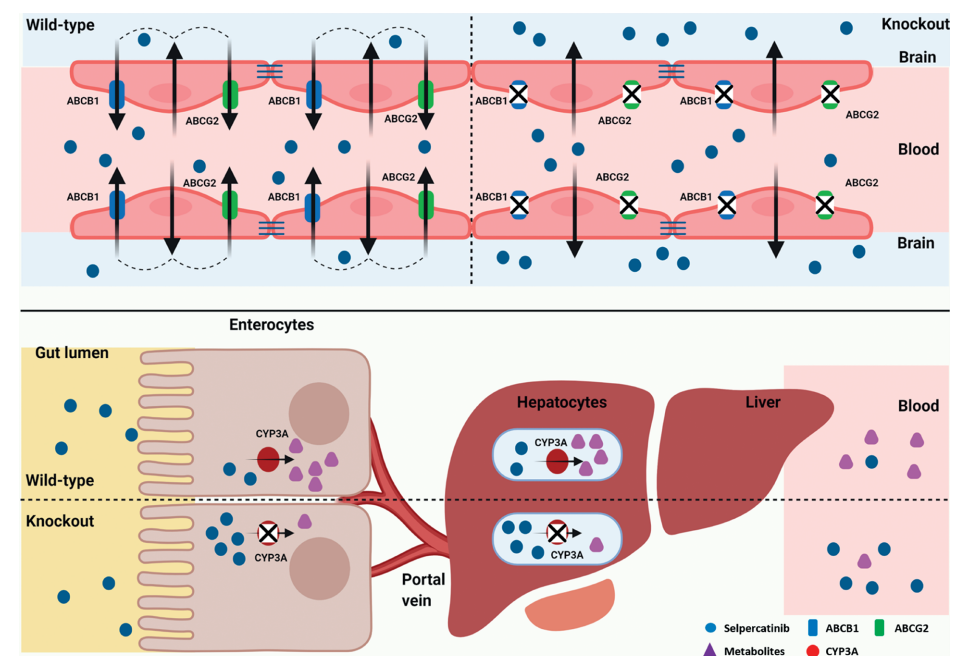
ABSTRACT

Selpercatinib is a targeted FDA-approved oral small-molecule inhibitor for treatment of rearranged during transfection (RET) proto-oncogene mutation-positive cancer. Using genetically modified mouse models, we investigated the roles of the multidrug efflux transporters ABCB1 and ABCG2, the OATP1A/1B uptake transporters, and the drug-metabolizing CYP3A complex in selpercatinib pharmacokinetics. Selpercatinib was efficiently transported by hABCB1 and mAbcg2, but not hABCG2, and was not a substrate of human OATP1A2, -1B1 or -1B3 in vitro. In vivo, the brain and testis penetration were increased by 3.0- and 2.7-fold in *Abcb1a/1b*^{-/-} mice and by 6.2- and 6.4-fold in *Abcb1a/1b;Abcg2*^{-/-} mice, respectively. *Oatp1a/1b* deficiency did not alter selpercatinib pharmacokinetics. The ABCB1/ABCG2 inhibitor elacridar boosted selpercatinib brain penetration in wild-type mice to the levels seen in *Abcb1a/1b;Abcg2*^{-/-} mice. *Cyp3a*^{-/-} mice showed a 1.4-fold higher plasma AUC_{0-4h} than wild-type mice, which was then 1.6-fold decreased upon transgenic overexpression of human CYP3A4 in liver and intestine. In summary, ABCG2 and especially ABCB1 limit brain and testis penetration of selpercatinib. Elacridar coadministration could mostly reverse these effects, without causing acute toxicity. CYP3A-mediated metabolism can limit selpercatinib oral exposure and hence its tissue concentrations. These insights may be useful in the further clinical development of selpercatinib.

Keywords: Selpercatinib, Cytochrome P450-3A, Oral exposure, Rearranged during transfection (RET) receptor kinase, Slco1a/1b, P-glycoprotein/ABCB1, Brain accumulation

Abbreviations:

ABC: ATP-binding cassette; ABCB1: ATP-binding cassette sub-family B member 1; ABCG2: ATP-binding cassette sub-family G member 2; BCRP: breast cancer resistance protein; CYP: Cytochrome P450; Cyp3aXAV: Cyp3a knockout mice with specific expression of human CYP3A4 in liver and intestine; LC-MS/MS: liquid chromatography coupled with tandem mass spectrometry; MDCK: Madin-Darby canine kidney; m (as prefix): mouse; OATP: Organic-anion-transporting polypeptide; P-gp: P-glycoprotein; RET: The rearranged during transfection (RET) proto-oncogene; SLCO: organic solute carrier family; TKI: tyrosine kinase inhibitor.



1. INTRODUCTION

The rearranged during transfection (RET) proto-oncogene encodes a receptor tyrosine kinase for members of the glial cell line-derived neurotrophic factor (GDNF) family of extracellular signaling molecules¹. Mutations in the RET genes can lead to a number of human diseases. The loss of RET functions can irreversibly induce a syndrome characterized by intestinal obstruction known as Hirschsprung's disease. However, mutations causing increased activity of RET functions can result in tumor formation². RET tyrosine kinase receptors can be oncogenically activated by gene fusions or point mutations. RET fusions occur in different types of cancers, including lung cancers (1%-2%) and papillary thyroid cancers (10%-20%)³, whereas RET mutations affect mostly medullary thyroid cancers (MTCs)⁴. Next-generation sequencing (NGS) analysis for numerous different types of patient tumors has uncovered that RET alterations can also occur in other tumor types (albeit at low frequency), including ovarian epithelial carcinoma and salivary gland adenocarcinoma⁵.

Until recently, some multikinase inhibitors (MKIs) with nonselective RET inhibitory activity have been available for patients with RET-altered cancers. For example, there were some clinical trials with cabozantinib for RET-mutant MTCs^{6,7} and RET fusion-positive lung cancers⁸, but results were underwhelming with considerable side-effects. Similar modest activity results were found for another drug, vandetanib, in advanced or metastatic medullary thyroid cancer⁹ and advanced non-small-cell lung cancer¹⁰. Other MKIs with potential RET activity include sunitinib, sorafenib, alectinib, nintedanib, and ponatinib. However, it is unclear if these drugs are likely to achieve improved responses compared to cabozantinib and vandetanib^{11,12}. To some extent, the low activity of these inhibitors may be due to the low affinity and/or specificity for RET inhibition and substantial 'off-target' side-effects would limit the RET inhibition functions¹³. Thus the limitations of these MKIs may prevent potent RET pathway inhibition and subsequently yield poor pharmacokinetic (PK) properties and weak anti-RET positive tumor efficacy.

Unlike these non-specific inhibitors, selpercatinib (LOXO-292, RETEVMO, Compound CID: 134436906) is a novel, highly selective, ATP-competitive small molecule RET inhibitor, which has nanomolar potency against diverse RET alterations. In a clinical phase 1 study, it showed 77% overall response rate in RET fusion-positive cancers, with intracranial activity and 45% overall response rate in RET-mutant medullary thyroid cancer¹⁴. In May 2020, selpercatinib (RETEVMO, Eli Lilly Company) was approved by the FDA for metastatic RET fusion-positive non-small cell lung cancer (NSCLC) in adult patients and advanced or metastatic RET-mutant medullary thyroid cancer (MTC) in adult and pediatric (≥ 12 years old) patients¹⁵. However, the information on selpercatinib pharmacokinetic properties is still limited.

Multidrug efflux transporters of the ATP-binding cassette (ABC) protein family, especially P-glycoprotein (P-gp; ABCB1) and breast cancer resistance protein (BCRP; ABCG2), and influx transporters such as the organic anion transporting polypeptides (OATPs) can affect drug absorption, distribution, metabolism and excretion (ADME). They have a broad substrate specificity and can thus influence the safety and efficacy profiles of many specific drugs¹⁶⁻¹⁸. ABCB1 and ABCG2 are highly expressed in the apical membrane of epithelia in a variety of tissues, including small intestine, liver and kidney. Also, they are abundant in the luminal membrane of physiological barriers, such as the blood-brain barrier (BBB), blood-testis barrier (BTB) and blood-placenta barrier (BPB)¹⁹. Therefore, the intestinal absorption, biliary and urinary excretion and also the accumulation in the central nervous system of many anti-tumor drugs, including numerous tyrosine kinase inhibitors (TKIs), are restricted by ABCB1 and/or ABCG2. This interaction often results in reduced systemic exposure after oral administration (in short oral exposure) or poor brain penetration^{20,21}. As brain metastases can occur in different tumor types, especially lung cancer, the potential interaction between selpercatinib and ABCB1/ABCG2 *in vivo* may not only limit selpercatinib oral exposure but also its brain accumulation, and thus affect therapeutic efficacy for brain metastases in lung cancer patients.

Besides the ABC efflux transporters, OATP uptake transporters, encoded by SLCO genes, are sodium-independent transmembrane uptake transporters²²⁻²⁵. With high expression in the main detoxification organ liver and possibly the small intestine, both primary locations for first-pass drug metabolism, they mediate the tissue uptake of many endogenous substrates, as well as exogenous compounds, such as hormones, toxins, and numerous drugs^{16,24-27}. As a member of the OATP uptake transporters, the SLCO1A/1B transporters are of particular interest considering their high expression in the liver²⁴ and their key roles in hepatic uptake and hence plasma clearance of several drug substrates, including many anti-tumor drugs^{26,28,29}. Thus, it is important to investigate whether selpercatinib is a substrate of the SLCO1A/1B transporters and whether this can influence selpercatinib oral exposure and organ distribution.

The multidrug-metabolizing Cytochrome P450 3A (CYP3A) enzyme complex is the most abundant CYP enzyme in human liver, the main detoxification organ, but also in the small intestine. It therefore plays a significant role in the oxidative metabolism of approximately half of the drugs currently in clinical use. As metabolic breakdown is one of the main elimination pathways for drugs, CYP3A activity can markedly affect the plasma exposure and thus tissue levels of certain drugs³⁰. Consequently, the oral exposure, therapeutic efficacy, and the potential toxicity of drugs may be influenced by the high degree of inter- and intra-individual variation that is known to occur for the CYP3A enzyme.

The primary aim of this study was to study ABCB1/ABCG2 and SLCO1A/1B (OATP1A/1B) transport functions *in vitro* by transepithelial transport and uptake assays, respectively, and clarify the *in*

vivo impact of ABCB1/ABCG2, SLCO1A/1B and CYP3A enzymes on selpercatinib pharmacokinetic behavior, including oral exposure and organ distribution by using appropriate genetically modified mouse models. We also further studied the effect of co-administration of the ABCB1 and ABCG2 inhibitor elacridar on selpercatinib plasma exposure and tissue distribution.

2. MATERIALS AND METHODS

2.1 Cell lines and transport assays

Polarized Madin-Darby Canine Kidney (MDCK-II) cell lines and subclones stably transduced with either human (h) ABCB1, hABCG2, or mouse (m) Abcg2 cDNA were generated in the Netherlands cancer institute between 1995 and 2005. The characteristic growth and drug transport properties, including inhibitor sensitivity, were regularly checked and commonly used in our recent studies, and the proper identity and functionality of these polarized epithelial cells were confirmed. The transepithelial transport experiments were performed as described previously²⁰. Briefly, transepithelial transport assays were performed on microporous polycarbonate membrane filters (3.0 µm pore size, 12 mm diameter, Transwell 3402, Corning, NY, USA). The parental cells and subclones were seeded at a density of 2.5×10^5 cells per well and cultured for 3 days to allow formation of an intact monolayer. Membrane tightness was assessed by measurement of transepithelial electrical resistance (TEER) before and after the transport phase.

In the inhibition experiments, 5 µM zosuquidar (ABCB1 inhibitor) and/or 5 µM Ko143 (ABCG2/Abcg2 inhibitor) were used during the transport experiments. Cells were pre-incubated with one or a combination of the inhibitors for 1 h in both apical and basolateral compartments. The transport phase was started (t = 0) by replacing the medium in either the apical or the basolateral compartment with fresh DMEM including 10% (v/v) fetal bovine serum (FBS) and selpercatinib at 5 µM, as well as the appropriate inhibitor(s). Plates then were kept at 37°C in 5% (v/v) CO₂ during the experiment, and 50 µl aliquots were taken from the acceptor compartment at 1, 2, 4, and 8 hours (h), and stored at -30°C until LC-MS/MS measurement of the selpercatinib concentrations. Experiments were performed in triplicate and the mean transport is shown in the figure. Active transport was expressed using the transport ratio (r), which is defined as the amount of apically directed drug transport divided by basolaterally directed drug translocation after 8 h.

2.2 Cellular uptake assays

HEK293 cells, vector-transfected or human (h)SLCO1A2, hSLCO1B1 or hSLCO1B3 cDNA-transfected were kind gifts from Prof. Werner Siegmund and Dr. Markus Keiser (University of Greifswald, Greifswald, Germany)³¹. All the HEK293 cell lines were maintained in DMEM supplemented with 10% (v/v) FBS, 1% penicillin-streptomycin mix at 37°C in 5% (v/v) CO₂ and 500 µg/ml G418. Cells were first seeded in 12-well plates [coated with 50 mg/l poly (l-lysine) and 50 mg/l poly (l-ornithine)] at a density of 1.0×10^5 cells/well. For the uptake study, in order to

induce the expression of OATP transporters, the cell culture medium was replaced with culture medium supplemented with 5 mM sodium butyrate 24 h before performing uptake assay.

The uptake transport study was performed as described previously²⁰. Briefly, cells were first washed twice and pre-incubated with Krebs-Henseleit solution at 37°C for 15 min, uptake was initiated by adding Krebs-Henseleit buffer containing 5 µM selpercatinib or 0.2 µM rosuvastatin as positive control. The Krebs-Henseleit solution was prepared from Krebs-Henseleit buffer modified powder and supplemented with 25 mM NaHCO₃ and 2.5 mM CaCl₂ adjusted to pH 6.4 with 1 M HCL. At 2.5 min, the incubation buffer was removed and uptake was terminated by adding 1 ml of ice-cold Krebs-Henseleit buffer, followed by two times washing with 1 ml of ice-cold Krebs-Henseleit buffer. Afterwards, cells were lysed with 150 µl of 0.2 N NaOH 15 min at room temperature and cell lysates were transferred into 1.5 ml Eppendorf tubes and stored at -30°C until the next day. The cellular protein amount was determined by the Bradford method using 10 µl of the cell lysates with bovine serum albumin as a standard. LC-MS/MS measurements of the selpercatinib and rosuvastatin concentrations were performed for cell lysates. Experiments were performed in independent triplicates and the mean transport is shown in the figure. Like for the transepithelial transport assay, n = 3 was considered sufficient for the selpercatinib and rosuvastatin uptake results.

2.3 Animals

Mice were housed and handled according to institutional guidelines complying with Dutch and EU legislation. All experimental animal protocols were evaluated and approved by the institutional animal care and use committee. Wild-type, *Abcb1a/1b*^{-/-}, *Abcg2*^{-/-}, *Abcb1a/1b;Abcg2*^{-/-}, *Slco1a/1b*^{-/-} male mice, and *Cyp3a*^{-/-} and *Cyp3aXAV* female mice, all of a >99% FVB genetic background, were used between 9 and 16 weeks of age. These mouse strains are continually used for pharmacokinetic studies with various drugs, confirming their proper identity and functionality^{20,32} and ongoing studies. Animals were kept in a temperature-controlled environment with 12-h light and 12-h dark cycle and they received a standard diet (Transbreed, SDS Diets, Technilab-BMI, Someren, The Netherlands) and acidified water *ad libitum*. All experimental animal protocols (WP9450, 9669, 9760), including power calculations, designed under the nationally approved DEC/CCD project AVD301002016595 were evaluated and approved by the institutional animal care and use committee in the Netherlands cancer institute.

2.4 Drug solutions

For oral administration, selpercatinib was dissolved in dimethyl sulfoxide (DMSO) at a concentration of 20 mg/ml and further diluted with polysorbate 20, absolute ethanol and 5% glucose water, resulting in a final working solution of 1 mg/ml [DMSO : polysorbate 20 : absolute ethanol : 5% glucose water = 5 : 15 : 15 : 65, (v/v/v/v)]. Elacridar hydrochloride was dissolved in DMSO (53 mg/ml) in order to get 50 mg elacridar base per ml DMSO. The stock solution was

further diluted with a mixture of polysorbate 20, absolute ethanol and 5% glucose water to yield a concentration of 5 mg/ml elacridar [DMSO : polysorbate 20 : absolute ethanol : 5% glucose water = 10 : 15 : 15 : 60, (v/v/v/v)]. All dosing solutions were prepared freshly on the day of the experiment.

2.5 Plasma and organ pharmacokinetics of selpercatinib in mice

In order to minimize variation in absorption because of oral administration, mice were first fasted for 3 h before selpercatinib (10 mg/kg) was administered orally, using a blunt-ended needle. For the 4-h transporter experiments, tail vein blood samples were collected at 0.125, 0.25, 0.5, 1, and 2 h time points after oral administration, respectively. For the CYP3A 8-h experiments, tail vein blood sampling was performed at 0.25, 0.5, 1, 2, and 4 h, respectively. While for elacridar inhibition experiments, tail vein blood samples were collected at 0.125, 0.25, 0.5, and 1 h time points after oral administration, respectively. Blood sample collection was performed using microvettes containing dipotassium-EDTA. At the last time point in each experiment (2, 4 or 8 h), mice were anesthetized with 5% isoflurane and blood was collected by cardiac puncture. Blood samples were collected in Eppendorf tubes containing heparin as an anticoagulant. The mice were then sacrificed by cervical dislocation and brain, liver, kidney, lung, small intestine and testis were rapidly removed. Plasma was isolated from the blood by centrifugation at 9,000g for 6 min at 4°C, and the plasma fraction was collected and stored at -30°C until analysis. Organs were homogenized with 4% (w/v) bovine serum albumin and stored at -30°C until analysis. Relative tissue-to-plasma ratio after oral administration was calculated by determining the selpercatinib tissue concentration relative to selpercatinib plasma concentration at the last time point.

2.6 LC-MS/MS analysis

Selpercatinib concentrations in DMEM/FBS (9/1, v/v) (Invitrogen, Waltham, MA, USA) cell culture medium, plasma samples, and organ homogenates were determined using a validated liquid chromatography-tandem mass spectrometry assay³³.

2.7 Materials

Selpercatinib was purchased from Chemgood (Glen Allen, VA, USA). Zosuquidar and elacridar HCl were obtained from Sequoia Research Products (Pangbourne, UK). Ko143 was from Tocris Bioscience (Bristol, UK). Bovine Serum Albumin (BSA) Fraction V was obtained from Roche Diagnostics GmbH (Mannheim, Germany). Glucose water 5% w/v was from B. Braun Medical Supplies, Inc. (Melsungen, Germany). Isoflurane was purchased from Pharmachemie (Haarlem, The Netherlands) and heparin (5000 IU ml⁻¹) was from Leo Pharma (Breda, The Netherlands). Other chemicals used in the selpercatinib detection assay were described before³³. All other chemicals and reagents were obtained from Sigma-Aldrich (Steinheim, Germany).

2.8 Data and Statistical analysis

Pharmacokinetic parameters were calculated by non-compartmental methods using the PK solver software³⁴. The area under the plasma concentration-time curve (AUC) was calculated using the trapezoidal rule, without extrapolating to infinity. The peak plasma concentration (C_{max}) and the time of maximum plasma concentration (T_{max}) were estimated from the original (individual mouse) data. One-way analysis of variance (ANOVA) was used when multiple groups were compared and the *Tukey post hoc* correction was used to accommodate multiple testing. The two-sided unpaired Student's t-test was used when treatments or differences between two specific groups were compared using the software GraphPad Prism 8 (GraphPad Software Inc., La Jolla, CA, USA). All the data were log-transformed before statistical tests were applied. Differences were considered statistically significant when $P < 0.05$. All data are presented as geometric mean \pm SD.

3. RESULTS

3.1 *In vitro* transport of selpercatinib

We tested *in vitro* transepithelial transport of selpercatinib using polarized monolayers of Madin-Darby Canine Kidney (MDCK-II) parental cells and its subclones overexpressing human (h) ABCB1, hABCG2, or mouse (m) Abcg2. Selpercatinib (5 μ M) was not transported in the apical direction in the parental MDCK-II cell line with or without ABCB1 inhibitor zosuquidar ($r = 1.0$, Figure 1A and $r = 0.9$, Figure 1B), suggesting that selpercatinib transport could not be mediated by the low amount of endogenous canine ABCB1 present in the MDCK-II cells³⁵. In MDCK-II cells transduced with hABCB1, there was clear apically directed transport of selpercatinib ($r = 6.8$, Figure 1C), which was completely inhibited by zosuquidar ($r = 1.0$, Figure 1D).

To suppress any potential confounding influence of endogenous canine ABCB1 activity, the following experiments on ABCG2-mediated transport were done in the presence of the inhibitor zosuquidar. In addition, the ABCG2 inhibitor Ko143 was used to inhibit the transport activity of hABCG2 and mAbcg2. In MDCK-II cells transduced with hABCG2, there was no active apically directed transport of selpercatinib ($r = 1.0$, Figure 1E), and this was not changed upon Ko143 addition ($r = 0.9$, Figure 1F). We observed strong apically directed transport of selpercatinib in cells overexpressing mouse Abcg2 ($r = 8.8$) and this was abrogated by addition of Ko143 ($r = 1.0$, Figure 1G and H).

Selpercatinib thus appears to be efficiently transported by hABCB1 and mAbcg2, but not by hABCG2 or canine ABCB1.

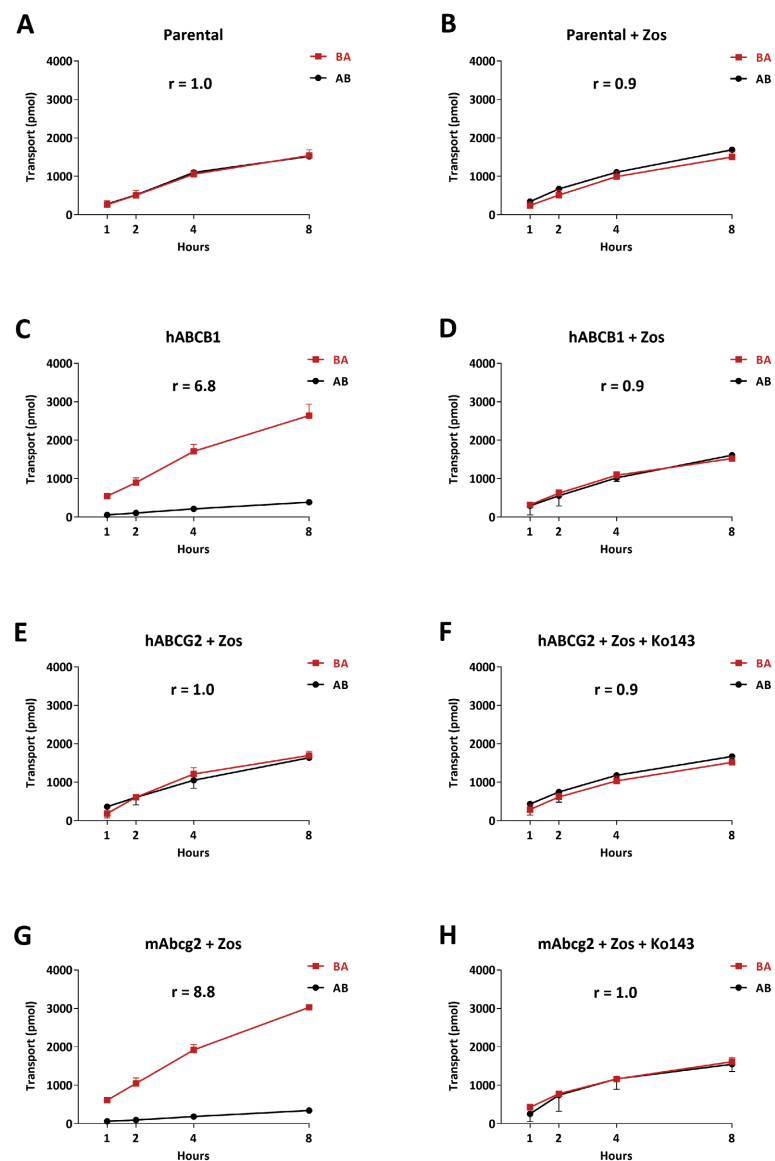


Figure 1. Transepithelial transport of selpercatinib (5 μ M) assessed in MDCK-II cells either non-transduced (A, B), transduced with hABCB1 (C, D), hABCG2 (E, F) or mAbcg2 (G, H) cDNA. At $t = 0$ h, drug was applied in the donor compartment and the concentrations in the acceptor compartment at $t = 1, 2, 4$ and 8 h were measured and plotted as cumulative amount of selpercatinib transported per well (pmol) in the graphs ($n = 3$). B, D–H: Zosuquidar (Zos, 5 μ M) was applied to inhibit human and/or endogenous canine ABCB1. F and H: the ABCG2 inhibitor Ko143 (5 μ M) was applied to inhibit ABCG2/Abcg2-mediated transport. r , relative transport ratio. AB (\bullet), translocation from the apical to the basolateral compartment; BA (\blacksquare), translocation from the basolateral to the apical compartment. Points, mean; bars, S.D.

3.2 Impact of ABCB1, ABCG2 and SLC01A/1B on selpercatinib plasma pharmacokinetics and tissue disposition

In order to study whether the ABCB1A/1B, ABCG2 and OATP1A/1B transporters affect selpercatinib systemic exposure after oral administration (oral exposure) and subsequent tissue disposition *in vivo*, we performed a 4-h pharmacokinetic pilot study in male wild-type, *Abcb1a/1b;Abcg2*^{-/-} and *Slco1a/1b*^{-/-} mice using oral administration of 10 mg/kg selpercatinib. This dose in mice results in systemic selpercatinib exposure of the same order of magnitude as seen in patients. As shown in Figure 2A–B and Table 1, after rapid initial absorption, it took around one to two hours to reach the maximum plasma concentration of selpercatinib in all tested strains, with a slow transition to elimination up to 4 hours. Mice with a combined knockout of *Abcb1a/1b* (*Mdr1*) and *Abcg2* (*Bcrp*) had a similar plasma C_{max} ($8,582 \pm 2,160$ ng/ml) as wild-type mice, but *mOatp1a/1b* deficiency led to significantly increased selpercatinib concentrations in plasma with a 1.5-fold higher C_{max} compared to wild-type mice ($11,625 \pm 1,614$ vs $7,862 \pm 1,814$ ng/ml, $P < 0.05$). However, plasma exposures of selpercatinib over 4 hours (AUC_{0-4h}) in both *Abcb1a/1b;Abcg2*^{-/-} ($30,188 \pm 7,632$ ng/ml*h) and *Slco1a/1b*^{-/-} ($36,197 \pm 5,255$ ng/ml*h) mice were not significantly different from those in wild-type mice ($26,649 \pm 6,360$ ng/ml*h).

Brain, liver, kidney, small intestine (SI), small intestine contents (SIC), testis, lung and spleen concentrations of selpercatinib 4 h after oral administration were analyzed. Notably, the selpercatinib brain-to-plasma ratio (0.030) in wild-type mice was quite low, suggesting poor brain penetration of selpercatinib at 4 h (Table 1). The brain concentrations and brain-to-plasma ratios in *Abcb1a/1b;Abcg2*^{-/-} mice were increased by 18.6-fold and 15.3-fold, respectively, compared to those in wild-type mice (Figure 2C–D and Table 1). The *Slco1a/1b*^{-/-} mice also showed enhanced brain concentrations and brain-to-plasma ratios by factors of 1.5-fold and 1.3-fold, respectively. However, these increases were quite limited compared to those in the *Abcb1a/1b;Abcg2*^{-/-} mice. We further observed similar results in testis, with low testis-to-plasma ratio (0.12) in wild-type mice, a significant increase up to 0.76 (6.3-fold) in *Abcb1a/1b;Abcg2*^{-/-} mice and a limited increase to 0.15 (1.3-fold) in *Slco1a/1b*^{-/-} mice (Figure 2E–F and Table 1).

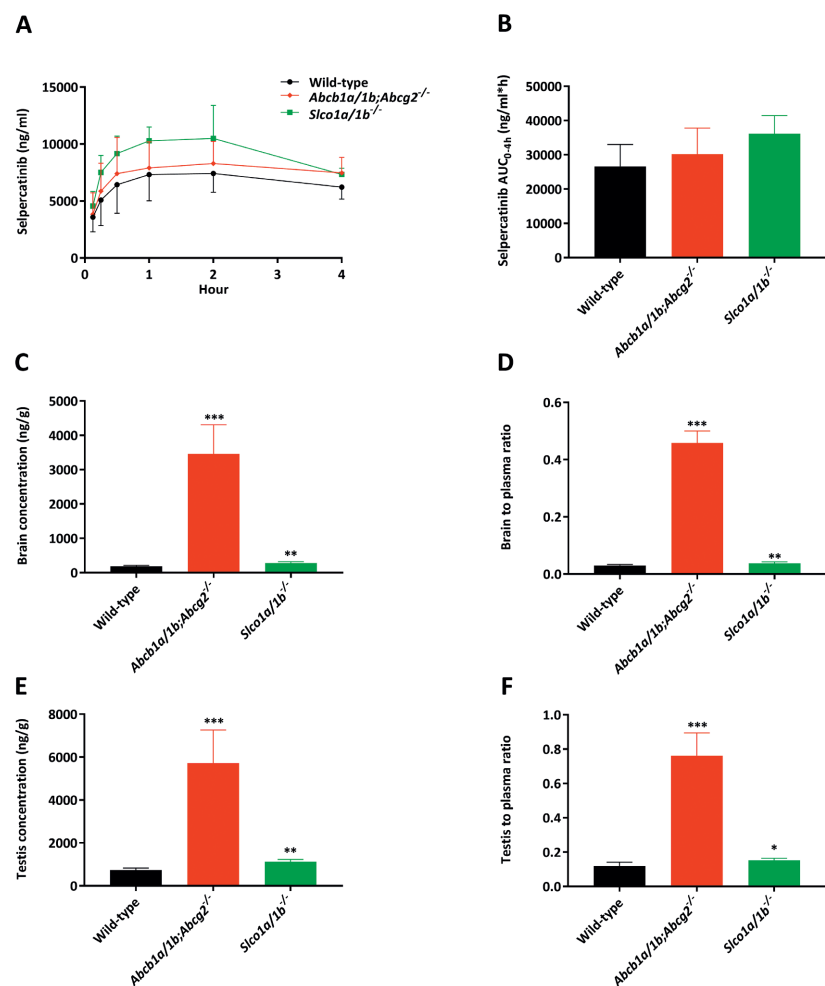


Figure 2. Plasma concentration-time curves (A), plasma AUC_{0-4h} (B), brain concentration (C), brain-to-plasma ratio (D), testis concentration (E) and testis-to-plasma ratio (F) of selpercatinib in male wild-type, *Abcb1a/1b;Abcg2*^{-/-} and *Slco1a/1b*^{-/-} mice over 4 h after oral administration of 10 mg/kg selpercatinib. Data are given as mean ± S.D. (n = 6 - 7). *, $P < 0.05$; **, $P < 0.01$; ***, $P < 0.001$ compared to wild-type mice. Statistical analysis was applied after log-transformation of linear data.

Whereas the other tissue-to-plasma ratios, including liver, kidney, lung and spleen, were not meaningfully altered between the three strains (liver shown in Figure 3A-B and Table 1, other data shown in Supplemental Figure 2), we observed markedly lower small intestine contents-to-plasma ratios in *Abcb1a/1b;Abcg2*^{-/-} mice compared to wild-type mice (0.30-fold, Figure 3E-F and Table 1). A lower small intestine contents percentage of total dose was also observed in *Abcb1a/1b;Abcg2*^{-/-} mice (Figure 3G-H). These results may therefore point to more rapid absorption of intestinal selpercatinib in the absence of *Abcb1a/1b* and *Abcg2*, or to reduced hepatobiliary excretion of the absorbed selpercatinib, or to a combination of both processes.

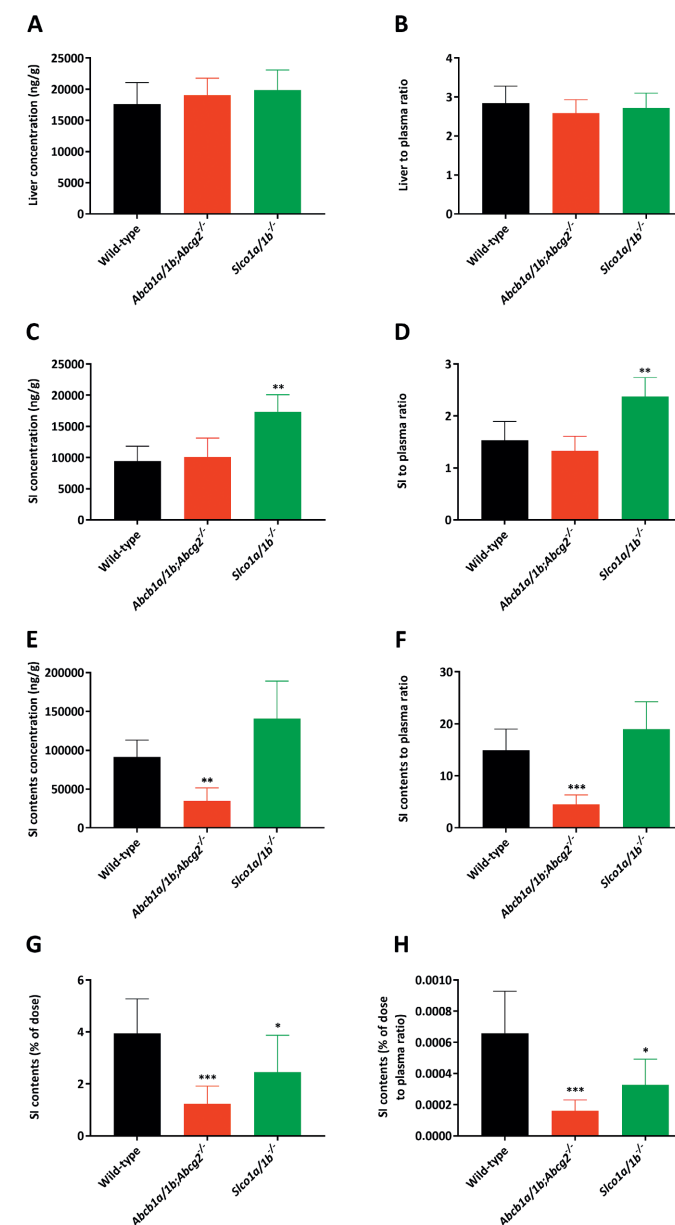


Figure 3. Liver, small intestine and small intestine contents concentrations (A, C, E), liver, small intestine- and small intestine contents-to-plasma ratios (B, D, F), small intestine contents as percentage of dose (G) and small intestine contents percentage of dose-to-plasma ratio (H) of selpercatinib in male wild-type, *Abcb1a/1b;Abcg2*^{-/-} and *Slco1a/1b*^{-/-} mice over 4 h after oral administration of 10 mg/kg selpercatinib. SI: small intestine. Data are given as mean ± S.D. (n = 6 - 7). *, $P < 0.05$; **, $P < 0.01$; ***, $P < 0.001$ compared to wild-type mice. Statistical analysis was applied after log-transformation of linear data.

Table 1. Plasma and organ pharmacokinetic parameters of selpercatinib in male wild-type, *Abcb1a/1b;Abcg2*^{-/-} and *Slco1a/1b*^{-/-} mice over 4 h after oral administration of 10 mg/kg selpercatinib.

| Parameter | Genotype | | |
|-----------------------------------|---------------|---------------------------------------|---------------------------------|
| | Wild-type | <i>Abcb1a/1b;Abcg2</i> ^{-/-} | <i>Slco1a/1b</i> ^{-/-} |
| AUC _{0-4h} , ng/ml*h | 26649 ± 6360 | 30188 ± 7632 | 36197 ± 5255 |
| Fold change AUC _{0-4h} | 1.0 | 1.1 | 1.4 |
| C _{max} , ng/ml | 7862 ± 1814 | 8582 ± 2160 | 11625 ± 1614* |
| T _{max} , h | 1.8 ± 1.2 | 1.6 ± 1.2 | 1.7 ± 0.52 |
| C _{brain} , ng/g | 186 ± 23 | 3454 ± 855*** | 278 ± 42** |
| Fold increase C _{brain} | 1.0 | 18.6 | 1.5 |
| Brain-to-plasma ratio | 0.030 ± 0.004 | 0.46 ± 0.04*** | 0.038 ± 0.005** |
| Fold increase ratio | 1.0 | 15.3 | 1.3 |
| C _{liver} , ng/g | 17593 ± 3471 | 19077 ± 2696 | 19916 ± 3174 |
| Fold increase C _{liver} | 1.0 | 1.1 | 1.1 |
| Liver-to-plasma ratio | 2.8 ± 0.4 | 2.6 ± 0.3 | 2.7 ± 0.4 |
| Fold increase ratio | 1.0 | 0.93 | 1.0 |
| C _{SIC} , ng/g | 91051 ± 22029 | 34929 ± 16659* | 140998 ± 48076 |
| Fold change C _{SIC} | 1.0 | 0.38 | 1.5 |
| SIC-to-plasma ratio | 14.9 ± 4.1 | 4.5 ± 1.8*** | 19.0 ± 5.3 |
| Fold increase ratio | 1.0 | 0.30 | 1.3 |
| C _{testis} , ng/g | 730 ± 103 | 5726 ± 1535*** | 1121 ± 107** |
| Fold increase C _{testis} | 1.0 | 7.8 | 1.5 |
| Testis-to-plasma ratio | 0.12 ± 0.02 | 0.76 ± 0.13*** | 0.15 ± 0.01* |
| Fold increase ratio | 1.0 | 6.3 | 1.3 |

AUC_{0-4h}, area under plasma concentration-time curve; C_{max}, maximum concentration in plasma; T_{max}, time point (h) of maximum plasma concentration; C_{brain}, brain concentration; C_{liver}, liver concentration; SIC, small intestine contents; C_{SIC}, small intestine contents concentration; C_{testis}, testis concentration; Data are given as mean ± S.D. (n = 6 - 7). *, P < 0.05; **, P < 0.01; ***, P < 0.001 compared to wild-type mice. Statistical analysis was applied after log-transformation of linear data.

It is worth noting that in wild-type mice most tissue-to-plasma ratios for liver, kidney, and small intestine (all >1) were far higher than observed for the brain (0.030) and even testis (0.12), suggesting a strong impact of the blood-brain-barrier (BBB) and blood-testis-barrier (BTB) on tissue accumulation of selpercatinib. Despite the dramatically increased selpercatinib brain levels in *Abcb1a/1b;Abcg2*^{-/-} mice, we did not observe any abnormal external behavior in these mice. This contrasts with the TKI drug brigatinib, for which we observed severe and even lethal acute toxicity in *Abcb1a/1b;Abcg2*^{-/-} mice²¹. Also *Slco1a/1b*^{-/-} mice did not show any abnormal external behavior due to selpercatinib.

3.3 *In vitro* uptake of selpercatinib

In the pilot study, we observed a relatively higher plasma concentration of selpercatinib in *Slco1a/1b*^{-/-} mice. There is high expression of OATP1A/1B transporters in the liver, and they have

clear effects on tissue distribution and elimination of a variety of substrates²⁰. We therefore evaluated whether selpercatinib can be transported by human OATP1A2, OATP1B1 or OATP1B3 *in vitro* using HEK293 cells transduced with cDNAs for these transporter proteins. However, we did not observe any significant increase in the uptake of selpercatinib in any of these transgenic cell lines compared to their vector control cells (Figure 4A). Rosuvastatin, as a positive control substrate, was efficiently taken up by all the OATP-overexpressing cell lines, demonstrating that all the OATP proteins transduced in the HEK293 cells are functional (Figure 4B). Taken together, these results indicate that selpercatinib is not a substantial transport substrate of human OATP1A2, -1B1 or -1B3 as measured in HEK293 cells *in vitro*.

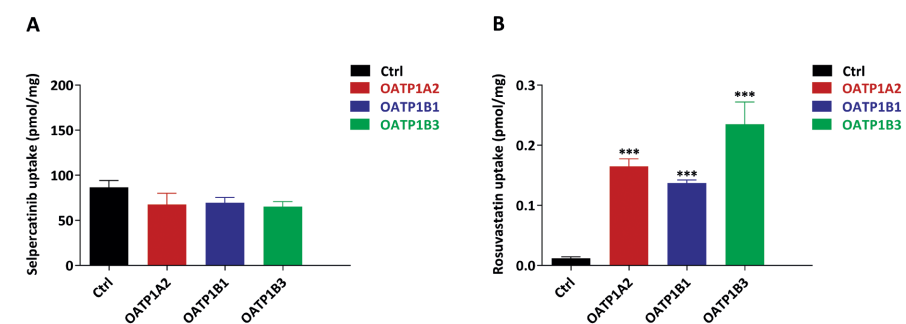


Figure 4. *In vitro* uptake of selpercatinib (A) and positive control rosuvastatin (B) by human OATP1A2, OATP1B1 and OATP1B3. Uptake of 5 μM selpercatinib and 0.2 μM rosuvastatin were measured after 2.5 min incubation using vector-transfected (control) or OATP1A2-, OATP1B1- or OATP1B3- overexpressing HEK293 cells. n = 3, data are given as mean ± S.D. *, P < 0.05; **, P < 0.01; ***, P < 0.001 compared to control group.

3.4 ABCB1 and ABCG2 limit selpercatinib brain and testis exposure

We next performed a more extensive main experiment and studied the separate and combined functions of *Abcb1a/1b* and *Abcg2* in selpercatinib pharmacokinetic behavior, including oral exposure and tissue distribution. In order to assess tissue distribution at a comparatively high plasma exposure, 10 mg/kg selpercatinib was administered orally to wild-type, *Abcb1a/1b*^{-/-}, *Abcg2*^{-/-}, and *Abcb1a/1b;Abcg2*^{-/-} mice, and the experiment was terminated at 4 h. Single deficiency of either mAbcb1 or mAbcg2 resulted in higher selpercatinib plasma exposure, with the plasma AUC_{0-4h} increased in both *Abcb1a/1b*^{-/-} (37,024 ± 9,634 ng/ml*h, 1.6-fold, P < 0.01) and *Abcg2*^{-/-} mice (39,056 ± 6,710 ng/ml*h, 1.7-fold, P < 0.01) (Figure 5 and Table 2). In *Abcb1a/1b;Abcg2*^{-/-} mice, the selpercatinib plasma AUC_{0-4h} was also increased up to 1.6-fold compared to wild-type mice (38,986 ± 4,711 ng/ml*h vs 23,670 ± 2,469 ng/ml*h, P < 0.01). This result contrasts somewhat with the pilot study, where *Abcb1a/1b;Abcg2*^{-/-} mice did not show a significantly higher plasma exposure than wild-type mice. This difference was mainly due to a higher plasma concentration in *Abcb1a/1b;Abcg2*^{-/-} mice in the main study, where the C_{max} was increased from 8,582 ng/ml in the pilot study up to 11,015 ng/ml. However, the difference between these two

sets of data was small, and did not alter tissue penetration effects of *Abcb1* and *Abcg2*, especially in brain and testis.

In spite of this modest discrepancy, the single *Abcb1a/1b* deficiency, but not *Abcg2* deficiency, profoundly increased the brain concentration by 4.8-fold compared to wild-type mice. However, this increase was even larger in mice with a combination deficiency of both *Abcb1a/1b* and *Abcg2* (10.2-fold) compared to wild-type mice. The brain-to-plasma ratio of selpercatinib was again very low (0.077) in wild-type mice, but was increased to 0.23 (3.0-fold) by single *mAbcb1* deficiency and further up to 0.48 (6.2-fold) by combined *mAbcb1* and *mAbcg2* deficiency (Figure 5C-D; Table 2). Notably, due to the higher brain concentration of selpercatinib in wild-type mice in the main study, this difference (6.2-fold) was lower than that observed in the pilot study (15.3-fold). Nonetheless, these results reveal that *Abcb1a/1b* can restrict selpercatinib brain accumulation and the further increased drug exposure in *Abcb1a/1b/Abcg2*^{-/-} brain demonstrates that, in the absence of *Abcb1a/1b* activity, *Abcg2* still limits selpercatinib brain penetration. Qualitatively similar results were obtained for selpercatinib testis penetration. Although the wild-type testis-to-plasma ratio was substantially higher (0.15) than for brain, the relative increased ratios in *Abcb1a/1b*^{-/-} (2.7-fold) and *Abcb1a/1b/Abcg2*^{-/-} (6.4-fold) mice were similar compared to those for brain (Figure 5E-F; Table 2). The data indicate that *Abcb1a/1b* and, to a lesser extent, *Abcg2* can strongly reduce the brain accumulation of selpercatinib, while testis accumulation was similarly affected.

In the main experiment we observed significantly lower liver-to-plasma ratios in *Abcg2*^{-/-} and *Abcb1a/1b/Abcg2*^{-/-} mice (Figure 6A-B), which had not been obvious in *Abcb1a/1b/Abcg2*^{-/-} mice in the pilot study. In theory it could be that the ABC transporters normally concentrate selpercatinib in the intrahepatic bile, and that loss of this process results in relatively reduced overall liver levels of the drug in the knockout strains. Indeed, the concentrations, the tissue-to-plasma ratios and the percentage of dose of selpercatinib in the small intestinal contents were reduced in *Abcb1a/1b*^{-/-} and especially *Abcb1a/1b/Abcg2*^{-/-} mice compared to wild-type mice (Figure 6 and Table 2). This finding was consistent with the pilot results and could again suggest a more rapid and extensive absorption of selpercatinib across the intestinal wall in the absence of intestinal *Abcb1a/1b* activity (essentially because of loss of an intestinal excretion process), or reduced hepatobiliary recirculation of absorbed selpercatinib through biliary excretion mediated by *Abcb1a/1b* in the bile canaliculi of the liver, or a combination of both processes. No meaningful differences were found in the other tissues analyzed (Supplemental Figure 3).

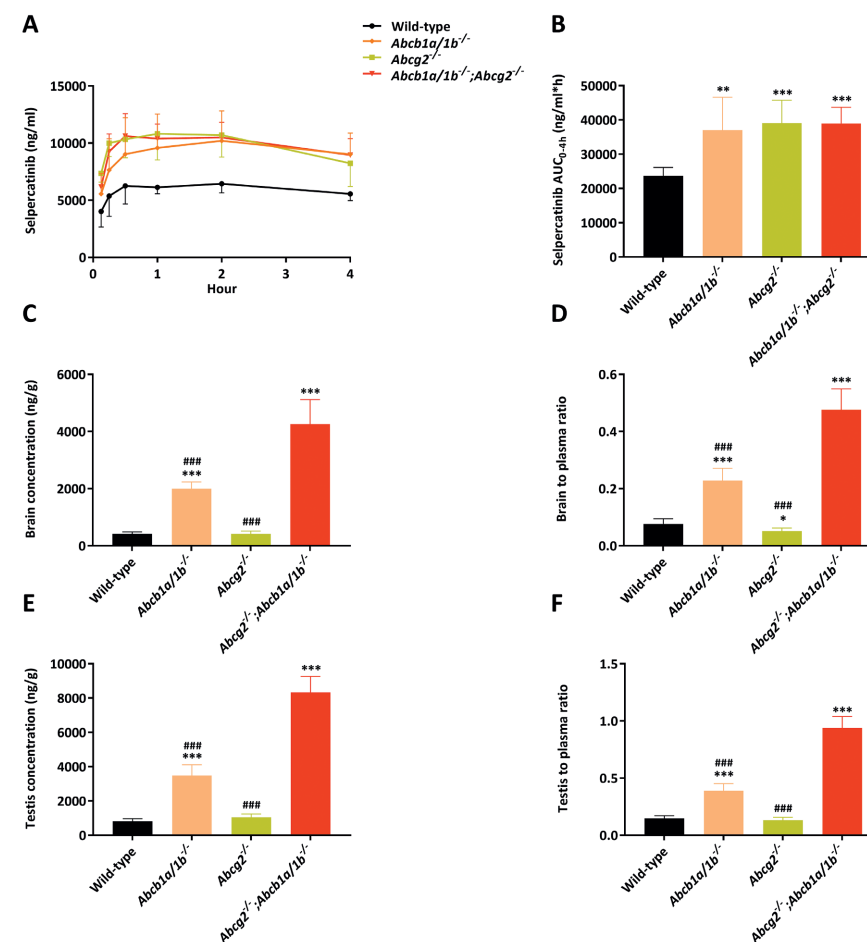


Figure 5. Plasma concentration-time curves (A), plasma AUC_{0-4h} (B), brain concentration (C), brain-to-plasma ratio (D), testis concentration (E) and testis-to-plasma ratio (F) of selpercatinib in male wild-type, *Abcb1a/1b*^{-/-}, *Abcg2*^{-/-} and *Abcb1a/1b/Abcg2*^{-/-} mice over 4 h after oral administration of 10 mg/kg selpercatinib. Data are given as mean \pm S.D. (n = 6). *, $P < 0.05$; **, $P < 0.01$; ***, $P < 0.001$ compared to wild-type mice; #, $P < 0.05$; ##, $P < 0.01$; ###, $P < 0.001$ compared to *Abcb1a/1b/Abcg2*^{-/-} mice. Statistical analysis was applied after log-transformation of linear data.

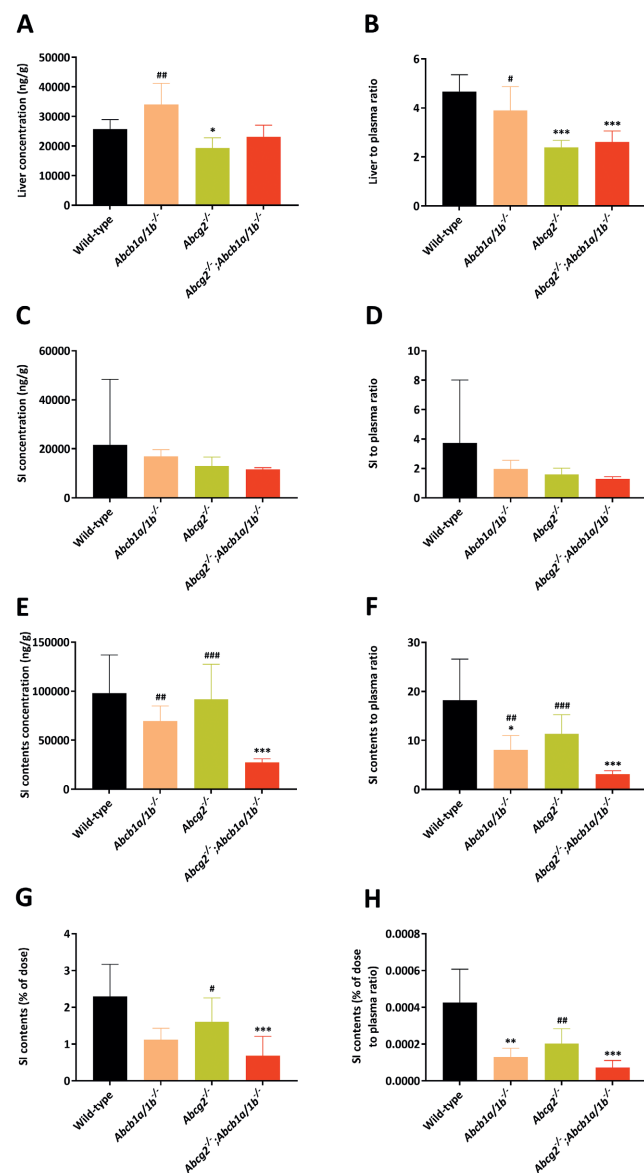


Figure 6. Liver, small intestine and small intestine contents concentrations (A, C, E), liver, small intestine- and small intestine contents-to-plasma ratios (B, D, F), small intestine contents as percentage of dose (G) and small intestine contents percentage of dose-to-plasma ratio (H) of selpercatinib in male wild-type, *Abcb1a/1b*^{-/-}, *Abcg2*^{-/-} and *Abcb1a/1b*^{-/-};*Abcg2*^{-/-} mice 4 h after oral administration of 10 mg/kg selpercatinib. SI: small intestine. Data are given as mean ± S.D. (n = 6). *, *P* < 0.05; **, *P* < 0.01; ***, *P* < 0.001 compared to wild-type mice; #, *P* < 0.05; ##, *P* < 0.01; ###, *P* < 0.001 compared between *Abcb1a/1b*^{-/-};*Abcg2*^{-/-} and *Slco1a/1b*^{-/-} mice. Statistical analysis was applied after log-transformation of linear data.

Table 2. Plasma and organ pharmacokinetic parameters of selpercatinib in male wild-type, *Abcb1a/1b*^{-/-}, *Abcg2*^{-/-} and *Abcb1a/1b*^{-/-};*Abcg2*^{-/-} mice over 4 h after oral administration of 10 mg/kg selpercatinib.

| Parameter | Genotype | | | |
|----------------------------------|---------------|---------------------------------|-----------------------------|---|
| | Wild-type | <i>Abcb1a/1b</i> ^{-/-} | <i>Abcg2</i> ^{-/-} | <i>Abcb1a/1b</i> ^{-/-} ; <i>Abcg2</i> ^{-/-} |
| AUC _{0-4h} , ng/ml*h | 23670 ± 2469 | 37024 ± 9634** | 39056 ± 6710*** | 38986 ± 4711*** |
| Fold change AUC _{0-4h} | 1.0 | 1.6 | 1.7 | 1.6 |
| C _{max} , ng/ml | 6908 ± 761 | 10338 ± 2641** | 11447 ± 2155*** | 11015 ± 1653** |
| T _{max} , h | 1.6 ± 1.4 | 1.8 ± 1.3 | 1.4 ± 0.74 | 1.5 ± 1.3 |
| C _{brain} , ng/g | 420 ± 66 | 1998 ± 233***### | 418 ± 102### | 4263 ± 853*** |
| Fold change C _{brain} | 1.0 | 4.8 | 1.0 | 10.2 |
| Brain-to-plasma ratio | 0.077 ± 0.018 | 0.23 ± 0.04***### | 0.052 ± 0.011***### | 0.48 ± 0.07*** |
| Fold change ratio | 1.0 | 3.0 | 0.68 | 6.2 |
| C _{Liver} , ng/g | 25737 ± 3219 | 34014 ± 7169## | 19334 ± 3483* | 23157 ± 3900 |
| Fold increase C _{Liver} | 1.0 | 1.3 | 0.75 | 0.90 |
| Liver-to-plasma ratio | 4.7 ± 0.7 | 3.9 ± 1.0# | 2.4 ± 0.3*** | 2.6 ± 0.5*** |
| Fold change ratio | 1.0 | 0.83 | 0.51 | 0.55 |
| C _{SI} , ng/g | 21649 ± 26731 | 16952 ± 2729 | 12967 ± 3639 | 11576 ± 734 |
| Fold increase C _{SI} | 1.0 | 0.83 | 0.60 | 0.53 |
| SI-to-plasma ratio | 3.7 ± 4.3 | 2.0 ± 0.6 | 1.6 ± 0.4 | 1.3 ± 0.1 |
| Fold change ratio | 1.0 | 0.54 | 0.43 | 0.35 |
| C _{SIC} , ng/g | 98083 ± 38906 | 69396 ± 15655## | 91686 ± 35700### | 27386 ± 3533*** |
| Fold increase C _{SIC} | 1.0 | 0.71 | 0.93 | 0.28 |
| SIC-to-plasma ratio | 18.2 ± 8.5 | 8.1 ± 2.9*## | 11.4 ± 3.9### | 3.1 ± 0.68*** |
| Fold change ratio | 1.0 | 0.45 | 0.63 | 0.17 |
| SIC percentage of dose, % | 2.3 ± 0.9 | 1.1 ± 0.3 | 1.6 ± 0.7# | 0.69 ± 0.52*** |
| Fold change ratio | 1.0 | 0.48 | 0.70 | 0.30 |
| C _{testis} , ng/g | 810.8 ± 148.4 | 3477 ± 634.1***### | 1049 ± 192.2### | 8328 ± 934.8*** |
| Fold change C _{testis} | 1.0 | 4.3 | 1.3 | 10.3 |
| Testis-to-plasma ratio | 0.15 ± 0.02 | 0.39 ± 0.06***### | 0.13 ± 0.03### | 0.94 ± 0.10*** |
| Fold change ratio | 1.0 | 2.7 | 0.90 | 6.4 |

Data are given as mean ± S.D. (n = 6). AUC_{0-4h}, area under the plasma concentration-time curve; C_{max}, maximum concentration in plasma; T_{max}, time point (h) of maximum plasma concentration; C_{brain}, brain concentration; C_{Liver}, liver concentration; SI, small intestine (tissue); C_{SI}, small intestine tissue concentration; SIC, small intestine contents; C_{SIC}, small intestine contents concentration; C_{testis}, testis concentration; *, *P* < 0.05; **, *P* < 0.01; ***, *P* < 0.001 compared to wild-type mice; #, *P* < 0.05; ##, *P* < 0.01; ###, *P* < 0.001 compared between *Abcb1a/1b*^{-/-};*Abcg2*^{-/-} mice. Statistical analysis was applied after log-transformation of linear data.

3.5 Effect of the dual ABCB1 and ABCG2 inhibitor elacridar on selpercatinib brain accumulation

In view of the poor selpercatinib penetration into wild-type brain and the potential therapeutic benefit of enhancing selpercatinib brain accumulation, we investigated to what extent the dual ABCB1 and ABCG2 inhibitor elacridar could increase brain accumulation of selpercatinib.

We also assessed whether elacridar influences selpercatinib disposition and distribution in other tissues. Oral elacridar has a T_{max} of about 4 h in mice. To ensure complete inhibition of the BBB ABC transporters, elacridar (50 mg/kg) or vehicle was administered orally 2 h prior to oral selpercatinib administration (10 mg/kg) to wild-type and *Abcb1a/1b;Abcg2*^{-/-} mice. Plasma and brain selpercatinib levels were assessed 2 h after selpercatinib administration. The selpercatinib plasma concentration was still high at this time point, making the impact of the BBB transporters especially relevant. In the vehicle-treated strains, the selpercatinib plasma AUC_{0-2h} was not significantly different between the strains, and pretreatment with elacridar did not result in meaningful alterations (Figure 7A-B and Table 3). In the absence of elacridar, the brain concentration and brain-to-plasma ratio of selpercatinib were 22.5-fold and 17-fold higher in *Abcb1a/1b;Abcg2*^{-/-} mice than in wild-type mice, respectively ($P < 0.001$). Elacridar pretreatment markedly increased these values in wild-type mice by 13.2- and 11.5-fold, respectively ($P < 0.001$), resulting in levels close to those observed in *Abcb1a/1b;Abcg2*^{-/-} mice with or without elacridar pretreatment (Figure 7C-D and Table 3). Since these parameters were not significantly altered by elacridar in *Abcb1a/1b;Abcg2*^{-/-} mice, the pharmacokinetic effect of elacridar appears to be specifically mediated by the inhibition of mAbcb1a/1b and mAbcg2 in the BBB. Qualitatively similar but more modest differences were seen in testis, suggesting elacridar inhibition functions also applied in the BTB (Figure 7E-F). Unlike for the brain and testis, the liver distribution of selpercatinib was not noticeably affected by elacridar treatment in either mouse strain (Table 3). Also other tissues tested did not show marked differences concerning tissue-to-plasma ratios (Supplemental Figure 4).

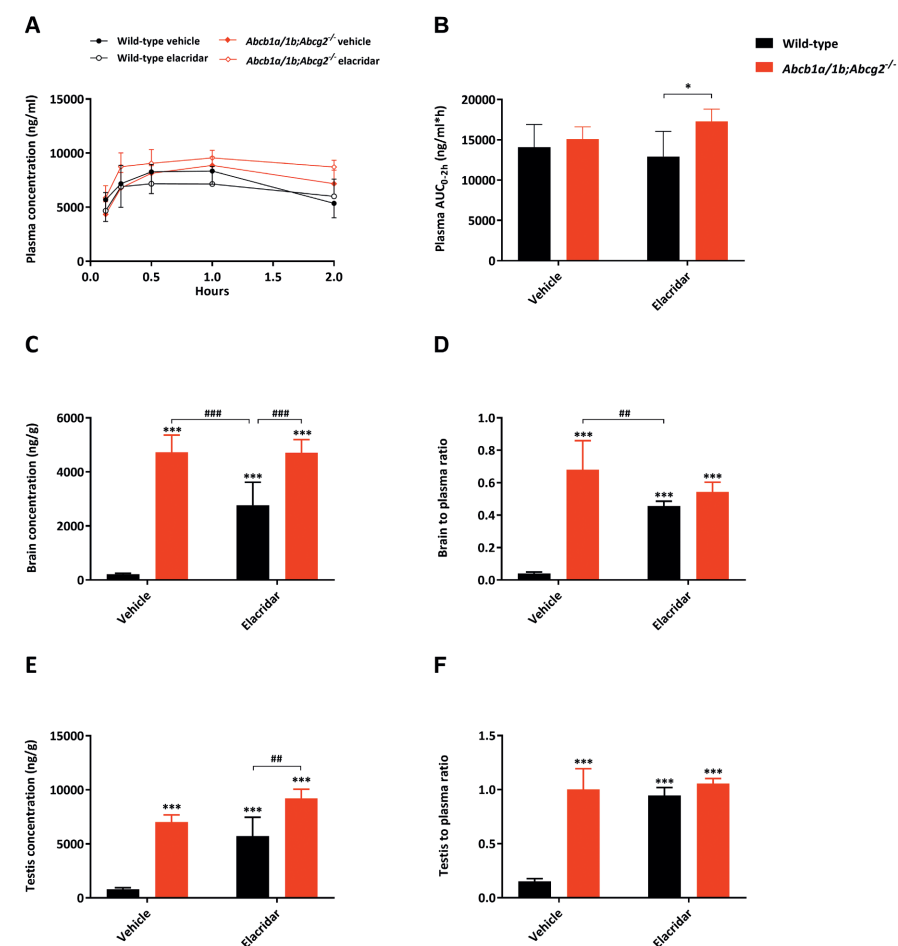


Figure 7. Plasma concentration-time curves (A), plasma AUC_{0-2h} (B), brain concentration (C), brain-to-plasma ratio (D), testis concentration (E) and testis-to-plasma ratio (F) of selpercatinib in male wild-type and *Abcb1a/1b;Abcg2*^{-/-} mice over 2 h after oral administration of 10 mg/kg selpercatinib with or without co-administration of elacridar. Data are given as mean \pm S.D. ($n = 6$). *, $P < 0.05$; **, $P < 0.01$; ***, $P < 0.001$ compared to wild-type mice. Statistical analysis was applied after log-transformation of linear data.

Table 3. Plasma and organ pharmacokinetic parameters of selpercatinib in male wild-type and *Abcb1a/1b;Abcg2*^{-/-} mice over 2 h after oral administration of 10 mg/kg selpercatinib with or without elacridar.

| Parameter | Genotype/Groups | | | |
|-------------------------------------|-----------------|---------------------------------------|----------------|---------------------------------------|
| | Vehicle | | Elacridar | |
| | Wild-type | <i>Abcb1a/1b;Abcg2</i> ^{-/-} | Wild-type | <i>Abcb1a/1b;Abcg2</i> ^{-/-} |
| AUC _{0-2h} , ng/ml*h | 14092 ± 2816 | 15098 ± 1503 | 12928 ± 3121 | 17294 ± 1513# |
| Fold change AUC _{0-2h} | 1.0 | 1.1 | 0.92 | 1.2 |
| C _{max} , ng/ml | 8739 ± 1560 | 8865 ± 792 | 7466 ± 1848 | 9617 ± 776# |
| T _{max} , h | 0.75 ± 0.27 | 1.0 ± 0.0# | 0.50 ± 0.27 | 0.79 ± 0.33 |
| C _{brain} , ng/g | 210 ± 40 | 4726 ± 638***### | 2765 ± 851*** | 4713 ± 484***### |
| Fold increase C _{brain} | 1.0 | 22.5 | 13.2 | 22.4 |
| Brain-to-plasma ratio | 0.041 ± 0.009 | 0.68 ± 0.18***### | 0.46 ± 0.03*** | 0.54 ± 0.06*** |
| Fold increase ratio | 1.0 | 17 | 11.5 | 13.5 |
| C _{Liver} , ng/g | 18134 ± 2604 | 21445 ± 2330 | 20028 ± 4435 | 23628 ± 4827 |
| Fold increase C _{Liver} | 1.0 | 1.2 | 1.1 | 1.3 |
| Liver-to-plasma ratio | 3.5 ± 0.8 | 3.1 ± 0.7 | 3.4 ± 0.3 | 2.7 ± 0.4 |
| Fold change ratio | 1.0 | 0.89 | 1.0 | 0.77 |
| C _{SI + SIC} , ng/g | 37604 ± 13607 | 18845 ± 3628** | 26630 ± 6802 | 21226 ± 929* |
| Fold increase C _{SI + SIC} | 1.0 | 0.50 | 0.71 | 0.56 |
| SI + SIC-to-plasma ratio | 7.0 ± 1.9 | 2.7 ± 0.8***### | 4.6 ± 1.3* | 2.4 ± 0.2***### |
| Fold change ratio | 1.0 | 0.39 | 0.66 | 0.34 |
| C _{testis} , ng/g | 788 ± 159 | 7020 ± 664*** | 5709 ± 1744*** | 9202 ± 856***### |
| Fold increase C _{testis} | 1.0 | 8.9 | 7.2 | 11.7 |
| Testis-to-plasma ratio | 0.15 ± 0.03 | 1.0 ± 0.2*** | 0.94 ± 0.08*** | 1.1 ± 0.05*** |
| Fold change ratio | 1.0 | 6.7 | 6.3 | 7.3 |

Data are given as mean ± S.D. (n = 6). AUC_{0-2h}, area under the plasma concentration-time curve; C_{max}, maximum concentration in plasma; T_{max}, time point (h) of maximum plasma concentration; C_{brain}, brain concentration; C_{Liver}, liver concentration; SI, small intestine (tissue); SIC, small intestine contents; C_{SI + SIC}, small intestine tissue together with small intestine contents concentration; C_{testis}, testis concentration; *, P < 0.05; **, P < 0.01; ***, P < 0.001 compared to vehicle treated wild-type mice; #, P < 0.05; ##, P < 0.01; ###, P < 0.001 compared to elacridar treated wild-type mice; ^, P < 0.05; ^^, P < 0.01; ^^, P < 0.001 compared between vehicle treated *Abcb1a/1b;Abcg2*^{-/-} and elacridar treated *Abcb1a/1b;Abcg2*^{-/-} mice. Statistical analysis was applied after log-transformation of linear data.

3.6 Impact of CYP3A on selpercatinib plasma exposure and tissue distribution

Many drugs and prodrugs are metabolized by CYP3A, which can therefore restrict their oral exposure. To assess the impact of CYP3A on selpercatinib *in vivo*, we next performed an 8 h pharmacokinetic study in female wild-type, *Cyp3a*^{-/-} and Cyp3aXAV mice (with human CYP3A4 specific transgene expression in liver and intestine in a mouse Cyp3a-deficient background). Selpercatinib (10 mg/kg) was administered orally after 2-3 h of fasting, blood samples were taken

at several time points and organs were collected at last time point (8 h). The oral selpercatinib plasma AUC_{0-8h} in *Cyp3a*^{-/-} mice was significantly higher (72,243 ± 5,642 ng/ml*h, 1.4-fold, P < 0.01) than that in wild-type mice (52,251 ± 6,922 ng/ml*h), while Cyp3aXAV mice showed a plasma AUC_{0-8h} (45,755 ± 3,460 ng/ml*h) which was reduced again to roughly the levels seen in wild-type mice (Figure 8 and Table 4). However, regarding the tissue distribution at 8 h, the observed differences in absolute tissue concentrations for brain, liver, kidney, small intestine, testis, lung and spleen among the strains reflected the plasma AUC_{0-8h} differences, without substantial alterations in corresponding tissue-to-plasma ratios (Supplemental Figure 5 and 6 and Table 4). Collectively, these results indicate that selpercatinib is substantially metabolized by mouse CYP3A and human CYP3A4, which markedly affects the oral exposure and, consequently, the tissue levels of selpercatinib.

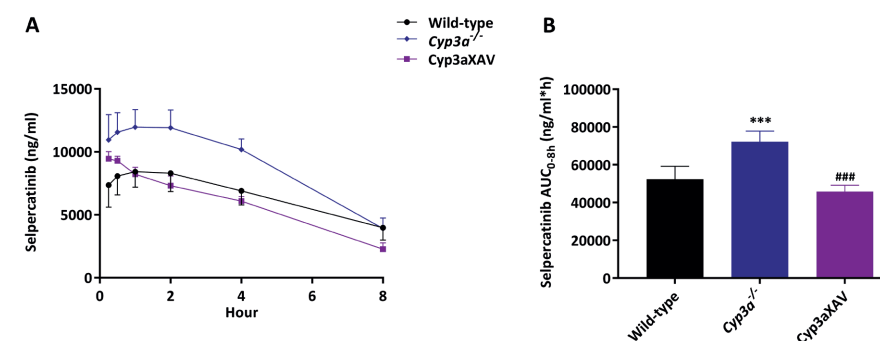


Figure 8. Plasma concentration-time curves (A) and plasma AUC_{0-8h} (B) of selpercatinib in female wild-type, *Cyp3a*^{-/-} and Cyp3aXAV mice 8 h after oral administration of 10 mg/kg selpercatinib. Data are given as mean ± S.D. (n = 6 - 7). *, P < 0.05; **, P < 0.01; ***, P < 0.001 compared to wild-type mice; #, P < 0.05; ##, P < 0.01; ###, P < 0.001 compared between *Cyp3a*^{-/-} and Cyp3aXAV mice. Statistical analysis was applied after log-transformation of linear data

Table 4. Plasma and organ pharmacokinetic parameters of selpercatinib in female wild-type, *Cyp3a*^{-/-} and *Cyp3aXAV* mice over 8 h after oral administration of 10 mg/kg selpercatinib.

| Parameter | Genotype | | |
|---------------------------------|---------------|-----------------------------|------------------|
| | Wild-type | <i>Cyp3a</i> ^{-/-} | <i>Cyp3aXAV</i> |
| AUC _{0-8h} , ng/ml*h | 52251 ± 6922 | 72243 ± 5642*** | 45755 ± 3460### |
| Fold change AUC _{0-8h} | 1.0 | 1.4 | 0.88 |
| C _{max} , ng/ml | 8556 ± 1299 | 12295 ± 1311*** | 9477 ± 548## |
| T _{max} , h | 1.5 ± 1.3 | 1.4 ± 1.3 | 0.29 ± 0.10*# |
| C _{brain} , ng/g | 82.4 ± 16.8 | 86.2 ± 24.2 | 51.0 ± 15.2*## |
| Fold change C _{brain} | 1.0 | 1.0 | 0.62 |
| Brain-to-plasma ratio | 0.021 ± 0.002 | 0.022 ± 0.002 | 0.022 ± 0.002 |
| Fold change ratio | 1.0 | 1.0 | 1.0 |
| C _{liver} , ng/g | 8255 ± 1615 | 7896 ± 1274 | 4386 ± 755***### |
| Fold change C _{liver} | 1.0 | 1.0 | 0.53 |
| Liver-to-plasma ratio | 2.1 ± 0.3 | 2.1 ± 0.2 | 2.0 ± 0.2 |
| Fold change ratio | 1.0 | 1.0 | 1.0 |
| C _{SI} , ng/g | 7302 ± 1116 | 6384 ± 930 | 5030 ± 347***# |
| Fold change C _{SI} | 1.0 | 0.87 | 0.69 |
| SI-to-plasma ratio | 1.9 ± 0.4 | 1.7 ± 0.3 | 2.3 ± 0.6 |
| Fold change ratio | 1.0 | 0.89 | 1.2 |
| C _{SIC} , ng/g | 83866 ± 51955 | 44922 ± 15127 | 48515 ± 13654 |
| Fold change C _{SIC} | 1.0 | 0.54 | 0.58 |
| SIC-to-plasma ratio | 20.0 ± 7.9 | 11.5 ± 3.3* | 22.3 ± 7.5## |
| Fold change ratio | 1.0 | 0.58 | 1.1 |
| SIC percentage of dose, % | 2.5 ± 0.9 | 1.4 ± 0.6* | 1.5 ± 0.5 |
| Fold change % | 1.0 | 0.56 | 0.60 |

Data are given as mean ± S.D. (n = 6 - 7). AUC_{0-8h}, area under plasma concentration-time curve; C_{max}, maximum concentration in plasma; T_{max}, time point (h) of maximum plasma concentration; C_{brain}, brain concentration; C_{liver}, liver concentration; SI, small intestine (tissue); C_{SI}, small intestine tissue concentration; SIC, small intestine contents; C_{SIC}, small intestine contents concentration; *, P < 0.05; **, P < 0.01; ***, P < 0.001 compared to wild-type mice; #, P < 0.05; ##, P < 0.01; ###, P < 0.001 compared between *Cyp3a*^{-/-} and *Cyp3aXAV* mice. Statistical analysis was applied after log-transformation of linear data.

4. DISCUSSION AND CONCLUSIONS

In the current study, we found that the RET inhibitor selpercatinib is efficiently transported by human ABCB1 and mouse *Abcg2* *in vitro*. The brain-to-plasma ratio of selpercatinib was found to be low (0.030 - 0.077) in wild-type mice, indicating relatively poor brain penetration of selpercatinib. This could be increased by a factor as high as 17-fold (ranging from 6.2- to 17-fold) in *Abcb1a/1b;Abcg2*^{-/-} mice. We obtained qualitatively similar results for the impact of the ABC transporters on limiting selpercatinib testis penetration, with increases as high as 6.7-fold upon deficiency of both *Abcb1* and *Abcg2*. Thus our results demonstrate that ABCB1

and ABCG2 in the blood-brain-barrier (BBB) could profoundly limit the brain penetration of selpercatinib, although ABCG2 showed a more modest effect. Similar functions of ABCB1 and ABCG2 also showed up in the blood-testis-barrier (BTB), albeit somewhat less pronounced. Oral coadministration of the ABCB1/ABCG2 inhibitor elacridar could further mostly reverse these functions. Despite the increased plasma and tissue exposure, we did not observe any abnormal external behavior indicative of acute toxicity caused by selpercatinib in the *Abcb1a/1b;Abcg2*^{-/-} mice (nor in the *Slco1a/1b*^{-/-} and *Cyp3a*^{-/-} mice). *Slco1a/1b* deficiencies did not significantly alter selpercatinib pharmacokinetics. Of note, at the dose used in our study (10 mg/kg), the relative pharmacokinetic parameters, including average T_{max} (~2 h), C_{max} (~8,000 ng/ml) and AUC_{0-8h} (52,251 ng/ml*h) of selpercatinib in wild-type mice, were of the same order of magnitude as those observed in patients (T_{max} is 2 hours with average C_{max} 2,980 ng/ml and AUC_{0-24h} 51,600 ng/ml*h).

In the small intestine contents, we further observed a clearly decreased concentration and SIC-to-plasma ratio of selpercatinib in the absence of *Abcb1a/1b*, and these values were even lower when both *Abcb1a/1b* and *Abcg2* were deficient (P < 0.01). As explained earlier, this suggests that both *Abcb1a/1b* and *Abcg2*, but mainly *Abcb1a/1b*, can either reduce net intestinal uptake by mediating direct efflux of selpercatinib across the intestinal wall back into the intestinal lumen, or the hepatobiliary excretion of selpercatinib, or a combination of both processes. No notable changes in tissue distribution were observed in other tissues due to the ABC transporter deficiencies, including liver, kidney, lung and spleen.

Oncogenic RET fusions occur infrequently in diverse types of cancer, including NSCLC (1-2%), and more frequently in papillary thyroid cancers (10-20%). Frequencies in other rare solid tumors are even lower. Although infrequent, RET fusions appear to be associated with a high risk of brain metastases, which was demonstrated by the finding that the cumulative incidence of CNS lesions in RET-positive NSCLC patients is higher than that in ROS1-positive patients³⁶. Thus, it is worthwhile to investigate whether selpercatinib can achieve high intrinsic BBB permeability, and the potential effects due to interaction of selpercatinib with ABCB1 and ABCG2 in the BBB. Of note, mouse has a relatively higher ABCB1 (2.3-fold) protein and lower ABCG2 (2.5-fold) protein expressed in the blood-brain-barrier. However, there is high chance that our findings may also be applied in humans, considering of the similar level of ABCB1 and ABCG2 protein expression (range from 3.2 to 14.2 fmol/mg). While this project was ongoing, the FDA approved selpercatinib (Food and Drug Administration, 2020)¹⁵. According to its guidelines, selpercatinib is a substrate of ABCB1 and ABCG2. However, in our *in vitro* results, selpercatinib was a good substrate of human ABCB1 and mouse *Abcg2*, but not of human ABCG2. Despite this, the guidelines appear in accordance with our *in vivo* data, especially in BBB and BTB, where ABCB1 displayed a main protective function, while ABCG2 had a smaller effect.

The observed strong interactions of selpercatinib with ABCB1 and ABCG2 could well result in poor brain penetration also in humans, potentially limiting therapeutic efficacy. So far, there is little direct documentation about human selpercatinib brain penetration or accumulation. Drilon et al. (2020) reported that selpercatinib was designed to penetrate the central nervous system (CNS) and had been shown in preclinical models to have antitumor activity in the brain. In the Phase 1–2 clinical trial, 38 of 105 patients had investigator-assessed CNS metastasis at baseline and 11 patients were deemed to have measurable lesions. Among these 11 patients, the percentage with an objective intracranial response was 91% (10 of 11 patients; 95% CI, 59 to 100) according to independent review, including 3 complete responses (27%), 7 partial responses (64%), and 1 stable disease³⁷. However, our results show that selpercatinib indeed has a poor brain penetration in wild-type mice, mainly due to the activity of ABCB1 in BBB. This ABCB1 P-glycoprotein function may be of relevance for further increasing therapeutic efficacy against brain metastases in RET-mutated NSCLC, in case ABCB1 in the human brain has a similar impact as in the mouse brain. If so, looking ahead for a broader clinical use of selpercatinib, we could also use this insight to improve (boost) brain concentration of selpercatinib using pharmacological inhibitors of P-glycoprotein, such as elacridar. From our results, oral co-administration of elacridar did not alter the overall plasma exposure of selpercatinib. Importantly, however, brain distribution of selpercatinib was profoundly improved in wild-type mice by elacridar (from 0.041 to 0.46, 11.5-fold) without any abnormal external behavior, albeit not to as high a level as seen in vehicle-treated *Abcb1a/1b;Abcg2*^{-/-} mice (0.68, 17.0-fold). We thus demonstrated that extensive inhibition of *Abcb1* in the BBB could be achieved using a clinically realistic co-administration schedule.

However, more drug accumulation in brain may also induce CNS toxicity, as we observed in a previous study with the ALK/EGFR inhibitor brigatinib. We found sometimes severe and lethal toxicity of oral brigatinib in mice with genetic knockout or pharmacological inhibition of *mAbcb1a/1b* and *mAbcg2*²¹. Related to this, recently selpercatinib was also being investigated in combination with previously registered anticancer drugs like crizotinib in patients with RET-positive NSCLC to overcome MET mutated resistance³⁸. According to the FDA documentation and our previous study^{39,40}, crizotinib is a substrate and also an inhibitor of ABCB1. Given the marked drug-drug interaction between selpercatinib and elacridar, any attempt to apply efficacious ABCB1/ABCG2 inhibitors in patients together with selpercatinib should be carefully monitored, even though no noticeable signs of acute selpercatinib CNS toxicity were observed in our study.

We further found that selpercatinib oral exposure in mice was modestly restricted by mouse *Cyp3a* (1.4-fold) and similarly by human CYP3A4 when compared to wild-type mice. This demonstrates that the metabolic clearance of selpercatinib is substantially influenced by human CYP3A4. Despite the clear differences in tissue concentrations among mouse strains, we did not observe any meaningful changes in corresponding tissue-to-plasma ratios. This

suggests that mouse *Cyp3a* and human CYP3A4 have little effect on relative selpercatinib tissue distribution and that the absolute tissue concentration differences only reflected the plasma concentration differences among the mouse strains. Consistent with the FDA declaration, our results indicate a clear *in vivo* interaction of selpercatinib and CYP3A. Thus, the body exposure and metabolic clearance of selpercatinib would likely be noticeably affected by variable CYP3A activity in patients, due to either drug-drug interactions or genetic polymorphisms, potentially compromising its therapeutic effect and safety. This further emphasizes the importance to critically monitor clinical dosing of selpercatinib due to individual CYP3A activity variation and/or when administering selpercatinib together with CYP3A inducers and/or inhibitors.

In summary, ABCG2 and especially ABCB1 can limit the oral exposure and brain and testis penetration of selpercatinib, as well as its intestinal disposition. To the best of our knowledge, this is the first study documenting that elacridar can improve selpercatinib brain accumulation. Additionally, CYP3A-mediated metabolism can markedly reduce selpercatinib oral exposure and thus its tissue concentrations. The obtained insights and principles may potentially be used to further enhance the therapeutic application and efficacy of selpercatinib, especially for brain metastases in RET fusion/mutation positive NSCLC patients.

ACKNOWLEDGEMENTS

This work was funded in part by the Chinese Scholarship Council through a scholarship to Y.W. (CSC Scholarship No. 201506240107).

AUTHOR CONTRIBUTIONS

Yaogeng Wang and Alfred H. Schinkel designed the study, analyzed the data and wrote the manuscript. Alfred H. Schinkel administered and supervised the project. Yaogeng Wang, Rolf W. Sparidans, Sander Potters and Rahime Şentürk performed the experimental parts of the study. Maria C. Lebre contributed reagents, materials, and mice. Jos H. Beijnen and Rolf W. Sparidans supervised the bioanalytical part of the studies and checked the content and language of manuscript. All authors commented on the manuscript and approved the final version.

CONFLICTS OF INTEREST STATEMENT

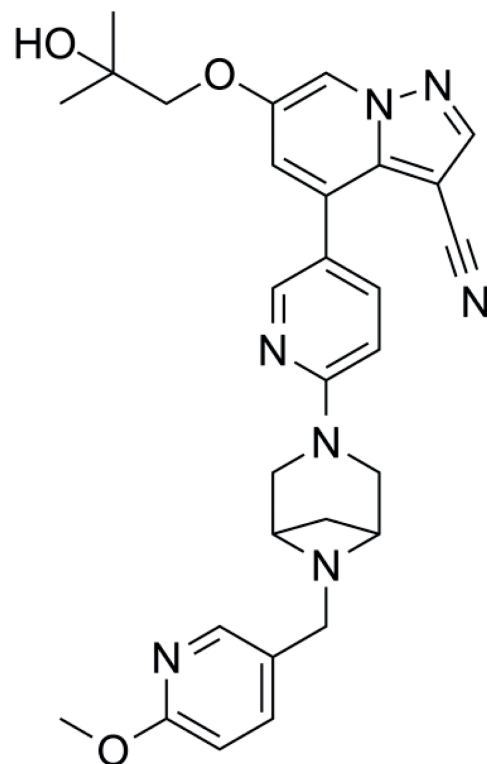
The research group of Alfred Schinkel receives revenue from commercial distribution of some of the mouse strains used in this study. The graphical abstract was made with Biorender.com. The remaining authors declare no conflict of interest.

REFERENCE

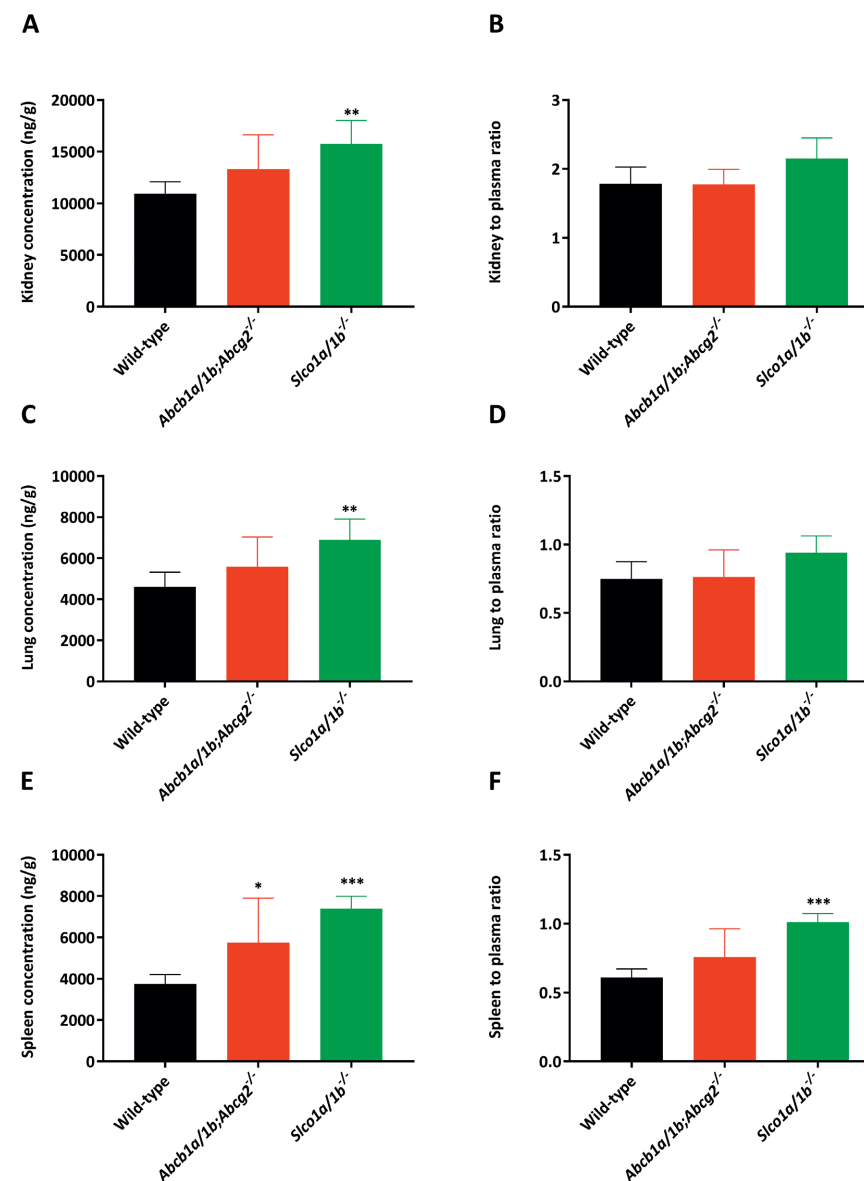
1. Manié, S., Santoro, M., Fusco, A. & Billaud, M. The RET receptor: function in development and dysfunction in congenital malformation. *Trends in Genetics* **17**, 580-589 (2001).
2. Ibanez, C.F. Structure and physiology of the RET receptor tyrosine kinase. *Cold Spring Harbor Perspectives in Biology* **5**(2013).
3. Stransky, N., Cerami, E., Schalm, S., Kim, J.L. & Lengauer, C. The landscape of kinase fusions in cancer. *Nature Communications* **5**, 4846 (2014).
4. Ji, J.H., et al. Identification of Driving ALK Fusion Genes and Genomic Landscape of Medullary Thyroid Cancer. *Plos Genetics* **11**, e1005467 (2015).
5. Kato, S., et al. RET Aberrations in Diverse Cancers: Next-Generation Sequencing of 4,871 Patients. *Clinical Cancer Research* **23**, 1988-1997 (2017).
6. Elisei, R., et al. Cabozantinib in progressive medullary thyroid cancer. *Journal of Clinical Oncology* **31**, 3639-3646 (2013).
7. Kurzrock, R., et al. Activity of XL184 (Cabozantinib), an oral tyrosine kinase inhibitor, in patients with medullary thyroid cancer. *Journal of Clinical Oncology* **29**, 2660-2666 (2011).
8. Drilon, A., et al. Cabozantinib in patients with advanced RET-rearranged non-small-cell lung cancer: an open-label, single-centre, phase 2, single-arm trial. *Lancet Oncology* **17**, 1653-1660 (2016).
9. Wells, S.A., Jr., et al. Vandetanib in patients with locally advanced or metastatic medullary thyroid cancer: a randomized, double-blind phase III trial. *Journal of Clinical Oncology* **30**, 134-141 (2012).
10. Yoh, K., et al. Vandetanib in patients with previously treated RET-rearranged advanced non-small-cell lung cancer (LURET): an open-label, multicentre phase 2 trial. *Lancet Respiratory Medicine* **5**, 42-50 (2017).
11. Sabari, J.K., Siau, E.D. & Drilon, A. Targeting RET-rearranged lung cancers with multikinase inhibitors. *Oncoscience* **4**, 23-24 (2017).
12. Gautschi, O., et al. Targeting RET in Patients With RET-Rearranged Lung Cancers: Results From the Global, Multicenter RET Registry. *Journal of Clinical Oncology* **35**, 1403-1410 (2017).
13. Subbiah, V. & Cote, G.J. Advances in Targeting RET-Dependent Cancers. *Cancer Discovery* **10**, 498-505 (2020).
14. Alexander Drilon, et al. A phase 1 study of LOXO-292, a potent and highly selective RET inhibitor, in patients with RET-altered cancers. in *ASCO* (2018).
15. Food and Drug Administration. Center for Drug Evaluation and Research of the US Department of Health and Human Service, Food and Drug Administration. Multi-discipline Review (2020). Available from: https://www.accessdata.fda.gov/drugsatfda_docs/label/2020/213246s0001bl.pdf.
16. Nigam, S.K. What do drug transporters really do? *Nature Reviews Drug Discovery* **14**, 29-44 (2014).
17. Russel, F.G.M. Transporters: Importance in Drug Absorption, Distribution, and Removal. 27-49 (2010).
18. Giacomini, K.M., et al. Membrane transporters in drug development. *Nature Reviews Drug Discovery* **9**, 215-236 (2010).
19. Schinkel, A.H. & Jonker, J.W. Mammalian drug efflux transporters of the ATP binding cassette (ABC) family: an overview. *Advanced Drug Delivery Reviews* **55**, 3-29 (2003).
20. Wang, Y., et al. OATP1A/1B, CYP3A, ABCB1, and ABCG2 limit oral availability of the NTRK inhibitor larotrectinib, while ABCB1 and ABCG2 also restrict its brain accumulation. *British Journal of Pharmacology* **177**, 3060-3074 (2020).
21. Li, W., et al. P-glycoprotein and breast cancer resistance protein restrict brigatinib brain accumulation and toxicity, and, alongside CYP3A, limit its oral availability. *Pharmacological Research* **137**, 47-55 (2018).
22. Roth, M., Obaidat, A. & Hagenbuch, B. OATPs, OATs and OCTs: the organic anion and cation transporters of the SLCO and SLC22A gene superfamilies. *British Journal of Pharmacology* **165**, 1260-1287 (2012).
23. Hagenbuch, B. & Gui, C. Xenobiotic transporters of the human organic anion transporting polypeptides (OATP) family. *Xenobiotica* **38**, 778-801 (2008).
24. Hagenbuch, B. & Meier, P.J. Organic anion transporting polypeptides of the OATP/ SLC21 family: phylogenetic classification as OATP/ SLCO superfamily, new nomenclature and molecular/functional properties. *Pflügers Archiv. European Journal of Physiology* **447**, 653-665 (2004).

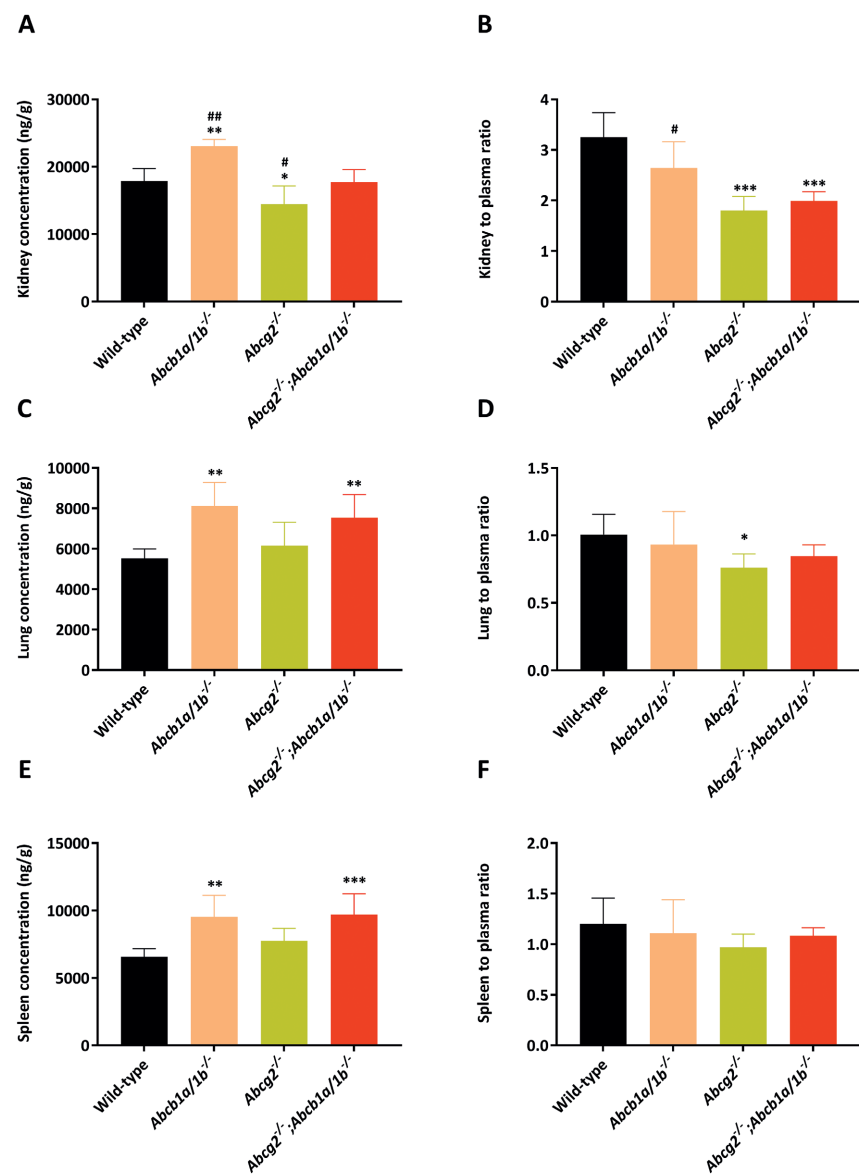
25. Hagenbuch, B. & Meier, P.J. The superfamily of organic anion transporting polypeptides. *Biochimica et Biophysica Acta* **1609**, 1-18 (2003).
26. Thakkar, N., Lockhart, A.C. & Lee, W. Role of Organic Anion-Transporting Polypeptides (OATPs) in Cancer Therapy. *The AAPS Journal* **17**, 535-545 (2015).
27. Cheng, X., Maher, J., Chen, C. & Klaassen, C.D. Tissue distribution and ontogeny of mouse organic anion transporting polypeptides (Oatps). *Drug Metabolism and Disposition* **33**, 1062-1073 (2005).
28. Shitara, Y., et al. Clinical significance of organic anion transporting polypeptides (OATPs) in drug disposition: their roles in hepatic clearance and intestinal absorption. *Biopharmaceutics and Drug Disposition* **34**, 45-78 (2013).
29. Kalliokoski, A. & Niemi, M. Impact of OATP transporters on pharmacokinetics. *British Journal of Pharmacology* **158**, 693-705 (2009).
30. Guengerich, F.P. Cytochrome P-450 3A4: regulation and role in drug metabolism. *Annual Review of Pharmacology and Toxicology* **39**, 1-17 (1999).
31. Peters, J., et al. Clarithromycin is absorbed by an intestinal uptake mechanism that is sensitive to major inhibition by rifampicin: results of a short-term drug interaction study in foals. *Drug Metabolism and Disposition* **40**, 522-528 (2012).
32. Wang, Y., et al. ABCB1 and ABCG2, but not CYP3A4 limit oral availability and brain accumulation of the RET inhibitor pralsetinib. *Pharmacological Research* **172**, 105850 (2021).
33. Şentürk, R., Wang, Y., Schinkel, A.H., Beijnen, J.H. & Sparidans, R.W. Quantitative bioanalytical assay for the selective RET inhibitors selpercatinib and pralsetinib in mouse plasma and tissue homogenates using liquid chromatography-tandem mass spectrometry. *Journal of Chromatography. B: Analytical Technologies in the Biomedical and Life Sciences* **1147**, 122131 (2020).
34. Zhang, Y., Huo, M., Zhou, J. & Xie, S. PKSolver: An add-in program for pharmacokinetic and pharmacodynamic data analysis in Microsoft Excel. *Computer Methods and Programs in Biomedicine* **99**, 306-314 (2010).
35. Simoff, I., et al. Complete Knockout of Endogenous Mdr1 (Abcb1) in MDCK Cells by CRISPR-Cas9. *Journal of Pharmaceutical Sciences* **105**, 1017-1021 (2016).
36. Drilon, A., et al. Frequency of Brain Metastases and Multikinase Inhibitor Outcomes in Patients With RET-Rearranged Lung Cancers. *Journal of Thoracic Oncology* **13**, 1595-1601 (2018).
37. Drilon, A., et al. Efficacy of Selpercatinib in RET Fusion-Positive Non-Small-Cell Lung Cancer. *New England Journal of Medicine* **383**, 813-824 (2020).
38. Rosen, E.Y., et al. Overcoming MET-Dependent Resistance to Selective RET Inhibition in Patients with RET Fusion-Positive Lung Cancer by Combining Selpercatinib with Crizotinib. *Clinical Cancer Research* (2020).
39. Tang, S.C., et al. Increased oral availability and brain accumulation of the ALK inhibitor crizotinib by coadministration of the P-glycoprotein (ABCB1) and breast cancer resistance protein (ABCG2) inhibitor elacridar. *International Journal of Cancer* **134**, 1484-1494 (2014).
40. Food and Drug Administration. Center for Drug Evaluation and Research of the US Department of Health and Human Service, Food and Drug Administration. Multi-discipline Review (2011). Available from: https://www.accessdata.fda.gov/drugsatfda_docs/label/2021/202570s0301bl.pdf.

SUPPLEMENTAL MATERIALS

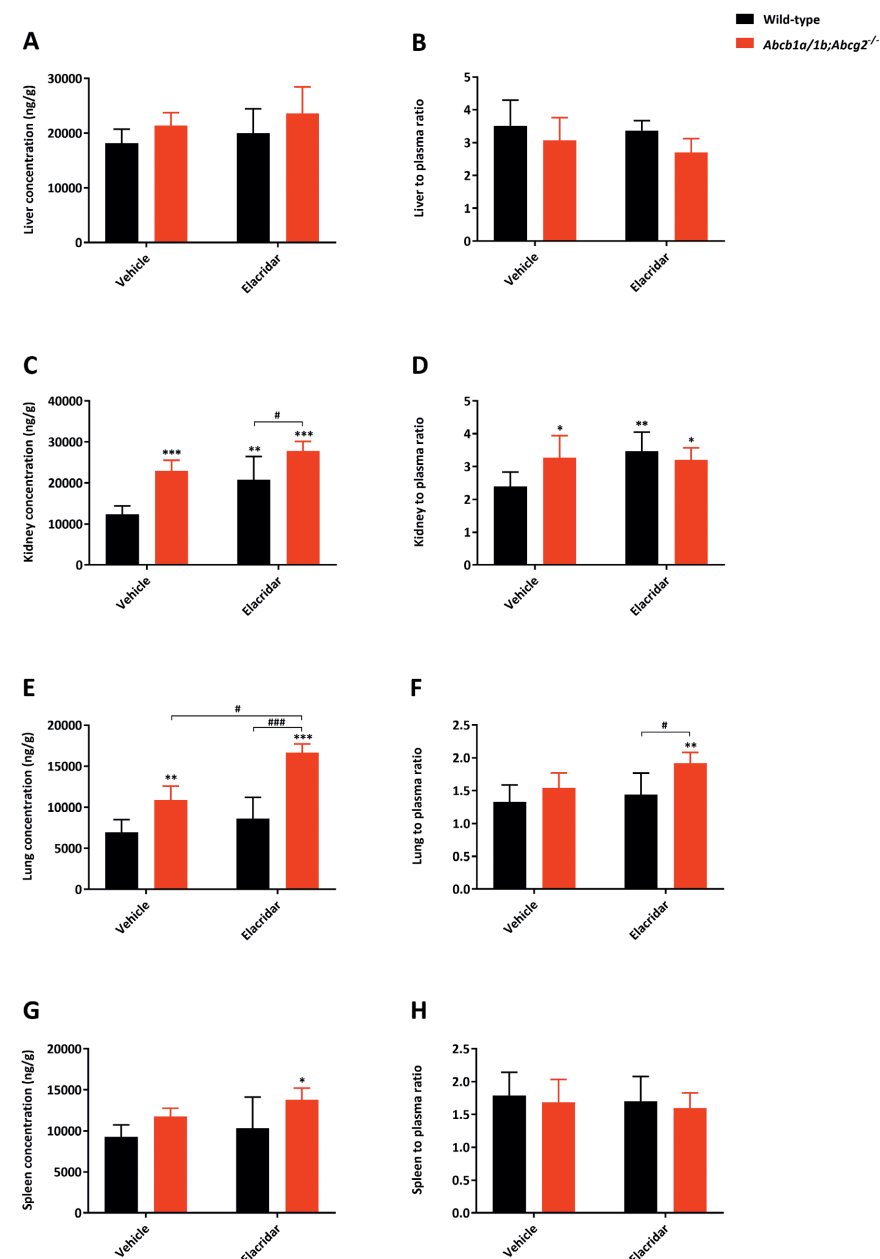


Supplemental Figure 1. Molecular structure of selpercatinib (RETEVMO, LOXO-292, 525.61 g/mol).

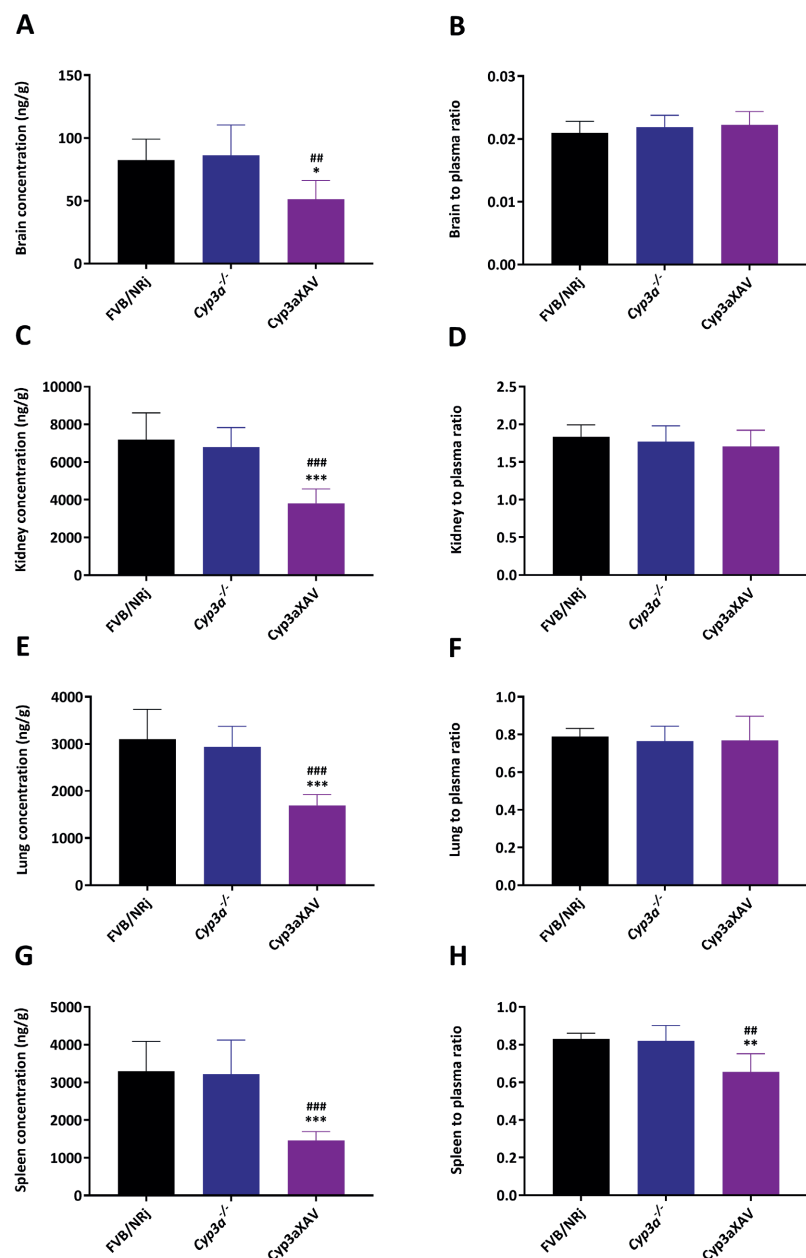
Supplemental Figure 2. Tissue concentrations (A, C, E) and tissue-to-plasma ratios (B, D, F) of selpercatinib in male wild-type, *Abcb1a/1b;Abcg2*^{-/-} and *Slco1a/1b*^{-/-} mice 4 h after oral administration of 10 mg/kg selpercatinib (n = 6 - 7). *, *P* < 0.05; **, *P* < 0.01; ***, *P* < 0.001 compared to wild-type mice. Statistical analysis was applied after log-transformation of linear data.



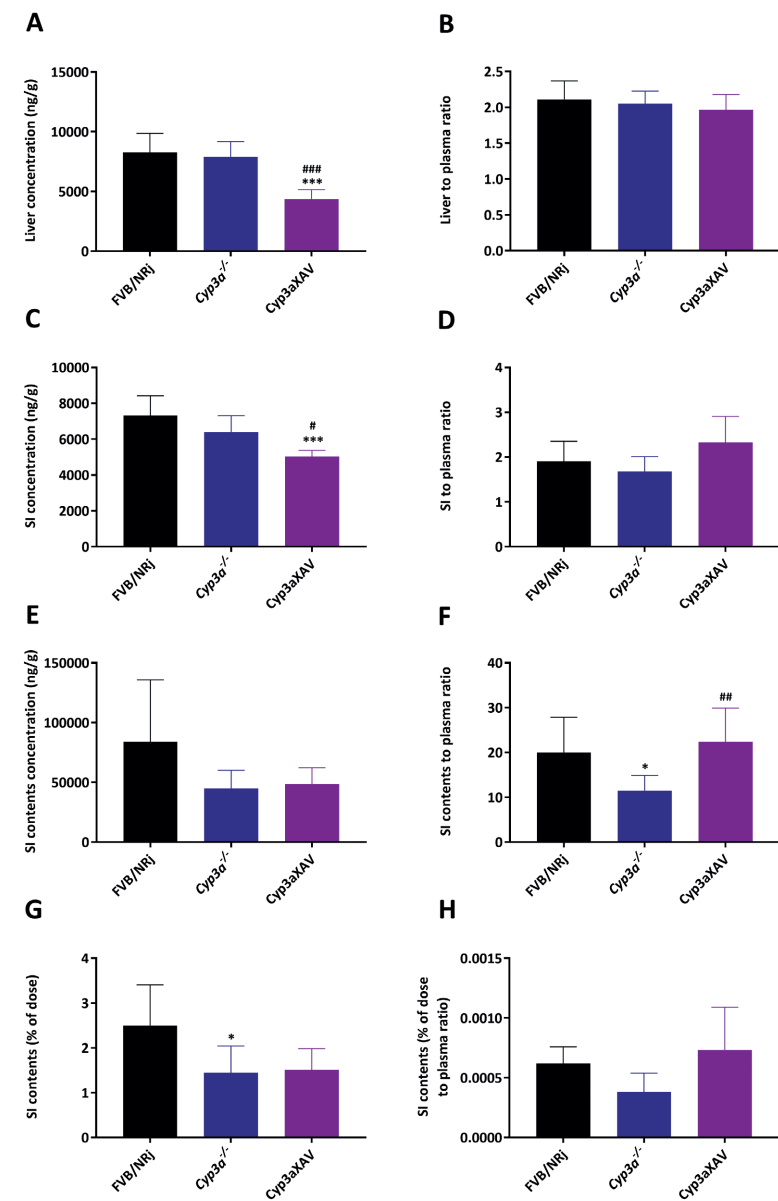
Supplemental Figure 3. Tissue concentrations (A, C, E) and tissue-to-plasma ratios (B, D, F) of selpercatinib in male wild-type, *Abcb1a/1b*^{-/-}, *Abcg2*^{-/-} and *Abcb1a/1b*^{-/-};*Abcg2*^{-/-} mice 4 h after oral administration of 10 mg/kg selpercatinib (n = 6). *, P < 0.05; **, P < 0.01; ***, P < 0.001 compared to wild-type mice; #, P < 0.05; ##, P < 0.01; ###, P < 0.001 compared to *Abcb1a/1b*;*Abcg2*^{-/-} mice. Statistical analysis was applied after log-transformation of linear data.



Supplemental Figure 4. Tissue concentrations (A, C, E, G) and tissue-to-plasma ratios (B, D, F, H) of selpercatinib in male wild-type and *Abcb1a/1b*;*Abcg2*^{-/-} mice over 2 h after oral administration of 10 mg/kg selpercatinib with or without co-administration of elacridar. Data are given as mean ± S.D. (n = 6). *, P < 0.05; **, P < 0.01; ***, P < 0.001 compared to wild-type mice; #, P < 0.05; ##, P < 0.01; ###, P < 0.001 compared among other groups. Statistical analysis was applied after log-transformation of linear data.



Supplemental Figure 5. Tissue concentrations (A, C, E, G) and tissue-to-plasma ratios (B, D, F, H) of selpercatinib in female wild-type, *Cyp3a*^{-/-} and *Cyp3aXAV* mice over 8 h after oral administration of 10 mg/kg selpercatinib. Data are given as mean \pm S.D. (n = 6 - 7). *, $P < 0.05$; **, $P < 0.01$; ***, $P < 0.001$ compared to wild-type mice; #, $P < 0.05$; ##, $P < 0.01$; ###, $P < 0.001$ compared between *Cyp3a*^{-/-} and *Cyp3aXAV* mice. Statistical analysis was applied after log-transformation of linear data.



Supplemental Figure 6. Liver, small intestine and small intestine contents concentrations (A, C, E), liver, small intestine- and small intestine contents-to-plasma ratios (B, D, F), small intestine contents as percentage of dose (G) and small intestine contents percentage of dose-to-plasma ratio (H) of selpercatinib in female wild-type, *Cyp3a*^{-/-} and *Cyp3aXAV* mice over 8 h after oral administration of 10 mg/kg selpercatinib. Data are given as mean \pm S.D. (n = 6 - 7). *, $P < 0.05$; **, $P < 0.01$; ***, $P < 0.001$ compared to wild-type mice; #, $P < 0.05$; ##, $P < 0.01$; ###, $P < 0.001$ compared between *Cyp3a*^{-/-} and *Cyp3aXAV* mice. Statistical analysis was applied after log-transformation of linear data.

Supplemental Table 1. Pharmacokinetic parameters of selpercatinib in male wild-type, *Abcb1a/1b;Abcg2*^{-/-} and *Sico1a/1b*^{-/-} mice over 4 h after oral administration of 10 mg/kg selpercatinib.

| Parameter | Genotype | | |
|-----------------------------------|-----------------|---------------------------------------|---------------------------------|
| | Wild-type | <i>Abcb1a/1b;Abcg2</i> ^{-/-} | <i>Sico1a/1b</i> ^{-/-} |
| AUC _{0-4h} , ng/ml*h | 26,649 ± 6,360 | 30,188 ± 7,632 | 36,197 ± 5,255 |
| Fold change AUC _{0-4h} | 1.0 | 1.1 | 1.4 |
| C _{max} , ng/ml | 7,862 ± 1,814 | 8,582 ± 2,160 | 11,625 ± 1,614* |
| T _{max} , h | 1.8 ± 1.2 | 1.6 ± 1.2 | 1.7 ± 0.52 |
| C _{brain} , ng/g | 186 ± 23 | 3,454 ± 855*** | 278 ± 42** |
| Fold increase C _{brain} | 1.0 | 18.6 | 1.5 |
| Brain-to-plasma ratio | 0.030 ± 0.004 | 0.46 ± 0.04*** | 0.038 ± 0.005** |
| Fold increase ratio | 1.0 | 15.3 | 1.3 |
| C _{liver} , ng/g | 17,593 ± 3,471 | 19,077 ± 2,696 | 19,916 ± 3,174 |
| Fold increase C _{liver} | 1.0 | 1.1 | 1.1 |
| Liver-to-plasma ratio | 2.8 ± 0.4 | 2.6 ± 0.3 | 2.7 ± w0.4 |
| Fold increase ratio | 1.0 | 0.93 | 1.0 |
| C _{sic} , ng/g | 91,051 ± 22,029 | 34,929 ± 16,659* | 140,998 ± 48,076 |
| Fold change C _{sic} | 1.0 | 0.38 | 1.5 |
| SIC-to-plasma ratio | 14.9 ± 4.1 | 4.5 ± 1.8*** | 19.0 ± 5.3 |
| Fold increase ratio | 1.0 | 0.30 | 1.3 |
| C _{testis} , ng/g | 730 ± 103 | 5,726 ± 1,535*** | 1,121 ± 107** |
| Fold increase C _{testis} | 1.0 | 7.8 | 1.5 |
| Testis-to-plasma ratio | 0.12 ± 0.02 | 0.76 ± 0.13*** | 0.15 ± 0.01* |
| Fold increase ratio | 1.0 | 6.3 | 1.3 |

AUC_{0-4h}, area under plasma concentration-time curve; C_{max}, maximum concentration in plasma; T_{max}, time point (h) of maximum plasma concentration; C_{brain}, brain concentration; C_{liver}, liver concentration; SIC, small intestine contents; C_{sic}, small intestine contents concentration; C_{testis}, testis concentration;. Data are given as mean ± S.D. (n = 6-7). *, P < 0.05; **, P < 0.01; ***, P < 0.001 compared to wild-type mice. Statistical analysis was applied after log-transformation of linear data.



CHAPTER 4.4

ABCB1 AND ABCG2, BUT NOT CYP3A4 LIMIT ORAL AVAILABILITY AND BRAIN ACCUMULATION OF THE RET INHIBITOR PRALSETINIB

Yaogeng Wang¹, Rolf W. Sparidans², Sander Potters³, Maria C. Lebre ¹, Jos H. Beijnen^{1,2,4}, Alfred H. Schinkel¹

¹The Netherlands Cancer Institute, Division of Pharmacology, Plesmanlaan 121, 1066 CX Amsterdam, The Netherlands.

²Utrecht University, Faculty of Science, Department of Pharmaceutical Sciences, Division of Pharmacology, Universiteitsweg 99, 3584 CG Utrecht, The Netherlands.

³Leiden university, Faculty of Science, Leiden Academic Centre for Drug Research (LACDR), Einsteinweg 55, 2300 RA Leiden, The Netherlands.

⁴The Netherlands Cancer Institute, Department of Pharmacy & Pharmacology, Plesmanlaan 121, 1066 CX Amsterdam, The Netherlands.

ABSTRACT

Background and Purpose

Pralsetinib is an FDA-approved oral small-molecule inhibitor for treatment of rearranged during transfection (RET) proto-oncogene fusion-positive non-small cell lung cancer. We investigated how the efflux transporters ABCB1 and ABCG2, the SLCO1A/1B uptake transporters and the drug-metabolizing enzyme CYP3A influence pralsetinib pharmacokinetics.

Experimental Approach

In vitro, transepithelial pralsetinib transport was assessed. *In vivo*, pralsetinib (10 mg/kg) was administered orally to relevant genetically modified mouse models. Pralsetinib concentrations in cell medium, plasma samples and organ homogenates were measured using liquid chromatography-tandem mass spectrometry.

Key Results

Pralsetinib was efficiently transported by human (h)ABCB1 and mouse (m)Abcg2, but not hABCG2. *In vivo*, mAbcb1a/1b markedly and mAbcg2 slightly limited pralsetinib brain penetration (6.3- and 1.8-fold, respectively). Testis distribution showed similar results. *Abcb1a/1b;Abcg2*^{-/-} mice showed 1.5-fold higher plasma exposure, 23-fold increased brain penetration, and 4-fold reduced recovery of pralsetinib in the small intestinal content. mSlco1a/1b deficiency did not affect pralsetinib oral availability or tissue exposure. Oral coadministration of the ABCB1/ABCG2 inhibitor elacridar boosted pralsetinib plasma exposure (1.3-fold) and brain penetration (19.6-fold) in wild-type mice. Additionally, pralsetinib was a modest substrate of mCYP3A, but not of hCYP3A4, which did not noticeably restrict the oral availability or tissue distribution of pralsetinib.

Conclusions and Implications

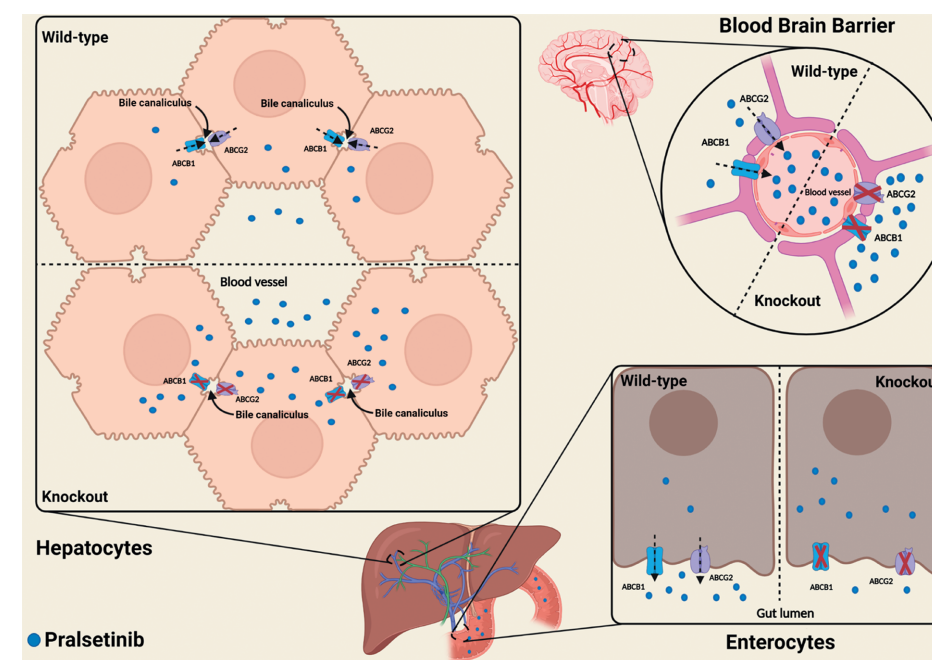
SLCO1A/1B and CYP3A4 are unlikely to affect the pharmacokinetics of pralsetinib, but ABCG2 and especially ABCB1 markedly limit its brain and testis penetration, as well as oral availability. These effects are mostly reversed by oral coadministration of the ABCB1/ABCG2 inhibitor elacridar. These insights may be useful in the further clinical development of pralsetinib.

Keywords: Pralsetinib, Cytochrome P450-3A, Oral availability, P-glycoprotein/ABCB1, BCRP/ABCG2, Brain accumulation

Chemical compounds: Cabozantinib (PubChem CID: 25102847); Elacridar (PubChem CID: 119373); Pralsetinib (PubChem CID: 129073603); Selpercatinib (PubChem CID: 134436906); Vandetanib (PubChem CID: 3081361); Zosuquidar (PubChem CID: 3036703).

Abbreviations:

ABC: ATP-binding cassette; ABCB1: ATP-binding cassette sub-family B member 1; ABCG2: ATP-binding cassette sub-family G member 2; BBB: blood-brain-barrier; BCRP: breast cancer resistance protein; BTB: blood-testis-barrier; CYP: Cytochrome P450; Cyp3aXAV: Cyp3a knockout mice with specific expression of human CYP3A4 in liver and intestine; h (as prefix): human; LC-MS/MS: liquid chromatography coupled with tandem mass spectrometry; MDCK: Madin-Darby canine kidney; m (as prefix): mouse; Multikinase inhibitors (MKIs); OATP: Organic-anion-transporting polypeptide; P-gp: P-glycoprotein; RET: Rearranged during transfection (RET) proto-oncogene; SLCO: organic anion solute carrier family; TKI: tyrosine kinase inhibitor.



1. INTRODUCTION

The rearranged during transfection (RET) proto-oncogene encodes a receptor tyrosine kinase for members of the glial cell line-derived neurotrophic factor (GDNF) family of extracellular signalling molecules^{1,2}. RET is a single-pass transmembrane protein with a typical intracellular tyrosine kinase domain and is involved in many different physiological and developmental functions. When mutated, loss of RET causes the absence of enteric ganglia from the distal colon (Hirschsprung's disease) and congenital megacolon, demonstrating an important role of RET in the development of the enteric nervous system³. RET mutations occur in most medullary thyroid cancers (MTCs)⁴, whereas RET fusions occur in various types of cancer, including 1%–2% of lung cancers, up to 10%–20% of papillary thyroid cancers, and albeit rarely, in many other solid tumors⁵. Besides, RET alterations have also been uncovered at low frequency by next generation sequencing (NGS) of large numbers of patient tumors in other tumor types, including ovarian epithelial carcinoma and salivary gland adenocarcinoma⁶.

Although some multikinase inhibitors (MKIs) with nonselective RET inhibitory activity have been available to treat RET-altered cancers, patients have derived only modest benefit from these so far, with unexpected side-effects⁷. For example, cabozantinib was used for RET-mutant MTCs⁸ and RET fusion-positive lung cancers⁹ and vandetanib for advanced or metastatic medullary thyroid cancer¹⁰ and advanced non-small-cell lung cancer¹¹. However in 2020, the FDA approved two highly selective, ATP-competitive small-molecule RET inhibitors, selpercatinib (LOXO-292, RETEVMO, Eli Lilly)¹² and pralsetinib (Blu-667, GAVRETO, Roche)¹³. Both can be applied for the treatment of adults with metastatic RET-fusion positive non-small cell lung cancer (NSCLC), yielding higher objective response rates (ORRs) of 68% and 58%, respectively, compared to other multikinase inhibitors, such as cabozantinib therapy with an ORR of only 28%^{14,15}. According to the guidelines, the recommended dose in adults is 160 mg twice daily for selpercatinib¹² and 400 mg once daily for pralsetinib¹³. Besides, they were designed to have high bioavailability and significant central nervous system (CNS) penetration, which may induce more efficient therapy for brain metastasis occurring in NSCLC patients. However, compared to selpercatinib, the information on pralsetinib pharmacokinetic properties is still limited.

Drug absorption, distribution, metabolism and excretion (ADME) can be influenced by certain efflux and influx transporters such as the ATP-binding cassette (ABC) transporters and the organic anion transporting polypeptides (OATPs). They can thus influence the pharmacokinetics, and hence the safety and efficacy profiles of specific drugs^{16–18}. Considering the high expression of the ABC drug efflux transporters P-glycoprotein (P-gp; ABCB1) and breast cancer resistance protein (BCRP; ABCG2) at the apical membrane of enterocytes, hepatocytes and renal tubular epithelial cells, they could potentially limit intestinal absorption of their substrates or mediate their direct intestinal, hepatobiliary or renal excretion. Moreover, ABCB1 and ABCG2 are also

highly expressed in brain capillary endothelial cells of the blood-brain barrier (BBB), where their efflux capacity can protect the central nervous system (CNS) from exogenous toxic compounds¹⁹. Conversely, limited exposure of the brain to anticancer drugs because of these transporters may reduce their therapeutic efficacy, especially against brain metastases^{20–23}. In addition, ABC transporters are also expressed in many tumor types, potentially mediating multidrug resistance against anticancer drugs¹⁹. As pralsetinib targets different tumor types with RET fusions that may develop brain metastases (especially lung cancer), it is important to know whether pralsetinib is transported by ABCB1 and/or ABCG2 *in vivo*, potentially affecting its oral availability and brain accumulation.

Organic anion-transporting polypeptides (OATPs), encoded by SLCO genes, are sodium-independent transmembrane uptake transporters for endogenous and exogenous compounds like hormones, toxins, and numerous drugs²⁴. The SLCO1A/1B proteins are of particular interest because of their broad substrate specificities and their high expression in the liver where they may affect oral availability and liver disposition of certain drugs^{25–29}. Thus, we wanted to know whether pralsetinib is a substrate of SLCO1A/1B and whether this can influence pralsetinib oral availability and organ distribution.

Besides these transporters, the multidrug-metabolizing Cytochrome P450 3A (CYP3A) enzyme complex is responsible for most Phase I drug metabolism. CYP3A4 is the most abundant CYP enzyme in human liver, and involved in the metabolism of about 50% of the currently used drugs, resulting in drug inactivation or sometimes also activation^{30–32}. CYP3A enzymes have high variation in activity between, but also within individuals due to drug–drug interactions and genetic polymorphisms. This can cause oral availability and plasma exposure differences among patients, which may dramatically influence their therapeutic efficacy and toxicity.

The primary aim of this study was to clarify the *in vivo* roles of ABCB1, ABCG2 and SLCO1A/1B (OATP1A/1B) as well as CYP3A in modulating oral availability and/or brain accumulation of pralsetinib by transepithelial pralsetinib transport assay *in vitro* and using appropriate genetically modified mouse models. We also studied the effect of co-administration of the ABCB1 and ABCG2 inhibitor elacridar on pralsetinib overall exposure and tissue distribution.

2. MATERIALS AND METHODS

2.1 Cell lines and transport assays

Polarized dog kidney-derived Madin-Darby Canine Kidney (MDCK-II) cells and their stably transduced subclones expressing human (h) ABCB1, hABCG2, or mouse (m) Abcg2 cDNA were used and cultured as described^{33,34}. Transepithelial transport assays were performed on microporous polycarbonate membrane filters (3.0 µm pore size, 12 mm diameter, Transwell

3414). Parental and variant subclones were seeded at a density of 2.5×10^5 cells per well and cultured for 3 days to form an intact monolayer. Membrane tightness was assessed by measurement of transepithelial electrical resistance (TEER) using an Epithelial Volt-Ohm Meter (Merck Millipore, Darmstadt, Germany) before and after the transport phase.

For inhibition experiments, 5 μ M zosuquidar (ABCB1 inhibitor) and/or 5 μ M Ko143 (ABCG2/Abcg2 inhibitor) were used during the transport experiments. Cells were pre-incubated with one or a combination of the inhibitors for 1 h in both apical and basolateral compartments. The transport phase was started ($t = 0$) by replacing the medium in either the apical or the basolateral compartment with fresh DMEM including 10% (v/v) fetal bovine serum (FBS) and pralsetinib at 5 μ M, as well as the appropriate inhibitor(s). Plates then were kept at 37°C in 5% (v/v) CO₂ during the experiment, and 50 μ l aliquots were taken from the acceptor compartment at 1, 2, 4, and 8 h, and stored at -30°C until LC-MS/MS measurement of the pralsetinib concentrations. Experiments were performed in triplicate and the mean transport is shown in the figure. Active transport was expressed using the transport ratio r , i.e., the amount of apically directed drug transport divided by basolaterally directed drug translocation after 8 hours (h).

2.2 Animals

Mice were housed and handled according to institutional guidelines complying with Dutch and EU legislation. All experimental animal protocols were evaluated and approved by the institutional animal care and use committee. Wild-type (both female and male), *Abcb1a/1b*^{-/-} (male), *Abcg2*^{-/-} (male), *Abcb1a/1b;Abcg2*^{-/-} (male), *Slco1a/1b*^{-/-} (male), *Cyp3a*^{-/-} (female) and *Cyp3aXAV* (female) mice, all of a >99% FVB genetic background, were used between 9 and 16 weeks of age. Animals were kept in a temperature-controlled environment with 12-h light and 12-h dark cycle and they received a standard diet (Transbreed, SDS Diets, Technilab – BMI) and acidified water *ad libitum*.

2.3 Drug solutions

For oral administration, pralsetinib was dissolved in dimethyl sulfoxide (DMSO) at a concentration of 50 mg/ml and further diluted with polysorbate 20, absolute ethanol and 5% glucose water, resulting in a final working solution of 1 mg/ml in [DMSO : Polysorbate 20 : absolute ethanol : 5% glucose water = 2 : 15 : 15 : 68, (v/v/v/v)]. Elacridar hydrochloride was dissolved in DMSO (53 mg/ml) in order to get 50 mg elacridar base per ml DMSO. The stock solution was further diluted with a mixture of polysorbate 20, absolute ethanol and 5% glucose water to yield an elacridar concentration of 5 mg/ml in [DMSO : Polysorbate 20 : absolute ethanol : 5% glucose water = 10 : 15 : 15 : 60, (v/v/v/v)]. All dosing solutions were prepared freshly on the day of the experiment.

2.4 Plasma and organ pharmacokinetics of pralsetinib in mice

In order to minimize variation in absorption because of oral administration, mice were first fasted for 3 h before pralsetinib (10 mg/kg) was administered orally, using a blunt-ended needle. For

the 4 h transporter pilot experiments, tail vein blood samples were collected at 0.125, 0.25, 0.5, 1, and 2 h time points after oral administration, respectively. For the 2 h transporter main experiments and elacridar inhibition experiments, tail vein blood samples were collected at 0.125, 0.25, 0.5, and 1 h time points after oral administration, respectively. For the 8 h CYP3A experiments, tail vein blood sampling was performed at 0.25, 0.5, 1, 2, and 4 h, respectively. Blood sample (~50 μ l) collection was performed using microvettes containing dipotassium-EDTA. At the last time point in each experiment (2, 4, or 8 h), mice were anesthetized with 5% isoflurane and blood was collected by cardiac puncture in Eppendorf tubes containing heparin as an anticoagulant. The mice were then sacrificed by cervical dislocation and brain, liver, kidney, lung, small intestine (SI), small intestine contents (SIC) and testis were rapidly removed. Plasma was isolated from the blood by centrifugation at 9,000g for 6 min at 4°C, and the plasma fraction was collected and stored at -30°C until analysis. Organs were homogenized with 4% (w/v) bovine serum albumin and stored at -30°C until analysis. The relative tissue-to-plasma ratio after oral administration was calculated by determining the pralsetinib tissue concentration relative to the pralsetinib plasma concentration at the last time point.

2.5 LC-MS/MS analysis

Pralsetinib concentrations in DMEM/FBS (9/1, v/v) (Invitrogen, Waltham, MA, USA) cell culture medium, plasma samples, and organ homogenates were determined using a validated liquid chromatography-tandem mass spectrometry assay as described³⁵.

2.6 Materials

Pralsetinib was purchased from MedChemExpress (Monmouth Junction, NJ, USA). Zosuquidar and elacridar HCl were obtained from Sequoia Research Products (Pangbourne, UK). Ko143 was from Tocris Bioscience (Bristol, UK). Bovine Serum Albumin (BSA) Fraction V was obtained from Roche Diagnostics GmbH (Mannheim, Germany). Glucose water 5% w/v was from B. Braun Medical Supplies (Melsungen, Germany). Isoflurane was purchased from Pharmachemie (Haarlem, The Netherlands), heparin (5000 IU ml⁻¹) was from Leo Pharma (Breda, The Netherlands). All other chemicals used in the pralsetinib detection assay were described before³⁵. All other chemicals and reagents were obtained from Sigma-Aldrich (Steinheim, Germany).

2.7 Data and Statistical analysis

Pharmacokinetic parameters were calculated by non-compartmental methods using the PK solver software³⁶. The area under the plasma concentration-time curve (AUC) was calculated using the trapezoidal rule, without extrapolating to infinity. The peak plasma concentration (C_{max}) and the time of maximum plasma concentration (T_{max}) were estimated from the original (individual mouse) data. One-way analysis of variance (ANOVA) was used when multiple groups were compared and the Bonferroni *post hoc* correction was used to accommodate multiple testing. The two-sided unpaired Student's t-test was used when treatments or differences

between two specific groups were compared using the software GraphPad Prism7 (GraphPad Software, La Jolla, CA, USA). All the data were log-transformed before statistical tests were applied. Differences were considered statistically significant when $P < 0.05$. All data are presented as mean \pm SD.

3. RESULTS

3.1 *In vitro* transport of pralsetinib

Transepithelial drug transport was tested by using polarized monolayers of Madin-Darby Canine Kidney (MDCK-II) parental cells and various ABC transporter-overexpressing derivative cell lines. No significant transport of pralsetinib (5 μ M) by the low-level endogenous canine *Abcb1* present in the parental MDCK-II cells³⁷ was observed either without or with ABCB1 inhibitor zosuquidar ($r = 1.2$, Figure 1A and $r = 1.2$, Figure 1B). In cells overexpressing hABCB1, there was strong apically directed transport of pralsetinib ($r = 19$, Figure 1C), which could be completely inhibited by zosuquidar ($r = 1.0$, Figure 1D).

Zosuquidar was added to inhibit any possible contribution of endogenous canine *Abcb1* in subsequent experiments with MDCK-II cells overexpressing hABCG2 and mAbcg2. The ABCG2 inhibitor Ko143 was used to inhibit the transport activity of hABCG2 and mAbcg2. In hABCG2-overexpressing MDCK-II cells, there was no detectable apically directed transport of pralsetinib in the absence or presence of Ko143 ($r = 1.0$, Figure 1E; $r = 0.9$, Figure 1F). We also observed marked apically directed transport of pralsetinib in cells overexpressing mouse *Abcg2* ($r = 7.1$) and this was virtually abrogated by Ko143 ($r = 1.0$, Figure 1G and H).

Pralsetinib thus appears to be efficiently transported by hABCB1 and mAbcg2, but not by hABCG2 and canine ABCB1 *in vitro*.

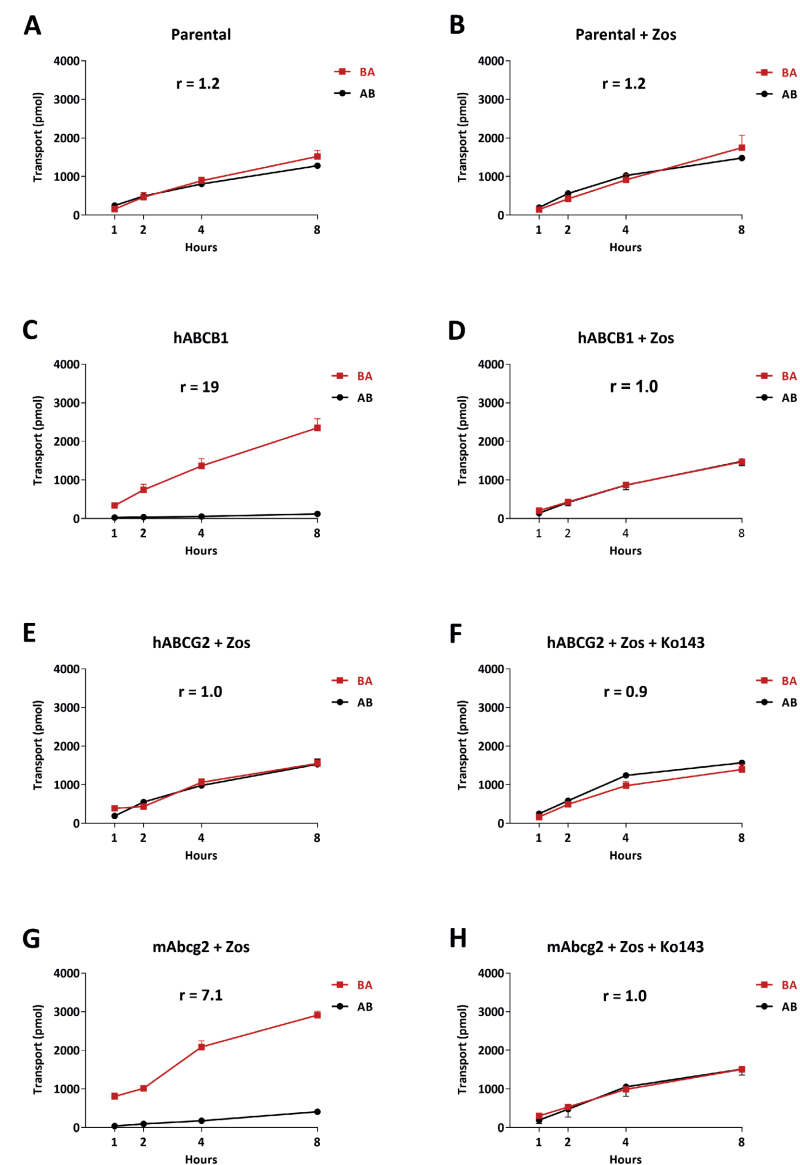


Figure 1. Transepithelial transport of pralsetinib (5 μ M) assessed in MDCK-II cells either non-transduced (A, B), transduced with hABCB1 (C, D), hABCG2 (E, F) or mAbcg2 (G, H) cDNA. At $t = 0$ h, drug was applied in the donor compartment and the concentrations in the acceptor compartment at $t = 1, 2, 4$ and 8 h were measured and plotted as pralsetinib transport (pmol) in the graph ($n = 3$). B, D–H: Zosuquidar (Zos, 5 μ M) was applied to inhibit human and/or endogenous canine ABCB1. F and H: the ABCG2 inhibitor Ko143 (5 μ M) was applied to inhibit ABCG2/Abcg2-mediated transport. r , relative transport ratio. AB (\bullet), translocation from the apical to the basolateral compartment; BA (\blacksquare), translocation from the basolateral to the apical compartment. Points, mean; bars, S.D.

3.2 Impact of ABCB1, ABCG2 and SLCO1A/1B on pralsetinib plasma pharmacokinetics and tissue disposition

Pralsetinib is orally administered in the clinic, so we performed a 4 h oral pharmacokinetic pilot study in male wild-type, *Abcb1a/1b;Abcg2*^{-/-} and *Slco1a/1b*^{-/-} mice using 10 mg/kg pralsetinib to study the possible impact of ABCB1A/1B, ABCG2 and OATP1A/1B on oral bioavailability and tissue disposition of pralsetinib. As shown in Supplemental figure 2 and Supplemental table 1, even though *Abcb1a/1b;Abcg2*^{-/-} mice had slightly higher plasma exposure of pralsetinib compared to wild-type mice, there was no statistically significant difference in AUC or C_{max} of pralsetinib between them. However, the last time point (4 h) in *Abcb1a/1b;Abcg2*^{-/-} mice did show a significantly higher plasma concentration, suggesting a somewhat delayed pralsetinib elimination in this strain. It took around two hours to reach the maximum plasma concentration of pralsetinib for these two mouse strains (average C_{max} in wild-type and *Abcb1a/1b;Abcg2*^{-/-} mice are 6202 ng/ml and 6962 ng/ml, respectively), indicating that absorption of this compound is not very rapid as compared to many other TKI drugs in mice³⁸⁻⁴¹. Notably, the T_{max} and C_{max} results obtained in our mouse models are of the same order of magnitude as those observed in patients (T_{max} ranging from 2 to 4 hours with average C_{max} 2830 ng/ml).

Brain, liver, kidney, small intestine (SI), small intestine contents (SIC), testis, lung and spleen concentrations of pralsetinib 4 h after oral administration were also assessed. The pralsetinib brain-to-plasma ratio (0.022) in wild-type mice was very low, suggesting poor brain penetration of pralsetinib (Supplemental table 1). The brain concentration and brain-to-plasma ratio in *Abcb1a/1b;Abcg2*^{-/-} mice were increased by 44.9-fold and 32.3-fold, respectively, compared to those in wild-type mice (Supplemental figure 3 and Supplemental table 1). *Slco1a/1b*^{-/-} mice also showed somewhat enhanced brain concentrations and brain-to-plasma ratios by 1.7-fold and 1.5-fold, respectively. Likewise in testis, the testis-to-plasma ratio was low in wild-type mice (0.13), and combined *Abcb1* and *Abcg2* deficiency could increase the ratio to 0.71 (5.5-fold increase).

Tissue-to-plasma ratios in other organs were not meaningfully altered among the three strains (Supplemental figure 4 and Supplemental figure 5). However, for the small intestine content (SIC) matrix, we found that the percentage of dose recovered was markedly decreased in *Abcb1a/1b;Abcg2*^{-/-} mice compared to wild-type mice (0.11, 9-fold Supplemental figure 5E and Supplemental table 1). These results may indicate that pralsetinib was absorbed more rapidly across the gut wall or that there was reduced hepatobiliary excretion of the absorbed pralsetinib in the absence of both *Abcb1a/1b* and *Abcg2*.

In wild-type mice most tissue-to-plasma ratios for liver, kidney, and small intestine (all >1) were far higher than those observed for the brain (0.022) and even testis (0.13), suggesting the strong impact of the blood-brain-barrier (BBB) and blood-testis-barrier (BTB) on reducing tissue accumulation of pralsetinib. We did not observe any sign of acute spontaneous toxicity

of pralsetinib in any of the three mouse strains, even though there was a dramatic increase in pralsetinib brain accumulation in *Abcb1a/1b;Abcg2*^{-/-} mice.

As shown in Supplemental figure 2 and Supplemental table 1, the pralsetinib plasma AUC_{0-4h}, C_{max} and T_{max} were not significantly different between wild-type and *Slco1a/1b*^{-/-} mice. With respect to tissues, even though the deficiency of *mSlco1a/1b* slightly increased brain-to-plasma ratio (from 0.022 to 0.034), lung-to-plasma ratio, and kidney-to-plasma ratio, and decreased liver-to-plasma ratio (from 3.4 to 2.7), the changes were limited. We also did not find any significant differences in pralsetinib percentage of dose recovered in SIC between wild-type and *Slco1a/1b*^{-/-} mice (Supplemental figure 3, 4 and 5). Taken together, these results indicate that pralsetinib pharmacokinetics is not substantially influenced by SLCO1A/1B activity.

3.3 ABCB1 and ABCG2 limit pralsetinib brain and testis exposure

The separate and combined functions of *Abcb1a/1b* and *Abcg2* in modulating oral bioavailability and tissue distribution of pralsetinib were subsequently studied by administering pralsetinib (10 mg/kg) orally to wild-type, *Abcb1a/1b*^{-/-}, *Abcg2*^{-/-}, and *Abcb1a/1b;Abcg2*^{-/-} mice. The experiment was terminated at 2 h, when pralsetinib plasma levels were still close to the C_{max}. As shown in Figure 2 and Table 1, single deficiency of either *mAbcb1* or *mAbcg2* resulted in higher pralsetinib plasma exposure, with the plasma AUC_{0-2h} increased in both *Abcb1a/1b*^{-/-} (1.5-fold, P < 0.01) and *Abcg2*^{-/-} (1.2-fold, albeit not statistically significant) mice (Table 1). Such increase also showed up in combination *Abcb1a/1b;Abcg2*^{-/-} mice, 1.6-fold compared to wild-type mice (P < 0.01). *Abcb1a/1b* activity appeared to be the main factor limiting plasma exposure.

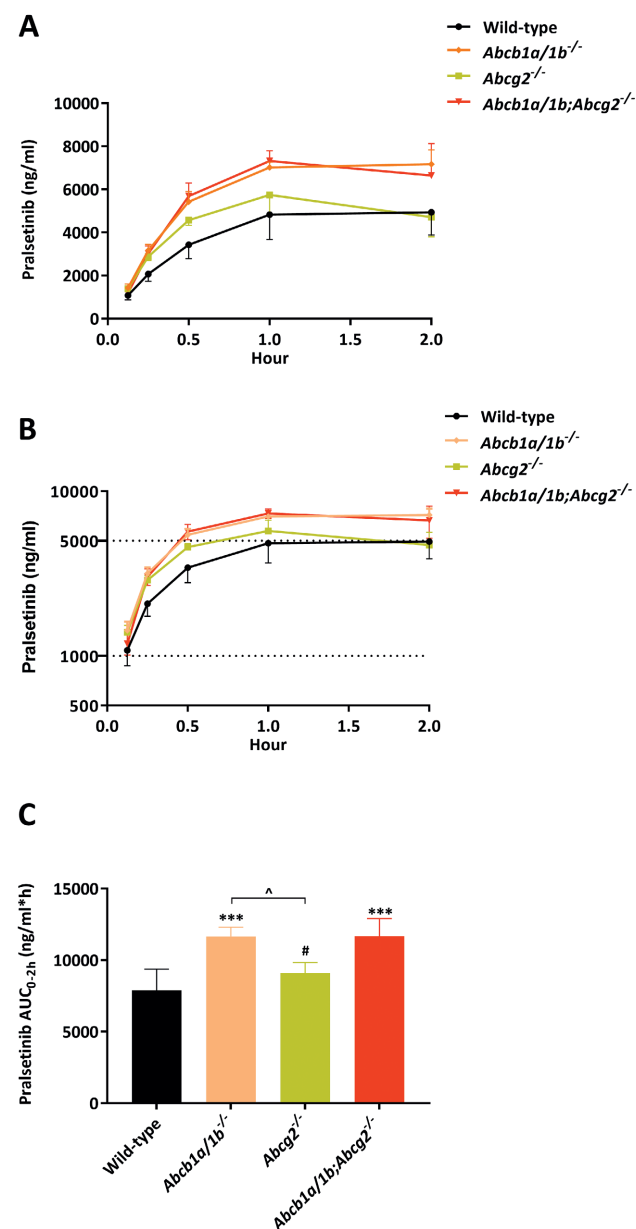


Figure 2. Plasma concentration-time curves (A), semi-log plot of plasma concentration-time curves (B) and plasma AUC_{0-2h} (C) of pralsetinib in male wild-type, *Abcb1a/1b*^{-/-}, *Abcg2*^{-/-} and *Abcb1a/1b;Abcg2*^{-/-} mice over 2 h after oral administration of 10 mg/kg pralsetinib. Data are given as mean ± S.D. (n = 6). *, P < 0.05; **, P < 0.01; ***, P < 0.001 compared to wild-type mice; #, P < 0.05; ##, P < 0.01; ###, P < 0.001 compared to *Abcb1a/1b;Abcg2*^{-/-} mice. Statistical analysis was applied after log-transformation of linear data.

Pralsetinib brain concentrations in *Abcb1a/1b*^{-/-} and *Abcb1a/1b;Abcg2*^{-/-} mice were profoundly increased by 9.5-fold and 30.4-fold respectively, and only slightly increased by 1.8-fold in *Abcg2*^{-/-} mice compared to wild-type mice. The brain-to-plasma ratio of pralsetinib was again very low (0.040) in wild-type mice, but could be increased to 0.25 (6.3-fold) due to single mAbcb1 deficiency and further up to 0.92 (23-fold) by combined mAbcb1 and mAbcg2 deficiency (Figure 3A-B; Table 1). Again, this increase was limited in mAbcg2-deficient mice (0.072, 1.8-fold). These results reveal that *Abcb1a/1b* and *Abcg2* can both restrict pralsetinib brain penetration, although *Abcb1a/1b* is the dominant player. In the absence of *Abcb1a/1b* activity, *Abcg2* noticeably limits pralsetinib brain penetration (by about 3.7-fold), while when *Abcg2* is absent, *Abcb1a/1b* could still take over almost the whole transport function. Qualitatively similar results were obtained for pralsetinib testis penetration, although the wild-type testis-to-plasma ratio was substantially higher (0.060), and the relative increases in ratios in *Abcb1a/1b*^{-/-} (4.5-fold) and *Abcb1a/1b;Abcg2*^{-/-} (7.8-fold) mice were more modest than observed for brain (Figure 3C-D; Table 1). These data indicate that *Abcb1a/1b* and, to a lesser extent, *Abcg2* can strongly reduce the brain accumulation of pralsetinib, while testis accumulation was more modestly affected.

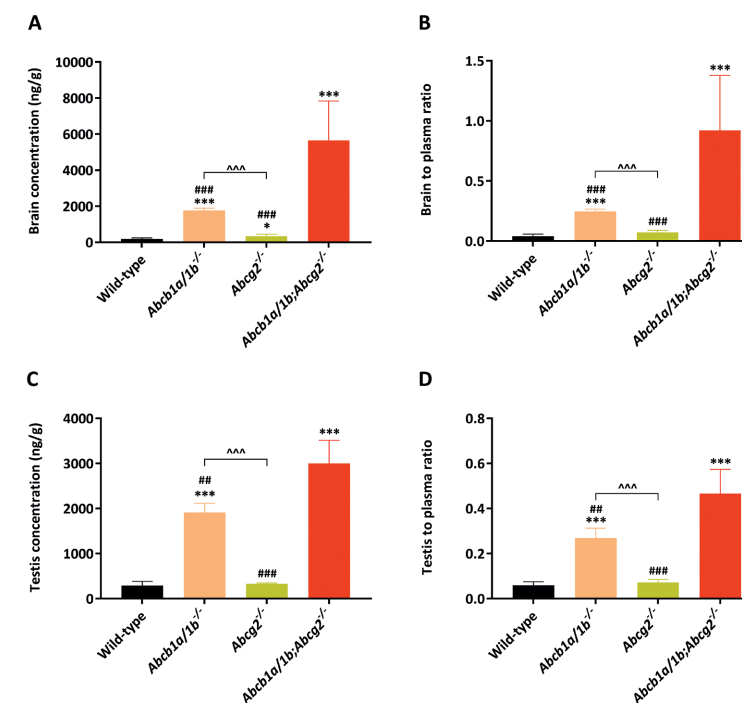


Figure 3. Brain and testis concentrations (A and C) and tissue-to-plasma ratios (B and D) of pralsetinib in male wild-type, *Abcb1a/1b*^{-/-}, *Abcg2*^{-/-} and *Abcb1a/1b;Abcg2*^{-/-} mice over 2 h after oral administration of 10 mg/kg pralsetinib. Data are given as mean ± S.D. (n = 6). *, P < 0.05; **, P < 0.01; ***, P < 0.001 compared to wild-type mice; #, P < 0.05; ##, P < 0.01; ###, P < 0.001 compared to *Abcb1a/1b;Abcg2*^{-/-} mice. Statistical analysis was applied after log-transformation of linear data.

With respect to other organs, we observed lower SI-to-plasma ratios in *Abcb1a/1b*^{-/-} and *Abcb1a/1b/Abcg2*^{-/-} mice (Supplemental figure 7B), which did not show up in *Abcg2*^{-/-} mice. As small intestine often mainly reflects the small intestine contents concentrations, we also analyzed related parameters of the SIC. Indeed, the SIC percentage of total dose values were markedly reduced from 12.0% to 3.2% in *Abcb1a/1b*^{-/-} mice (0.27-fold) and to 2.9% in *Abcb1a/1b;Abcg2*^{-/-} mice (0.24-fold) compared to wild-type mice, whereas this decrease was much less in *Abcg2*^{-/-} mice (7.1%, 0.59-fold) (Supplemental figure 7 and Table 1). These findings were consistent with our pilot results. They may indicate a more rapid and extensive absorption of pralsetinib across the intestinal wall in the absence of intestinal *Abcb1a/1b* activity (essentially because of loss of an intestinal excretion process), or reduced hepatobiliary recirculation of absorbed pralsetinib through biliary excretion mediated by *Abcb1a/1b* in the bile canaliculi of the liver, or a combination of both processes. No meaningful differences were found in tissue-to-plasma ratios of other tissues (Supplemental figure 6).

Table 1. Plasma and organ pharmacokinetic parameters of pralsetinib in male wild-type, *Abcb1a/1b*^{-/-}, *Abcg2*^{-/-} and *Abcb1a/1b;Abcg2*^{-/-} mice over 2 h after oral administration of 10 mg/kg pralsetinib.

| Parameter | Genotype | | | |
|----------------------------------|---------------|---------------------------------|-----------------------------|---------------------------------------|
| | Wild-type | <i>Abcb1a/1b</i> ^{-/-} | <i>Abcg2</i> ^{-/-} | <i>Abcb1a/1b;Abcg2</i> ^{-/-} |
| AUC _{0-2h} , ng/ml.h | 7898 ± 1469 | 11657 ± 643*** | 9094 ± 747# | 11663 ± 1248*** |
| Fold change AUC _{0-2h} | 1.0 | 1.5 | 1.2 | 1.5 |
| C _{max} , ng/ml | 5181 ± 1117 | 7301 ± 520** | 5890 ± 833# | 7510 ± 631*** |
| T _{max} , h | 1.5 ± 0.55 | 1.7 ± 0.52 | 1.3 ± 0.61 | 1.3 ± 0.52 |
| C _{brain} , ng/g | 186 ± 62 | 1774 ± 125***### | 339 ± 107*### | 5658 ± 2176*** |
| Fold change C _{brain} | 1.0 | 9.5 | 1.8 | 30.4 |
| Brain-to-plasma ratio | 0.040 ± 0.018 | 0.25 ± 0.017***### | 0.072 ± 0.017### | 0.92 ± 0.46*** |
| Fold change ratio | 1.0 | 6.3 | 1.8 | 23 |
| C _{liver} , ng/g | 16558 ± 1976 | 23385 ± 3547** | 18702 ± 2187# | 24295 ± 3712*** |
| Fold increase C _{liver} | 1.0 | 1.4 | 1.1 | 1.5 |
| Liver-to-plasma ratio | 3.4 ± 0.47 | 3.3 ± 0.50 | 4.1 ± 1.3 | 3.8 ± 0.75 |
| Fold change ratio | 1.0 | 0.97 | 1.2 | 1.1 |
| C _{si} , ng/g | 20412 ± 2964 | 14214 ± 2372 | 20994 ± 5971 | 14344 ± 4333 |
| Fold change C _{si} | 1.0 | 0.70 | 1.0 | 0.70 |
| SI-to-plasma ratio | 4.3 ± 1.2 | 2.0 ± 0.23** | 4.8 ± 2.3## | 2.2 ± 0.70** |
| Fold change ratio | 1.0 | 0.47 | 1.1 | 0.51 |
| SIC percentage of dose, % | 12.0 ± 3.8 | 3.2 ± 1.5*** | 7.1 ± 1.9## | 2.9 ± 1.3*** |
| Fold change ratio | 1.0 | 0.27 | 0.59 | 0.24 |
| C _{testis} , ng/g | 287 ± 95 | 1910 ± 206***## | 327 ± 23### | 2997 ± 515*** |
| Fold change C _{testis} | 1.0 | 6.7 | 1.1 | 10.4 |
| Testis-to-plasma ratio | 0.060 ± 0.016 | 0.27 ± 0.044***## | 0.071 ± 0.014### | 0.47 ± 0.11*** |
| Fold change ratio | 1.0 | 4.5 | 1.2 | 7.8 |

Data are given as mean ± S.D. (n = 6). AUC_{0-2h}, area under the plasma concentration-time curve; C_{max}, maximum concentration in plasma; T_{max}, time point (h) of maximum plasma concentration; C_{brain}, brain concentration; C_{liver}, liver concentration; SI, small intestine (tissue); C_{si}, small intestine tissue concentration; SIC, small intestine contents; C_{testis}, testis concentration; *, P < 0.05; **, P < 0.01; ***, P < 0.001 compared to wild-type mice; #, P < 0.05; ##, P < 0.01; ###, P < 0.001 compared to *Abcb1a/1b;Abcg2*^{-/-} mice. Statistical analysis was applied after log-transformation of linear data.

3.4 Effect of the dual ABCB1 and ABCG 2 inhibitor elacridar on pralsetinib brain accumulation

As pralsetinib penetration into wild-type brain was markedly restricted by ABCB1 and ABCG2 activity, we investigated to what extent the dual ABCB1 and ABCG2 inhibitor elacridar could increase brain accumulation of pralsetinib, and whether it would influence pralsetinib disposition and distribution in other tissues. This approach may potentially be used for enhancing pralsetinib brain accumulation and therapeutic efficacy. Considering that the elacridar plasma exposure peak occurs approximately 4 h after oral administration in mice, elacridar (50 mg/kg) or vehicle was administered orally 2 h prior to oral pralsetinib administration (10 mg/kg) to wild-type and *Abcb1a/1b;Abcg2*^{-/-} mice. Plasma and brain pralsetinib levels were assessed 2 hours later, at which time point pralsetinib plasma concentrations were still high, making the impact of the BBB transporters especially relevant. When elacridar was absent, the pralsetinib plasma AUC_{0-2h} was significantly (1.5-fold) increased in *Abcb1a/1b;Abcg2*^{-/-} mice compared to wild-type mice, consistent with preceding experiments. Pre-treatment with elacridar increased plasma pralsetinib AUC_{0-2h} by 1.3-fold in wild-type mice, and did not alter exposure in *Abcb1a/1b;Abcg2*^{-/-} mice (Figure 4 and Table 2).

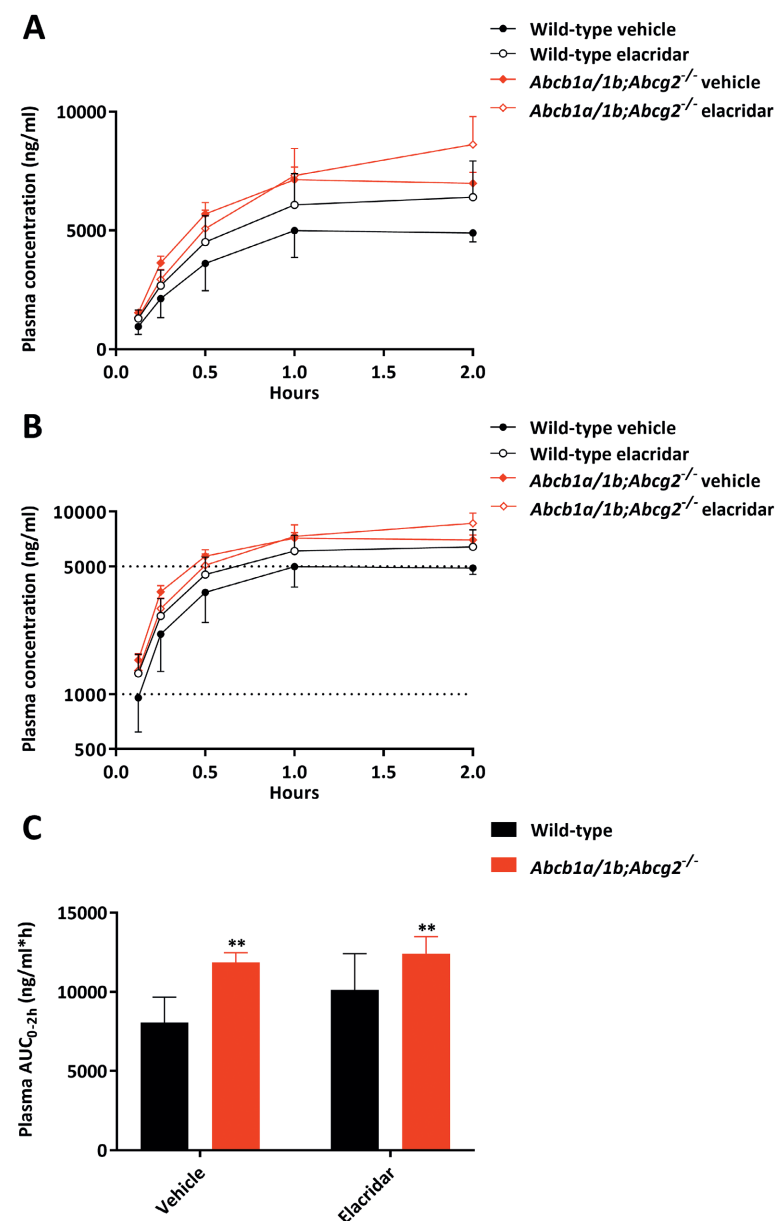


Figure 4. Plasma concentration-time curves (A), semi-log plot of plasma concentration-time curves (B) and plasma AUC_{0-2h} (C) of pralsetinib in male wild-type and *Abcb1a/1b;Abcg2^{-/-}* mice over 2 h after oral administration of 10 mg/kg pralsetinib with or without co-administration of elacridar. Data are given as mean \pm S.D. (n = 6). *, $P < 0.05$; **, $P < 0.01$; ***, $P < 0.001$ compared to wild-type mice. Statistical analysis was applied after log-transformation of linear data.

With respect to tissues, in the absence of elacridar, the brain concentration and brain-to-plasma ratio of pralsetinib was 45.9-fold and 31.9-fold higher in *Abcb1a/1b;Abcg2^{-/-}* than in wild-type mice, respectively ($P < 0.001$), (Figure 5A-B and Table 2). Elacridar pre-treatment markedly increased these parameters in wild-type mice by 26.2- and 19.6-fold, respectively ($P < 0.001$), yielding a level similar to that in elacridar pre-treated *Abcb1a/1b;Abcg2^{-/-}* mice (35.5- and 20.0-fold, respectively). While the data indicate extensive inhibition of *Abcb1a/1b* and *Abcg2* activity in the BBB by elacridar, the brain penetration in both elacridar co-administration groups was somewhat (about 40%) lower than that in vehicle-treated *Abcb1a/1b;Abcg2^{-/-}* mice. This suggested a modest additional effect of elacridar, somewhat lowering brain penetration of pralsetinib independent of the ABC transporters. Unlike for brain, for testis the enhanced pralsetinib penetration by elacridar only showed up in wild-type mice, suggesting full inhibition of ABC transporter functions in the BTB by elacridar (Figure 5C-D and Table 2). Relative drug penetration in most other tissues (liver, kidney, lung and spleen) was not meaningfully altered by elacridar in wild-type or *Abcb1a/1b;Abcg2^{-/-}* mice (Supplemental figure 8 B, D, F and H).

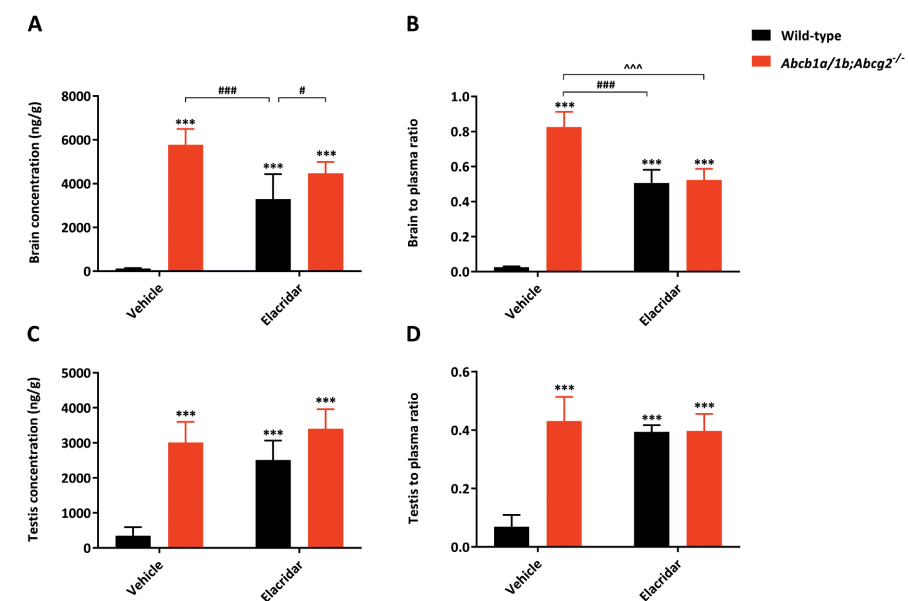


Figure 5. Brain and testis concentrations (A and C) and tissue-to-plasma ratios (B and D) of pralsetinib in male wild-type and *Abcb1a/1b;Abcg2^{-/-}* mice over 2 h after oral administration of 10 mg/kg pralsetinib with or without co-administration of elacridar. Data are given as mean \pm S.D. (n = 6). *, $P < 0.05$; **, $P < 0.01$; ***, $P < 0.001$ compared to wild-type mice; #, $P < 0.05$; ##, $P < 0.01$; ###, $P < 0.001$ compared to elacridar-treated wild-type mice; ^, $P < 0.05$; ^^, $P < 0.01$; ^^, $P < 0.001$ compared between vehicle-treated *Abcb1a/1b;Abcg2^{-/-}* and elacridar-treated *Abcb1a/1b;Abcg2^{-/-}* mice. Statistical analysis was applied after log-transformation of linear data.

In accordance with our previous results, there was a large amount of pralsetinib in the intestinal lumen at 2 h in wild-type mice, with 20.2% of dose recovered in SI+SIC. This was markedly reduced to 8.4% upon elacridar co-administration (Supplemental figure 9). Even though there was a small difference in recovered pralsetinib between *Abcb1a/1b;Abcg2^{-/-}* mice with elacridar (11.7%) compared with *Abcb1a/1b;Abcg2^{-/-}* mice without elacridar (7.5%), the results became virtually identical after correction for the plasma concentrations (Supplemental figure 9D). Taken together, these results suggest that the mouse *Abcb1a/1b* and *Abcg2* in the small intestine and/or the bile canaliculi of the liver were completely inhibited by the elacridar treatment, resulting in decreased recovery of pralsetinib in the small intestine contents.

Table 2. Plasma and organ pharmacokinetic parameters of pralsetinib in male wild-type and *Abcb1a/1b;Abcg2^{-/-}* mice over 2 h after oral administration of 10 mg/kg pralsetinib with or without inhibitor elacridar.

| Parameter | Genotype/Groups | | | |
|-----------------------------------|-----------------|--------------------------------------|-----------------|--------------------------------------|
| | Vehicle | | Elacridar | |
| | Wild-type | <i>Abcb1a/1b;Abcg2^{-/-}</i> | Wild-type | <i>Abcb1a/1b;Abcg2^{-/-}</i> |
| AUC _{0-2h} , ng/ml.h | 8067 ± 1605 | 11860 ± 608** | 10119 ± 2299 | 12416 ± 1074** |
| Fold change AUC _{0-2h} | 1.0 | 1.5 | 1.3 | 1.5 |
| C _{max} , ng/ml | 5297 ± 816 | 7360 ± 256** | 6432 ± 1519 | 8845 ± 773***## |
| T _{max} , h | 1.5 ± 0.55 | 1.3 ± 0.5 | 1.8 ± 0.41 | 1.8 ± 0.41 |
| C _{brain} , ng/g | 126 ± 20 | 5778 ± 722***### | 3300 ± 1136*** | 4474 ± 517***# |
| Fold increase C _{brain} | 1.0 | 45.9 | 26.2 | 35.5 |
| Brain-to-plasma ratio | 0.026 ± 0.0038 | 0.83 ± 0.086***### | 0.51 ± 0.075*** | 0.52 ± 0.063***^^^ |
| Fold increase ratio | 1.0 | 31.9 | 19.6 | 20.0 |
| C _{liver} , ng/g | 19030 ± 1412 | 23756 ± 3170* | 21837 ± 4105 | 25303 ± 1378** |
| Fold increase C _{liver} | 1.0 | 1.2 | 1.1 | 1.3 |
| Liver-to-plasma ratio | 3.9 ± 0.13 | 3.4 ± 0.30 | 3.5 ± 0.29 | 3.0 ± 0.49*** |
| Fold change ratio | 1.0 | 0.87 | 0.90 | 0.77 |
| SI + SIC percentage of dose, % | 20.2 ± 2.2 | 7.5 ± 2.7*** | 8.4 ± 1.8*** | 11.7 ± 1.3***^^ |
| Fold change ratio | 1.0 | 0.37 | 0.42 | 0.58 |
| C _{testis} , ng/g | 348 ± 245 | 3011 ± 590*** | 2511 ± 553*** | 3402 ± 559*** |
| Fold increase C _{testis} | 1.0 | 8.7 | 7.2 | 9.8 |
| Testis-to-plasma ratio | 0.069 ± 0.041 | 0.43 ± 0.083*** | 0.39 ± 0.023*** | 0.40 ± 0.059*** |
| Fold change ratio | 1.0 | 6.2 | 5.7 | 5.8 |

Data are given as mean ± S.D. (n = 6). AUC_{0-2h}, area under the plasma concentration-time curve; C_{max}, maximum concentration in plasma; T_{max}, time point (h) of maximum plasma concentration; C_{brain}, brain concentration; C_{liver}, liver concentration; SI, small intestine (tissue); SIC, small intestine contents; C_{testis}, testis concentration; *, P < 0.05; **, P < 0.01; ***, P < 0.001 compared to vehicle treated wild-type mice; #, P < 0.05; ##, P < 0.01; ###, P < 0.001 compared to elacridar treated wild-type mice; ^, P < 0.05; ^^, P < 0.01; ^^, P < 0.001 compared between vehicle-treated *Abcb1a/1b;Abcg2^{-/-}* and elacridar-treated *Abcb1a/1b;Abcg2^{-/-}* mice. Statistical analysis was applied after log-transformation of linear data.

3.5 Impact of CYP3A on pralsetinib plasma pharmacokinetics and tissue disposition

To investigate the possible *in vivo* impact of mouse *Cyp3a* and human CYP3A4 on pralsetinib pharmacokinetics, we performed an 8 h study in female wild-type, *Cyp3a^{-/-}* and *Cyp3aXAV* mice (*Cyp3a^{-/-}* mice with transgenic expression of human CYP3A4 in liver and intestine). Pralsetinib (10 mg/kg) was administered orally after 2-3 h of fasting, blood samples were taken at several time points, and at 8 h organs were collected. The pralsetinib plasma AUC_{0-8h} in *Cyp3a^{-/-}* mice was significantly higher (1.4-fold, P < 0.01) than that in wild-type mice (Figure 6 and Table 3). *Cyp3a^{-/-}* mice had a similar T_{max} as wild-type mice (about 2 h), but the difference between the two mouse strains occurred mainly during the first 4 h. After that, the relative elimination was similar between the strains (Figure 6B). These data suggest that mCyp3a modestly reduces pralsetinib exposure, presumably mainly by first-pass (intestinal?) metabolism. Intriguingly, for the *Cyp3aXAV* mice we observed a similar plasma profile as in *Cyp3a^{-/-}* mice up till 2 hours, but after that, *Cyp3aXAV* mice showed a markedly slower relative elimination of pralsetinib than *Cyp3a^{-/-}* mice (Figure 6B). This unexpected result not only suggests that human CYP3A4 metabolized pralsetinib very little *in vivo*, but also that an alternative pralsetinib elimination mechanism was down-regulated in *Cyp3aXAV* mice.

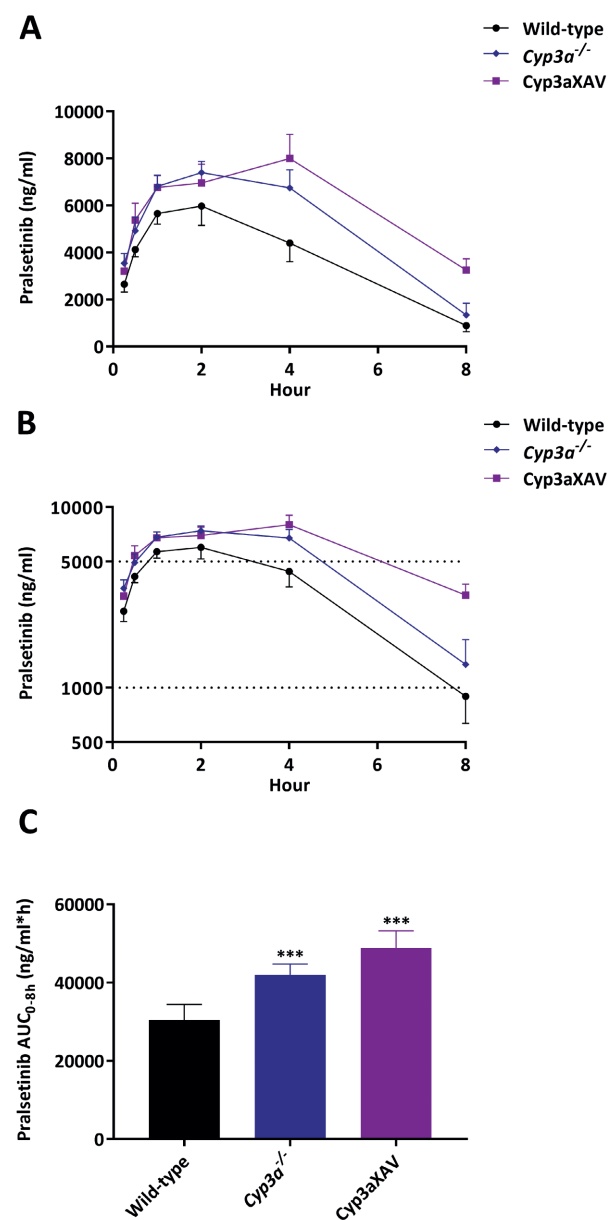


Figure 6. Plasma concentration-time curves (A), semi-log plot of plasma concentration-time curves (B) and plasma AUC_{0-8h} (C) of pralsetinib in female wild-type, *Cyp3a*^{-/-} and *Cyp3aXAV* mice 8 h after oral administration of 10 mg/kg pralsetinib. Data are given as mean ± S.D. (n = 6). *, *P* < 0.05; **, *P* < 0.01; ***, *P* < 0.001 compared to wild-type mice; #, *P* < 0.05; ##, *P* < 0.01; ###, *P* < 0.001 compared between *Cyp3a*^{-/-} and *Cyp3aXAV* mice. Statistical analysis was applied after log-transformation of linear data.

Interestingly, the average pralsetinib plasma AUC_{0-8h} in wild-type and *Cyp3aXAV* mice were 30427 ng/ml*h and 48865 ng/ml*h (Table 3), respectively, whereas 400 mg pralsetinib once daily in patients yielded a plasma AUC_{0-24h} of 43900 ng/ml*h. The overall pralsetinib plasma exposure in mice in our study and in human patients is therefore quite similar. With respect to the tissue distribution at 8 h, the observed differences in absolute tissue concentrations between the strains in brain, liver, testis, lung, and spleen mostly reflected the differences in plasma concentrations: the tissue-to-plasma ratios were not substantially altered between the strains, perhaps excepting the clearing organs kidney and small intestine (Supplemental figure 10 and 11). Collectively, these results suggest that pralsetinib is modestly metabolized by mouse *Cyp3a*, but not by human CYP3A4. In addition, the elimination of pralsetinib may be in part controlled by an (as yet unidentified) detoxification mechanism other than CYP3A, that is down-regulated in *Cyp3aXAV* mice. This unknown detoxification mechanisms is unlikely to be a hepatic OATP transporter, as the liver-to-plasma ratio was unchanged in the *Cyp3aXAV* mice (Supplemental Figure 10), but it might be an apical ABC transporter, given the slightly reduced SI- and SIC-to plasma ratios in these mice (Supplemental Figure 11). However, these shifts are so modest that downregulation of a pralsetinib-metabolizing enzyme is also a distinct possibility.

Table 3. Plasma and organ pharmacokinetic parameters of pralsetinib in female wild-type, *Cyp3a*^{-/-} and *Cyp3aXAV* mice over 8 h after oral administration of 10 mg/kg pralsetinib.

| Parameter | Genotype | | |
|---------------------------------|----------------|-----------------------------|--------------------|
| | Wild-type | <i>Cyp3a</i> ^{-/-} | <i>Cyp3aXAV</i> |
| AUC _{0-8h} , ng/ml.h | 30427 ± 3975 | 41904 ± 2860*** | 48865 ± 4339***## |
| Fold change AUC _{0-8h} | 1.0 | 1.4 | 1.6 |
| C _{max} , ng/ml | 6067 ± 721 | 7525 ± 517** | 8210 ± 816*** |
| T _{max} , h | 1.8 ± 0.41 | 2.0 ± 1.10 | 3.7 ± 0.82*# |
| C _{brain} , ng/g | 26.5 ± 10.0 | 41.5 ± 11.5* | 95.6 ± 16.9***### |
| Fold change C _{brain} | 1.0 | 1.6 | 3.6 |
| Brain-to-plasma ratio | 0.030 ± 0.0058 | 0.032 ± 0.0054 | 0.030 ± 0.0055 |
| Fold change ratio | 1.0 | 1.1 | 1.0 |
| C _{liver} , ng/g | 2796 ± 947 | 3889 ± 1152 | 9111 ± 1103***### |
| Fold change C _{liver} | 1.0 | 1.4 | 3.3 |
| Liver-to-plasma ratio | 3.1 ± 0.28 | 3.0 ± 0.27 | 2.8 ± 0.48 |
| Fold change ratio | 1.0 | 0.97 | 0.90 |
| C _{si} , ng/g | 4286 ± 686 | 6142 ± 1791* | 10244 ± 1798***### |
| Fold change C _{si} | 1.0 | 1.4 | 2.4 |
| SI-to-plasma ratio | 5.0 ± 0.91 | 4.8 ± 1.0 | 3.1 ± 0.22***## |
| Fold change ratio | 1.0 | 0.96 | 0.62 |
| SIC percentage of dose | 3.1 ± 1.3 | 6.0 ± 1.3** | 8.7 ± 2.6*** |
| Fold change % | 1.0 | 1.9 | 2.8 |

Data are given as mean ± S.D. (n = 6). AUC_{0-8h}, area under plasma concentration-time curve; C_{max}, maximum concentration in plasma; T_{max}, time point (h) of maximum plasma concentration; C_{brain}, brain concentration. C_{liver}, liver concentration; SI, small intestine (tissue); C_{si}, small intestine tissue concentration; SIC, small intestine contents; C_{SIC}, small intestine contents concentration; *, *P* < 0.05; **, *P* < 0.01; ***, *P* < 0.001 compared to wild-type mice; #, *P* < 0.05; ##, *P* < 0.01; ###, *P* < 0.001 compared between *Cyp3a*^{-/-} and *Cyp3aXAV* mice. Statistical analysis was applied after log-transformation of linear data.

4. DISCUSSION AND CONCLUSIONS

This study shows that the RET inhibitor pralsetinib is a transported substrate by ABCB1 and ABCG2 and these transporters affect the *in vivo* bioavailability and distribution of pralsetinib in mice. *In vitro*, pralsetinib was transported very efficiently by human ABCB1 and mouse Abcg2, but not by human ABCG2 and this transport could be completely inhibited by specific small-molecule ABCB1 and ABCG2 inhibitors. The oral availability of pralsetinib was modestly restricted by ABCB1. Moreover, ABCB1 P-gp in the blood-brain-barrier (BBB) could strongly restrict the brain penetration of pralsetinib, while ABCG2 had a more modest effect. Similar functions of ABCB1 and ABCG2 also showed up in the blood-testis-barrier (BTB), albeit somewhat less pronounced. Despite the highly increased brain concentration (30.4-fold), no acute spontaneous pralsetinib toxicity was observed in the *Abcb1a/1b;Abcg2*^{-/-} mice. Of note, at the dose used in our study, the average T_{max} (~2 h), C_{max} (5000-6000 ng/ml) and AUC_{0-8h} (30427 ng/ml*h) of pralsetinib in wild-type mice were of the same order of magnitude as those observed in patients (T_{max} ranging from 2 to 4 hours with average C_{max} 2830 ng/ml and AUC_{0-24h} 43900 ng/ml*h)¹³.

We also observed a markedly decreased percentage of dose of pralsetinib remaining in the small intestine contents in the absence of *Abcb1a/1b*, and this decrease was not further enhanced when both *Abcb1a/1b* and *Abcg2* were deficient. This suggests that *Abcb1a/1b*, but not *Abcg2*, can mediate either the direct efflux of pralsetinib across the intestinal wall (also reducing net intestinal uptake) or the hepatobiliary excretion of pralsetinib or a combination of both processes. No substantial changes in tissue distribution due to the ABC transporter deficiencies were found in other tissues including liver, kidney, lung and spleen. OATP1A/1B proteins also did not show a substantial influence on pralsetinib distribution in mice. Taking everything together, our results appear to be generally in line with FDA documentation, in which pralsetinib is mentioned to be a substrate of P-gp and BCRP, but not a substrate of the organic anion transporting polypeptides OATP1B1 and OATP1B3 *in vitro*.

It is striking that the impact of *Abcb1a/1b* and *Abcg2* on the relative brain penetration of pralsetinib (~23-fold reduction) is far higher than on the oral availability of this drug (~1.5-fold reduction). The most likely explanations for this apparent discrepancy are that: 1), the drug concentration in the small intestinal lumen shortly after drug administration is far higher than in the blood that exposes the BBB, making initial saturation of the ABC transporters in the intestine more likely; 2), the overall xenobiotic permeability of the intestinal epithelium, containing countless uptake systems for various nutrients, will likely be much higher than that for the highly selective BBB, which makes it harder for the ABC efflux transporters to effectively counteract a substantial influx of pralsetinib in the intestine; 3), there are likely more alternative drug detoxification systems (e.g., drug-metabolizing systems) in the small intestine and liver for pralsetinib than in the BBB, which makes the relative contribution of the ABC transporters in

restricting pralsetinib levels more limited in the small intestine than in the BBB. 4), we further cannot exclude that the membrane density of the ABC transporters in the BBB is higher than in the small intestine, but because of the intestinal microvilli it is hard to give exact numbers on such parameters.

RET fusions occur in lung cancers with a frequency of 1%–2%. In 2018, Drilon et al⁴² focused on the frequency, responsiveness, and overall outcomes in RET-rearranged advanced NSCLC patients with central nervous system (CNS) metastases. They showed that the frequency of CNS involvement in these patients is 25% at diagnosis, but lifetime prevalence can reach almost 50%. Furthermore, the cumulative incidence of CNS lesions in RET-positive NSCLC patients is higher than in ROS1-positive but lower than in ALK-positive patients. They also found a low intracranial response rate when these patients were treated with various multikinase inhibitors. However, these outcomes could be due to the limited efficacy of multikinase inhibitors in RET-rearranged NSCLC patients. Whereas for pralsetinib, according to the clinical phase 1/2 trial results and the FDA document¹³, responses in intracranial lesions were observed in 4 out of 8 patients including 2 patients with a CNS complete response in metastatic RET fusion-positive NSCLC previously treated with platinum chemotherapy patients. Based on our data, brain penetration of pralsetinib was actually quite low in wild-type mice and this low penetration could be enhanced by up to 32.3-fold due to both ABCB1 and ABCG2 deficiency or inhibition. This brain accumulation enhancement might perhaps further benefit treatment of the NSCLC brain metastasis patients. As also tumors that themselves express significant levels of ABCB1 and/or ABCG2 might become relatively drug resistant, there could be an added benefit to such an inhibitor approach^{19,43}.

Therefore, in order to further investigate the potential benefit of ABC efflux transporter inhibition, aiming to obtain higher drug efficacy, especially in brain, we tested a potentially clinically realistic schedule to largely or completely inhibit both ABCB1a/1b and ABCG2 in the BBB by co-administration of the pharmacological inhibitor elacridar. Pre-treatment with elacridar increased oral availability of pralsetinib in wild-type mice. Moreover, brain distribution of pralsetinib was profoundly improved in wild-type mice by elacridar (from 0.026 to 0.51, 19.6-fold), albeit not to as high a level as seen in vehicle-treated *Abcb1a/1b;Abcg2*^{-/-} mice (0.83, 31.9-fold). Unexpectedly, brain distribution of pralsetinib in *Abcb1a/1b;Abcg2*^{-/-} mice with elacridar was lower than that in *Abcb1a/1b;Abcg2*^{-/-} mice without elacridar, suggesting that some other pralsetinib transport system (perhaps mediating pralsetinib brain uptake) might be affected by elacridar. Our findings on elacridar efficacy could provide a rationale for enhanced treatment of brain metastasis of NSCLC patients by boosting brain penetration of pralsetinib using co-administration of an efficacious ABCB1/ABCG2 inhibitor. Of note, we previously observed severe CNS toxicity in a brigatinib pharmacokinetic study in *Abcb1a/1b;Abcg2*^{-/-} or elacridar-treated wild-type mice⁴⁴. Although there was no acute toxicity observed in mice in the current study,

any attempts to enhance pralsetinib overall exposure or brain accumulation in patients using ABCB1/ABCG2 inhibitors should first be carefully monitored for safety.

We further found that pralsetinib oral availability in mice was somewhat restricted by mouse Cyp3a (1.4-fold), but this increased plasma exposure was not rescued by human CYP3A4 expressed in *Cyp3a*-deficient mice. We did not observe any meaningful changes in tissue-to-plasma ratios, suggesting that the differences in tissue concentrations simply reflected the different plasma concentrations among the three mouse strains. These results suggest that CYP3A, and especially human CYP3A4, may not play a substantial role in the metabolic clearance of pralsetinib. It is worth noting that our results seem partly in contradiction with the FDA data, which indicate that pralsetinib is primarily metabolized by CYP3A4 and to a lesser extent by CYP2D6 and CYP1A2, *in vitro*. However, our results suggest that there may be one or more other, as yet unidentified, pralsetinib detoxification (elimination) systems downregulated when CYP3A4 is reintroduced, which is/are responsible for the modest pharmacokinetic changes that we observed among the strains. We have previously observed similar compensatory phenomena for the metabolism of midazolam by Cyp3a in Cyp3a knockout mice^{45,46}. Nonetheless, the most likely interpretation of our data is that CYP3A4 itself is not an important determinant of pralsetinib pharmacokinetics in mice.

However, according to FDA guidelines, when pralsetinib (200 mg, QD) was co-administered with the strong CYP3A inhibitor itraconazole (200 mg, QD) in patients, this increased the pralsetinib C_{max} by 84% and AUC_{0-12h} by 251%. Conversely, co-administration of the CYP3A inducer rifampin (600 mg, QD) with pralsetinib (400 mg, QD) decreased the pralsetinib C_{max} by 30% and the AUC_{0-12h} by 68% in the clinic. Both findings would be consistent with a significant role for CYP3A in clearing pralsetinib in humans. However, we'd like to emphasize that itraconazole can not only inhibit CYP3A, but also ABCB1. Studies have shown that many of the clinical drug interactions that occur between itraconazole and other drugs are caused by the inhibition of ABCB1 P-gp activity, as well as by the inhibition of CYP3A-mediated metabolism⁴⁷⁻⁴⁹. Moreover, rifampin is also not a completely specific CYP3A inducer. It has been shown that rifampin could also induce many other CYP enzyme family members, as well as some drug transporter proteins, such as intestinal and hepatic P-gp^{50,51}. As mentioned above, other pralsetinib detoxification systems may exist and considering that pralsetinib is a good substrate of ABCB1, there is a chance that the increased pralsetinib exposure by itraconazole is due to the inhibition of ABCB1. Furthermore, the decreased pralsetinib exposure by rifampin might be due to the induced function of other CYP enzymes and/or ABCB1 in the FDA drug-drug interaction studies.

In summary, ABCG2 and especially ABCB1, but not OATP1A/1B, can limit the oral availability and brain penetration of pralsetinib. Furthermore, elacridar co-administration could markedly enhance the brain accumulation of oral pralsetinib. Additionally, CYP3A may not be the

primary factor responsible for pralsetinib metabolism and elimination *in vivo*, and some other detoxification systems may mediate the elimination of pralsetinib instead. The obtained insights and principles may potentially be used to further enhance the therapeutic application and efficacy of pralsetinib, especially for treatment of brain metastases in NSCLC patients.

ACKNOWLEDGEMENTS

This work was funded in part by the Chinese Scholarship Council (CSC Scholarship No. 201506240107 to Y.W.). We gratefully acknowledge Rahime Şentürk for the development and validation of the bioanalytical LC-MS/MS assay at the Utrecht University.

AUTHOR CONTRIBUTIONS

Yaogeng Wang and Alfred H. Schinkel designed the study, analyzed the data and wrote the manuscript. Alfred H. Schinkel administered and supervised the project. Yaogeng Wang, Rolf W. Sparidans, and Sander Potters performed the experimental parts of the study. Maria C. Lebre contributed reagents, materials, and mice. Jos H. Beijnen and Rolf W. Sparidans supervised the bioanalytical part of the studies and checked the content and language of manuscript. All authors commented on and approved the manuscript for submission.

DECLARATION OF INTEREST

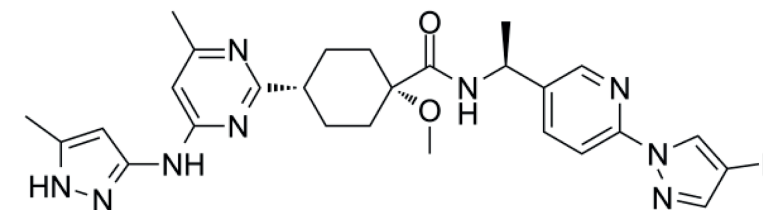
The research group of Alfred Schinkel receives revenue from commercial distribution of some of the mouse strains used in this study. The remaining authors declare no conflict of interest.

REFERENCES

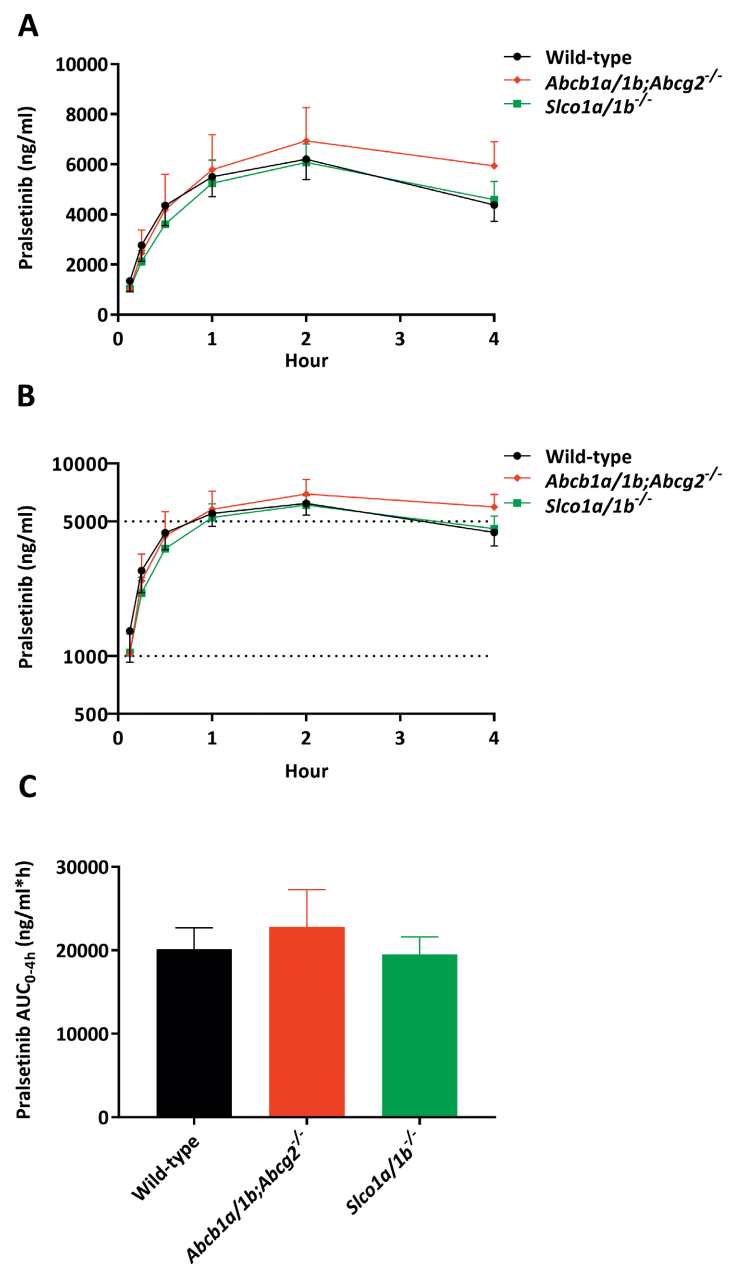
- Manié, S., Santoro, M., Fusco, A. & Billaud, M. The RET receptor: function in development and dysfunction in congenital malformation. *Trends in Genetics* **17**, 580-589 (2001).
- Arighi, E., Borrello, M.G. & Sariola, H. RET tyrosine kinase signaling in development and cancer. *Cytokine and Growth Factor Reviews* **16**, 441-467 (2005).
- Ibanez, C.F. Structure and physiology of the RET receptor tyrosine kinase. *Cold Spring Harbor Perspectives in Biology* **5**(2013).
- Ji, J.H., et al. Identification of Driving ALK Fusion Genes and Genomic Landscape of Medullary Thyroid Cancer. *Plos Genetics* **11**, e1005467 (2015).
- Stransky, N., Cerami, E., Schalm, S., Kim, J.L. & Lengauer, C. The landscape of kinase fusions in cancer. *Nature Communications* **5**, 4846 (2014).
- Kato, S., et al. RET Aberrations in Diverse Cancers: Next-Generation Sequencing of 4,871 Patients. *Clinical Cancer Research* **23**, 1988-1997 (2017).
- Drilon, A., Hu, Z.L., Lai, G.G.Y. & Tan, D.S.W. Targeting RET-driven cancers: lessons from evolving preclinical and clinical landscapes. *Nature Reviews: Clinical Oncology* **15**, 151-167 (2018).
- Elisei, R., et al. Cabozantinib in progressive medullary thyroid cancer. *Journal of Clinical Oncology* **31**, 3639-3646 (2013).
- Drilon, A., et al. Cabozantinib in patients with advanced RET-rearranged non-small-cell lung cancer: an open-label, single-centre, phase 2, single-arm trial. *Lancet Oncology* **17**, 1653-1660 (2016).
- Wells, S.A., Jr., et al. Vandetanib in patients with locally advanced or metastatic medullary thyroid cancer: a randomized, double-blind phase III trial. *Journal of Clinical Oncology* **30**, 134-141 (2012).
- Yoh, K., et al. Vandetanib in patients with previously treated RET-rearranged advanced non-small-cell lung cancer (LURET): an open-label, multicentre phase 2 trial. *Lancet Respiratory Medicine* **5**, 42-50 (2017).
- Food and Drug Administration. Center for Drug Evaluation and Research of the US Department of Health and Human Service, Food and Drug Administration. Multi-discipline Review (2020). Available from: https://www.accessdata.fda.gov/drugsatfda_docs/label/2020/213246s000lbl.pdf.
- Food and Drug Administration. Center for Drug Evaluation and Research of the US Department of Health and Human Service, Food and Drug Administration. Multi-discipline Review (2020). Available from: https://www.accessdata.fda.gov/drugsatfda_docs/label/2020/213721s000lbl.pdf.
- Alexander Drilon, et al. A phase 1 study of LOXO-292, a potent and highly selective RET inhibitor, in patients with RET-altered cancers. in *ASCO* (2018).
- Subbiah, V., et al. Precision Targeted Therapy with BLU-667 for RET-Driven Cancers. *Cancer Discovery* **8**, 836-849 (2018).
- Nigam, S.K. What do drug transporters really do? *Nature Reviews Drug Discovery* **14**, 29-44 (2014).
- Russel, F.G.M. Transporters: Importance in Drug Absorption, Distribution, and Removal. 27-49 (2010).
- Giacomini, K.M., et al. Membrane transporters in drug development. *Nature Reviews Drug Discovery* **9**, 215-236 (2010).
- Schinkel, A.H. & Jonker, J.W. Mammalian drug efflux transporters of the ATP binding cassette (ABC) family: an overview. *Advanced Drug Delivery Reviews* **55**, 3-29 (2003).
- Tang, S.C., et al. Increased oral availability and brain accumulation of the ALK inhibitor crizotinib by coadministration of the P-glycoprotein (ABCB1) and breast cancer resistance protein (ABCG2) inhibitor elacridar. *International Journal of Cancer* **134**, 1484-1494 (2014).
- Tang, S.C., et al. Impact of P-glycoprotein (ABCB1) and breast cancer resistance protein (ABCG2) gene dosage on plasma pharmacokinetics and brain accumulation of dasatinib, sorafenib, and sunitinib. *Journal of Pharmacology and Experimental Therapeutics* **346**, 486-494 (2013).
- Lagas, J.S., et al. Breast cancer resistance protein and P-glycoprotein limit sorafenib brain accumulation. *Molecular Cancer Therapeutics* **9**, 319-326 (2010).
- Kodaira, H., Kushihara, H., Ushiki, J., Fuse, E. & Sugiyama, Y. Kinetic analysis of the cooperation of P-glycoprotein (P-gp/Abcb1) and breast cancer resistance protein (Bcrp/Abcg2) in limiting the brain and testis penetration of erlotinib, flavopiridol, and mitoxantrone. *Journal of Pharmacology and Experimental Therapeutics* **333**, 788-796 (2010).
- Hagenbuch, B. & Meier, P.J. Organic anion transporting polypeptides of the OATP/ SLC21 family: phylogenetic classification as OATP/ SLCO superfamily, new nomenclature and molecular/functional properties. *Pflügers Archiv. European Journal of Physiology* **447**, 653-665 (2004).
- van de Steeg, E., van Esch, A., Wagenaar, E., Kenworthy, K.E. & Schinkel, A.H. Influence of human OATP1B1, OATP1B3, and OATP1A2 on the pharmacokinetics of methotrexate and paclitaxel in humanized transgenic mice. *Clinical Cancer Research* **19**, 821-832 (2013).
- van de Steeg, E., et al. Complete OATP1B1 and OATP1B3 deficiency causes human Rotor syndrome by interrupting conjugated bilirubin reuptake into the liver. *Journal of Clinical Investigation* **122**, 519-528 (2012).
- van de Steeg, E., et al. Organic anion transporting polypeptide 1a/1b-knockout mice provide insights into hepatic handling of bilirubin, bile acids, and drugs. *Journal of Clinical Investigation* **120**, 2942-2952 (2010).
- Kalliokoski, A. & Niemi, M. Impact of OATP transporters on pharmacokinetics. *British Journal of Pharmacology* **158**, 693-705 (2009).
- van de Steeg, E., et al. Methotrexate Pharmacokinetics in Transgenic Mice with Liver-Specific Expression of Human Organic Anion-Transporting Polypeptide 1B1 (SLCO1B1). *Drug Metabolism and Disposition* **37**, 277-281 (2008).
- van Herwaarden, A.E., et al. Knockout of cytochrome P450 3A yields new mouse models for understanding xenobiotic metabolism. *Journal of Clinical Investigation* **117**, 3583-3592 (2007).
- Lynch, T. & Price, A. The effect of cytochrome P450 metabolism on drug response, interactions, and adverse effects. *American Family Physician* **76**, 391-396 (2007).
- Guengerich, F.P. Cytochrome P-450 3A4: regulation and role in drug metabolism. *Annual Review of Pharmacology and Toxicology* **39**, 1-17 (1999).
- Bakos, E., et al. Characterization of the amino-terminal regions in the human multidrug resistance protein (MRP1). *Journal of Cell Science* **113 Pt 24**, 4451-4461 (2000).
- Evers, R., et al. Drug export activity of the human canalicular multispecific organic anion transporter in polarized kidney MDCK cells expressing cMOAT (MRP2) cDNA. *Journal of Clinical Investigation* **101**, 1310-1319 (1998).
- Şentürk, R., Wang, Y., Schinkel, A.H., Beijnen, J.H. & Sparidans, R.W. Quantitative bioanalytical assay for the selective RET inhibitors selipercatinib and pralsetinib in mouse plasma and tissue homogenates using liquid chromatography-tandem mass spectrometry. *Journal of Chromatography. B: Analytical Technologies in the Biomedical and Life Sciences* **1147**, 122131 (2020).
- Zhang, Y., Huo, M., Zhou, J. & Xie, S. PKSolver: An add-in program for pharmacokinetic and pharmacodynamic data analysis in Microsoft Excel. *Computer Methods and Programs in Biomedicine* **99**, 306-314 (2010).
- Simoff, I., et al. Complete Knockout of Endogenous Mdr1 (Abcb1) in MDCK Cells by CRISPR-Cas9. *Journal of Pharmaceutical Sciences* **105**, 1017-1021 (2016).
- Wang, J., et al. Brain accumulation of tivozanib is restricted by ABCB1 (P-glycoprotein) and ABCG2 (breast cancer resistance protein) in mice. *International Journal of Pharmaceutics* **581**, 119277 (2020).
- Li, W., et al. P-glycoprotein (MDR1/ABCB1) controls brain accumulation and intestinal disposition of the novel TGF- β signaling pathway inhibitor galunisertib. *International Journal of Cancer* **146**, 1631-1642 (2020).
- Wang, J., et al. P-glycoprotein (MDR1/ABCB1) and Breast Cancer Resistance Protein (BCRP/ABCG2) affect brain accumulation and intestinal disposition of encorafenib in mice. *Pharmacological Research* **129**, 414-423 (2018).
- Wang, Y., et al. OATP1A/1B, CYP3A, ABCB1, and ABCG2 limit oral availability of the NTRK inhibitor larotrectinib, while ABCB1 and ABCG2 also restrict its brain accumulation. *British Journal of Pharmacology* **177**, 3060-3074 (2020).
- Drilon, A., et al. Frequency of Brain Metastases and Multikinase Inhibitor Outcomes in Patients With RET-Rearranged Lung Cancers. *Journal of Thoracic Oncology* **13**, 1595-1601 (2018).
- Robey, R.W., et al. Revisiting the role of ABC transporters in multidrug-resistant cancer. *Nature Reviews: Cancer* **18**, 452-464 (2018).
- Li, W., et al. P-glycoprotein and breast cancer resistance protein restrict brigatinib brain accumulation and toxicity, and, alongside CYP3A, limit its oral availability. *Pharmacological Research* **137**, 47-55 (2018).

45. van Waterschoot, R.A., *et al.* Intestinal cytochrome P450 3A plays an important role in the regulation of detoxifying systems in the liver. *FASEB Journal* **23**, 224-231 (2009).
46. van Waterschoot, R.A., *et al.* Midazolam metabolism in cytochrome P450 3A knockout mice can be attributed to up-regulated CYP2C enzymes. *Molecular Pharmacology* **73**, 1029-1036 (2008).
47. Lilja, J.J., Backman, J.T., Laitila, J., Luurila, H. & Neuvonen, P.J. Itraconazole increases but grapefruit juice greatly decreases plasma concentrations of celiprolol. *Clinical Pharmacology and Therapeutics* **73**, 192-198 (2003).
48. Kaukonen, K.M., Olkkola, K.T. & Neuvonen, P.J. Itraconazole increases plasma concentrations of quinidine. *Clinical Pharmacology and Therapeutics* **62**, 510-517 (1997).
49. Partanen, J., Jalava, K.M. & Neuvonen, P.J. Itraconazole increases serum digoxin concentration. *Pharmacology and Toxicology* **79**, 274-276 (1996).
50. Elmeligy, M., Vourvahis, M., Guo, C. & Wang, D.D. Effect of P-glycoprotein (P-gp) Inducers on Exposure of P-gp Substrates: Review of Clinical Drug-Drug Interaction Studies. *Clinical Pharmacokinetics* **59**, 699-714 (2020).
51. Chen, J. & Raymond, K. Roles of rifampicin in drug-drug interactions: underlying molecular mechanisms involving the nuclear pregnane X receptor. *Annals of Clinical Microbiology and Antimicrobials* **5**, 3 (2006).

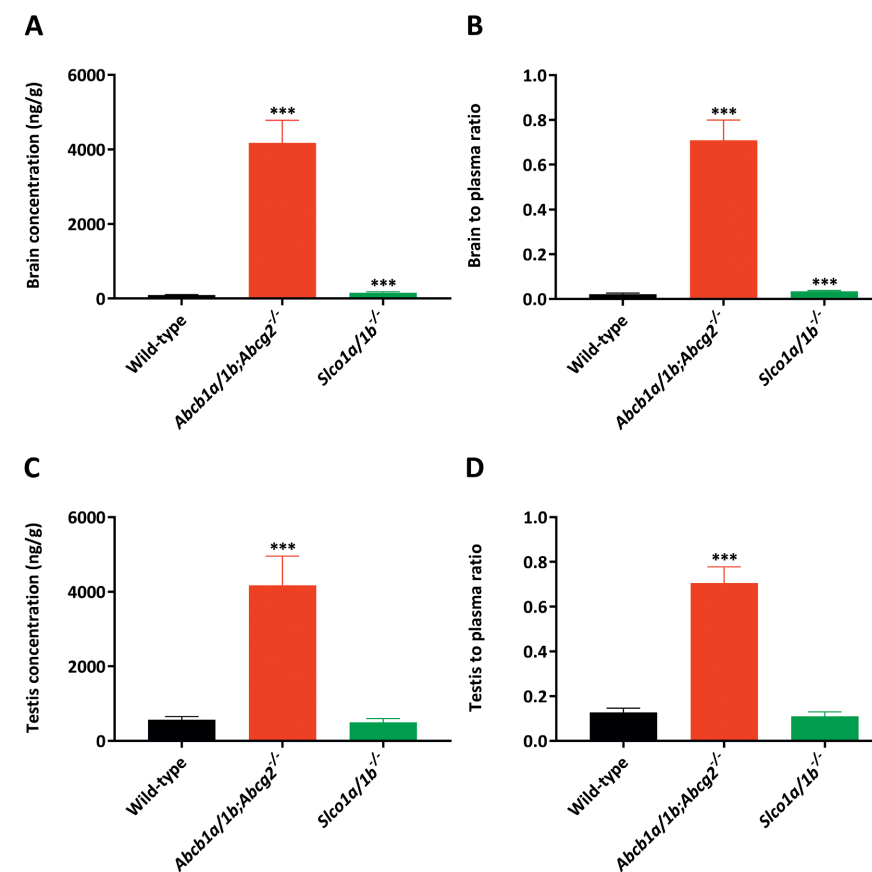
SUPPLEMENTAL MATERIALS



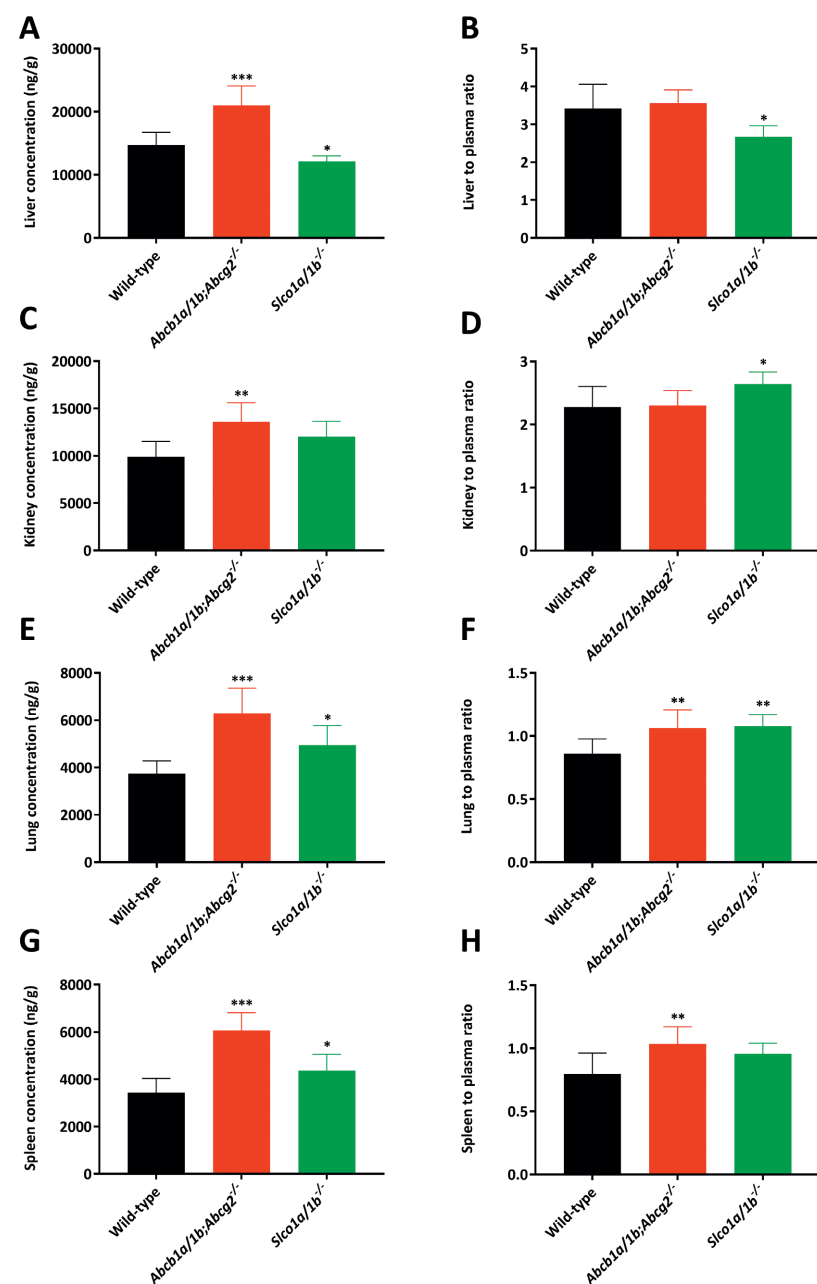
Supplemental Figure 1. Molecular structure of pralsetinib (GAVRETO, BLU-667, 533.61 g/mol).



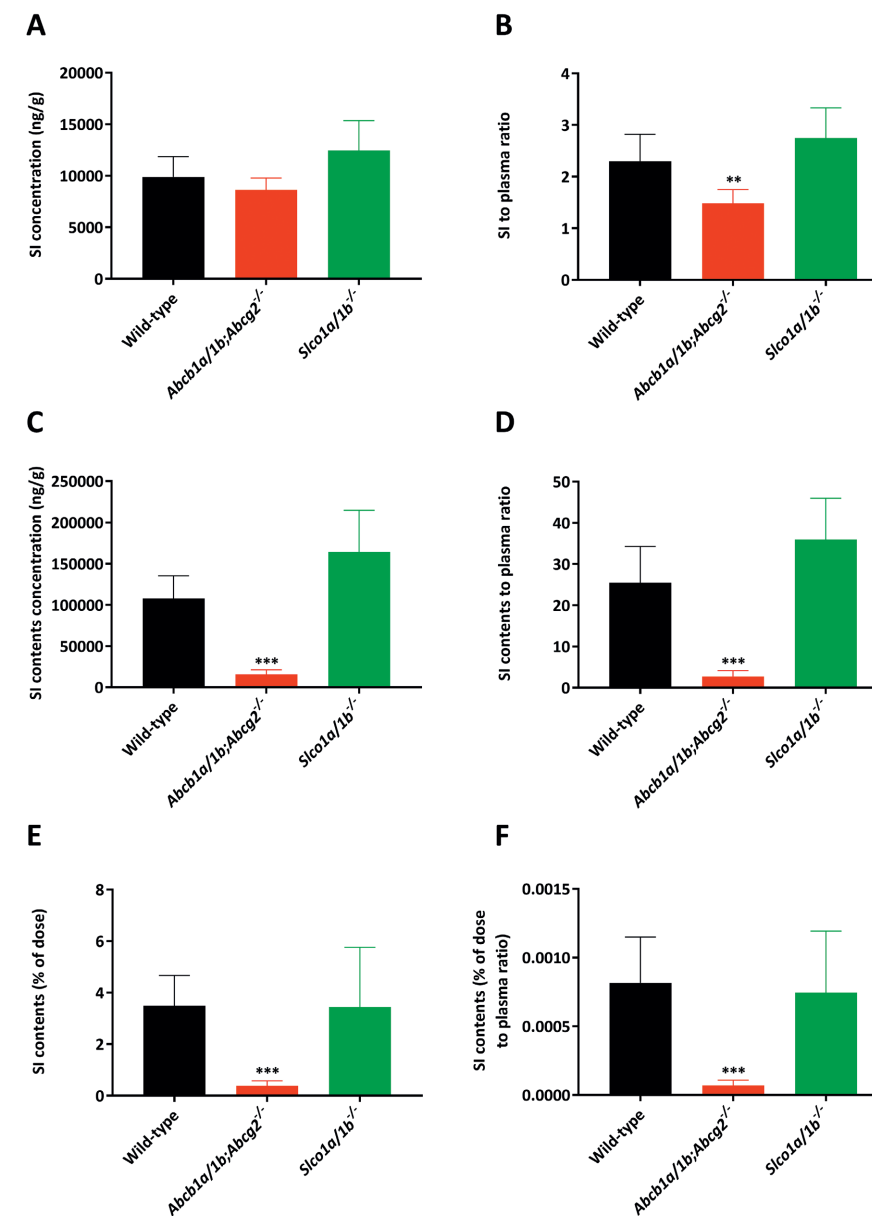
Supplemental Figure 2. Plasma concentration-time curves (A), semi-log plot of plasma concentration-time curves (B) and plasma AUC_{0-4h} (C) of pralsetinib in male wild-type, *Abcb1a/1b;Abcg2*^{-/-} and *Slco1a/1b*^{-/-} mice over 4 h after oral administration of 10 mg/kg pralsetinib. Data are given as mean \pm S.D. (n = 6 - 7). Statistical analysis was applied after log-transformation of linear data.



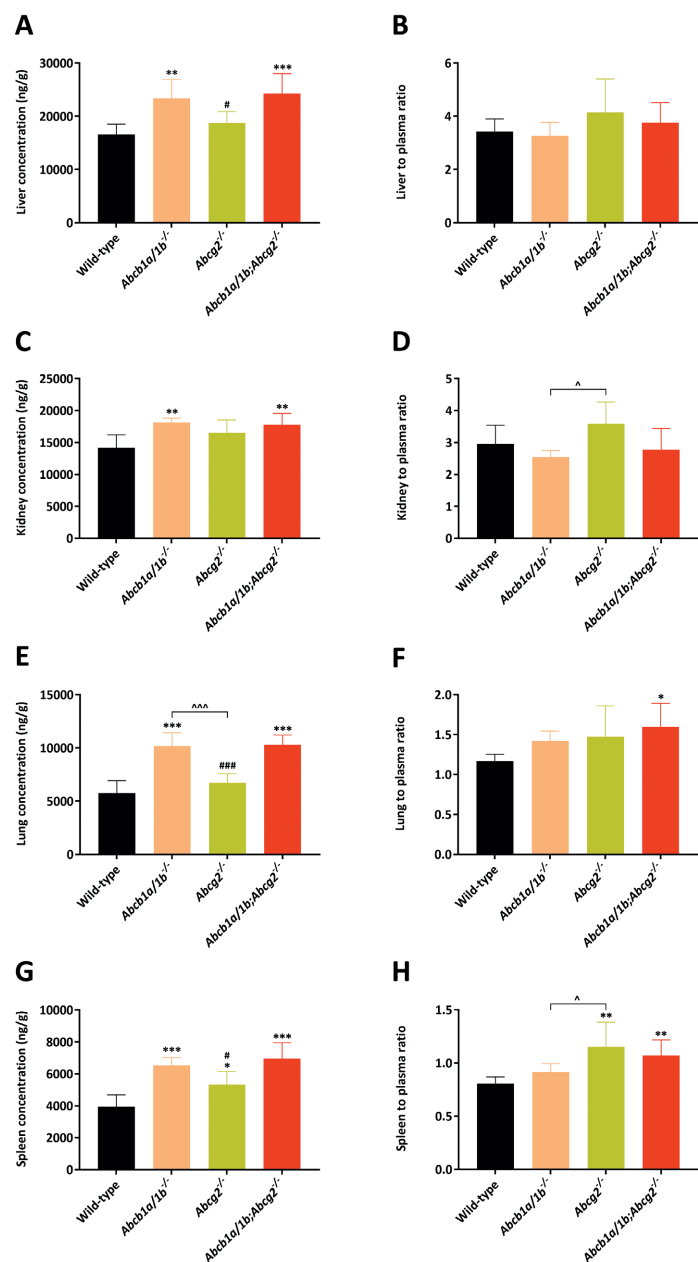
Supplemental Figure 3. Brain concentration (A), brain-to-plasma ratio (B), testis concentration (C) and testis-to-plasma ratio (D) of pralsetinib in male wild-type, *Abcb1a/1b;Abcg2*^{-/-} and *Slco1a/1b*^{-/-} mice 4 h after oral administration of 10 mg/kg pralsetinib (n = 6 - 7). *, $P < 0.05$; **, $P < 0.01$; ***, $P < 0.001$ compared to wild-type mice. Statistical analysis was applied after log-transformation of linear data.



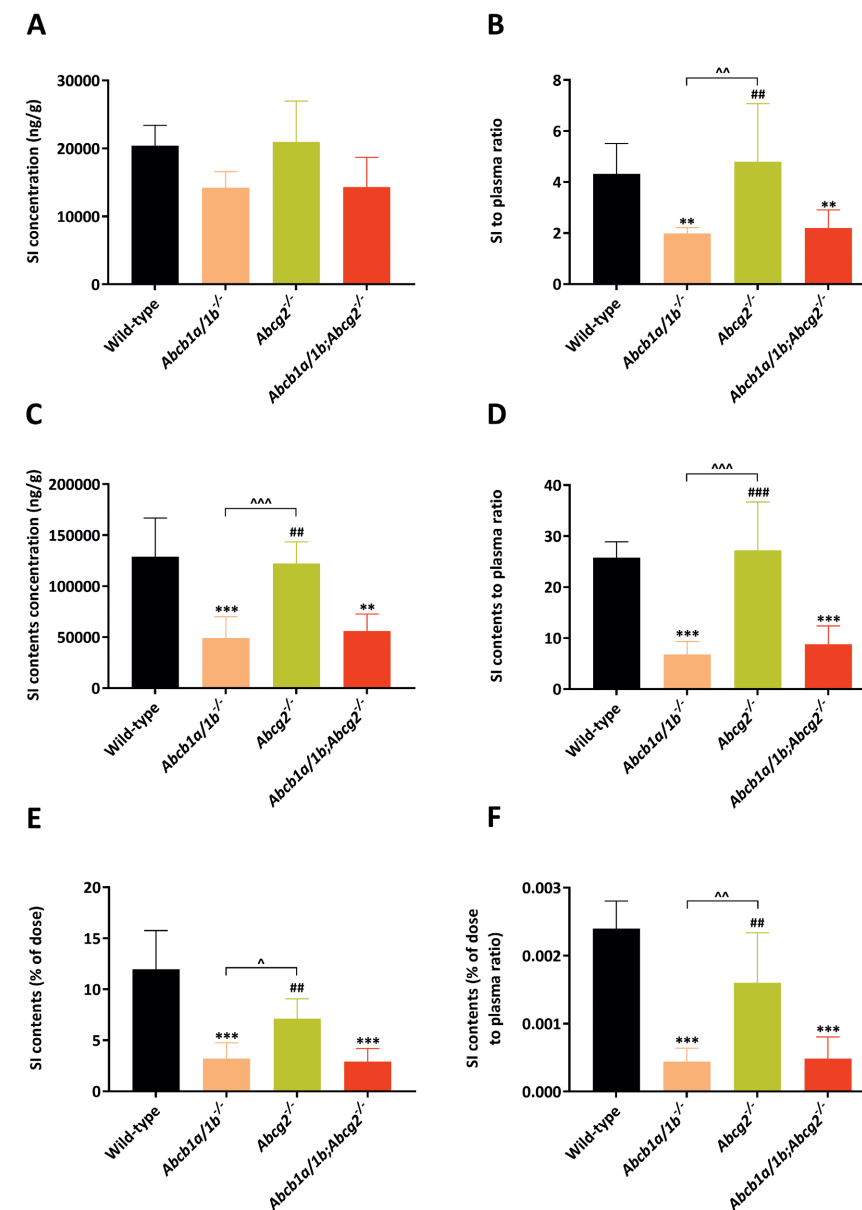
Supplemental Figure 4. Tissue concentrations (A, C, E, G) and tissue-to-plasma ratios (B, D, F, H) of pralsetinib in male wild-type, *Abcb1a/1b;Abcg2*^{-/-} and *Slco1a/1b*^{-/-} mice 4 h after oral administration of 10 mg/kg pralsetinib (n = 6 - 7). *, $P < 0.05$; **, $P < 0.01$; ***, $P < 0.001$ compared to wild-type mice. Statistical analysis was applied after log-transformation of linear data.



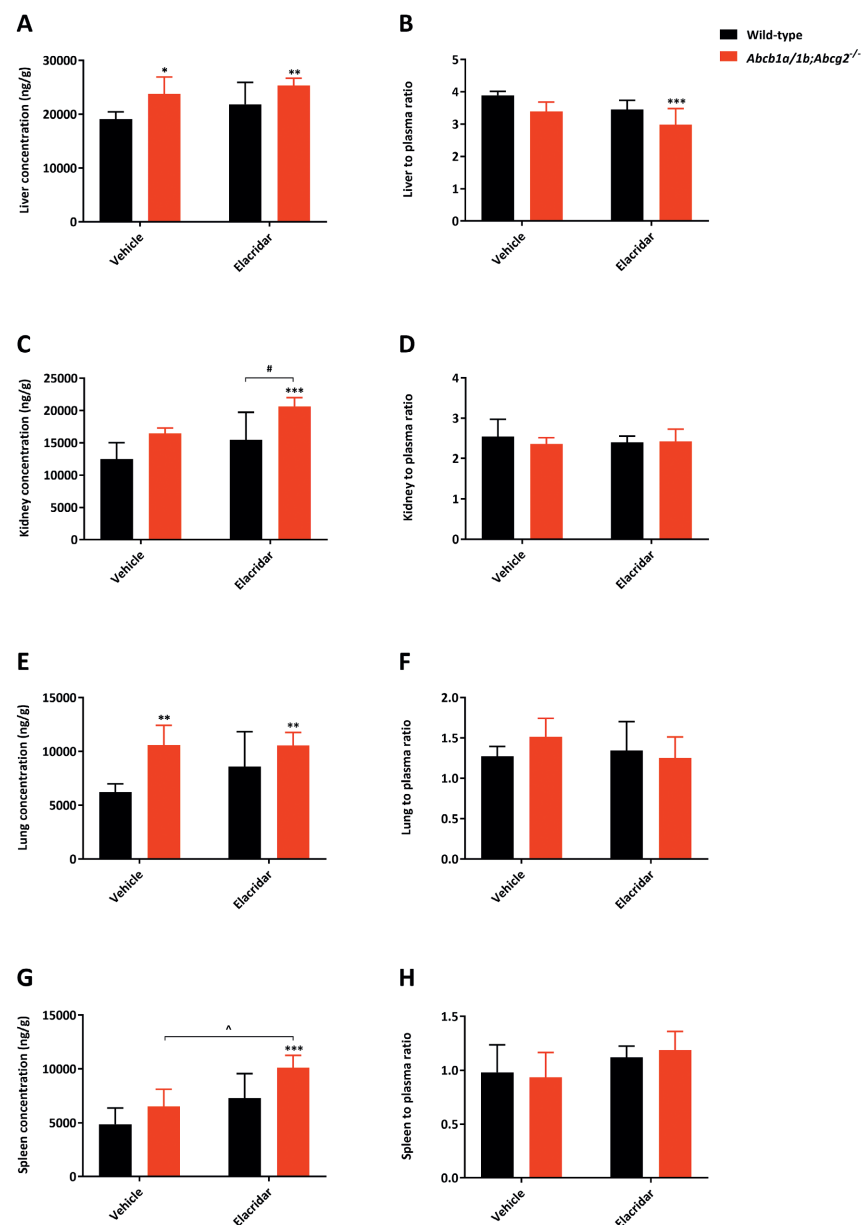
Supplemental Figure 5. Small intestine and small intestine contents concentrations (A and C), small intestine- and small intestine contents-to-plasma ratios (B and D), small intestine contents as percentage of dose (E) and small intestine contents percentage of dose-to-plasma ratio (F) of pralsetinib in male wild-type, *Abcb1a/1b;Abcg2*^{-/-} and *Slco1a/1b*^{-/-} mice over 4 h after oral administration of 10 mg/kg pralsetinib. SI: Small intestine. Data are given as mean \pm S.D. (n = 6 - 7). *, $P < 0.05$; **, $P < 0.01$; ***, $P < 0.001$ compared to wild-type mice. Statistical analysis was applied after log-transformation of linear data.



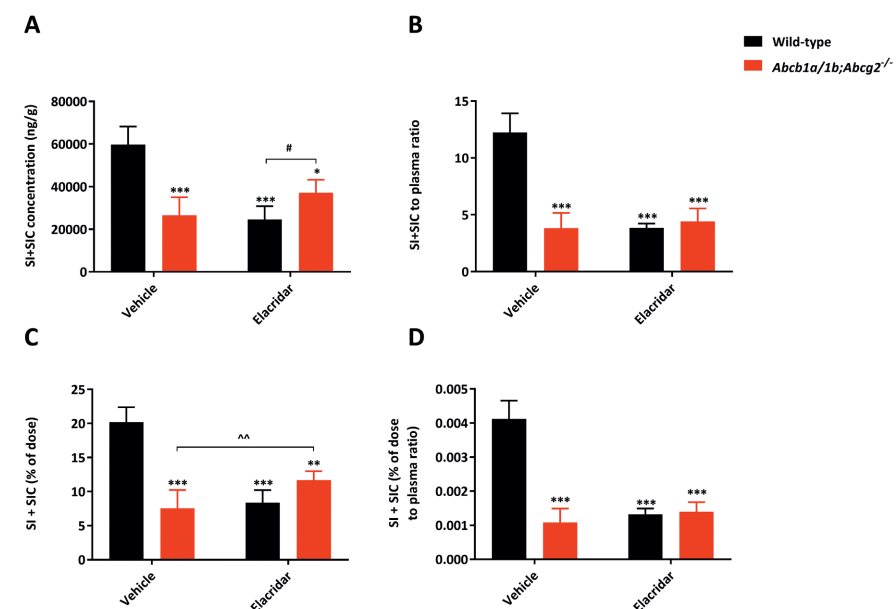
Supplemental Figure 6. Tissue concentrations (A, C, E, G) and tissue-to-plasma ratios (B, D, F, H) of pralsetinib in male wild-type, *Abcb1a/1b*^{-/-}, *Abcg2*^{-/-} and *Abcb1a/1b;Abcg2*^{-/-} mice 2 h after oral administration of 10 mg/kg pralsetinib (n = 6). *, $P < 0.05$; **, $P < 0.01$; ***, $P < 0.001$ compared to wild-type mice; #, $P < 0.05$; ##, $P < 0.01$; ###, $P < 0.001$ compared to *Abcb1a/1b;Abcg2*^{-/-} mice. Statistical analysis was applied after log-transformation of linear data.



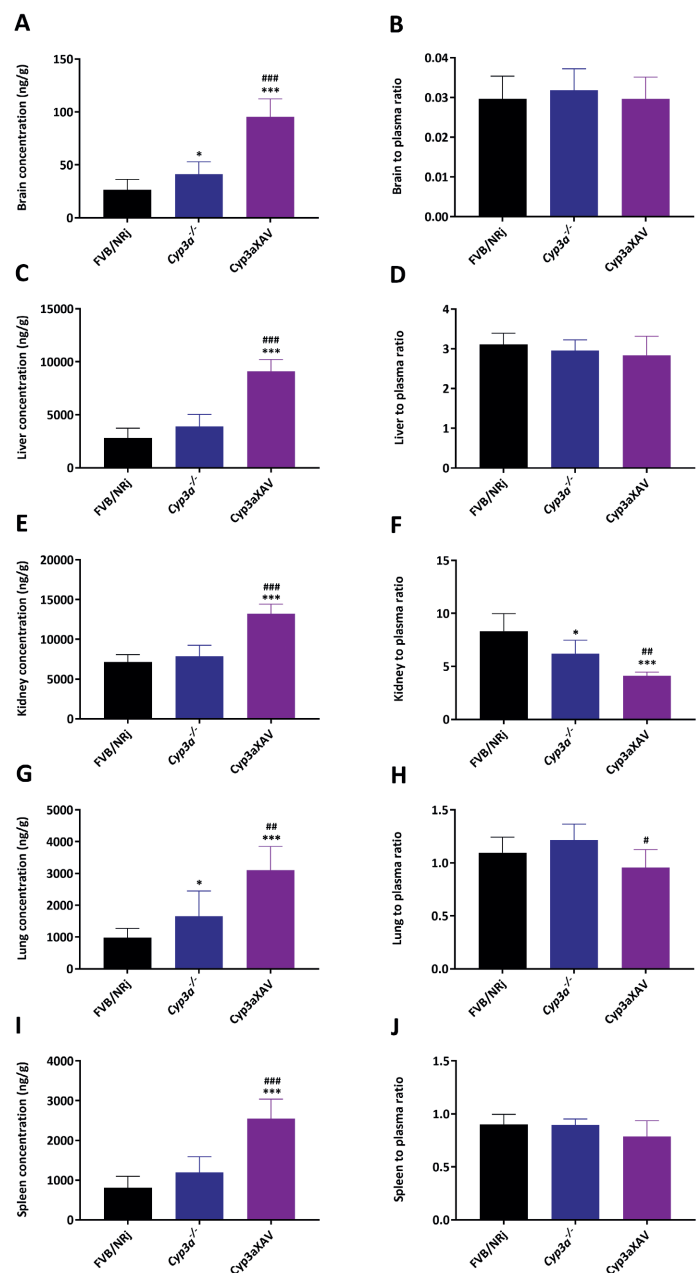
Supplemental Figure 7. Small intestine and small intestine contents concentrations (A and C), small intestine- and small intestine contents-to-plasma ratios (B and D), small intestine contents as percentage of dose (E) and small intestine contents percentage of dose-to-plasma ratio (F) of pralsetinib in male wild-type, *Abcb1a/1b*^{-/-}, *Abcg2*^{-/-} and *Abcb1a/1b;Abcg2*^{-/-} mice 2 h after oral administration of 10 mg/kg pralsetinib. SI: Small intestine. Data are given as mean \pm S.D. (n = 6). *, $P < 0.05$; **, $P < 0.01$; ***, $P < 0.001$ compared to wild-type mice; #, $P < 0.05$; ##, $P < 0.01$; ###, $P < 0.001$ compared to *Abcb1a/1b;Abcg2*^{-/-} mice. Statistical analysis was applied after log-transformation of linear data.



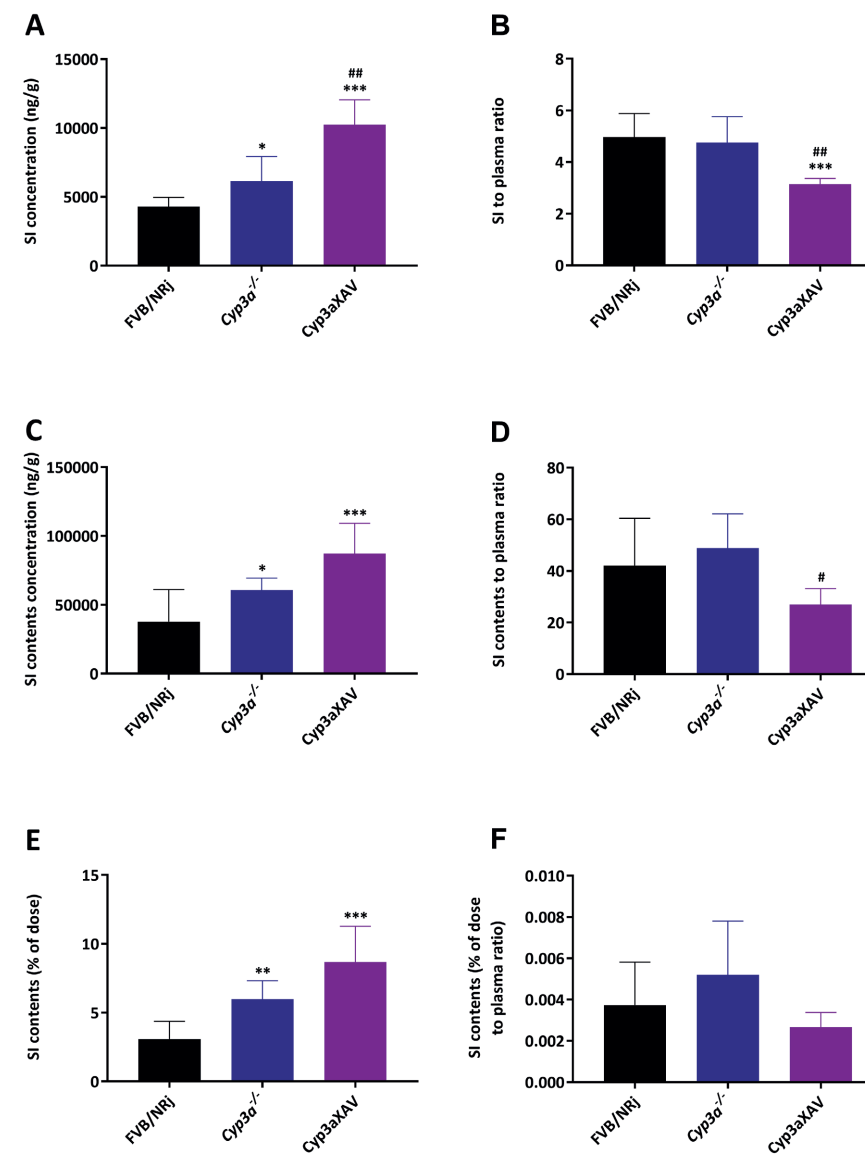
Supplemental figure 8. Tissue concentrations (A, C, E, G) and tissue-to-plasma ratios (B, D, F, H) of pralsetinib in male wild-type and *Abcb1a/1b;Abcg2^{-/-}* mice over 2 h after oral administration of 10 mg/kg pralsetinib with or without co-administration of elacridar. Data are given as mean \pm S.D. (n = 6). *, $P < 0.05$; **, $P < 0.01$; ***, $P < 0.001$ compared to wild-type mice; #, $P < 0.05$; ##, $P < 0.01$; ###, $P < 0.001$ compared to elacridar-treated wild-type mice; ^, $P < 0.05$; ^^, $P < 0.01$; ^^, $P < 0.001$ compared between vehicle-treated *Abcb1a/1b;Abcg2^{-/-}* and elacridar-treated *Abcb1a/1b;Abcg2^{-/-}* mice. Statistical analysis was applied after log-transformation of linear data.



Supplemental figure 9. Small intestine together with small intestine contents (SI + SIC) concentrations (A), SI + SIC-to-plasma ratios (B), SI+SIC percentage of total dose (C) and SI+SIC percentage of total dose to plasma ratio (D) of pralsetinib in male wild-type and *Abcb1a/1b;Abcg2^{-/-}* mice over 2 h after oral administration of 10 mg/kg pralsetinib with or without co-administration of elacridar. SI, small intestinal tissue; SIC, small intestine contents. Data are given as mean \pm S.D. (n = 6). *, $P < 0.05$; **, $P < 0.01$; ***, $P < 0.001$ compared to wild-type mice; #, $P < 0.05$; ##, $P < 0.01$; ###, $P < 0.001$ compared to elacridar-treated wild-type mice; ^, $P < 0.05$; ^^, $P < 0.01$; ^^, $P < 0.001$ compared between vehicle-treated *Abcb1a/1b;Abcg2^{-/-}* and elacridar-treated *Abcb1a/1b;Abcg2^{-/-}* mice. Statistical analysis was applied after log-transformation of linear data.



Supplemental Figure 10. Tissue concentrations (A, C, E, G, I) and tissue-to-plasma ratios (B, D, F, H, J) of pralsetinib in female wild-type, *Cyp3a*^{-/-} and *Cyp3aXAV* mice over 8 h after oral administration of 10 mg/kg pralsetinib. Data are given as mean \pm S.D. (n = 6). *, $P < 0.05$; **, $P < 0.01$; ***, $P < 0.001$ compared to wild-type mice; #, $P < 0.05$; ##, $P < 0.01$; ###, $P < 0.001$ compared between *Cyp3a*^{-/-} and *Cyp3aXAV* mice. Statistical analysis was applied after log-transformation of linear data.



Supplemental figure 11. Small intestine and small intestine contents concentrations (A and C), small intestine- and small intestine contents-to-plasma ratios (B and D), small intestine contents as percentage of dose (E) and small intestine contents percentage of dose-to-plasma ratio (F) of pralsetinib in female wild-type, *Cyp3a*^{-/-} and *Cyp3aXAV* mice over 8 h after oral administration of 10 mg/kg pralsetinib. Data are given as mean \pm S.D. (n = 6). *, $P < 0.05$; **, $P < 0.01$; ***, $P < 0.001$ compared to wild-type mice; #, $P < 0.05$; ##, $P < 0.01$; ###, $P < 0.001$ compared between *Cyp3a*^{-/-} and *Cyp3aXAV* mice. Statistical analysis was applied after log-transformation of linear data.

Supplemental Table 1. Pharmacokinetic parameters, brain concentrations, and brain-to-plasma ratios of pralsetinib in male wild-type, *Abcb1a/1b;Abcg2*^{-/-} and *Slco1a/1b*^{-/-} mice over 4 h after oral administration of 10 mg/kg pralsetinib.

| Parameter | Genotype | | |
|---|----------------|---------------------------------------|---------------------------------|
| | Wild-type | <i>Abcb1a/1b;Abcg2</i> ^{-/-} | <i>Slco1a/1b</i> ^{-/-} |
| AUC _{0-4h} ^{pl} , ng/ml.h | 20129 ± 2581 | 22844 ± 4435 | 19519 ± 2102 |
| Fold change AUC _{0-4h} ^{pl} | 1.0 | 1.1 | 0.97 |
| C _{max} ^{pl} , ng/ml | 6202 ± 805.7 | 6962 ± 1303 | 6138 ± 586.1 |
| T _{max} ^{pl} , h | 2.0 ± 0.00 | 2.3 ± 0.76 | 2.3 ± 0.76 |
| C _{brain} ^{pl} , ng/g | 93 ± 14.4 | 4175 ± 606*** | 154 ± 29*** |
| Fold increase C _{brain} ^{pl} | 1.0 | 44.9 | 1.7 |
| Brain-to-plasma ratio | 0.022 ± 0.0048 | 0.71 ± 0.090*** | 0.034 ± 0.0045*** |
| Fold increase ratio | 1.0 | 32.3 | 1.5 |
| C _{liver} ^{pl} , ng/g | 14714 ± 2031 | 21044 ± 3054*** | 12085 ± 930* |
| Fold increase C _{liver} ^{pl} | 1.0 | 1.4 | 0.82 |
| Liver-to-plasma ratio | 3.4 ± 0.64 | 3.6 ± 0.34 | 2.7 ± 0.29* |
| Fold increase ratio | 1.0 | 1.1 | 0.79 |
| SIC percentage of dose, % | 3.5 ± 1.2 | 0.38 ± 0.20*** | 3.5 ± 2.3 |
| Fold change ratio | 1.0 | 0.11 | 1.0 |
| C _{testis} ^{pl} , ng/g | 566 ± 88 | 4174 ± 785*** | 498 ± 98 |
| Fold increase C _{testis} ^{pl} | 1.0 | 7.4 | 0.88 |
| Testis-to-plasma ratio | 0.13 ± 0.019 | 0.71 ± 0.072*** | 0.11 ± 0.021 |
| Fold change ratio | 1.0 | 5.5 | 0.85 |

AUC_{0-4h}^{pl}, area under plasma concentration-time curve; C_{max}^{pl}, maximum concentration in plasma; T_{max}^{pl}, time point (h) of maximum plasma concentration; C_{brain}^{pl}, brain concentration; C_{liver}^{pl}, liver concentration; SIC, small intestine contents; C_{testis}^{pl}, testis concentration; Data are given as mean ± S.D. (n = 6 - 7). *, P < 0.05; **, P < 0.01; ***, P < 0.001 compared to wild-type mice. Statistical analysis was applied after log-transformation of linear data.



CHAPTER 5

CONCLUSIONS AND PERSPECTIVES

CONCLUSIONS AND PERSPECTIVES

The carboxylesterase family plays a quite important role in the activation and/or detoxification of many (pro-)drugs, as well as in lipid metabolism, energy expenditure and homeostasis. In **Part I** of this thesis we studied the pharmacological and physiological functions of the drug-metabolizing enzyme carboxylesterase 2 (CES2/Ces2), using genetically modified mouse models. The pharmacokinetic profiles, efficacy and safety of drugs can be markedly influenced by drug transporters (especially ABCB1/ABCG2 and/or SLCO1A1/1B) and drug-metabolizing enzymes (particularly CYP3A). In **Part II** of the thesis, such potential effects were investigated for three small-molecule inhibitors, including larotrectinib (the first selective inhibitor for TRK receptors), selpercatinib and pralsetinib (the first two selective inhibitors for RET receptors), using relevant genetically modified cell lines and mouse strains. In addition, in order to explore possible drug-drug interaction effects, we performed inhibition (boosting) experiments for larotrectinib and analyzed the resulting pharmacokinetic changes.

PART I. PHARMACOLOGICAL AND PHYSIOLOGICAL FUNCTIONS OF THE CARBOXYLESTERASE 2 COMPLEX

As a member of the esterase enzyme family, carboxylesterases (CES) are mainly known as enzymes involved in detoxification and metabolism of (pro-)drugs and environmental toxicants¹⁻⁴. In addition, carboxylesterases have also been demonstrated to hydrolyze endogenous esters and thioesters, including lipids and some of these enzymes have been shown to play important physiological functions in lipid metabolism and energy homeostasis⁵. Within these carboxylesterases, CES1 and CES2 are thought to be the two most important members with the widest functional ramifications. Human (h) CES2 is expressed mainly in liver and intestine, but especially abundant in intestine. It can hydrolyze carboxylesters as well as amide and thioester linkages in both exogenous and endogenous compounds. With 47% amino acid identity, hCES1 and hCES2 exhibit distinct substrate specificities to some extent. However, they also have very extensive substrate overlap. hCES1 preferentially catalyzes the hydrolysis of compounds esterified with a small alcohol group, while hCES2 hydrolyzes compounds with a relatively small acyl group and large alcohol group⁴. Given the importance of CES1 and CES2 in both pharmacology and physiology, it is worthwhile to systemically investigate the specific roles of both CES1 and CES2 in pre-clinical models, especially using genetically modified mouse models.

The pharmacological functions of CES2

Until recently, there were limited reports on CES2-related mouse models, including hepatic Ces2c knockdown, human CES2 liver expression and Ces2c intestinal overexpression⁶⁻⁸. However, all of these mouse models still had a full (wild-type) mouse Ces2 background. For instance, Li et al. knocked down or overexpressed mouse Ces2c in liver with a short hairpin (sh)RNA against

Ces2c or recombinant adenovirus encoding *Ces2c*, respectively, in a wild-type C57BL/6 strain background⁸. Considering the complications that may be induced by the presence of the other six functional mouse Ces2 proteins, we generated and characterized a mouse *Ces2* cluster knockout (all *Ces2* genes deleted) mouse strain (*Ces2*^{-/-}). Based on *Ces2*^{-/-} mice, a human CES2 liver-specific expression mouse strain without mouse Ces2 background (*Ces2*^{-/-}A) was generated. In addition, because of the high enterocyte hCES2 expression, a human CES2 intestine-specific expression mouse strain with the mouse *Ces2* deletion background was also successfully made (*Ces2*^{-/-}V). With these two transgenic mouse models, we aimed to analyze the specific roles of hepatic CES2 and intestinal CES2 pharmacological functions, and estimate the contributions of CES2 with different tissue locations in different ester (pro-)drug hydrolysis processes. We found that vinorelbine was a very good substrate of mouse (m) *Ces2* protein(s), but perhaps not of human CES2. m*Ces2* can markedly influence the metabolism of vinorelbine into its active metabolite deacetylvinorelbine. In addition, similar to CES1, CES2 was strongly involved in the first-step metabolic activation of capecitabine, but without affecting 5-FU exposure. All of this indicates the importance of proper pre-clinical models, which may provide powerful tools for drug design, development, and for investigating the ADME properties of specific drugs *in vivo*.

The physiological functions of CES2

We also explored the potential physiological functions of CES2 based on the mouse models we obtained. The absence of mouse *Ces2* did not affect body weight development, and had no influence on oral lipid absorption and hepatic lipid secretion, which is consistent with recent studies^{7,8}. However, we did observe some physiological alterations due to mouse *Ces2* deficiency, including increased local liver lipid accumulation in males, and clearly increased plasma cholesterol with limited triglyceride changes in both genders. Probably related to this, the disruption of lipid homeostasis in liver may further induce remote white adipose tissue adipositis⁹, glucose dysregulation and insulin resistance¹⁰. Indeed, *Ces2*^{-/-} mice showed significant white adipose tissue (WAT) adipositis, and slightly higher glucose exposure in both glucose and insulin tolerance tests compared to wild-type mice. Interestingly, we found that overexpression of human CES2 either in liver or intestine, but especially in intestine, could reverse the phenotypes we obtained in *Ces2*-deficient mice to some extent. For instance, both hepatocyte and enterocyte hCES2, but especially enterocyte hCES2, alleviated WAT adipositis and liver lipid over-accumulation in males, could decrease plasma triglyceride and cholesterol concentrations, and improve glucose tolerance and insulin sensitivity in both genders compared to *Ces2*^{-/-} mice. Even though all our analyses were performed under medium-fat diet conditions, our results are mostly in line with recent studies by other groups⁶⁻⁸. Besides this, the different expression locations of hCES2 also induce as yet unexplained complications. For example, we observed a clear bodyweight increase in *Ces2*^{-/-}A mice, but a decrease in *Ces2*^{-/-}V mice. The mechanism behind this is still unclear and will need to be further explored in the future, but this suggests that different physiological functions of CES2 due to different local tissue expression

may exist. All in all, the results we obtained demonstrated a relatively positive role of CES2 in energy metabolism processes and glucose homeostasis. This could help us to further explore potential solutions for the metabolic syndrome problem.

Possible future research lines

In the preceding **Part I** chapters of the current thesis, we have mentioned some implications which deserve to be further explored in the future. Here, we summarize the potential future work and application insights based on the performed CES2 studies, including, but not limited to, the following aspects:

1) The single *Ces2* cluster knockout and related human *CES2* transgenic mice provide powerful tools for the exploration of *Ces2*-specific functions in both pharmacology and physiology. However, all of the above-mentioned mouse models still have *Ces1* enzymes present in the body, including *Ces1c* which is abundant in blood. This may partly or completely obscure *Ces2* pharmacological functions when a target drug is a shared substrate of both CES2 and CES1. Thus, a combined *Ces1* and *Ces2* cluster knockout mouse strain might be very useful, assuming that it would be viable and amenable for studies. Further, based on this mouse model, transgenic human CES1 expressed in the liver and CES2 expressed in liver and/or intestine could be generated. With a more extensive carboxylesterase-deficient background mouse model, and humanized CES transgenic mouse models, perhaps more sensitive and accurate studies could be performed to evaluate the separate and specific roles of human CES1 or CES2 in physiological and drug ADME processes. However, not limited to this, another hepatic and intestinal esterase, arylacetamide deacetylase (AADAC), also shares many exogenous (xenobiotic) and endogenous substrates with CES enzymes. Therefore, generation of a triple knockout mouse strain (*Ces1*-, *Ces2*-, and *AADAC*-deficient) and related humanized mouse models can be also considered, again of course assuming that such strains would be viable and amenable to functional studies. Of note, the possibility of (partial) functional compensation in these various genetically modified mouse models by altered expression of functionally related esterases or of other detoxifying proteins can certainly not be excluded.

2) CES2 can hydrolyze its substrates in both intestine and liver. This combined metabolism process (first-pass intestinal and hepatic metabolism) brings up some implications for drug design as well. Therapeutic agents often cause intestinal diarrhea¹¹, and this includes chemotherapies¹² or targeted therapies¹² or even immunotherapies¹³. Considering this situation, in order to prevent or alleviate treatment-induced diarrhea, some protective drug candidates specifically targeting the intestine (enterocytes) may be developed. While still quite theoretical, by appropriate engineering of these compounds with ester moieties, it might be possible to have their pharmacodynamically active compound “arrest in” or “escape from” the enterocytes due to enterocyte-specific esterase activity. This could enhance their efficacy and/or limit their toxicity

as much as possible. Similar principles might be applied for liver-targeting drugs, depending on the tissue-specific expression and activity of esterases.

PART II. THE EFFECTS OF DRUG TRANSPORTERS AND CYP3A ENZYMES ON THE PHARMACOKINETICS OF SELECTIVE ANTI-TUMOR SMALL MOLECULAR INHIBITORS

The pharmacological functions of the ABCB1 and ABCG2 efflux transporters

It has been well established that drug efflux and influx transporters such as the ATP-binding cassette (ABC) transporters and the organic anion transporting polypeptides (OATPs), as well as the drug-metabolizing enzyme CYP3A, can influence drug ADME processes with broad substrate specificity¹⁴⁻¹⁶. In this thesis, we investigated the pharmacological functions of the two most prominent ABC drug efflux transporters, ABCB1 (P-glycoprotein: P-gp) and ABCG2 (breast cancer resistance protein: BCRP) for the selective small-molecular tyrosine kinase inhibitors (TKIs) larotrectinib, seliprecatinib and pralsetinib. This was done both *in vitro*, by using transwell transport assays and *in vivo*, by using the single and combination knockout mouse models of ABCB1 and ABCG2. Only for larotrectinib we observed a clearly increased systemic exposure of larotrectinib when either ABCB1 or ABCG2 was deficient, and an even further increase when both ABCB1 and ABCG2 were absent. While this was not always significant, similar trends showed up for the other two TKIs. This apparent oral bioavailability discrepancy may be mainly due to the different physicochemical properties of the specific TKIs, or perhaps the presence of differential high-capacity uptake systems in the epithelial cells, or possibly both. All of these three TKIs theoretically have a high capacity of passive bio-membrane penetration (lipophilic efficiency, $LipE \geq 5$)¹⁷, which might suggest high intestinal absorption due to passive diffusion. This suggests that the epithelial drug exporting systems may dominate the systemic exposure differences between the three TKIs. Indeed, *in vitro* trans-well results revealed that larotrectinib was much more efficiently transported by ABCB1 and ABCG2 compared to seliprecatinib or pralsetinib. The complete deficiency of ABCB1 and/or ABCG2, especially in hepatocytes and/or enterocytes, as well as in renal epithelial cells, would thus markedly increase the larotrectinib overall systemic exposure, but less so for seliprecatinib or pralsetinib.

Probably related to this, a pronounced reduction in intestinal lumen recovery of all of these three TKIs due to the absence of ABCB1 and ABCG2 was also observed (most for larotrectinib, moderately for pralsetinib and least for seliprecatinib). This phenomenon could suggest a more extensive absorption of drug across the intestinal wall in the absence of intestinal ABC transporter activity (essentially because of loss of an intestinal excretion process), or reduced hepatobiliary excretion of the absorbed drug normally mediated by these transporters in the bile canaliculi of the liver, or a combination of both processes. The absolute amount, as well as percentage recovery of dose, in the intestine contents was decreased for all three orally

administered TKIs, but only larotrectinib showed clearly increased systemic exposure in the ABCB1 and/or ABCG2 knockout mice. We would like to emphasize here that a reduced drug amount in the gut lumen does not necessarily mean that there is a noticeably increased drug exposure in the systemic circulation. As the absolute amount of drug recovered from the small intestine is in most cases only a limited percentage of the total amount of drug absorbed, the impact on the systemic levels of the drug may be quite limited. Thus in the cases of selpercatinib and pralsetinib, there were no obvious overall systemic exposure increases observed when ABCB1 and/or ABCG2 were absent.

Interestingly, unlike the oral bioavailability differences, the brain penetration of all of these three inhibitors was clearly restricted by ABCB1 and/or ABCG2 in the blood-brain barrier (BBB). BBB endothelial cells are tightly connected with low permeability and high density of the ABC transporters¹⁸. In addition, the BBB is highly selective, and generally allows only the mediated uptake of a few specific compounds, such as nutrients and signaling molecules essential for brain function¹⁸. In contrast, the intestinal epithelium, while presenting an important functional barrier between the outside world and the systemic circulation, needs to be able to absorb a large number and variety of nutritional compounds. It must therefore be equipped with a large number of functional uptake systems, many of which may facilitate the uptake of oral drugs. Moreover, there is a much higher concentration of drugs in the small intestinal lumen (after oral drug administration) than in the blood exposing the brain. Intestinal drug is therefore much more likely to saturate the intestinal ABC transporter activity. These considerations also suggest that many intestinal-type drug uptake systems are likely absent from the BBB, or only lowly expressed, making the ABC transporter-mediated efflux (counteracting this modest influx) more effective and noticeable in the brain.

However, enhanced drug accumulation in the brain can have positive and negative effects. On the one hand, this may improve the therapeutic effects for specific medicines, especially those targeting cancer brain metastasis and/or central nervous system diseases. On the other hand, this may also induce potential central nervous system toxicity. Even though we have not observed this in our pre-clinical studies with larotrectinib, selpercatinib, and pralsetinib, we have seen acute and even lethal CNS toxicity for some other TKIs in *Abcb1a/1b;Abcg2*-deficient mice¹⁹. These insights may provide some suggestions for optimizing the clinical usage of larotrectinib, selpercatinib and pralsetinib, especially when considering drug-drug interactions with powerful ABCB1 and ABCG2 inhibitors.

The pharmacological functions of SLCO1A/1B (OATP1A/1B) uptake transporters

As some of the most important members of the solute carrier organic anion (SLCO) uptake transporter family (also known as organic anion transporting polypeptides: OATPs), the SLCO1A/1B proteins (OATP1A/1B) are highly expressed in the liver and intestine, and are responsible for the

uptake of a wide variety of drugs²⁰⁻²³. We previously generated *Slco1a/1b*^{-/-} mice, and human SLCO1B1 or -1B3 liver-specific transgenic mice based on *Slco1a/1b*^{-/-} mice²²⁻²⁴. With these mouse models, we confirmed the important pharmacological and physiological functions of SLCO1A/1B with a series of studies²⁰⁻²⁸. Therefore, we also performed pharmacokinetic studies with the three above-mentioned TKIs in the SLCO1A/1B-related mouse models. Our results revealed that mouse *Slco1a/1b* clearly limited the oral exposure, as well as liver- and intestine-to-plasma-ratios of larotrectinib. We further found that larotrectinib is a likely substrate of human SLCO1A2 *in vitro*, but not of human SLCO1B1 or -1B3. The latter negative result was further confirmed in a follow-up *in vivo* study with SLCO1B1 and -1B3 humanized mice. All of this suggests that the observed uptake effect was mainly due to mSlco1a1 and/or mSlco1a4, and perhaps *Slco1b2*, in the mouse liver. The deficiency of hepatic sinusoidal mOatp1 leads to relatively reduced larotrectinib uptake into the liver and consequently higher larotrectinib levels in the blood. The decreased accumulation of larotrectinib in the liver may then also result in relatively reduced hepatobiliary excretion of larotrectinib, restricting the amount of larotrectinib returned to the intestinal lumen. Of note, despite the considerable expression level of some *Slco1a/1b* transporters in the BBB and blood-testis barrier (BTB), there were no noticeable effects on larotrectinib brain and testis penetration. This may be because the abundant ABC efflux transporters ABCB1 and ABCG2 are also present in the BBB and BTB, where they have been demonstrated to avidly transport larotrectinib, potentially overwhelming the uptake functions of SLCO1A/1B.

However, such clear uptake effects of SLCO1A/1B were not seen for the other two drugs (selpercatinib and pralsetinib). Even though we found a non-significant increase in oral exposure of selpercatinib in *Slco1a/1b*^{-/-} mice, the liver or intestinal drug accumulation was not influenced. In addition, the *in vitro* uptake results suggested that selpercatinib was not a human SLCO1A2, -1B1 or -1B3 substrate. Taken all this together, the selpercatinib and pralsetinib pharmacokinetic properties were not, or at least not significantly, affected by SLCO1A/1B uptake transporters.

Larotrectinib is, to our knowledge, the first targeted TKI anticancer drug for which the disposition of the parent compound is demonstrated to be strongly affected by mouse *Slco1a/1b* proteins (Oatps). For some targeted drugs, such as sorafenib, the disposition of the negatively charged glucuronide metabolite can be strongly affected, but impact on the parent compound is minimal. It therefore appears that pharmaceutical companies are relatively efficient in developing targeted anticancer drugs that are minimal OATP substrates. Pharmaceutical companies may mainly test the uptake effects by *in vitro* uptake experiments with transduced cell lines, such as SLCO1A2, -1B1, -1B3 or -2B1 overexpressing HEK293 cells. However, SLCO-mediated uptake of certain substrates can be cell-type dependent for as yet unknown reasons, so a negative result does not necessarily mean that a substrate cannot be transported under any circumstances²⁹. We therefore would still recommend vigilance in recognizing possible SLCO-mediated drug-drug

interactions during the clinical application of specific drug candidates, for example, larotrectinib in our case.

The pharmacological functions of the CYP3A enzyme complex

As crucial detoxification systems, Cytochrome P450 3A (CYP3A) enzymes are involved in the metabolism of around half of the current clinically used drugs^{30,31}. Considering their important pharmacological functions, we previously generated and characterized Cyp3a knockout mice (*Cyp3a*^{-/-}), and human CYP3A4 liver- and intestine-specific transgenic mice (*Cyp3aXAV*)³²⁻³⁴. These mouse strains have shown to be useful models in multiple pharmacokinetic studies, and CYP3A enzymes were demonstrated to markedly influence a number of specific drug candidates^{32,35,36}. In this thesis, we explored the pharmacological effects of CYP3A for larotrectinib, selpercatinib and pralsetinib. The results revealed that the oral availability of larotrectinib and selpercatinib, but not pralsetinib, can be significantly restricted by CYP3A, especially for larotrectinib. The effect of Cyp3a and CYP3A4 was mainly seen in the different plasma oral exposures, without any meaningful changes in tissue-to-plasma ratios for larotrectinib and selpercatinib. It is very likely that the substantial intestinal and hepatic first-pass metabolism and elimination functions of CYP3A for larotrectinib and selpercatinib will have markedly influenced their overall systemic and tissue exposure and thus efficacy. However, with respect to pralsetinib, the results suggest that CYP3A, and especially human CYP3A4, may not play a substantial role in its metabolic clearance. The increased oral exposure of pralsetinib we observed in CYP3AXAV mice suggested there may be one or more other, as yet unidentified, pralsetinib detoxification (elimination) systems which are downregulated when CYP3A4 is reintroduced. These systems might be responsible for the modest pharmacokinetic changes that we observed among the strains. We have previously observed similar compensatory phenomena for the metabolism of midazolam by Cyp3a in Cyp3a knockout mice, where upregulation of several Cyp2c enzymes metabolizing midazolam just about compensated for the reduced midazolam metabolism by the absence of Cyp3a³⁷. Nonetheless, the most likely interpretation of our data is that CYP3A4 itself is not an important determinant of pralsetinib pharmacokinetics in mice.

Given the importance of CYP enzyme families in pharmacology, pharmaceutical companies generally need to identify the potential metabolizing functions of CYP enzymes before their drug under development gets approved, especially for CYP3A. Of note, CYP3A levels among human donors can vary as much as 40-fold in both liver and small intestine, which can markedly affect the drug metabolism process and consequently therapeutic efficacy of substrate drugs³⁸. These large inter- and intra-individual differences can come from various controlling factors of gene expression and enzyme activity, such as circulating hormones, or drugs and food-derived xenobiotics, or from genetic polymorphisms³⁸. Thus, a good understanding of CYP3A enzyme pharmacology functions with respect to a specific drug is essential.

Drug-drug interaction studies

Potential drug-drug interactions (DDI) may profoundly affect drug pharmacokinetics (ADME processes associated with both treatment failure or toxicity) and pharmacodynamics³⁹. The pharmacokinetic profiles of all of the three small-molecule inhibitors we studied were markedly influenced by the ABCB1 and ABCG2 transporters, especially the brain accumulation. It has been well established that co-administration of elacridar, a dual inhibitor of ABCB1 and ABCG2, could improve both oral exposure and brain penetration (one of our particular interests) of several TKIs^{19,40-42}. Therefore, we performed drug-drug interaction studies for these three small-molecule inhibitors together with elacridar. Co-administration of elacridar in wild-type mice generated a similar profile as seen in the ABC transporter genetically modified mouse strain (ABCB1 and ABCG2 combination knockout mice). In detail, elacridar could markedly increase the oral availability of larotrectinib, as well as that of pralsetinib (moderately but significantly), but not of selpercatinib. Consistent with the plasma exposure results, decreased intestinal lumen recovery measured as percentage of the dose was observed very clearly for larotrectinib, significantly for pralsetinib, and slightly but not significantly for selpercatinib. In contrast, the blood-brain-barrier showed relatively similar drug accumulation enhancement effects by elacridar among the three TKIs. The obtained data and comparison with the results seen in the ABC transporter knockout mice demonstrate that elacridar efficiently inhibits ABCB1 and ABCG2 transport functions in both the enterohepatic system and the BBB.

As larotrectinib is also a quite substantial substrate of the SLCO1A/1B uptake transporters and CYP3A enzymes, we also explored the potential drug-drug interactions of larotrectinib with rifampin (a prototypical Slco1a/1b inhibitor)^{28,43} or ritonavir (a prototypical CYP3A enzyme inhibitor)^{35,36}. Somewhat to our surprise, in the rifampin study, we observed not only larotrectinib liver-to-plasma ratio decreases, but also intestinal contents-to-plasma ratio decreases. This indicates that, besides inhibiting hepatic Slco1a/1b transporters, other larotrectinib-handling systems must have been influenced by rifampin. It is known that oral rifampin can also inhibit enterocyte ABCB1 (P-gp), without affecting hepatic ABCB1 or renal transporters^{44,45}, resulting in reduced efflux of digoxin, an excellent ABCB1 substrate, into the intestinal lumen. As larotrectinib is also an excellent ABCB1 substrate, it is very likely that a similar process applies in our mouse models: inhibition of intestinal ABCB1 by the high concentration of oral rifampin present in the intestinal lumen results in reduced direct intestinal excretion and increased net absorption of larotrectinib. This explains the strongly reduced small intestine combined with small intestinal content levels of larotrectinib upon rifampin treatment. Such extra inhibition effects were also observed in ritonavir boosting experiments, where ritonavir, administered as a CYP3A inhibitor, unexpectedly also enhanced the overall systemic exposure of larotrectinib in *Cyp3a*^{-/-} mice. While ritonavir primarily inhibits CYP3A-mediated metabolism, it is known that it can also inhibit ABCB1^{46,47}. As we found that ritonavir strongly reduced both liver and small intestine combined with small intestinal content distribution of larotrectinib even in *Cyp3a*^{-/-} mice, the most likely

explanation is that ritonavir could also inhibit ABCB1 in both small intestine and liver, thus enhancing the larotrectinib exposure even when Cyp3a is absent.

Taken together, the drug-drug interaction studies revealed that the drug transporter or drug-metabolizing enzyme inhibitors can alter the specific drug pharmacokinetic properties and thus possibly influence its safety and efficacy profiles. Still, the observations from the larotrectinib case that some known possibly co-administered inhibitors such as rifampin (for OATPs) and ritonavir (for CYP3A) can simultaneously affect some other important detoxification systems does pose a potential risk that needs to be carefully considered. Even though no signs of spontaneous toxicity of larotrectinib, selpercatinib or pralsetinib showed up in any of the tested mouse strains in our experiments, given the complications we observed, any attempt to apply “specific” inhibitors or combination therapy regimens in patients together with these TKIs should be carefully monitored.

Possible future research lines

Some implications from **Part II** of the current thesis, also considering future research lines, are as follows:

1) The generation of humanized mouse models with ABCB1 and/or ABCG2 specifically expressed in the BBB can be considered. In fact, there have been some attempts to express human ABCB1 in the BBB with human *ABCB1* cDNA fused to the translational start ATG of the mouse *Abcb1a* and/or *Abcb1b* gene. Both attempts failed, with negligible expression levels of the human ABCB1 protein, probably because of unexpected alternative splicing and/or alternative polyadenylation, or perhaps other unknown reasons^{48,49}. However, considering the crucial pharmacological functions of ABCB1 and ABCG2, it is worthwhile to further explore the possibility of developing humanized ABCB1/ABCG2 strains, especially with BBB-specific expression;

2) Specific inhibitors, such as elacridar, can efficiently inhibit ABC efflux transporter activities in mice. On the one hand, this suggests the potential application of ABC transporter inhibitors in the clinic to further enhance the efficacy of target drugs. During the last several decades, investment in the clinical development of ABCB1/ABCG2 inhibitors has been virtually absent, mostly as a result of disappointing trials in the early 1990s concerning efforts to reverse multidrug resistance in clinical tumors. A lot of the early generation inhibitors suffered from toxicity, while newer generation agents largely failed from lack of clinical response, which may be partially due to poor oral availability (for instance for elacridar) and/or poor preselection of the tumors included in these studies^{50,51}. Inspired by the insights of part I, perhaps specific ester (pro-)drugs can be developed for ABC transporter inhibitors in order to improve their oral availability, with release of the active form when subjected to the first-pass esterase metabolism in intestine and liver. If this principle works, the overall exposure of active inhibiting compound targeting

ABCB1/ABCG2 will thus be increased, which may provide efficient inhibition functions even at the BBB. On the other hand, potential central nervous system (CNS) toxicity due to drug-drug interactions or even genetic polymorphisms may also be a concern. In a previous study in our group, brigatinib over-accumulation in the brain due to genetic knockout or pharmacological inhibition of mAbcb1a/1b and mAbcg2 induced severe CNS toxicity in mice¹⁹. In addition, recently, Baudou et al. reported a case of a 13-year-old boy who displayed severe adverse effects after a normal therapeutic dose of ivermectin was administered. This turned out to be caused by a complete genetic ABCB1 deficiency⁵². Thus, any attempts to enhance the overall exposure or brain accumulation of target drugs in patients using ABCB1/ABCG2 inhibitors, as well as the application of combination therapy regimens which involve strong ABCB1/ABCG2 substrates, should first be carefully monitored for safety.

SUMMARY

In **Part I** of the thesis, we generated and characterized several CES2-related gene modified mouse models to systematically explore the specific pharmacological and physiological roles of CES2. Based on these new mouse models, CES2 was demonstrated to strongly affect vinorelbine and capecitabine metabolism, and to improve lipid and glucose homeostasis. In **Part II** of the thesis, we demonstrated the effects of ABC transporters (ABCB1 and ABCG2), SLCO uptake transporters (SLCO1A/1B) and the CYP3A metabolizing enzyme on larotrectinib, selpercatinib and pralsetinib pharmacokinetics using relevant gene-modified mouse strains. In addition, such effects can be also influenced by drug-drug interactions. The insights obtained in the current thesis provide more theoretical and practical information for better understanding of the potential pharmacological and/or physiological functions of different detoxification systems. This information can be useful for initial drug design, during further drug development, and for optimization of the final clinical drug regimens and therapeutic applications.

REFERENCE

- Yoshida, T., *et al.* Difference in substrate specificity of carboxylesterase and arylacetamide deacetylase between dogs and humans. *European Journal of Pharmaceutical Sciences* **111**, 167-176 (2018).
- Casey Laizure, S., Herring, V., Hu, Z., Witbrodt, K. & Parker, R.B. The Role of Human Carboxylesterases in Drug Metabolism: Have We Overlooked Their Importance? *Pharmacotherapy* **33**, 210-222 (2013).
- Staudinger, J.L., Xu, C., Cui, Y.J. & Klaassen, C.D. Nuclear receptor-mediated regulation of carboxylesterase expression and activity. *Expert Opinion on Drug Metabolism & Toxicology* **6**, 261-271 (2010).
- Imai, T. Human carboxylesterase isozymes: catalytic properties and rational drug design. *Drug Metabolism and Pharmacokinetics* **21**, 173-185 (2006).
- Lian, J., Nelson, R. & Lehner, R. Carboxylesterases in lipid metabolism: from mouse to human. *Protein Cell* (2017).
- Maresch, L.K., *et al.* Intestine-Specific Overexpression of Carboxylesterase 2c Protects Mice From Diet-Induced Liver Steatosis and Obesity. *Hepatology communications* **3**, 227-245 (2019).
- Ruby, M.A., *et al.* Human Carboxylesterase 2 Reverses Obesity-Induced Diacylglycerol Accumulation and Glucose Intolerance. *Cell Reports* **18**, 636-646 (2017).
- Li, Y., *et al.* Carboxylesterase 2 prevents liver steatosis by modulating lipolysis, endoplasmic reticulum stress, and lipogenesis and is regulated by hepatocyte nuclear factor 4 alpha in mice. *Hepatology* **63**, 1860-1874 (2016).
- Azzu, V., Vacca, M., Virtue, S., Allison, M. & Vidal-Puig, A. Adipose Tissue-Liver Cross Talk in the Control of Whole-Body Metabolism: Implications in Nonalcoholic Fatty Liver Disease. *Gastroenterology* **158**, 1899-1912 (2020).
- Samuel, V.T., Petersen, K.F. & Shulman, G.I. Lipid-induced insulin resistance: unravelling the mechanism. *Lancet* **375**, 2267-2277 (2010).
- Yu, Y., *et al.* Two birds, one stone: hesperetin alleviates chemotherapy-induced diarrhea and potentiates tumor inhibition. *Oncotarget* **9**, 27958-27973 (2018).
- Stein, A., Voigt, W. & Jordan, K. Chemotherapy-induced diarrhea: pathophysiology, frequency and guideline-based management. *Therapeutic Advances in Medical Oncology* **2**, 51-63 (2010).
- Weber, J.S., Yang, J.C., Atkins, M.B. & Disis, M.L. Toxicities of Immunotherapy for the Practitioner. *Journal of Clinical Oncology* **33**, 2092-2099 (2015).
- Nigam, S.K. What do drug transporters really do? *Nature Reviews Drug Discovery* **14**, 29-44 (2014).
- Russel, F.G.M. Transporters: Importance in Drug Absorption, Distribution, and Removal. 27-49 (2010).
- Giacomini, K.M., *et al.* Membrane transporters in drug development. *Nature Reviews Drug Discovery* **9**, 215-236 (2010).
- Roskoski, R., Jr. Properties of FDA-approved small molecule protein kinase inhibitors: A 2022 update. *Pharmacological Research* **175**, 106037 (2021).
- Luissint, A.C., Artus, C., Glacial, F., Ganeshamoorthy, K. & Couraud, P.O. Tight junctions at the blood brain barrier: physiological architecture and disease-associated dysregulation. *Fluids Barriers CNS* **9**, 23 (2012).
- Li, W., *et al.* P-glycoprotein and breast cancer resistance protein restrict brigatinib brain accumulation and toxicity, and, alongside CYP3A, limit its oral availability. *Pharmacological Research* **137**, 47-55 (2018).
- Durmus, S., *et al.* In vivo disposition of doxorubicin is affected by mouse Oatp1a/1b and human OATP1A/1B transporters. *International Journal of Cancer* **135**, 1700-1710 (2014).
- Zimmerman, E.I., *et al.* Contribution of OATP1B1 and OATP1B3 to the disposition of sorafenib and sorafenib-glucuronide. *Clinical Cancer Research* **19**, 1458-1466 (2013).
- van de Steeg, E., van Esch, A., Wagenaar, E., Kenworthy, K.E. & Schinkel, A.H. Influence of human OATP1B1, OATP1B3, and OATP1A2 on the pharmacokinetics of methotrexate and paclitaxel in humanized transgenic mice. *Clinical Cancer Research* **19**, 821-832 (2013).
- van de Steeg, E., *et al.* Organic anion transporting polypeptide 1a/1b-knockout mice provide insights into hepatic handling of bilirubin, bile acids, and drugs. *Journal of Clinical Investigation* **120**, 2942-2952 (2010).
- van de Steeg, E., *et al.* Methotrexate Pharmacokinetics in Transgenic Mice with Liver-Specific Expression of Human Organic Anion-Transporting Polypeptide 1B1 (SLCO1B1). *Drug Metabolism and Disposition* **37**, 277-281 (2008).
- Shitara, Y., *et al.* Clinical significance of organic anion transporting polypeptides (OATPs) in drug disposition: their roles in hepatic clearance and intestinal absorption. *Biopharmaceutics and Drug Disposition* **34**, 45-78 (2013).
- Iusuf, D., van de Steeg, E. & Schinkel, A.H. Functions of OATP1A and 1B transporters in vivo: insights from mouse models. *Trends in Pharmacological Sciences* **33**, 100-108 (2012).
- van de Steeg, E., *et al.* Methotrexate pharmacokinetics in transgenic mice with liver-specific expression of human organic anion-transporting polypeptide 1B1 (SLCO1B1). *Drug Metabolism and Disposition* **37**, 277-281 (2009).
- Salphati, L., *et al.* Evaluation of organic anion transporting polypeptide 1B1 and 1B3 humanized mice as a translational model to study the pharmacokinetics of statins. *Drug Metabolism and Disposition* **42**, 1301-1313 (2014).
- de Graan, A.J., *et al.* Influence of polymorphic OATP1B-type carriers on the disposition of docetaxel. *Clinical Cancer Research* **18**, 4433-4440 (2012).
- Lynch, T. & Price, A. The effect of cytochrome P450 metabolism on drug response, interactions, and adverse effects. *American Family Physician* **76**, 391-396 (2007).
- Guengerich, F.P. Cytochrome P-450 3A4: regulation and role in drug metabolism. *Annual Review of Pharmacology and Toxicology* **39**, 1-17 (1999).
- van Waterschoot, R.A., *et al.* Intestinal cytochrome P450 3A plays an important role in the regulation of detoxifying systems in the liver. *FASEB Journal* **23**, 224-231 (2009).
- van Herwaarden, A.E., van Waterschoot, R.A. & Schinkel, A.H. How important is intestinal cytochrome P450 3A metabolism? *Trends in Pharmacological Sciences* **30**, 223-227 (2009).
- van Herwaarden, A.E., *et al.* Knockout of cytochrome P450 3A yields new mouse models for understanding xenobiotic metabolism. *Journal of Clinical Investigation* **117**, 3583-3592 (2007).
- Hendriks, J.J., *et al.* Oral co-administration of elacridar and ritonavir enhances plasma levels of oral paclitaxel and docetaxel without affecting relative brain accumulation. *British Journal of Cancer* **110**, 2669-2676 (2014).
- ter Heine, R., *et al.* An integrated pharmacokinetic model for the influence of CYP3A4 expression on the in vivo disposition of lopinavir and its modulation by ritonavir. *Journal of Pharmaceutical Sciences* **100**, 2508-2515 (2011).
- van Waterschoot, R.A., *et al.* Midazolam metabolism in cytochrome P450 3A knockout mice can be attributed to up-regulated CYP2C enzymes. *Molecular Pharmacology* **73**, 1029-1036 (2008).
- Lamba, J.K., Lin, Y.S., Schuetz, E.G. & Thummel, K.E. Genetic contribution to variable human CYP3A-mediated metabolism. *Advanced Drug Delivery Reviews* **54**, 1271-1294 (2002).
- Palleria, C., *et al.* Pharmacokinetic drug-drug interaction and their implication in clinical management. *Journal of Research in Medical Sciences* **18**, 601-610 (2013).
- Li, W., *et al.* ABCB1 and ABCG2 Restrict Brain and Testis Accumulation and, Alongside CYP3A, Limit Oral Availability of the Novel TRK Inhibitor Selitrectinib. *Molecular Cancer Therapeutics* **20**, 1173-1182 (2021).
- Li, W., *et al.* P-glycoprotein (MDR1/ABCB1) controls brain accumulation and intestinal disposition of the novel TGF- β signaling pathway inhibitor galunisertib. *International Journal of Cancer* **146**, 1631-1642 (2020).
- Li, W., *et al.* Oral coadministration of elacridar and ritonavir enhances brain accumulation and oral availability of the novel ALK/ROS1 inhibitor lorlatinib. *European Journal of Pharmaceutics and Biopharmaceutics* **136**, 120-130 (2019).
- Durmus, S., *et al.* Preclinical Mouse Models To Study Human OATP1B1- and OATP1B3-Mediated Drug-Drug Interactions in Vivo. *Molecular Pharmaceutics* **12**, 4259-4269 (2015).
- Reitman, M.L., *et al.* Rifampin's acute inhibitory and chronic inductive drug interactions: experimental and model-based approaches to drug-drug interaction trial design. *Clinical Pharmacology and Therapeutics* **89**, 234-242 (2011).
- Greiner, B., *et al.* The role of intestinal P-glycoprotein in the interaction of digoxin and rifampin. *Journal of Clinical Investigation* **104**, 147-153 (1999).

46. Gutmann, H., Fricker, G., Drewe, J., Toeroek, M. & Miller, D.S. Interactions of HIV protease inhibitors with ATP-dependent drug export proteins. *Molecular Pharmacology* **56**, 383-389 (1999).
47. Drewe, J., *et al.* HIV protease inhibitor ritonavir: a more potent inhibitor of P-glycoprotein than the cyclosporine analog SDZ PSC 833. *Biochemical Pharmacology* **57**, 1147-1152 (1999).
48. Krohn, M., *et al.* Humanization of the Blood-Brain Barrier Transporter ABCB1 in Mice Disrupts Genomic Locus - Lessons from Three Unsuccessful Approaches. *European Journal of Microbiology & Immunology* **8**, 78-86 (2018).
49. Sadiq, M.W., *et al.* Validation of a P-Glycoprotein (P-gp) Humanized Mouse Model by Integrating Selective Absolute Quantification of Human MDR1, Mouse Mdr1a and Mdr1b Protein Expressions with In Vivo Functional Analysis for Blood-Brain Barrier Transport. *PLoS One* **10**, e0118638 (2015).
50. Lai, J.I., Tseng, Y.J., Chen, M.H., Huang, C.F. & Chang, P.M. Clinical Perspective of FDA Approved Drugs With P-Glycoprotein Inhibition Activities for Potential Cancer Therapeutics. *Frontiers in Oncology* **10**, 561936 (2020).
51. Dash, R.P., Jayachandra Babu, R. & Srinivas, N.R. Therapeutic Potential and Utility of Elacridar with Respect to P-glycoprotein Inhibition: An Insight from the Published In Vitro, Preclinical and Clinical Studies. *European Journal of Drug Metabolism and Pharmacokinetics* **42**, 915-933 (2017).
52. Baudou, E., *et al.* Serious Ivermectin Toxicity and Human ABCB1 Nonsense Mutations. *New England Journal of Medicine* **383**, 787-789 (2020).



CHAPTER 6

SUMMARY

6.1 SUMMARY

A number of broad-specific detoxification systems, including drug transporters and metabolizing enzymes, can protect the body from various toxins, and dramatically influence drug absorption, metabolism, distribution and elimination (ADME) processes, as well as in some cases physiological homeostasis. In view of the likely importance of carboxylesterase 2 in pharmacological and physiological processes, we generated and characterized several CES2-related genetically modified mouse models, and then applied these in pre-clinical drug metabolism and physiology-metabolic studies in **Part I** of this thesis. In **Part II** of this thesis, the potential pharmacokinetic effects of drug transporters (especially ABCB1/ABCG2 and/or OATP1A/1B) and metabolizing enzymes (particularly CYP3A) were investigated for three small-molecule tyrosine kinase inhibitors (TKIs), as well as their role in drug-drug interactions.

PART I. PHARMACOLOGICAL AND PHYSIOLOGICAL FUNCTIONS OF THE CARBOXY-LESTERASE 2 COMPLEX

In **chapter 1.1**, we review the pharmacological functions of the main esterase enzymes, including carboxylesterase (CES) 1 and 2, and arylacetamide deacetylase (AADAC). Considering that CES and AADAC are present in both intestine and liver, they may play important roles in intestinal and hepatic elimination of oral drugs (first-pass metabolism). These processes can profoundly influence the overall exposure, the efficacy, and even the safety of specific ester (pro-)drugs. We summarize their specific substrates and inhibitors, relevant genetic polymorphisms, hepatic or intestinal roles in drug metabolism and available pre-clinical mouse models for various research needs. In **chapter 1.2** we provide a brief introduction to the physiological functions of the above-mentioned esterase enzymes. We also summarize the findings on physiological effects of specific esterases in previous studies, including in lipid metabolism and glucose/insulin homeostasis, as well as related metabolic syndromes, such as Non-Alcoholic Fatty Liver Disease (NAFLD), diabetes and atherosclerosis.

Chapter 2 reports on the generation of several CES2-related mouse models, including full mouse *Ces2* cluster deletion mice (*Ces2*^{-/-}), and two humanized CES2 transgenic mouse strains with human CES2 expression either in liver or intestine of *Ces2*^{-/-} mice (*Ces2*^{-/-A} or *Ces2*^{-/-V}). The CES2 genetically engineered mouse models were generated efficiently, were viable and fertile, and demonstrated the important functions of CES2 in vinorelbine and capecitabine metabolism. Moreover, a significant role of CES2 in improving lipid metabolism and glucose homeostasis was confirmed. These mouse models are expected to facilitate development of several (pro-) drug classes and to improve drug administration regimens. In addition, with these models, better understanding of CES2 involvement in energy metabolism processes and thus deeper physiological insights can be obtained. This could help us to further explore potential solutions for the metabolic syndrome problem.

PART II. THE EFFECTS OF DRUG TRANSPORTERS AND CYP3A ENZYMES ON THE PHARMACOKINETICS OF SELECTIVE ANTI-TUMOR SMALL MOLECULAR INHIBITORS

In **Chapter 3**, we briefly introduce the pharmacokinetic effects of drug transporters, including the ABC efflux transporters ABCB1 and ABCG2, and the OATP uptake transporters (OATP1A/1B), as well as the drug-metabolizing enzyme complex CYP3A. The respective family members, expression levels and tissue locations, genetic polymorphisms, and potential drug-drug interactions (DDI) with specific transporters or enzymes are discussed.

Larotrectinib is an FDA-approved oral small-molecule inhibitor for the treatment of neurotrophic tropomyosin receptor kinase (NTRK) fusion-positive cancer. **Chapter 4.1** explores whether the pharmacokinetic properties of larotrectinib can be influenced by the above-mentioned transporters and CYP3A. We found that ABCG2 and especially ABCB1 can limit the oral availability and brain penetration of larotrectinib. In addition, OATP1A/1B (most likely the OATP1A proteins) can restrict larotrectinib systemic exposure by mediating hepatic uptake of larotrectinib and thus, presumably, facilitating its hepatobiliary excretion. Additionally, CYP3A-mediated metabolism can strongly reduce larotrectinib oral availability and thus its tissue concentrations. The obtained insights and investigated principles may potentially be used to further enhance the therapeutic application and efficacy of larotrectinib, especially for brain metastases in NSCLC and for glioblastoma patients.

Considering that larotrectinib pharmacokinetic behavior can be affected by multiple factors, including, but perhaps not limited to, ABC transporters, OATP1A, and CYP3A, in **chapter 4.2** we performed drug-drug interaction studies by co-administering larotrectinib with elacridar (ABCB1/ABCG2 inhibitor), rifampin (OATP1A/1B inhibitor) and ritonavir (CYP3A inhibitor), respectively. The results revealed that elacridar enhances both larotrectinib plasma and tissue exposure and especially relative brain penetration, which might be therapeutically relevant. Moreover, rifampin enhances larotrectinib systemic exposure, most likely by inhibiting mOatp1a/1b, but probably also hepatic and/or intestinal mAbcb1 activity. Similar to rifampin, dual-inhibition functions of ritonavir affecting both CYP3A enzymes and hepatic and/or intestinal Abcb1 transport enhanced larotrectinib oral availability. Such insights may be used to further optimize the clinical-therapeutic application of larotrectinib.

Similar pharmacokinetic studies were performed for selpercatinib and pralsetinib, two highly selective, ATP-competitive small-molecule RET inhibitors, in **chapters 4.3** and **4.4**, respectively. Briefly, ABCG2 and especially ABCB1 can limit the oral availability and brain and testis penetration of both selpercatinib and pralsetinib. Furthermore, elacridar co-administration could markedly enhance the brain accumulation of oral selpercatinib and pralsetinib. There was no clear evidence that either of these two inhibitors is a good transport substrate of OATP1A/1B. In addition, CYP3A-mediated metabolism could markedly reduce selpercatinib oral availability and thus

its tissue concentrations, but not for pralsetinib. This suggests that some other detoxification systems may mediate the elimination of pralsetinib instead. The obtained insights may potentially be used to further enhance the therapeutic application and efficacy of selpercatinib or pralsetinib, especially for brain metastases in RET fusion/mutation positive NSCLC patients.

In conclusion, in this thesis we demonstrated the value of knockout and humanized transgenic mouse models to investigate the pharmacological and physiological properties of the CES2 enzyme complex. Moreover, a mouse *Ces1* and *Ces2* cluster combination knockout mouse strain was developed and characterized, and successfully applied to explore the combined and separate contributions of each cluster in specific drug metabolism processes, which further demonstrated the important pharmacological functions of carboxylesterase enzymes. Moreover, we explored and added some insights into the roles of drug transporters (ABCB1, ABCG2 and OATP1A/1B) and the drug-metabolizing enzyme CYP3A in pharmacokinetic behavior of several anti-tumor small-molecule inhibitors, as well as related drug-drug interaction effects. All in all, we believe that the obtained new mouse models and pharmacological and physiological insights will provide further useful information and support for improved drug discovery and development, and eventually clinical-therapeutic application regimens.

6.2 SAMENVATTING

Een aantal specifieke ontgiftingssystemen, waaronder geneesmiddel transporters en metaboliserende enzymen, beschermen het lichaam tegen verschillende toxische stoffen en kunnen een dramatische invloed hebben op absorptie, metabolisme, distributie en eliminatie (ADME) processen van geneesmiddelen. In sommige gevallen beïnvloeden zij ook de fysiologische homeostase. Gebaseerd op het feit dat carboxylesterase 2 een belangrijke rol zou kunnen spelen in farmacologische en fysiologische processen, hebben we verschillende CES2-gerelateerde genetisch gemodificeerde muismodellen gegenereerd. Deze zijn vervolgens toegepast in preklinische geneesmiddelmetabolisme en fysiologische studies in **deel I** van dit proefschrift. In **deel II** van dit proefschrift zijn de mogelijke farmacokinetische effecten van efflux transporters (met name ABCB1/ABCG2), influx transporters (OATP1A/1B) en cytochroom P450 enzymen (met name CYP3A) onderzocht voor drie klein-molecuul tyrosine kinase remmers (TKI's), evenals hun rol in de interacties tussen geneesmiddelen.

Deel I. Farmacologische en fysiologische functies van het carboxylesterase 2 complex

In **hoofdstuk 1.1** bespreken we de farmacologische functies van de belangrijkste esterase-enzymen waaronder carboxylesterase (CES) 1 en 2 en arylacetamide deacetylase (AADAC). Aangezien zowel de CES als de AADAC enzymen aanwezig zijn in de darm en de lever, kunnen zij een belangrijke rol spelen bij de hepatische en intestinale eliminatie van orale geneesmiddelen (first-pass metabolisme). Deze processen kunnen de algehele blootstelling, de werkzaamheid en zelfs de veiligheid van specifieke ester-bevattende (pro-)geneesmiddelen drastisch beïnvloeden. In dit hoofdstuk wordt een samenvatting gegeven van specifieke substraten en inhibitoren van deze enzymen, relevante genetische polymorfismen, de rol van de lever en de darm in het metabolisme van geneesmiddelen en beschikbare preklinische muismodellen voor verschillende onderzoeksvragen. In **hoofdstuk 1.2** geven we een korte inleiding op de fysiologische functies van de bovengenoemde esterase-enzymen. De bevindingen over de fysiologische effecten van specifieke esterases in eerdere onderzoeken, waaronder in het lipidenmetabolisme en glucose/insuline homeostase, evenals in gerelateerde metabole syndromen zoals niet-alcoholische leververvetting (NAFLD), diabetes en atherosclerose staan in dit hoofdstuk beschreven.

In **hoofdstuk 2** wordt een overzicht gegeven van CES2-gerelateerde muismodellen, waaronder de volledige muis *Ces2* clusterdeletie muizen (*CES2*^{-/-}) en twee gehumaniseerde CES2 transgene muisstammen met humane CES2 expressie in de lever of darm van *Ces2*^{-/-} muizen (*Ces2*^{-/-A} of *Ces2*^{-/-V}). De genetisch gemodificeerde muismodellen van CES2 zijn zeer efficiënt gegenereerd, levensvatbaar en vruchtbaar en demonstreerden de belangrijke functies van CES2 in het metabolisme van vinorelbine en capecitabine. Bovendien werd een significante rol van CES2 bij het verbeteren van het lipidenmetabolisme en de glucosehomeostase bevestigd. De verwachting

van deze muismodellen is dat ze de ontwikkeling van verschillende (pro-)geneesmiddelklassen vergemakkelijken en hun toedieningsregime kunnen verbeteren. Daarnaast kunnen deze modellen gebruikt worden om meer inzicht te verkrijgen in diepere fysiologische aspecten en een mogelijkheid bieden om onderzoek te doen naar metabole syndromen.

Deel II. Het farmacokinetisch effect van geneesmiddel transporters en het CYP3A enzym op selectieve anti-tumor klein-molecuul remmers

In **hoofdstuk 3** introduceren we de farmacokinetische effecten van de geneesmiddeltransporters, met name de ABCB1 en ABCG2 transporters en de OATP transporters (OATP1A/1B), evenals het CYP3A enzym. De familieleden, expressieniveaus, weefselexpressie, genetische polymorfismen en potentiële geneesmiddelinteracties (DDI) met specifieke transporters of enzymen worden besproken.

Larotrectinib is een door de FDA goedgekeurde klein-molecuul remmer voor de behandeling van tropomyosinereceptor kinase (NTRK) fusie-positieve kanker. In **hoofdstuk 4.1** onderzochten we of de farmacokinetische eigenschappen van larotrectinib beïnvloed kunnen worden door de bovengenoemde transporters en het CYP3A enzym. De resultaten lieten zien dat de ABCG2 transporter en in hogere mate de ABCB1 transporter de orale beschikbaarheid en de hersenpenetratie van larotrectinib kunnen beperken. Daarnaast zijn de OATP1A/1B transporters betrokken bij de beperking van de systematische blootstelling van larotrectinib, door het aanzienlijk verhogen van de opname in de lever en aldus de hepatobiliaire excretie te vergemakkelijken. Ten derde verlaagt CYP3A de orale beschikbaarheid en de weefselconcentratie significant, door het metaboliseren van larotrectinib.

Deze studies geven meer inzicht in de farmacologische functies van de verschillende transporters en het CYP3A enzym. De verkregen inzichten kunnen potentieel bijdrage aan het verbeteren van de therapeutische toepassing en werkzaamheid van larotrectinib, met name voor hersenmetastasen bij NSCLC en glioblastoma patiënten. De farmacokinetische processen van larotrectinib kunnen beïnvloed worden door meerdere factoren, waaronder de ABC en OATP1 transporters en CYP3A. In **hoofdstuk 4.2** onderzochten we de interactie tussen larotrectinib en elacridar (ABCB1/ABCG2 remmer), rifampicine (OATP1A/1B remmer) en ritonavir (CYP3A remmer). De resultaten lieten zien dat elacridar zowel de plasma- als weefselblootstelling van larotrectinib verbetert. Daarnaast zagen we dat de hersenpenetratie significant was verhoogd, wat therapeutisch relevant kan zijn. De gecombineerde toediening met rifampicine resulteerde in een verhoogde systemische blootstelling van larotrectinib, waarschijnlijk door de remming van mOatp1a/1b, maar ook door de hepatische en/of intestinale mAbcb1-activiteit. Vergelijkbaar met rifampicine, resulteerde de gecombineerde remming van ritonavir, die zowel de CYP3A-enzymen als de Abcb1 transporters in de lever en/of de darmen kan beïnvloeden, in een verhoogde

orale beschikbaarheid van larotrectinib. Deze resultaten kunnen worden ingezet om de klinisch-therapeutische toepassing van larotrectinib verder te optimaliseren.

Vergelijkbare farmacokinetische studies werden uitgevoerd voor selpercatinib en pralsetinib, twee zeer selectieve ATP-competitieve klein-molecuul RET-remmers. In **hoofdstukken 4.3 en 4.4** tonen we aan dat ABCG2 en vooral ABCB1 de orale beschikbaarheid en penetratie van selpercatinib en pralsetinib in de hersenen en testis beperken. De toediening van elacridar in combinatie met selpercatinib of pralsetinib verhoogde de hersenaccumulatie aanzienlijk. Er kon niet aangetoond worden dat een van deze twee RET-remmers een transportsubstraat van OATP1A/1B is. Het CYP3A-gemedieerde metabolisme kon de orale beschikbaarheid en de weefselconcentraties van selpercatinib significant verminderen, maar ditzelfde effect werd niet gezien voor pralsetinib. Dit suggereert dat andere ontgiftingssystemen betrokken zijn bij de eliminatie van pralsetinib. Deze bevindingen kunnen mogelijk gebruikt worden om de therapeutische toepassing en werkzaamheid van selpercatinib en pralsetinib verder te verbeteren, met name voor NSCLC patiënten met RET-fusie/mutatie-positieve hersenmetastasen.

Concluderend, in dit proefschrift tonen we aan dat knock-out en transgene muismodellen van grote waarde zijn tijdens het onderzoek naar de farmacologische en fysiologische eigenschappen van het CES2 enzym complex. Ten eerste presenteren we de ontwikkeling en karakterisering van een *Ces1* en *Ces2* cluster combinatie knock-out muisstam, die we succesvol hebben toegepast om de afzonderlijke en gecombineerde bijdrage van elke cluster aan specifieke metabolismeprocessen van geneesmiddelen te onderzoeken. Daarnaast werden er belangrijke farmacologische functies van de carboxylesterase-enzymen verder aangetoond. Ten tweede verkregen we nieuwe belangrijke inzichten in de rol van efflux en influx transporters (ABCB1, ABCG2 en OATP1A/1B) en het enzym CYP3A in farmacokinetische processen van verschillende anti-tumorremmers, evenals gerelateerde geneesmiddel-interactie effecten. Al met al zijn we van mening dat de verkregen nieuwe muismodellen en farmacologische en fysiologische inzichten van belang zullen zijn tijdens de ontdekking en ontwikkeling van geneesmiddelen en hun uiteindelijke klinisch-therapeutische toepassing.

6.3中文总结

人体存在着许多包括药物代谢酶和药物转运蛋白在内地许多解毒/排毒体系。这些体系有着广泛地底物特异性，在保护机体免受各种毒物侵害的同时，也显著地影响着药物地吸收、分布、代谢和外排(ADME)，有时甚至也影响着机体的生理代谢平衡。在药物代谢酶中，羧酸酯酶是一种主要催化酯、硫酸酯和酰胺键水解的药物代谢酶，参与了大量的临床药物代谢。羧酸酯酶2 (CES2) 作为肠道主要的羧酸酯酶亚型，介导大部分口服前药进入血液循环前的首过水解代谢过程，也介导内源性物质的代谢，如胆固醇酯和甘油三酯的水解，进而在脂质代谢平衡中发挥重要作用。鉴于此，在本论文的第一部分，我们建立并表征了CES2相关的转基因小鼠模型，并在此基础上研究了CES2对抗肿瘤药物的药理学作用，同时也研究了CES2潜在的生理学功能。除此之外，药物跨膜有机阴离子摄取转运多肽(OATP)、ATP-结合盒外排转运蛋白(ABC)以及细胞色素P450酶系(以CYP3A家族最为重要)广泛地分布在机体的重要解毒和排毒器官中，这些药物转运蛋白和代谢酶影响着药物的药理学特性。在本论文的第二部分中，我们利用已经构建好的相关小鼠模型，结合转运蛋白抑制剂，研究了转运蛋白和CYP3A代谢酶对抗肿瘤小分子靶向药物的药代动力学的影响，从而阐述和验证它们的药理学功能以及之间的相互作用。

第一部分 羧酸酯酶2的药理学及生理学功能

在本论文的第一章第一节中，我们主要回顾并讨论了包括羧酸酯酶(CES)和芳基乙酰胺脱乙酰酶(AADAC)在内的人体主要酯酶的药理学功能。基于酯酶CES(尤其是CES1和2)和AADAC在肝脏和肠道中的高表达，这些酯酶在某些口服底物药的肠道首过效应以及后续的肝脏代谢过程中发挥了异常重要的作用，从而显著地影响特定药物的血液暴露量，药物疗效甚至其安全性。在本小节中，我们总结了羧酸酯酶(CES1和CES2)以及芳基乙酰胺脱乙酰酶(AADAC)的特异性底物和抑制剂，基因的多态性及其影响，肝脏和肠道酯酶在药物代谢中的作用以及现阶段为满足不同研究需要构建的相关酯酶基因敲除或转基因小鼠模型。在本论文第一章第二节中，我们对上述提到的不同酯酶的生理学功能进行了简述。在此基础上，我们总结了近些年来针对不同酯酶在生理学方面的研究进行了总结，这包括酯酶在脂质代谢和稳态或者糖代谢和稳态中的具体作用以及和脂代谢或糖代谢相关的代谢性疾病，例如非酒精性脂肪肝、糖尿病和动脉粥样硬化等的关系。

本论文的第二章阐述了几种羧酸酯酶2相关的小鼠模型，包括小鼠Ces2全基因簇敲除模型(Ces2^{-/-})，和在此基础上建立的两种分别在肝脏中或肠道中表达人CES2基因的两种人源化小鼠模型(Ces2^{-/-}A和Ces2^{-/-}V)。该三种基因编辑小鼠品系的构建均被证实是有效的、成功的以及具有正常的寿命周期和繁殖效率。通过对该三种小鼠品系的药理学研究，我们发现羧酸酯酶2在两种化疗药物长春瑞滨(Vinorelbine)和卡培他滨(Capecitabine)的代谢中发挥了非常重要的作用。除此之外，我们也证实了羧酸酯酶2在改善脂质代谢和维持糖类正常稳态中所发挥的积极作用。可见，我们所构建的羧酸酯酶2相关的小鼠模型可以帮助提升对某些种类的药物整体药理学认知，特别是酯类药物的早期药物发现，中期药物优化以及后期临床的药物应用。

第二部分 药物转运蛋白和药物代谢酶CYP3A对抗肿瘤小分子靶向药物的药物代谢动力学特性的影响

在本论文第三章中，我们对药物转运蛋白和药物代谢酶CYP3A对药物的药代动力学特性的影响进行了简述。基于重要性的考量，我们对药物转运蛋白家族中的ATP-结合盒(ATP-binding cassette, ABC)外排转运蛋白家族中的两个重要蛋白P-糖蛋白(ABCB1)和乳腺癌抗性蛋白(ABCG2)以及有机阴离子摄取转运多肽家族中的OATP1A/1B进行了较为详细的论述。其中包括，各个药物转运蛋白家族或药物代谢细胞色素P450酶系的家族成员，组织分布和表达量，基因的多态性和潜在的特性行针对特定药物转运蛋白或代谢酶的药物互作影响。

拉罗替尼(Larotrectinib)是一款美国食品药品监督管理局(FDA)批准的用于治疗神经源性酪氨酸激酶受体(NTRK)融合癌症的口服小分子抑制剂。在本论文第四章第一节中，我们探索了第三章所述的药物转运蛋白和代谢酶对拉罗替尼药代动力学上的影响。结果发现，P-糖蛋白(ABCB1)和乳腺癌抗性蛋白(ABCG2)，尤其是ABCB1显著降低了拉罗替尼在血液和脑部的药物暴露量。其次，有机阴离子摄取转运多肽OATP1A/1B也能明显制约其在血液中的药物浓度，这是由于肝脏表达的OATP1A/1B可以主动摄取血液中的拉罗替尼，从而加速肝脏外排药物至胆汁中，最终被清除到体外。此外，结果显示拉罗替尼也是CYP3A酶的底物，CYP3A酶的过表达显著地降低了其血液药物暴露量和组织中的药物浓度。本章以上发现对提高拉罗替尼的药效以及优化临床的实际应用提供了理论支撑，尤其是对发生脑转移的NTRK融合阳性的非小细胞肺癌(NSCLC)和胶质母细胞瘤患者，更具有实际临床意义。

上述发现说明拉罗替尼的药代特性可以被多种药物转运蛋白或药物代谢酶影响，包括但不限于上述提到的ATP-结合盒(ABC)外排转运蛋白家族成员ABCB1和ABCG2，有机阴离子摄取转运多肽OATP1A/1B和药物代谢酶CYP3A。基于此，在第四章第二节中，利用相关基因编辑小鼠模型，在口服拉罗替尼的同时，我们分别给予依克立达(Elacridar, ABCB1和ABCG2抑制剂)、利福平(Rifampin, OATP1A/1B抑制剂)和利托那韦(Ritonavir, CYP3A酶抑制剂)，以此探索药物互作对拉罗替尼的潜在影响。结果表明，依克立达(Elacridar)有效地提升了拉罗替尼在血液和组织中的浓度，同时也大幅度提升了拉罗替尼在脑部的渗透，从而提高拉罗替尼的药效作用。此外，利福平(Rifampin)通过对小鼠OATP1A/1B的抑制以及对肝脏或肠道ABCB1的潜在抑制作用，也显著提高了拉罗替尼的血液浓度。与利福平类似，利托那韦(Ritonavir)也表现出潜在的对CYP3A代谢酶和肝脏或肠道ABCB1的双重抑制作用，从而显著提高了拉罗替尼的口服利用率。综上所述进一步加深了药物互作对拉罗替尼药物代谢影响的理解，也为优化拉罗替尼的临床用药打下基础。

塞尔帕替尼(Selpercatinib)和普拉西替尼(Pralsetinib)是两款FDA批准的针对转染原癌基因(transfection proto-oncogene gene, RET)融合阳性肿瘤的小分子靶向ATP-竞争性抑制剂。对此两个抗肿瘤小分子抑制剂的药代动力学研究结果和论述展示在本轮中第四章第三节和第四小节中。具体而言，ABCB1和ABCG2可以明显地提高两种药物的血液浓度以及脑部和睾丸的药物渗透。在分别共同给药的情况下，Elacridar可以大幅增加两种药物在脑中的浓

度·但并不影响他们的口服利用度和其他器官组织分布。小鼠OATP1A/1B对该两种药物的药代动力学影响并不明显。此外·CYP3A代谢酶可以显著降低Selpercatinib的血液暴露量及组织中的药物浓度·然而CYP3A酶对Pralsetinib的代谢作用则并不明显。这说明机体内仍有其他更重要的代谢体系介导Pralsetinib的代谢。相同地·上述结果可以帮助我们更好地理解塞尔帕替尼(Selpercatinib)和普拉西替尼(Pralsetinib)药物代谢动力学特性。在临床上·我们的发现为该两种药物的临床应用和优化提供了理论支持·使RET受体融合/突变阳性的癌症患者·尤其是脑转移患者受益。

第综上所述·首先·通过羧酸酯酶2相关基因敲出小鼠和人源化转基因小鼠模型的建立和表征·本论文扩展了对现有羧酸酯酶2在药理和生理方面的功能的认知。其次·本论文也探索了ABC外排转运蛋白·OATP摄取转运蛋白或CYP3A药物代谢酶对不同抗肿瘤小分子抑制剂的药物代谢动力学特性的影响。再次·通过对上述转运蛋白或CYP3A代谢酶化学抑制剂与Larotrectinib共同给药·证实了药物互作对特定药物药理药代的显著影响。总之·本论文的各种研究中可以帮助我们更多地了解各种药物转运蛋白和药物代谢酶在药理药代·甚至生理学上的作用。为更好地提高治疗药物的疗效并预测药物间的相互作用提供了强有力的理论支撑。此外·我们也认为在药物转运蛋白和代谢酶的生理·药理和毒理的领域仍有许多未知·也值得我们在后续工作中更深入地探讨。



APPENDICES

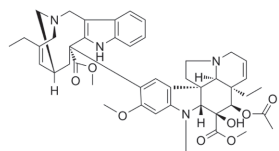
CHEMICAL STRUCTURES

CURRICULUM VITAE

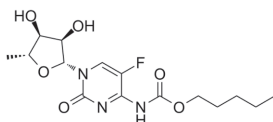
PUBLICATIONS

ACKNOWLEDGEMENTS

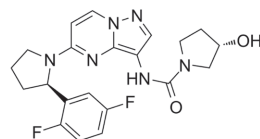
CHEMICAL STRUCTURES



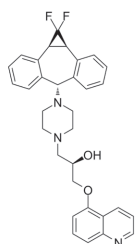
Vinorelbine
MW 778.95



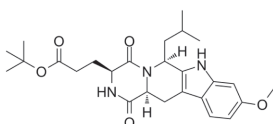
Capecitabine
MW 359.35



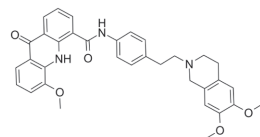
Larotrectinib
MW 428.44



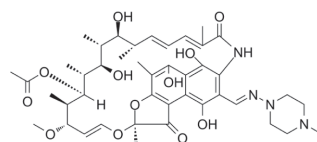
Zosuquidar
MW 527.62



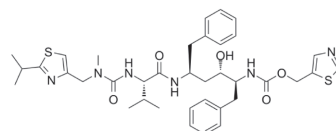
Ko143
MW 469.58



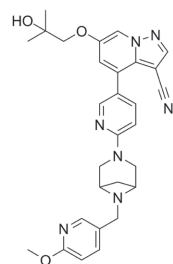
Elacridar
MW 563.65



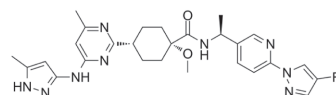
Rifampin
MW 822.95



Ritonavir
MW 720.95



Selpercatinib
MW 525.61



Pralsetinib
MW 533.61

CURRICULUM VITAE

Yaogeng WANG was born on January 27th 1990 in Puyang, Henan Province, P.R. China. After graduated from the Puyang No.1 senior high school, he started his bachelor study at the School of life Science in Sichuan Agriculture University (China), major in bio-engineering. He obtained his B.Sc. degree in 2012. Afterwards, he was enrolled as a master student in West China hospital, Sichuan University. His master program focused on the fundamental oncology research (The influences of complement-dependent immune response effects on the therapeutic effect of breast cancer with Herceptin and the mechanism of this process) and bio-bank optimization research, under the supervision of Prof. Yanping Wang. In the year of 2015, he finished his master program and obtained his master degree. After that, he obtained a scholarship of the China Scholarship Council-Utrecht University PhD program, under the supervision of Prof. Jos H. Beijnen and Dr. Alfred H. Schinkel at the department of Pharmacology, The Netherlands Cancer Institute. During the PhD period, he mainly focused on the pharmacological and physiological functions of carboxylesterase 2 (CES2) family, and drug transporters and Cytochrome P450 3A (CYP3A) enzymes pharmacokinetic effects of anti-tumor small molecule inhibitors, which have been described in the current thesis. After receiving his PhD degree, he will be further trained as a clinical pharmacologist in China.

PUBLICATIONS

1. **Wang, Y.**, Sparidans, R.W., Wang, J., Li, W., Lebre, M.C., Beijnen, J.H. & Schinkel, A.H. Rifampin and ritonavir increase oral availability and elacridar enhances overall exposure and brain accumulation of the NTRK inhibitor larotrectinib. *European Journal of Pharmaceutics and Biopharmaceutics* **170**, 197-207 (2022).
2. **Wang, Y.**, Sparidans, R.W., Potters, S., Şentürk, R., Lebre, M.C., Beijnen, J.H. & Schinkel, A.H. P-Glycoprotein (ABCB1/MDR1) and BCRP (ABCG2) Limit Brain Accumulation and Cytochrome P450-3A (CYP3A) Restricts Oral Exposure of the RET Inhibitor Selpercatinib (RETEVMO). *Pharmaceutics* **14**, (2021).
3. **Wang, Y.**, Sparidans, R.W., Potters, S., Lebre, M.C., Beijnen, J.H. & Schinkel, A.H. ABCB1 and ABCG2, but not CYP3A4 limit oral availability and brain accumulation of the RET inhibitor pralsetinib. *Pharmacological Research* **172**, 105850 (2021).
4. **Wang, Y.**, Sparidans, R.W., Li, W., Lebre, M.C., Beijnen, J.H. & Schinkel, A.H. OATP1A/1B, CYP3A, ABCB1, and ABCG2 limit oral availability of the NTRK inhibitor larotrectinib, while ABCB1 and ABCG2 also restrict its brain accumulation. *British Journal of Pharmacology* **177**, 3060-3074 (2020).
5. Şentürk, R., **Wang, Y.**, Schinkel, A.H., Beijnen, J.H. & Sparidans, R.W. Quantitative bioanalytical assay for the selective RET inhibitors selpercatinib and pralsetinib in mouse plasma and tissue homogenates using liquid chromatography-tandem mass spectrometry. *Journal of Chromatography B: Analytical Technologies in the Biomedical and Life Sciences* **1147**, 122131 (2020).
6. Martínez-Chávez, A., Rosing, H., Gan, C., **Wang, Y.**, Schinkel, A.H. & Beijnen, J.H. Bioanalytical method for the simultaneous quantification of irinotecan and its active metabolite SN-38 in mouse plasma and tissue homogenates using HPLC-fluorescence. *Journal of Chromatography B: Analytical Technologies in the Biomedical and Life Sciences* **1149**, 122177 (2020).
7. Li, W., Sparidans, R., El-Lari, M., **Wang, Y.**, Lebre, M.C., Beijnen, J.H. & Schinkel, A.H. P-glycoprotein (ABCB1/MDR1) limits brain accumulation and Cytochrome P450-3A (CYP3A) restricts oral availability of the novel FGFR4 inhibitor fisogatinib (BLU-554). *International Journal of Pharmaceutics* **573**, 118842 (2020).

8. Li, W., Tibben, M., **Wang, Y.**, Lebre, M.C., Rosing, H., Beijnen, J.H. & Schinkel, A.H. P-glycoprotein (MDR1/ABCB1) controls brain accumulation and intestinal disposition of the novel TGF-beta signaling pathway inhibitor galunisertib. *International Journal of Cancer* (2019).
9. Li, W., Sparidans, R.W., **Wang, Y.**, Lebre, M.C., Beijnen, J.H. & Schinkel, A.H. Oral coadministration of elacridar and ritonavir enhances brain accumulation and oral availability of the novel ALK/ROS1 inhibitor lorlatinib. *European Journal of Pharmaceutics and Biopharmaceutics* **136**, 120-130 (2019).
10. Sparidans, R.W., **Wang, Y.**, Schinkel, A.H., Schellens, J.H.M. & Beijnen, J.H. Quantitative bioanalytical assay for the tropomyosin receptor kinase inhibitor larotrectinib in mouse plasma and tissue homogenates using liquid chromatography-tandem mass spectrometry. *Journal of Chromatography B: Analytical Technologies in the Biomedical and Life Sciences* **1102-1103**, 167-172 (2018).
11. Li, W., Sparidans, R.W., **Wang, Y.**, Lebre, M.C., Wagenaar, E., Beijnen, J.H. & Schinkel, A.H. P-glycoprotein (MDR1/ABCB1) restricts brain accumulation and cytochrome P450-3A (CYP3A) limits oral availability of the novel ALK/ROS1 inhibitor lorlatinib. *International Journal of Cancer* **143**, 2029-2038 (2018).
12. Li, W., Sparidans, R.W., **Wang, Y.**, Lebre, M.C., Beijnen, J.H. & Schinkel, A.H. P-glycoprotein and breast cancer resistance protein restrict brigatinib brain accumulation and toxicity, and, alongside CYP3A, limit its oral availability. *Pharmacological Research* **137**, 47-55 (2018).
13. **Wang, Y.**, Zheng, H., Chen, J., Zhong, X., Wang, Y., Wang, Z. & Wang, Y. The Impact of Different Preservation Conditions and Freezing-Thawing Cycles on Quality of RNA, DNA, and Proteins in Cancer Tissue. *Biopreservation and Biobanking* **13**, 335-347 (2015).
14. Wu, Y., **Wang, Y.**, Qin, F., Wang, Z., Wang, Y., Yang, Y., Zheng, H. & Wang, Y. CD55 limits sensitivity to complement-dependent cytolysis triggered by heterologous expression of alpha-gal xenoantigen in colon tumor cells. *American Journal of Physiology: Gastrointestinal and Liver Physiology* **306**, G1056-1064 (2014).

ACKNOWLEDGEMENTS

Many people can pass by during one's life. During my Ph.D period, I met many nice people who helped me a lot, both from scientific side and living side. Time flies, and I gained a lot in the whole Ph.D journey, and of course also paid a lot. I cannot appreciate more with the supports from all of you, which helped me finalize my Ph.D study.

First of all, I would like to thank Dr. Alfred Schinkel, a wisdom and kind supervisor. For these years, I learnt a lot from you, not only knowledge but also scientific thinking, which taught me how to be a real scientist or researcher. And my promotor Prof. Jos Beijnen, thank you for all the suggestions and comments, which optimized my research. The most important, you inspired me and initiated my interests to clinical pharmacology aspect. All in all, I was happy to do research under the cooperation supervising of both of you, and enjoyed the way we doing science, from bed to bench and then back to bed or from human to mice and back to human.

Dr. Rolf Sparidans, thank you for your massive time input and efforts on my projects. You are an extremely efficient expert in bio-analysis. Dr. Hilde Rosing, I am always impressed by your kindness and friendliness, you can always find some solutions to support my project in our pharmacy department.

All the former and current members of the Schinkel group at the NKI: Els, you were my first teacher when I came here to start my experiment. You are so experienced technician, even though sometimes strict, I can always obtain good results under your training. Cristina, thanks for the help, not only the mice and materials arrangement but also the good suggestions on my projects. Alejandra, Changpei, Jamie, Jing, Margarida, Nancy, Sander, Senchuan, Stephanie, Wenlong and Xiaozhe, all of you helped, supported and inspired me though the past several years. Besides, many thanks for Jamie helping me to translate the summary part of this thesis from English to Dutch.

Many thanks to all the co-authors in this thesis, for all the contributions to my projects.

Thank all the members of my OIO committee. All the helpful and suggestive comments during my PhD study, improved my thesis to a better level.

I also would like to express my gratitude to the Netherlands Cancer Institute. All the staff, especially the transgenic facility, animal facility, pathology department and clinical chemistry lab colleagues. Whenever I had some problems, you always could find solutions to solve them. The most important, our H3 pharmacology department and NKI pharmacy department, where I spent all my PhD study here, for the nice atmosphere for both science and living.

Lizi (Lance), Yuejiao and Hugo, thanks for massive supports and wonderful food from your family, as well as every nice moment shared with you!

To all the Chinese former and current colleagues and friends in the NKI: Changpei, Chong, Cun, Guotai, Haojie, Jing, Ji-Ying, Li Li, Liqin, Ruiqi, Shuqing, Tao, Wenlong, Xiangjun, Xiaohang, Xiaohu, Xinyao, Xuhui, Xuefei, Xuezheng, Yanling, Yuchen, Yuhang et al. I still remember all the nice talk, funny games and great moments with all of you. For Shuqing, who helped me designed this excellent scientific cover, thanks!

To my Chinese literature teacher in the junior high(middle) school who influenced me through the life, Mr. Guozhu Wang (王国柱 先生), for the passion, open-minding and positive attitude to this world, which made me from a boy to a man. My master supervisor Prof. Yanping Wang (王艳萍 先生) and Prof. Hong Zheng (郑鸿 先生), thanks for leading me into medicine science, initiating my interests in cancer research. And all the colleagues who helped me during my master, especially Zhu Wang. I missed all of you, and the City of Chengdu!

My parents, thank for the encourages and unconditional supports through the years since I was born, I owe you too much. To my parents-in-law, too many help from you, which released my stress. The last but most important, to my love, my wife, Wei, a honest, sincere and beautiful lady. I was so lucky to meet you, and without your support, I cannot make it. Cannot find any words to express my appreciation!

